Investigating functional roles of conserved microRNAs in the endometrium of placental mammals

Jessica Charlotte Edge

Submitted in accordance with the requirements for the degree of Doctor of Philosophy

The University of Leeds

School of Molecular and Cellular Biology

September 2023

Intellectual Property and Publication Statement

I confirm that the work submitted is my own, except where work which has formed part of jointly authored publications has been included. My contribution and the other authors to this work has been explicitly indicated below. I confirm that appropriate credit has been given within the thesis where reference has been made to the work of others.

Chapter 2, 3 and 4 contain data which is published in:

MicroRNAs emerging coordinate with placental mammals alter pathways in endometrial epithelia important for endometrial function

Laura Hume, Jessica C. Edge, Haidee Tinning, Dapeng Wang, Alysha S. Taylor, Vladimir Ovchinnikov, Annika V. Geijer-Simpson, Pavle Vrljicak, Jan J. Brosens, Emma S. Lucas, Nigel A.B. Simpson, Jayne Shillito, Karen Forbes, Mary J. O'Connell, and Niamh Forde

iScience, 2023

Author contributions:

Experimental work in this paper was carried out by myself for transfections of Ishikawa cells with microRNAs of interest and subsequent proteomic data analysis.

N.F., M.O'C., K.F., E.S.L., J.J.B., N.A.B.S., and J.S. conceived of the project and designed experiments.

L.H., J.C.E., and H.T. performed experiments. D.W., A.S.T., V.O., A.V.G.S., and P.V. performed data analysis. N.F., J.C.E., and L.H. drafted the manuscript. All authors provided components of the manuscript and contributed to editing drafts of the manuscript.

Analysis of protein was performed by Bristol Proteomics Facility.

Acknowledgements

"I am always doing that which I cannot do, in order that I may learn how to do it.” - Pablo Picasso

"The measure of intelligence is the ability to change." - Albert Einstein

These two quotes perfectly summarise my PhD experience. Research by its very nature is unknown territory, and the last 4 years have taught me perseverance, adaptability, and resilience, whilst I learned how to do the things that I could not do. Inevitably, there are a list of people without whom this project would be impossible, who deserve recognition, and my sincere gratitude, for the significant roles they have played.

First and foremost, I would like to thank my fantastic primary supervisor, Professor Niamh Forde. Niamh, quite simply I would never have embarked on this journey if it was not for the enthusiasm you inspired in me, and I certainly could not have finished it. Thank you for your support, guidance, and understanding. Thank you for letting me cry in your office whenever my experiments failed (which happened more than I care to admit), and for being integral to me becoming the scientist I am today. To my amazing co-supervisors, Dr Karen Forbes, and Dr Mary O'Connell, thank you so much for all of your encouragement, help, and advice. My supervisor meetings have always been a joy to take part in and I am privileged to have worked under three such incredible, successful women.

I have met many wonderful people during this PhD. To all of the colleagues I have had the pleasure of working alongside throughout this journey, past and present members of the Forde and Forbes labs, thank you for the support, friendship, and forcing me to start liking cake. I would like to thank Haidee Tinning in particular, who has always answered my stupid questions, bounced ideas back and forth, replied to my panicked texts, and looked after cells or long-term experiments if I have been away from the lab. Furthermore, thank you to LeedsOmics and Bristol Proteomics Facility for their assistance in RNASeq and Proteomic analyses.

To my parents, thank you for always believing in me and pushing me to achieve my best, as well as supporting my many changes of heart throughout my education - we all knew I'd get there eventually. Thank you also to you both, and my grandparents, for attempting to read everything I have ever written throughout my PhD; including academic papers I am an author on, despite not understanding a word of it. I love you all.

To Kieran, there aren't words to express how grateful I am to you for your support, and always reminding me of my achievements when I needed to hear it. You are patient, encouraging and inspiring, knowing exactly when to use each. Thank you for doing everything in your power to help, from driving me to Uni in the middle of the night, to letting me practise my presentations over and over, and making a genuine effort to learn, understand and remember everything I study. I simply could not have done this without you, I love you.

Special mentions go to my friends - I wish I could name you all here - for helping me maintain my sanity, and letting me vent about everything and anything, as well as the 1903 HP team for keeping me full of coffee and wonderful food throughout the long process of writing up. I can't forget to acknowledge my puppy Bobby, who did not realise he would be taking on a role as my therapy animal throughout the last year - being present as moral support for nearly every hour of writing; and who only dived on my laptop keyboard when it was absolutely necessary...

And finally, it would not be appropriate to submit this thesis without acknowledging the help of a dear friend who is sadly no longer with us. Darren Duke, thanks must go to you for rescuing my entire laptop memory with ALL of my (stupidly not backed up) data and writing on it. You helped me without hesitation at a moment’s notice during lockdown when I had no other options, physically angle-grinding down your tools to the right size to get into the back of my laptop and rescue my files. Without your kindness I'd have lost so much work. I promise I've backed up everything ever since. You are so missed... thank you, Daz.

Abstract

Early pregnancy events like implantation strategies are diverse amongst eutherian mammals. Some molecular signals between embryo and endometrium during the peri-implantation period of pregnancy are conserved *e.g.,* progesterone, whilst others are species-specific, such as those involved in maternal recognition of pregnancy. MicroRNAs are one key set of molecules which may be involved in conservation or diversification of early pregnancy events. Recently, our lab identified a set of microRNAs which arose concurrent with eutherian mammals and were subsequently never lost. Three (miR-340-5p, -542-3p and -671-5p) are differentially expressed following progesterone treatment. We hypothesised that these miRNAs modify endometrial protein expression, facilitating receptivity to implantation. To investigate mechanistically, Ishikawa cells (n=3) were transfected with miRNA mimics, inhibitors, and controls for 48hrs. Protein was extracted and TMT mass spectrometry performed. Statistical significance was calculated using paired T-Tests and Benjamini-Hochberg correction. Differential expression of miRNAs significantly altered many endometrial epithelial proteins. Functions significantly enriched include metabolism, localisation, and endoplasmic reticulum stress - involved in decidualisation, important to implantation. Many altered proteins were associated with proliferation, which may be important for establishing receptivity. To investigate functionally, embryo-like spheroids (trophoblast cell line) were added to transfected Ishikawa cells to determine spheroid attachment. MiR-542-3p significantly reduced attachment, and some miRNA combinations also altered embryo attachment. We propose these miRNAs are involved in altering protein abundance, having implications for endometrial receptivity to embryo implantation. Finally, 2 novel 3D models of the endometrium were developed. A 3D multicellular human endometrial model using Alvetex scaffolds - where miRNAs of interest could be differentially expressed - showed reduced proliferation following overexpression of miR-340-5p, miR-542-3p and miR-671-5p. Bovine endometrial organoids derived from endometrial glands were shown, by RNASeq, to be progesterone responsive. These models provide tools to investigate endometrial receptivity and implantation, allowing species comparison to understand the diversity in reproductive strategies.

Table of Contents

List of Figures

List of Tables

List of Supplementary Material

Available in separate documents.

Supplementary Figure 1: Proteins altered in endometrial epithelial cells following treatment with miR-340-5p mimic and/or inhibitor compared to miRDB predicted targets.
Supplementary Figure 2: Proteins altered in endometrial epithelial cells following treatment with miR-542-3p mimic and/or inhibitor compared to miRDB predicted targets.
Supplementary Figure 3: Proteins altered in endometrial epithelial cells following treatment with miR-671-5p mimic and/or inhibitor compared to miRDB predicted targets.

Supplementary Table 1: List of proteins significantly altered in abundance in response to non-targeting mimic and miR-340-5p mimic. Final column lists proteins solely altered by miR-340-5p mimic once off target effects are removed ($p<0.05$), n=3. Corresponds to Figure 2.10.
Supplementary Table 2: List of proteins significantly more or less abundant in response to miR-340-5p mimic (n=3). Corresponds to Figure 2.12.
Supplementary Table 3: List of proteins significantly altered in abundance in response to non-targeting inhibitor and miR-340-5p inhibitor. Final column lists proteins solely altered by miR-340-5p inhibitor once off target effects are removed ($p<0.05$), n=3. Corresponds to Figure 2.13.
Supplementary Table 4: List of proteins significantly more or less abundant in response to miR-340-5p inhibitor (n=3). Corresponds to Figure 2.14.
Supplementary Table 5: List of proteins significantly altered in abundance in response to miR-340-5p mimic, inhibitor, both ($p<0.05$), n=3. Corresponds to Figure 2.15.
Supplementary Table 6: List of proteins significantly altered in abundance in response to miR-340-5p mimic and inhibitor (n=3) in the same direction or opposite directions. Corresponds to Figure 2.16.
Supplementary Table 7: List of proteins significantly altered in abundance in response to miR-340-5p mimic and/or inhibitor, miRDB predicted targets of miR-340-5p. Final column lists genes common to altered proteins in miR-340-5p mimic and/or inhibitor and a miRDB predicted target ($p<0.05$), n=3. Corresponds to Figure 2.17.
Supplementary Table 8: List of proteins significantly altered in abundance in response to miR-340-5p mimic and/or inhibitor, miRDB Predicted targets and P4 regulated genes which are predicted targets of miR-340-5p by Targetscan ($p<0.05$), n=3. Corresponds to Figure 2.18.
Supplementary Table 9A: List of gene names in segments of Venn diagram in Figure 2.19 comparing endometrial biopsy RNASeq data with proteins altered in abundance in response to differential expression of miR-340-5p. Corresponds to Figure 2.19
Supplementary Table 9B: RNASeq data for human endometrial biopsies for mRNAs matching 1192 proteins changed in response to miR-340-5p mimic. Refers to Figure 2.19.
Supplementary Table 9C: RNASeq data for human endometrial biopsies for mRNAs matching 267 proteins changed in response to miR-340-5p inhibitor. Refers to Figure 2.19.

Supplementary Table 9D: RNASeq data for human endometrial biopsies for mRNAs matching 59 proteins changed in response to miR-340-5p mimic AND inhibitor. Refers to Figure 2.19.
Supplementary Table 10: List of proteins significantly altered in abundance in response to non-targeting mimic and miR-542-3p mimic. Final column lists proteins solely altered by miR-542-3p mimic once off target effects are removed ($p<0.05$), n=3. Corresponds to Figure 3.6.
Supplementary Table 11: List of proteins significantly more or less abundant in response to miR-542-3p mimic (n=3). Corresponds to Figure 3.8.
Supplementary Table 12: List of proteins significantly altered in abundance in response to non-targeting inhibitor and miR-542-3p inhibitor. Final column lists proteins solely altered by miR-542-3p inhibitor once off target effects are removed ($p<0.05$), n=3. Corresponds to Figure 3.9.
Supplementary Table 13: List of proteins significantly more or less abundant in response to miR-542-3p inhibitor (n=3). Corresponds to Figure 3.10.
Supplementary Table 14: List of proteins significantly altered in abundance in response to miR-542-3p mimic, inhibitor, both ($p<0.05$), n=3. Corresponds to Figure 3.11.
Supplementary Table 15: List of proteins significantly altered in abundance in response to miR-542-3p mimic and inhibitor (n=3) in the same direction or opposite directions. Corresponds to Figure 3.12.
Supplementary Table 16: List of proteins significantly altered in abundance in response to miR-542-3p mimic and/or inhibitor, miRDB predicted targets of miR-542-3p. Final column lists genes common to altered proteins in miR-542-3p mimic and/or inhibitor and a miRDB predicted target ($p<0.05$), n=3. Corresponds to Figure 3.13.
Supplementary Table 17: List of proteins significantly altered in abundance in response to miR-542-3p mimic and/or inhibitor, miRDB Predicted targets and P4 regulated genes which are predicted targets of miR-542-3p by Targetscan ($p<0.05$), n=3. Corresponds to Figure 3.14.
Supplementary Table 18A: List of gene names in segments of Venn diagram in Figure 3.15 comparing endometrial biopsy RNASeq data with proteins altered in abundance in response to differential expression of miR-542-3p. Corresponds to Figure 3.15
Supplementary Table 18B: RNASeq data for human endometrial biopsies for mRNAs matching 1080 proteins changed in response to miR-542-3p mimic. Refers to Figure 3.15.
Supplementary Table 18C: RNASeq data for human endometrial biopsies for mRNAs matching 714 proteins changed in response to miR-542-3p inhibitor. Refers to Figure 3.15**.**
Supplementary Table 18D: RNASeq data for human endometrial biopsies for mRNAs matching 181 proteins changed in response to miR-542-3p mimic AND inhibitor. Refers to Figure 3.15.
Supplementary Table 19: List of proteins significantly altered in abundance in response to non-targeting mimic and miR-671-5p mimic. Final column lists proteins solely altered by miR-671-5p mimic once off target effects are removed ($p<0.05$), n=3. Corresponds to Figure 4.6.
Supplementary Table 20: List of proteins significantly more or less abundant in response to miR-671-5p mimic (n=3). Corresponds to Figure 4.8.
Supplementary Table 21: List of proteins significantly altered in abundance in response to non-targeting inhibitor and miR-671-5p inhibitor. Final column lists

proteins solely altered by miR-671-5p inhibitor once off target effects are removed ($p<0.05$), n=3. Corresponds to Figure 4.9.

Supplementary Table 22: List of proteins significantly more or less abundant in response to miR-671-5p inhibitor (n=3). Corresponds to Figure 4.10.

Supplementary Table 23: List of proteins significantly altered in abundance in response to miR-671-5p mimic, inhibitor, both ($p<0.05$), n=3. Corresponds to Figure 4.11.

Supplementary Table 24: List of proteins significantly altered in abundance in response to miR-671-5p mimic and inhibitor (n=3) in the same direction or opposite directions. Corresponds to Figure 4.12.

Supplementary Table 25: List of proteins significantly altered in abundance in response to miR-671-5p mimic and/or inhibitor, miRDB predicted targets of miR-671-5p. Final column lists genes common to altered proteins in miR-671-5p mimic and/or inhibitor and a miRDB predicted target ($p<0.05$), n=3. Corresponds to Figure 4.13.

Supplementary Table 26: List of proteins significantly altered in abundance in response to miR-671-5p mimic and/or inhibitor, miRDB Predicted targets and P4 regulated genes which are predicted targets of miR-671-5p by Targetscan ($p<0.05$), n=3. Corresponds to Figure 4.14.

Supplementary Table 27A: List of gene names in segments of Venn diagram in Figure 4.15 comparing endometrial biopsy RNASeq data with proteins altered in abundance in response to differential expression of miR-671-5p. Corresponds to Figure 4.15.

Supplementary Table 27B: RNASeq data for human endometrial biopsies for mRNAs matching 1063 proteins changed in response to miR-671-5p mimic. Refers to Figure 4.15.

Supplementary Table 27C: RNASeq data for human endometrial biopsies for mRNAs matching 362 proteins changed in response to miR-671-5p inhibitor. Refers to Figure 4.15.

Supplementary Table 27D: RNASeq data for human endometrial biopsies for mRNAs matching 87 proteins changed in response to miR-671-5p mimic AND inhibitor. Refers to Figure 4.15.

Supplementary Table 28: List of proteins comparing significantly altered in abundance in response to miR-340-5p, miR-542-3p and miR-671-5p mimic and/or inhibitor ($p<0.05$), n=3. Corresponds to Figure 4.17.

Supplementary Table 29: List of proteins comparing significantly altered in abundance in response to miR-340-5p, miR-542-3p and miR-671-5p mimic ($p<0.05$), n=3. Corresponds to Figure 4.18.

Supplementary Table 30: List of proteins comparing significantly increased in abundance in response to miR-340-5p, miR-542-3p and miR-671-5p mimic ($p<0.05$), n=3. Corresponds to Figure 4.19.

Supplementary Table 31: List of proteins comparing significantly decreased in abundance in response to miR-340-5p, miR-542-3p and miR-671-5p mimic ($p<0.05$), n=3. Corresponds to Figure 4.19.

Supplementary Table 32: List of proteins comparing significantly altered in abundance in response to miR-340-5p, miR-542-3p and miR-671-5p inhibitor ($p<0.05$), n=3. Corresponds to Figure 4.20.

Supplementary Table 33: List of proteins comparing significantly increased in abundance in response to miR-340-5p, miR-542-3p and miR-671-5p inhibitor ($p<0.05$), n=3. Corresponds to Figure 4.21.

Abbreviations

ABAM	Anti-biotic anti-mycotic
ANXA2	Annexin A2
BSA	Bovine serum albumin
cAMP	Cyclic adenosine monophosphate
CCNA2	Cyclin A2
CD55	Complement decay-accelerating factor
CDK14	Cyclin-dependent kinase 14
Cdk2	Cyclin-dependent kinase 2
Cdx2	Caudal type homeobox 2
CLDN4	Claudin 4
Cox-2	Cyclooxygenase-2
CST3	Cystatin C
CUL5	Cullin 5
Cyclic AMP	Cyclic adenosine monophosphate
dNK cells	Decidual natural killer cells
DMEM	Dulbecco's Modified Eagle Medium
DOHaD	Developmental Origins of Health and Disease
Drosha	Drosha ribonuclease III
DSCs	Decidualised stromal cells
E2	Oestrogen
ECACC	European Collection of Authenticated Cell Cultures
EGF	Epidermal growth factor
ER	Endoplasmic reticulum
ER-α	Oestrogen receptor alpha
ERAD	Endoplasmic reticulum-associated degradation

ESCRT	Endosomal sorting complex required for transport machinery
ESCs	Endometrial stromal cells
ESR1	Oestrogen receptor 1
EV	Extracellular vesicle
FBLN1	Fibulin 1
FBS	Fetal Bovine Serum
FGF	Fibroblast growth factor
FOXO1	Forkhead box O1
FSH	Follicle stimulating hormone
GDM	Gestational diabetes mellitus
GnRH	Gonadotrophin releasing hormone
GREB1	Growth regulation by oestrogen in breast cancer 1
GSP	Glutamine, streptomycin and penicillin
Hand2	Hand and Neural Crest Derivatives Expressed 2
HBSS	Hanks' balanced salt solution
hCG	Human chorionic gonadotropin
Hoxa10	Homeobox A10
HSPG2	Heparan sulphate proteoglycan 2
HUVECs	Human umbilical vein endothelial cells
IFNG	Interferon-γ
IFNT	Interferon tau
Ihh	Indian hedgehog
IVF	in vitro fertilisation
JAK3	Janus kinase 3
KMD1A	Lysine-specific demethylase 1A
let-7	Lethal-7

LH	Luteinising hormone
LIF	Leukaemia inhibitory factor
MAPK	Mitogen-activated protein kinase
MET	Mesenchymal to epithelial transition
miRNA	MicroRNA
mRNA	Messenger RNA
MRP	Maternal recognition of pregnancy
MUC-1	Mucin-1
Nanog	Nanog homeobox
NFIA	Nuclear Factor I A
NO	Nitric oxide
Oct4	Octamer-binding transcription factor 4
P4	Progesterone
PAR1	Partitioning defective complex
PBS	Phosphate buffered saline
PCA	Principal component analysis
PCOS	Polycystic ovary syndrome
PGE2	Prostaglandin E2
PGR	Progesterone receptor
PNO1	Partner of NOB1 homolog
Poly-A	Poly adenylated
Pre-miRNA	Precursor miRNA
Pri-miRNA	Primary microRNA
PRR11	Proline rich 11
PTGS2	Prostaglandin-endoperoxide synthase 2
PTRH2	Peptidyl-tRNA hydrolase 2
PVP	Polyvinylpyrrolidone
RanGTP	RAS-related nuclear protein-guanosine-5’-triphosphate-ase

RIF	Recurrent implantation failure
RISC	RNA induced silencing complex
ROS	Reactive oxygen species
RT	Reverse transcription
SDC-1	Syndecan-1
SDC-3	Syndecan-3
Sox2	SRY-box transcription factor 2
STAT	Signal transducer and activator of transcription
STRING	Search tool for the retrieval of interacting genes/proteins
Tead4	TEA domain transcription factor 4
TGF	Transforming growth factor beta 1
TGFβR2	Transforming growth factor beta receptor type 2
TJs	Tight junctions
TMT	Tandem Mass Tag
TNF	Tumour necrosis factor
TP53I11	Tumour protein p53-inducible protein 11
UPR	Unfolded protein response
UTR	Untranslated region
ZNF346	Zinc finger protein 346

Chapter 1 Introduction

1.1 Placental Mammals

The Mammalia are a class of animals characterised by being warm-blooded, with specific mammalian traits of body hair, lactation, three middle ear ossicles and a singular lower jawbone (Anthwal et al., 2013). Within the class Mammalia, there are two extant subclasses: Prototheria, which is made up of the Monotremata - egg laying monotremes; and the Theria, consisting of the Metatheria *i.e.,* marsupials, and the eutheria – commonly known as placental mammals (Rawlings, Makwana, Taylor, et al., 2021). A placenta is present in some form in all species within the Theria, though the term placental mammals usually alludes to eutherians only, as the marsupial placenta does not represent a typical placenta - more aptly referred to as a 'placenta-like structure' (Roberts et al., 2016). For this thesis, any further mention of placental mammals will refer specifically to eutherians, *i.e*., humans, ruminants, primates, mice. Marsupial gestation and placentation are generally shorter than that of the eutherian mammals, with specialised, temporally regulated changes in lactation supporting the offspring after birth until fully developed (Guernsey et al., 2017). Alternatively, the eutherian gestation is usually longer, with a placenta persisting throughout, carrying out its roles in gas and nutrient exchange along with hormone production and immune system protection (Rankin and Clauss, 2021).

The divergence of characteristics between eutherian mammals and marsupials does not stop at the placenta. Eutherians lack epipubic bones - allowing for expansion of the abdomen to accommodate a pregnancy (Dunwell et al., 2017). There are dental differences between the eutherians and marsupials, with the majority of marsupial species possessing a single generation of teeth, whereas eutherians undergo 2 generations of nearly all teeth (Nievelt and Smith, 2005). Litter size and frequency of pregnancy also differ greatly within eutherian mammals, as well as between eutherians and marsupials (Hamilton et al., 2011). Many aspects of the remainder of this chapter will discuss, compare, and contrast reproductive processes using human and bovine as example species due to their diverse reproductive phenotypes.

1.2 Hormonal Regulation of the Menstrual/Estrous Cycle

In humans, the cyclic pattern of preparing the uterus for a pregnancy followed by either: sloughing of the lining of the uterus in the absence of a blastocyst to re-start the cycle, or supporting the pregnancy in the event of fertilisation, is known as the menstrual cycle; and usually lasts approximately 28 days (Critchley et al., 2020). An overview of the menstrual cycle, consisting of the proliferative - or follicular - phase, and the secretory - or luteal - phase is shown in Figure 1.1. In most other mammals, for example bovine, the reproductive cycle is known as the estrous cycle (Forde et al., 2011), with similarities and differences to the menstrual cycle, which will be highlighted.

The driving factor of both the menstrual and estrous cycles is gonadotropin releasing hormone (GnRH), produced in the hypothalamus in the brain, and secreted in frequent pulses; which are more frequent in the follicular phase of the cycle, and less regular in the luteal phase (Barbieri, 2014). Several molecules are involved in stimulating or inhibiting GnRH to control its pulsatile expression; norepinephrine and kisspeptin induce GnRH whereas progesterone (P4), beta-endorphin and interleukin-1 are known to inhibit its expression (Tsutsumi and Webster, 2009). This process can be altered by the female's environment, as adverse conditions resulting in factors like poor nutrition or stress cause fewer GnRH pulses. This has a knock-on effect on the menstrual cycle and can result in no ovulation, as it would be unfavourable for a pregnancy to occur in these conditions (Barbieri, 2014).

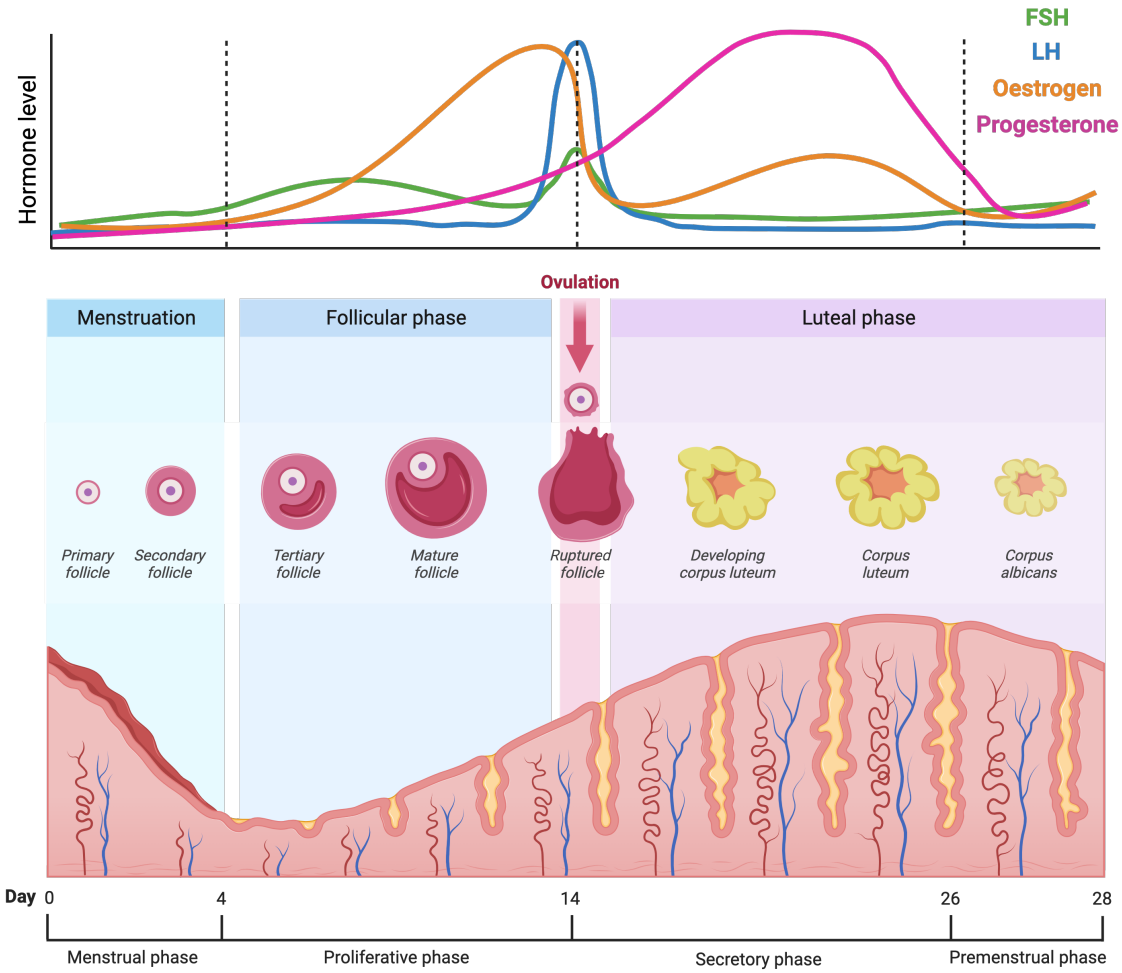

Figure 1.1: *Overview of the human menstrual cycle*.
Image shows representative thickness of the endometrium, oocyte development and hormone levels of progesterone (pink), oestrogen (yellow), follicle stimulating hormone (FSH - green) and luteinizing hormone (LH - blue) during menstruation, follicular phase, ovulation and luteal phase. Figure created using Biorender.com

In mammals, pulses of GnRH trigger the release of both follicle stimulating hormone (FSH) and luteinising hormone (LH), which are produced in the anterior pituitary (Tsutsumi and Webster, 2009). Less frequent pulses of GnRH approximately 2-4 hours apart in the follicular phase result in FSH release, and as these pulses become more regular (~30 minutes apart) this triggers the LH surge at the time of ovulation (Bernard et al., 2010). Throughout this time, primordial follicles in the ovary continuously begin to grow to form primary follicles and secondary follicles until they reach tertiary follicle (characterised by an antral cavity) (Figure 1.1) (McGee and Hsueh, 2000). The developing follicle is surrounded by granulosa cells, and outside of this, from the secondary follicle stage onwards, theca cells (Skinner et al., 2008). Early development of the primordial follicle is FSH independent, as surrounding granulosa cells lack FSH receptor, whereas FSH receptor becomes expressed in granulosa cells at the secondary follicle stage - thought to be induced by androgens (Kishi et al., 2018). At this stage, the follicles come into contact with the blood supply by development of small arterioles; and the stromal cells surrounding the granulosa cells align to form the thecal layer (Gougeon, 2003). Tertiary follicles can only bypass atresia and mature in the presence of rising concentrations of FSH - which a small number achieve (McGee and Hsueh, 2000). The follicles which persist at this point acquire LH receptors expressed on the granulosa cells - induced by actions of FSH (Kishi et al., 2018). The actions of FSH on FSH receptor, along with LH interaction with LH-receptor on the granulosa cells, both result in production of cyclic adenosine monophosphate (cAMP) (Zeleznik, 2004). This means that the requirement for FSH in follicular development is reduced, the follicle is now responsive to FSH and LH, whereas previously it was responsive only to FSH. Each cycle, only 1 of these follicles becomes dominant and results in ovulation, with the rest undergoing atresia (Fauser and Van Heusden, 1997). Surrounding theca cells produce androgens which are required by the granulosa cells for FSH induced production of oestrogen (E2) in response to the low concentrations of LH (Skinner, 2005). Due to the production of E2 from the dominant follicle, FSH production is suppressed, meaning there is no growth in other premature follicles (Barbieri, 2014). Despite the reduction in FSH, the dominant follicle is able to continue to grow, due to its expression of FSH receptors with a higher receptivity for FSH (Kumar and Sait, 2011), as well as becoming responsive to LH (Zeleznik, 2004). High concentrations of E2 result in positive feedback to the pituitary, provoking a GnRH mediated LH surge at the middle of the cycle which triggers final maturation and subsequently ovulation of the oocyte (Wallach et al., 1995).

During the LH surge, non-dominant follicles regress, as it is thought they have a lower maximum responsivity to LH than the dominant follicle (Kumar and Sait,

2011). Immediately following the LH surge, the LH receptor is downregulated on granulosa cells, before being upregulated again later in the luteal phase (Yung et al., 2014). A number of signalling pathways important for ovulation are activated by the LH surge. The mitogen-activated protein kinase (MAPK) pathway is activated - which is required for oocyte maturation and ovulation by inducing production of epidermal growth factor (EGF) like ligands (Robker et al., 2018). These ligands activate the EGF receptor on the cumulus cells (the granulosa cells immediately surrounding and closely associated with the oocyte) essentially communicating the LH-surge to allow an ovulatory response and expansion of the cumulus-oocyte complex (Park et al., 2004). Knockdown of MAPK signalling also results in failure of the follicle to rupture, meaning the oocyte is not released (Fan et al., 2009). Expression of progesterone receptor (PGR) is activated following the LH surge, and also plays a role in rupture of the follicle by controlling cytokine production and presence of immune cells (Robker et al., 2018). Ovulation of an oocyte marks the beginning of the luteal, or secretory phase of the menstrual cycle. Humans as well as cows usually ovulate a single oocyte, whereas other species such as pigs ovulate many oocytes at once, and sheep may ovulate 1 or more oocyte, varying between breeds (Hunter et al., 2004).

The remains of the follicle from which the oocyte was ovulated becomes a structure known as the corpus luteum, which is infiltrated by the generation of new blood vessels due to remodelling of the surrounding cells (Messinis et al., 2009). Triggered by the LH surge which caused ovulation of the mature oocyte, the granulosa cells are reprogrammed into luteal cells, occurring in a matter of hours (Stocco et al., 2007). The luteal cells undergo cell cycle arrest (Green et al., 2000), and cell cycle regulators such as cyclin-dependent kinase 2 (*Cdk2*) and cyclin D2 are downregulated by the LH surge (Richards et al., 1998; Green et al., 2000). Other genes are thought to be induced at this stage and involved in the process of luteinization, including P4 receptor (Park and Mayo, 1991) and cyclooxygenase-2 (*Cox-2)* (Lim et al., 1997). Structurally, the membrane of the follicle is disrupted, resulting in an influx of theca cells, endothelial cells and fibroblasts (Green et al., 2000), and angiogenesis establishes a blood supply to the corpus luteum (Reynolds et al., 2000).

The corpus luteum is responsible for production of P4, which is the main hormone acting during the luteal phase to prepare the uterus for an imminent pregnancy (Nagy et al., 2021). Should pregnancy not occur, the corpus luteum regresses due to the absence of human chorionic gonadotropin (hCG), or IFNT in bovine; this ceases P4 production and triggers cell death (Devoto et al., 2009). The molecular mechanism of luteolysis is not fully understood, with

$PGF_{2\alpha}$ produced by the endometrium hypothesised to drive luteolysis, by activating cell death pathways (Jonczyk et al., 2019). Cell death is thought to occur in luteolysis primarily by caspase dependent apoptosis, and molecules which have been found to be mediators of the process are tumour necrosis factor-α (TNF), interferon-γ (IFNG) and nitric oxide (NO) (Teeli et al., 2019). Endothelin-1 is also thought to play a role (Girsh et al., 1996).

Decreasing concentrations of P4 removes the P4 mediated downregulation of GnRH pulses, resulting in them becoming more frequent, which increases production of E2 and stimulates follicular development (McCracken et al., 1999). Reduction of P4 also results in the commencement of menstruation in humans, where shedding of the lining of the uterus occurs leading to repair, and the cycle is repeated (Critchley et al., 2001). In non-pregnant animals, rather than sloughing of the endometrium as in humans, the tissue is reabsorbed to re-start the estrous cycle (Radi et al., 2009).

As mentioned, there are some similarities and differences between the menstrual cycle in humans and estrous cycle in most other mammals. The bovine reproductive cycle lasts a shorter time than that of humans: approximately 18-24 days; the follicular phase spanning 4-6 of those days and the luteal phase the remaining 14-18 days (Forde et al., 2011). Similarly to humans, GnRH, FSH, LH, P4 and E2 hormonally control the transition from follicular phase, to ovulation, to luteal phase in the estrous cycle (Roche, 1996). Also, the corpus luteum produced from the site of ovulation governs the length of the luteal phase; with its regression and luteolysis occurring in the absence of a conceptus, due to lack of P4, causing the cycle to restart (Forde et al., 2011).

1.3 Uterine Receptivity to Implantation

The innermost lining of the uterus is named the endometrium. Its purpose is to support a pregnancy, by providing a receptive implantation site for an embryo and promoting its growth and development (Marquardt et al., 2019). The endometrium is comprised of an epithelial layer made up of luminal epithelial cells - the site of implantation, and glandular epithelial cells, secretions of which support a blastocyst; as well as a stromal layer (Lessey and Young, 2019a). The supporting stromal cell layer in humans is responsible for proliferation, decidualization (Section 1.6) and remodelling (Queckbörner et al., 2020). The events preceding successful implantation require a carefully tuned orchestration of events and signalling which result in an appropriately developed embryo meeting an optimally primed endometrium. The period during which this is possible is referred to as the window of receptivity, and to achieve this, the endometrium must establish receptivity to implantation (Large and DeMayo, 2012). The key hormones involved in establishing endometrial receptivity are E2 and P4. As described in Section 1.2, during the proliferative phase of the menstrual cycle, E2 is the primary hormone. Endometrial receptivity depends on appropriate pre-priming with E2 - which drives proliferation of the endometrium (Moustafa and Young, 2020). Oestrogen receptor alpha (ER-α) is highly expressed in endometrial epithelial cells during the proliferative phase, with its expression greatly reduced around the window of receptivity in all Eutherians (Dorostghoal et al., 2018). Following ovulation, P4 is the active hormone working to create a receptive endometrium. It is also thought to play a role in immune tolerance of the embryo by the maternal immune system (Lessey and Young, 2019b). In all mammalian endometrium that has been studied, the nuclear progesterone receptor (PR) is present in two forms – PRA and PRB – and the receptor can be located in the nucleus or membranous. Expression of the PR is controlled by E2 and P4 which up- and down-regulate it, respectively (Graham and Clarke, 1997). P4 also negatively regulates ER, explaining its reduction in the secretory phase (Evans and Leavitt, 1980). P4 and PR interaction is essential for uterine receptivity, demonstrated in a knockout mouse model which resulted in implantation failure and lack of decidualisation; rendering the mice infertile (Wetendorf and DeMayo, 2012).

P4 has many different effects on the endometrium which function to establish receptivity. One of these effects in humans is that P4 drives cyclic stromal cell decidualisation, which is discussed in section 1.6. Presence of P4 also halts epithelial proliferation (Marquardt et al., 2019). This is thought to be carried out by upregulation of downstream P4 target Hand and Neural Crest Derivatives Expressed 2 (Hand2) (Q. Li et al., 2011). *Hand2* results in downregulation of

multiple fibroblast growth factors, and this inhibits epithelial proliferation. Other downstream targets have been associated with implantation. Indian hedgehog (*Ihh*) which is upregulated by P4 signalling is necessary for communication between epithelial and stromal cells, with *Ihh* only present in the epithelial cells, yet its targets, which are only present in stromal cells, respond to *Ihh* induction (Takamoto et al., 2002). As the endometrium requires extensive coordination of multiple cell types to achieve receptivity, the absence of cross communication between epithelial and stromal cells is inconceivable. Homeobox A10 (*Hoxa10*) is regulated by P4 and is present in the epithelial cells of the endometrium early after ovulation, before becoming expressed in stromal cells during decidualisation (Satokata et al., 1995; Ma et al., 1998). *Hoxa10* is thought to be involved in endometrial receptivity as knockdown mouse models display a reduced success rate for embryo attachment (Benson et al., 1996).

The range of functions and cell types P4 is involved in along with the large number of targets which work synchronously to establish endometrial receptivity highlight the importance of correct P4 signalling in successful implantation. In humans, decidualisation - which is P4 regulated - is a major requirement for endometrial receptivity.

1.4 Embryo Development

Fertilisation of the human oocyte occurs in the oviduct and refers to the fusion of a single spermatozoa with an oocyte; amalgamating the maternal and paternal chromosomes; and producing a zygote (Georgadaki et al., 2016). The human zygote is then subjected to a number of cell divisions over the course of the next 6 to 7 days, forming a diploid cell, to a 4-cell embryo, followed by 8-cell embryo and next a morula (Figure 1.2) (Weatherbee et al., 2021).

In humans, a blastocyst is then formed from the morula, through the stages of compaction, internalisation and lumen formation (Shahbazi, 2020). Compaction increases the cell-cell contact between the blastomeres, meaning they have less contact with the surrounding material (Maître, 2017). Mouse embryos have been used to study the mechanism of compaction, and this revealed that the actomyosin cytoskeleton drives this process by creating tension in the membranes and producing pulsatile contractions (Shahbazi, 2020). E-cadherin is also involved in compaction, where it is a major component of the filopodia -

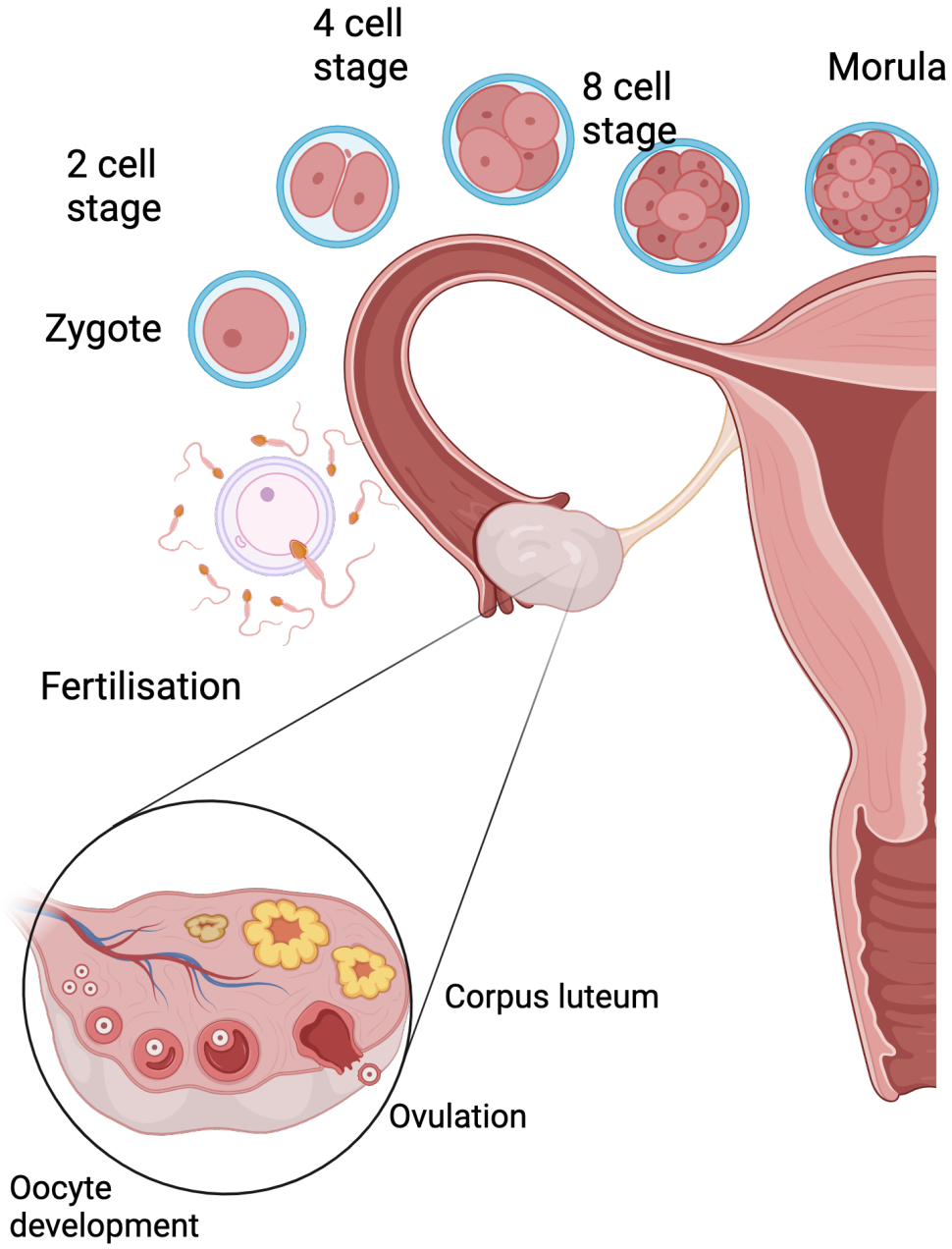

Figure 1.2: *Diagram of early human embryo development.*
Diagram shows oocyte development to ovulation in the ovary, followed by fertilisation and production of a zygote through cell cleavages resulting in a morula. Figure created using Biorender.com

which are cell protrusions - that are responsible for adhering the cells of the embryo together (Fierro-González et al., 2013).

The next process of rearranging blastomeres to fully encapsulate a number inside other cells is known as internalisation, and these cells are sorted so that those destined for inner cell mass are inside. Insights into this process come from polarisation of mouse embryo models, where E-cadherin and other proteins associated with adhesion localise basolaterally, and cytoskeletal proteins along with others such as partitioning defective complex (PAR1) localise apically (Shahbazi, 2020). Molecularly, in mice it has been shown that protein kinase C induces this process (Zhu et al., 2017). Both polarity and cell position are involved in determining whether the cell is destined for inner cell mass or trophectoderm fate; and interestingly, inside cells lose their polarity, resulting in them becoming part of the inner cell mass (Chen et al., 2010). Gene expression profiles in the two cell types are different, with octamer-binding transcription factor 4 (*Oct4),* SRY-box transcription factor 2 (*Sox2)* and Nanog homeobox (*Nanog)* expressed in the inner cell mass, whereas caudal type homeobox 2 (*Cdx2)* and TEA domain transcription factor 4 (*Tead4)* is expressed in the trophectoderm (Chen et al., 2010).

The developing blastocyst then forms a lumen known as the blastocoel which becomes filled with fluid (Gauster et al., 2022) This fluid moves from outside the blastocyst to inside by osmosis, causing the production of small fluid-filled lumens that merge into one large lumen that undergoes expansion due to hydrostatic pressure inside the blastocyst (Shahbazi, 2020). The inner cell mass develops into the embryo, and cells around the outside differentiate to form the trophectoderm - which will become the placenta (Firmin and Maître, 2021). Surrounding the blastocyst is an extracellular matrix known as the zona pellucida, through which a blastocyst must hatch before it is able to implant in the endometrium (Seshagiri et al., 2016). Mechanical pressure is thought to initiate blastocyst hatching (Seshagiri et al., 2009), with production of proteases to assist in the process (Seshagiri et al., 2016).

Many eutherian mammals show common characteristics of embryo development. The bovine embryo at early stages is round and also contains an inner cell mass and trophectoderm, with a zona pellucida surrounding it (Spencer, 2013). Blastocyst formation also undergoes stages of compaction, internalisation and lumen formation, (Iwata et al., 2014); with hatching occurring in the same way as in humans, with mechanical pressure and proteases; although bovine conceptuses reach this stage 2 days later than humans (Seshagiri et al., 2016). Following hatching, the embryo is known as a conceptus, which begins to elongate - a process driven by maternal secretions -

in preparation for implantation by day 20 (Lonergan and Forde, 2014). The histotroph - which refers to the uterine luminal fluid and contains maternal endometrial secretions - controls the process of elongation, and the composition of this is regulated by P4 production by the corpus luteum (Sánchez et al., 2018), as well as IFNT produced by the conceptus (Brooks et al., 2014). The histotroph is not well characterised, and contains amino acids, proteins, sugars and lipids (Brooks et al., 2014). Endometrial secretions are required for elongation, as a gland knockout model in sheep results in failed conceptus elongation (Spencer and Gray, 2006); and elongation is not possible to recapitulate *in vitro*, but blastocysts which are transferred back to a receptive uterus will elongate (Clemente et al., 2009).

The difference in eutherian mammal embryogenesis compared with marsupial embryogenesis highlights the reproductive differences that diverged. The marsupial embryo completely lacks an inner cell mass, featuring only a single layer of trophoblast cells; leaving it unknown how the marsupial embryo determines which cells become the embryo (Renfree, 2010).

1.5 Decidualisation

Decidualisation - in those species which undergo this process - of the endometrium describes the process during which endometrial stromal cells (ESCs) undergo differentiation and vast morphological changes to become decidual cells; which are more epithelial-like (Ng et al., 2020). This process occurs in humans cyclically, irrespective of the presence of a fertilised embryo, approximately 6 days post ovulation in preparation to support a pregnancy (Okada et al., 2018). During decidualisation, there is also an increase in immune cells in the endometrium, mainly uterine natural killer cells (Kajihara et al., 2013). These cells are able to modulate tissue remodelling and trophoblast invasion in the endometrium to aid implantation (Zhang and Wei, 2021). A diagram displaying the main features of decidualisation is shown in Figure 1.3.

As discussed, P4 is vital for priming of the endometrium to establish receptivity to implantation, and P4 also drives decidualisation through activation of PR-B, which is highly expressed in stromal cells at this stage of the menstrual cycle (Okada et al., 2018). Furthermore, upregulation of prolactin is caused by P4, which drives decidualisation (Maslar et al., 1986). Although the molecular mechanisms behind controlling decidualisation are far from clear, a number of molecules have been found to be involved. Cyclic AMP is integral to decidualisation - increasing sensitivity of ESCs to P4, and cyclic AMP alone is sufficient to induce decidualisation *in vitro* (Logan et al., 2013). Regulation of downstream targets by cyclic AMP and P4 weave a network of signals that

result in decidualisation. Forkhead box O1 (*FOXO1*) is P4 responsive, and is greatly increased at the onset of decidualisation - with its knockdown in decidualising cells resulting in differential expression of more than 500 downstream genes (Kajihara et al., 2013). *HAND2* is another P4 regulated gene without which decidualisation is markedly impaired, and is upregulated during decidualization not only in humans but mice too - suggesting involvement of *HAND2* in decidualisation is conserved between species (Huyen and Bany, 2011).

Decidualisation results in an alteration in secretions from the cells, with prolactin (PRL) and insulin-like growth factor binding protein 1 (IGFBP1) found to be the most highly expressed proteins following decidualisation (Gellersen and Brosens, 2014). PRL has been studied in early pregnancy and is suggested to have involvement in trophoblast invasion and implantation, as its knockdown causes failure of embryos to implant (Jabbour and Critchley, 2001). This is corroborated by Stefanoska et al., (2013), who's *in vitro* modelling also concludes that PRL aids trophoblast invasion. There is further evidence that PRL has a role in stimulating angiogenesis - an important feature of placentation (Corbacho et al., 2002). Similarly, IGFBP1 was shown to encourage invasion and migration of trophoblast cells (Gleeson et al., 2001).

Decidualisation occurs in some other species within eutherian mammals to different extents (however not all eutherian mammals undergo decidualisation), and this is usually representative of the invasiveness of the trophoblast in that species. Those with more invasive implantation strategies (*i.e.,* humans) experience extensive decidualisation, whereas those with less invasive pregnancies (*i.e.,* pigs) display more limited decidualisation (Gellersen and Brosens, 2003). Very few species other than humans carry out spontaneous decidualisation - that is, without the need for signals from the blastocyst - only non-human primates and a small selection of non-primates such as elephant shrews and bats along with the spiny mouse (Ng et al., 2020). This perhaps provides an explanation as to why humans and a select number of other species have a menstrual cycle, which culminates in the shedding of endometrial tissue that was prepared for receipt of a blastocyst when one does not materialise (Emera et al., 2012). In mice, decidualisation is dependent on the presence of an embryo, and does not occur until implantation is initiated, with the process occurring locally to the site of implantation (Zhao et al., 2017). In animals which do not undergo invasive implantation, such as ruminants, decidualisation does not take place (MacIntyre et al., 2002), again highlighting the correlation between invasiveness of implantation and decidualisation.

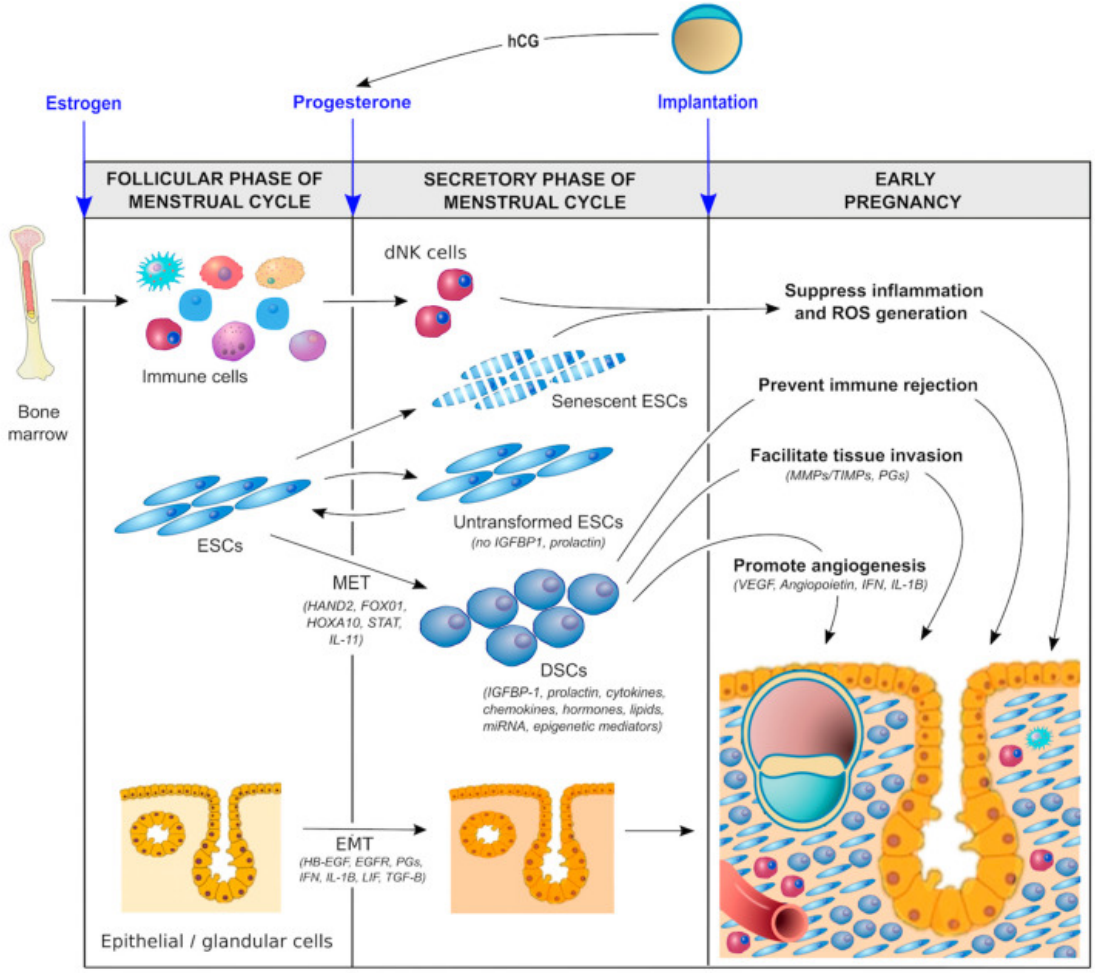

Figure 1.3: *Diagram showing the process of human endometrial stromal cell decidualisation.*
Endometrial stromal cells (ESCs) undergo differentiation and morphological changes reminiscent of mesenchymal to epithelial transition (MET) in response to progesterone and factors such as *HAND2* and *FOXO1* in the secretory phase of the menstrual cycle irrespective of presence of an embryo. This results in decidual cells (DSCs) which secrete IGFBP1 and PRL. Decidualisation also causes an increase in immune cell population in the endometrium, mainly uterine natural killer cells. The result of these processes assists in implantation of a blastocyst and maintenance of a pregnancy. EMT - Epithelial to mesenchymal transition, ROS - Reactive oxygen species, hCG - human chorionic gonadotrophin, dNK - decidual natural killer cells (Ng et al., 2020).

1.6 Maternal Recognition of Pregnancy

Maternal recognition of pregnancy (MRP) is the process that results in sustained production of P4, which is integral for pregnancy to occur (Raheem, 2017). In the circumstance where an oocyte has been fertilised, in order for implantation and pregnancy, the corpus luteum must assume responsibility for P4 production. This means that the corpus luteum must persist, and not regress as it would in the non-pregnant menstrual cycle (Michael Roberts et al., 1996). For this process to happen, the embryo must communicate its presence to the maternal reproductive system via the pregnancy recognition signal MRP molecule (Raheem, 2017).

Where P4 is a conserved pregnancy associated molecule; the MRP molecule is species specific and differs amongst eutherian mammals. In humans, hCG produced by trophoblast cells in the embryo signifies MRP (Ticconi et al., 2007). hCG is a glycoprotein hormone and is one of the earliest molecules produced by the embryo to communicate its presence to the mother (d'Hauterive et al., 2022). *In vivo* studies in non-human primates show that presence of their respective CG in the uterus causes effects on gene expression in both luminal and glandular epithelial cells, as well as the stromal cells in the endometrium (Fazleabas et al., 1999). Glycodelin was elevated in the glandular epithelial cells in response to CG treatment - a protein highly expressed in the endometrium during early pregnancy. Epithelial plaque formation is a physiological response during pregnancy in baboons, usually occurring at the site of implantation; where treatment with CG caused plaque to form over the full luminal epithelium. The authors suggest that the plaque response is due to blastocyst secreted CG. This multi-cellular response demonstrates the direct action of CG in the endometrium resulting in MRP, and the ability of CG to participate in priming of the uterus to facilitate implantation. Furthermore, hCG has been shown to reduce apoptosis in the endometrium (Lovely et al., 2005), potentially functioning as a mechanism to avoid menstruation. Furthermore, hCG has roles in trophoblast activity and immune regulation (Ticconi et al., 2007). The initial function in order to sustain a pregnancy, is that hCG induces P4 production from the corpus luteum - which was previously produced in response to LH (Cole, 2010). As LH concentration is drastically reduced shortly after ovulation, hCG is required to continue this stimulation of P4. Following the initial 3-4 weeks of pregnancy, once the placenta is established, this becomes the main producer of P4 (Cole, 2010). It was also found that hCG has a role in inducing endometrial stromal cell decidualisation through upregulation of *Cox-2* and prostaglandin E_2 (PGE_2) which causes decidual cell differentiation (Han et al., 1999).

Alternatively, in cows and sheep, interferon tau (IFNT) is the MRP molecule (Bauersachs et al., 2006). This molecule is a type I interferon secreted by the trophectoderm cells of the conceptus, and functions to avoid luteolysis by inhibiting oxytocin receptor expression (Forde and Lonergan, 2017). This mechanism results in IFNT mediated prevention of endometrial secreted prostaglandin $F_{2\alpha}$ ($PGF_{2\alpha}$). This is also achieved by inhibiting ER-α in sheep as well as oxytocin; signalling of which would normally induce $PGF_{2\alpha}$ production to luteinize the corpus luteum (Niswender et al., 2000; Basavaraja et al., 2017). The MRP molecule in pigs is estradiol-17 β, which carries out a similar role to MRP in ruminants, in that it diverts from the cycle by suppressing $PGF_{2\alpha}$ production (Okano, 1997).

1.7 Implantation

Implantation amongst eutherian mammals is varied. Invasiveness is the main source of variation observed; with some species performing more invasive implantation strategies, and others less so (McGowen et al., 2014). Human implantation is highly invasive, whereas bovine implantation is superficial, with the fetal cells attaching to the endometrium but not invading into the underlying tissue (Imakawa et al., 2017). Understanding the mechanisms behind these different strategies may provide insight and identify treatment targets to improve implantation success in patients suffering from infertility due to failure of the embryo to implant.

The process of embryo implantation in humans consists of 3 steps: 1) apposition, 2) adhesion and 3) invasion, shown in Figure 1.4. The first stage - apposition - involves the blastocyst becoming properly aligned with the endometrium at the site where it will implant, mechanisms of which are not completely understood (Ashary et al., 2018). Apposition results in weak initial contact between the endometrium and blastocyst (Su and Fazleabas, 2015). It is likely that selectins are involved in this process, with L-selectin expressed by the blastocyst thought to be responsible for this initial stage (Genbacev et al., 2003; Fazleabas and Kim, 2003). Mucin-1 (MUC-1), a negative regulator of adhesion, is also implicated here; hypothesised to be upregulated in regions of the endometrium to avoid blastocyst implantation at unfavourable sites (Achache and Revel, 2006). Consistent with this, at the implantation site *MUC-1* is downregulated - the culmination of these findings suggesting that *MUC-1* ensures the correct timing and location for implantation to occur. In fact, it was shown that the size of the *MUC-1* allele is significantly different between fertile and infertile women (Horne et al., 2001). During apposition, the inner cell mass is able to migrate within the blastocyst to be oriented towards the endometrium,

meaning any part of the blastocyst's outside has the capacity for apposition and attachment (Su and Fazleabas, 2015).

Adhesion is the next stage of implantation, where a stable, physical connection between the blastocyst and epithelial endometrium is established (Staun-Ram and Shalev, 2005). Molecules from cytokines to adhesion molecules have been identified as important for this stage of implantation, examples of which will be discussed here (Achache and Revel, 2006).The blastocyst is thought to activate cleavage of MUC-1 at the site of implantation to stop its anti-adhesive effects and facilitate implantation (Meseguer et al., 2001). The cytokine leukaemia inhibitory factor (LIF) is expected to play a role in adhesion stage of implantation - with an increase in expression at the window of implantation in fertile women (Charnock-Jones et al., 1994). Further evidence for this is presented in mouse models where competent embryos in LIF knockdown females are unable to implant (Stewart et al., 1992). LIF is also present in bovine endometrium and dynamically expressed throughout early pregnancy (Oshima et al., 2003). Interleukin-6 (IL-6) is a proinflammatory cytokine and is upregulated in the endometrium at the time of implantation, leading to it being linked to successful implantation (Cork et al., 2002). Reduced expression of IL-6 is found in the endometrium of patients with recurrent miscarriage (Jasper et al., 2007).

The final stage of implantation known as invasion describes the process during which trophoblast cells belonging to the blastocyst migrate and invade into the endometrial stromal layer (Ochoa-Bernal and Fazleabas, 2020). These cells invade between the cells in the epithelial layer with the purpose of making contact with the maternal vascular system (Su and Fazleabas, 2015). They are able to degrade the basement membrane to achieve this, by forming structures called invadopodia (Giudice, 1999). The trophectoderm differentiates, forming 2 distinct cell types: cytotrophoblasts and syncytiotrophoblasts (Costa, 2016). Commencement of invasion is by the syncytiotrophoblast cells, which are located on the outer region of the trophectoderm (Bischof and Campana, 1997). Structures known as lacunae form within the syncytiotrophoblast layer which begin as small pockets of fluid but later combine and become filled with maternal blood producing the intervillous spaces (Latendresse and Founds, 2015). This contact with the maternal blood persists throughout the pregnancy and acts as an interface – a barrier which allows transport of gas and proteins. Extravillous trophoblasts also differentiate from cytotrophoblasts and are responsible for invading of the maternal endometrium, participating in remodelling of uterine spiral arteries leading to dilated arteries allowing improved transport of blood (Cartwright et al., 2010).

The stages of implantation in other eutherian mammals are relatively similar up until the point where attachment has been established (Lee and DeMayo, 2004). At this point, species such as ruminants diverge from the process seen in humans as they do not undergo invasive implantation, rather achieving implantation by superficially attaching to the endometrium (Imakawa et al., 2017). However, in these species, the conceptus has elongated before the stages of apposition and attachment, so bears morphological differences (McGowen et al., 2014). Bovine trophoblast cells form structures in the form of cytoplasmic projections which are able to adhere the conceptus to the microvilli of the endometrium (Guillomot et al., 1981). Rodents undergo an intermediate level of invasiveness, where uterine invagination surrounds the blastocyst (Lee and DeMayo, 2004).

It is very difficult to fully decipher the exact mechanisms involved in implantation due to ethical considerations; and the knowledge that strategies differ so much between species means that principles learned from animal models are not always applicable in humans (Aghajanova et al., 2008). This emphasises the importance and requirement for accurate *in vitro* models if we wish to expand our understanding.

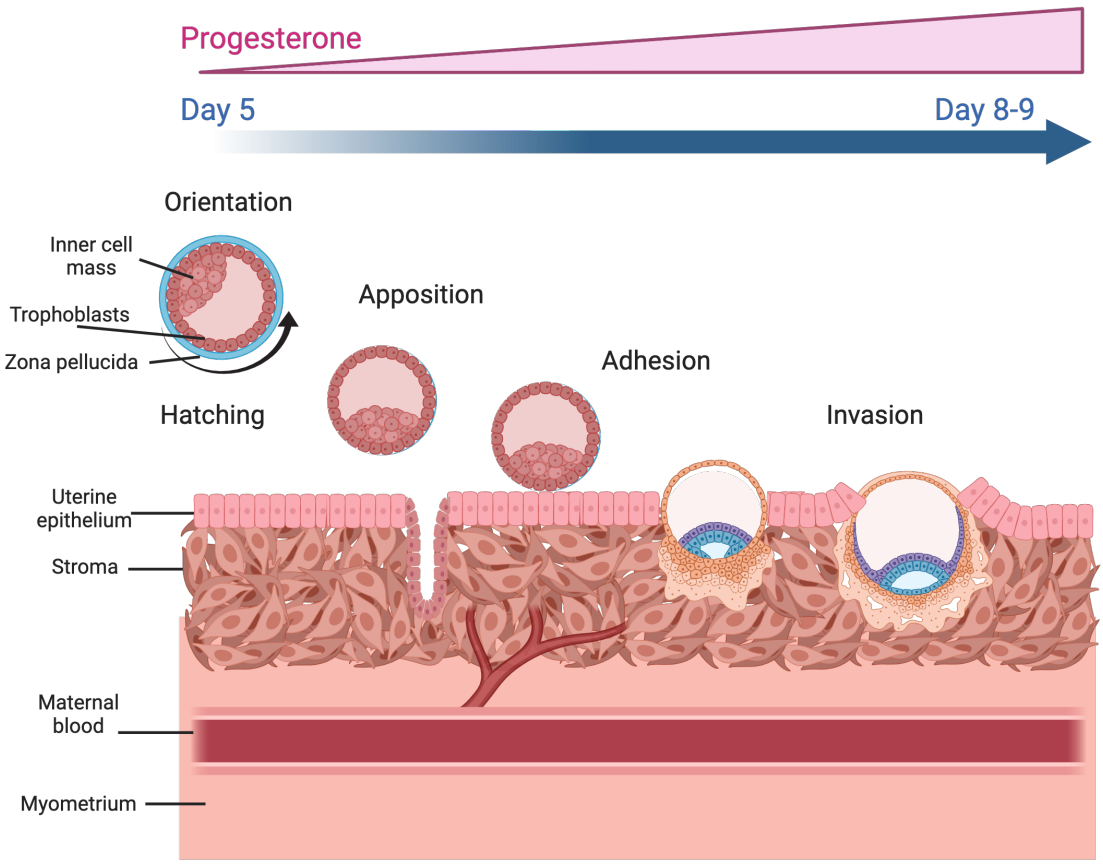

Figure 1.4: *Diagram detailing the stages of implantation in humans.* The blastocyst hatches and undergoes orientation and apposition where it establishes weak connections with the epithelial layer of the endometrium. Following this, stronger physical contact is made known as adhesion, via molecules such as cytokines and adhesion molecules. Invasion is the final stage of implantation where the trophoblast cells invade the underlying stromal cells. During this time progesterone is increasing in concentration. Figure created with Biorender.com

1.8 The Placenta

The placenta is a specialised organ formed from fetal tissues during pregnancy that is vital for correct development (Gude et al., 2004). Severe complications can arise if the placenta is misformed or does not function correctly, such as miscarriage or still birth (Napso et al., 2018). Morphologically, Eutherian placentas vary greatly in many aspects, likely due to differences in reproductive strategies amongst species, or perhaps because of nutrient allocation for the mother vs the offspring (Knox and Baker, 2008). Features of the placenta which can differ between species are the morphology, interdigitation - that is, the level of contact between maternal and fetal blood supply, and the degree of invasiveness - how many layers separate the maternal and fetal tissue (Gundling Jr and Wildman, 2015). Each of these characteristics have a number of different phenotypes that are displayed across the eutherian mammals. There are 5 different shapes of placenta (Figure 1.5): 1) discoid - a disk like shape, the hypothesised ancestral placenta and the shape observed in human pregnancy; 2) bidiscoid - which consists of 2 disk like placental shapes and is present in rodents, 3) cotyledonary - an arrangement of placental structures appearing in patches known as caruncles, present in bovine; 4) zonary - forms a structure which circles the fetus, which occurs in most carnivores; and 5) diffuse - spans the length of the fetal membrane, present in pigs (Wildman et al., 2006; Furukawa et al., 2014; Gundling Jr and Wildman, 2015). Interdigitation is characterised by the branching of the trophectoderm cells, which make up the outer epithelial layer of the blastocyst (Alarcon and Marikawa, 2022). These fall into 5 categories - 3 of which are branching, from most branching to least: labyrinthine, trabecular and villous; and 2 of which are folded: folded and lamellar (Gundling Jr and Wildman, 2015). A visual representation of the different types of interdigitation is shown in Figure 1.6. Finally, there are 3 patterns of invasiveness as shown in, the most invasive being that observed in humans: haemochorial, where the fetal cells are in immediate contact with the maternal blood, allowing the most efficient nutrient exchange (Enders et al., 1998). The intermediately degree of invasive known as endotheliochorial - present in ovine - has less contact with the maternal blood than haemochorial, but not as little contact as epitheliochorial invasiveness, which possesses the most layers of tissue between fetal and maternal blood supplies - as seen in bovine (Klisch and Mess, 2007; Montiel et al., 2013).

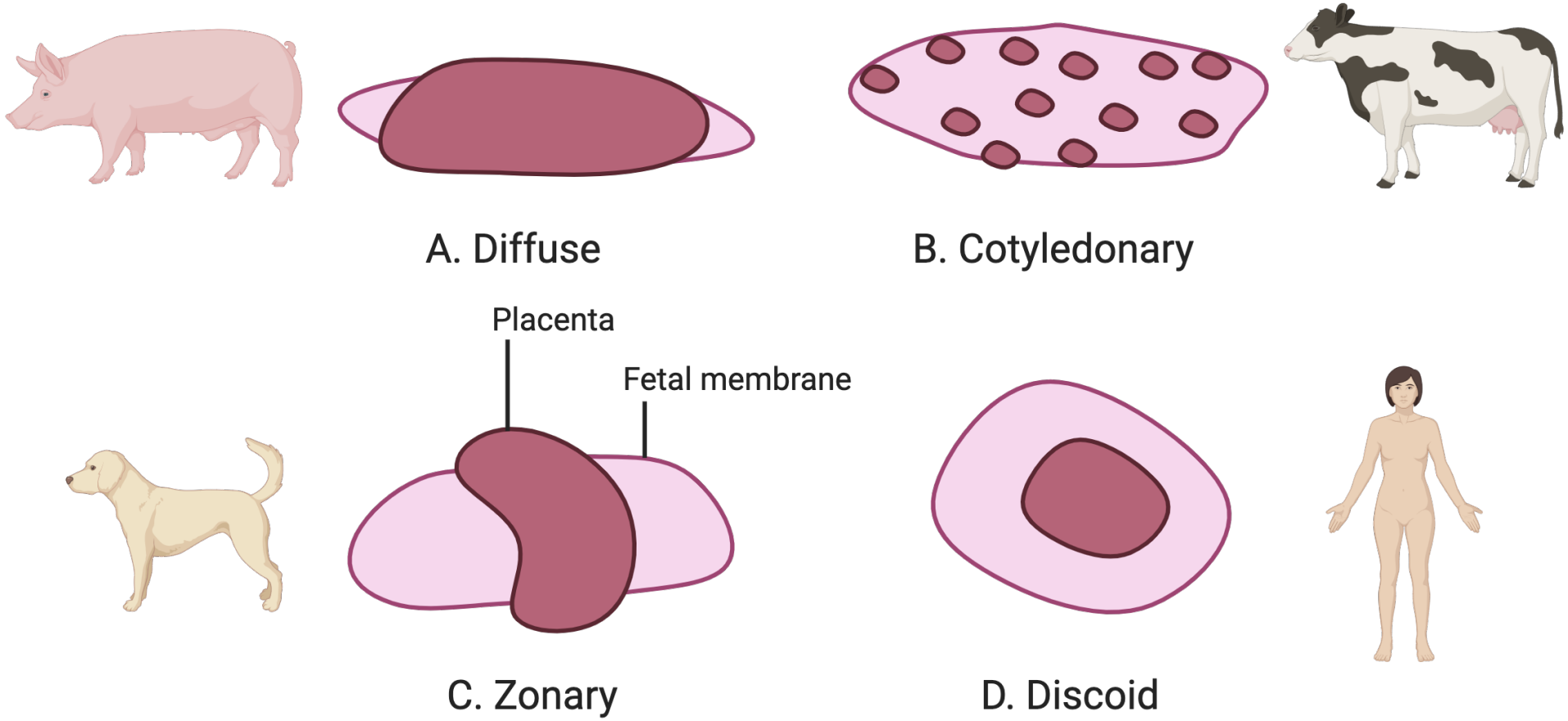

Figure 1.5: *Visual representation of the different shapes of placenta observed across the Eutherian mammals, with example species in which these phenotypes are found.*
Figure created with Biorender.com

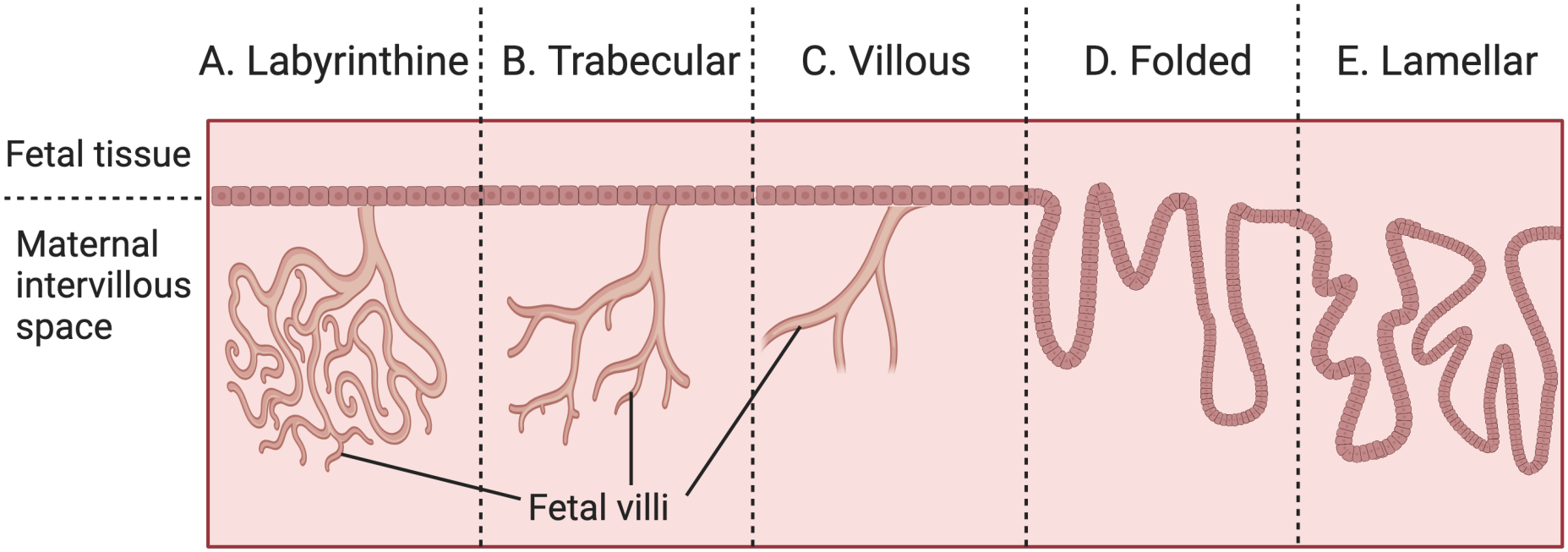

Figure 1.6: *Diagram showing placental interdigitation.*
Visual representation of the different types of interdigitation - which is the level of branching of the trophectoderm cells - found in different eutherian mammals. Figure created with Biorender.com.

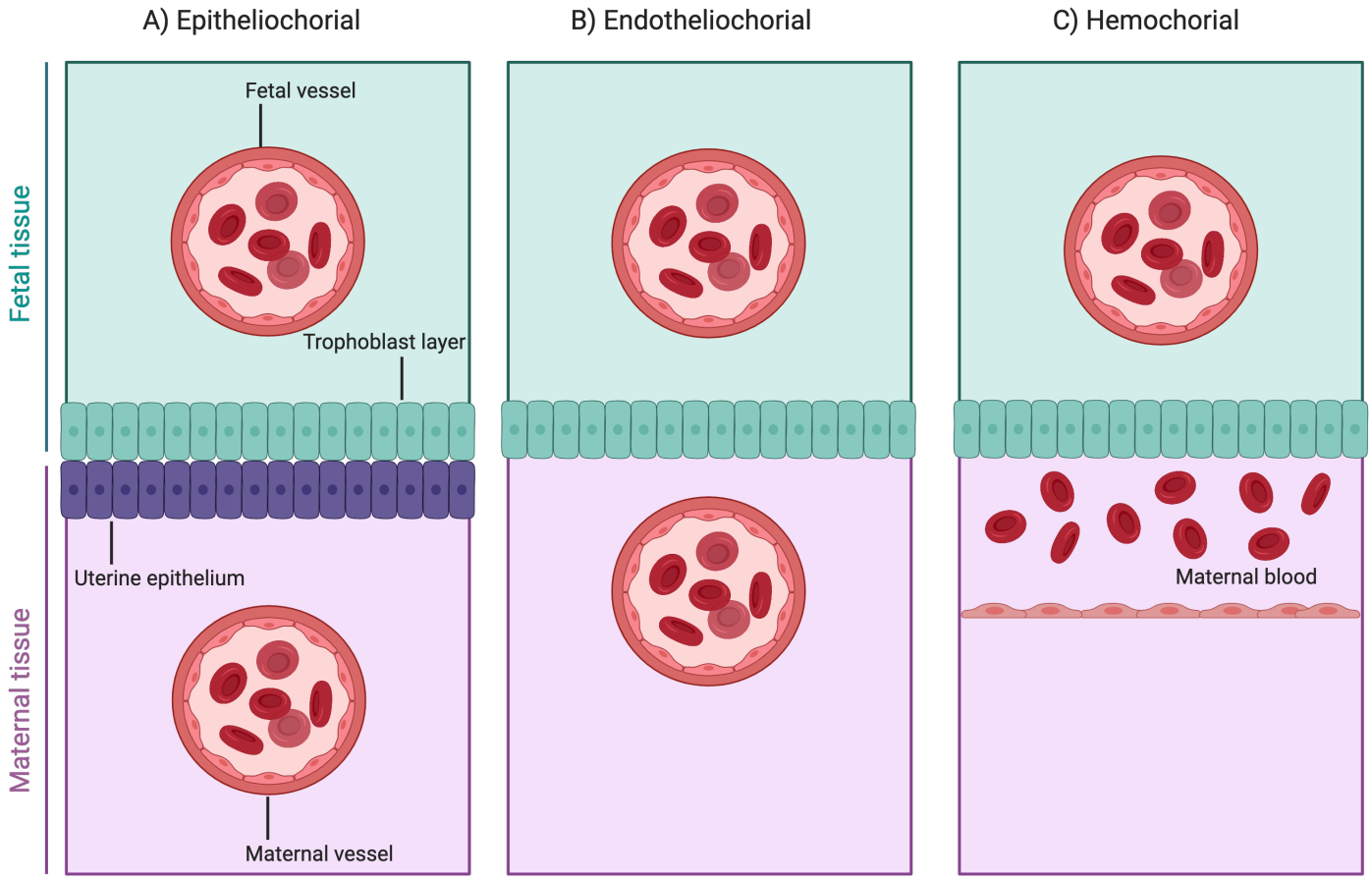

Figure 1.7: *Visual representation of the three patterns of invasiveness seen in different eutherian mammals*.
Figure created with Biorender.com

For placentation, it is evident that humans and bovine display very different phenotypes, with the human placenta being very invasive and the bovine being non-invasive. These differences in placental structure and function demonstrate the high level of reproductive diversity across the placental mammals and outline a basis for a range of reproductive strategies even if they are considered solely from the perspective of the placenta.

This project will focus on endometrial function in humans, using bovine as a comparative species. This is due to the vast differences in embryo development, implantation strategy and placentation observed between the two species, which have been discussed previously in this chapter. These species are appropriate for comparison, as both species are described as mono-ovulatory - meaning they usually ovulate a single oocyte (Abedal-Majed and Cupp, 2019), however display very opposite phenotypes when considering early pregnancy events. It is for these reasons that these species will be used comparatively to investigate implantation strategies.

1.9 MicroRNAs

It is thought that much of the complexity and variation between species could be due to non-coding, regulatory regions of the genome, with approximately 98% of human genetic material falling into this category (Mattick, 2001). This is exemplified by humans and *Caenorhabditis elegans possessing* a remarkably similar number of protein coding genes - around 20,000 - yet the differences in organismal complexity and morphology between these two organisms are vast. Explaining these differences solely in relation to protein coding genes therefore is not possible; gene number cannot be solely correlated with complexity as each have a similar number of genes (Prasanth and Spector, 2007). Therefore, another mechanism must be involved, and it has been shown that non-coding RNAs also play a role in epigenetic gene regulation - that is, alteration of gene expression without changes to the DNA sequence (Wei et al., 2017).

MicroRNAs (miRNAs) are a type of non-coding RNA, meaning that they don't encode for proteins (R. Zhao et al., 2022). They are single stranded molecules, usually consisting of around 22 nucleotides in length, and are known to regulate expression of genes in over 270 species (Li et al., 2018). In humans, miRNAs are suggested to make up to ~5% of the genome (Macfarlane and Murphy, 2010) and regulate as much as 60% of protein coding genes (Shu et al., 2017). They are dynamically regulated and involved in the control of a huge range of processes (Catalanotto et al., 2016), some of which will be discussed here.

MiRNAs were initially discovered in 1993, with the identification of *lin-4* in *C.elegans*, which originally was thought to be a protein coding RNA. However, it became apparent that the sequence was complimentary to the 3' untranslated region (UTR) of *lin-14* - which was found to be downregulated by *lin-4* (Lee et al., 1993; Wightman et al., 1993). *Lethal-7* (*let-7*) was another *C.elegans* miRNA which was found early on in the investigation into miRNAs (Reinhart et al., 2000). This miRNA is conserved amongst mammals and flies - mammals have multiple isoforms, whereas flies share the isoform found in *C.elegans* - but is absent from the plant kingdom (Lee et al., 2016). The expression of *let-7* in these diverse species displayed similar patterns temporally, indicating that the roles in which this miRNA was involved are likely similar across species (Pasquinelli et al., 2000). Since their discovery, miRNAs have been detected in different kingdoms including Animalia and Plantae, as well as viruses - and many are conserved within kingdoms (Bartel, 2009). More than half of *C.elegans* miRNAs have a human equivalent, as do almost half of *Drosophila melanogaster* miRNAs, emphasising the conservation during evolution, and thus their importance indicated by their retention (Ibáñez-Ventoso et al., 2008). It was thought that no

miRNAs were conserved between plants and animals, until 2 (miR-854 and miR-855) were identified by Arteaga-Vázquez et al., (2006) in *Arabidopsis thaliana*. However, there are major differences in the way in which plant miRNAs function, with plant miRNAs usually matching targets with perfect or almost perfect sequence complementarity, and usually target single sites within the protein coding region (Millar and Waterhouse, 2005). These differences highlight the evolution of miRNAs on different lineages specific for developmental complexity within kingdoms (Millar and Waterhouse, 2005). Emergence of novel miRNAs can often be identified at times of morphological innovation, such as the introduction of a new organ - like the placenta (Hosseini et al., 2018).

1.9.1 Synthesis

The synthesis of a miRNA is a multi-step process - Figure 1.8 shows a visual representation of this, along with the location of each stage. The majority of miRNAs are produced via the canonical animal miRNA synthesis pathway. This begins in the nucleus with transcription of the miRNA gene by RNA Polymerase II to produce a primary miRNA (pri-miRNA) transcript - a stem loop with poly adenylated (poly-A) tail and 5' cap (Lee et al., 2004). MiRNA synthesis is generally performed by RNA Polymerase II, however it has been shown that RNA Polymerase III is capable of transcribing some human miRNA genes (Borchert et al., 2006). From this, the pri-miRNA is processed by the microprocessor complex, which results in the formation of a precursor miRNA (pre-miRNA). Endoribonuclease Drosha (Drosha ribonuclease III) is part of this microprocessor complex which is responsible for cleavage of the pri-miRNA, before the resulting pre-miRNA is exported from the nucleus to the cytoplasm (Annese et al., 2020). RanGTP (RAS-related nuclear protein-guanosine-5’-triphosphate-ase) and the Exportin 5 protein, recognise the structure of the pre-miRNA created during cleavage; but not the sequence - allowing for non-specific recognition of multiple pre-miRNAs. These molecules protect the pre-miRNA from degradation and mediate transport out of the nucleus into the cytoplasm (Okada et al., 2009).

The next stage of biogenesis is cleavage of the terminal loop by RNase III endonuclease Dicer, and the structure is now known as a mature miRNA duplex (Doyle et al., 2013). Either of the strands which form the miRNA duplex can become the mature miRNA, and the nomenclature used for the miRNA is dependent on the directionality of the strand. The miRNA can either be named miRNA-5p or miRNA-3p, with the strand originating from the 5' end, or 3' end of the pre-miRNA, respectively (Annese et al., 2020). One of these strands is selected to be loaded into the Argonaute protein of the RNA-induced silencing complex (RISC) - the selection process of which is mostly unknown; but is

theorized to be related to factors such as weak binding at the 5' end, as well as dependent on the cell type in which the miRNA is produced, the stage of embryo development or even disease status of the cell (Meijer et al., 2014). The other strand, known as the passenger strand, is degraded (O'Brien et al., 2018). The miRNA loaded into the RISC complex can now interact with its target messenger RNAs (mRNA) (Hayder et al., 2018).

There are 2 non-canonical pathways of miRNA synthesis. The first is the Drosha independent pathway, where pre-miRNA-like molecules are produced by splicing of introns of mRNA and known as miRtrons; rather than through processing by the microprocessor (Ruby et al., 2007). This pathway is also seen for 7-methylguanosine-capped pre-miRNA, which is exported from the nucleus by Exportin 1 and also bypasses the microprocessor. This method results in a strong 3' bias (O'Brien et al., 2018). Both of these forms of pre-miRNAs produced by the Drosha independent pathway go on to Dicer processing as usual (Ruby et al., 2007). The second pathway of non-canonical biogenesis utilises RNA produced by Drosha which is too short for Dicer processing known as short hairpin RNA. Argonaute 2 rather than Dicer is necessary for this pathway to produce the mature miRNA (Cheloufi et al., 2010; Yang et al., 2010).

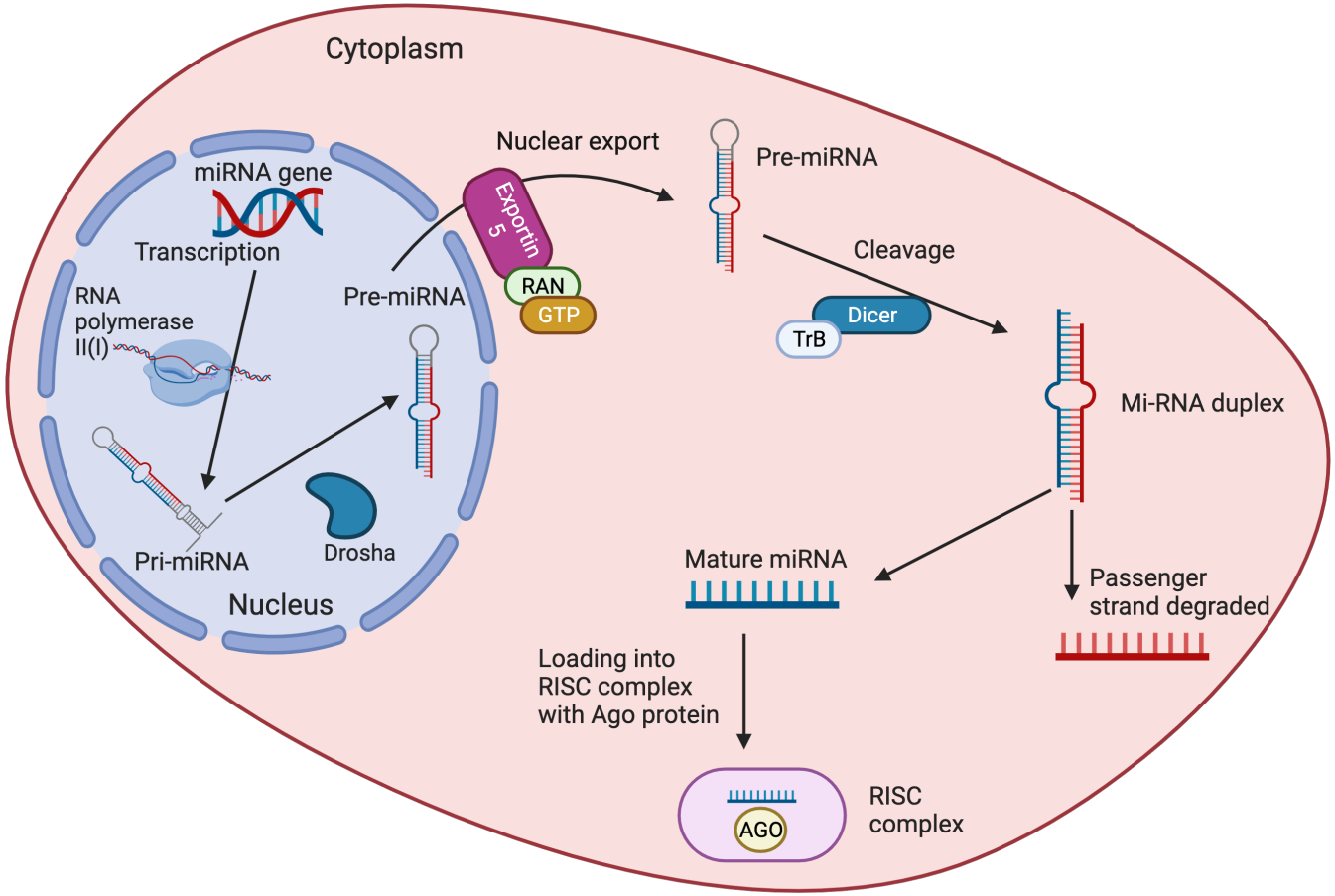

Figure 1.8: *Stages of microRNA biosynthesis with necessary enzymes and proteins.*
MiRNA gene is transcribed into pri-miRNA which is processed into pre-miRNA and exported from the nucleus. Cleavage results in the mature miRNA of which the guide strand is loaded into a RISC complex and the passenger strand degraded. The miRNA can now interact with its targets. Created with Biorender.com

1.9.3 Function

Initially, it was thought that miRNAs target mRNA by exact matching of the target with their seed sequence - a 6-8 nucleotide region beginning within the first 8 nucleotides from the 5' end of the miRNA (Ellwanger et al., 2011). However, seed sequence alone is not always adequate to ensure target matching; with other features surrounding the site such as local AU richness or distance to co-expressed miRNAs found to be important (Grimson et al., 2007). MiRNAs which share a seed sequence are termed a miRNA family, usually possessing the same predicted targets; and miRNAs which are highly conserved tend to have a higher number of predicted targets (Bartel, 2009).

Animal miRNAs were originally thought to only target the 3' UTR of its target mRNA, but have also been shown to interact with the 5' UTR and promoter regions as well (Broughton et al., 2016). Binding of the miRNA-RISC complex to the target mRNA 3' UTR by exact, or almost exact base pairing results in Argonaute 2 mediated cleavage of the mRNA and degradation (Bushati and Cohen, 2007). More commonly, miRNAs undergo imperfect pairing with the target mRNA 3' UTR which causes repression of translation; the stage of translation at which this occurs is debated (Huntzinger and Izaurralde, 2011). It is thought that binding of the miRNA to the 5' UTR also results in downregulation of gene expression, however the mechanisms and evidence are inconclusive (Gu et al., 2014; O'Brien et al., 2018). Some evidence suggests that miRNAs completely inhibit the initiation of the translation process - perhaps by stopping the initiation factor binding, whereas others present opposing studies that find repression at subsequent stages during translation (Wu and Belasco, 2008). It is unclear which of these methods is the accurate description for miRNA mediated translation repression, or whether this is achieved by a combination of different methods in various situations.

Studies have also shown that gene silencing is not the only function of miRNAs. Binding of certain miRNAs to the promoter region of its target gene can upregulate expression (Place et al., 2008). It is thought that a miRNA and its target can experience various types of regulation - increased or decreased expression, depending on developmental stage or cellular environmental requirements (Bartel, 2009).

MiRNAs are able to function within a cell, but can also be transported by extracellular vesicles (EVs) to a different cell (Boon and Vickers, 2013). EVs are small structures consisting of a phospholipid bilayer capable of carrying cargo including miRNAs, mRNA and protein from one cell to another (Nguyen et al., 2016). The contents of an EV are purposely packaged for transport, as the EV

cargo does not represent the original cell's transcriptome (Oggero et al., 2019). This process of transporting miRNAs may be employed in cell-cell communication during early pregnancy.

1.9.4 MicroRNAs in Pregnancy

MiRNAs are integral for pregnancy success, best illustrated by a complete failure to achieve a pregnancy in mice when miRNA processing machinery Dicer is knocked down (Hong et al., 2008). As miRNAs regulate a large repertoire of genes, they are involved in a huge number of biological processes including proliferation, differentiation, metabolism and apoptosis (Catalanotto et al., 2016). Regulation of genes by correct expression of miRNA is important in many aspects of pregnancy (detailed below), with their dysregulation leading to complications such as preeclampsia, fetal growth restriction, early pregnancy loss, and preterm labour (Cai et al., 2017).

MiRNAs are present in the endometrium, and have been found to be important for endometrial receptivity to implantation (Shekibi et al., 2022). A study comparing miRNA expression in endometrial biopsies of women suffering from recurrent implantation failure (RIF), with those undergoing assisted reproduction techniques who attained a pregnancy after one embryo transfer found 105 significantly differentially expressed miRNAs between the groups (Shi et al., 2017). Similar work comparing RIF patient endometrial biopsy miRNA expression with that of fertile women found 10 upregulated and 3 downregulated miRNAs (Revel et al., 2011). Comparison of these miRNAs with previously differentially expressed mRNAs and predicted targets highlighted a group of genes of which 80% were targeted by miR-23b and miR-145. Functional analysis of these genes showed involvement in processes important for implantation such as cell adhesion, suggesting that these two miRNAs play a role in endometrial receptivity to implantation. In fact, overexpression of another miR-23 family member - miR-23a-3p - in endometrial epithelial cells was shown to increase embryo attachment rate in an *in vitro* model (Huang et al., 2020).

Circulating miRNAs in the blood are often described in detail in studies concerning areas such as cancer, however this approach is not helpful in detecting differences in menstrual cycle stage, as serum miRNAs do not appear to be correlated (Rekker et al., 2013). Notwithstanding, during pregnancy, some serum concentrations of miRNA display significant differences between first and third trimester - miR-526a and miR-527 are altered 600 fold (Gilad et al., 2008). More intricately, Légaré et al., (2022) demonstrated temporal changes in the presence and concentration of miRNAs in the plasma of women throughout the

first trimester of pregnancy. These were thought to be related to development of the fetus and adaptation of the maternal system to accommodate the offspring. Potentially, these could be used as markers to measure gestational age of the pregnancy.

As previously stated, abnormally altered expression of miRNAs during pregnancy can result in severe complications, many associated with dysregulation in the placenta (Ali et al., 2021). MiRNA expression in the placenta and serum have been investigated in relation to preeclampsia (Cirkovic et al., 2021), which is a hypertensive disorder that affects approximately 5-7% of pregnancies (Rana et al., 2019). MiR-185 and miR-210 were found to be dysregulated in the placenta of preeclamptic patients (Pineles et al., 2007). MiR-210 has also been found to influence invasion of trophoblast cells, inhibiting this process when overexpressed in these cells; and was upregulated in the serum in preeclamptic patients (Anton et al., 2013). These findings suggest that this miRNA may be an appropriate serum biomarker for preeclampsia, as well as suggesting a mechanism in trophoblast invasion for which miR-210 is responsible. Altered expression of miRNA has been described in fetal growth restriction cases, with several miRNAs implicated. MiR-424 was found to be significantly overexpressed in the placenta of these patients (Huang et al., 2013) as well as miR-141 (Tang et al., 2013), in cooperation with their targets MEK1 and PLAG1, respectively. MiRNA dysregulation has also been associated with early pregnancy loss, with a study comparing placental tissue and maternal serum miRNA expression from early pregnancy loss patients with same gestational age abortions (Hosseini et al., 2018). This investigation revealed 4 miRNAs (miR-125a-3p, miR-423-5p, miR-575 and miR-3663-3p) that are upregulated in placenta in early pregnancy loss cases, with 2 miRNAs (let-7c and miR-122) upregulated and 1 (miR-135a) downregulated in maternal serum. Pre-term birth is another adverse pregnancy complication miRNAs have been linked to. Burris et al., (2023) uncovered 95 miRNAs which are significantly upregulated in cervical swabs from patients who experiences pre-term birth. Three of these: miR-30e-3p, miR-199b, and miR-143, have been previously described in relation to pre-term birth (Elovitz et al., 2014).

The results of these studies demonstrate the range of reproductive processes miRNAs are involved in and have an effect on. They provide evidence for their dysregulation causing adverse effects, from failure of the pregnancy to implant, to negative complications during gestation.

1.9.5 Conserved MicroRNAs

The emergence of novel miRNAs is often coincident with an expansion of developmental complexity, for example the emergence of the eutherian mammals (Guerra-Assunção and Enright, 2012; Hayder et al., 2018). During the emergence of Eutheria, the placenta - a novel organ, was produced; and the reproductive system was evolving new strategies for implantation and extended gestation (Hosseini et al., 2018). Conserved miRNAs are also able to develop new roles in the functions associated with novel organs and processes (Guerra-Assunção and Enright, 2012). Over the course of evolution, miRNAs have undergone duplications, retaining more than one copy, and neofunctionalization has occurred; resulting in new roles for existing miRNAs (Mohammed et al., 2014; McCreight et al., 2017). This has also been observed through a switch in favouring selection of 3p strand to 5p strand or *vice versa* which results in an alteration of function (Liu et al., 2008). These methods of developing new miRNAs or novel miRNA functions highlight the capacity for increasing developmental complexity during evolution, and the role that miRNAs play in this process.

Previous work from our collaboration has identified a core toolkit of miRNA families which arose coincident with the placenta and were never subsequently lost (Taylor et al., 2023). Eleven of these miRNA families: miR-28, -127, -185, -188, -324, -331, -378, -423, -433, -505 and -542 arose at the root of the Eutherians (Figure 1.9). MiR-671 is another eutherian mammal retained miRNA family, which is also present in the Tasmanian devil, and miR-340 is conserved in all Theria studied (Figure 1.9). Each of these miRNAs and their targets are linked to reproductive functions in the literature, these are detailed below. A number of these miRNAs are linked together by a systematic review in the same pregnancy condition: miR-127, -185, -188, -378 and -542 were all noted to be differentially expressed in preeclamptic patients (Harapan and Andalas, 2015). MiR-127 was recognised as downregulated in preeclampsia (Timofeeva et al., 2018) and research into other reproductive functions showed that it is involved in placentomegaly in mice - a complication characterised by an abnormally large placenta (Ito et al., 2015). The mechanism of this is thought to be due to miR-127 targeting of retrotransposon-like gene 1, and this miRNA may interact with miR-433 (Chen et al., 2013). MiR-127-3p has also been discovered to be downregulated in placental tissue from patients suffering from recurrent miscarriage, as well as in the serum (Yang et al., 2018). Furthermore, in epithelial ovarian cancer, miR-127-3p is described as a tumour suppressor when overexpressed, by inhibiting processes such as proliferation and invasion (Bi et al., 2016).

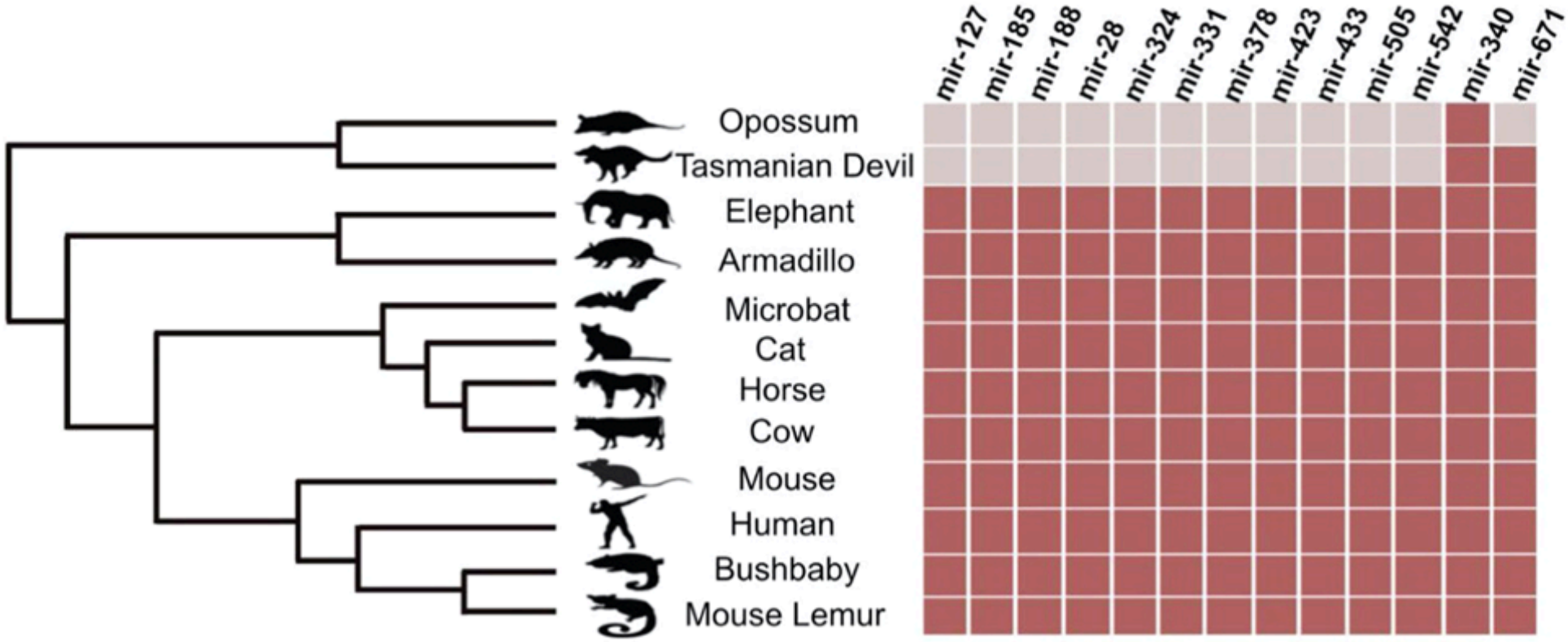

Figure 1.9: *Phylogenetic tree of Theria and Eutheria depicting presence and absence of miRNA families in different species.* Presence of miRNA is depicted by dark red, and absence by pale red. Taken with permission from (Taylor et al., 2023).

MiR-185, which was also described as dysregulated in preeclampsia (Harapan and Andalas, 2015), has been linked to pre-term birth (Cook et al., 2019) where it is upregulated in human plasma. In other reproductive investigations, miR-185-5p was elevated in blood from the umbilical cord of late onset fetal growth restricted babies (Loscalzo et al., 2021). MiR-188 was another miRNA altered in preeclampsia - where it was found to be downregulated in preeclampsia patients (Zhong et al., 2019). An upregulation of miR-188-3p has also been identified in polycystic ovary syndrome (PCOS), along with its targets - which were also associated with PCOS (Dai and Jiang, 2021). MiR-324 which was dysregulated in preeclampsia (Harapan and Andalas, 2015), was also found to be upregulated in embryonic placental tissue of ectopic pregnancies, and found to be regulating kisspeptin 1 - a placental regulation gene (Romero-Ruiz et al., 2019). Additionally, miR-324 expression was found to be downregulated in the plasma of patients who had a premature birth compared to those who had a normal gestation period (Fallen et al., 2018). As well as those miRNAs identified by the systematic review, miR-423-5p, which is overexpressed in patients with preeclampsia, has been described to have an inhibitory effect on processes of migration and invasion of trophoblast cells (Guo et al., 2018). It was also identified as upregulated in preeclampsia by Timofeeva et al., (2018). In bovine, miR-423 is suggested to be a circulating biomarker of early pregnancy (Ioannidis and Donadeu, 2016).

Two of the miRNAs - miR-331-5p and miR-378a-3p were linked to premature birth. MiR-331-5p overexpression is associated with spontaneous pregnancy loss in pigs (Wessels et al., 2013). This miRNA is oppositely connected to macrosomia - a condition where the offspring has an unusually large birth weight - miR-331-5p is downregulated (Ge et al., 2015). Early pregnancy loss is thought to be associated with miR-378a-3p downregulation in decidual cells, resulting in their apoptosis (Hong et al., 2018). This is interesting, as miR-378a-5p modulates trophoblast cell survival, with roles in development of the placenta, and displaying reduced expression in patients with preeclampsia (Luo et al., 2012).

Other pregnancy conditions were linked to miR-433 through the detection of miR-433 in maternal plasma (Miura et al., 2010); and a significant increase of miR-433-3p in patients with gestational diabetes was recently identified (Elhag and Al Khodor, 2023). This miRNA was identified in Bovine to be upregulated during pregnancy at day 19 of gestation (Gebremedhn et al., 2018). MiR-28 is also reported in bovine reproductive tissues - it is associated with bovine mammary gland epithelial cells - as discussed lactation is a mammal specific

trait (Li et al., 2015). This miRNA is also found to be secreted by the embryo and suggested to be involved in implantation (Kamijo et al., 2022).

Finally, there are very limited studies concerning miR-505 in reproductive systems - with some links to a tumour suppressive role in endometrial cancer (S. Chen et al., 2016). Endometritis is an infertility causing inflammatory disease of the female reproductive system, of which miR-505 is thought to be a regulator of; having anti-inflammatory effects (J. Liu et al., 2020).

Three of the conserved miRNAs: miR-340-5p (discussed in detail in Chapter 2), miR-542-3p (detailed in Chapter 3) and miR-671-5p (discussed in Chapter 4) were shown to be significantly upregulated in human endometrial epithelial cells in response to P4 (Edge et al., 2023). Overall, the fact that all of these miRNAs are conserved across Eutherians, and are heavily implicated in reproductive processes or pathologies, suggests that they have regulatory roles in the conservation or diversification of reproductive strategies that have evolved. This thesis will investigate and examine the functional roles of the 3 evolutionarily conserved, P4 regulated miRNAs in the endometrium of eutherian mammals.

1.10 Hypotheses

This thesis tests the hypotheses that:

1) Evolutionarily conserved, progesterone regulated microRNAs, miR-340-5p, miR-542-3p and miR-671-5p, modify protein coding regions of human endometrial epithelial cells and may facilitate endometrial receptivity to implantation.

2) Altering these microRNAs in an *in vitro* model will have an effect on endometrial function and embryo implantation.

1.11 Aims of This Thesis

The aims of this thesis are to:

1) Investigate whether differential expression of evolutionarily conserved, progesterone regulated microRNAs - miR-340-5p, miR-542-3p and miR-671-5p - alter the proteome in the endometrium.

2) Understand which pathways altered proteins are associated with in order to deduce their mechanistic roles in facilitating implantation.

3) Model implantation using an *in vitro* technique to study the functional effect of conserved, progesterone regulated microRNAs.

4) Produce novel, three dimensional models of the endometrium in human and bovine species that can be used to investigate endometrial function and implantation.

Chapter 2 Investigating the Mechanistic Effect of MiR-340-5p in the Endometrium

2.1 Introduction

2.1.1 Progesterone Control of Endometrial Receptivity

The hormone P4 is a signalling molecule which is conserved across the eutherian mammals (Marinić and Lynch, 2020). P4 is critically involved in priming of the endometrium to be receptive to implantation of an appropriately developed embryo (Young, 2013). Production of P4 during the luteal phase suppresses oestrogen receptor 1 expression (ESR1) and there is an increase in P4 receptors (Lessey et al., 1988). This also causes inhibition of endometrial epithelial cell proliferation and activates stromal cell proliferation in preparation for embryo implantation and decidualization (Marquardt et al., 2019). Luminal epithelial tight junctions (TJs) as well as adherens junctions become disrupted as epithelial differentiation takes place, to allow for invasion of the embryo (Bhurke et al., 2016). Many targets of P4 are involved in establishing endometrial receptivity. For example, Indian Hedgehog, (Ihh) which is upregulated in response to P4 in the endometrial epithelium (Lee et al., 2006), has been found to function as a growth factor for endometrial cells in mouse, where it becomes highly expressed in the epithelial cells around the time of implantation (Matsumoto et al., 2002). At this time, downstream targets of Ihh - Noggin, Patched, and GLI family zinc finger 1 and 2 are upregulated in the stromal cells, resulting in increased proliferation. This demonstrates a mechanism for Ihh mediating stromal cell proliferation. Experiments in mice inducing Ihh knockout or downstream target COUP-TFII knockout causes failure of the embryo to implant (Lee et al., 2006). As previously mentioned, P4 expression inhibits epithelial proliferation. It was discovered that its target Hand and Neural Crest Derivatives Expressed 2 (Hand2) suppresses multiple members of the fibroblast growth factor family (FGF) - specifically Fgf1, Fgf2, Fgf9 and Fgf18, which results in inhibited epithelial cell proliferation. FGFs usually activate the FGFR-ERK1/2 pathway, which promote epithelial proliferation. Hand2 suppresses these growth factors. Without Hand2 and this inhibitory mechanism, implantation failure occurs as epithelial cells continue to proliferate (Q. Li et al., 2011). These studies accentuate the necessity for appropriate P4 signalling and regulation of the endometrium for establishing endometrial receptivity.

2.1.2 Non-coding Elements

Throughout evolution, developmental complexity in the vertebrate lineage has increased - at times dramatically - initially thought to be brought about by two events of genome duplication (Sidow, 1996). This theory is not irrefutable, as when fossil morphology is considered, genome duplication does not solely explain the evolutionary patterns observed (Donoghue and Purnell, 2005). When a new morphological innovation occurs, genome duplication can be responsible for some of this. However, a study of protein coding gene families with relation to complexity found that a small number of families are involved, but others are described as conservative expansions - functioning to assist with adaptation rather than development (Vogel and Chothia, 2006). The relationship between genome expansion and developmental complexity is more complicated. Gene regulatory networks governed by non-coding elements of the genome such as microRNAs (miRNAs) are suggested to play a role in increasing complexity - for example, the amount of non-coding RNA transcribed by mammals is more than an order of magnitude greater than that of a fly (Heimberg et al., 2008). Sempere et al. (2006) demonstrate that whilst vertebrates, jellyfish and sponges have fairly similar amount of genetic material at their disposal, miRNAs which are absent in jellyfish and sponges and their expression in specific vertebrate tissues are likely to be accountable for development of more complex structures. Further, this paper discusses data that suggests miRNA expansion was implicated in the development of kidneys in the Nephrozoa clade. They emphasise that an amplification in number of miRNAs and their regulatory mechanisms may add complexity to existing genetic systems allowing formation of organs which were not present previously. Whilst the number of possible miRNA targets have remained reasonably stable - in that, the genome has not drastically increased in size - it is likely that an increasing number would come under miRNA regulation. This would push towards 'fine tuning' of developmental processes rather than providing a broad range for phenotypic plasticity - thus creating new functions for 'old' genes (Sempere et al., 2006).

In fact, emergence of miRNAs often occurs coincident with a burst of developmental complexity throughout evolution, such as at a point of novel organ formation - like the placenta (Guerra-Assunção and Enright, 2012; Hayder et al., 2018). Hertel et al. (2006) uncover 3 miRNA expansions occurring correspondent to central developmental changes, one occasion being the emergence of eutherian mammals.

As described in Chapter 1, Section 1.9, miRNAs are a key group of molecules which interact in many biological processes post-transcriptionally; from proliferation and differentiation to apoptosis and immune response; with implications in many diseases (Paul et al., 2018). MiRNAs are dynamically regulated, with roles in up- or down-regulating gene expression, post-transcriptional RNA degradation and splicing (Catalanotto et al., 2016). The presence of miRNAs during reproductive processes is essential. Figure 2.1 demonstrates the number of miRNAs involved in every process between production of gametes and implantation illustrating the importance of miRNAs in early pregnancy. Loss of the components of the miRNA production pathway has a huge negative impact on fertility (Reza et al., 2019). Studies in mice have shown that knockdown of *Dicer1* caused miR-503 dysregulation and ovary degeneration (Stefanski et al., 2019). MiR-675-5p is shown to play an important role in extravillous trophoblast invasion which is vital for successful implantation in humans, despite previously being shown to negatively regulate growth in these cells (Ogoyama et al., 2021). A systematic review of patients with preeclampsia reports that 7 miRNAs are upregulated (miR-16, -20a, 29b, -125b-1-3p -155, -181a and -210) whereas 6 others were downregulated (miR-17, -19b1, -195, -376c, 378a-5p and -675) in the patients' trophoblast cells which had an inhibitory effect on proliferation and differentiation (Harapan and Andalas, 2015). A specific signature of these miRNAs was found to be linked to trophoblast apoptosis when miR-29b is increased and miR-376c and 378a-5p are decreased.

Evidence in the literature has shown miRNAs are involved in endometrial receptivity to implantation, with an additional group which have adverse effects on receptivity (Shekibi et al., 2022). MiR-let-7-a/g, which are under the control of P4 and E2, have been found to improve receptivity in the endometrium by suppression of Wnt signalling (Li et al., 2020). This study demonstrated higher rates of embryo attachment with increased let-7-a, as well as outgrowth rate and area when let-7-g is highly expressed. β-catenin (a key Wnt signalling molecule) shows opposing patterns of expression to let-7 during the implantation period suggesting it is downregulated in response to let-7. Wnt signalling has a negative impact on implantation as high Wnt signalling results in reduced implantation success. Several miRNAs are suggested to be differentially expressed in the endometrium specifically at the time of receptivity, (miR-30b and -30d upregulated, miR-494 and -923 downregulated), suggesting that they may contribute to endometrial receptivity (Altmäe et al., 2013). Implantation is significantly reduced in humans following overexpression of miR-145 (Kang et al., 2015). This is achieved via its target IGF1R, which, during the receptive phase of the normal human endometrium, is upregulated, and

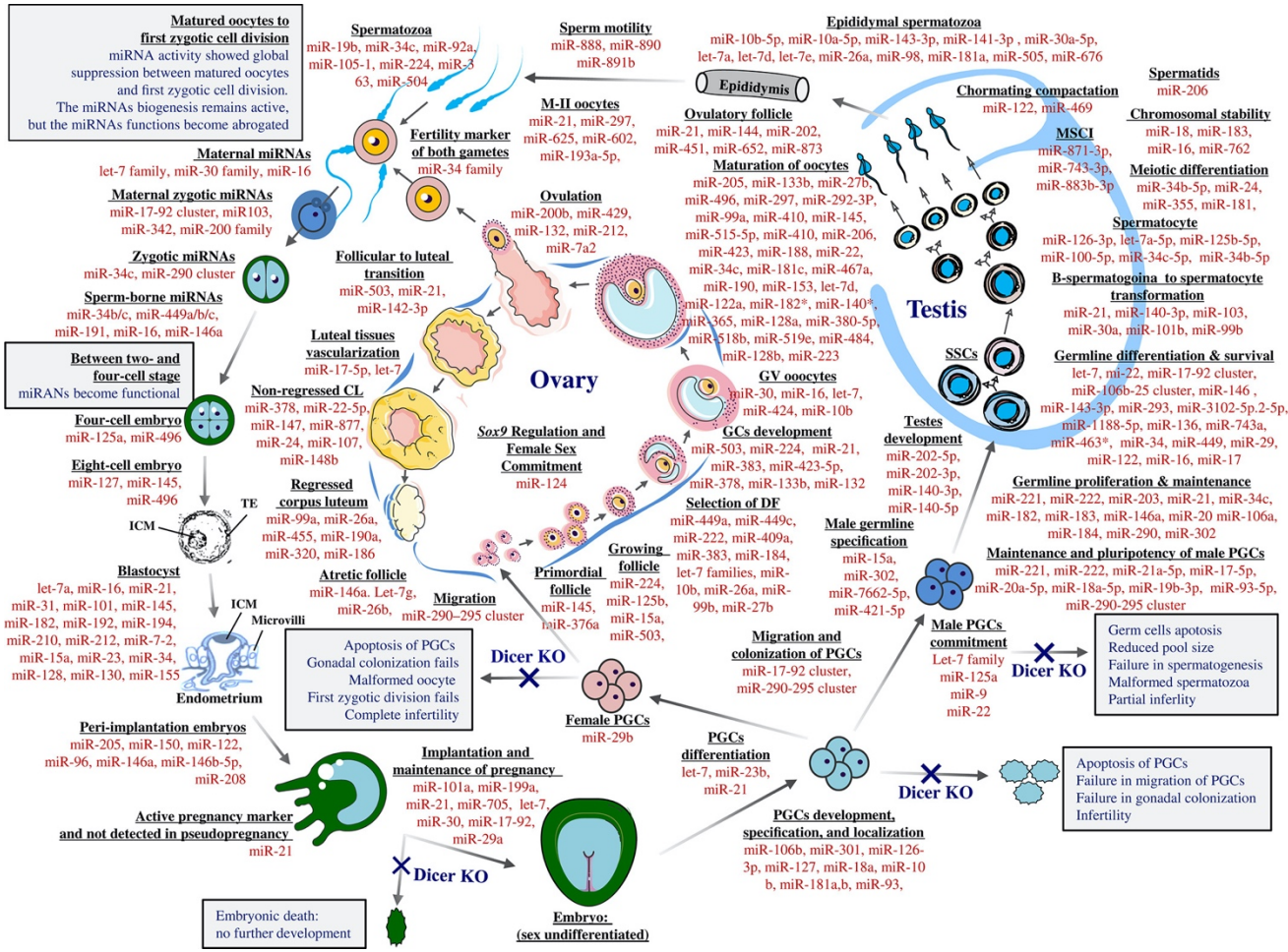

Figure 2.1: *MicroRNAs involved in reproductive processes.*
Diagram displaying the huge range of microRNAs involved in every aspect of early reproduction, from gamete development to implantation (Reza et al., 2019).

knockdown causes impaired implantation. This hypothesis is reaffirmed experimentally through use of a target protector for IGF1R which reverses the negative effect of miR-145 on implantation. MiR-145 is upregulated in patients with recurrent implantation failure (RIF), and experiments to investigate this effect showed significant reduction in PAI-1 expression when miR-145 is overexpressed (X. Liu et al., 2020). PAI-1 is also downregulated in women suffering from RIF, suggesting it is involved in the process of implantation and regulated by miR-145 expression. A further study found a set of miRNAs which were differentially expressed in RIF patients - 10 were upregulated (miR-23b, -27b, -99a, -139-5p, -145, -150, -195, -342-3p, -374b, -652) and 3 downregulated (miR-32, -628-5p, -874). These studies demonstrate that different miRNAs play important roles in mechanisms associated with implantation and endometrial receptivity vital for successful pregnancy, however they are not conclusive. A summary image of miRNAs implicated in endometrial receptivity in the literature is shown in Figure 2.2.

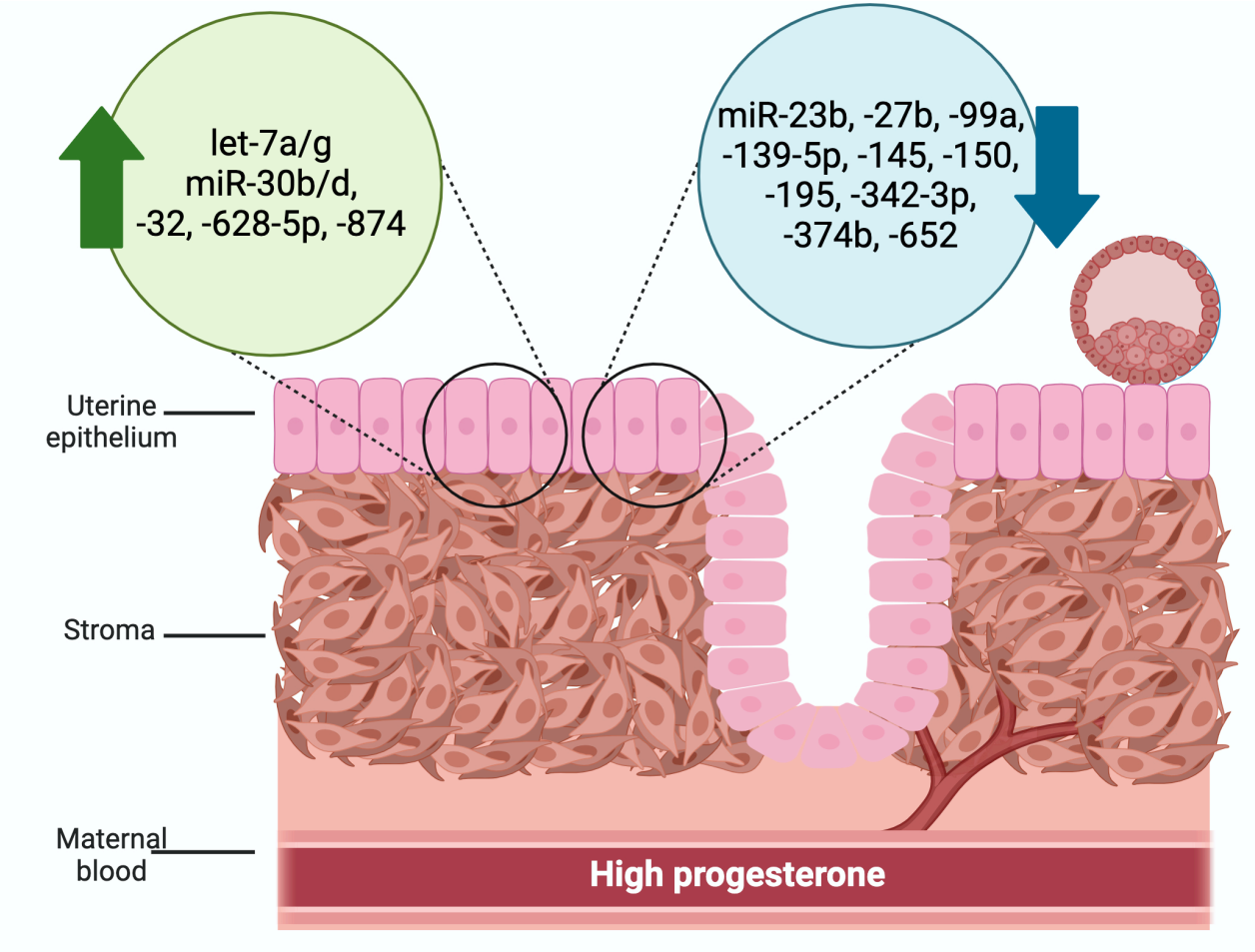

Figure 2.2: *Summary of differentially expressed microRNAs in a receptive endometrium.*
Diagram summarising microRNAs which are reported to be upregulated (green) and downregulated (blue) in a receptive endometrium primed for embryo implantation. Figure created using Biorender.com.

2.1.3 MiR-340-5p

Previous work by our group identified a specific group of miRNA families which evolved at the same time as the eutherian mammals and was never subsequently lost (Taylor et al., 2023). This core toolkit consisting of miR-28, -127, -185, -188, -324, -331, -340, -378, -423, -433, -505, -542 and -671 was present in all species studied since, emphasising their importance, and functions of predicted targets associates them with reproductive functions. Further investigation into these conserved miRNAs revealed that miR-340-5p is differentially expressed in response to P4. Specifically, when treated for 24 hrs with 10μg/ml P4, miR-340-5p expression was increased in comparison to controls (Edge et al., 2023). Understanding the roles of these miRNAs may explain some of the conservation or diversification of early pregnancy strategies between eutherian mammals.

MiR-340-5p is a tumor suppressor in a number of cancers. (Z. Li et al., 2019). For example, it's expression was downregulated in cancer lines which were more invasive, suggesting that a reduction of miR-340-5p plays a role in increasing proliferation in epithelial breast cancer cells (Wu et al., 2011). This suggests miR-340-5p may also be involved in controlling proliferation of epithelial cells in the endometrium. Overexpression of miR-340-5p in hepatocellular carcinoma inhibits tumor growth along with processes including migration, invasion and proliferation by reducing expression of *JAK1* (Yuan et al., 2017). *JAK1* is an activator of the signal transducer and activator of transcription (*STAT*) pathway known to regulate processes including invasion, apoptosis and growth. MiR-340-5p also reduced downstream targets of *STAT3* which could explain the mechanism for the inhibition of invasion seen in hepatocellular carcinoma. As these are epithelial cells, it is possible that miR-340-5p regulates the *STAT3* pathway in some way in the endometrium to facilitate implantation and endometrial receptivity. Glioblastoma also has downregulated miR-340-5p. Interestingly, patients who survive longer than 1 year have higher expression of miR-340-5p than those who survive less than 1 year (Fiore et al., 2016). MiR-340-5p was found here to target *NRAS*, which is upstream of the mitogen-activated protein kinase (MAPK) signalling pathway. Consequently, miR-340-5p may be regulating proliferation and cell cycle in the endometrium via the *NRAS* mediated MAPK signalling pathway.

In relation to reproductive biology, expression of miR-340-5p has already been characterised in gestational diabetes mellitus (GDM), where it was found to be one of the 5 miRNAs most significantly upregulated in maternal blood in pregnancies affected by GDM (Stirm et al., 2018). It was also reported that

dysregulation of miR-340-5p in the placenta results in vulnerability to activity-based anorexia in mice - particularly in females - due to altered expression during gestational programming (Schroeder et al., 2018). Alteration of miR-340-5p expression is also observed in patients with endometriosis, where it is downregulated in the plasma and upregulated in endometrial mesenchymal stem-like cells, which are cells associated with the pathogenesis of endometriosis (Bahramy et al., 2021). Additional links to endometriosis have been identified, with miR-340-5p displaying low expression in patients (Papari et al., 2020). It is thought that dysregulation of MAPK signalling is involved in the development of endometriosis (Bora and Yaba, 2021). Specifically, when overexpressed, miR-340-5p was found to target and inactivate MAP3K2, thus causing abnormal MAPK signalling. This resulted in reduced migration and invasiveness, reducing progression of endometriosis - explaining why it is downregulated in patients. Further investigation showed overexpression of miR-340-5p negatively affects invasiveness and migration in endometrial stromal cells (Wan et al., 2022). This implies that miR-340-5p may have a role in regulating aspects of implantation in the endometrium via the MAPK pathway. A summary of systems in which miR-340-5p is implicated is shown in Figure 2.3.

Whilst miR-340-5p has been studied in various cancer and pregnancy conditions, as well as in functions which are required for pregnancy, it has not yet been described specifically in relation to implantation.

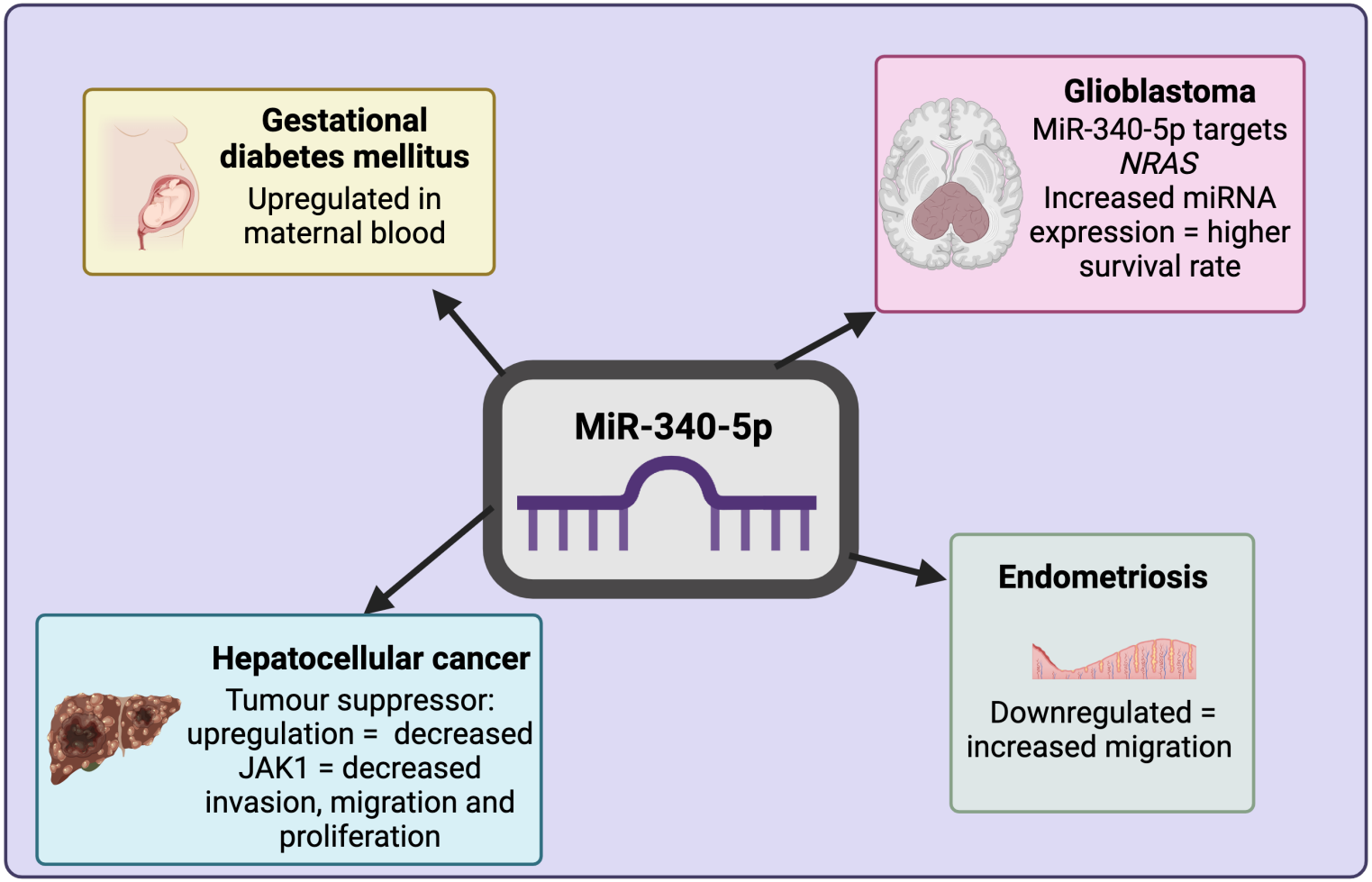

Figure 2.3: *Summary figure illustrating systems in which miR-340-5p is reported in the literature to play a role.* Figure created using Biorender.com

2.2 Hypothesis and Aims

2.2.1 Hypothesis

We hypothesise that an evolutionarily conserved microRNA which is altered by progesterone - miR-340-5p - modifies the expression of protein coding regions of human endometrial epithelial cells and may facilitate receptivity to implantation in humans.

2.2.2 Aims

The aim of this chapter is to:

1) Evaluate the change in proteomic response in the endometrial epithelium following over or under expression of miR-340-5p, by use of microRNA mimics and inhibitors.

2) Examine pathways differentially abundant proteins are involved in to understand functional relevance of upregulated miR-340-5p in response to progesterone.

This seeks to unravel the role which miR-340-5p plays in the endometrium and its implications for implantation and endometrial receptivity.

2.3 Materials and Methods

2.3.1 Cell Culture

All cell culture processes were performed in a sterile tissue culture hood, using sterile filtered pipette tips and 70% ethanol. Size 75cm^2 and 25cm^2 cell culture treated flasks were used to grow the cultures. Light microscopy was used to assess confluency and quality.

2.3.1.1 Ishikawa (immortalized endometrial epithelial) cells

Ishikawa cells (adenocarcinoma endometrial epithelial cells) (ECACC # 99040201) were used as a model of endometrial epithelial cells as they are an immortalised model representative of a hormonally respondent epithelial layer of an human endometrium. For all experiments cells were passaged in culture when they reached >70% confluency.

Culture media consisting of 1:1 Dulbecco's Modified Eagle Medium (DMEM) and Hams' F12 was supplemented with 10% Fetal Bovine Serum (FBS) and glutamine, streptomycin and penicillin (GSP). Prior to use, media, phosphate buffered saline (without Ca^{2+} / Mg^{2+}) (PBS) and trypsin were warmed in a water bath to 37^{o}C. To passage cells, culture media was aspirated from the flask, followed by two washes with PBS to remove any remaining serum which would cause inhibition of trypsinisation. Trypsin EDTA was diluted with PBS to 0.025% and 5ml was added to dissociate the cell monolayer, detaching them from the flask. This was then incubated for 2-3 min at 37^{o}C for trypsinisation to occur. Light microscopy was used to assess cell shape and detachment to ensure cells were rounded up and floating in suspension. Five millilitres of culture media were added to halt trypsin action to avoid damage to cells and the suspension was transferred to a falcon tube and centrifuged at 500 g for 5 min. Supernatant was aspirated and the resulting pellet was washed in PBS and centrifuged at 500 g for 5 mins. After aspiration of the supernatant again, the cell pellet was resuspended in an appropriate amount of culture media dependent on whether the cells are to be used for plating for experimentation or splitting into new flasks for further growth.

2.3.2 MicroRNA Mimic and Inhibitor Transfection

A diagram of workflow for the process of transfection and subsequent proteomic analysis is shown in Figure 2.4.

2.3.2.1 Transfection Optimisation

Optimisations of transfection reagent volume for siRNA transfection of Ishikawa cells were carried out to assess best transfection efficiency with minimised effect on cells.

Cells were plated at approximately 100,000 cells per well with 500μl culture media (media described in Chapter 2, section 2.3.1.1) in 24 well plates. Twenty-four hrs later, 25nM fluorescent labelled miRNA (Ambion, Cy3 Labelled Pre-MiR Negative Control #1) was added to the cells with a range of volumes of Lipofectamine 2000 (Invitrogen). The range of transfection reagent volumes was chosen according to manufacturer recommendations. Treatments were carried out in biological duplicate.

Treatments were as follows; each treatment was applied in 400μl culture media:

1. Control: 100μl opti-MEM media
2. Transfection reagent control: 100μl opti-MEM media + 1.5μl Lipofectamine 2000
3. MiRNA control: 100μl opti-MEM media + 25nM miRNA
4. 0.5μl treatment: 100μl opti-MEM media + 25nM miRNA + 0.5μl Lipofectamine 2000
5. 1μl treatment: 100μl opti-MEM media + 25nM miRNA + 1μl Lipofectamine 2000
6. 1.5μl treatment: 100μl opti-MEM media + 25nM miRNA + 1.5μl Lipofectamine 2000

Treatments 2-5 were added to the wells by diluting fluorescent miRNA in opti-MEM media. In duplicate, 0.5μl of lipofectamine 2000 was added to 49.5μl of opti-MEM, 1μl of lipofectamine 2000 added to 49μl opti-MEM and 1.5μl lipofectamine 2000 added to 48.5μl opti-MEM, as per manufacturer's instructions, and left to incubate for 5 min at room temperature. Transfection reagent only controls were carried out in the same way along with controls without lipofectamine 2000. To each of these tubes, 50μl of miRNA diluted in opti-MEM was added (except for control and transfection reagent control, which received 50μl opti-MEM alone) to result in 25nM of miRNA to be added per well. Tubes were incubated for 20 min at RT. During this time, culture media was removed from the cells, which were then washed twice with 500μl PBS, and 400μl culture media was replaced. Next, 100μl of each treatment was pipetted into the corresponding well and the plate was gently shaken to mix.

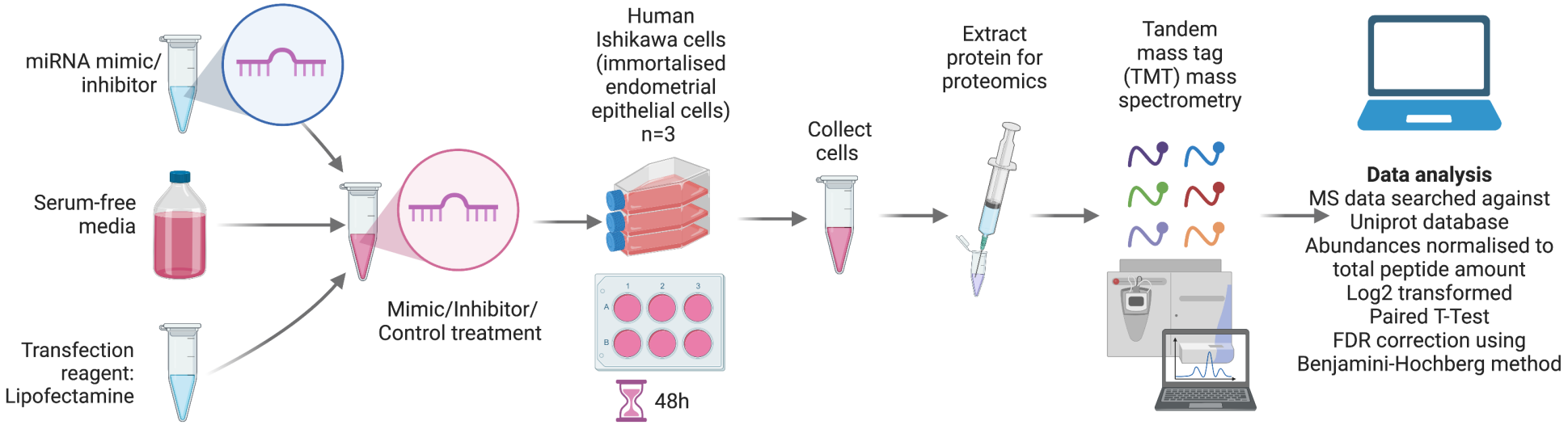

Figure 2.4: *Schematic diagram of workflow of processes for proteomic analysis of Ishikawa cells (n=3) transfected with microRNA mimics and inhibitors of interest.*
Ishikawa cells in 1.6ml antibiotic and serum free media were treated with: 1) control - 400µl optiMEM media, 2) lipofectamine only control - 1µl lipofectamine 2000 in 400µl optiMEM media, 3-6) 80pmol miR-340-5p mimic, inhibitor, non-targeting mimic or non-targeting inhibitor in 400µl optiMEM media. Cells were treated for 48 hrs at 37°C 5% CO_2. Cells are then collected, and protein extracted using RIPA buffer for protein analysis by TMT mass spectrometry before data analysis.

Plates were incubated for 24 hrs at 37°C, 5% CO_2. Then, media was removed, and cells were washed twice with 500µl PBS. Culture media was replaced, and cells were taken for fluorescent imaging. Using the EVOS microscope at 20X objective, 3 fields of view from each well were randomly selected and photographs taken using bright-field and red fluorescent light (553/568nm). Images were processed and merged using ImageJ. Number of cells present were counted followed by number of transfected cells defined as those showing red fluorescence within the cell. Only cells of which the perimeter was fully within the field of view were counted. The percentage of cells transfected was calculated from this information. Once imaging was complete, cells were trypsinised and two counts were conducted for live or dead cells using trypan blue stain to establish percentage of cell death for each treatment. Results were averaged between the two replicates.

2.3.2.2 Mimic and Inhibitor Transfection

Following the outcome of transfection reagent optimisation in Chapter 2, Section 2.3.2.1, transfection of Ishikawa cells with miR-340-5p mimic and inhibitor was carried out. MiRNA mimics and inhibitors obtained from Horizon Discovery were re-suspended to a 100µM stock by a brief centrifuge (to ensure all contents were at the bottom of the tube), followed by addition of 20µl sterile water. Tubes were mixed thoroughly by manual pipetting before being placed on an orbital shaker at ~80RPM for 30 min at room temperature. They were then aliquoted and stored at -20°C.

Ishikawa cells were plated in a 6 well plate at 200,000 cells per well in complete media (1:1 DMEM:F12, 10% FBS, 1% GSP) and incubated for 24 hrs at 37°C, 5% CO_2. Each mimic and inhibitor as well as non-targeting controls were made up using 40nM of the mimic, inhibitor, or non-targeting control (manufacturers guidelines) in 200µl optiMEM media and mixed gently. Separately to this, for each treatment, 4µl lipofectamine 2000 was added to 200µl optiMEM media, mixed, and incubated for 5 min at room temperature. Post-incubation, per treatment, these two tubes were combined, mixed and incubated for 20 min at room temperature, with the exception of the control, which did not contain lipofectamine 2000. Treatments were carried out in biological replicate of n=3, technical replicate of n=2 resulting in 2 sets of samples for future RNASeq and proteomic analysis. During this time, media was removed from cells which were then washed three times with PBS. Following this, 1.6ml of media (1:1 DMEM:F12, 10% EV-depleted serum, antibiotic-free) was added to the Ishikawa cells. Next, 400µl of the mimic/inhibitor with lipofectamine treatment was added to cells, and the plate was rocked to mix, followed by a 48 hr incubation at 37°C, 5% CO_2. After 48 hrs, media was removed from the cells and transferred to 2ml

Eppendorfs for extracellular vesicle (EV) - processing for future potential EV analysis. Cells were harvested (described in detail in 3.2.3) by being washed twice with PBS and lifted by trypsinisation, transferred to an Eppendorf and centrifuged at 500 g for 5 min. The supernatant was removed leaving the cell pellet and this was snap frozen and stored at -80^{o}C.

2.3.2.3 Cell harvesting

Any cells cultured in plates or flasks that were to be harvested for subsequent analysis were collected in the following way.

Media was aspirated from wells/flasks and cells subjected to two PBS washes. Trypsin EDTA/PBS was added, and cells were incubated at 37^{o}C for 2-3 min. Following observation with a light microscope to ensure dissociation, an equal volume of media was added to halt trypsinisation. Cells were collected using a pipette and employing repeated manual pipetting to guarantee all cells are detached from the surface. If some cells remain difficult to collect, a cell scraper was used to physically detach them. They were then transferred to Eppendorf tubes where they were centrifuged at 500 g for 5 min before resuspension in PBS, then a repeated centrifuge cycle. The supernatant was aspirated, and cells could be snap frozen and stored at -80^{o}C until required.

2.3.3 RNA Analysis

2.3.3.1 RNA extraction for separate microRNA enriched fraction (<200nt) and mRNA fraction (>200nt)

RNA extraction was carried out using MiRNeasy Mini Kit (Qiagen, UK) according to manufacturer's instructions. Samples were thawed slowly on ice followed by addition of 700μl QIAzol Lysis Reagent. They were then vortexed for ~1 min to homogenize. The samples were then left at room temperature for 5 min to dissociate the nucleoprotein complexes. Chloroform (140μl) was added, and tubes shaken vigorously for thorough mixing before centrifugation at 4^{o}C for 5 min at 12,000 g. The upper phase containing RNA was collected and transferred to a new tube where 70% ethanol (350μl) was added and thoroughly mixed. The sample was passed through an RNeasy mini spin column by centrifugation at 8000 g for 15 seconds. Flow through, which contains the miRNA-enriched fraction, was transferred to a new tube. To this, 450μl of 100% ethanol was added and mixed followed by pipetting into an RNeasy MinElute spin column. This underwent centrifugation at 8000 g for 15 seconds and the flow through was discarded. Next, 500μl of buffer RPE was added and centrifuged at 8000 g for 15 seconds with the flow through being disposed of. Then, 80% ethanol was added (500μl) and centrifuged at 8000 g for 2 min

before the column was transferred to a new collection tube and centrifuged at 8000 g for 5 min with the lid open. The spin column was then placed in the collection eppendorf and 14μl of RNase free water was added and then centrifugation at 8000 g for 1 min eluted the miRNA enriched fraction.

Into the original column containing the >200nt fraction, 700μl buffer RWT was added. This was centrifuged at 8000 g for 15 seconds. An on-column DNase digestion step was then performed using an RNase-Free DNase Set (Qiagen, UK). A wash with Buffer RWT (350μl) and 15 second centrifugation at 8000 g precedes addition of DNase I (10μl DNAse I stock in 70μl Buffer RDD). This is then incubated for 15 min at RT, before a second Buffer RWT wash followed by a repeat centrifugation. All flow through was discarded at each centrifugation step. Next, Buffer RPE (500μl) was added twice to the column and centrifuged for 15 seconds at 8000 g in between. A 2 min centrifugation at 8000 g was carried out to dry the membrane followed by a 1 min centrifugation at full speed with the lid open in a new collection tube. RNA was then eluted from the column by placing in a collection Eppendorf, adding 50μl of RNase-free water and centrifuging for 1 min at 8000 g. The RNA could then be snap frozen for future use.

2.3.3.2 RNA quantification

RNA concentration was quantified using the Nanodrop N1000 spectrophotometer (Thermo Fisher Scientific, USA). Prior to each measurement, the nanodrop was blanked using 2μl sterile water. RNA was kept on ice whilst concentrations were measured by depositing 2μl of the sample onto the arm of the nanodrop.

2.3.3.3 cDNA conversion for microRNA analysis

According to concentrations of RNA obtained from the nanodrop, RNA was diluted to a final concentration of 5ng/μl using DNase/ RNase free water. Following manufacturer's instructions, the miRCURY LNA RT Kit (Qiagen) was used to reverse transcribe RNA into cDNA. Two microlitres of each sample was added to a reaction mix consisting of 5μl DNase/RNase free water, 2μl 5x miRCURY RT reaction buffer and 1μl 10x miRCURY RT enzyme mix containing the reverse transcription (RT) enzyme. A pool of RNA from each sample was created to use as a negative RT control where the RT enzyme mix was replaced with DNase/RNase free water. cDNA conversion was carried out using a 96 well thermal cycler to incubate at 42^{o}C for 1 hr, before 95^{o}C for 5 min to inactivate the reaction. cDNA could then be stored overnight at 4^{o}C or longer term at -20^{o}C to be used for subsequent analysis.

2.3.3.4 MicroRNA qPCR

Quantitative real-time PCR was carried out to demonstrate over and under expression of the miRNAs of interest following transfection with mimics and inhibitors. MiRNA cDNA was diluted 1:60 in RNase-free water. A reaction mix consisting of (per sample) 5μl 2x miRCURY SYBR Green Master Mix, 1μl PCR primer mix for miR-340-5p, 1μl RNase-free water was added to 3μl of diluted cDNA per well. PCRs for each treatment were performed in biological triplicate. The PCR plate was then briefly centrifuged and then placed in the LightCycler 96. The programme was as follows: PCR initial heat activation - 2 min at 95°C, 40 cycles of 2 step cycling; consisting of denaturation for 10 seconds at 95°C then annealing and extension for 60 seconds at 56°C, ending with a melt curve analysis from 60-95°C. Raw Ct values were extracted using LightCycler 96 software and subjected to data analysis. Any miRNA which was not detected was given the value 40 (the highest possible cycle threshold). ΔCt values were normalised by subtracting the global mean of 5S normaliser from each value. The transformation $2^{-\Delta Ct}$ was calculated for each value to show normalised absolute expression of miRNA.

2.3.4 Proteomic Analysis

2.3.4.1 Protein extraction

Cell pellets were resuspended in 250μl RIPA buffer (components in Table 2.1) and incubated on ice for 15-30 min. The suspension was then mixed by manual pipetting before being passed through a 21'G needle and syringe to homogenise. Samples were then centrifuged at maximum speed for 1 min and the supernatant (containing protein) transferred to a new Eppendorf where it was frozen for future analysis.

Table 2.1:*Components of RIPA buffer used for protein extraction of miRNA mimic and inhibitor transfected Ishikawa cells (n=3).*

Reagent	**2.5 ml (μl)**	**Final concentration**
5 M NaCl	75	150 mM NaCl
10% IGEPAL	250	1% IGEPAL
10% Sodium deoxycholate (DOC)	125	0.5% Sodium deoxycholate (DOC)
10% SDS	25	0.1% SDS
1 M Tris (pH 7.4)	62.5	25 mM Tris (pH 7.4)
Protease Inhibitor Cocktail (25x)	100	1x Protease Inhibitor Cocktail
ddH_2O	1862.5	

2.3.4.2 Quantitative proteomic analysis

Quantitative proteomic analysis and initial statistics were carried out by Bristol Proteomics Facility. Methods in Chapter 2, Sections 2.3.3.3 and 2.3.3.4 are provided by them.

2.3.4.2.1 Tandem Mass Tag Labelling and High pH reversed-phase chromatography.

Overnight digestion of 50µg per sample was carried out using trypsin (1.25µg at 37^{o}C) before labelling with Tandem Mass Tag (TMT) eleven plex reagents following manufacturer's instructions (Thermo Scientific) in order for the labelled samples to be pooled. Desalting by SepPak cartridge (Waters, USA) of 100µg of pooled sample was performed and eluate evaporated before resuspension in buffer A (Table 2.2) followed by fractionation by high pH reversed-phase chromatography using the Ultimate 3000 liquid chromatography system (Thermo Scientific). This consisted of loading the sample onto an XBridge BEH C18 Column (130Å, 3.5 µm, 2.1 mm X 150 mm, Waters, UK) in buffer A (Table 2.2) An increasing gradient spanning 0-95% of buffer B for 60 min was used to elute peptides. This produced 15 fractions which were evaporated and resuspended in 1% formic acid. An Orbitrap Fusion Lumos mass spectrometer (Thermo Scientific) was used to perform nano-LC MSMS to analyse samples.

2.3.4.2.2 Nano-LC Mass Spectrometry

Reversed-phase chromatography fractions with high pH were fractionated again using an Ultimate 3000 nano-LC system with Orbitrap Fusion Lumos mass spectrometer (Thermo Scientific). The peptides (in 1% vol/vol formic acid) were injected onto an Acclaim PepMap C18 nano-trap column (Thermo Scientific) before washing with 0.5% vol/vol acetonitrile 0.1% vol/vol formic acid. Then, peptides were resolved on an Acclaim PepMap C18 reverse phase analytical column (250mm x 75µm) (Thermo Scientific) for a duration of 150 min on an organic gradient consisting of the segments in Table 2.3. A stainless-steel emitter was used for nano-electrospray ionization (2.0kV, capillary temperature 300^{o}C, internal diameter 30 µm) to ionize peptides.

Table 2.2: *Reagents and their compositions used for Tandem Mass Tagging and Nano-LC Mass Spectrometry.*

Reagent	**Composition**
Buffer A	20mM ammonium hydroxide pH 10
Buffer B	20mM ammonium hydroxide in acetonitrile pH 10
Solvent A	0.1% formic acid
Solvent B	Aqueous 80% acetonitrile in 01% formic acid

Table 2.3: *Organic gradient segments, solvents and timing used for fractionation of peptide samples during Nano-LC Mass Spectrometry.*

Segment	**Percentage Solvent B in Solvent A** (Table 2.2) **(%)**	**Time (min)**
1	1-6	1
2	6-15	58
3	15-32	58
4	32-40	5
5	40-90	1
6	90	6
7	1	1

An Orbitrap Fusion Lumos mass spectrometer with Xcalibur 3.0 software (Thermo Scientific) in data-dependent acquisition mode using SPS-MS3 workflow was used to obtain spectra. A resolution of 120,000 was used to collect FTMS1 spectra with 50ms maximum injection time and automatic gain control target of 200,000. Monoisotopic peak determination was set as 'Peptide' with intensity threshold set to 5000, before precursors were filtered according to charge state (including charge states 2-7). A dynamic window of 60s +/- 10ppm was used to remove previously interrogated precursors. A quadrupole isolation window of 0.7m/z was used to isolate MS2 precursors. An automatic gain control target of 10,000 was used to collect ITMS2 spectra when the maximum injection time was set to 70ms with CID collision energy at 35%.

A resolution of 50,000 was used to collect FTMS3 with automatic gain control target also at 50,000 when the maximum injection time was 105ms. High energy collision dissociation at normalised collision energy of 60% was used to fragment precursors. Up to 10 MS2 fragment ions could be included in the FTMS3 scan by synchronous precursor selection.

2.3.4.3 Proteomic statistical analysis

The software Proteome Discoverer 2.1 (PD2.1, Thermo Scientific) was used initially to process and quantify raw data along with establishing protein groupings. This was later improved, and master protein selection achieved, using an in-house script at Bristol Proteomics Facility. This script increases effectiveness of biological trend identification whilst minimising loss of quality of the data. On 14/1/2021 the proteomic data was searched against the human Uniprot database using SEQUEST HT algorithm and later updated on 15/11/2021. Conditions were set as follows: peptide precursor mass tolerance at 10ppm and 0.6Da MS/MS tolerance. Variable modification search criteria consisted of: 1) oxidation of methionine (+15.995Da) 2) acetylation of the protein N-terminus (+42.011Da) and 3) methionine loss plus acetylation of the protein N-terminus (-89.03Da). Fixed modifications include: 1) carbamidomethylation of cysteine (+57.021Da) and 2) addition of the TMT mass tag (+229.162Da) to peptide N-termini and lysine. A limit of 2 missed cleavages was set as acceptable and searches included full tryptic digestion. A false discovery rate filter of 5% was applied.

Normalisation was carried out for each sample for protein abundance relative to total peptide amount before being Log_2 transformed to achieve a more normal distribution. Paired T-tests were used to calculate statistical significance ($p<0.05$) between each condition and the Benjamini-Hochberg method used for

false discovery rate correction. At this point of the analysis data was exported to excel.

2.3.4.3.1 PCA Plots

The FactoMineR package was used to calculate principal component analysis (PCA) before plotting using ggplot2 package. The main source of variance was indicated by plotting PC1 and PC2 against each other, as well as showing any further trends with a second PCA plot consisting of PC3 and PC4.

2.3.4.3.2 Volcano Plots

Proteins for each comparison of two treatment groups were plotted in a volcano plot depicting the $-\log^{10}$ p value on the y axis and the $\log_2$ fold change on the x axis. Statistical significance is denoted as follows: those which have values of $p<0.05$ are shown in yellow and those which have values of $p<0.05$ and $>1\text{Log}_2$ fold change are coloured in red.

2.3.3.5 Proteomic results analysis

Data was first filtered to remove proteins which appeared in the contaminant database. For each test comparison, eg. Non-targeting mimic vs miR-340-5p mimic, all proteins whose t-test value was statistically significant ($p<0.05$) were used. Protein lists then underwent Venn diagram analysis by gene name to remove those which were changed in abundance in response to the non-targeting control. Venn diagrams were produced using Venny (Oliveros, n.d.) and then re-drawn manually in Graphpad Prism. The list of proteins significantly changed in response to the non-targeting mimic vs control was compared to the list of proteins significantly changed after treatment with miR-340-5p mimic. Those which overlapped in the centre of the diagram were excluded due to altered abundance by the non-targeting mimic and so were likely to be due to off-target effects. Any proteins which were missing a gene name were included using their accession number instead. Some lists had multiple proteins with the same gene name due to there being different fragments or forms of the same protein altered in abundance. Identical steps were carried out for miR-340-5p inhibitor vs non-targeting inhibitor. Proteins identified by this analysis which were discussed further were selected through their involvement in related pathways in the literature. Proteins were also compared to RNASeq data from 36 human endometrial biopsies collected 4-12 days following a positive home ovulation test. Women aged 31-36 were recruited with between 0-9 previous losses, and went on to have either live birth, ongoing pregnancy or miscarriage outcomes (Lipecki et al., 2022).

2.4 Results

2.4.1 Optimising Transfection Reagent Volume

To determine which volume of transfection reagent - Lipofectamine 2000 - to use within the range of manufacturer's recommended volumes, transfection efficiency and cell death at different volumes was assessed (Figure 2.5). Treatment with 1.5μl of Lipofectamine 2000 resulted in a transfection efficiency of 100%, however cell death was elevated to over 26%. This is in comparison to 1μl Lipofectamine 2000 which showed over 99% transfection efficiency whilst cell death was 16%. Reducing the Lipofectamine 2000 volume to 0.5μl still resulted in a high transfection efficiency of 96%, but only reduced cell death by 5%, not as much as reducing the volume from 1.5μl to 1μl. For this reason, to ensure highest possible transfection efficiency and a middle compromise on cell death, 1μl Lipofectamine was selected as the optimum transfection reagent volume for 24 well plates. This was to be scaled up or down depending on well size.

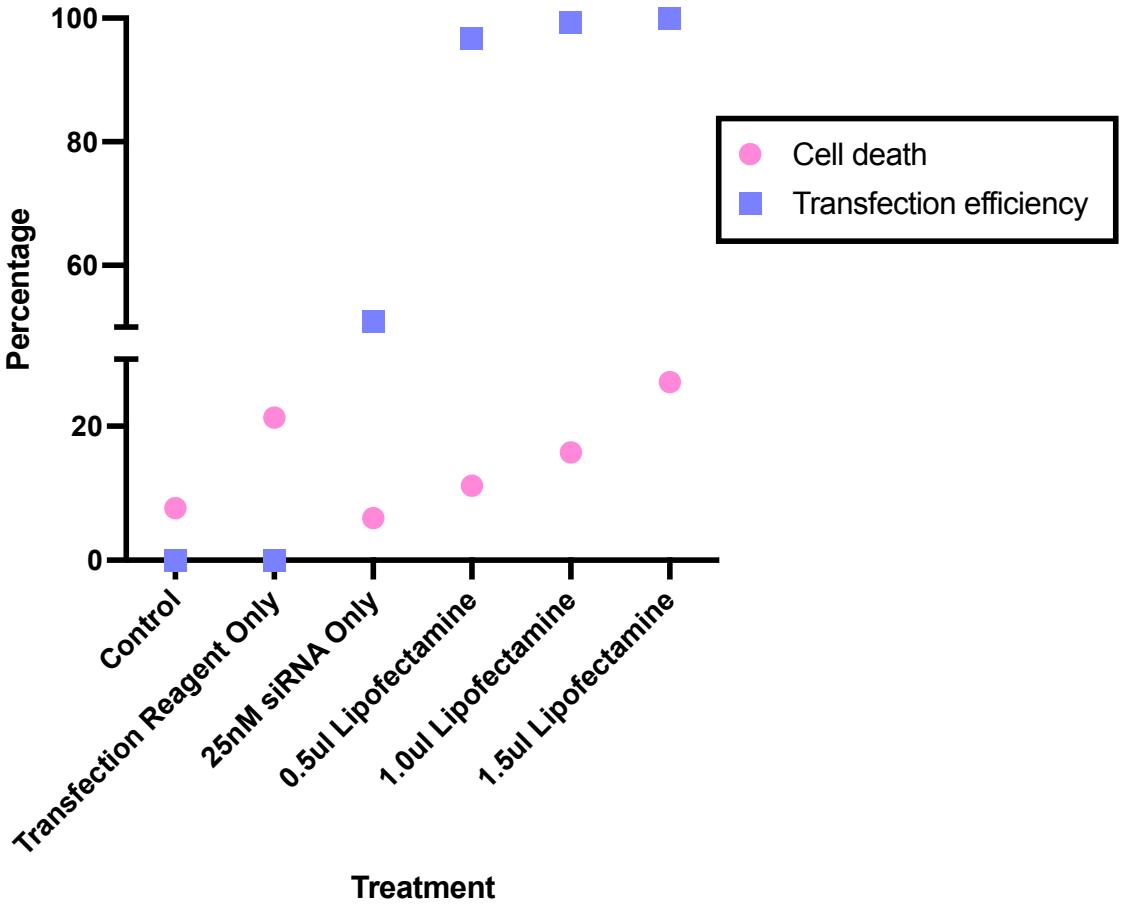

Figure 2.5: *Optimising transfection efficiency vs cell death*
Graph to show percentage cell death and percentage transfection efficiency 24 hrs after transfection of Ishikawa cells (endometrial epithelial cell line) with 25nM fluorescent siRNA of Ishikawa cells (n=2) using different volumes (0.5μl, 1.0μl and 1.5μl) of transfection reagent (Lipofectamine 2000). Cell death was recorded by counting number of alive and dead cells post-transfection by trypan blue staining, and transfection efficiency by counting number of cells containing fluorescent miRNA in 3 images taken at random across the well.

2.4.2 qPCR Results

A qPCR was performed on RNA from transfected Ishikawa cells to confirm over and under expression of miR-340-5p following transfection with miR-340-5p mimic and inhibitor. MiR-340-5p was significantly ($p<0.0001$) over expressed in endometrial epithelial cells in response to miR-340-5p mimic compared to control, lipofectamine only control, non-targeting mimic, and miR-340-5p inhibitor (Figure 2.6). This demonstrates that treatment with miR-340-5p mimic increases expression of this miRNA.

MiR-340-5p was not significantly differentially expressed in response to miR-340-5p inhibitor (Figure 2.6). Nevertheless, the expression values appear very slightly reduced and less variable compared to controls, despite being statistically non-significant.

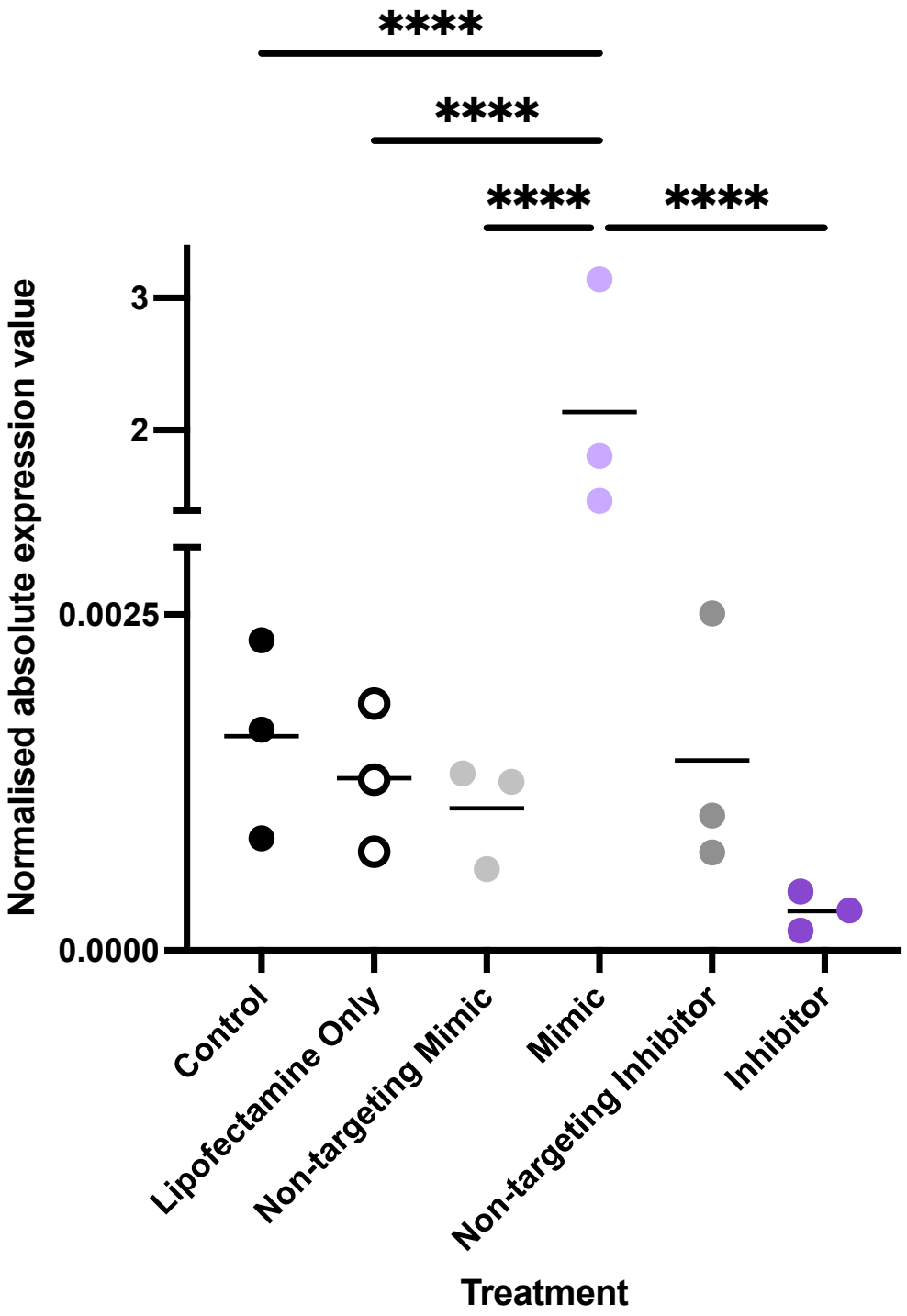

Figure 2.6: *Absolute expression values of miR-340-5p normalised to 5s following endometrial epithelial cell transfection (Ishikawa cell line, 48hr, n=3 biological replicates) with miR-340-5p mimic and inhibitor.*
Treatments were each added to 1.6ml antibiotic and serum free media and consisted of i) Control - 400μl optiMEM media only, ii) Lipofectamine only control - 4μl lipofectamine in 400μl optiMEM media, iii-vi) 80pmol of non-targeting mimic, miR-340-5p mimic, non-targeting inhibitor or miR-340-5p inhibitor in 400μl optiMEM media. Statistical significance following a one way ANOVA and multiple comparisons test is denoted by **** $p<0.0001$.

2.4.3 Proteomics Results

2.4.3.1 PCA Plots

Initial analysis by a Principal component analysis (PCA) showed clear clustering of one biological repeat, emphasising the effect of this on the variance of the data. The biological repeat n=1 appears to cluster together regardless of treatment towards the right and bottom. Different treatments for n=2 and n=3 generally cluster close to each other based on treatment type and treatments involving the mimic or inhibitor for miR-340-5p fall mostly in the upper section of the plot (Figure 2.7). A PCA plot of PC3 and PC4 which explains less of the data's variance (10.8% and 9.3% as opposed to 27% and 18.9% for PC1 and PC2 respectively) shows a very obvious clustering of miR-340-5p mimic in the upper left section of the plot, whilst controls tend to lie furthest to the right (Figure 2.8).

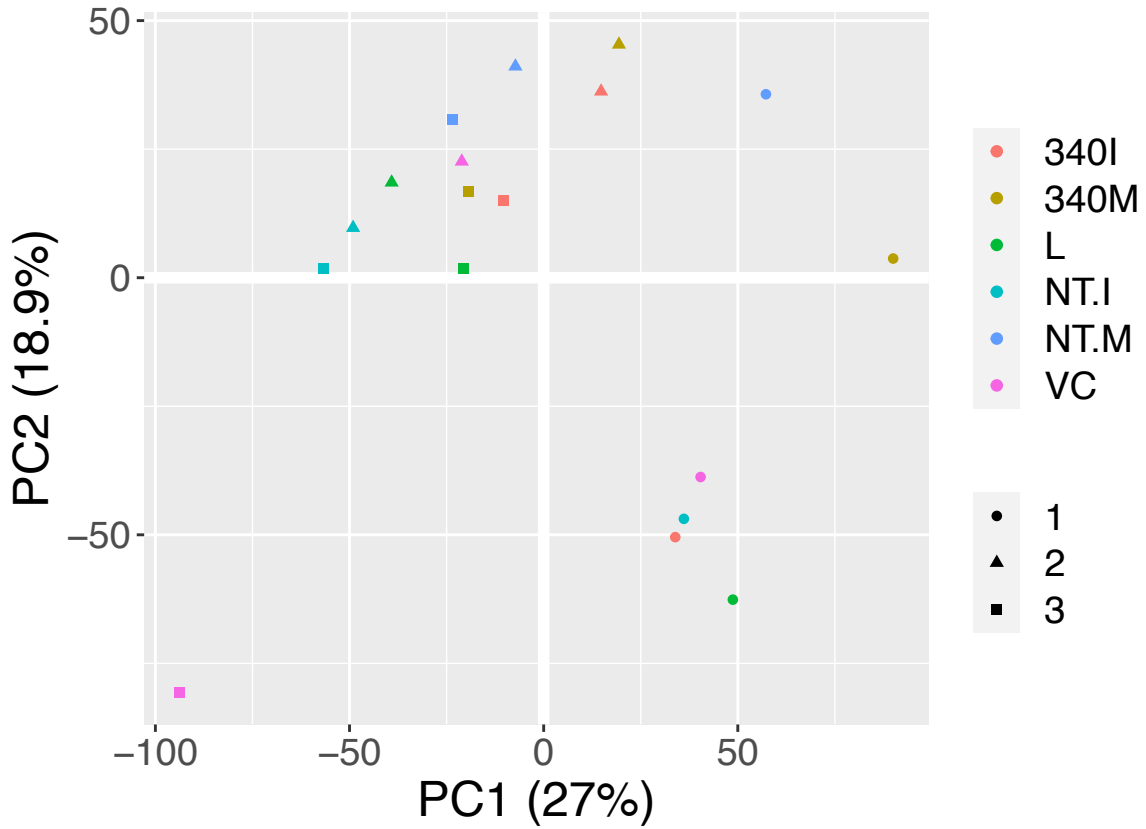

Figure 2.7: *PCA plot (PC1 and PC2) for miR-340-5p overexpression or under expression in Ishikawa cells.*
PCA (principal component analysis) plot of PC1 and PC2 for Ishikawa cells (n=3 - biological repeats shown by circle, triangle and square) transfected for 48 hrs with miR-340-5p mimic (340M), miR-340-5p inhibitor (340I), non-targeting mimic control (NT.M), non-targeting inhibitor control (NT.I), lipofectamine transfection reagent only (L) or media control (VC). Produced by Bristol Proteomics Facility.

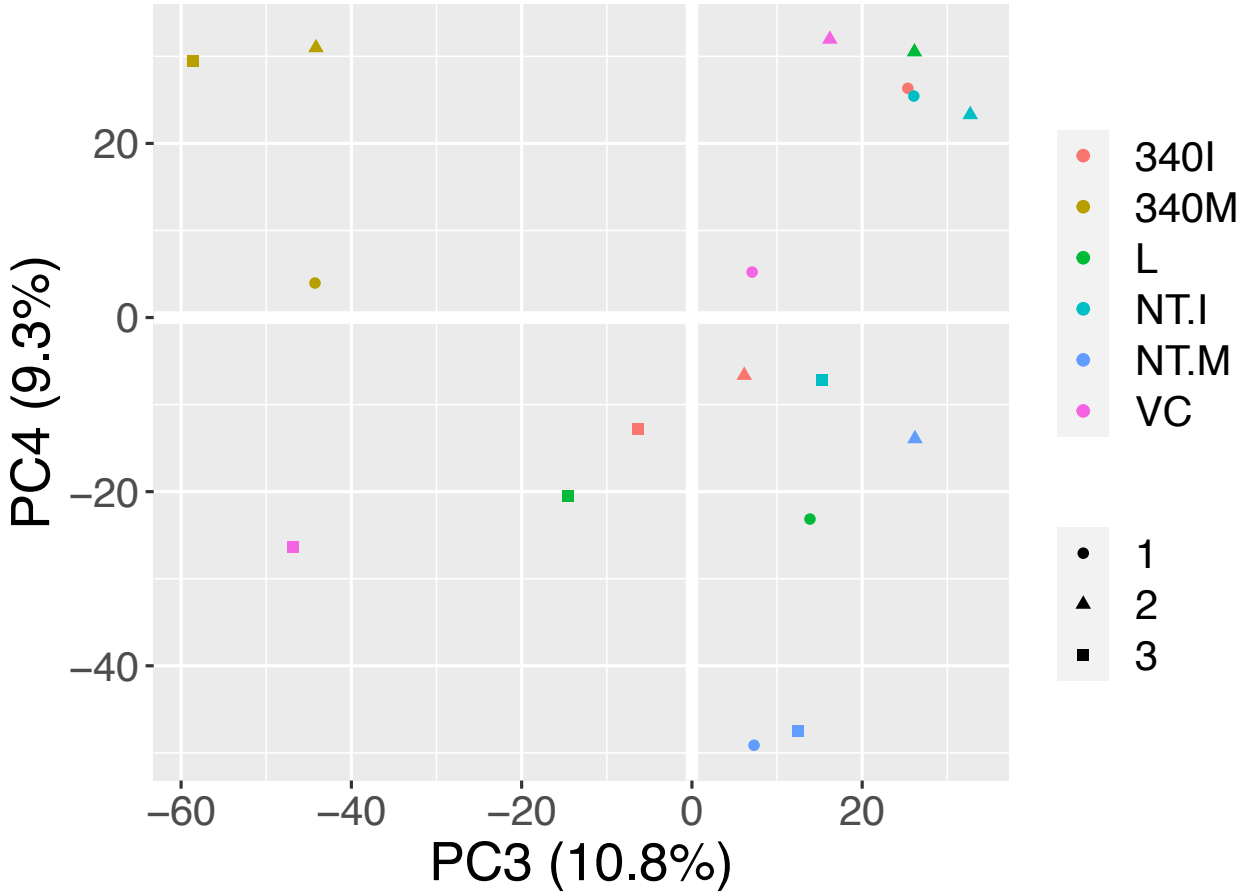

Figure 2.8: *PCA plot (PC3 and PC4) for miR-340-5p overexpression or under expression in Ishikawa cells.*
PCA (principal component analysis) plot of PC3 and PC4 for Ishikawa cells (n=3 - biological repeats shown by circle, triangle and square) transfected for 48 hrs with miR-340-5p mimic (340M), miR-340-5p inhibitor (340I), non-targeting mimic control (NT.M), non-targeting inhibitor control (NT.I), lipofectamine transfection reagent only (L) or media control (VC). Produced by Bristol Proteomics Facility.

2.4.3.2 Protein abundance following overexpression of miR-340-5p

Ishikawa cells were treated with non-targeting controls to ensure that differentially abundant proteins were due to the specific miRNA of interest and not just the presence of any miRNA. Non-targeting mimic and inhibitor altered the abundance of 958 and 467 proteins, respectively. Treatment with miR-340-5p mimic changed abundance of 1743 proteins whilst treatment with miR-340-5p inhibitor caused a change in abundance of 412 proteins ($p<0.05$). To remove non-specific effects a workflow (Figure 2.9) shows the removal of proteins altered by non-targeting controls to generate lists of proteins changed by the mimic, inhibitor, or both, only. There were 374 proteins which were changed in both non-targeting and mir-340 mimic targeting treatment which were excluded from those changed in response to the miR-340-5p targeting mimic to remove off-target effects. A total of 1369 proteins remained after these were removed, which were differentially abundant specifically in response to overexpression of miR-340-5p (Figure 2.10A). These proteins were enriched in biological processes including oxidation-reduction (141 proteins) and in cellular components such as the envelope (153 proteins), organelle envelope (153 proteins) and mitochondria (196 proteins) (Figure 2.10B). The biological process they were most commonly associated with was metabolic process (908 proteins), and a number were involved in developmental process (427 proteins) as well as reproduction (90 proteins) (Figure 2.10C). This group of proteins was broken down further into those which were more abundant and those which were less - a visual representation of this process is displayed in Figure 2.11. Of the 1369 altered proteins, 614 proteins were more abundant following treatment with miR-340-5p mimic, and 763 were less abundant in comparison to non-targeting control (Figure 2.12 and Figure 2.12). These include duplicate protein gene names with different accession numbers (such as different fragments of a singular protein) are counted as a single protein when determining significantly differentially abundant proteins but are considered separately when analysing in more depth in which direction each protein was changed.

Interestingly, enriched KEGG pathways associated with the 614 proteins which are more abundant following miR-340-5p overexpression include cadherin binding (32 proteins) and cell adhesion molecule binding (41 proteins) (Figure 2.12B). The 763 proteins which are less abundant when miR-340-5p expression is inhibited show enrichment in various KEGG pathways centred around cell metabolic processes (Figure 2.12C).

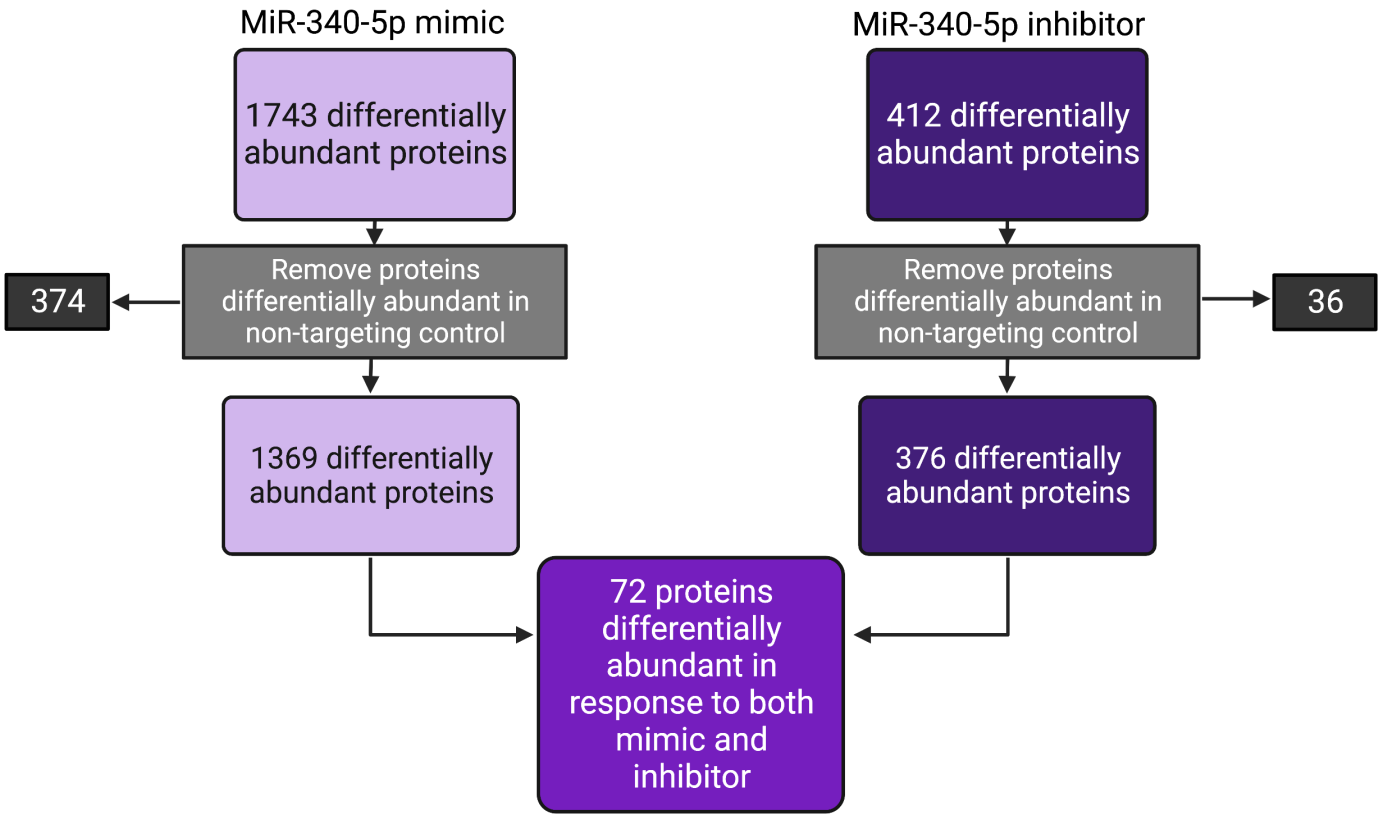

Figure 2.9: *Schematic diagram to summarise workflow for establishing lists of differentially abundant proteins for miR-340-5p mimic or inhibitor and those which are common to both.*
Lists of proteins differentially abundant in response to the mimic (1743) or inhibitor (412) were collated followed by removal of those which were also differentially abundant in response to the corresponding non-targeting control, leaving only proteins which are changed specifically in response to miR-340-5p mimic (1369) or miR-340-5p inhibitor (376). These lists were compared to deduce a list of proteins changed in response to both over and under expression of miR-340-5p (72).

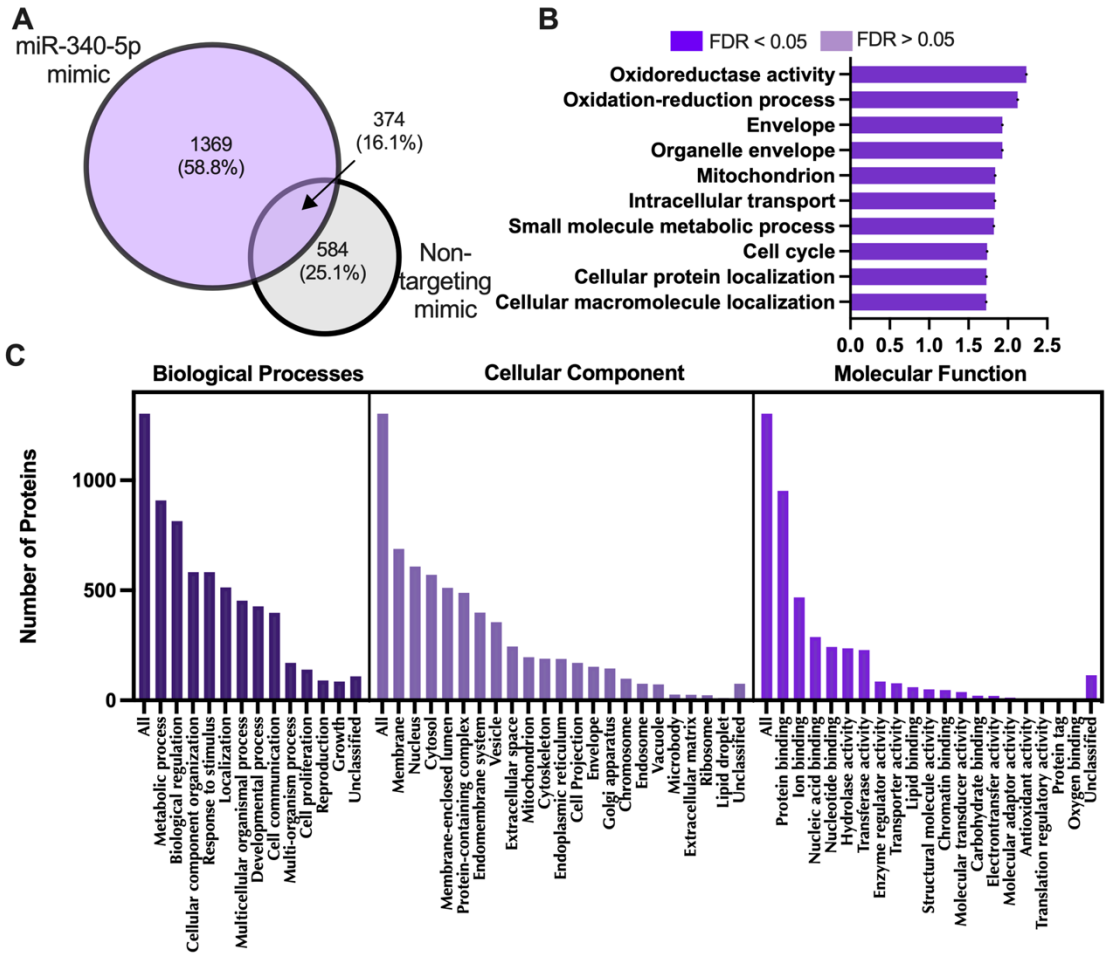

Figure 2.10: *Proteins altered in endometrial epithelial cells (Ishikawa) following treatment with miR-340-5p mimic.*
A) Venn diagram depicting total number of significantly differentially expressed proteins ($p<0.05$) following transfection of Ishikawa cells (n=3 biological replicates, 48 hrs) with miR-340-5p mimic (LHS) and non-targeting mimic (RHS). **B**) Enriched KEGG pathways associated with miR-340-5p mimic regulated proteins (FDR<0.05). **C**) WebGestalt overrepresentation analysis of biological process, cellular component, and molecular function categories for identified significantly differentially expressed proteins in response to miR-340-5p mimic (total of 1369). (Supplementary Table 1).

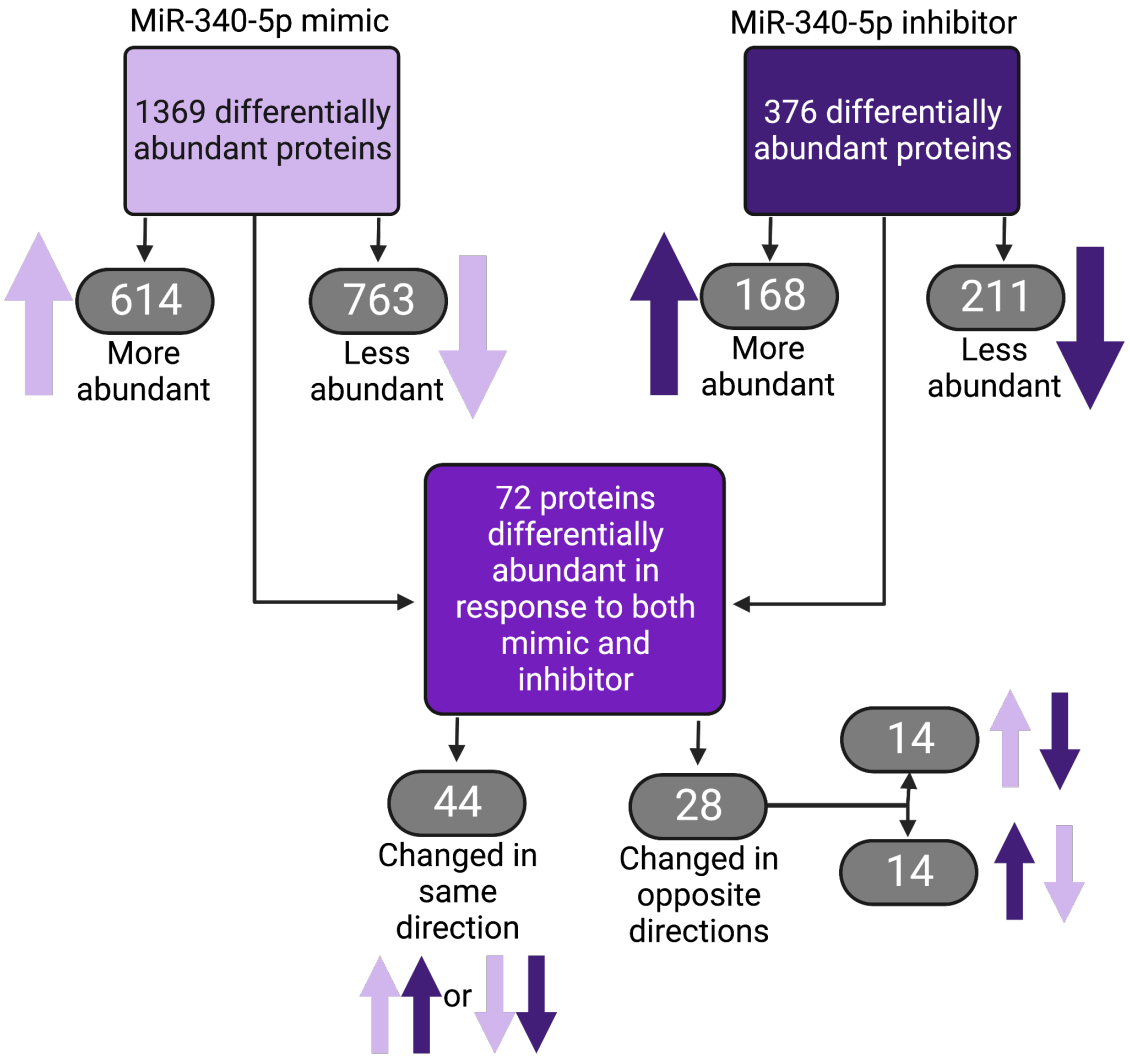

Figure 2.11: *Schematic diagram to demonstrate break down of numbers of proteins more or less abundant in response to altered expression of miR-340-5p.*
Diagram shows the number of proteins altered in abundance to be more or less abundant than the non-targeting mimic in response to miR-340-5p mimic or inhibitor. Also shows whether proteins that were changed in abundance in response to both miR-340-5p mimic or miR-340-5p inhibitor were changed in the same way (*i.e.,* both treatments result in more or less abundant) or opposite ways (*e.g.*, one treatment results in more abundant and one in less). Counts of proteins more or less abundant include duplicate gene names with different accession numbers.

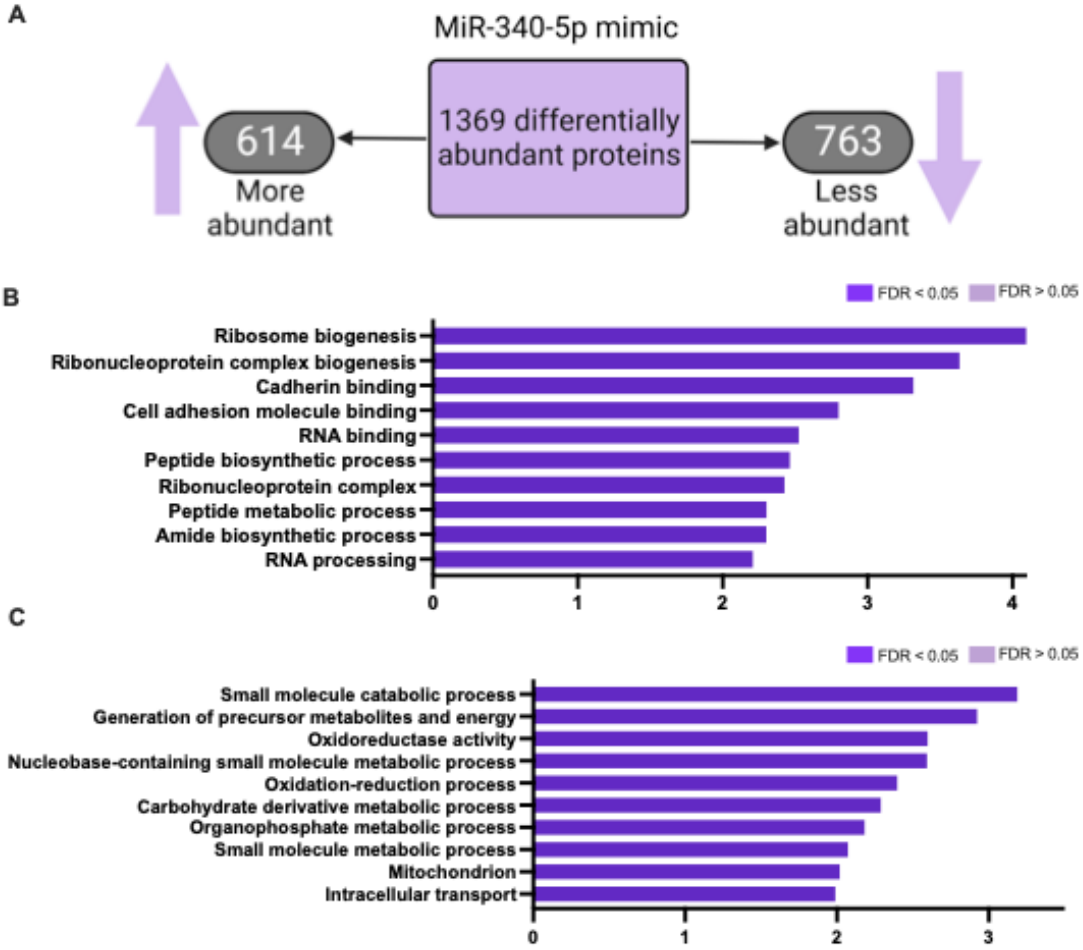

Figure 2.12: *Break down of numbers of proteins altered in abundance following 48 hr treatment of endometrial epithelial cells (n=3) with miR-340-5p mimic with regards to whether proteins were more or less abundant compared to non-targeting mimic control.*
Includes duplicate gene names with different accession numbers. **A**) Distribution of 1369 proteins altered in response to miR-340-5p mimic into categories of 'more abundant' or 'less abundant'. **B**) Enriched KEGG pathways associated with proteins which are more abundant in response to miR-340-5p mimic (FDR<0.05). **C**) Enriched KEGG pathways associated with proteins which are less abundant in response to miR-340-5p mimic (FDR<0.05). (Supplementary Table 2).

2.4.3.3 Protein abundance following inhibition of miR-340-5p

Once 36 proteins were removed from the total of 412 proteins changed in abundance by miR-340-5p inhibitor through exclusion of proteins also changed by the non-targeting inhibitor, 376 proteins exhibited altered abundance in response to miR-340-5p inhibitor (Figure 2.13A). These proteins are significantly enriched more than can be expected by chance in KEGG pathways involving multiple transport processes such as nuclear (22 proteins), nucleocytoplasmic (22 proteins), intracellular (68 proteins) and protein transport (65 proteins) (Figure 2.13B). This suggests these proteins changed in abundance by reduced expression of miR-340-5p are likely to play roles in or have an effect on the aforementioned various transport pathways. The cellular components that these proteins are localised to is most commonly the nucleus (169 proteins) followed by the cell membrane (161 proteins) and protein binding is the most overrepresented molecular function (259 proteins) (Figure 2.13C).

Of the 376 differentially abundant proteins in response to treatment with miR-340-5p inhibitor, 211 were less abundant following miR-340-5p inhibition, and 168 were more abundant (Figure 2.14A). Proteins which are less abundant following treatment with miR-340-5p inhibitor show significant enrichment in intracellular transport (42 proteins), with non-significant enrichment in symbiont process (21 proteins) (Figure 2.14C). This is particularly interesting as this suggests the interaction between invading trophoblast cells and maternal epithelium may evoke similar mechanisms involved in symbiont process as the genetically different cells encounter the maternal cells.

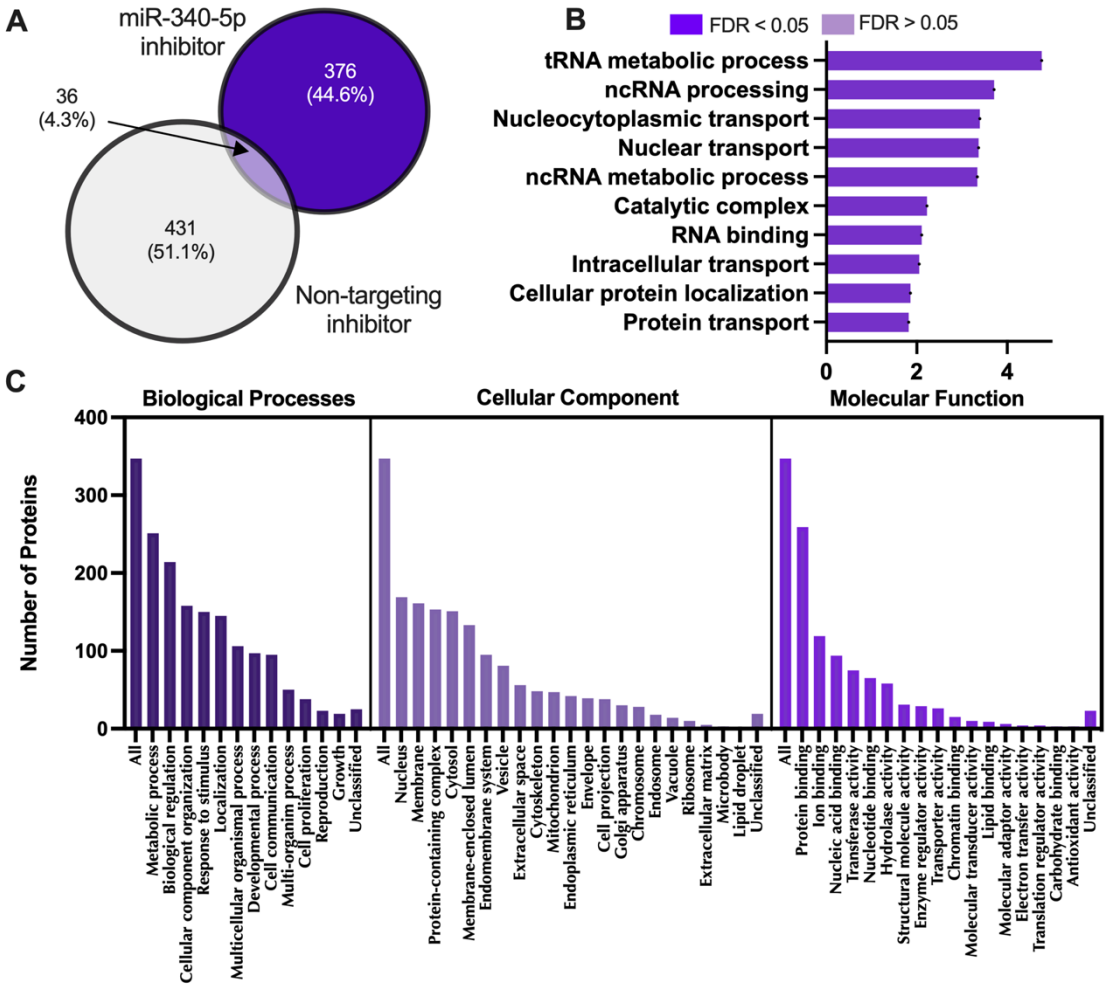

Figure 2.13: *Proteins altered in endometrial epithelial cells (Ishikawa) following treatment with miR-340-5p inhibitor.*
A) Venn diagram demonstrating total number of significantly altered proteins ($p<0.05$) following transfection of ishikawa cells (n=3 biological replicates, 48 hrs) with miR-340-5p inhibitor (RHS) and non-targeting inhibitor (LHS). **B**) Enriched KEGG pathways associated with miR-340-5p inhibition regulated proteins (FDR<0.05). **C**) WebGestalt overrepresentation analysis of biological process, cellular component, and molecular function categories for identified significantly differentially expressed proteins in response to miR-340-5p inhibitor (total of 376). (Supplementary Table 3).

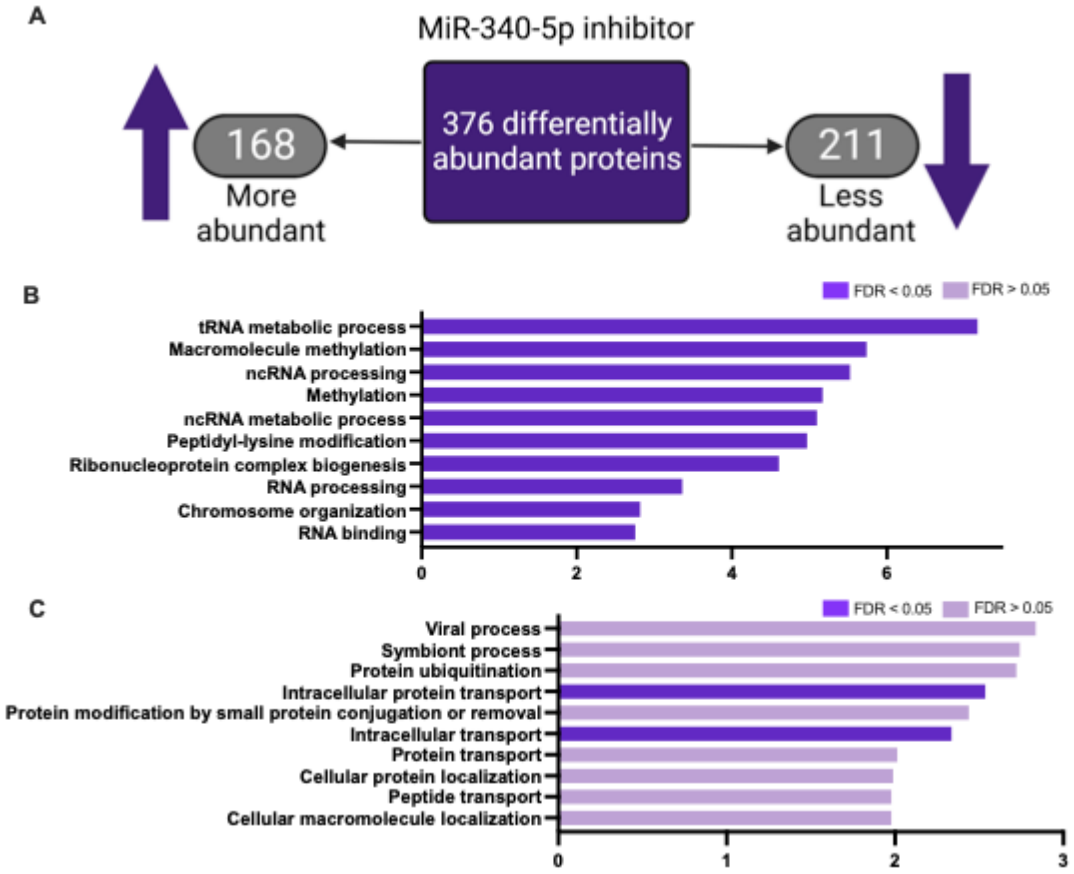

Figure 2.14: *Break down of numbers of proteins altered in abundance following 48 hr treatment of endometrial epithelial cells (n=3) with miR-340-5p inhibitor with regards to whether proteins were more or less abundant compared to non-targeting inhibitor control.*
Includes duplicate gene names with different accession numbers. **A**) Distribution of 376 proteins altered in response to miR-340-5p inhibitor into categories of 'more abundant' or 'less abundant'. **B**) Enriched KEGG pathways associated with proteins which are more abundant in response to miR-340-5p inhibitor (FDR<0.05). **C**) Enriched KEGG pathways associated with proteins which are less abundant in response to miR-340-5p inhibitor (FDR<0.05). (Supplementary Table 4).

2.4.3.4 Proteins altered in abundance in response to over and under expression of miR-340-5p

When comparing proteins altered by miR-340-5p mimic and those changed by miR-340-5p inhibitor, there were 72 proteins in common (Figure 2.15A). These proteins were not significantly enriched in any functions - likely due to the small number - but were non-significantly overrepresented in transport processes as well as redox response (Figure 2.15B-C).

Of these 72 common proteins, 28 were differentially abundant in opposite directions following treatment with miR-340-5p mimic vs miR-340-5p inhibitor (*i.e.*, protein is more abundant following treatment with mimic, and less abundant following treatment with inhibitor, or vice versa). Of the 28 proteins, there were 14 which were increased by overexpression and decreased by inhibition, and 14 which were increased by inhibition and decreased by overexpression. Forty-four proteins were changed in the same way (both treatments result in protein being more abundant or less abundant) (Figure 2.11). There were no significantly overrepresented KEGG pathways associated with these proteins, likely due to the small sample sizes (Figure 2.16).

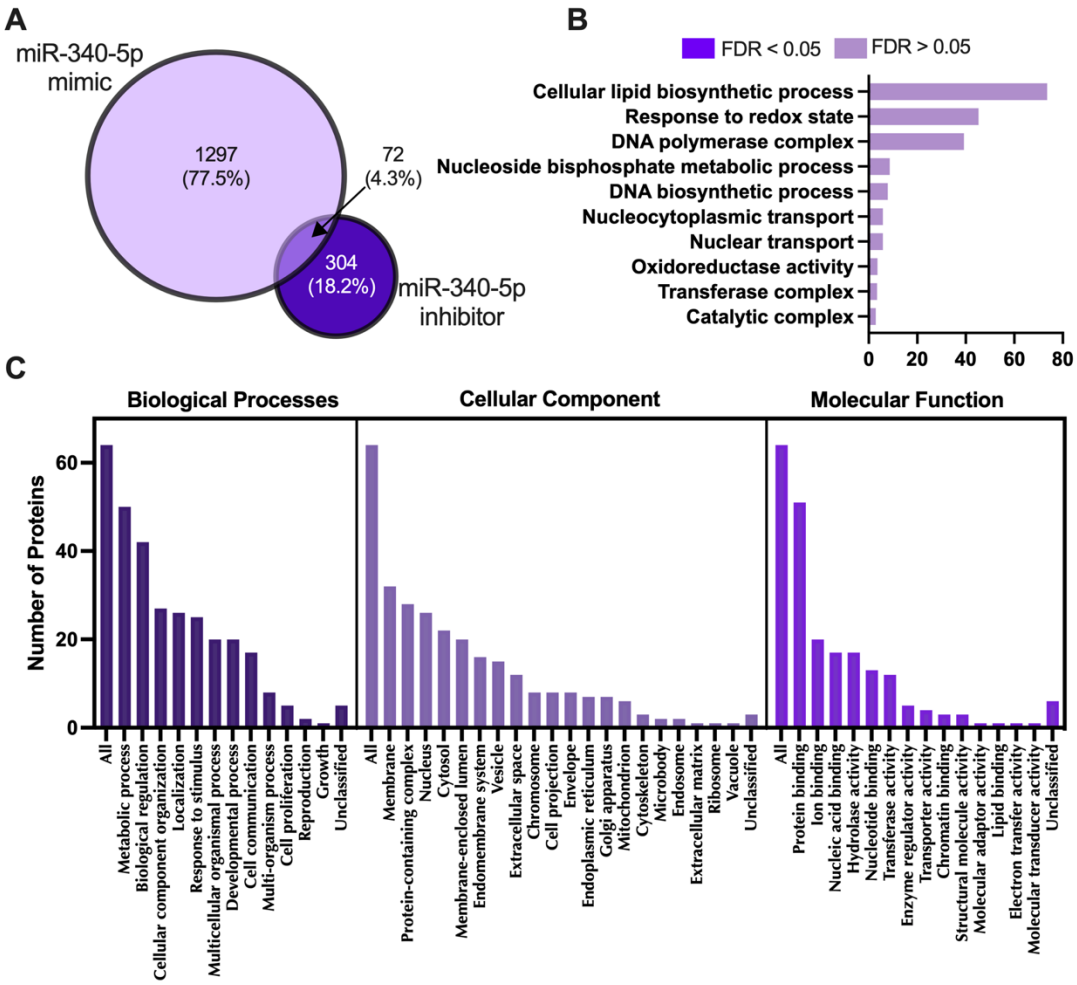

Figure 2.15: *Proteins altered in endometrial epithelial cells (Ishikawa) following treatment with miR-340-5p mimic or inhibitor.*
A) Venn diagram demonstrating total number of significantly altered proteins ($p<0.05$) following transfection of ishikawa cells (n=3 biological replicates, 48 hrs) with either miR-340-5p mimic (LHS) or inhibitor (RHS). **B**) Enriched KEGG pathways associated with miR-340-5p mimic and inhibition regulated proteins (FDR<0.05). **C**) WebGestalt overrepresentation analysis of biological process, cellular component, and molecular function categories for identified significantly differentially expressed proteins in response to miR-340-5p mimic and inhibitor (total of 72). (Supplementary Table 5).

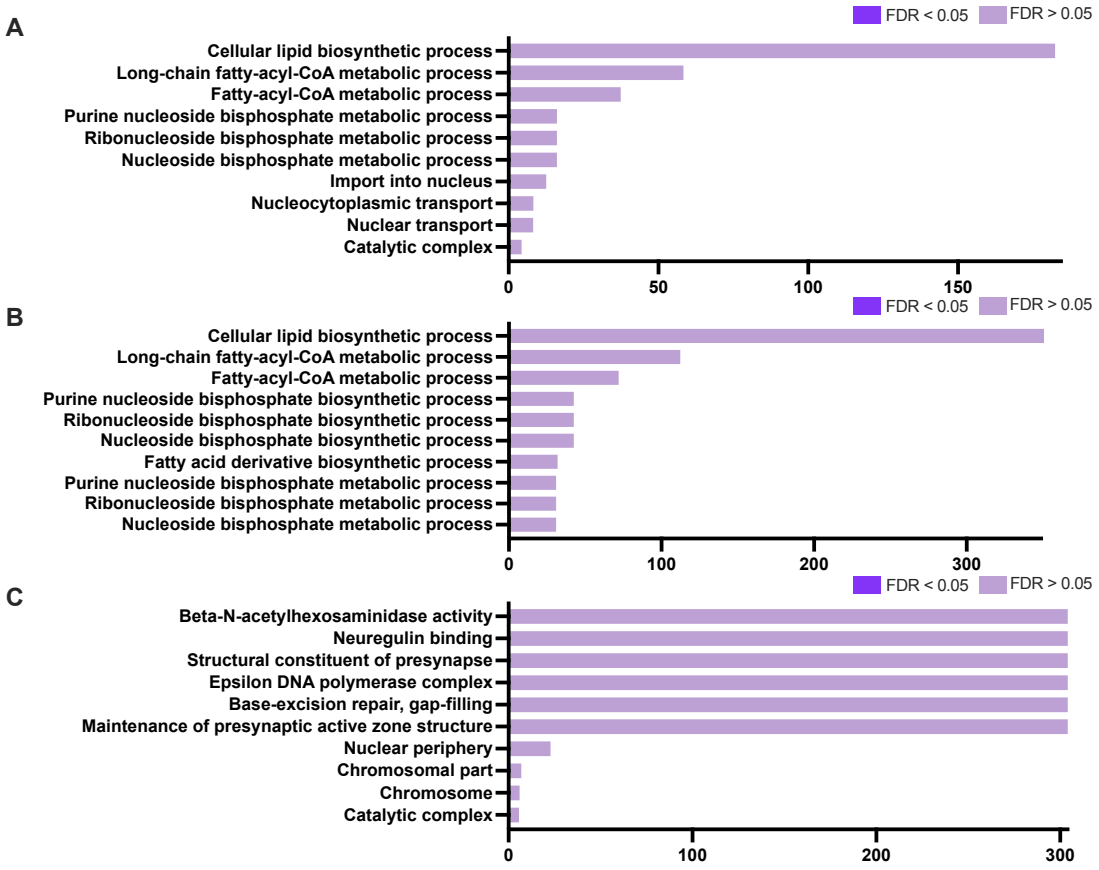

Figure 2.16: *Enriched KEGG pathways associated with proteins which are altered in Ishikawa cells (n=3) following transfection (48 hrs) by both miR-340-5p mimic and inhibitor.*
A) Enriched KEGG pathways for proteins altered in the *same* way by miR-340-5p mimic and inhibitor (*i.e.*, both increased or both decreased in abundance) (FDR<0.05). **B**) Enriched KEGG pathways for proteins increased by miR-340-5p overexpression and decreased by miR-340-5p inhibition (FDR<0.05). **C**) Enriched KEGG pathways for proteins decreased by miR-340-5p overexpression and increased by miR-340-5p inhibition (FDR<0.05). (Supplementary Table 6).

2.4.3.5 Proteins confirmed *in vitro* as targets of miR-340-5p, compared with miRDB predicted targets, and P4 regulated *in vitro* targets

MiRDB was used to predict 2102 targets of miR-340-5p. To determine how many of these *in vitro* identified targets of miR-340-5p were predicted by mirDB, these lists were compared. Of the 2102 predicted targets, only 274 were confirmed *in vitro* by transfection with miR-340-5p mimic and/or inhibitor (Supplementary Figure 1) These proteins were significantly enriched in mRNA 3'-UTR binding (8 proteins) as well as cadherin binding (17 proteins) (Supplementary Figure 1).

Next, *in vitro* confirmed targets, miRDB predicted targets and those mRNAs altered by P4 in endometrial epithelial cells from previous work (Edge et al., 2023) were compared. A total of 171 proteins were predicted to be targets by miRDB as well as being altered *in vitro* by treatment with miR-340-5p mimic and/or inhibitor as well as in endometrial epithelial cells treated with P4. This resulted in 171 proteins that fit all 3 categories (Figure 2.17A). Further analysis was carried out on this list of proteins; they were non-significantly ($p>0.05$) overrepresented in adherens junction assembly (6 proteins) and organization (8 proteins) (Figure 2.17B-C) which are important for joining epithelial cells together and their organization may be involved in invasion through the epithelial layer during implantation, vital for early pregnancy. They are also represented in cellular response to hormone stimulus (18 proteins) and symbiont process (19 proteins).

Finally, it was necessary to determine whether the list of *in vitro* proteins altered in abundance by transfection of miR-340-5p mimic or miR-340-5p inhibitor were present in RNASeq data from human endometrial biopsy samples (Lipecki et al., 2022). Of the proteins altered by miR-340-5p mimic, 94% of their corresponding mRNAs were detected in patient samples. Furthermore, only 13 of 1251 mRNAs that corresponded to altered proteins were absent from 1 or more of n=36 samples. Ninety percent of proteins affected by inhibition of miR-340-5p were identified in RNASeq data, with only 5 of 326 mRNAs not present in all of the 36 patient samples. There were 59 of each of these sets of proteins which were changed by both mimic and inhibitor whose mRNA was found in patient samples (Figure 2.18).

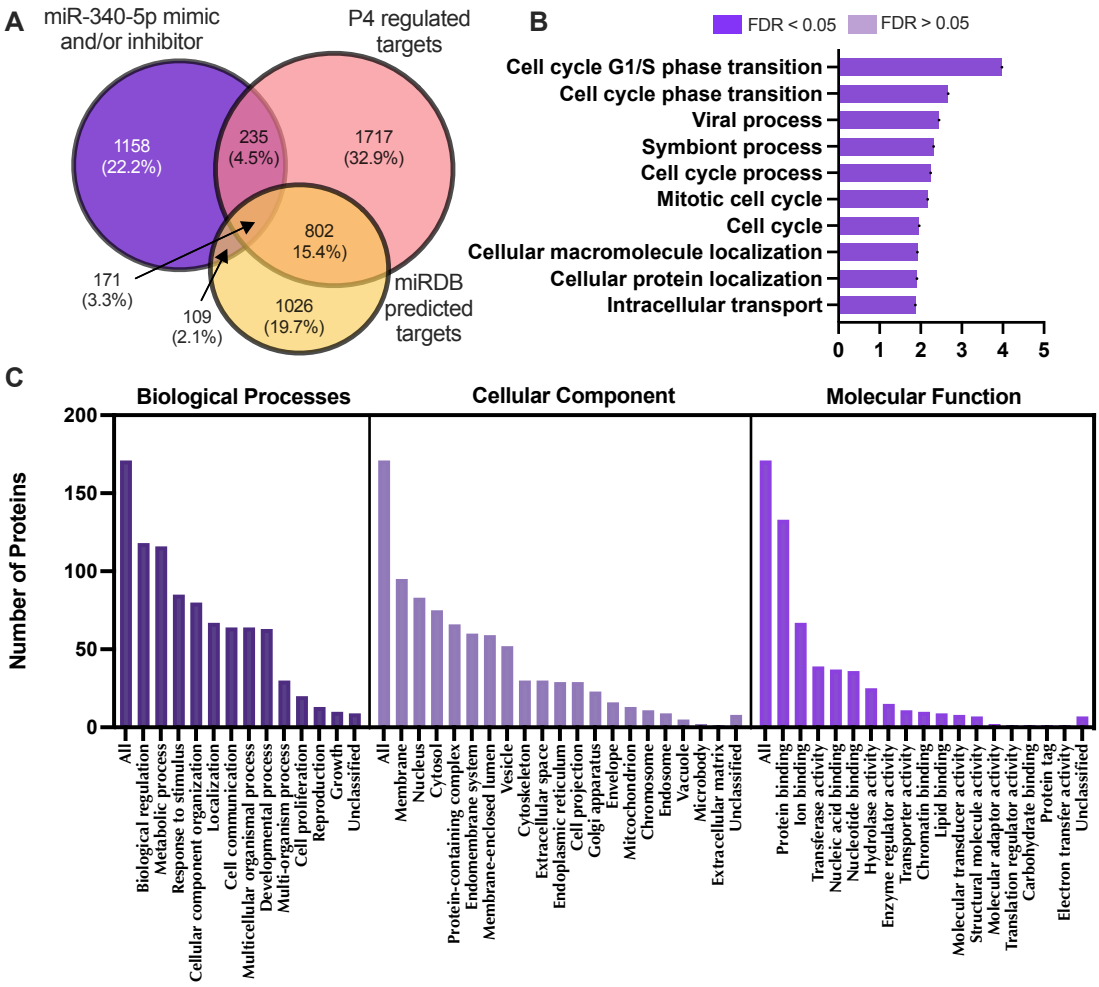

Figure 2.17: *Proteins significantly altered in abundance in response to miR-340-5p mimic and/or inhibition compared to miRDB predicted targets and P4 regulated mRNAs.*
A) Venn diagram showing total number of proteins significantly altered in abundance ($p<0.05$) following transfection of ishikawa cells (n=3 biological replicates, 48 hrs) with miR-340-5p mimic and/or inhibitor vs miRDB predicted targets vs progesterone regulated mRNAs (Edge et al., 2023). **B)** Enriched KEGG pathways associated with miR-340-5p mimic and/or inhibitor regulated proteins, miRDB predicted targets and P4 regulated mRNAs overlap (FDR<0.05). **C)** WebGestalt overrepresentation analysis of biological process, cellular component, and molecular function categories for identified significantly differentially abundant proteins in response to miR-340-5p mimic and/or inhibition, predicted targets and P4 regulated mRNAs overlap. (Supplementary Table 8).

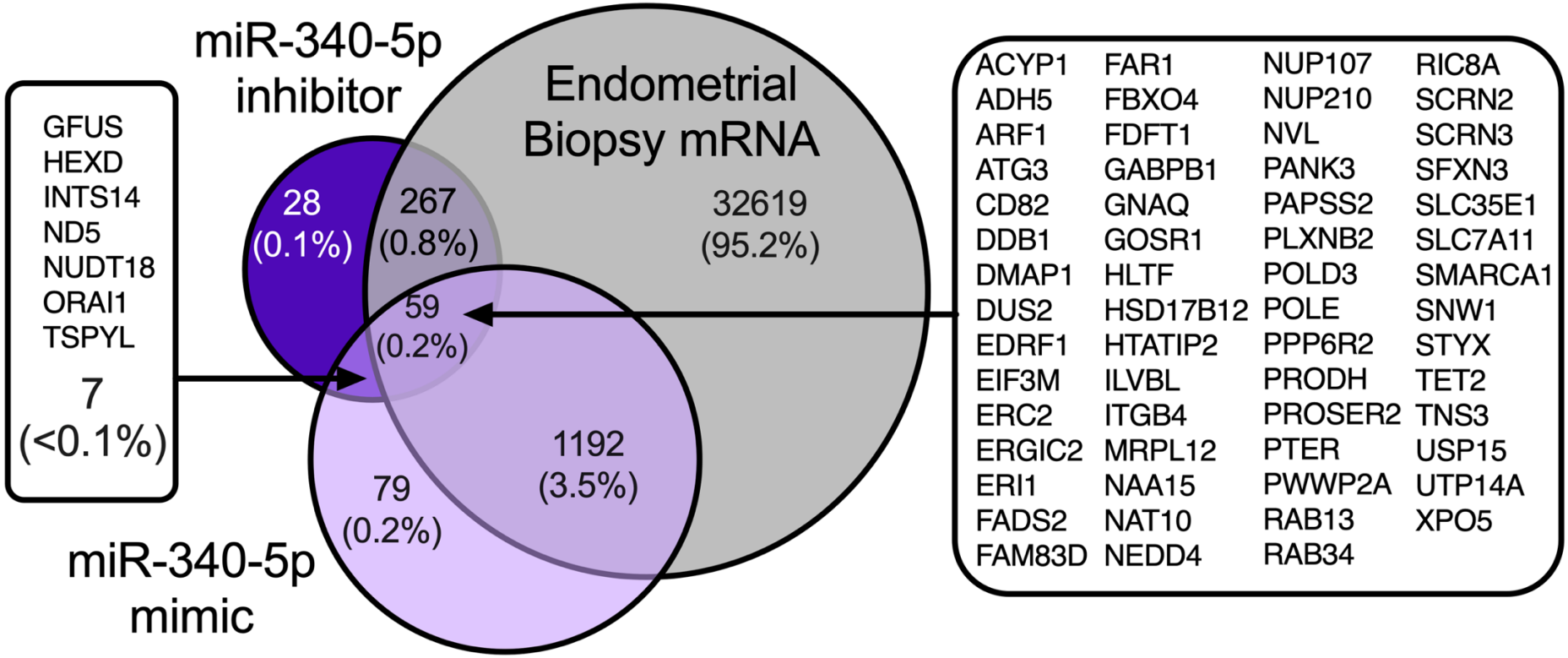

Figure 2.18: *Comparison of miR-340-5p regulated proteins with mRNA from human endometrial biopsies.*
Comparison of proteins significantly altered in abundance ($p<0.05$) in following transfection of endometrial epithelial (Ishikawa) cells (n=3 biological replicates, 48 hrs) with miR-340-5p mimic and/or inhibitor compared to RNASeq data from human endometrial biopsies (n=36 biological repeats, biopsies taken 4-12 days following ovulation)(Lipecki et al., 2022). Listed proteins display 7 which are altered by both over and under expression of miR-340-5p, but are not detected in biopsies, suggesting they are not present physiologically; and 59 proteins which are altered in response to both over and under expression of miR-340-5p and were detected in endometrial biopsies, suggesting they are direct targets and physiologically relevant in primary endometrial tissue (Longer lists of proteins in each section of Venn diagram can be found in Supplementary Table 9A-D).

2.4.3.6 Differential protein abundance

A visual representation of the number of proteins significantly differentially abundant in response to either the miR-340-5p mimic or inhibitor is present as a volcano plot in Figure 2.19 shows proteins which are significantly different in number ($p<0.05$) and highly significantly different ($p<0.05$ and $>1 Log_2FC$) or ($p<0.05$ and >-1 Log_2FC) between the two groups.

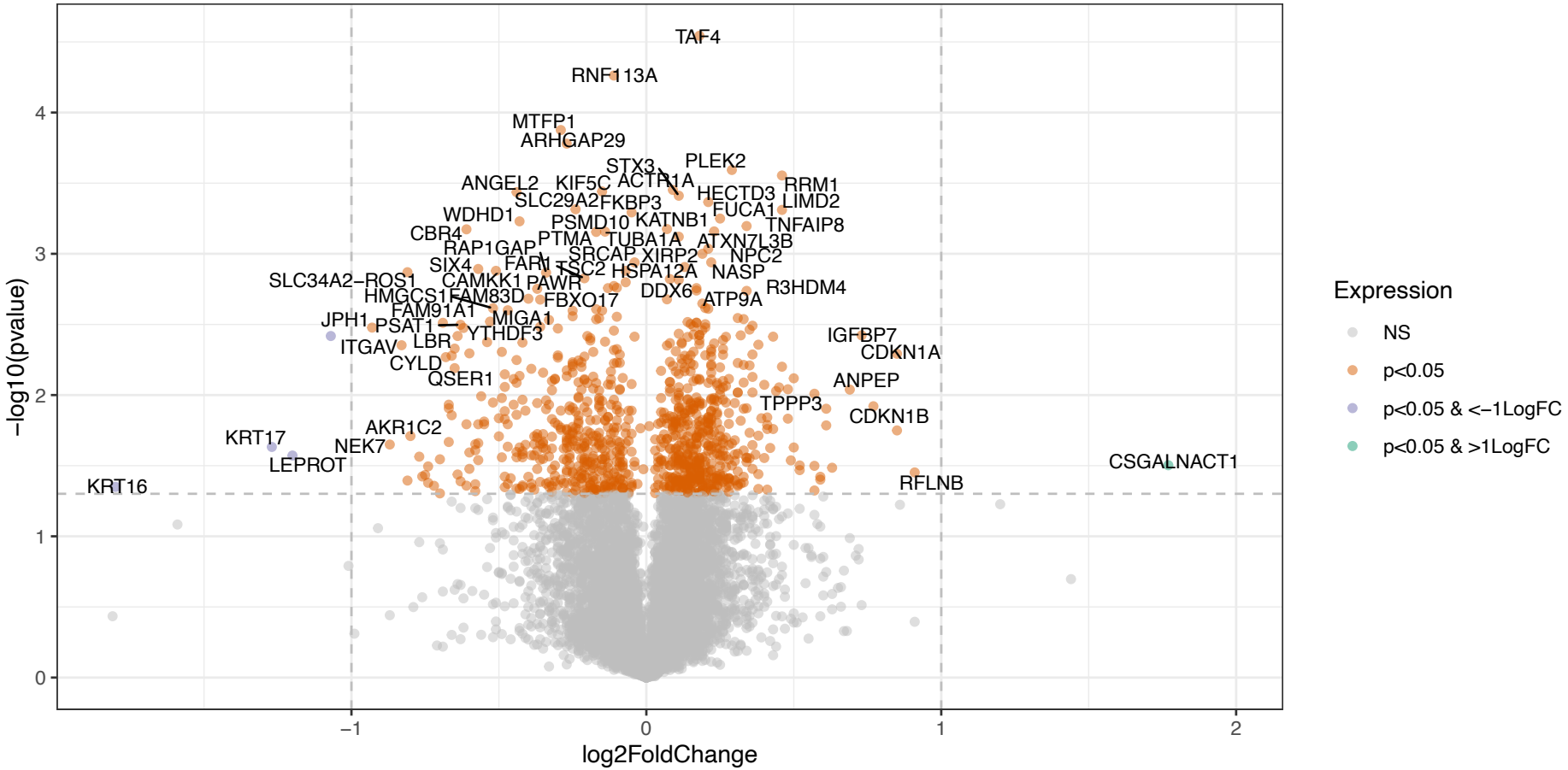

Figure 2.19: *Volcano plot showing abundance of proteins present in Ishikawa cells (n=3) transfected for 48 hrs with either miR-340-5p mimic or inhibitor highlighting those which are significantly differentially abundant between the two groups.*
Proteins which are significantly differentially abundant ($p<0.05$) between the two treatments are shown in orange, proteins which are highly significantly decreased in abundance ($p<0.05$ and $>-1\text{Log}_2\text{FC}$) are coloured purple, and those which are highly significantly increased in abundance abundant ($p<0.05$ and $>1\text{Log}_2\text{FC}$) are coloured green.

2.5. Discussion

This chapter tested the hypothesis that a miRNA which is evolutionarily conserved across eutherian mammals and is regulated by P4, modifies the expression of protein coding regions of the genome, and may facilitate receptivity to implantation in humans. Eutherian mammals show a diverse range of implantation strategies therefore it was hypothesised that the eutherian-mammal-specific conserved miRNAs would play a role in establishing the similarities or diversities observed across species (Taylor et al., 2021). Previous work from our lab demonstrated that miR-340-5p is upregulated in response to P4 *in vitro* in endometrial epithelial cells. To begin to unravel the function of this modification, I investigated the proteome of the endometrial epithelial cell layer when treated with miR-340-5p mimic or inhibitor.

Confirmation of miR-340-5p over or under expression in Ishikawa cells was first carried out, resulting in significant overexpression of the miRNA in response to miR-340-5p mimic transfection. There was no significant difference in miR-340-5p expression between miR-340-5p inhibitor transfected cells and controls, however the expression was detected by qPCR to be slightly decreased. This is likely due to the method in which the miRIDIAN inhibitors function. These inhibitors bind to the miRNA of interest and stop its activity, but do not degrade the miRNA. Therefore, when the miRNA is extracted from the cells, miR-340-5p will still be present and detectable by PCR, however in vitro it would be non-functional.

Over and under expression of miR-340-5p in Ishikawa cells resulted in alterations in abundance of many proteins. Following downstream analysis using Webgestalt (Liao et al., 2019) of proteins altered by miR-340-5p mimic, it was found that oxidation reduction process along with oxidoreductase activity were two of the most overrepresented pathways these proteins are involved in. Fetal oxidative stress is linked to cardiovascular disease in adult life - referred to as the Developmental Origins of Health and Disease (DOHaD) (Rodríguez-Rodríguez et al., 2018) demonstrating that the *in utero* environment in which an individual is gestated can cause increased susceptibility to diseases such as diabetes and cardiovascular disease later in life (Bianco-Miotto et al., 2017). Reactive oxygen species (ROS) function as signalling molecules during pregnancy as well as playing a role in placentation (Rodríguez-Rodríguez et al., 2018). During very early pregnancy, the embryo is extremely vulnerable to oxidative stress, and low redox state favours proliferation and differentiation (Dennery,

2010). This suggests that a function of increased expression of miR-340-5p, triggered by P4 present at this stage of the cycle, is to regulate redox processes to keep them tightly controlled at this crucial time of development.

Interestingly, proteomic analysis revealed 28 proteins which were significantly differentially abundant in opposite directions following both over and under expression of miR-340-5p - *eg.,* a protein is more abundant following overexpression and less abundant following inhibition (Figure 2.11 and Figure 2.16B-C). This indicates these proteins are direct and important targets of miR-340-5p, suggesting that they are likely to be P4 regulated *in vivo* via P4 mediated upregulation of miR-340-5p. Unfortunately due to small sample size, this group of proteins was not significantly enriched in any biological processes in further analyses. The majority of processes which are highlighted as significantly overrepresented in response to miR-340-5p mimic and/or inhibitor, as well as those which are common to predicted targets or P4 regulated targets; centre around regulation of the cell cycle. This points towards miR-340-5p playing a role in controlling the endometrial epithelial cells rate of proliferation, growth, and apoptosis, to allow for implantation and successful pregnancy. Many studies investigating roles of miR-340-5p in other systems have findings which may be applicable to this work. A study considering the role of miR-340-5p in endometrial cancer cells determined that it acts as an anti-oncogene when overexpressed (Xie et al., 2016). Proliferation was significantly downregulated, and apoptosis triggered in an endometrial cancer cell line following miR-340-5p overexpression. This theory could be applicable to miR-340-5p expression in the endometrial epithelial cells. Rising concentrations of P4 result in halted epithelial cell proliferation in the endometrium which is required for priming of the endometrium to be receptive to embryo implantation (Marquardt et al., 2019). Here, miR-340-5p is overexpressed in endometrial epithelial cells to recapitulate the increase in miR-340-5p observed when treated with P4 previously (Edge et al., 2023). The function of miR-340-5p in inhibition of proliferation observed in the endometrial cancer cell line could be employed here in the priming of the endometrium by stopping epithelial cell proliferation during the luteal phase. Molecules thought to regulate proliferation and apoptosis in the endometrial cancer study include p27 KIP1, Bcl-2, Bax and Caspase-3 (Xie et al., 2016). The proteomic analysis conducted in epithelial cells overexpressing miR-340-5 also showed altered levels of Peptidyl-tRNA hydrolase 2 (PTRH2), also known as Bcl-2 inhibitor of transcription 1 which is involved in apoptotic processes. Caspase activity and apoptosis inhibitor 1 (CAAP) was significantly less abundant in Ishikawa cells following treatment with miR-340-5p mimic, suggesting that the process

of apoptosis is upregulated following an increase in miR-340-5p. Moreover, overrepresented biological processes of the list of proteins which meet all of the following criteria: 1) significantly differentially abundant following transfection with miR-340-5p mimic and/or inhibitor, 2) P4 regulated target and 3) miRDB predicted target (Figure 2.17); centre around regulation of the cell cycle. This further supports the suggestion that higher expression of miR-340-5p due to increasing P4 concentrations in circulation during the luteal phase functions to regulate cell cycle and death in endometrial epithelial proliferation.

Negative regulation of *PNO1* by miR-340-5p was observed in lung adenocarcinoma cells. This is determined to reduce proliferation and migration of malignant cells by downregulating Notch signalling (D. Liu et al., 2020). Interestingly, in my proteomic data, overexpression of miR-340-5p results in significant upregulation of *PNO1.* This opposite function in endometrial epithelial cells could be relevant as Notch signalling regulates many processes important in early pregnancy such as proliferation, differentiation, and adhesion (Cuman et al., 2014). It has been found that Notch ligands *Jagged1* and *DLL4* localise to the endometrial epithelium along with *Notch2* (Cuman et al., 2014). *Notch2* is also upregulated in this proteomic data. It may be that miR-340-5p upregulation causes increased *PNO1* which in turn increases Notch signalling pathways to facilitate endometrial receptivity through regulating processes like adhesion.

Tight junctions (TJs) are one of a number of different intercellular complexes and function to create an epithelial barrier between adjacent cells whilst allowing cell to cell transport and communication. Claudins are a group of transmembrane proteins that form TJs (Kozieł et al., 2020). It is thought that miRNAs are involved in epigenetic regulation of claudins, and that dysregulation is seen in many human cancers (Kwon, 2013). In this proteomic analysis, in response to treatment with miR-340-5p mimic performed to recreate the increase in miR-340-5p expression following P4 treatment, Claudin 4 (*CLDN4*) is significantly upregulated. In a meta-analysis with the objective to determine genes associated with endometrial receptivity, *CLDN4* was one of the most highly significantly upregulated biomarkers in endometrial biopsies during the window of implantation (Altmäe et al., 2017). *CLDN4* was also found to be elevated in the endometrial tissue distinctively during the time of implantation in humans before declining (Riesewijk et al., 2003). This is also observed in the rat uterus, where *CLDN4* peaks during implantation, with the suggestion that an increase in *CLDN4* in both luminal and glandular epithelial cells is P4 driven

(Nicholson et al., 2010). Similar results for increased expression of *CLDN4* were found in human luminal and glandular epithelial cells of the endometrium during the mid-luteal phase during which there is a high concentration of P4 (Carson et al., 2002). These studies demonstrate the importance of expression of *CLDN4* in the endometrium and its association with endometrial receptivity. Alternately, an investigation into the relationship between *CLDN4* expression and assisted reproductive technology outcome demonstrates weaker concentrations of *CLDN4* yield a better rate of successful pregnancies following in-vitro fertilisation (IVF) treatment compared to higher levels (Serafini et al., 2009). Oppositely, it has also been suggested that reduction of *CLDN4* is potentially linked to development of endometriosis (Gaetje et al., 2008; Pan et al., 2009). *CLDN4* has been shown to be upregulated in cancers, particularly ovarian cancer. Studying the altered gene expression in cells overexpressing *CLDN4,* as is the case in ovarian cancer, found that genes promoting angiogenesis were increased as well as production of angiogenic factors (Li et al., 2009). A separate investigation into knockdown of *CLDN4* in tumour cells displays a reduction in the ability of the cells to form TJs, which has an effect on processes such as attachment and invasion (Shang et al., 2012), suggesting that *CLDN4* is required for these mechanisms vital for implantation. It is known that TJs are important to endometrial receptivity, and they become disrupted following P4 stimulation of the endometrium to assist in invasion (Bhurke et al., 2016). If *CLDN4,* a key TJ component, peaks in the endometrium at the height of endometrial receptivity and then reduces, perhaps this is facilitating the subsequent invasion by disturbance of TJs. Overall, this indicates that temporally controlled and correct expression level of *CLDN4* is required, where over or under expression is detrimental to functions during the period of receptivity.

The group of proteins which are more abundant following overexpression of miR-340-5p interestingly demonstrate overrepresentation in processes including cell adhesion molecule binding and cadherin binding. Cadherin 6 is in both gene sets associated with these processes and is increased by overexpression of miR-340-5p. Cadherin 6 has previously been found to localise to the apical surface of the endometrial epithelium during the stage of endometrial receptivity (Singh and Aplin, 2015). Further, it has been found that presence of cadherin 6 is reduced in endometrial epithelial cells at the time during the window of receptivity in infertile women compared to fertile (Zhou et al., 2020). This study also discovered that knockdown of cadherin 6 in endometrial epithelial cells resulted in lessened ability of embryo-like trophoblast cell spheroids to attach to the epithelial cells. This, taken with the

findings of the proteomic data here, suggests a mechanism for embryo attachment consisting of cadherin 6 regulation by miR-340-5p overexpression in response to rising P4 concentration.

In addition to the systems already discussed which miR-340-5p participates in, this miRNA is involved in the development of osteosarcoma. Specifically, it is naturally downregulated in an epithelial osteosarcoma cell line U2OS; but when it is overexpressed, this results in increased apoptosis and reduced proliferation - suggesting that miR-340-5p acts as a tumor suppressor in this system also (Rongxin et al., 2019). Their study found that miR-340-5p was targeting *STAT3* to downregulate its expression. *STAT3* is also a target of miR-340-5p in this proteomic data where, oppositely to its role in osteosarcoma, it is upregulated in endometrial epithelial cells following overexpression of the miRNA. In mice, knockdown of *STAT3* in the endometrial epithelium results in failed embryo attachment and thus the mice are infertile (Hiraoka et al., 2020). This is particularly fascinating as it suggests that *STAT3* is required for embryo attachment and miR-340-5p may be upregulating the abundance of this protein to facilitate implantation.

As previously mentioned, *NRAS* is a target of miR-340-5p in glioblastoma patients which is part of the MAPK signalling pathway and appears to be controlling cell cycle and proliferation in this system (Fiore et al., 2016). *NRAS* is also more abundant in the endometrial epithelium in this proteomic study in response to miR-340-5p mimic which suggests that *NRAS* via MAPK signalling may be responsible for ensuring correct proliferation of the endometrial epithelium. The increase in miR-340-5p due to rising progesterone concentration may be in order to halt proliferation of the endometrial epithelial cells to allow implantation.

This study into the effect on the proteome of the epithelial endometrium following over- or under-expression of miRNAs which are altered by P4 has demonstrated that many pathways associated with various aspects of implantation are affected. Therefore, further work is required to fully understand the functional roles of these miRNAs and their implications in implantation. Implantation of an embryo into the endometrium is inefficient - is thought that implantation rates for natural conception sit at approximately 20-25% with similar rates of 25% observed in IVF (Simon and Laufer, 2012). It is also estimated that endometrial receptivity is the root cause in two thirds of failed implantation (Achache and Revel, 2006), demonstrating the importance of gaining a full understanding of processes in the endometrium during the window of receptivity. Identifying roles of these P4 regulated

miRNAs in the endometrium will assist in developing this understanding and could potentially lead to targets that can improve implantation efficiency.

This study utilises Ishikawa cells as a model for the epithelial layer of the endometrium, which introduces limitations. Ishikawa cells are not wholly representative of a functioning endometrial epithelium. This is further exacerbated by the fact that Ishikawa cells are a cancer cell line, and as discussed throughout this thesis, many miRNAs are dysregulated in cancer. A further concern with using cell lines in general is that they may undergo genetic drift or contamination following high numbers of passages, reducing the ability of the cells to behave physiologically (Hughes et al., 2007). For this reason, Ishikawa cells used for these experiments were not cultured for long periods of time. Notwithstanding, Ishikawa cells respond appropriately to many types of signalling in the way which primary endometrial epithelial cells do, including functional P4 receptors (Mo et al., 2006). Ishikawa cells are widely used in the reproductive biology field, are very well characterised compared to other endometrial cell lines, and possess functional hormone receptors for E2 and P4 as well as androgens (Mo et al., 2006). Priming of Ishikawa cells with E2 results in increased PR, and this is also decreased in response to P4 - which is physiologically relevant (Lessey et al., 1996). This thesis uses Ishikawa cells to represent an endometrial epithelial monolayer to identify potential pathways and mechanisms by which miR-340-5p is involved in to establish endometrial receptivity and implantation. Alternative cell line Hec-1A and RL95 cells are also E2 and P4 hormone responsive, however are also derived from an adenocarcinoma (Tamm et al., 2009). Endometrial organoids would be an excellent alternative to using cell lines, which are self-forming structures derived from primary endometrial epithelial cells, and these can be produced from healthy tissue or diseased tissues for comparison (Guo et al., 2023). Primary endometrial cells from endometrial biopsies would improve the reliability of this study but were unable to be used in this case due to cost, consumable availability and time. Therefore, comparing results from this work to profiling of endometrial biopsies to confirm that the proteins identified were indeed present in patient samples - of which >94% were - increased confidence in these results.

Currently, it is difficult to fully investigate implantation due to a lack of appropriate models, as mechanisms of implantation are very different between species, meaning animal models of human implantation are not sufficient (Paria et al., 2002). For this reason, accurate, advanced *in vitro* models of human implantation and the human endometrium are required to further advance our knowledge, which are currently lacking.

In conclusion, these data demonstrate that altered expression of miR-340-5p changes the abundance of many proteins. Overexpression results in 1369 proteins changed, inhibition affects 376 proteins, and 72 of these are changed by both. These data are not consistent with target prediction software, highlighting the poor reliability of these tools. A reasonably small number (406) of the 2366 proteins altered by either miR-340-5p mimic and/or inhibitor were detected as P4 regulated in previous work. It is probable that many of the proteins which are absent from RNASeq data are those which are less abundant in response to increased miR-340-5p, or that they are those which are changed in abundance in response to inhibition of miR-340-5p, which is not what happens in response to increased P4. The fact that some RNASeq data is not found in the proteomic data is unsurprising as this is likely due to the way in which miRNAs work, in that miR-340-5p is stopping this RNA being translated into protein.

In conclusion, we propose that this evolutionarily conserved, P4 regulated miRNA - miR-340-5p, along with its protein targets, regulate endometrial epithelial cell proliferation to establish endometrial receptivity. Also, we note that it may play a role in pathways involving *Notch* signalling to control proliferation and adhesion, as well as regulating proteins involved with apoptosis, the cell cycle and endometrial receptivity; and so the function of miR-340-5p could contribute to successful pregnancy. A summary of findings from this Chapter is provided in Table 2.4 and Figure 2.20.

Table 2.4: Summary of key proteins altered by differential expression of miR-340-5p in endometrial epithelial (Ishikawa) cells and their physiologically relevant functions in other system(s).

Protein	Effect on protein abundance following differential expression of miR-340-5p	Role in other system(s)	Reference
Cadherin 6	*Increased* by miR-340-5p overexpression	Localisation to endometrial epithelial apical surface during window of receptivity Reduced in endometrial epithelial cells during the window of receptivity in infertile women compared to fertile women. When knocked down, shows *in vitro* reduced embryo attachment	(Singh and Aplin, 2015) (Zhou et al., 2020)
STAT3 Signal transducer and activator of transcription 3	*Increased* by miR-340-5p overexpression	Tumour suppressor in epithelial osteosarcoma cell line U2OS Knockdown in endometrial epithelium in mice reduces embryo attachment	(Rongxin et al., 2019) (Hiraoka et al., 2020)
PTRH2 Peptidyl-tRNA hydrolase 2	*Decreased* by miR-340-5p overexpression	Bcl-2 regulates proliferation and apoptosis in endometrial cancer. PTRH2 is also known as Bcl-2 inhibitor of transcription 1 and may regulate Bcl-2 and thus influence proliferation and apoptosis	(Xie et al., 2016)

CAAP Caspase activity and apoptosis inhibitor 1	*Decreased* by miR-340-5p overexpression	Caspase-3 regulates proliferation and apoptosis in endometrial cancer. CAAP may regulate Caspase-3 and consequently have an effect on proliferation and apoptosis	(Xie et al., 2016)
PNO1 Partner of NOB1 homolog	*Increased* by miR-340-5p overexpression	PNO1 downregulated by miR-340-5p in lung adenocarcinoma cells resulting in reduction of proliferation and migration	(D. Liu et al., 2020)
Notch2 Notch receptor 2	*Increased* by miR-340-5p overexpression	PNO1 regulates Notch signalling, *Notch2* localises to endometrial epithelium.	(Cuman et al., 2014; D. Liu et al., 2020)
CLDN4 Claudin 4	*Increased* by miR-340-5p overexpression	One of the most highly significantly upregulated biomarkers during window of implantation in the endometrium Elevated during time of implantation in endometrium in humans Elevated in rat uterus in endometrial luminal and glandular epithelial cells at the time of implantation Increased in human endometrial luminal and glandular epithelial cells during mid-luteal phase	(Altmäe et al., 2017) (Riesewijk et al., 2003) (Nicholson et al., 2010) (Carson et al., 2002)

		Assisted reproductive technology outcomes show weaker concentration of CLDN4 yields better pregnancy rate following *in-vitro* fertilisation Decreased CLDN4 linked to endometriosis development	(Serafini et al., 2009) (Gaetje et al., 2008)

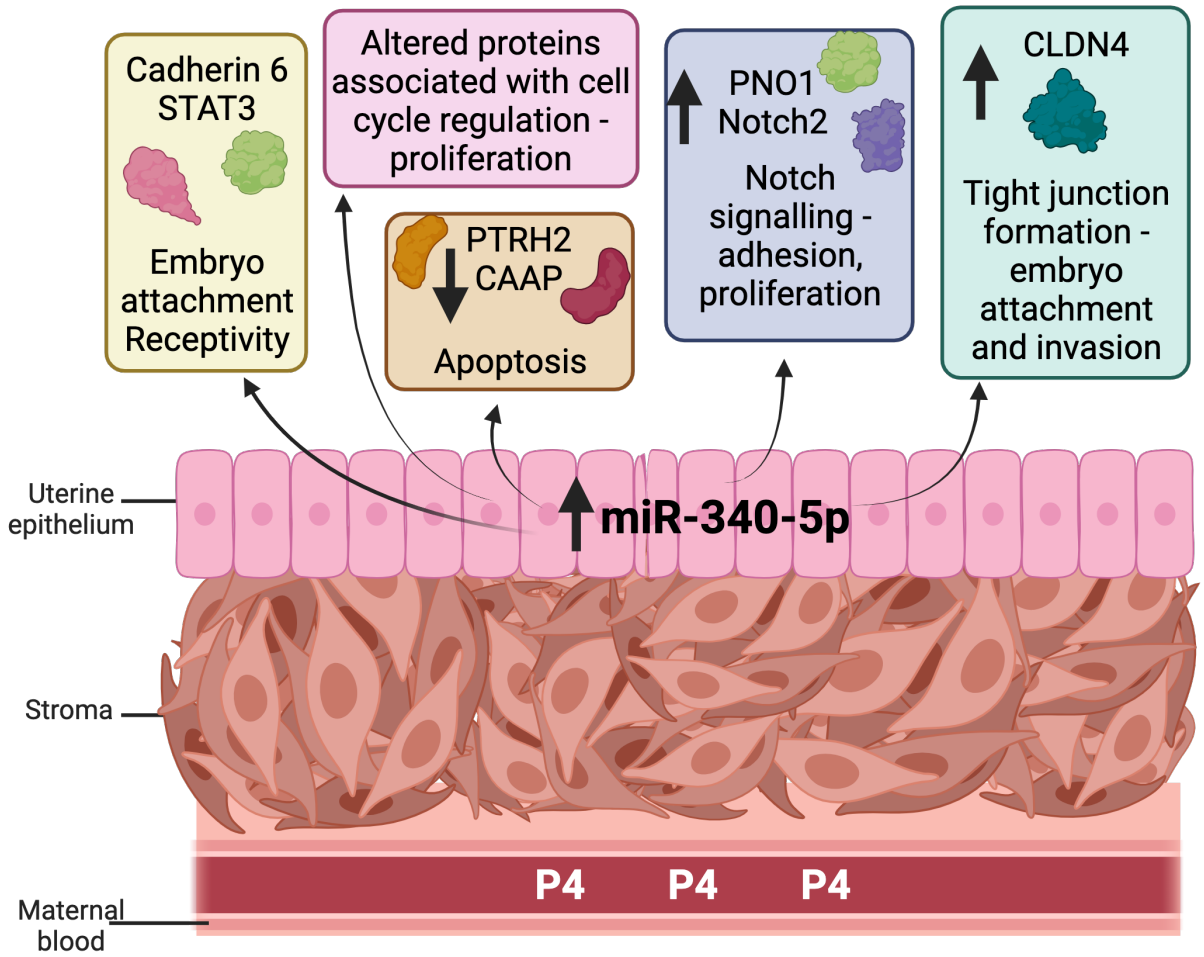

Figure 2.20: *Diagram summarising key proteins and processes altered by miR-340-5p in the endometrial epithelium which may be important for early pregnancy*.
Proteins included in figure are those altered in abundance by differentially expressed miR-340-5p and linked to endometrial function in the literature. Figure created using Biorender.com

Chapter 3 Investigating the Mechanistic Effect of MiR-542-3p in the Endometrium

3.1 Introduction

Establishing endometrial receptivity to implantation is a complex process, orchestrated by a collaboration of hormones and molecules in order to facilitate implantation of an embryo (Lessey and Young, 2019b). A major player in this process is the hormone P4, involvement of which is imperative to establish endometrial receptivity, being responsible for halting epithelial cell proliferation and switching to differentiation as well as endometrial remodelling and stromal cell proliferation (Bhurke et al., 2016) (discussed in detail in Chapter 1, Section 1.5, and further in Chapter 2, Section 2.1.1). As outlined in Chapter 2, Section 2.1.2, miRNAs are important molecules regulating many biological processes by modifying gene expression, and their dysregulation can have consequences resulting in disease phenotypes (Paul et al., 2018). Many miRNAs have reported involvement in endometrial receptivity to implantation, along with aspects of pregnancy and reproductive complications (Shekibi et al., 2022). However, research on their specific mechanisms and roles is deficient, meaning further investigation is required to allow understanding of these processes and identification of novel therapeutic targets.

3.1.1 MiR-542-3p

MiR-542-3p has previously been identified as an evolutionarily conserved miRNA amongst all extant eutherian mammals studied (Taylor et al., 2023), has been shown in previous work from our lab to be significantly overexpressed in response to P4 in an endometrial epithelial cell model (Edge et al., 2023). Twenty of its predicted targets fell under the category 'reproductive function', with 7 being exclusive to miR-542-3p and not present as a predicted target for any other miRNA found to be P4 regulated in this study.

Research into the functional role of miR-542-3p is lacking, its most frequent research focus being its participation in development of different cancers. In epithelial ovarian cancer cell lines, miR-542-3p functions as a tumour suppressor, where its overexpression has an inhibitory effect on proliferation along with invasion and migration via its target cyclin-dependent kinase 14 (CDK14) (J. Li et al., 2019). This may suggest that this mechanism is employed during P4 upregulation of miR-542-3p, functioning to inhibit proliferation of endometrial epithelial cells. In neuroblastoma, miR-542-3p plays a similar tumour suppressor role, where upregulation of it causes downregulation of *KDM1A* (Lysine-specific demethylase 1A) and *ZNF346* (Zinc finger protein 346) when overexpressed (Wei et al., 2020). Reduction of *KDM1A* in turn causes inhibition of proliferation, whereas upregulation of it reverses these effects. This supports the hypothesis that miR-542-3p plays a role in regulating cell

proliferation. A similar function was observed in colon cancer, where expression of miR-542-3p is downregulated (Yang et al., 2017). In this study, using a colon cancer epithelial cell line, it was shown that this downregulation of miR-542-3p inhibits apoptosis and increases viability, along with activation of PI3K/AKT signalling involving survivin, which is an apoptosis inhibitor and mitosis regulator. The opposite effects were demonstrated following overexpression of miR-542-3p (Yang et al., 2017). A study specifically investigating the role of miR-542-3p on cell proliferation found that overexpression caused reduced proliferation capabilities of human epithelial cells of lung carcinoma, cervical adenocarcinoma and breast adenocarcinoma (Yoon et al., 2010). Mechanistically it was shown again here that miR-542-3p targeted and reduced both mRNA and protein expression of survivin. This provides yet further evidence for the proposal that a role of miR-542-3p in human epithelial cells is regulating proliferation.

There are very limited studies concerning miR-542-3p in relation to reproductive biology. MiR-542-3p was identified as one of a set of miRNAs which was upregulated in the endometrial epithelium during the mid-secretory phase of the menstrual cycle (Kuokkanen et al., 2010), which is when the endometrium is receptive, and reinforces the finding of previous work from our lab (Edge et al., 2023). In endometrial stromal cells, miR-542-3p targets *IGFBP1* to inhibit decidualisation (Tochigi et al., 2017). Similarly, Qu et al., 2021 observed downregulation in human endometrial stromal cells, confirming integrin linked kinase (*ILK*) as a target. When overexpressing miR-542-3p, *ILK* is decreased, and expression of two downstream genes were affected: *SMAD2* and *TGF-β1*. This study also explored the effect of overexpression of miR-542-3p in mouse endometrium, resulting in decreased embryo implantation. It was hypothesised that these effects were due to miR-542-3p impairing decidualisation. These results highlight the function of miR-542-3p in the stromal cells and pose the question of whether the miRNA regulates the same genes in the epithelial layer of the endometrium. A summary figure of roles which miR-542-3p reportedly plays in different systems is provided in Figure 3.1.

The functional role of miR-542-3p in the endometrial epithelium is not described in the literature and has not been investigated with respect to endometrial receptivity and implantation. Clearly, further work is required to unravel this.

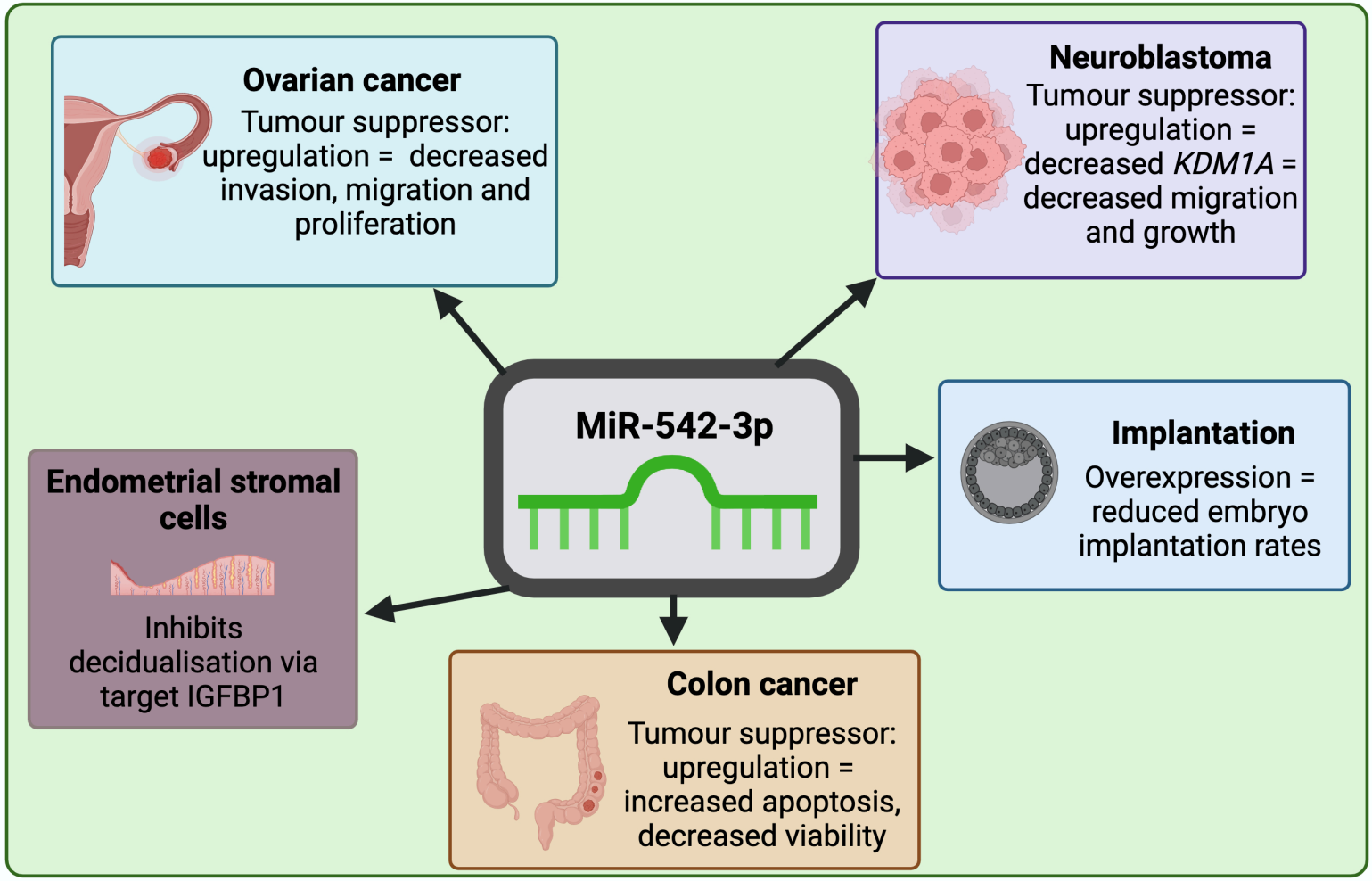

Figure 3.1: *Summary figure illustrating systems in which miR-542-3p is reported in the literature to play a role, and the outcomes in each system.*
Figure created using Biorender.com

3.2 Hypothesis and Aims

3.2.1 Hypothesis

We hypothesise that an evolutionarily conserved microRNA which is altered by progesterone - miR-542-3p - modifies the expression of protein coding regions of human endometrial epithelial cells and may facilitate receptivity to implantation in humans.

3.2.2 Aims

The aim of this chapter is to:

1) Decipher whether there is an alteration in the proteome of the endometrial epithelium following modification of miR-542-3p expression.

2) Deduce mechanistic relevance of progesterone induced upregulation of miR-542-3p, by investigating proteins altered in abundance and pathways they are involved in.

This seeks to discover the role that miR-542-3p plays in the endometrium, explaining its implications for implantation and endometrial receptivity.

3.3 Materials and Methods

3.3.1 Cell Culture

All cell culture processes were performed in a sterile tissue culture hood, using sterile filtered pipette tips and 70% ethanol. Size 75cm^2 and 25cm^2 cell culture treated flasks were used to grow the cultures. Light microscopy was used to assess confluency and quality.

3.3.1.1 Ishikawa (immortalized endometrial epithelial) cells

Ishikawa cells (ECACC # 99040201) which are an immortalized endometrial epithelial cell line were used as a hormonally responsive model of the epithelial layer of the human endometrium. As described in Chapter 2, Section 2.3.1.1, Ishikawa cells were maintained in culture and passaged at >70% confluency. Cells were grown in 1:1 Dulbecco's Modified Eagle Medium (DMEM) and Hams' F12 was supplemented with 10% FBS and glutamine, streptomycin and penicillin (GSP).

These cells were maintained and passaged according to the more detailed protocol in Chapter 2, Section 2.3.1.1.

3.3.2 MicroRNA Mimic and Inhibitor Transfection

The protocol for miRNA mimic and inhibitor transfection is provided in more detail in Chapter 2, Section 2.3.2. Briefly, with alterations for this chapter:

Optimisations were first carried out to determine the ideal transfection reagent volume to maximise transfection efficiency whilst minimising negative effects on cells (Chapter 2, Section 2.3.2.1). A volume of 1μl per well for a 24 well plate was selected, which was scaled up and down dependent on well size required for experiment.

Mimics and inhibitors (Horizon Discovery) for miR-542-3p were used and an identical protocol performed to Chapter 2, Section 2.3.2.2. The treatments for this chapter, which were added to 6 well plates containing 200,000 cells/well in 1.6ml of antibiotic and serum free media (n=3), for 48 hrs were as follows:

7. Control: 400μl opti-MEM media
8. Transfection reagent control: 400μl opti-MEM media + 4μl Lipofectamine 2000
9. Non-targeting mimic control: 400μl opti-MEM media + 4μl Lipofectamine 2000 + 80pmol non-targeting mimic
10. Non-targeting inhibitor control: 400μl opti-MEM media + 4μl Lipofectamine 2000 + 80pmol non-targeting inhibitor
11. MiR-542-3p mimic: 400μl opti-MEM media + 4μl Lipofectamine 2000 + 80pmol miR-542-3p mimic

12. MiR-542-3p inhibitor: 400μl opti-MEM media + 4μl Lipofectamine 2000 + 80pmol miR-542-3p inhibitor

Cells were harvested as described in Chapter 2, Section 2.3.2.3, using trypsin/EDTA 0.025%.

3.3 RNA Analysis

RNA was extracted using the MiRNeasy Mini Kit (Qiagen) according to manufacturer's instructions. No deviations from the method described in Chapter 2, Section 2.3.3.1 for this stage. RNA concentration was quantified using the Nanodrop N1000 spectrophotometer (Thermo Fisher Scientific, USA) as explained in Chapter 2, Section 2.3.3.2. RNA was reverse transcribed to cDNA for microRNA analysis using the miRCURY LNA RT Kit (Qiagen) according to manufacturer's instructions and detailed in Chapter 2, Section 2.3.3.3. A qRT-PCR was performed to confirm over and under expression of miR-542-3p in comparison to non-targeting controls prior to continuing to proteomic analysis. Primers for miR-542-3p were obtained from Qiagen and PCR carried out using miRCURY SYBR Green Kit (Qiagen). ΔCt values were normalised by subtracting the global mean of 5S normaliser from each value. The transformation $2^{-\Delta Ct}$ was calculated for each value to show normalised absolute expression of miRNA. (Full details are available in Chapter 2, Section 2.3.3.4).

3.4 Proteomic Analysis

Protein was extracted using a RIPA buffer as described in Chapter 2, Section 2.3.4.1, and quantitative proteomic analysis was carried out at Bristol Proteomics Facility. Stages of proteomic analysis carried out by Bristol Proteomic Facility are explained in Chapter 2, Section 2.3.4.2 but consist of:

1. Tandem Mass Tag Labelling and High pH reversed-phase chromatography.
2. Nano-LC Mass Spectrometry
3. Proteomic Statistical Analysis
4. Production of PCA and Volcano plots

3.4.1 Data Analysis

Data was then filtered to remove proteins which appeared in the contaminant database. For each comparison, *e.g.*, non-targeting mimic vs miR-542-3p mimic, all proteins whose t-test value was statistically significant ($p<0.05$) were used. Protein lists then underwent Venn diagram analysis by gene name to remove those which were changed in abundance in response to the non-targeting control. This was carried out by creating a Venn diagram comparing the list of proteins significantly changed in response to the non-targeting mimic vs control, to the list of proteins significantly changed after treatment with miR-542-3p mimic. Those which overlapped in the centre of the diagram were excluded due to altered abundance by the non-targeting mimic and so were likely to be due to off-target effects. Any proteins which were missing a gene name were included using their accession number instead. Some lists had multiple proteins with the same gene name due to there being different fragments or forms of the same protein altered in abundance. Identical steps were carried out for miR-542-3p inhibitor vs non-targeting inhibitor (as described in Chapter 2, Section 2.3.3.5). Proteins identified by this analysis which were discussed further were selected through their involvement in related pathways in the literature. Proteins were also compared to RNASeq data from 36 human endometrial biopsies collected 4-12 days following a positive home ovulation test. Women aged 31-36 were recruited with between 0-9 previous losses, and went on to have either live birth, ongoing pregnancy or miscarriage outcomes (Lipecki et al., 2022).

3.4 Results

3.4.1 qPCR Results

MiR-542-3p was significantly (p<000.1) overexpressed following treatment with miR-542-3p mimic compared to control, lipofectamine only control, non-targeting mimic and miR-542-3p inhibitor (Figure 3.2).

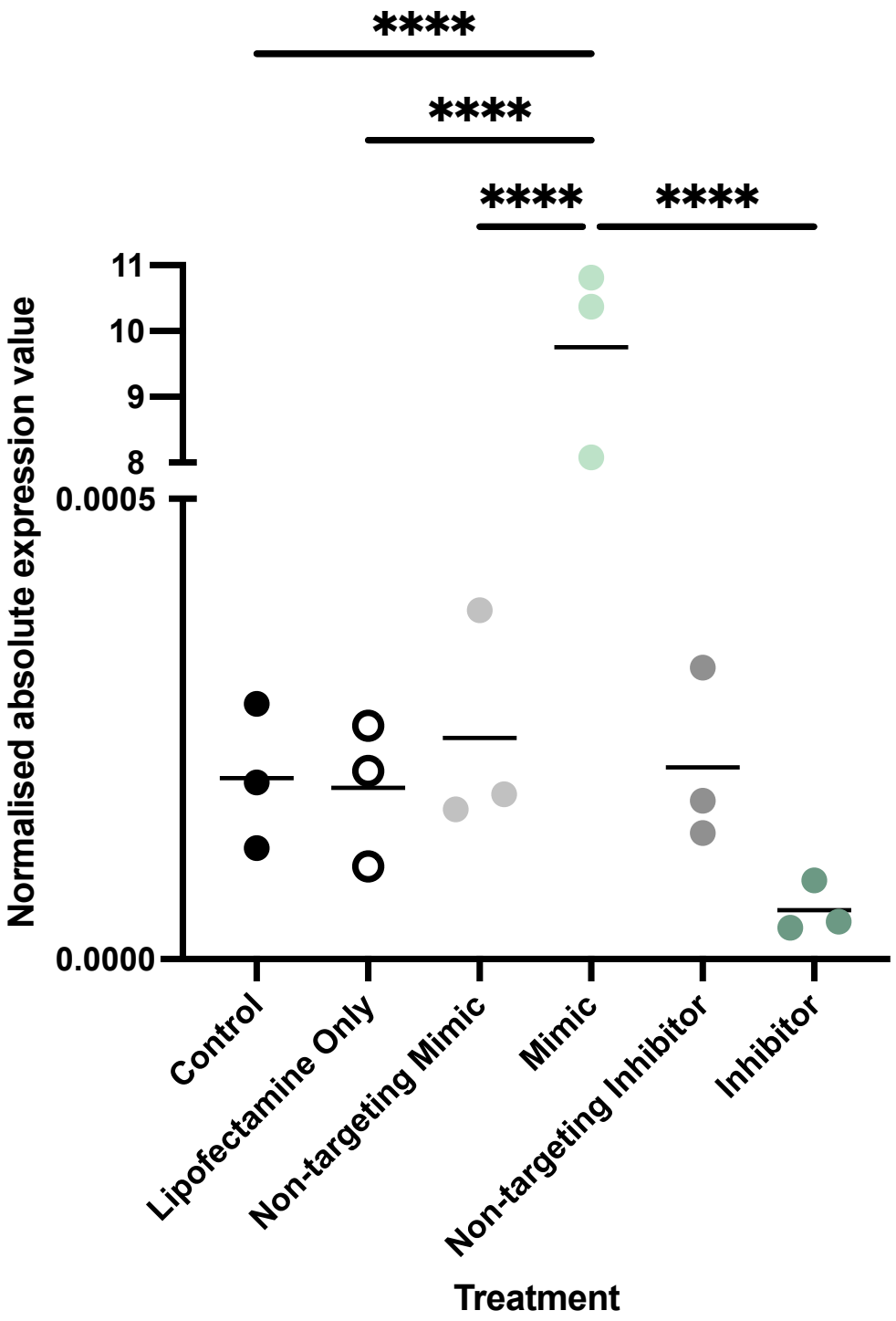

Figure 3.2: *Absolute expression values of miR-542-3p normalised to 5s following endometrial epithelial cell transfection (Ishikawa cell line, 48hr, n=3 biological replicates) with miR-542-3p mimic and inhibitor.*
Treatments were all added to 1.6ml antibiotic and serum free media and consisted of i) Control - 400ml optiMEM media only, ii) Lipofectamine only control - 4ml lipofectamine in 400ml optiMEM media, iii-vi) 80pmol of non-targeting mimic, miR-542-3p mimic, non-targeting inhibitor or miR-542-3p inhibitor in 400ml optiMEM media. Statistical significance following a one way ANOVA and multiple comparisons test is denoted by **** $p<0.0001$.

3.4.2 Proteomics Results

3.4.2.1 PCA Plot

A PCA (principal component analysis) plot for PC1 and PC2 of the data (Figure 3.3) demonstrates evident clustering of miR-542-3p treatment for all biological repeats in the lower right-hand corner of the graph, with its non-targeting control clustering further up the y axis. This illustrates the source of variation in the data. MiR-542-3p inhibitor is scattered further to the right of the plot than its corresponding non-targeting inhibitor control, and the other control and lipofectamine only control fall further to the left of the graph. The PCA plot of PC3 and PC4 (Figure 3.4) to infer any further sources of variation whilst displaying less of the variance (12.3% and 8.4% as opposed to 24.8% and 18.8% for PC1 and PC2) still shows an obvious clustering of miR-542-3p in the lower right-hand corner. The non-targeting mimic is plotted in the upper left of the graph, as far apart from the targeting mimic. MiR-542-3p inhibitor samples also cluster reasonably centrally, just to the northeast of the middle of the graph.

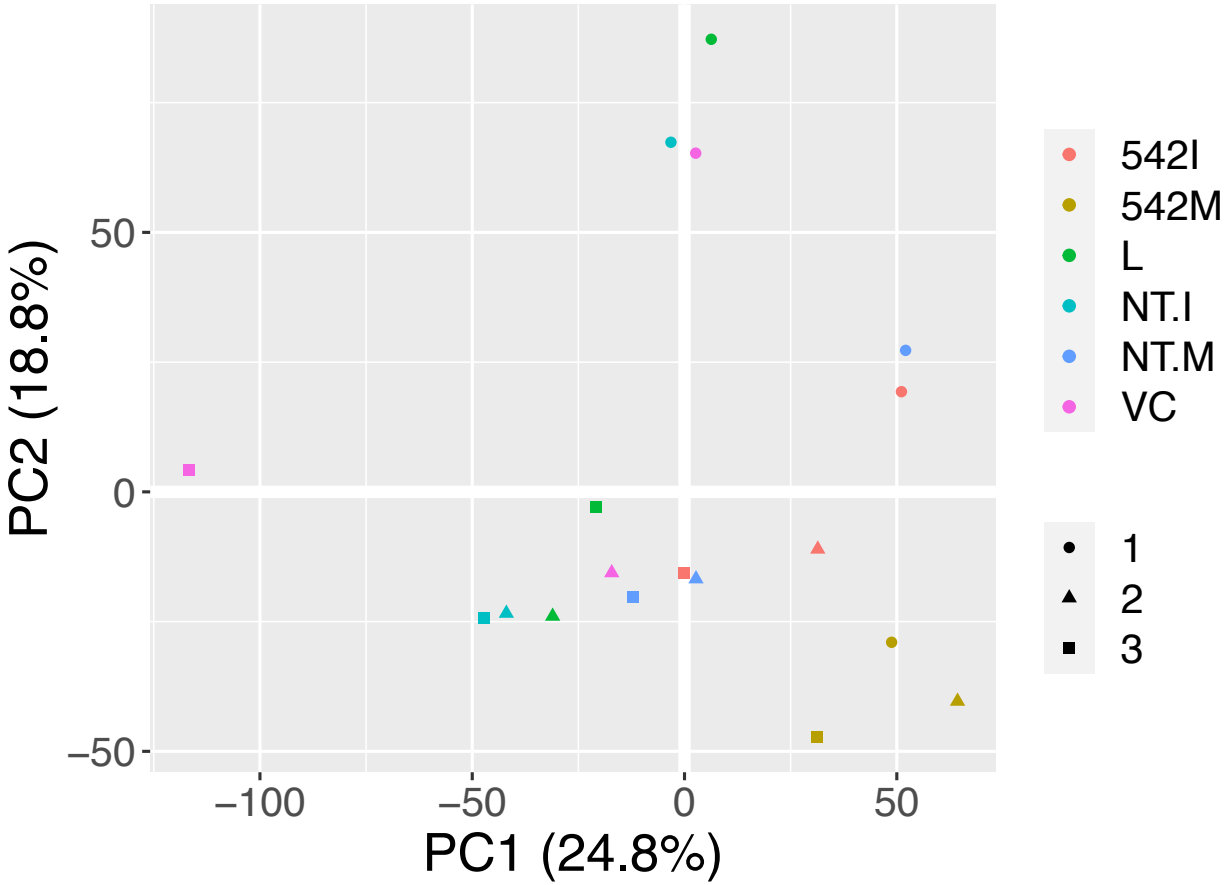

Figure 3.3: *PCA plot (PC1 and PC2) for miR-542-3p overexpression or under expression in Ishikawa cells.*
PCA (principal component analysis) plot of PC1 and PC2 for Ishikawa cells (n=3 - biological repeats shown by circle, triangle and square) transfected for 48 hrs with miR-542-3p mimic (542M), miR-542-3p inhibitor (542I), non-targeting mimic control (NT.M), non-targeting inhibitor control (NT.I), lipofectamine transfection reagent only (L) or media control (VC). Produced by Bristol Proteomics Facility.

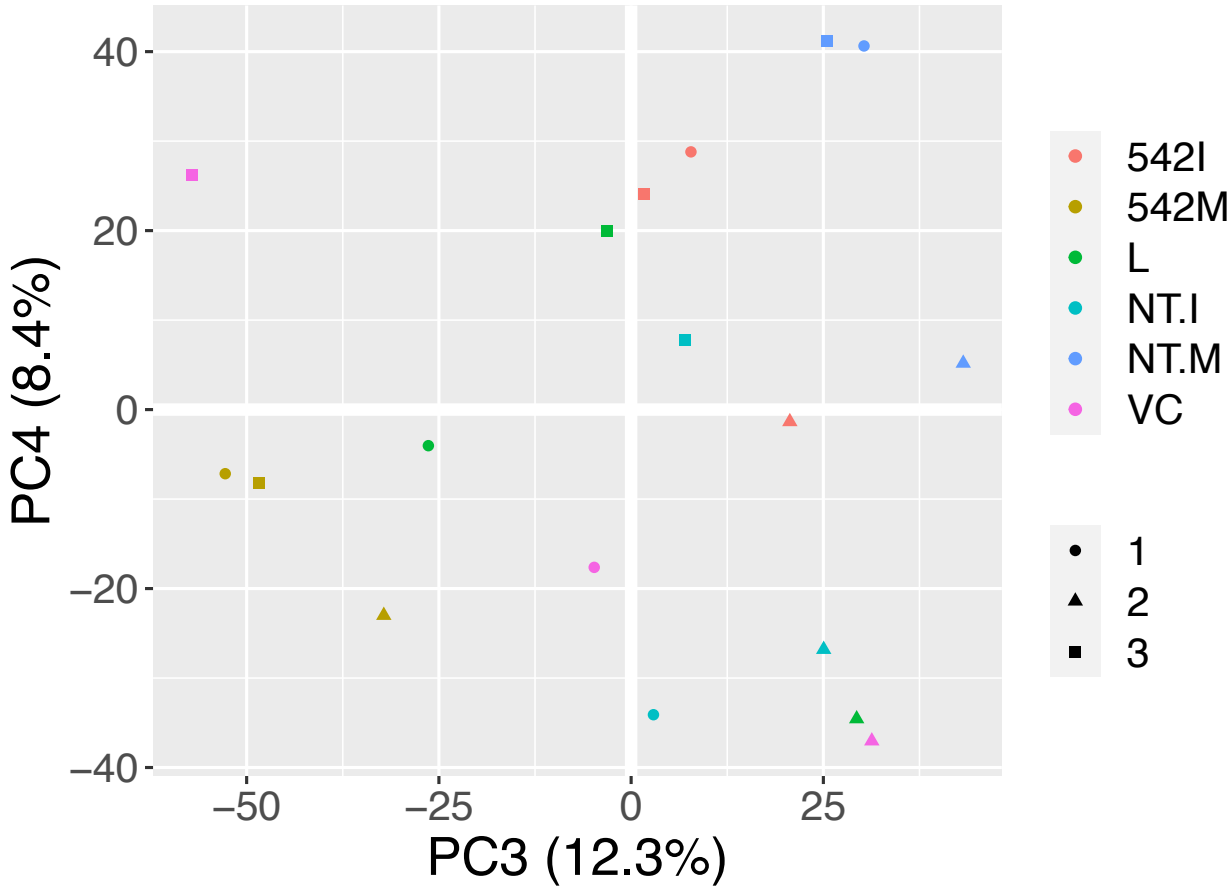

Figure 3.4: *PCA plot (PC3 and PC4) for miR-542-3p overexpression or under expression in Ishikawa cells.*
PCA (principal component analysis) plot of PC3 and PC4 for Ishikawa cells (n=3 - biological repeats shown by circle, triangle and square) transfected for 48 hrs with miR-542-3p mimic (542M), miR-542-3p inhibitor (542I), non-targeting mimic control (NT.M), non-targeting inhibitor control (NT.I), lipofectamine transfection reagent only (L) or media control (VC). Produced by Bristol Proteomics Facility.

3.4.2.2 Protein abundance following overexpression of miR-542-3p

Non-targeting controls were used to remove off target effects, meaning the resulting protein lists consisted only of those proteins altered in abundance specifically in response to the miR-542-3p over or under expression, not just the presence of a miRNA. A schematic of this process is shown in Figure 3.5. There were 1674 proteins changed by treatment with miR-542-3p mimic. Of these, 296 were also changed in the non-targeting control and so were removed, leaving a total of 1378 proteins changed specifically in response to miR-542-3p over expression (Figure 3.6A). This list was then separated into proteins which were more abundant - 661 proteins, or less abundant - 724 proteins in comparison to the non-targeting mimic control (Figure 3.7). Downstream analysis by Webgestalt revealed that proteins changed in either direction by over expression of miR-542-3p were significantly ($p<0.05$) enriched in biological processes including ribonucleoprotein complex biogenesis (89 proteins), intracellular transport (216 proteins), and cellular protein localisation (229), as well as in the cell cycle (217 proteins) (Figure 3.6B). They were most commonly located in the nucleus (690 proteins) and the largest number of proteins were involved in metabolic processes (936 proteins) (Figure 3.6C).

Downstream analysis after separation of proteins which were more abundant following treatment with miR-542-3p mimic revealed that these proteins were significantly ($p<0.05$) enriched in multiple different biological processes involving targeting or localisation of proteins to the endoplasmic reticulum. These proteins were also located in multiple parts of the ribosome (Figure 3.8A-B). Those proteins which were less abundant in response to miR-542-3p over expression are significantly ($p<0.05$) enriched in the previously mentioned biological processes of ribonucleoprotein complex biogenesis (53 proteins) and metabolism (DNA metabolic process - 89 proteins, and ncRNA metabolic process - 61 proteins) - highlighting the importance of this further categorising of the altered proteins. They were also enriched in the chromosome (89 proteins) (Figure 3.8C).

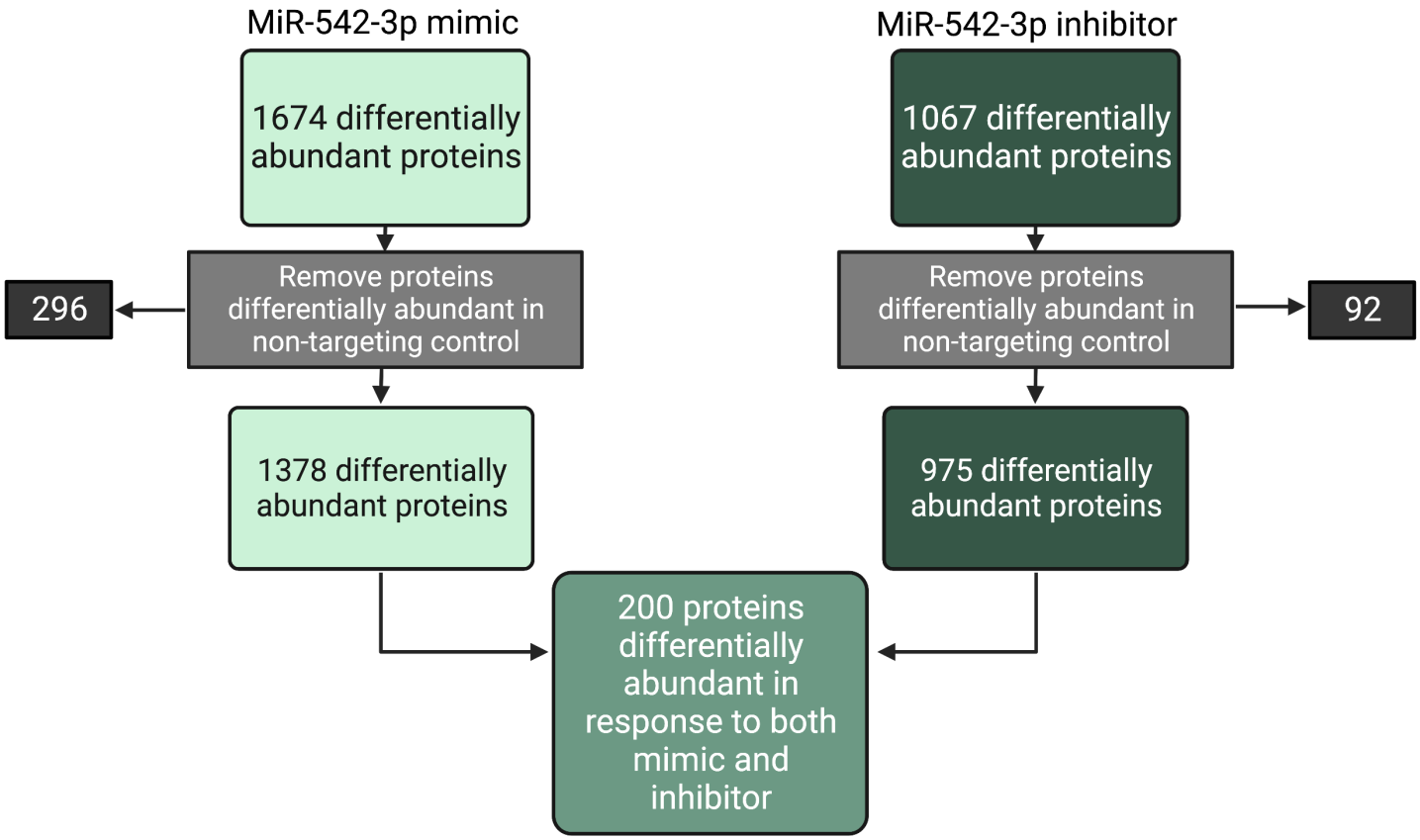

Figure 3.5: *Schematic diagram to summarise workflow for establishing lists of differentially abundant proteins for miR-542-3p mimic or inhibitor and those which are common to both.*
Lists of proteins differentially abundant in response to the mimic (1673) or inhibitor (1067) were collated followed by removal of those which were also differentially abundant in response to the corresponding non-targeting control, leaving only proteins which are changed specifically in response to miR-542-3p mimic (1378) or miR-542-3p inhibitor (975). These lists were compared to deduce a list of proteins changed in response to both over and under expression of miR-542-3p (72).

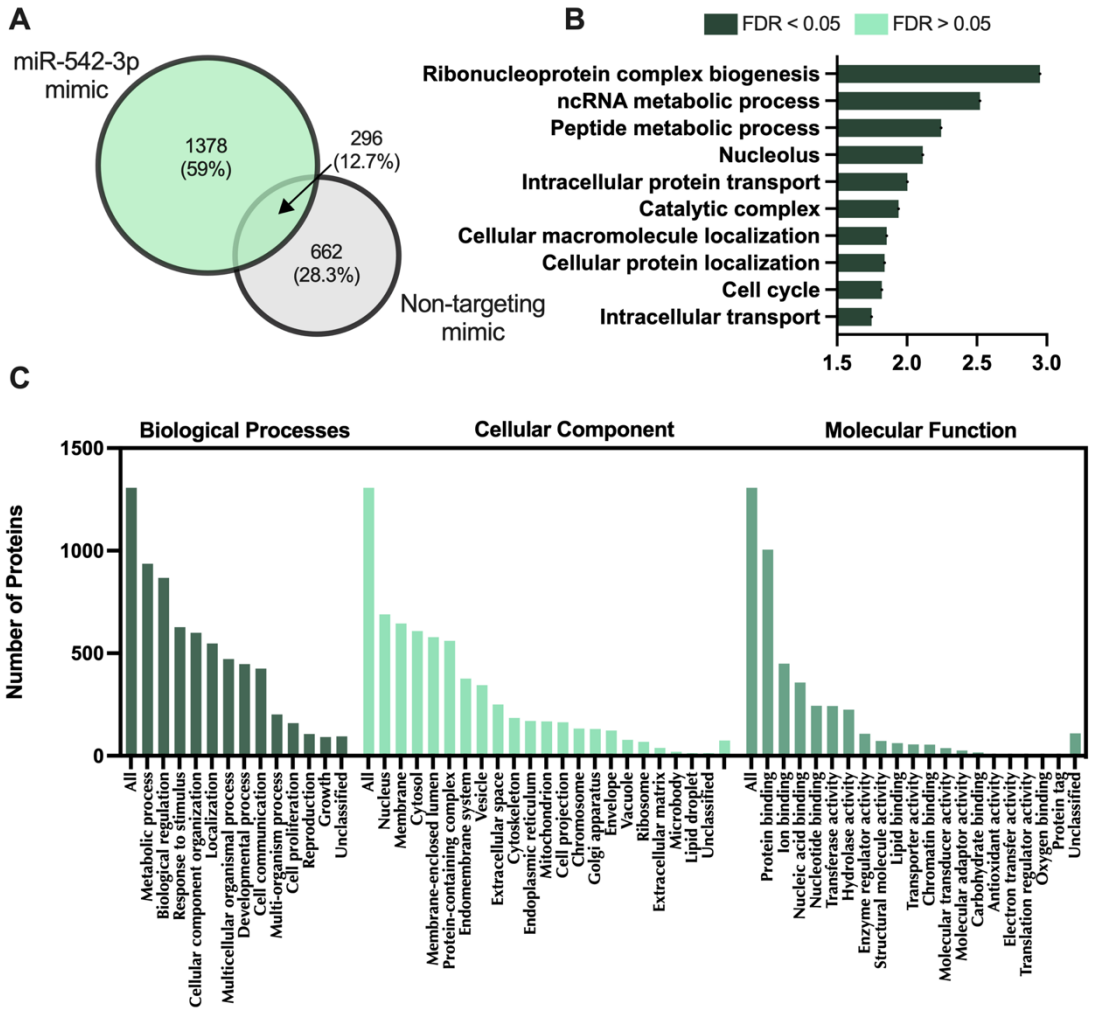

Figure 3.6: *Proteins altered in endometrial epithelial cells (Ishikawa) following treatment with miR-542-3p mimic.*
A) Venn diagram depicting total number of significantly differentially expressed proteins ($p<0.05$) following transfection of Ishikawa cells (n=3 biological replicates, 48 hrs) with miR-542-3p mimic (LHS) and non-targeting mimic (RHS). **B**) Enriched KEGG pathways associated with miR-542-3p mimic regulated proteins (FDR<0.05) **C**) WebGestalt overrepresentation analysis of biological process, cellular component, and molecular function categories for identified significantly differentially expressed proteins in response to miR-542-3p mimic (total of 1369). (Supplementary Table 10).

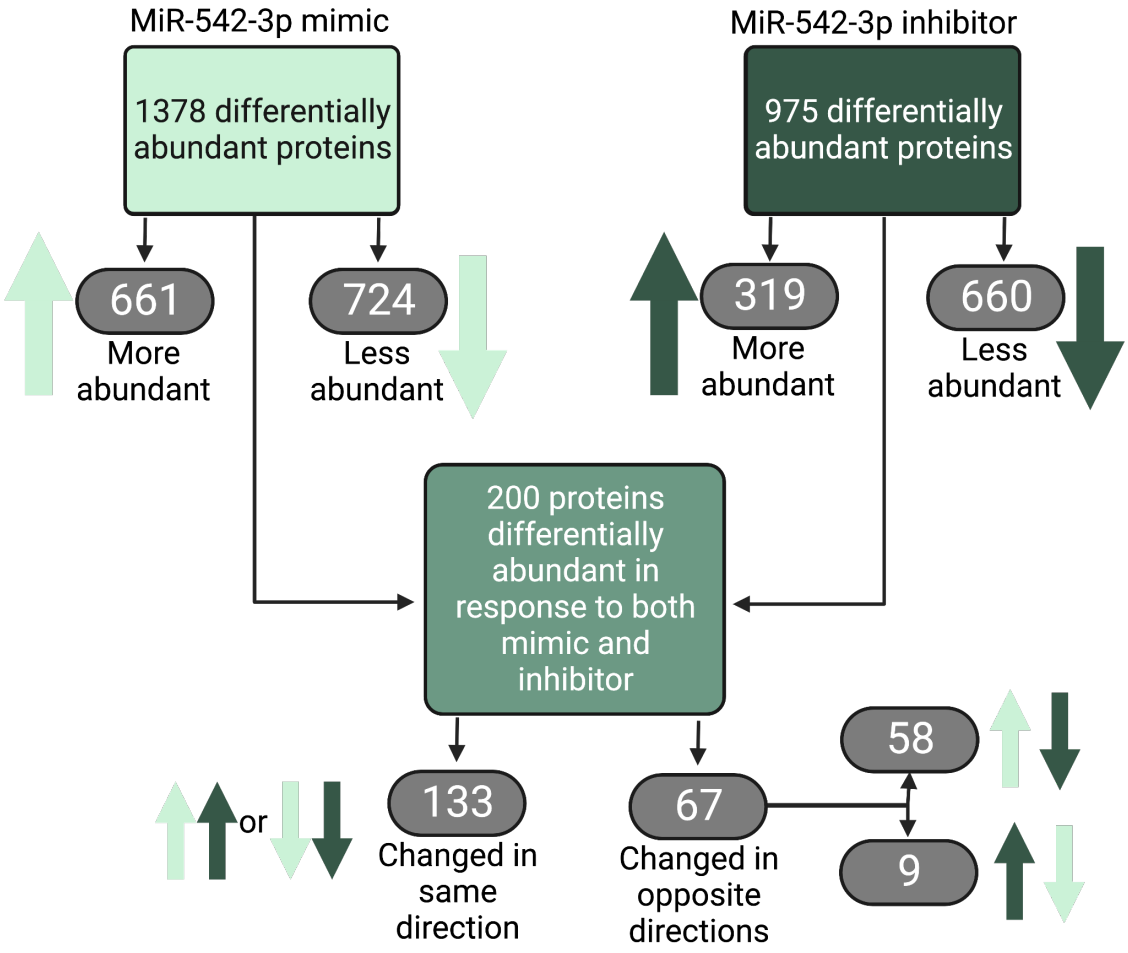

Figure 3.7: *Schematic diagram to demonstrate break down of numbers of proteins more or less abundant in response to altered expression of miR-542-3p.*
Diagram shows the number of proteins altered in abundance to be more or less abundant than the non-targeting mimic in response to miR-542-3p mimic or inhibitor. Also shows whether proteins that were changed in abundance in response to both miR-542-3p mimic or miR-542-3p inhibitor were changed in the same way (*i.e.*, both treatments result in more or less abundant) or opposite ways (*e.g.*, one treatment results in more abundant and one in less). Counts of proteins more or less abundant include duplicate gene names with different accession numbers.

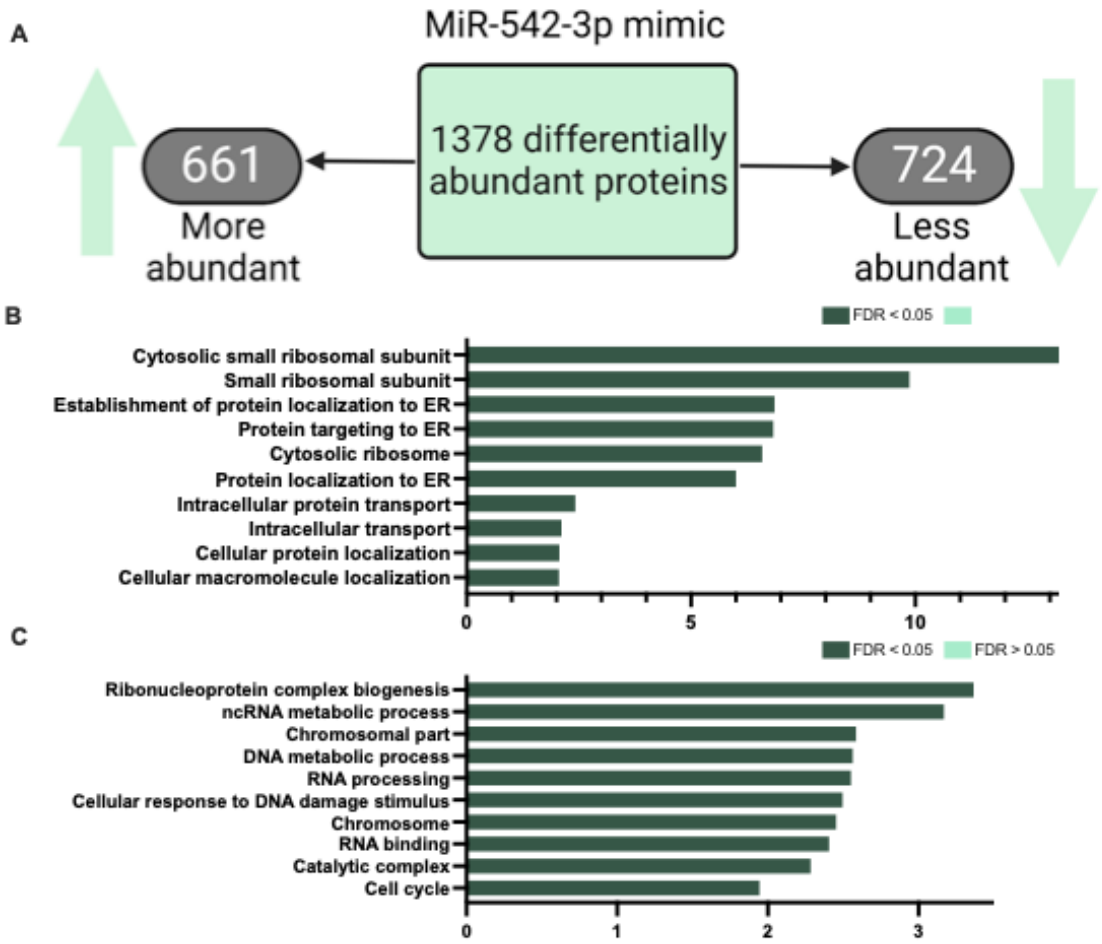

Figure 3.8: *Break down of numbers of proteins altered in abundance following 48 hr treatment of endometrial epithelial cells (n=3) with miR-542-3p mimic with regards to whether proteins were more or less abundant compared to non-targeting mimic control.*
Includes duplicate gene names with different accession numbers. **A**) Distribution of 1378 proteins altered in response to miR-542-3p mimic into categories of 'more abundant' or 'less abundant'. **B**) Enriched KEGG pathways associated with proteins which are more abundant in response to miR-542-3p mimic (FDR<0.05). **C**) Enriched KEGG pathways associated with proteins which are less abundant in response to miR-542-3p mimic (FDR<0.05). (Supplementary Table 11).

3.4.2.3 Protein abundance following inhibition of miR-542-3p

Inhibition of miR-542-3p in endometrial epithelial cells resulted in 1047 proteins significantly ($p<0.05$) altered in abundance. Ninety-two of these proteins were also changed in response to the non-targeting inhibitor and so were removed, leaving a list of 975 proteins deemed to be altered specifically in response to the inhibition of miR-542-3p (Figure 3.9A). These proteins were significantly ($p<0.05$) enriched in biological processes including RNA splicing (74 proteins) and processing (120 proteins) and mitotic cell cycle (106 proteins) (Figure 3.9B-C).

Further analysis was carried out by splitting of proteins into lists of those which are more abundant (319) following inhibition of miR-542-3p and those which were less abundant (660) (Figure 3.7 and Figure 3.10A). The proteins which were more abundant by treatment with miR-542-3p inhibitor are significantly ($p<0.05$) the previously mentioned proteins which are enriched in multiple biological processes concerning RNA and mRNA processing and splicing (Figure 3.10B). As well as this, these proteins are enriched in the ribonucleoprotein complex cellular component (65 proteins), which interestingly is associated with proteins which are downregulated by miR-542-3p mimic, demonstrating the opposite function of over and under expression of miR-542-3p. Proteins less abundant following inhibition of miR-542-3p are significantly ($p<0.05$) enriched in biological processes including cadherin binding (43 proteins) and cellular adhesion molecule binding (50 proteins) (Figure 3.10C).

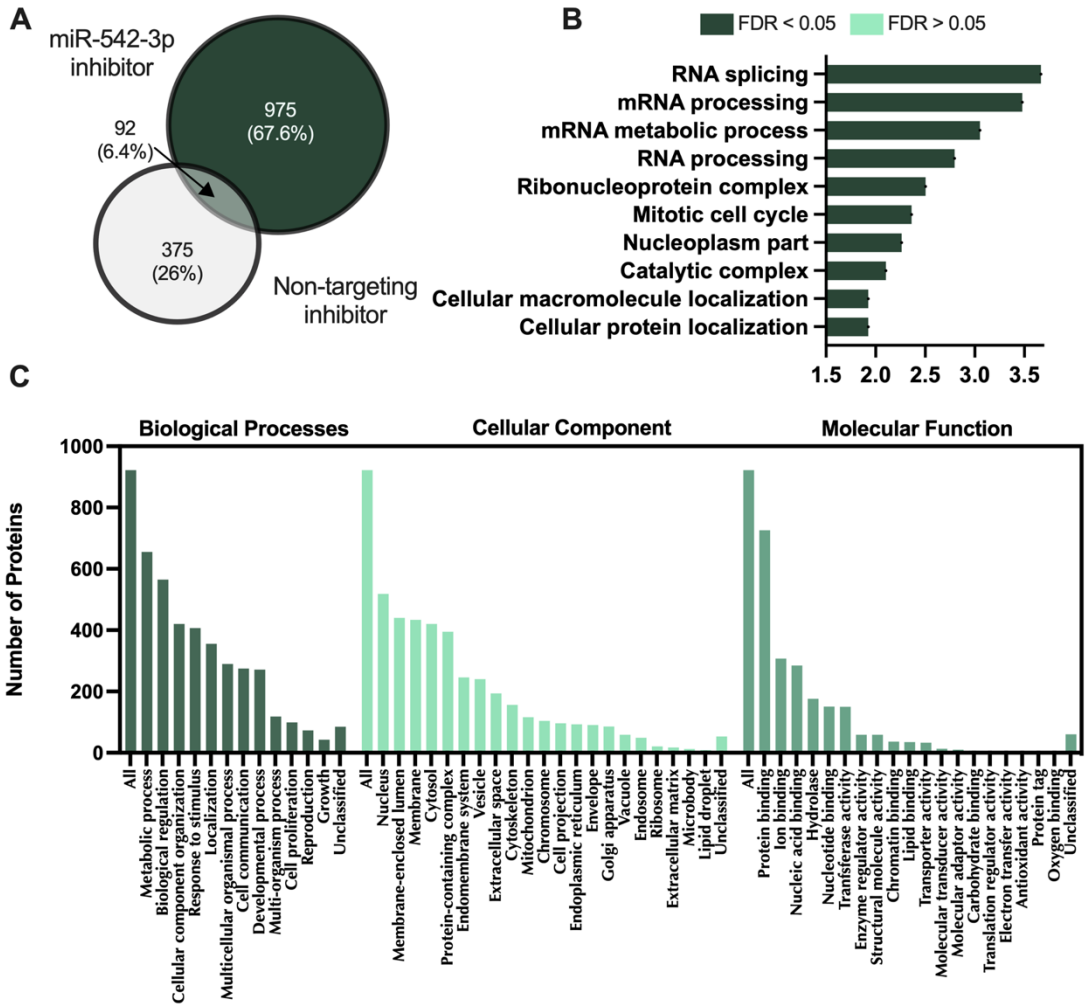

Figure 3.9: *Proteins altered in endometrial epithelial cells (Ishikawa) following treatment with miR-542-3p inhibitor.*
A) Venn diagram demonstrating total number of significantly altered proteins ($p<0.05$) following transfection of ishikawa cells (n=3 biological replicates, 48 hrs) with miR-542-3p inhibitor (RHS) and non-targeting inhibitor (LHS). **B**) Enriched KEGG pathways associated with miR-542-3p inhibition regulated proteins (FDR<0.05). **C**) WebGestalt overrepresentation analysis of biological process, cellular component, and molecular function categories for identified significantly differentially expressed proteins in response to miR-542-3p inhibitor (total of 975). (Supplementary Table 12).

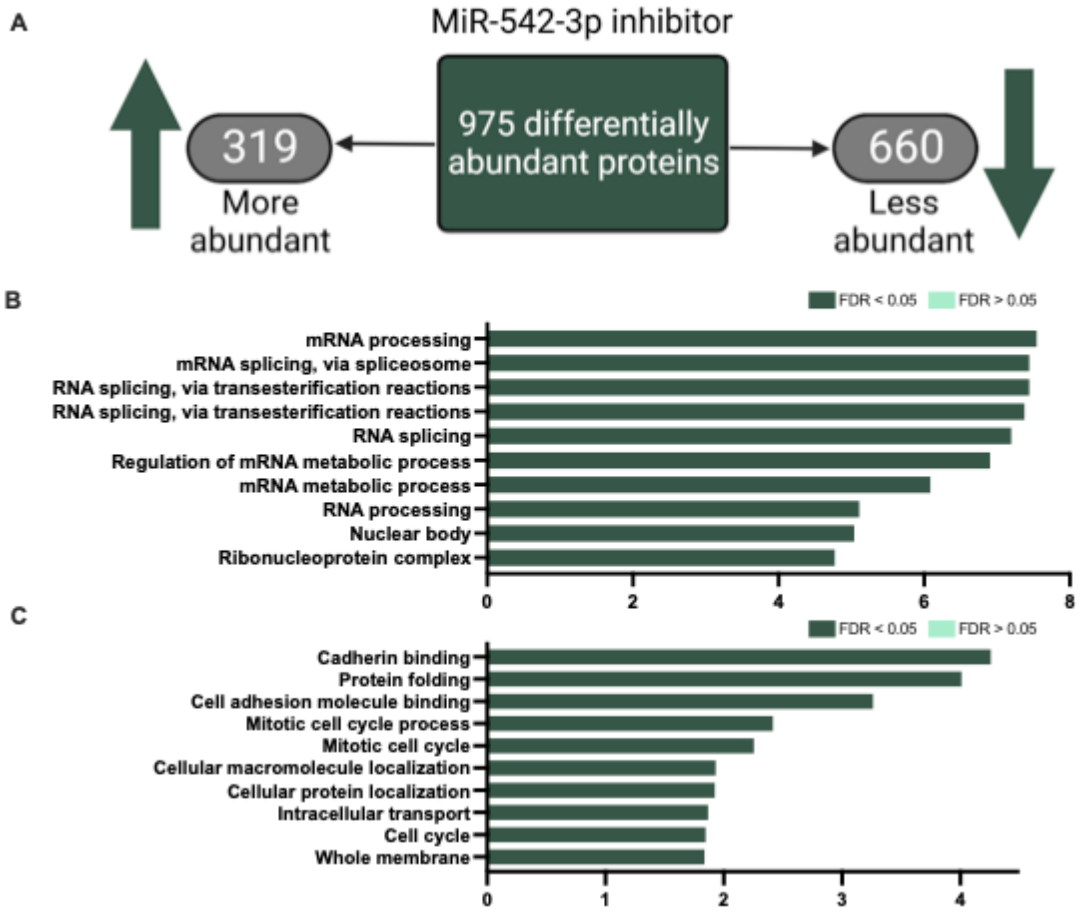

Figure 3.10: *Break down of numbers of proteins altered in abundance following 48 hr treatment of endometrial epithelial cells (n=3) with miR-542-3p inhibitor with regards to whether proteins were more or less abundant compared to non-targeting inhibitor control.*
Includes duplicate gene names with different accession numbers. **A**) Distribution of 975 proteins altered in response to miR-542-3p inhibitor into categories of 'more abundant' or 'less abundant'. **B**) Enriched KEGG pathways associated with proteins which are more abundant in response to miR-542-3p inhibitor (FDR<0.05). **C**) Enriched KEGG pathways associated with proteins which are less abundant in response to miR-542-3p inhibitor (FDR<0.05). (Supplementary Table 13).

3.4.2.4 Proteins altered in abundance in response to over and under expression of miR-542-3p

Proteins altered in response to miR-542-3p mimic were compared to those changed by miR-542-3p inhibitor to obtain a group of proteins which were altered in response to both (Figure 3.11A). Biological processes significantly ($p<0.05$) enriched for the 200 proteins changed by both treatments include golgi and organelle inheritance (4 proteins), cadherin binding (14 proteins) and protein folding (11 proteins) (Figure 3.11B-C).

More in depth analysis was carried out by dividing these 200 proteins into those which are changed in the *same* direction *e.g.,* more abundant in response to both mimic and inhibitor - 67 proteins - or in opposite directions: more abundant in response to mimic and less abundant in response to inhibitor - 58 proteins- or less abundant after overexpression and more abundant following inhibition - 9 proteins (Figure 3.7). The 67 proteins changed in the same direction are significantly ($p<0.05$) enriched in biological processes concerning cellular protein and macromolecule localisation (28 proteins) as well as heat shock protein binding (7 proteins) (Figure 3.12A). Cadherin binding is an interesting molecular function 10 of these proteins are involved in, but is not statistically significant (FDR>0.05).

Proteins (58) more abundant by treatment with miR-542-3p mimic and less abundant by inhibition of miR-542-3p are not significantly enriched ($p>0.05$) in any biological processes however show overrepresentation in positive regulation of anoikis (2 proteins) and regulation of protein stability (6 proteins) (Figure 3.12B). The 9 proteins for which the opposite is true (overexpression of miR-542-3p causes lessened abundance and inhibition causes increased abundance) also have no significant enrichment in biological processes, likely due to small sample size, but are overrepresented in chromosome organisation (4 proteins), chromatid segregation (2 proteins) and chromatid cohesion (2 proteins) (Figure 3.12C).

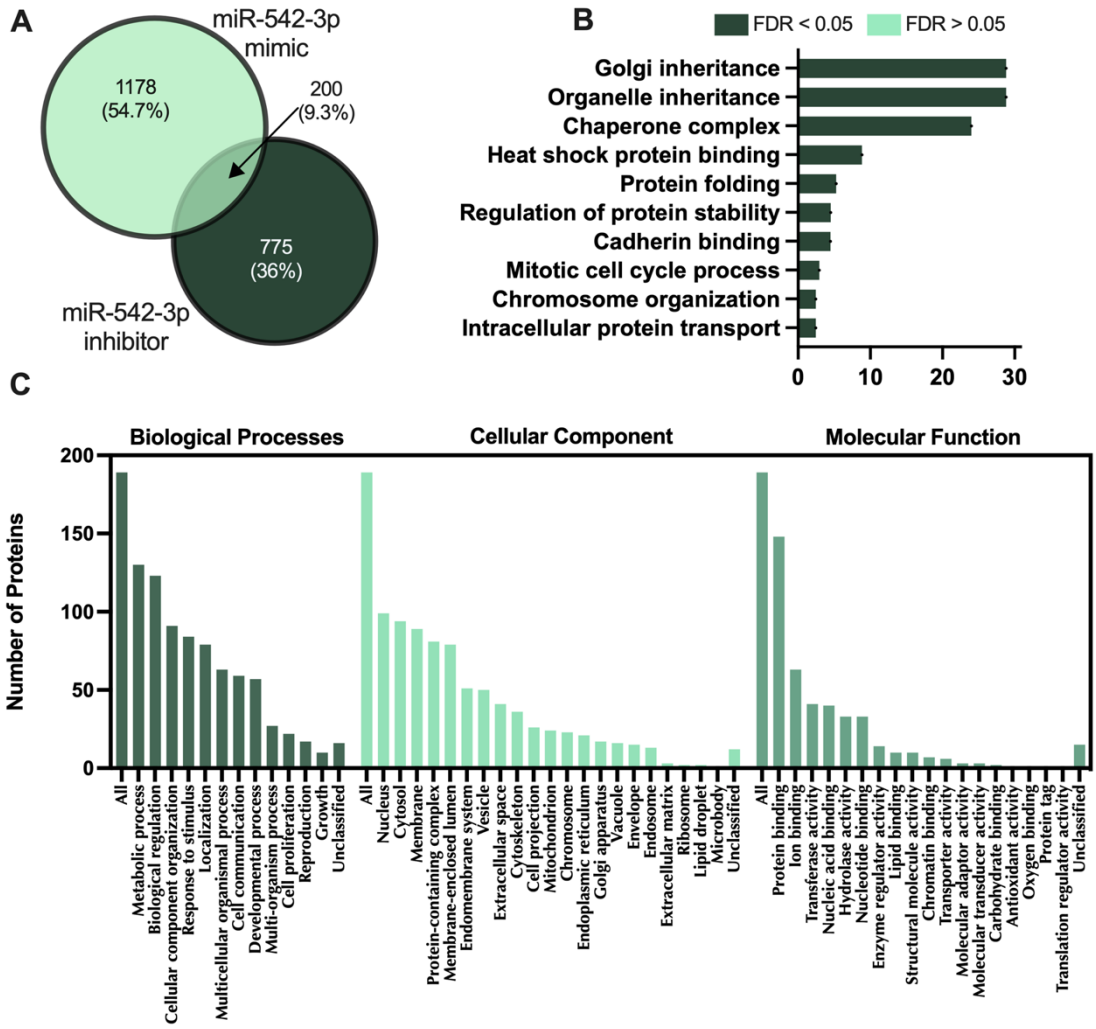

Figure 3.11: *Proteins altered in endometrial epithelial cells (Ishikawa) following treatment with miR-542-3p mimic or inhibitor.*
A) Venn diagram demonstrating total number of significantly altered proteins ($p<0.05$) following transfection of ishikawa cells (n=3 biological replicates, 48 hrs) with either miR-542-3p mimic (LHS) or inhibitor (RHS). **B**) Enriched KEGG pathways associated with miR-542-3p mimic and inhibition regulated proteins (FDR<0.05). **C**) WebGestalt overrepresentation analysis of biological process, cellular component, and molecular function categories for identified significantly differentially expressed proteins in response to miR-542-3p mimic and inhibitor (total of 200). (Supplementary Table 14).

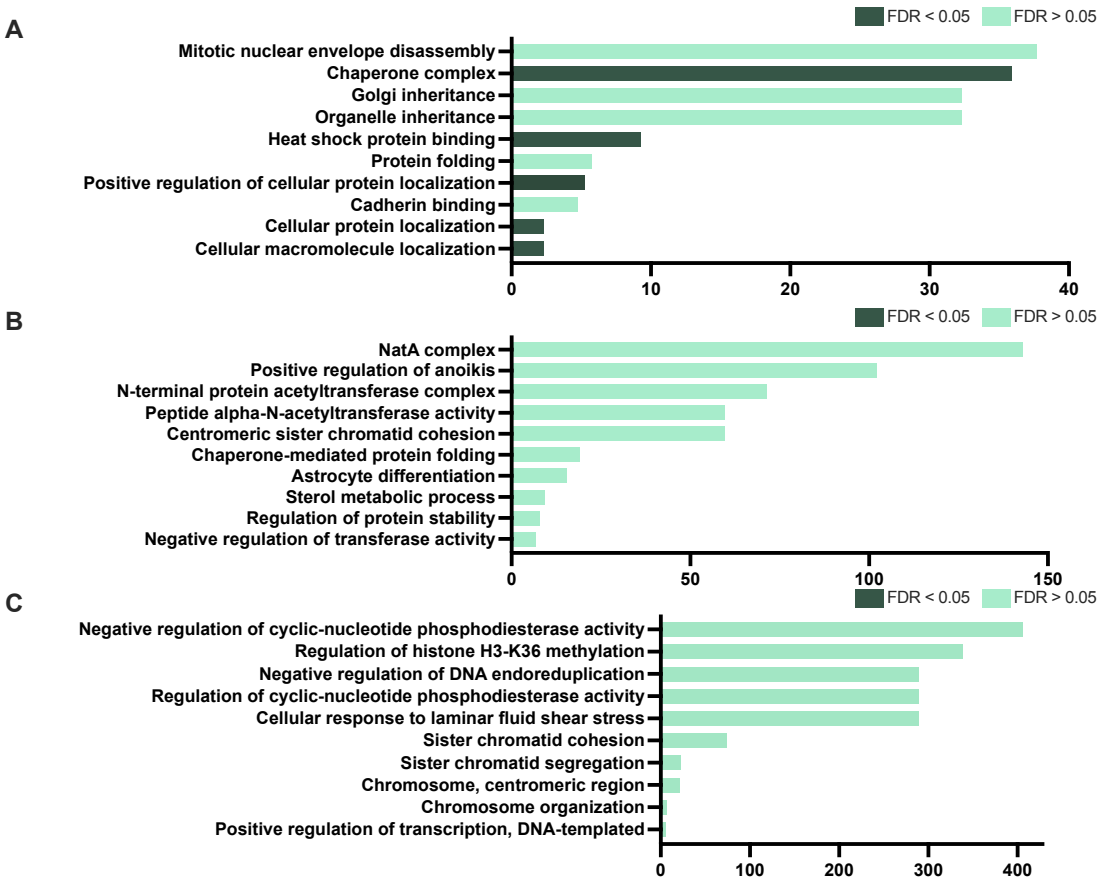

Figure 3.12: *Enriched KEGG pathways associated with proteins which are altered in Ishikawa cells (n=3) following transfection (48 hrs) by both miR-542-3p mimic and inhibitor.*
A) Enriched KEGG pathways for proteins altered in the *same* way by miR-542-3p mimic and inhibitor (*i.e.*, both increased or both decreased in abundance) (FDR<0.05). **B**) Enriched KEGG pathways for proteins increased by miR-542-3p overexpression and decreased by miR-542-3p inhibition (FDR<0.05). **C**) Enriched KEGG pathways for proteins decreased by miR-542-3p overexpression and increased by miR-542-3p inhibition (FDR<0.05). (Supplementary Table 15).

3.4.2.5 Proteins confirmed *in vitro* as targets of miR-542-3p, compared with miRDB predicted targets, and P4 regulated *in vitro* targets

In order to investigate functional relevance of altered proteins, miRDB was used to predict targets of miR-542-3p. Five hundred and eighty-eight targets were identified, and this list compared to proteins changed by miR-542-3p mimic and/or inhibitor *in vitro*. Only 100 of the predicted targets were changed in ishikawa cells treated with miR-542-3p mimic or inhibitor (Supplementary Figure 2A). This small sample size produced no significant ($p>0.05$) enrichment however shows overrepresentation in ubiquitin protein ligase binding (8 proteins) and protein kinase binding (11 proteins) (Supplementary Figure 2). MiRDB predicted targets, *in vitro* confirmed protein targets of miR-542-3p mimic and/or inhibitor and P4 regulated mRNAs in endometrial epithelial cells from previous work (Edge et al., 2023) were then compared. Only 46 proteins met all three conditions (Figure 3.13A). These proteins were non-significantly ($p>0.05$) overrepresented in multiple biological processes of protein localization and transport (Figure 3.13B-C). There were 328 of the *in vitro* proteins altered by miR-542-5p mimic or inhibitor which were also changed in response to P4 (Figure 3.13A).

Ultimately, investigation into whether the identified proteins changed in response to miR-542-3p mimic and/or inhibitor *in vitro* were present in RNASeq data from human endometrial biopsy samples was carried out (Lipecki et al., 2022). For 94% of proteins altered in abundance in response to miR-542-3p mimic, the corresponding mRNA was present in the RNASeq data (Figure 3.14). Of these 1261 proteins, only 11 were not present in all of the 36 clinical samples. Furthermore, 95% of proteins changed in abundance following inhibition of miR-542-3p were identified in mRNA data from endometrial biopsies, and only 8 of the 895 proteins altered by inhibition of miR-542-3p were missing from 1 or more patient sample.

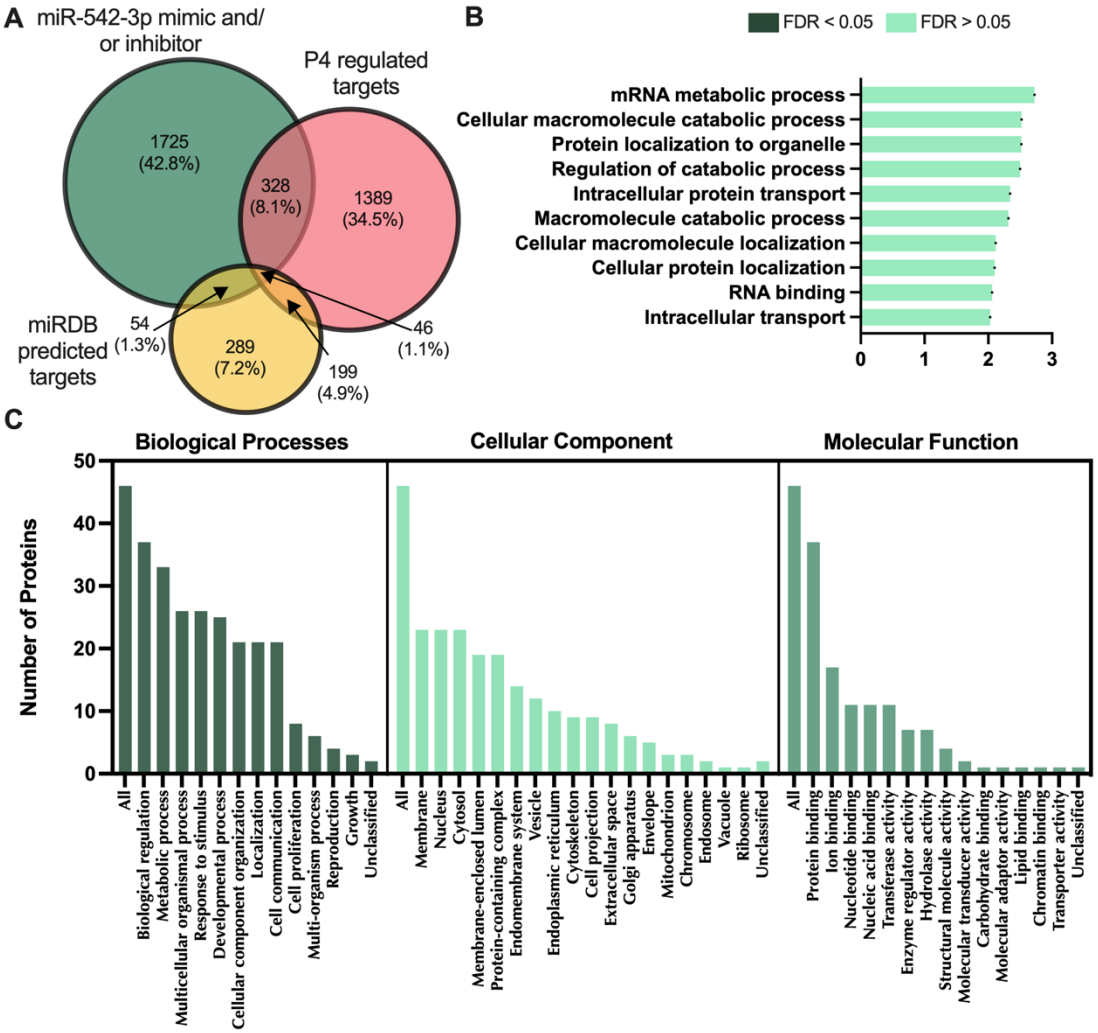

Figure 3.13: *Proteins significantly altered in abundance in response to miR-542-3p mimic and/or inhibition compared to miRDB predicted targets and P4 regulated mRNAs.*
A) Venn diagram showing total number of proteins significantly altered in abundance ($p<0.05$) following transfection of ishikawa cells (n=3 biological replicates, 48 hrs) with miR-542-3p mimic and/or inhibitor vs miRDB predicted targets vs progesterone regulated mRNAs (Edge et al., 2023)**. B**) Enriched KEGG pathways associated with miR-542-3p mimic and/or inhibitor regulated proteins, miRDB predicted targets and P4 regulated mRNAs overlap (FDR<0.05). **C**) WebGestalt overrepresentation analysis of biological process, cellular component, and molecular function categories for identified significantly differentially abundant proteins in response to miR-542-3p mimic and/or inhibition, predicted targets and P4 regulated mRNAs overlap. (Supplementary Table 17).

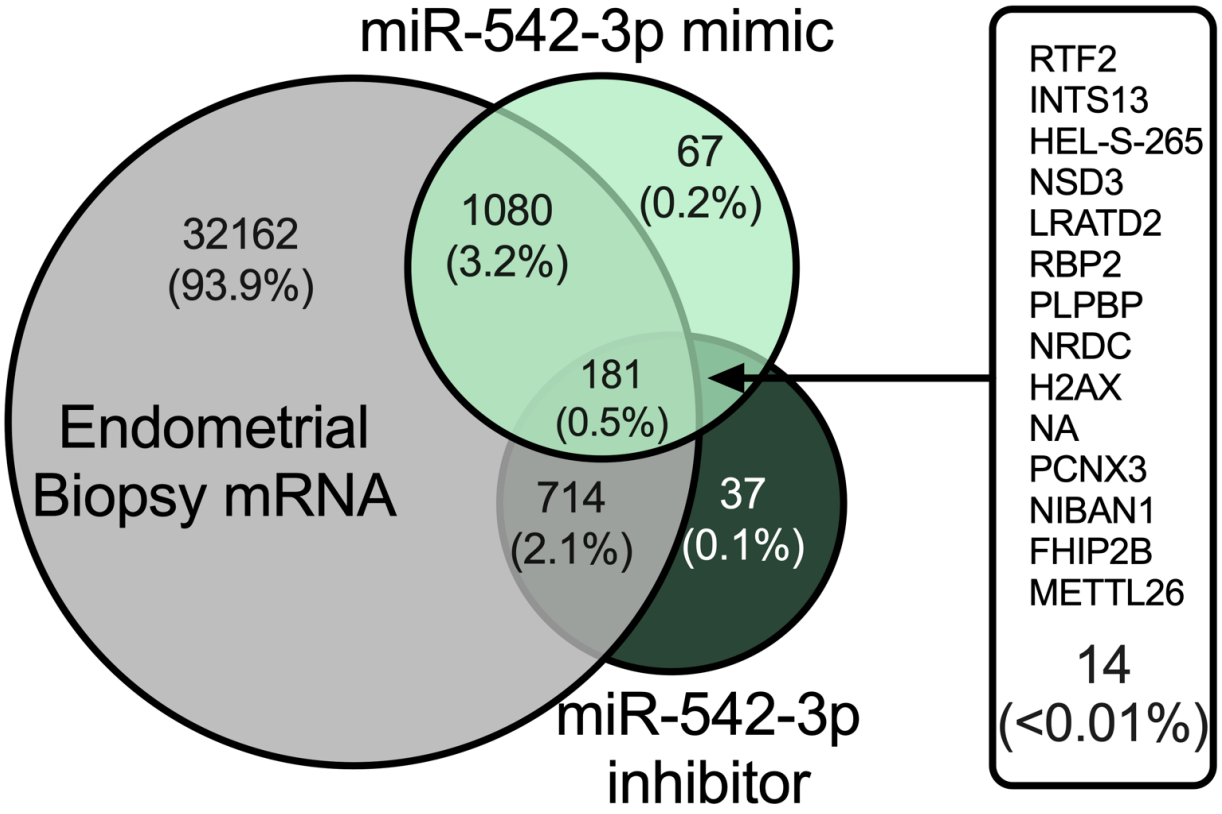

Figure 3.14: *Comparison of miR-542-3p regulated proteins with mRNA from human endometrial biopsies*
Comparison of proteins significantly altered in abundance ($p<0.05$) in following transfection of endometrial epithelial (Ishikawa) cells (n=3 biological replicates, 48 hrs) with miR-542-3p mimic and/or inhibitor compared to RNASeq data from human endometrial biopsies (n=36 biological repeats, biopsies taken 4-12 days following ovulation)(Lipecki et al., 2022). Listed proteins display 14 which are altered by both over and under expression of miR-542-3p, but are not detected in biopsies, suggesting they are not present physiologically. (Longer lists of proteins in each section of Venn diagram can be found in each section of Venn diagram can be found in Supplementary Table 18A-D).

3.4.2.6 Differential protein abundance

An example volcano plot (Figure 3.15) comparing proteins differentially abundant in response to miR-542-3p mimic vs miR-542-3p inhibitor exhibits the number of proteins significantly ($p<0.05$) and highly significantly ($p<0.05$ and $>1 Log_2FC$) or ($p<0.05$ and $>-1\ Log_2FC$) differentially abundant between the two treatment groups.

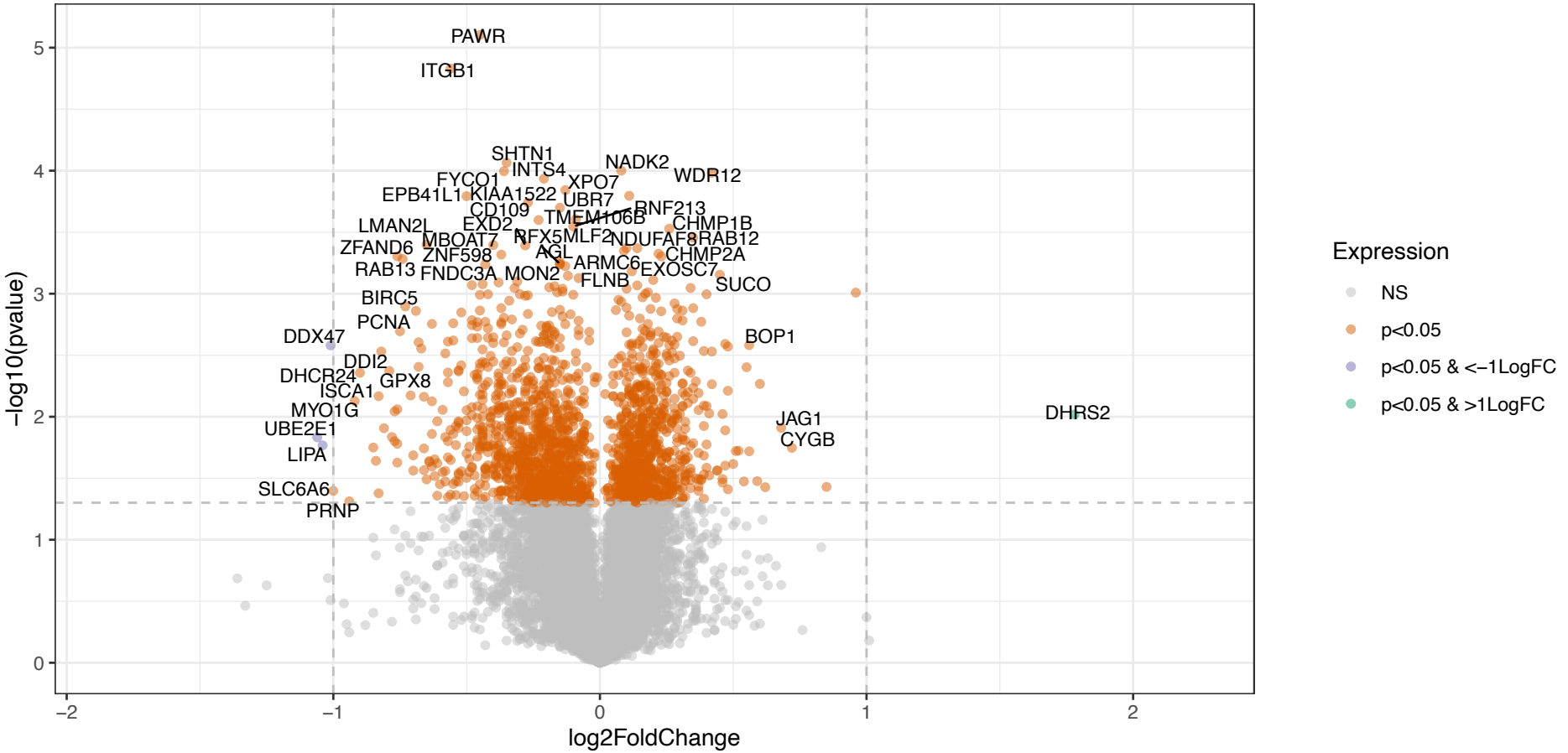

Figure 3.15: *Volcano plot showing abundance of proteins present in Ishikawa cells (n=3) transfected for 48 hrs with either miR-542-3p mimic or inhibitor highlighting those which are significantly differentially abundant between the two groups.*
Proteins which are significantly differentially abundant ($p<0.05$) between the two treatments are shown in orange, proteins which are highly significantly decreased in abundance ($p<0.05$ and $>-1Log_2FC$) are coloured purple, and those which are highly significantly increased in abundance abundant ($p<0.05$ and $>1Log_2FC$) are coloured green.

3.5 Discussion

This chapter tested the hypothesis that miR-542-3p - which is an evolutionarily conserved miRNA amongst eutherian mammals (Taylor et al., 2023), and is overexpressed in response to P4 (Edge et al., 2023) - modifies the proteome of the endometrium, potentially to facilitate receptivity to implantation. To investigate this, miR-542-3p was over and under expressed in Ishikawa cells to study the mechanisms altered by this miRNA. In this chapter, I have produced a list of proteins which were differentially abundant following treatment with miR-542-3p mimic or inhibitor, with many of their associated pathways relevant for implantation. Downstream analysis of these proteins was also conducted to determine which pathways they are involved in, which are likely regulated by P4 via miR-542-3p.

Proteomic analysis revealed 67 proteins which were altered in opposite directions following over or under expression of miR-542-3p - *ie.,* a protein was increased following miR-542-3p overexpression and decreased following inhibition, or vice versa (Figure 3.7 and Figure 3.12B-C). This suggests that these proteins may be direct targets of miR-542-3p and thus may be regulated by P4 *in vivo.* Fifty-eight of these were increased in abundance following overexpression of miR-542-3p, and decreased following inhibition. Although there are no significantly enriched biological processes associated with this group of proteins - likely due to protein group size - one of the non-significantly overrepresented functions was positive regulation of anoikis (Figure 3.12B). This is interesting as anoikis refers to the process through which cells undergo apoptosis following adhesion to a location which is inappropriate (Paoli et al., 2013). This highlights a role for P4 mediated, miR-542-3p upregulated proteins in regulating attachment of the blastocyst to avoid implantation at unsuitable locations in the endometrium, or perhaps ensuring that the blastocyst implants at a time that is temporally and developmentally correct.

As described in Chapter 3, Section 3.1.1, miR-542-3p overexpression caused downregulation of *ILK* in endometrial stromal cells. Interestingly, in this work in the endometrial epithelial cells, miR-542-3p overexpression causes an increase in protein abundance of ILK, and inhibition causes a reduction of ILK (Qu et al., 2021). This is particularly interesting as the protein is altered in opposite ways by over or under expression of miR-542-3p suggesting that it is a direct and important target of miR-542-3p. Furthermore, Chen et al., (2020) found that ILK was downregulated in the serum of idiopathic infertility patients, and that overexpressing ILK in endometrial epithelial cells has a negative effect on embryo attachment ability. They suggest that ILK is important for endometrial

receptivity; and propose that mechanistically loss of ILK inactivates Wnt/ β-catenin signalling which affects implantation. Overall, these studies and the data in this chapter argue that miR-542-3p regulates ILK as one of a number of mechanisms establishing endometrial receptivity.

Proteins which were less abundant following inhibition of miR-542-3p were significantly overrepresented in the biological process cadherin binding. Cadherins are adhesion molecules which are expressed in the endometrial luminal epithelium, and generally maintain cell-cell contact, tissue structure and polarity (Perez and Nelson, 2004; Zhou et al., 2020). Kokkinos et al., (2010) suggest that embryo implantation involves E-cadherin, with a reduction in expression resulting in loss of cell-cell adhesion in the endometrial epithelium assisting in implantation. Cadherin 6 is another adhesion molecule of which knockdown in endometrial epithelial cells causes reduced embryo adhesive ability (Zhou et al., 2020). A protein within the group which were found to be associated with cadherin binding following inhibition of miR-542-3p: annexin A2 (ANXA2), is found to be upregulated at the time of endometrial receptivity (Garrido-Gómez et al., 2012). In this study, when ANXA2 is inhibited in the endometrial epithelium, embryos are less able to attach to the endometrium, endometrial epithelial inhibition of ANXA2 also had a negative effect on trophoblast outgrowth. Finally, it was observed that wound healing was impaired whilst inhibiting ANXA2, meaning that the endometrium would be less able to undergo epithelial reconstitution following invasion of an embryo. It is interesting that inhibition of miR-542-3p causes a reduction in ANXA2 compared to untreated cells, as this appears to be important for attachment. This therefore suggests one of the functions of increased expression of miR-542-3p in response to P4 is to avoid loss of ANXA2 to facilitate attachment. ANXA2 has also been implicated in decidualization in the stromal layer of the endometrium, where its knockdown impairs this process in mice (Garrido-Gomez et al., 2020). Furthermore, endometrial stromal cells from women who had suffered from severe preeclampsia had significantly less ANXA2 protein and mRNA (Garrido-Gomez et al., 2020). This emphasises the necessity for appropriate expression of *ANXA2* in the endometrium at multiple stages and cells to allow a pregnancy to occur and progress.

Proteins more abundant following overexpression of miR-542-3p are significantly overrepresented in multiple processes concerning targeting of proteins to the endoplasmic reticulum (ER) and intracellular protein transport and localization. This suggests that miR-542-3p and its targets are involved in intracellular, as well as intercellular communication and signalling, perhaps communicating with the stromal cells to regulate decidualization.

Communication between the epithelial and stromal compartments of the endometrium appears to be important for decidualization, as removal of the epithelial cells in rats causes complete inhibition of the decidualization process (Lejeune et al., 1981). The precise cell to cell communication between these two layers of the endometrium is unclear, but there are some suggestions of key molecules in the literature. Transforming growth factor beta 1 (TGF-β1) is upregulated in the endometrium in response to P4 and is produced by the epithelial cells and secreted (Kim et al., 2005). Kim et al., (2005) found that adding TGF- β1 to stromal cells activated Smad signalling to instigate decidualization. Whilst TGF- β1 was not increased directly by miR-542-3p in this chapter data, TGF- β receptor type 2 (TGFβR2) was significantly increased following overexpression of miR-542-3p, perhaps demonstrating that miR-542-3p is involved in this pathway and function in some way. Notwithstanding, with the available discussed literature and the involvement of proteins altered in abundance by miR-542-3p in intra- and inter- cellular signalling; it is not unlikely that a function of miR-542-3p lies in the regulation of stromal cell decidualization.

Functionality of *survivin* was discussed in Chapter 3, Section 3.1.1, where overexpression of miR-542-3p caused reduced abundance of *survivin* - an apoptosis inhibitor, resulting in impaired ability of proliferation in a cancer model (Yoon et al., 2010). In contrast, in this chapter data, overexpression of miR-542-3p resulted in increased *survivin*, and inhibition of miR-542-3p reduced the abundance of *survivin* in the Ishikawa cells. In rodents, it was found that the blastocyst induces apoptosis in endometrial epithelial cells during implantation (Parr et al., 1987). Galán et al., 2000 revealed that in human endometrial epithelium, during apposition of an embryo before attachment, apoptosis is reduced. However, during the attachment stage of implantation, apoptosis is increased. Taken together, miR-542-3p overexpression - due to P4 - causing increased abundance of survivin may be functioning to inhibit apoptosis of endometrial epithelial during attachment stages of implantation. There is some evidence that *Syndecan-1* (*SDC-1*), is hormonally regulated, and elevated (although non-significantly) in endometrial epithelial cells during the secretory phase of the menstrual cycle (Lorenzi et al., 2011). The proteomic data in this chapter demonstrates increased abundance of SDC-1 in response to miR-542-3p overexpression in Ishikawa cells. This is interesting because SDC-1 has previously been implicated in 'fine tuning' of apoptosis during the menstrual cycle (Boeddeker et al., 2014), with *survivin* as a downstream target of *SDC-1.* Their study also showed that knockdown of *SDC-1* caused endometrial epithelial cells to be more responsive to embryonic signalling pertaining to apoptosis. Overall, decreased *SDC-1* in the endometrial epithelium caused

reduction of *survivin* resulting in increased apoptosis. In this *in vitro* proteomic study with miR-542-3p overexpression in Ishikawa cells, SDC-1 is increased as well as survivin, providing opposite evidence for downregulation of apoptosis to assist in embryo apposition. This suggests that dynamic, temporal, miR-542-3p induced regulation of apoptosis in the endometrium, potentially in conjunction with its targets *SDC-1* and *survivin*, is necessary for the different stages of implantation to occur. Another member of the syndecan family of transmembrane proteoglycans, syndecan 3 (SDC-3), is also upregulated by miR-542-3p overexpression in the Ishikawa cells. The literature fails to provide conclusive evidence on SDC-3 regulation in endometrial epithelial cells during the menstrual cycle, with no observed difference between phases (Germeyer et al., 2007), and there are no studies investigating its role in reproduction. Therefore, this work provides novel insight into hormonally modulated, secretory phase upregulation of SDC-3 in response to increased miR-340-5p. As a family, syndecans are associated with cell adhesion, invasion and migration (Afratis et al., 2017) - processes vital for implantation; spotlighting SDC-3 as a theoretical participant in implantation.

In a different system - neuroblastoma cells, *KDM1A* expression is regulated by miR-542-3p, where upregulation of miR-542-3p causes reduced *KDM1A* and inhibits proliferation (Wei et al., 2020). This work confirms *KDM1A* as a target of miR-542-3p and demonstrates that when endometrial epithelial cells are transfected with miR-542-3p to recapitulate the rise in expression due to P4, *KDM1A* is downregulated. These results reveal that miR-542-3p may be controlling proliferation of endometrial epithelial cells through its target *KDM1A*.

In conclusion, the results of this chapter lead to the suggestion that regulation of miR-542-3p by P4 plays a role in controlling endometrial epithelial cell proliferation to contribute to establishing endometrial receptivity. In addition, some evidence implies that miR-542-3p is involved in communication between epithelial and stromal cells in the endometrium and may be important for stromal cell decidualisation. Finally, it appears that miR-542-3p is necessary for processes controlling cadherin binding, which may have implications for implantation. A summary of findings from Chapter 3 is provided in Table 3.1 and Figure 3.16.

Table 3.1: Summary of key proteins altered by differential expression of miR-542-3p in endometrial epithelial (Ishikawa) cells and their physiologically relevant functions in other system(s).

Protein	Effect on protein abundance following differential expression of miR-542-3p	Role in other system(s)	Reference
Survivin	*Increased* in abundance following overexpression of miR-542-5p AND *decreased* in abundance following inhibition of miR-542-3p	Overexpression of miR-542-3p causes decreased *survivin* resulting in impaired proliferation in a cancer model	(Yoon et al., 2010)
SDC-1 Syndecan-1	*Increased* in abundance following overexpression of miR-542-3p	Hormonally regulated and elevated in endometrial epithelial cells during secretory phase of menstrual cycle Linked to 'fine-tuning' of apoptosis during menstrual cycle - *survivin* downstream target	(Lorenzi et al., 2011) (Boeddeker et al., 2014)
KDM1A Lysine demethylase 1A	*Decreased* in abundance following overexpression of miR-542-3p	*KDM1A* expression decreased by overexpression of miR-542-3p in neuroblastoma cells resulting in decreased proliferation	(Wei et al., 2020)

ILK Integrin-linked kinase	*Increased* in abundance following overexpression of miR-542-3p, AND *decreased* in abundance following inhibition of miR-542-3p	ILK downregulated in patients with idiopathic infertility and overexpression of ILK has negative effect on embryo attachment	(Chen et al., 2020)(Cuman et al., 2014; D. Liu et al., 2020)
TGFβR2 Transforming growth factor beta receptor 2	*Increased* in abundance following overexpression of miR-542-3p	Another member of the transforming growth factor beta receptor family - TGFβR1 is P4 regulated and produced by endometrial epithelial cells. TGFβR1 causes endometrial stromal cell decidualisation	(Kim et al., 2005)

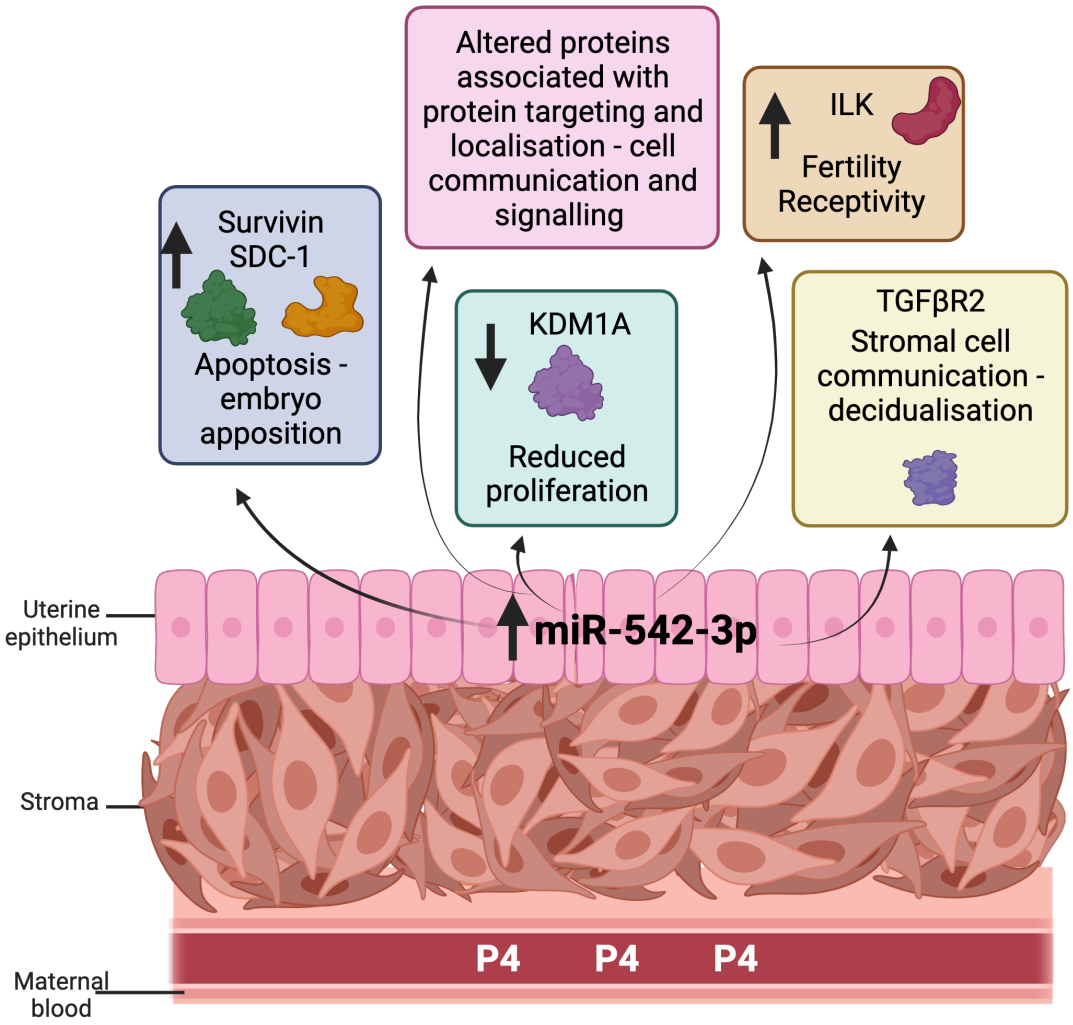

Figure 3.16: *Diagram summarising key proteins and processes altered by miR-542-3p in the endometrial epithelium which may be important for early pregnancy*.
Proteins included in figure are those altered in abundance by differentially expressed miR-542-3p and linked to endometrial function in the literature Figure created using Biorender.com

Chapter 4 Investigating the Mechanistic Effect of miR-671-5p in the Endometrium

4.1. Introduction

In order for pregnancy to occur, the endometrium must be optimally primed to allow for an embryo to attach to the epithelial cells, and invade into underlying stromal cells (Enciso et al., 2021). Coordinated production of steroid hormones E2 and P4 - E2 concentration highest in the proliferative phase of the menstrual cycle and P4 produced in the secretory phase - cooperate to establish endometrial receptivity (Moustafa and Young, 2020). E2 production and expression of its receptors is necessary prior to the window of implantation as this results in proliferation of the epithelial layer, however to prime the endometrium for implantation, P4 signalling downregulates E2 receptors (Lessey and Young, 2019b). P4 is vital to achieve endometrial receptivity. It is responsible for halting epithelial proliferation and activating differentiation, beginning stromal cell proliferation; along with remodelling and disruption of the adherens and tight junctions in the endometrium (Bhurke et al., 2016). Alongside P4, a plethora of molecules are involved in early pregnancy events including growth factors, cytokines and microRNAs (miRNAs) (Singh et al., 2011). MiRNAs are of interest in endometrial receptivity and implantation as they are relatively understudied in the literature with respect to the field of reproduction. Despite this, limited research shows a number are reported to play roles in reproductive systems (Shekibi et al., 2022) (Chapter 2, Section 2.1), but the extent of their involvement and understanding of the exact mechanisms is scarce.

4.1.1 MiR-671-5p

MiR-671-5p has previously been identified as an evolutionarily conserved miRNA present in all extant eutherian mammals studied (Taylor et al., 2023), and has been shown in previous work from our lab to be regulated by P4 - with overexpression in endometrial epithelial cells in response to P4 treatment (Edge et al., 2023). This suggests miR-671-5p must be important to some eutherian mammal specific mechanisms, due to the fact it is highly conserved, and also likely to have involvement in reproductive processes due to its upregulation in response to P4, which occurs at the time of endometrial receptivity and pregnancy.

There is minimal research concerning miR-671-5p in all fields, however it is modestly described for its roles in cancer. MiR-671-5p was observed to function as an oncogene in the development of prostate cancer, where higher expression signifies worse prognosis, as well as increased invasion, migration and proliferation of prostate cancer cells (PC-3 cell line - epithelial metastatic adenocarcinoma) (Z. Zhu et al., 2020). This was suggested mechanistically to

be due to miR-671-5p downregulation of NFIA (Nuclear Factor I A), and when NFIA was increased, effects on proliferative abilities were reversed. Conversely, miR-671-5p reportedly functions as a tumour suppressor in non-small cell lung cancer, where it's overexpression reduced invasion, proliferation and migration in the cancer (Ye et al., 2022). A proposed mechanism for this suppressive function was that overexpression of miR-671-5p downregulates MFAP3L, whilst replacement of MFAP3L causes a reversal of the negative proliferative and invasive effects. In glioblastoma, miR-671-5p is downregulated by MSI1, and this under expression of miR-671-5p results in increased migration and growth of tumour cells by its target *STAT3* (Lin et al., 2021). The fact that miR-671-5p is reported to function as both an oncogene and tumour suppressor highlights the dynamic roles this miRNA can play in different systems or pathways and suggests there may be a role in controlling proliferation in the endometrium. A similar effect was also observed in breast cancer, where miR-671-5p acted as a tumour suppressor again by decreasing proliferation and invasion through targeting and downregulating FOXM1 (Tan et al., 2019). In relation to reproductive biology, FOXM1 has also been implicated in endometrial stromal cells decidualization, where its deletion in mice results in defects in decidualization and thus reduced fertility - with a significant decrease in number of successful pregnancies compared to controls (Gao et al., 2015). FOXM1 is a key transcription factor involved in the cell cycle and was found to be highly expressed in the endometrium during the proliferative phase, lowly expressed during early secretory phase, and then increased in the late secretory phase of the human menstrual cycle (Jiang et al., 2015). This study found that presence of FOXM1 was important for human endometrial stromal cell proliferation as its absence causes proliferation inhibition. It also identified STAT3 as a target of FOXM1 during stromal cell decidualization. This evidence implies miR-671-5p may be involved in regulation of endometrial proliferation and decidualization (Jiang et al., 2015). Despite stromal cells being those which decidualize, communication between the stromal and epithelial layers may allow miR-671-5p and its targets to play a role in this process.

In a study analysing miRNA presence in uterine fluid from patients with recurrent implantation failure (RIF), miR-671-5p was significantly upregulated when compared to healthy patients who had proven fertility (von Grothusen et al., 2022). Further analysis in this paper examined target genes of dysregulated miRNAs, however it grouped the targets of all dysregulated miRNAs together so did not detail what miR-671-5p may be specifically responsible for mechanistically. Nevertheless, the grouped targets of the set of upregulated miRNAs include pathways important for implantation, suggesting that miR-671-5p dysregulation may play a role in RIF. Consequently, correct expression of

miR-671-5p in the endometrium could be necessary for successful establishment of pregnancy. A diagram in Figure 4.1 summarises the systems that miR-671-5p is implicated in.

The mechanisms of miR-671-5p in the epithelial endometrium are not described in the literature, with little evidence of its role in endometrial receptivity and implantation. Investigation into these mechanisms is necessary to provide us with a greater understanding of the processes behind successful pregnancy and reveal potential future therapeutic targets.

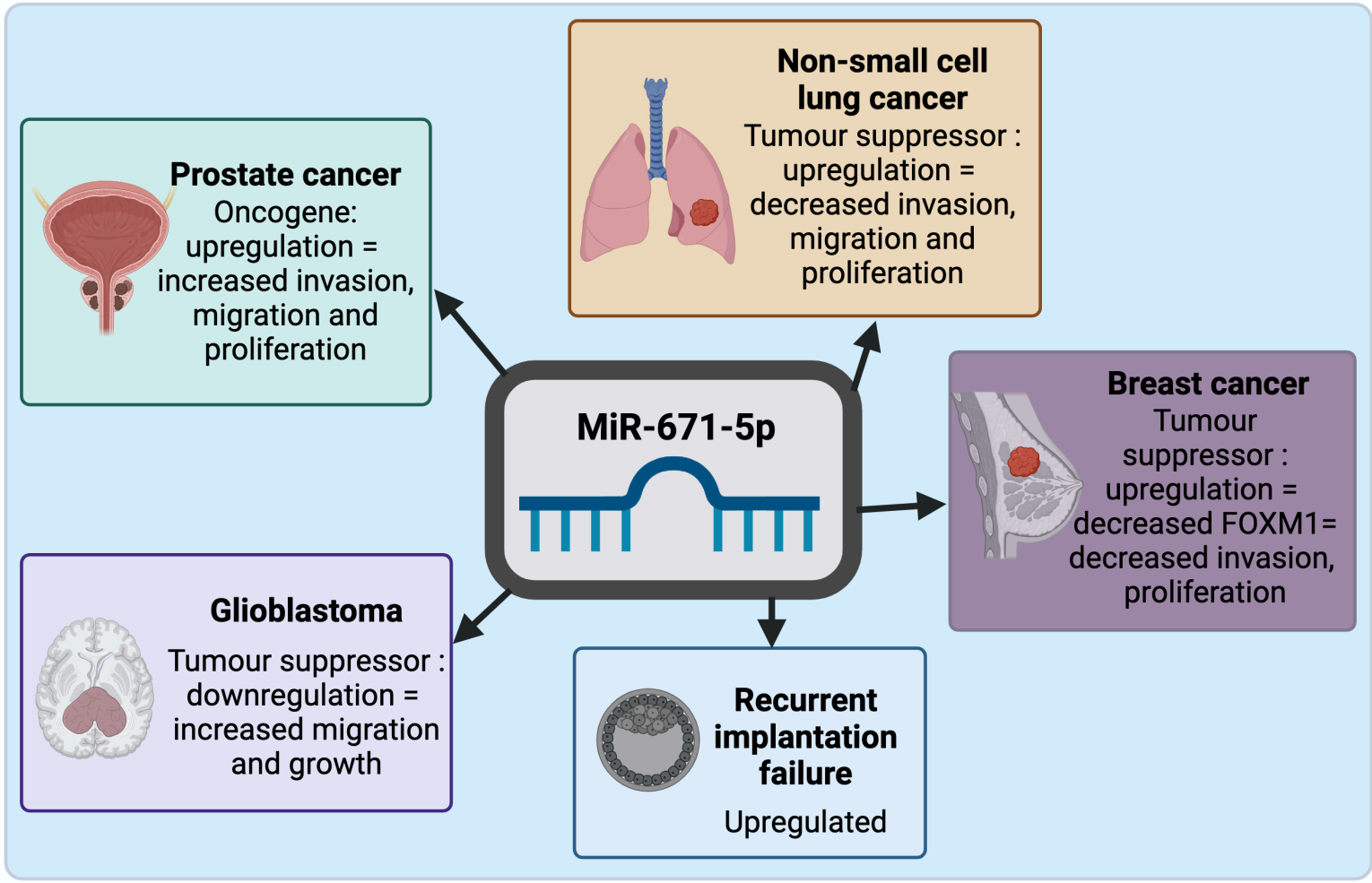

Figure 4.1: *Summary figure illustrating systems in which miR-671-5p is reported in the literature to play a role, and the outcomes in each system.*
Figure created using Biorender.com

4.2 Hypothesis and Aims

4.2.1 Hypothesis

This chapter tests the hypothesis that an evolutionarily conserved, progesterone regulated miRNA - miR-671-5p - modifies the expression of protein coding regions of human endometrial epithelial cells and may facilitate receptivity to implantation in humans.

4.2.2 Aims

The aim of this chapter is to:

1) Unravel whether there are alterations in the proteome of the endometrial epithelium after modifying miR-671-5p expression.

2) Understand mechanistic relevance of progesterone induced miR-671-5p upregulation through analysis of proteins altered in abundance, and investigation of pathways these proteins are involved in.

4.3 Materials and Methods

4.3.1 Cell Culture

All cell culture processes were performed in a sterile tissue culture hood, using sterile filtered pipette tips and 70% ethanol. Size 75cm^2 and 25cm^2 cell culture treated flasks were used to grow the cultures. Light microscopy was used to assess confluency and quality.

4.3.1.1 Ishikawa (immortalized endometrial epithelial) cells

Ishikawa cells (ECACC # 99040201) are an immortalized endometrial epithelial cell line employed here as a hormonally responsive epithelial layer model of the human endometrium. As previously described in Chapter 2, Section 2.3.1.1, Ishikawa cells were maintained in culture, with passaging taking place at >70% confluency. Culture media composition, maintenance and passaging protocols are detailed in Chapter 2, Section 2.3.1.1.

4.3.2 MicroRNA Mimic and Inhibitor Transfection

A detailed protocol for the miRNA mimic and inhibitor transfection carried out is provided in Chapter 2, Section 2.3.2. Briefly, with alterations for this chapter:

Initial optimisations were performed to confirm the correct volume of transfection reagent that resulted in maximum transfection efficiency but minimum harm to cells (Chapter 2, Section 2.3.2.1). The chosen volume of 1μl per well using a 24 well plate was scaled up or down dependent on well size used.

Mimics and inhibitors (Horizon Discovery) for miR-671-5p were used and the protocol executed as explained in Chapter 2, Section 2.3.2.2. Treatments were added to 6 well plates containing 200,000 cells/well with 1.6ml antibiotic and serum free media (n=3) for 48 hrs. Treatments are listed below:

13. Control: 400μl opti-MEM media
14. Transfection reagent control: 400μl opti-MEM media + 4μl Lipofectamine 2000
15. Non-targeting mimic control: 400μl opti-MEM media + 4μl Lipofectamine 2000 + 80pmol non-targeting mimic
16. Non-targeting inhibitor control: 400μl opti-MEM media + 4μl Lipofectamine 2000 + 80pmol non-targeting inhibitor
17. MiR-542-3p mimic: 400μl opti-MEM media + 4μl Lipofectamine 2000 + 80pmol miR-671-5p mimic
18. MiR-542-3p inhibitor: 400μl opti-ME M media + 4μl Lipofectamine 2000 + 80pmol miR-671-5p inhibitor

Cells were collected for subsequent analysis using trypsin/EDTA 0.025% following the protocol in Chapter 2, Section 2.3.2.3.

4.3.3 RNA Analysis

The MiRNeasy Mini Kit (Qiagen) was used to extract RNA following manufacturer's instructions and the protocol in Chapter 2, Section 2.3.3.1 with no chapter specific changes. Concentration of extracted RNA was then quantified using the Nanodrop N1000 spectrophotometer (Thermo Fisher Scientific, USA) which is detailed in Chapter 2, Section 2.3.3.2. A cDNA conversion was carried out to reverse transcribe RNA into cDNA utilizing the miRCURY LNA RT Kit (Qiagen) as explained in Chapter 2, Section 2.3.3.3 according to manufacturer's instructions. Samples then underwent qRT-PCR to confirm over and under expression of miR-671-5p compared to non-targeting controls. MiR-671-5p primers were purchased from Qiagen and PCR performed using miRCURY SYBR Green Kit (Qiagen). ΔCt values were calculated by subtracting the global mean of 5S normaliser from each value to normalise the data. Data was then transformed using $2^{-\Delta Ct}$ to show miRNA normalised absolute expression values. Detailed protocol is provided in Chapter 2, Section 2.3.3.4.

4.3.4 Proteomic Analysis

Protein was extracted using a RIPA buffer as described in Chapter 2, Section 2.3.4.1, and quantitative proteomic analysis was carried out at Bristol Proteomics Facility. Steps of proteomic analysis carried out by Bristol Proteomics Facility are explained in Chapter 2, Section 2.3.4.2 but consist of stages:

1. Tandem Mass Tag Labelling and High pH reversed-phase chromatography.
2. Nano-LC Mass Spectrometry
3. Proteomic Statistical Analysis
4. Production of PCA and Volcano plots

4.3.4.1 Data Analysis

Proteins that appeared in the contaminant database were removed by filtration. For each comparison, eg. Non-targeting mimic vs miR-671-5p mimic, all proteins whose t-test value was statistically significant ($p<0.05$) were used. Gene names were used to create Venn diagrams to remove any proteins that were also changed in abundance in response to the non-targeting control. The list of proteins changed in response to the non-targeting mimic vs control was compared in a Venn diagram, to the list of proteins significantly changed after treatment with miR-671-5p mimic. Any overlapping proteins in the centre of the diagram were excluded due to altered abundance by the non-targeting mimic and so were likely to be due to off-target effects. Accession numbers were used in replacement of gene name where this information was absent. Some lists had multiple proteins with the same gene name due to there being different fragments or forms of the same protein altered in abundance. Identical steps were carried out for miR-671-5p inhibitor vs non-targeting inhibitor (described in Chapter 2, Section 2.3.3.5). Proteins identified by this analysis which were discussed further were selected through their involvement in related pathways in the literature. Proteins were also compared to RNASeq data from 36 human endometrial biopsies collected 4-12 days following a positive home ovulation test. Women aged 31-36 were recruited with between 0-9 previous losses, and went on to have either live birth, ongoing pregnancy or miscarriage outcomes (Lipecki et al., 2022).

4.4 Results

4.4.1 qPCR Results

MiR-671-5p was significantly ($p<0.0001$) overexpressed after transfection of Ishikawa cells with miR-671-5p mimic in comparison to control, lipofectamine only control, non-targeting mimic and miR-671-5p inhibitor (Figure 4.2).

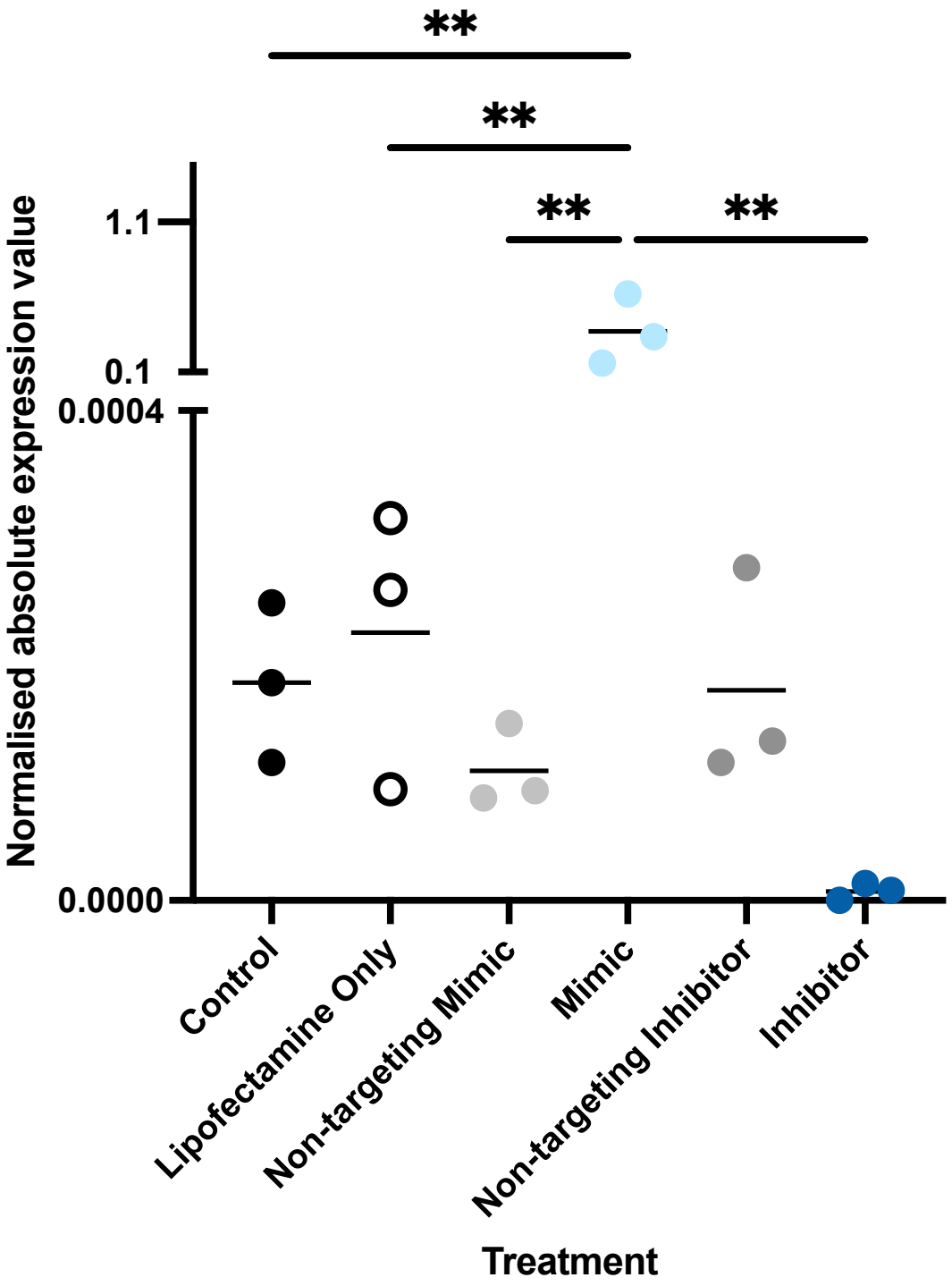

Figure 4.2: *Absolute expression values of miR-671-5p normalised to 5s following endometrial epithelial cell transfection (Ishikawa cell line, 48hr, n=3 biological replicates) with miR-671-5p mimic and inhibitor.*
Treatments were all added to 1.6ml antibiotic and serum free media and consisted of i) Control - 400μl optiMEM media only, ii) Lipofectamine only control - 4μl lipofectamine in 400μl optiMEM media, iii-vi) 80pmol of non-targeting mimic, miR-671-5p mimic, non-targeting inhibitor or miR-671-5p inhibitor in 400μl optiMEM media. Statistical significance following a one way ANOVA and multiple comparisons test is denoted by ** $p<0.005$.

4.4.2 Proteomics Results

4.4.2.1 PCA Plots

Using a PCA plot of principal components 1+2 (PC1, PC2) (Figure 4.3) to demonstrate treatment influence on the largest variance in the data, it is evident that samples cluster together depending on biological repeat. N=1 (circles) clusters down the right-hand side of the graph providing a visual representation for the variance caused by the differences in biological repeats. N=2 and N=3 appear to be more similar to each other, as these plots are mostly in the upper middle portion of the graph. A PCA plot of PC3 and PC4 (Figure 4.4) explains less of the variance of the data - 9.9% and 8.6% compared with 27.5% and 18.3% for PC1 and PC2 and is used to show other trends in the data. In this plot, there is obvious clustering of miR-671-5p mimic samples in the lower left corner, with the non-targeting mimic plotted as oppositely as possible in the upper right corner. MiR-671-5p inhibitor clusters together just to the northeast of the centre of the graph but does not show such clear separation from the controls as is seen with the mimic.

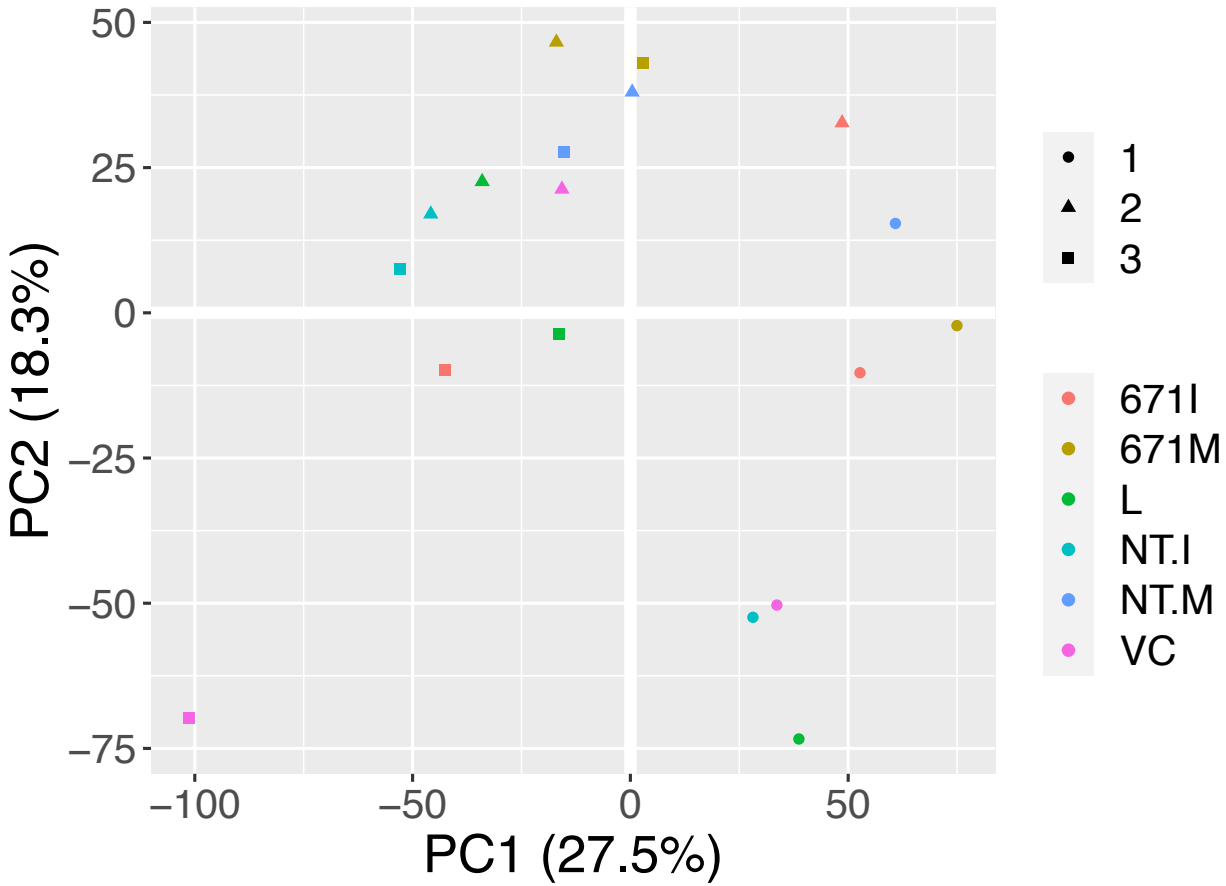

Figure 4.3: *PCA plot (PC1 and PC2) for miR-671-5p overexpression or under expression in Ishikawa cells.*
PCA (principal component analysis) plot of PC1 and PC2 for Ishikawa cells (n=3 - biological repeats shown by circle, triangle and square) transfected for 48 hrs with miR-340-5p mimic (340M), miR-340-5p inhibitor (340I), non-targeting mimic control (NT.M), non-targeting inhibitor control (NT.I), lipofectamine transfection reagent only (L) or media control (VC). Produced by Bristol Proteomics Facility.

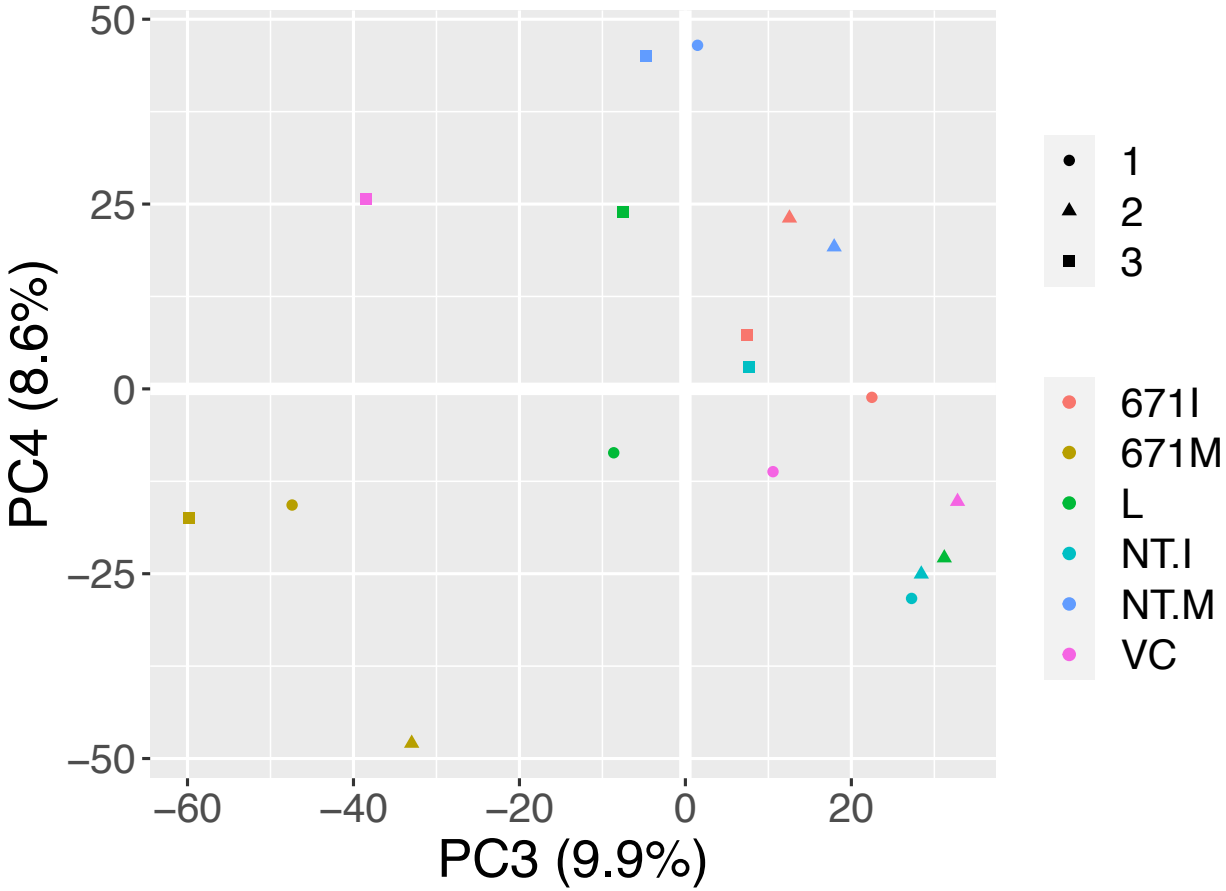

Figure 4.4: *PCA plot (PC3 and PC4) for miR-671-5p overexpression or under expression in Ishikawa cells.*
PCA (principal component analysis) plot of PC3 and PC4 for Ishikawa cells (n=3 - biological repeats shown by circle, triangle and square) transfected for 48 hrs with miR-671-5p mimic (671M), miR-671-5p inhibitor (671I), non-targeting mimic control (NT.M), non-targeting inhibitor control (NT.I), lipofectamine transfection reagent only (L) or media control (VC). Produced by Bristol Proteomics Facility.

4.4.2.2 Protein abundance following overexpression of miR-671-5p

For the purpose of ensuring that any proteins altered in abundance were changed specifically by treatment with miR-671-5p mimic or miR-671-5p inhibitor, non-targeting controls were used. A total of 958 and 467 proteins were changed by non-targeting mimic and non-targeting inhibitor, respectively. There were 1536 proteins differentially abundant following treatment with miR-671-5p mimic which were compared to the list changed by the non-targeting control, and any proteins appearing in both lists were removed. This process is shown in Figure 4.5. This left a total of 1252 proteins altered in abundance by overexpression of miR-671-5p in endometrial epithelial cells (Figure 4.6A). These proteins were significantly (FDR<0.05) overrepresented in multiple biological processes pertaining to transport (intracellular protein transport - 143 proteins, golgi vesicle transport - 65 proteins and vesicle mediated transport - 218 proteins) and localisation of proteins (231 proteins) (Figure 4.6B-C).

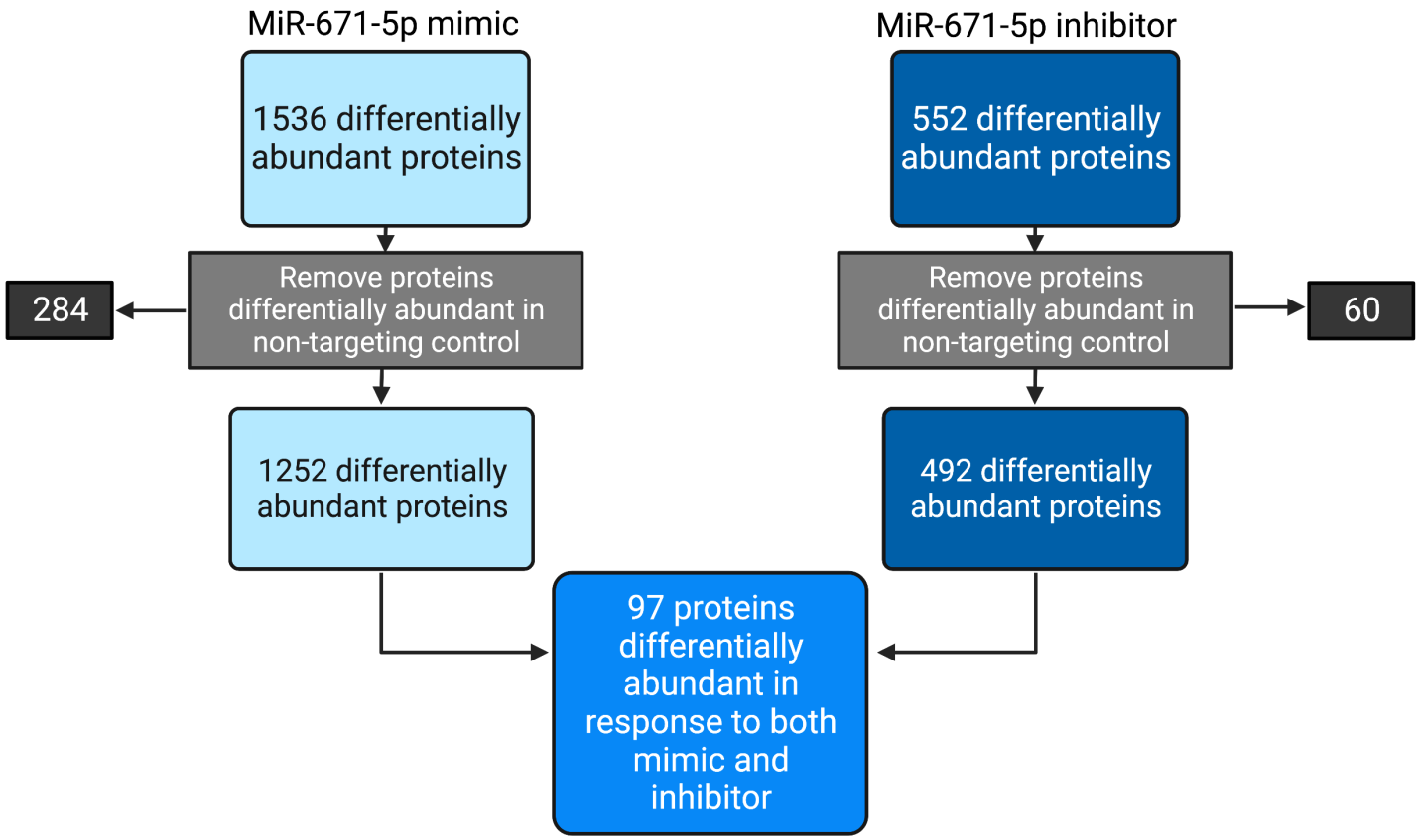

Figure 4.5: *Schematic diagram to summarise workflow for establishing lists of differentially abundant proteins for miR-671-5p mimic or inhibitor and those which are common to both.*
Lists of proteins differentially abundant in response to the mimic (1536) or inhibitor (552) were collated followed by removal of those which were also differentially abundant in response to the corresponding non-targeting control, leaving only proteins which are changed specifically in response to miR-671-5p mimic (1252) or miR-671-5p inhibitor (492). These lists were compared to deduce a list of proteins changed in response to both over and under expression of miR-671-5p (97).

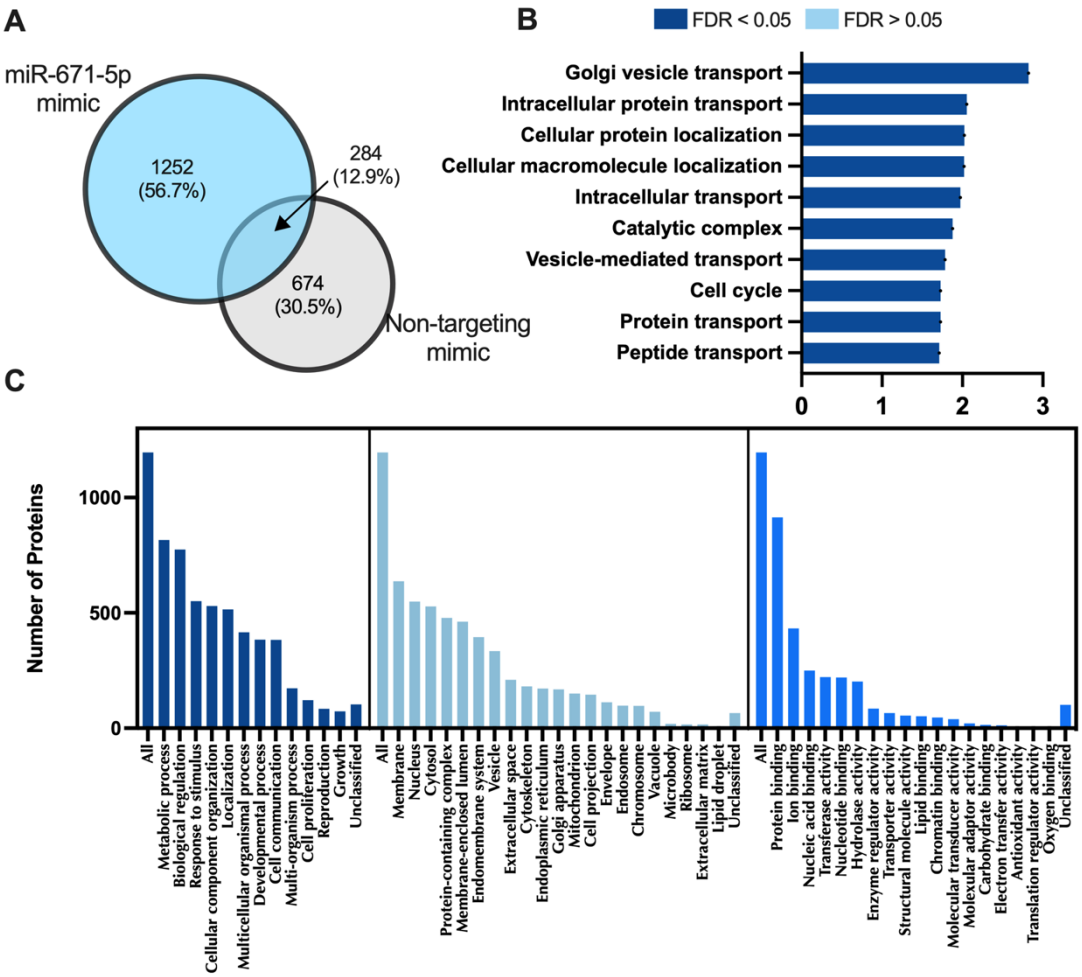

Figure 4.6: *Proteins altered in endometrial epithelial cells (Ishikawa) following treatment with miR-671-5p mimic.*
A) Venn diagram depicting total number of significantly differentially expressed proteins ($p<0.05$) following transfection of Ishikawa cells (n=3 biological replicates, 48 hrs) with miR-671-5p mimic (LHS) and non-targeting mimic (RHS). **B**) Enriched KEGG pathways associated with miR-671-5p mimic regulated proteins (FDR<0.05). **C**) WebGestalt overrepresentation analysis of biological process, cellular component, and molecular function categories for identified significantly differentially expressed proteins in response to miR-671-5p mimic (total of 1252). (Supplementary Table 19).

Further analysis of this set of proteins allows a break down into two lists, one containing proteins increased in abundance by miR-671-5p and one with those decreased in abundance (Figure 4.7). This further in-depth analysis counted proteins with the same gene names but different accession numbers - such as different fragments of a single protein - as separate proteins when examining in which direction they were changed. Initial analysis of overall proteins changed in abundance counted any duplicate gene names as one. Abundance of 670 proteins were increased following treatment with miR-671-5p mimic (Figure 4.8A), which are significantly (FDR<0.05) overrepresented in biological processes including organelle localization (45 proteins), golgi vesicle transport (38 proteins) and regulation of cell cycle (76 proteins) (Figure 4.8B). There were 589 decreased in response to miR-671-5p overexpression (Figure 4.8A), which were significantly (FDR<0.05) overrepresented in the cellular component the chaperone complex (11 proteins), as well as multiple localization (cellular protein localization - 110 proteins) and transport biological processes (intracellular transport - 108 proteins, protein transport - 190 proteins) (Figure 4.8C).

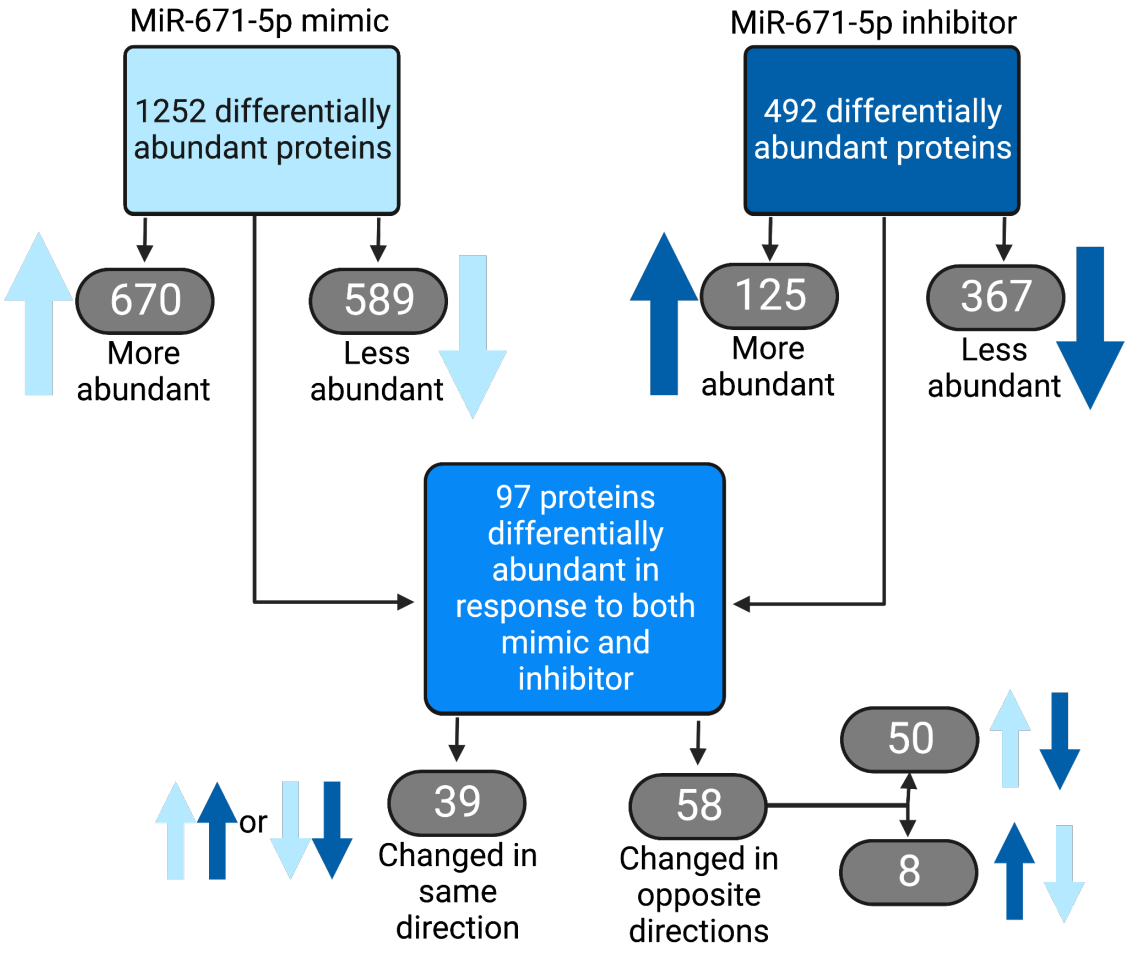

Figure 4.7: *Schematic diagram to demonstrate break down of numbers of proteins more or less abundant in response to altered expression of miR-671-5p.*
Diagram shows the number of proteins altered in abundance to be more or less abundant than the non-targeting mimic in response to miR-671-5p mimic or inhibitor. Also shows whether proteins that were changed in abundance in response to both miR-671-5p mimic or miR-671-5p inhibitor were changed in the same way (*i.e.*, both treatments result in more or less abundant) or opposite ways (*e.g.*, one treatment results in more abundant and one in less). Counts of proteins more or less abundant include duplicate gene names with different accession numbers.

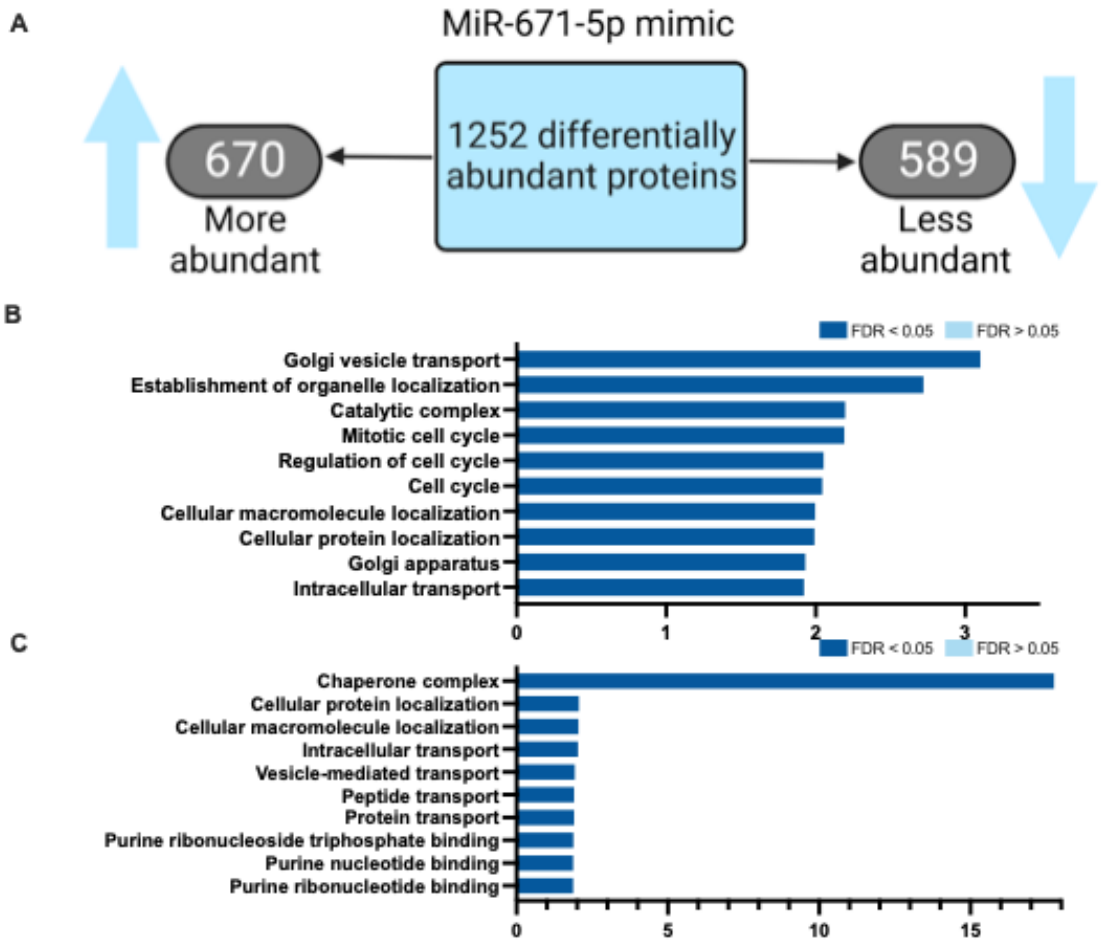

Figure 4.8: *Break down of numbers of proteins altered in abundance following 48 hr treatment of endometrial epithelial cells (n=3) with miR-671-5p mimic with regards to whether proteins were more or less abundant compared to non-targeting mimic control.*
Includes duplicate gene names with different accession numbers. **A**) Distribution of 1252 proteins altered in response to miR-671-5p mimic into categories of 'more abundant' or 'less abundant'. **B**) Enriched KEGG pathways associated with proteins which are more abundant in response to miR-671-5p mimic (FDR<0.05). **C**) Enriched KEGG pathways associated with proteins which are less abundant in response to miR-671-5p mimic (FDR<0.05). (Supplementary Table 20).

4.4.2.3 Protein abundance following inhibition of miR-671-5p

Following removal of 60 proteins also altered by the non-targeting inhibitor, miR-671-5p inhibition resulted in 492 differentially abundant proteins (Figure 4.9A). These proteins were significantly (FDR<0.05) overrepresented in cellular components the mitochondrion (71 proteins), whole membrane (74 proteins) and catalytic complex (64 proteins), as well as in biological processes associated with metabolism (rRNA metabolic process - 23 proteins, generation of precursor metabolites and energy - 33 proteins) (Figure 4.9B-C).

When examining the division of proteins within this group of 492 into those which are more, or less, abundant following inhibition of miR-671-5p, there were 125 and 367 respectively (Figure 4.10A). For the 125 which miR-671-5p inhibitor treatment caused increased abundance, the molecular function of translation was significantly (FDR<0.05) overrepresented (17 proteins), alongside biological processes such as ribosome biogenesis (11 proteins) and rRNA metabolic process (12 proteins) (Figure 4.10B). Oppositely, the 367 proteins which are less abundant in response to miR-671-5p inhibition demonstrate significant (FDR<0.05) overrepresentation in metabolism of many molecules including organophosphate (51 proteins), small molecules (82 proteins), organic acid (47 proteins), drugs (38 proteins) and carbohydrate derivatives (50 proteins) (Figure 4.10C). Interestingly, cellular protein localization is a biological process which is associated with proteins increased by miR-671-5p overexpression (121 proteins) (Figure 4.8B), but is also linked to those proteins which are decreased by miR-671-5p under expression (72 proteins) (Figure 4.10C), demonstrating the opposite activity of this process with opposing treatments.

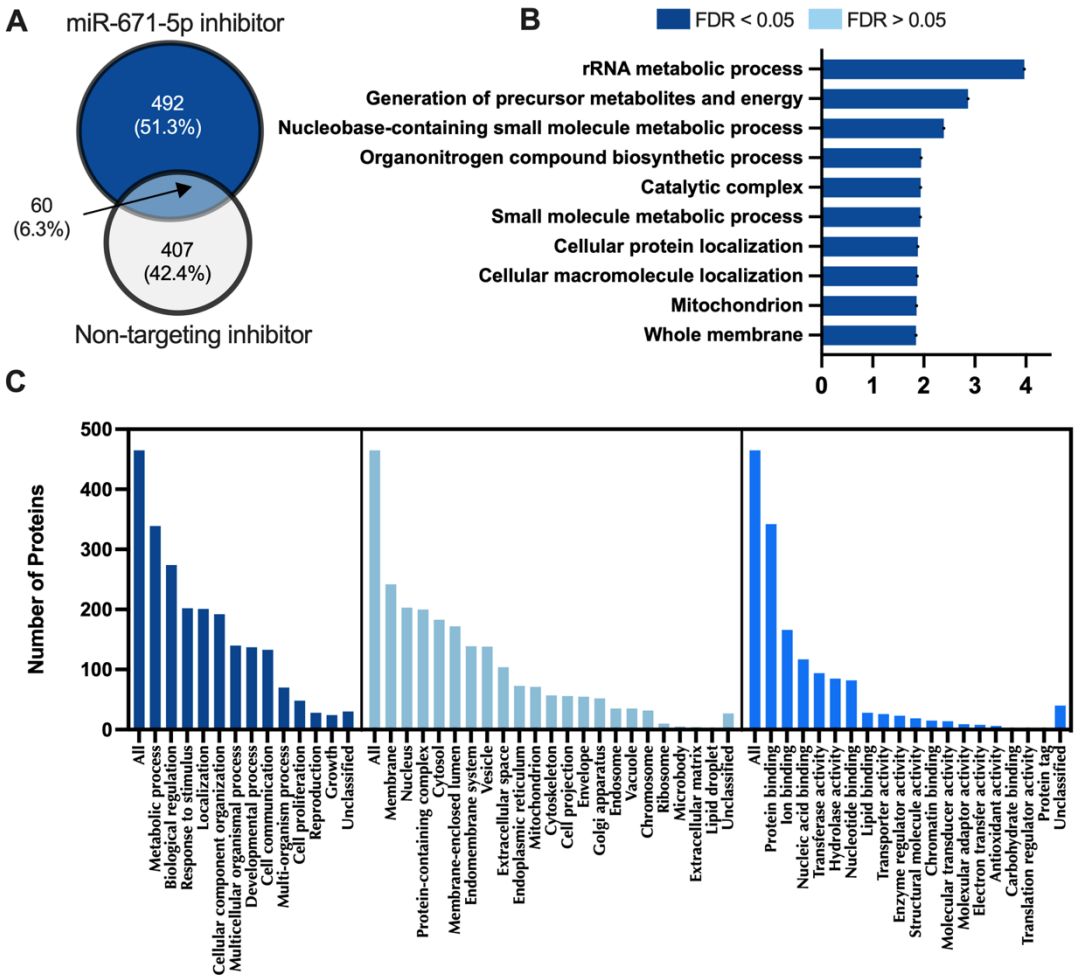

Figure 4.9: *Proteins altered in endometrial epithelial cells (Ishikawa) following treatment with miR-671-5p inhibitor.*
A) Venn diagram demonstrating total number of significantly altered proteins ($p<0.05$) following transfection of ishikawa cells (n=3 biological replicates, 48 hrs) with miR-671-5p inhibitor (top) and non-targeting inhibitor (bottom). **B**) Enriched KEGG pathways associated with miR-671-5p inhibition regulated proteins (FDR<0.05). **C**) WebGestalt overrepresentation analysis of biological process, cellular component, and molecular function categories for identified significantly differentially expressed proteins in response to miR-671-5p inhibitor (total of 492). (Supplementary Table 21).

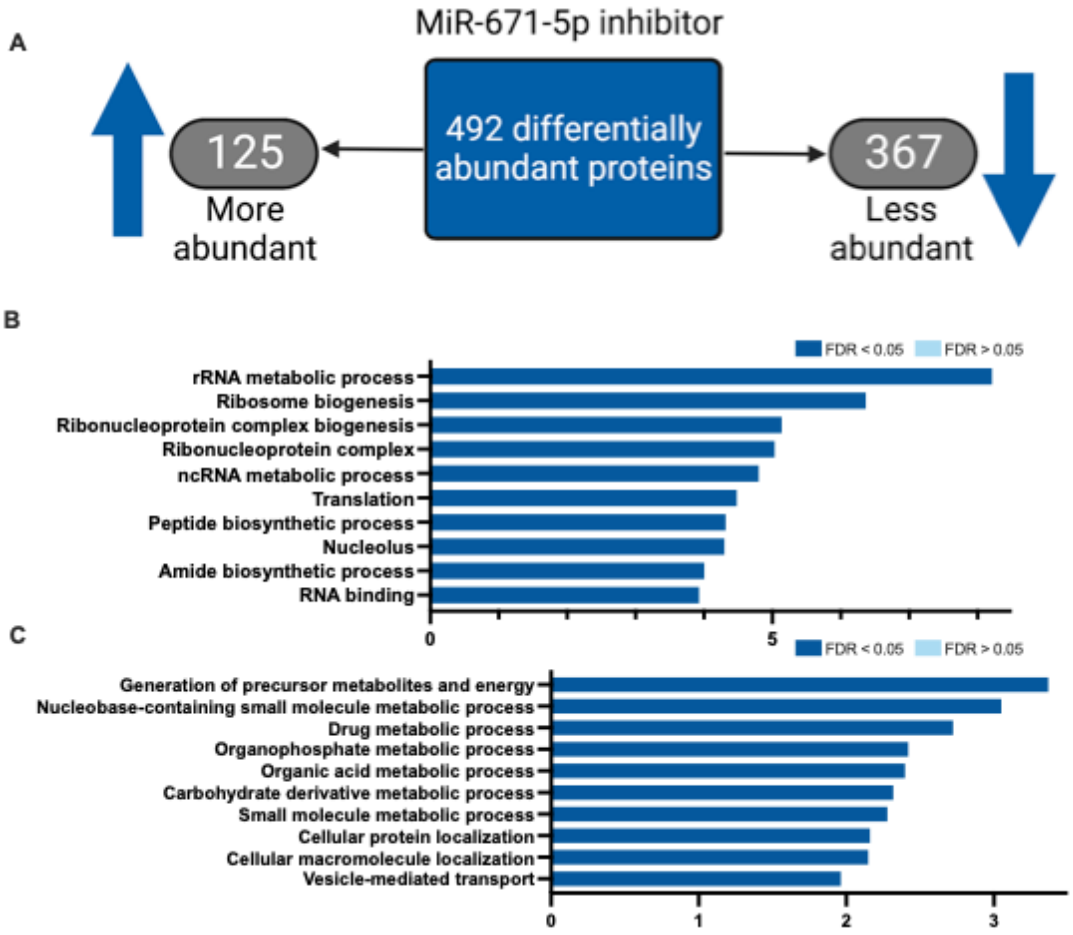

Figure 4.10: *Break down of numbers of proteins altered in abundance following 48 hr treatment of endometrial epithelial cells (n=3) with miR-671-5p inhibitor with regards to whether proteins were more or less abundant compared to non-targeting inhibitor control.*
Includes duplicate gene names with different accession numbers. **A**) Distribution of 492 proteins altered in response to miR-671-5p inhibitor into categories of 'more abundant' or 'less abundant'. **B**) Enriched KEGG pathways associated with proteins which are more abundant in response to miR-671-5p inhibitor (FDR<0.05). **C**) Enriched KEGG pathways associated with proteins which are less abundant in response to miR-671-5p inhibitor (FDR<0.05). (Supplementary Table 22).

4.4.2.4 Proteins altered in abundance in response to over and under expression of miR-671-5p

Comparison of proteins altered in abundance in response to miR-671-5p mimic, and those changed by miR-671-5p inhibitor provides a list of proteins common to both treatments, which consists of 97 proteins (Figure 4.11A). Four out of the 10 biological processes, molecular functions and cellular components for which these 97 proteins are significantly (FDR<0.05) overrepresented in centre around endoplasmic reticulum (ER) stress (negative regulation of response to ER stress - 5 proteins, negative regulation of endoplasmic reticulum unfolded protein response - 3 proteins, regulation of response to endoplasmic reticulum stress - 6 proteins, intrinsic apoptotic signaling pathway in response to endoplasmic reticulum stress - 5 proteins) (Figure 4.11B), a process important during early pregnancy. Their top biological process overall is biological regulation (62 proteins) (Figure 4.11C).

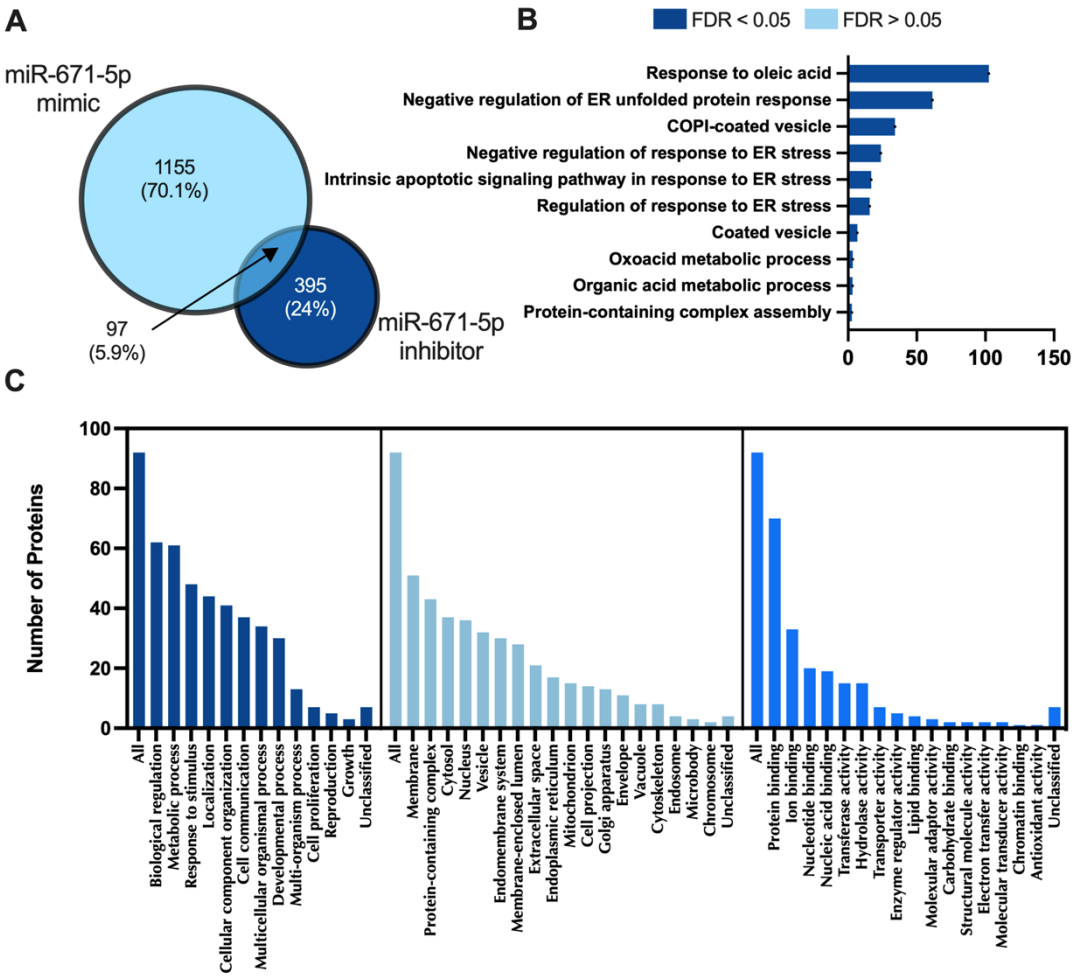

Figure 4.11: *Proteins altered in endometrial epithelial cells (Ishikawa) following treatment with miR-671-5p mimic or inhibitor.*
A) Venn diagram demonstrating total number of significantly altered proteins ($p<0.05$) following transfection of ishikawa cells (n=3 biological replicates, 48 hrs) with either miR-671-5p mimic (LHS) or inhibitor (RHS). **B**) Enriched KEGG pathways associated with miR-671-5p mimic and inhibition regulated proteins (FDR<0.05). **C**) WebGestalt overrepresentation analysis of biological process, cellular component, and molecular function categories for identified significantly differentially expressed proteins in response to miR-671-5p mimic and inhibitor (total of 97). (Supplementary Table 23).

Further investigation separated these proteins according to whether they were changed in the same way, or differently, in response to miR-671-5p mimic and inhibitor. This resulted in a group of 39 changed in the same direction (*i.e.,* in response to mimic and inhibitor treatment, the protein was more abundant in both cases, or less abundant in both cases) (Figure 4.7). Those proteins which were changed in the same way by either treatment (39) only had significant (FDR<0.05) overrepresentation in one molecular function which was response to oleic acid (3 proteins) (Figure 4.12A).

There were 50 proteins which were increased in abundance by overexpression of miR-671-5p but decreased following inhibition of miR-671-5p. Webgestalt analysis of proteins which were increased in abundance when miR-671-5p was overexpressed and decreased in abundance when inhibition of miR-671-5p was performed (50) are significantly (FDR<0.05) overrepresented in all of the previous biological processes linked to ER stress (Figure 4.12B). The fact that these processes are upregulated in response to over expression of miR-671-5p, and oppositely downregulated in response to inhibition, perhaps suggests that they are important processes miR-671-5p directly controls. COPI-coated vesicles (4 proteins) and coated vesicles (7 proteins) are cellular components for which these proteins are overrepresented, as well as biological processes concerning cellular protein localization (15 proteins).

Finally, 8 proteins were decreased by the mimic but increased by the inhibitor. This set of proteins which were decreased in abundance by miR-671-5p overexpression and increased in response to inhibition of miR-671-5p (8) are not significantly overrepresented in any biological processes, molecular functions or cellular components, likely due to the small sample size (Figure 4.12C). They are non-significantly most represented in testosterone dehydrogenase activity, PeBoW complex and neuregulin activity (1 protein each). It is likely that the processes these proteins are associated with are unrelated to their functions in the receptive endometrium as it has been shown that miR-671-5p is upregulated in response to progesterone (Edge et al., 2023), whereas these proteins are changed in the opposite situation.

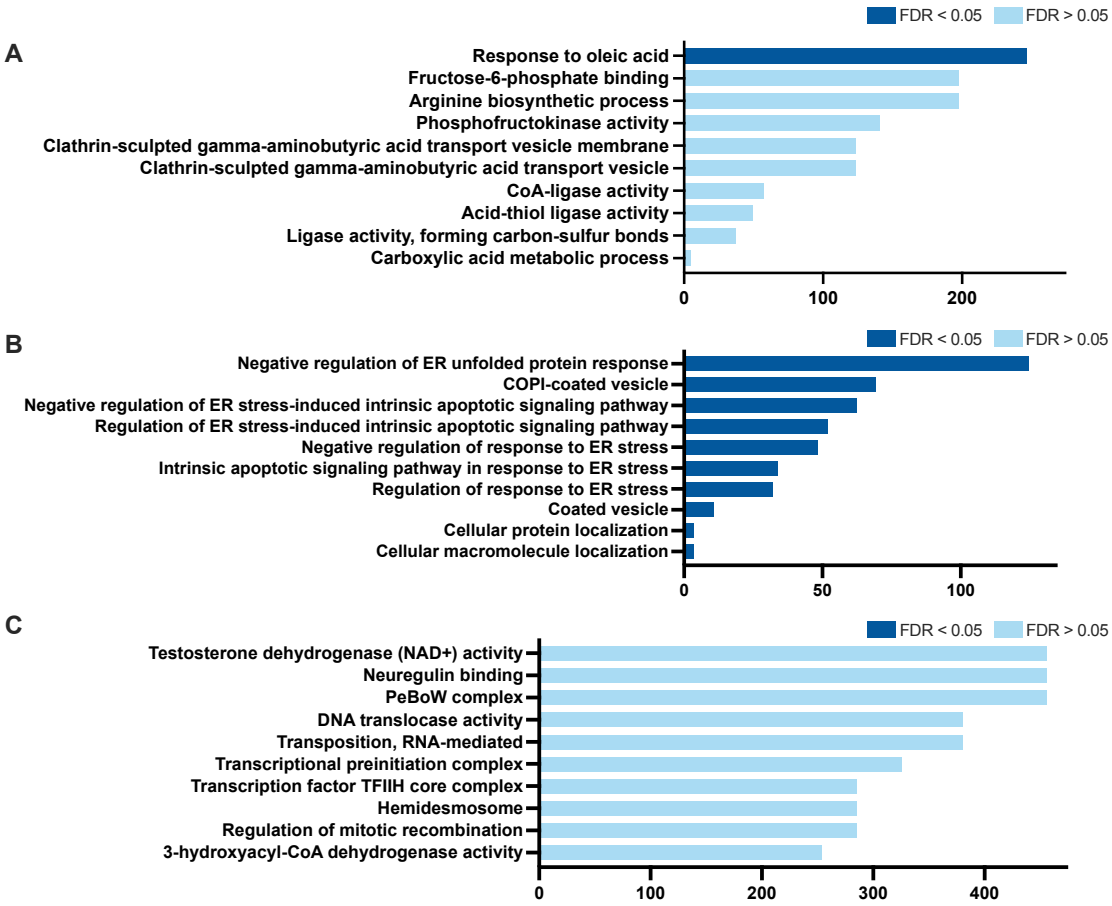

Figure 4.12: *Enriched KEGG pathways associated with proteins which are altered in Ishikawa cells (n=3) following transfection (48 hrs) by both miR-671-5p mimic and inhibitor.*

A) Enriched KEGG pathways for proteins altered in the *same* way by miR-671-5p mimic and inhibitor (*i.e.*, both increased or both decreased in abundance) (FDR<0.05). **B**) Enriched KEGG pathways for proteins increased by miR-671-5p overexpression and decreased by miR-671-5p inhibition (FDR<0.05). **C**) Enriched KEGG pathways for proteins decreased by miR-671-5p overexpression and increased by miR-671-5p inhibition (FDR<0.05). (Supplementary Table 24).

4.4.2.5 Proteins confirmed *in vitro* as targets of miR-671-5p, compared with miRDB predicted targets, and P4 regulated *in vitro* targets

Proteins which were changed in response to miR-671-5p mimic and/or inhibitor were compared to a list of predicted targets by miRDB. A small number - 95 - were common to both predicted targets and confirmed *in vitro* targets (Supplementary Figure 3A). Interestingly, despite this small sample size, their significantly (FDR<0.05) overrepresented biological processes still capture similar functions demonstrated by the previous analysis of just *in vitro* confirmed targets. For example, protein transport (18 proteins), vesicle-mediated transport (28 proteins) and cellular components of the golgi (golgi subcompartment - 17 proteins, golgi apparatus part - 17 proteins) all appear here (Supplementary Figure 3).

Confirmed *in vitro* targets and miRDB predicted targets were then compared with previous data of differentially expressed mRNAs in response to P4 in endometrial epithelial cells (Edge et al., 2023). Forty-six proteins satisfied all three categories (Figure 4.13A), so these proteins were subjected to further analysis. They were non-significantly (FDR>0.05) represented in biological processes of endocytosis (8 proteins) and multiple transport processes including golgi to lysosome (2 proteins) and vesicle-mediated transport (15 proteins). A cellular component they were represented in was the intrinsic component of the ER membrane (5 proteins) (Figure 4.13B-C).

Lastly, confirmation that the *in vitro* confirmed proteins altered in abundance in response to up or down regulated miR-671-5p were present in the human endometrium was required. Human endometrial biopsy sample RNASeq data was used (Lipecki et al., 2022) to achieve this. Of the proteins changed in abundance by miR-671-5p mimic, corresponding mRNAs for 94% were identified in RNASeq data (Figure 4.14). Of the 1,150 proteins, all but 8 were present in every one of the 36 patient samples. For proteins altered in abundance by miR-671-5p inhibitor, 95% had an mRNA counterpart in endometrial biopsy sample RNASeq data. There were only 8 which were absent from 1 or more patient samples.

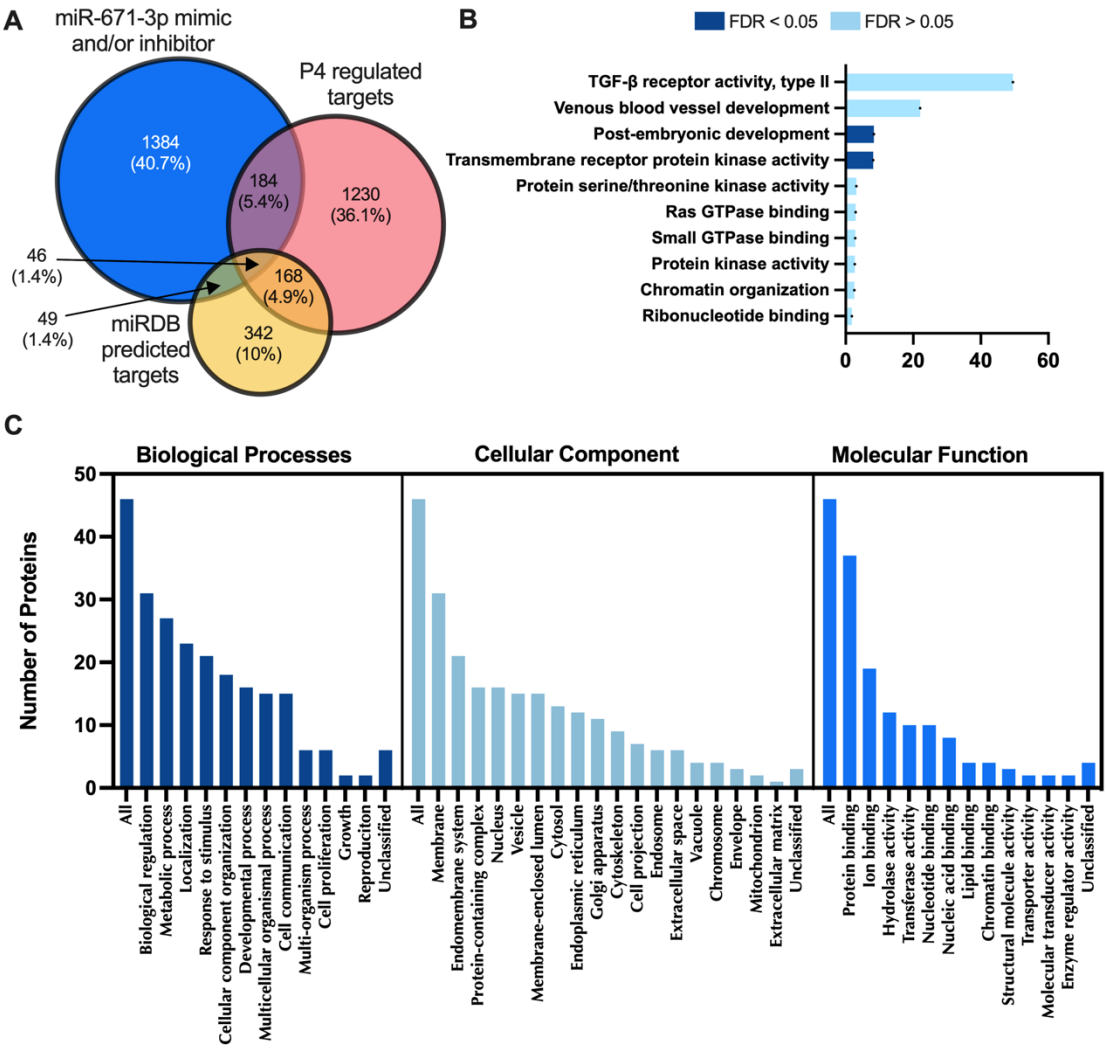

Figure 4.13: *Proteins significantly altered in abundance in response to miR-671-5p mimic and/or inhibition compared to miRDB predicted targets and P4 regulated mRNAs.*
A) Venn diagram showing total number of proteins significantly altered in abundance ($p<0.05$) following transfection of ishikawa cells (n=3 biological replicates, 48 hrs) with miR-671-5p mimic and/or inhibitor vs miRDB predicted targets vs progesterone regulated mRNAs (Edge et al., 2023). **B**) Enriched KEGG pathways associated with miR-671-5p mimic and/or inhibitor regulated proteins, miRDB predicted targets and P4 regulated mRNAs overlap (FDR<0.05). **C**) WebGestalt overrepresentation analysis of biological process, cellular component, and molecular function categories for identified significantly differentially abundant proteins in response to miR-671-5p mimic and/or inhibition, predicted targets and P4 regulated mRNAs overlap. (Supplementary Table 26).

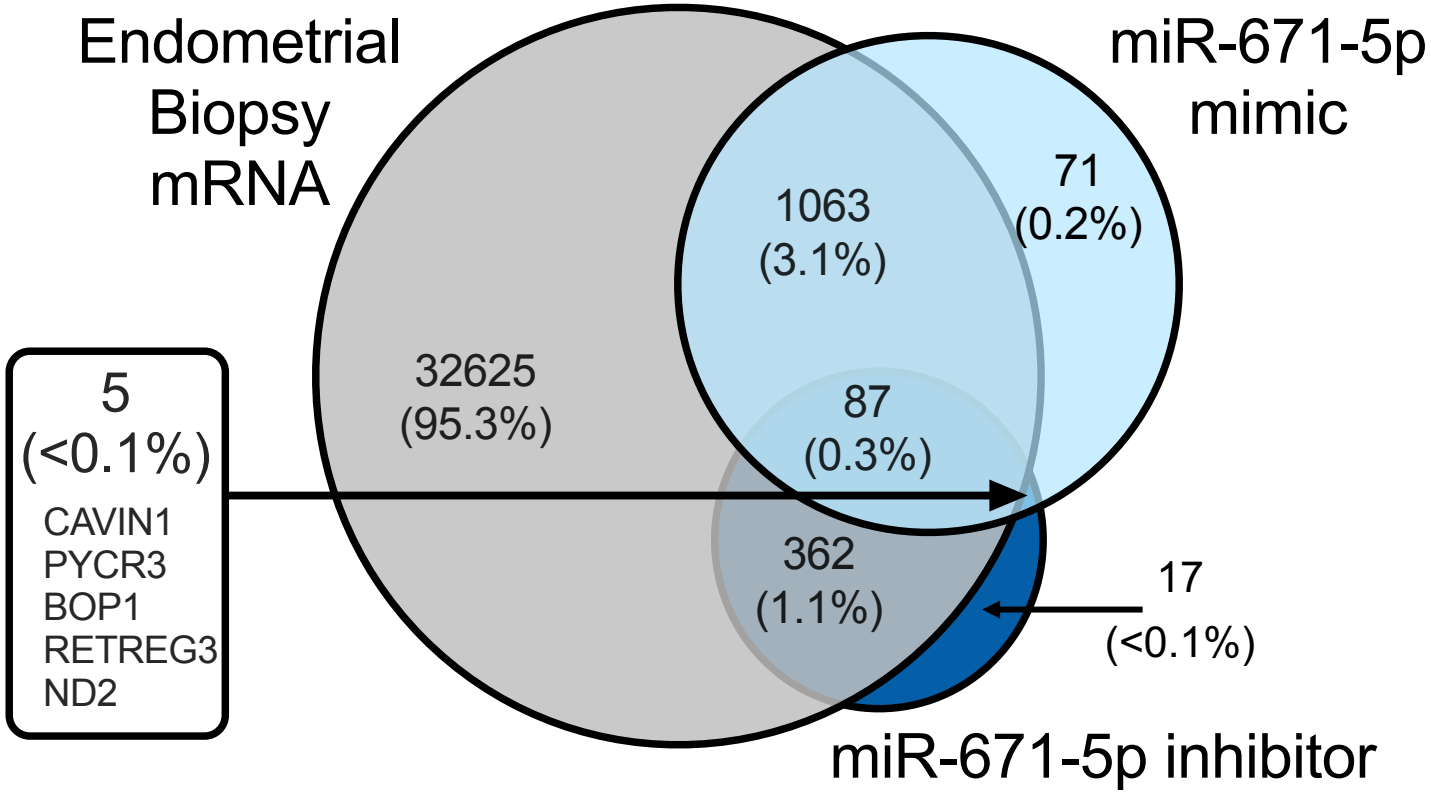

Figure 4.14: *Comparison of miR-671-5p regulated proteins with mRNA from human endometrial biopsies.*
Comparison of proteins significantly altered in abundance ($p<0.05$) in following transfection of endometrial epithelial (Ishikawa) cells (n=3 biological replicates, 48 hrs) with miR-671-5p mimic and/or inhibitor compared to RNASeq data from human endometrial biopsies (n=36 biological repeats, biopsies taken 4-12 days following ovulation)(Lipecki et al., 2022)**.** Listed proteins display 5 which are altered by both over and under expression of miR-671-5p, but are not detected in biopsies, suggesting they are not present physiologically. (Longer lists of proteins in each section of Venn diagram can be found in Supplementary Table 27A-D).

4.4.2.6 Differential protein abundance

Figure 4.15 is an example volcano plot showing the altered protein abundance in miR-671-5p mimic treated samples vs miR-671-5p inhibitor treated samples. Proteins displayed are significantly (orange - $p<0.05$), highly significantly (green - $p<0.05$ and $>1 Log_2FC$) or (purple - $p<0.05$ and >-1 Log_2FC) differentially abundant between these two treatment groups, highlighting the large number of proteins altered in response to this miRNA.

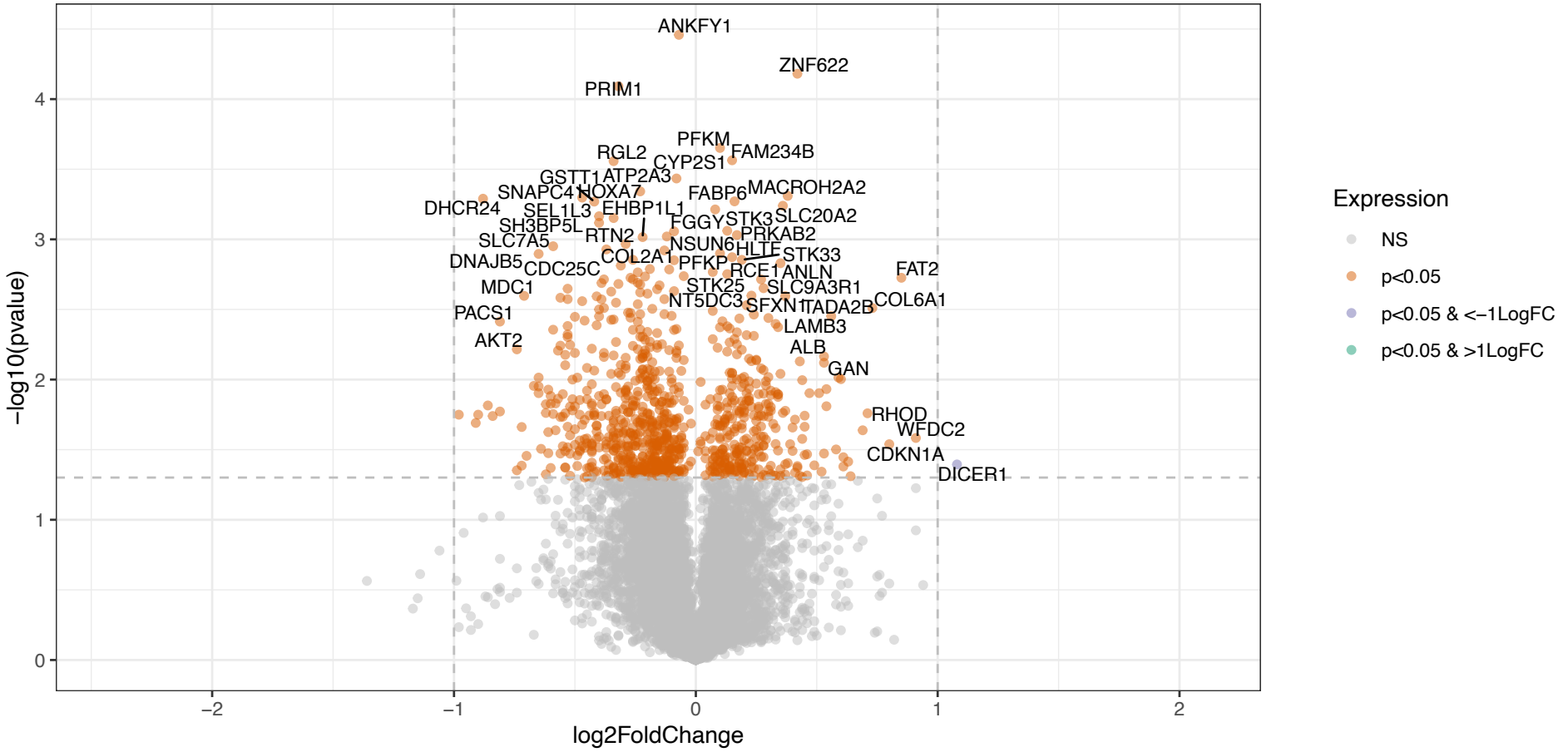

Figure 4.15: *Volcano plot showing abundance of proteins present in Ishikawa cells (n=3) transfected for 48 hrs with either miR-671-5p mimic or inhibitor highlighting those which are significantly differentially abundant between the two groups.*
Proteins which are significantly differentially abundant ($p<0.05$) between the two treatments are shown in orange, proteins which are highly significantly decreased in abundance ($p<0.05$ and $>-1Log_2FC$) are coloured purple, and those which are highly significantly increased in abundance abundant ($p<0.05$ and $>1Log_2FC$) are coloured green.

4.4.3 Comparison of miR-340-5p, miR-542-3p and miR-671 Proteomics Results

4.4.3.1 Proteins altered by mimic and/or inhibitors for miRNAs of interest

After analysis of each individual miRNA, results were compared between the miRNAs to determine whether they were altering abundance of the same proteins. Initially, lists of proteins changed by the mimic and/or the inhibitor for each miRNA were compared to each other (Figure 4.16A). There were 223 proteins differentially abundant in response to over and/or under expression of all 3 miRNAs. The top 10 significantly (FDR<0.05) overrepresented biological processes, cellular components and molecular functions are shown in Figure 4.16B. The ESCRT (endosomal sorting complex required for transport machinery) complex is the cellular component with the highest enrichment ratio, with 7 of the proteins altered by the miRNAs over and/or under expression also found in the gene set for ESCRT complex. Twenty-seven of the proteins were also overrepresented in the gene set for symbiont process, perhaps highlighting the use of these genes for the maternal epithelial cells to interact with a genetically different embryo.

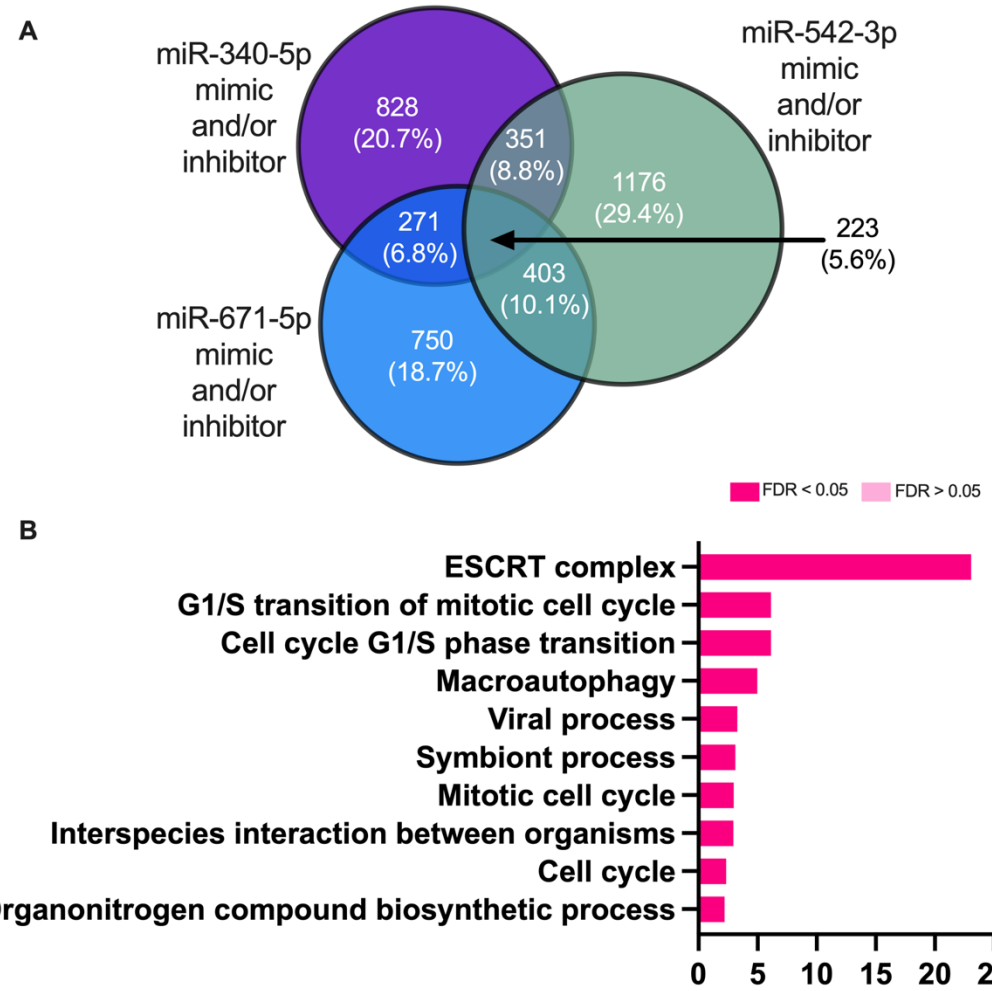

Figure 4.16: *Comparison of proteins differentially abundant in response to miR-340-5p, miR-542-3p and miR-671-5p mimic and/or inhibitor.*
A) Venn diagram showing comparison of differentially abundant proteins significantly altered in abundance ($p<0.05$) following transfection of Ishikawa cells (n=3 biological repeats, 48 hrs) with miR-340-5p mimic and/or inhibitor (purple), miR-542-3p mimic and/or inhibitor (green) or miR-671-5p mimic and/or inhibitor (blue). **B**) Enriched KEGG pathways associated with 233 proteins in common altered in abundance by all three of miR-340-5p mimic and/or inhibitor, miR-542-3p mimic and/or inhibitor and miR-671-5p mimic and/or inhibitor ($p<0.05$). (Supplementary Table 28).

4.4.3.2 Proteins altered by mimics for miRNAs of interest

When comparing proteins altered by each of the mimics for the 3 miRNAs, there is a set of 122 which are differentially abundant in response to miR-340-5p overexpression, miR-542-3p overexpression and miR-671-5p overexpression (Figure 4.17A). Five of these are still significantly (FDR<0.05) overrepresented in the ESCRT complex (Figure 4.17B). Cadherin binding is a biological process for which these proteins are overrepresented, with 11 differentially abundant proteins overlapping with this gene set. Most of the other top 10 biological processes, cellular components or molecular functions revolve around the cell cycle. Proper regulation of the cell cycle is important during establishment of endometrial receptivity and implantation.

Further analysis of proteins altered in abundance by all three of miR-340-5p mimic, miR-542-3p mimic and miR-671-5p mimic was carried out by splitting the proteins into those which were more abundant following treatment and those which were less abundant during treatment. There were 31 proteins significantly ($p<0.05$) more abundant following treatment with each of the miRNA mimics (Figure 4.18A), and 42 less abundant after overexpression of each of the miRNAs (Figure 4.18C). There were no significantly overrepresented processes associated with proteins increased in abundance in response to the miRNA mimics, however they had non-significant (FDR>0.05) representation in components of the ER and the ESCRT complex (Figure 4.18B). The proteins which were less abundant after treatment with each of the miRNA mimics had several significantly (FDR<0.05) overrepresented biological processes including autophagy - for which 9 of the proteins were in the gene set (Figure 4.18D). The same 9 were overrepresented in utilizing autophagic mechanism, and eight of these 9 were also overrepresented in the macroautophagy gene set.

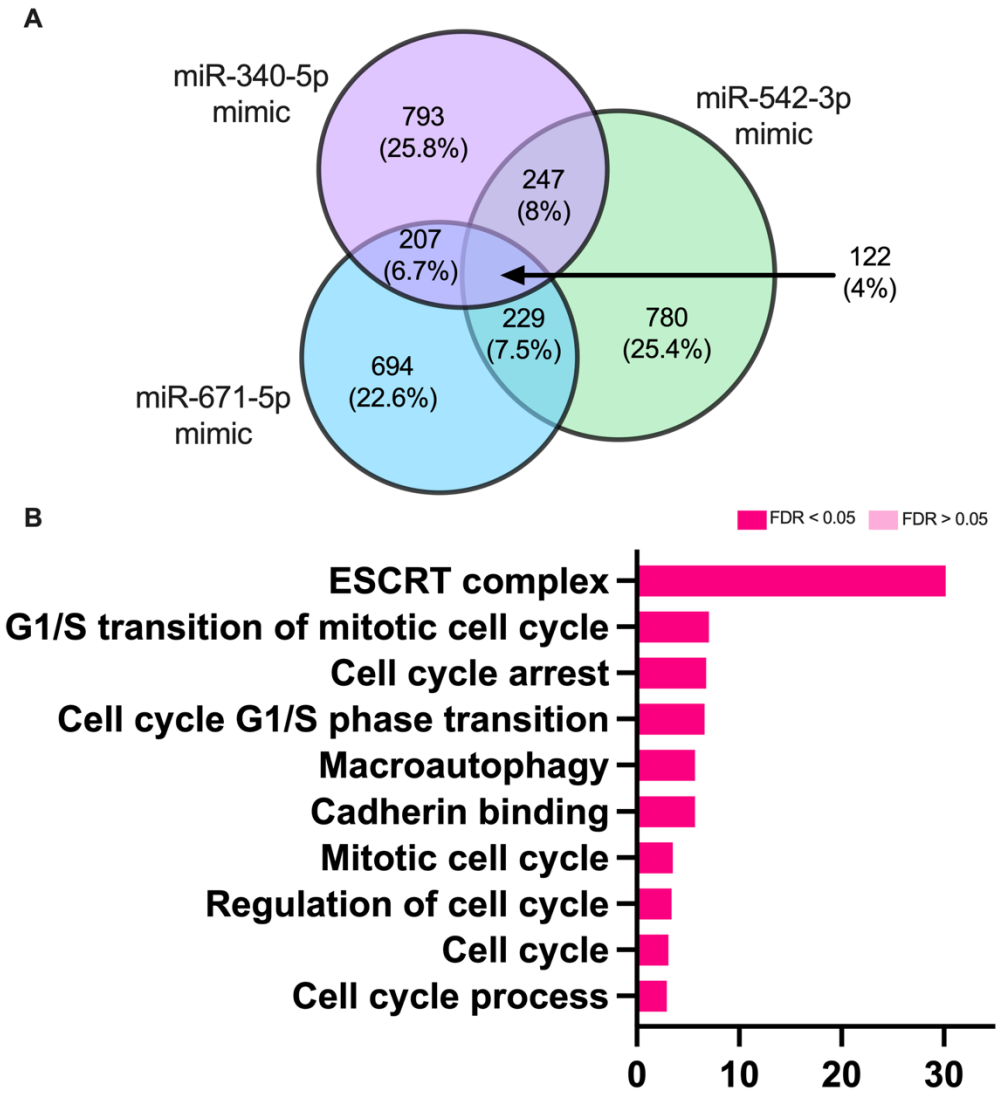

Figure 4.17: *Comparison of proteins differentially abundant in response to miR-340-5p, miR-542-3p and miR-671-5p mimic.*
A) Venn diagram showing comparison of differentially abundant proteins significantly altered in abundance ($p<0.05$) following transfection of Ishikawa cells (n=3 biological repeats, 48 hrs) with miR-340-5p mimic (purple), miR-542-3p mimic (green) or miR-671-5p mimic. **B**) Enriched KEGG pathways associated with 122 proteins in common altered in abundance by all three of miR-340-5p mimic, miR-542-3p mimic and miR-671-5p mimic ($p<0.05$). (Supplementary Table 29).

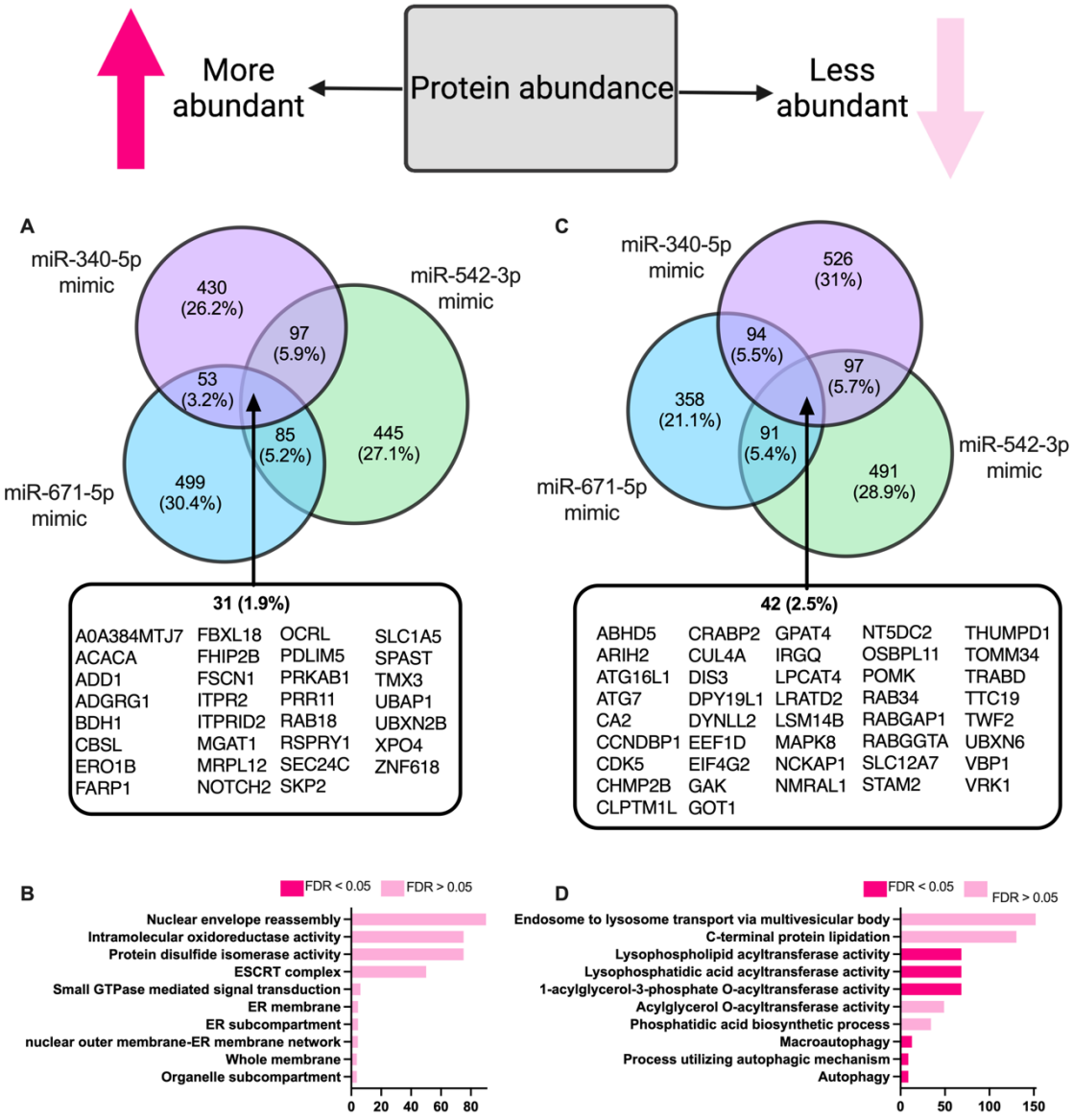

Figure 4.18: *Comparison of proteins **more** abundant in response to miR-340-5p, miR-542-3p and miR-671-5p mimic, and comparison of those which are **less** abundant.*
A) Venn diagram showing comparison of significantly **more** abundant proteins ($p<0.05$) following transfection of Ishikawa cells (n=3 biological repeats, 48 hrs) with miR-340-5p mimic (purple), miR-542-3p mimic (green) or miR-671-5p mimic. **B**) Enriched KEGG pathways associated with 31 proteins **more** abundant in response to all three of miR-340-5p mimic, miR-542-3p mimic and miR-671-5p mimic ($p<0.05$). **C**) Venn diagram showing comparison of significantly **less** abundant proteins ($p<0.05$) following transfection of Ishikawa cells (n=3 biological repeats, 48 hrs) with miR-340-5p mimic (purple), miR-542-3p mimic (green) or miR-671-5p mimic. **D**) Enriched KEGG pathways associated with 42 proteins **less** abundant in response to all three of miR-340-5p mimic, miR-542-3p mimic and miR-671-5p mimic ($p<0.05$). (Supplementary Table 30 and 31).

4.4.3.3 Proteins altered by inhibitors for miRNAs of interest

Inhibition of miRNAs miR-340-5p, miR-542-3p and miR-671-5p had a very small overlap of differentially abundant proteins of only 7 (Figure 4.19A). Downstream analysis of this set of proteins resulted in no significant overrepresentation in biological processes, likely due to having a small sample size. Non-significant (FDR>0.05) representation in pathways such as positive regulation of cellular respiration (1 protein) and protein stabilization (2 proteins) was found (Figure 4.19B).

Of the proteins altered in abundance for each of the 3 miRNAs, separation into those which were more abundant and those which were less abundant was carried out. A total of 2 proteins were more abundant in response to all 3 inhibition treatments (Figure 4.20A). Again, no significant overrepresentation was found for these proteins by Webgestalt analysis, but they seemed to be non-significantly (FDR>0.05) involved with RNA polymerase III action (Figure 4.20B). There were 5 proteins less abundant after treatment with miR-340-5p inhibitor, miR-542-3p inhibitor and miR-671-5p inhibitor (Figure 4.20C). Similarly, no significant overrepresentation in biological processes, cellular components or molecular functions were observed, however, interestingly golgi disassembly is presented here as a non-significant (FDR>0.05) representation for 1 of the proteins (Figure 4.20D). Functions involving the golgi apparatus were found to be associated with miR-671-5p mimic treatment in this chapter, potentially demonstrating the opposite effect occurs following inhibition of any of the P4 regulated miRNAs.

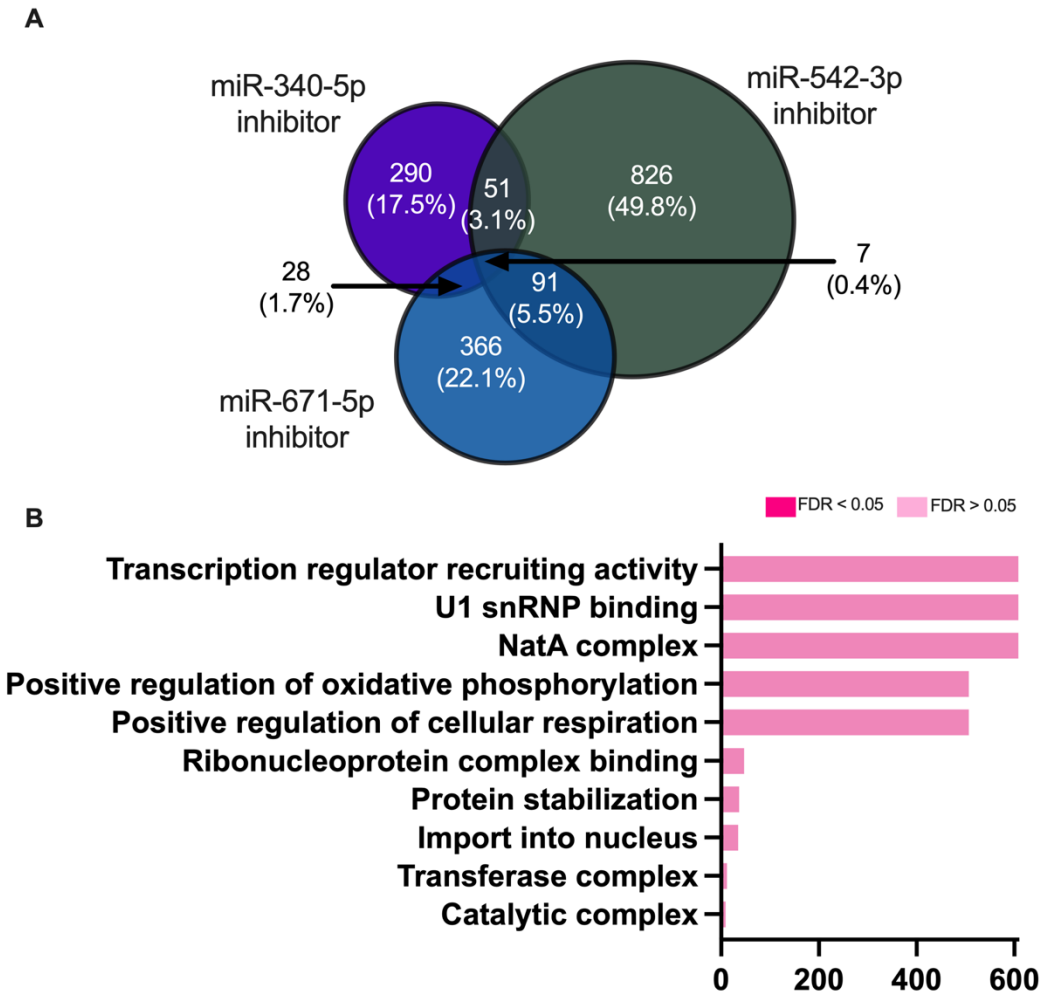

Figure 4.19: *Comparison of proteins differentially abundant in response to miR-340-5p, miR-542-3p and miR-671-5p inhibitor.*
A) Venn diagram showing comparison of differentially abundant proteins significantly altered in abundance ($p<0.05$) following transfection of Ishikawa cells (n=3 biological repeats, 48 hrs) with miR-340-5p inhibitor (purple), miR-542-3p inhibitor (green) or miR-671-5p inhibitor. **B**) Enriched KEGG pathways associated with 7 proteins in common altered in abundance by all three of miR-340-5p inhibitor, miR-542-3p inhibitor and miR-671-5p inhibitor ($p<0.05$). (Supplementary Table 32).

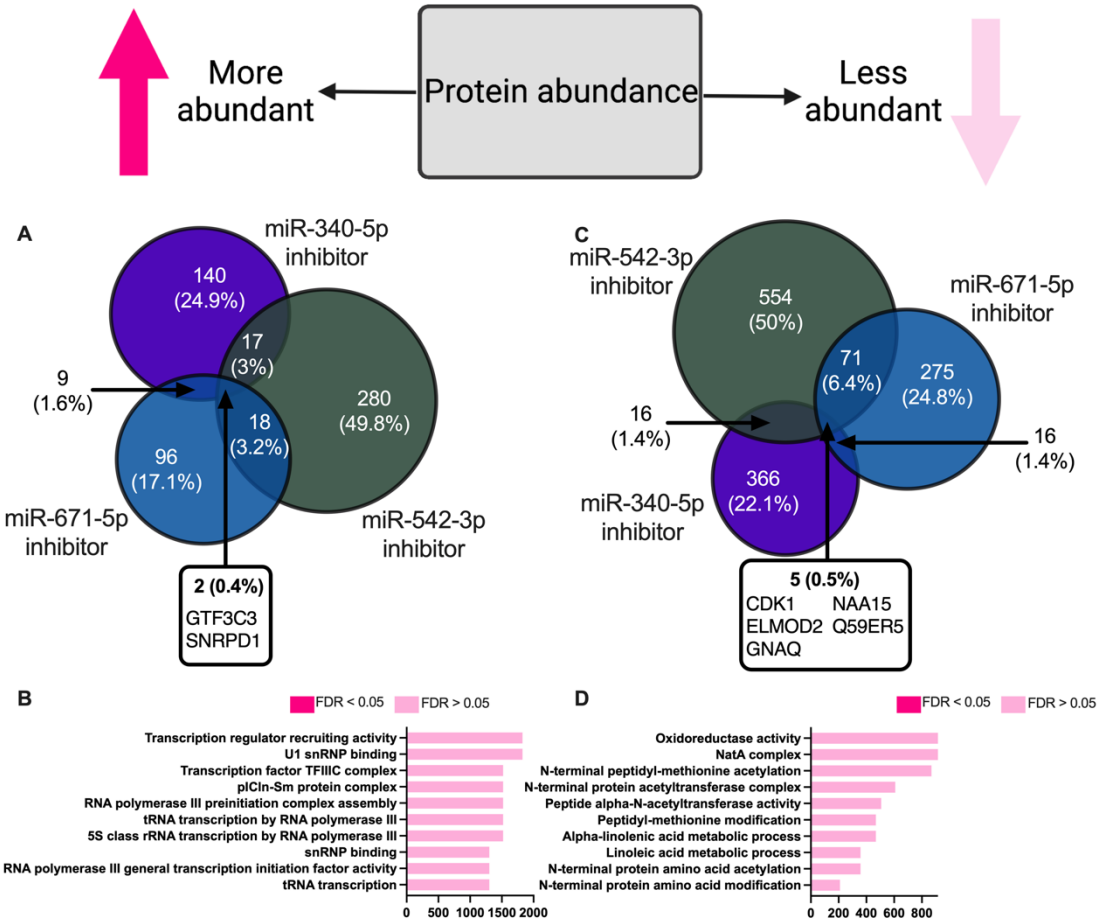

Figure 4.20: *Comparison of proteins **more** abundant in response to miR-340-5p, miR-542-3p and miR-671-5p inhibitor, and comparison of those which are **less** abundant.*

A) Venn diagram showing comparison of significantly **more** abundant proteins ($p<0.05$) following transfection of Ishikawa cells (n=3 biological repeats, 48 hrs) with miR-340-5p inhibitor (purple), miR-542-3p inhibitor (green) or miR-671-5p inhibitor. **B**) Enriched KEGG pathways associated with 2 proteins **more** abundant in response to all three of miR-340-5p inhibitor, miR-542-3p inhibitor and miR-671-5p inhibitor ($p<0.05$). **C**) Venn diagram showing comparison of significantly **less** abundant proteins ($p<0.05$) following transfection of Ishikawa cells (n=3 biological repeats, 48 hrs) with miR-340-5p inhibitor (purple), miR-542-3p inhibitor (green) or miR-671-5p inhibitor. **D**) Enriched KEGG pathways associated with 5 proteins **less** abundant in response to all three of miR-340-5p inhibitor, miR-542-3p inhibitor and miR-671-5p inhibitor ($p<0.05$). (Supplementary Table 33 and 34).

4.4.3.4 Proteins altered by mimic and inhibitor for each miRNA of interest

Lastly, proteins altered for each miRNA in response to both the mimic AND the inhibitor were compared between miRNAs (Figure 4.21A). No proteins satisfied all 3 categories. Small overlaps of proteins were found between each pair of miRNAs - 3 in common between miR-340-5p and miR-542-3p, 4 in both miR-340-5p and miR-671-5p, and a total of 9 proteins the same for miR-542-3p and miR-671-5p. Figure 4.21B and C demonstrate no statistically significant (FDR>0.05) overrepresented biological processes, cellular components or molecular functions for the 3 (Figure 4.21B) or 4 (Figure 4.21C) proteins common to miR-340-5p and miR-542-3p or miR-340-5p and miR-671-5p, respectively. Fascinatingly, for those 9 proteins which overlap between miR-542-3p and miR-671-5p, all of the most significantly (FDR<0.05) overrepresented functions are associated with ER stress response and unfolded protein response, despite the small sample size (Figure 4.21D).

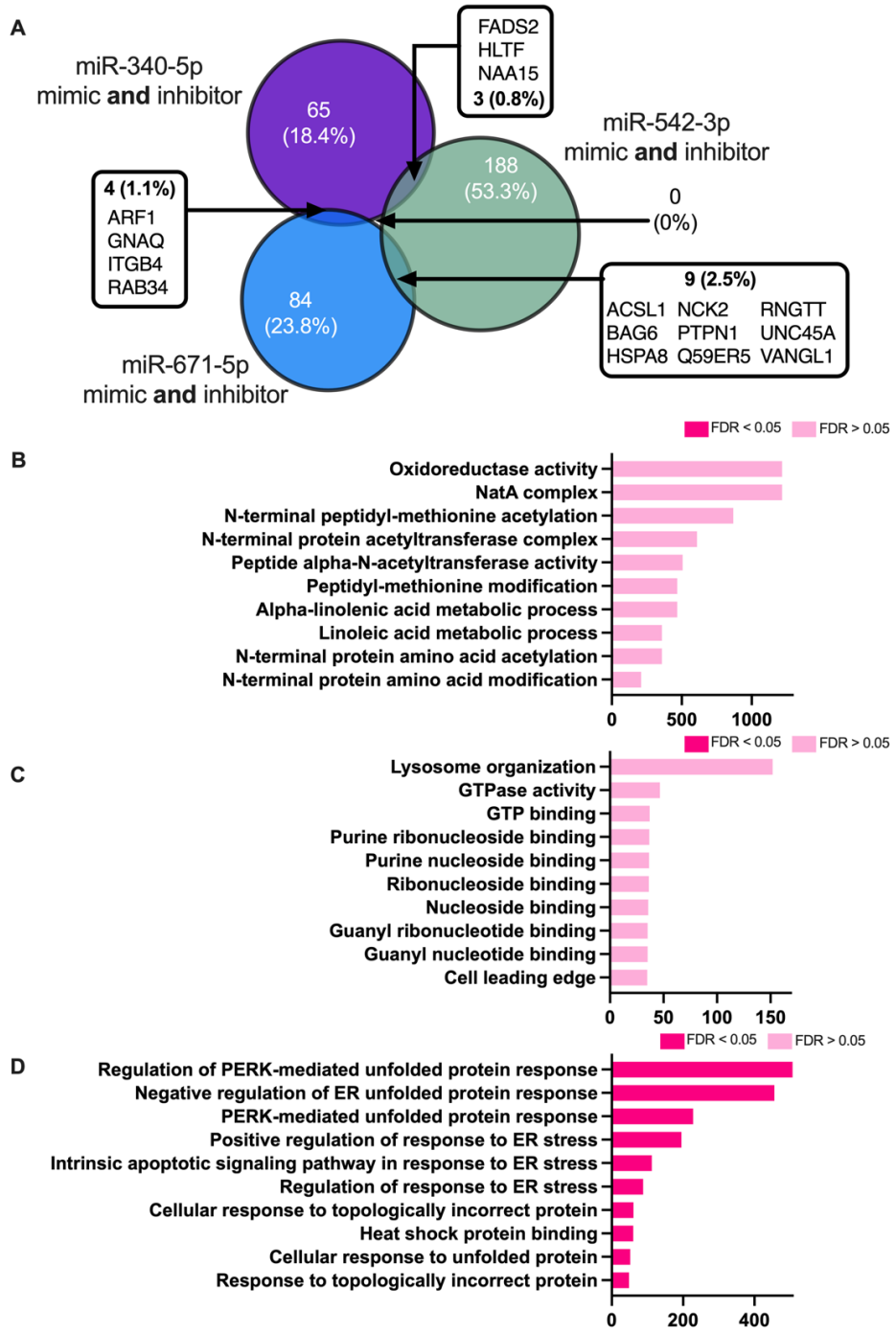

Figure 4.21: *Comparison of proteins differentially abundant in response to both miR-340-5p, miR-542-3p and miR-671-5p mimic **and** inhibitor.*
A) Venn diagram showing comparison of differentially abundant proteins significantly altered in abundance ($p<0.05$) following transfection of Ishikawa cells (n=3 biological repeats, 48 hrs) with miR-340-5p mimic **and** inhibitor (purple), miR-542-3p mimic **and** inhibitor (green) or miR-671-5p mimic **and** inhibitor. **B**) Enriched KEGG pathways associated with 3 proteins in common altered in abundance by miR-340-5p mimic **and** inhibitor as well as miR-542-3p mimic **and** inhibitor. **C**) Enriched KEGG pathways associated with 4 proteins in common altered in abundance by miR-340-5p mimic **and** inhibitor as well as miR-671-5p mimic **and** inhibitor ($p<0.05$). **D**) Enriched KEGG pathways associated with 9 proteins in common altered in abundance by miR-542-3p mimic **and** inhibitor as well as miR-671-5p mimic **and** inhibitor. (Supplementary Table 35).

4.5 Discussion

This chapter tested the hypothesis that an evolutionarily conserved, P4 regulated miRNA - miR-671-5p - modifies the expression of protein coding regions of the genome and may facilitate receptivity to implantation in humans. P4 signalling is vital for establishing endometrial receptivity, without which implantation is impossible (Taraborrelli, 2015). Previous work from our lab revealed that miR-671-5p is upregulated when endometrial epithelial cells are treated with P4 *in vitro.* To gain insight into the mechanistic purpose of this, the proteome of the endometrial epithelium after treatment with miR-671-5p mimic or inhibitor was examined. In this chapter, I have determined pathways that are associated with proteins which are differentially abundant in response to miR-671-5p over or under expression. These pathways are likely P4 regulated through overexpression of miR-671-5p. Furthermore, I have compared proteins altered by miR-671-5p with those altered by two other miRNAs of interest, P4 regulated, evolutionarily conserved miR-340-5p and miR-542-3p, to investigate whether their targets and purposes are similar. I have established pathways these protein targets common to each miRNA are involved in to examine the collaborative effect of these P4 regulated miRNAs in the endometrial epithelium.

4.5.1 Proteins altered in abundance in response to differential expression of miR-671-5p

Proteins changed in abundance by overexpression of miR-671-5p in endometrial epithelial cells highlighted many potential pathways associated with protein localization and transport. Those which are increased in abundance are mainly linked to roles in the cell cycle and golgi vesicle transport, whereas those which are decreased in abundance are mostly involved in localization and transport. At this stage of the cycle, proliferation is halted in endometrial epithelial cells. The fact that so many proteins associated with the cell cycle are upregulated following overexpression of miR-671-5p does not necessarily mean that proliferation is increased; rather, these proteins could be functioning to inhibit proliferation.

Cullin 5 (CUL5) is a protein upregulated by miR-671-5p and implicated in the molecular function regulation of cell cycle. This protein is observed in other systems to inhibit proliferation; in a rat endothelial cell line CUL5 overexpression causes reduced proliferation (Bradley et al., 2010). Furthermore, using a hamster ovary model, CUL5 was found to inhibit proliferation and cell growth by disruption of phosphorylation of MAPK which increased the concentration of p53 (Van Dort et al., 2003). This is interesting as in the current investigation, whilst p53 is not identified as significantly more abundant, tumour protein p53-

inducible protein 11 (TP53I11) is. This protein is induced by p53 and has been found to control proliferation and apoptosis in non-small cell lung cancer cells; with its downregulation associated with increased proliferation and its upregulation having an inhibitory effect - also under the control of another miRNA - miR-645 (B. Zhu et al., 2020). Taken together, this suggests that P4 induced upregulation of miR-671-5p controls and inhibits proliferation of endometrial epithelial cells in the early secretory phase through upregulation of CUL5 and TP53I11.

STAT3 is another protein increased in abundance in response to overexpression of miR-671-5p, and is also associated with regulation of cell cycle, with reports of its involvement in both up and down regulation of proliferation in different cancers (Tolomeo and Cascio, 2021). This protein is also highlighted as one which is upregulated by miR-340-5p overexpression, and as previously discussed in Chapter 2, absence of STAT3 in the endometrium results in implantation failure (Hiraoka et al., 2020). These results suggest that miR-340-5p and miR-671-5p may work together to increase STAT3 abundance to facilitate implantation and regulate proliferation. Further evidence for the necessity of STAT3 expression is provided by Pawar et al., (2013), where the knockdown of it in the endometrial epithelial cells causes infertility in mice due to failed embryo attachment. Additionally, inhibition of STAT3 in the epithelial cells causes impaired decidualization in the stromal cells. This emphasises the participation of the epithelial layer in the correct functioning of the stromal layer during early pregnancy events and highlights that cell-to-cell communication between the two cell types is present and important. This suggests that miR-671-5p upregulation in the endometrial epithelium is involved in communication with the stromal layer and plays a role in correct decidualization. In fact, there is evidence that miR-671-5p is itself transported between cells - with mesenchymal stem cells releasing extracellular vesicles containing miR-671-5p, which in this system has an effect on pulmonary inflammatory conditions (Lian et al., 2023). It is therefore not out of the question that miR-671-5p may be transported from epithelial cells to stromal cells to participate in decidualization processes. However, due to the previous evidence suggesting that STAT3 deletion in the epithelial cells affects stromal decidualization, the transport of proteins altered in abundance by P4 induced miR-671-5p overexpression to the stromal cells may explain some mechanisms more accurately.

Many of the overrepresented processes linked to the proteins that are changed in abundance in response to both over and under expression of miR-671-5p concern the regulation of endoplasmic reticulum (ER) stress. One of the ER's

roles is responsibility for the correct folding of proteins and performing posttranslational modifications to them (Braakman and Bulleid, 2011). When the capacity for the process of protein folding becomes saturated, the cell experiences ER stress, distinguished by the aggregation of misfolded proteins (Navid and Colbert, 2017). This triggers the unfolded protein response (UPR), which works to resolve the problem in three ways. Protein synthesis may be halted or slowed to avoid adding to the accumulated misfolded proteins. The UPR will also instigate removal of misfolded proteins by ER-associated degradation (ERAD) or through lysosomes (Read and Schröder, 2021). Expansion of the ER to accommodate more protein folding machinery and ability is another method of regulating ER stress (Walter and Ron, 2011). If ER stress is prolonged, the actions of the UPR may not be sufficient to reverse the stress, and this will usually trigger apoptosis (Tabas and Ron, 2011). During stromal cell decidualization, the resulting cells are required to produce a higher volume of proteins, and the UPR is triggered by ER stress caused by this (Soczewski et al., 2020). Inhibition of ER stress and UPR in stromal cells results in reduced invasive ability of the blastocyst into the endometrium (Grasso et al., 2018). With so many of the overrepresented processes centring around ER stress and UPR that are associated with proteins altered in abundance in response to miR-671-5p overexpression and inhibition, it is likely this miRNA is participating in stromal cell decidualization by regulating ER stress. There were 58 proteins which were altered in opposite ways in response to over or under expression of miR-671-5p, highlighting these proteins as direct targets of miR-671-5p, likely mediated by P4 *in vivo.* The 50 proteins which show increased abundance in response to miR-671-5p mimic and decreased abundance in response to miR-671-5p inhibition (Figure 4.12B) are significantly overrepresented in molecular functions of both regulation of response to ER stress and negative regulation of response to ER stress along with regulation and negative regulation of ER stress induced intrinsic apoptotic signalling pathway. This emphasises the necessity for - and involvement of miR-671-5p in - tightly controlled ER stress response and apoptosis; in that at least some level of ER stress and UPR is vital for decidualization and pregnancy - as demonstrated by prohibition of these processes having negative effects on blastocyst implantation (Grasso et al., 2018). The ER is also the origin of the secretory pathway, with many proteins destined for secretion travelling via the ER (Braakman and Bulleid, 2011). It is therefore not unconceivable that the proteins upregulated in response to miR-671-5p associated with ER stress response are secreted and intended to be received by the endometrial stromal cells. In fact, as already discussed; during ER stress, mechanisms are employed within the cell to minimise ER stress by downregulating transcription

of proteins. Therefore since 1) ER stress and UPR is required for implantation, 2) correct regulation of ER stress is vital and 3) protein synthesis is downregulated during UPR; it would be logical that regulatory proteins would be produced externally - *i.e*., in the epithelial cells - and transported to the stromal cells to carry out their functions. Overexpression of miR-671-5p was actually reported to play a role in promoting ER stress by upregulating an ER stress associated gene *ATP2A3* in epithelial cells in periodontitis (Sun and Zhu, 2023). In the current study, the protein encoded by this gene is not differentially abundant, however ATP2A2 protein is significantly increased in abundance - which is also an ER stress associated gene. Overall, this highlights, and provides more evidence for, the possibility that miR-671-5p produced in the epithelial cells regulates ER stress in the stromal cells through altering abundance of proteomes destined to be transported to the stromal layer and in turn facilitates the invasion stage of implantation. A summary of the findings in this Chapter which are associated with P4 mediated altered expression of miR-671-5p is shown in Figure 4.22 and Table 4.1.

Overall, these data demonstrate that miR-671-5p plays a role in modifying the proteome of the endometrial epithelium. It's up and down regulation causes changes in the abundance of 1252 and 492 proteins respectively, with 97 proteins in common. Target prediction software identifies a surprisingly small proportion of these *in vitro* confirmed targets - emphasising the unreliability of predicting miRNA targets. Only 230 of the 1614 proteins altered in abundance by either the miR-671-5p mimic and/or inhibitor treatment were identified in previous P4 regulated mRNAs (Edge et al., 2023). This may be due to the fact that P4 treatment increases expression of miR-671-5p, and so any proteins altered by inhibition of miR-671-5p would not be in the P4 regulated data. Subsequently, the proteins showing decreased abundance in response to overexpression of miR-671-5p would not be identified in P4 regulated data either.

In conclusion, we propose that miR-671-5p has a role in regulating the endometrial epithelial cell proteome in order to control cell proliferation. Furthermore, we suggest that miR-671-5p is involved in regulation of stromal cell decidualization via control of ER stress and UPR by epithelial to stromal cell communication and transport of target proteins.

Table 4.1: Summary of key proteins altered by differential expression of miR-671-5p in endometrial epithelial (Ishikawa) cells and their physiologically relevant functions in other system(s).

Protein	Effect on protein abundance following differential expression of miR-542-3p	Role in other system(s)	Reference
CUL5 Cullin 5	*Increased* in abundance following overexpression of miR-671-5p	Overexpression of CUL5 inhibits proliferation in rat endothelial cell line Inhibition of proliferation and cell growth	(Bradley et al., 2010) (Van Dort et al., 2003)
STAT3	*Increased* in abundance following overexpression of miR-671-5p	Involvement in up or down regulation of proliferation in various cancers Absence of STAT3 results in implantation failure	(Tolomeo and Cascio, 2021) (Hiraoka et al., 2020)
NCK2 - NCK adaptor protein 2, PTPN1 - Protein tyrosine phosphatase, non-receptor type 1, WFS1 - Wolframin ER transmembrane glycoprotein,	Altered in abundance by both miR-671-5p overexpression and underexpression	Significantly enriched in processes associated with regulation of endoplasmic reticulum (ER) stress and unfolded protein response (UPR). ER stress and UPR linked to endometrial decidualisation. Inhibition of this results in reduced embryo invasion	(Soczewski et al., 2020)(Grasso et al., 2018)

HYOU1 - hypoxia upregulated 1 UBE2G2 - ubiquitin conjugating enzyme E2 G2 BAG6 - Bcl2 associated athanogene 6			

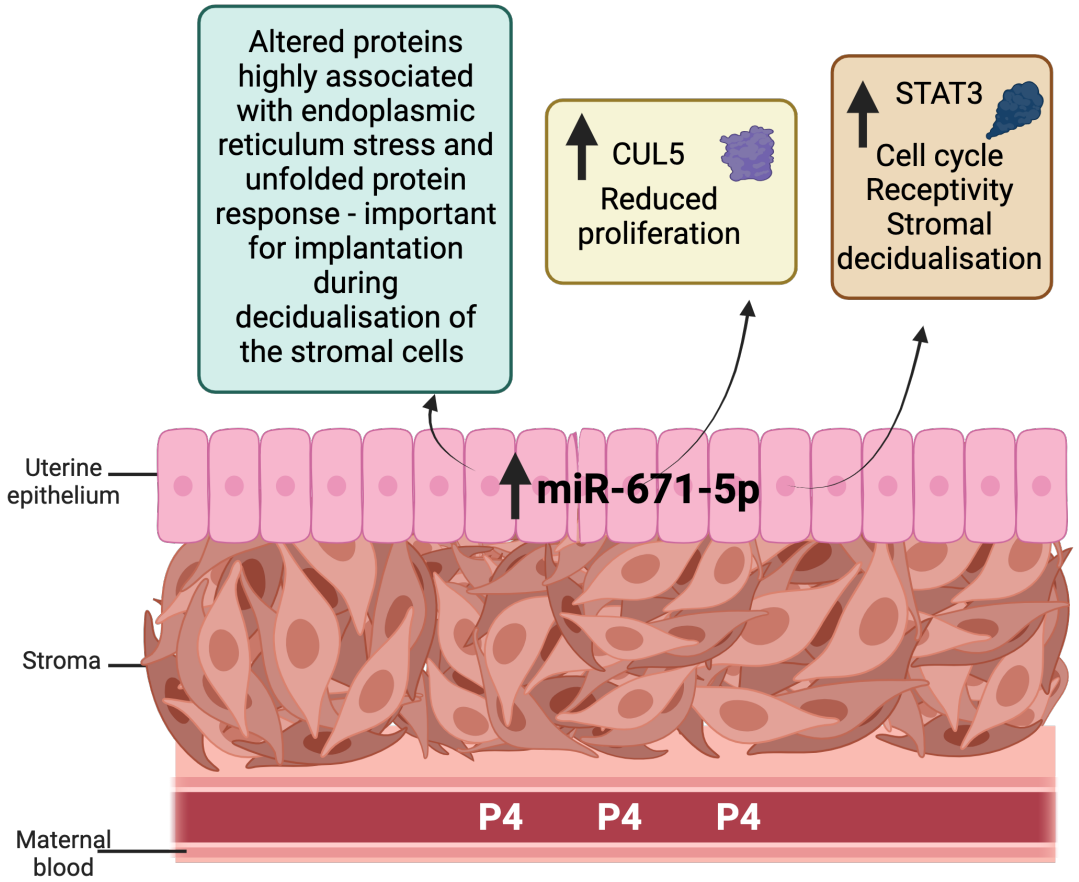

Figure 4.22: *Diagram summarising key proteins and processes altered by miR-671-5p in the endometrial epithelium which may be important for early pregnancy*.
Proteins included in figure are those altered in abundance by differentially expressed miR-671-5p and linked to endometrial function in the literature Figure created using Biorender.com

4.5.2 Comparing proteins altered in abundance by differential expression of miR-340-5p, miR-542-3p and miR-671-5p

Interestingly, similar results were seen when examining overrepresentation of proteins altered by both miR-671-5p mimic and inhibitor, and miR-542-3p mimic and inhibitor. Proteins displayed significant overrepresentation in multiple pathways surrounding positive and negative regulation of ER stress - suggesting miR-542-3p and its targets may also be involved in tightly controlling ER stress.

There are 223 differentially abundant proteins in response to differential expression (either up, down, or both) of miR-340-5p, miR-542-3p and miR-671-5p. An overrepresented pathway associated with these proteins is symbiont process - with 27 of the *in vitro* confirmed protein targets involved. A protein in this group - cyclin A2 (CCNA2) is less abundant following inhibition of miR-340-5p or miR-542-3p; and more abundant after overexpression of miR-671-5p. A study into CCNA2 expression and location in the endometrium of women undergoing IVF found that in the early proliferative phase, CCNA2 was mainly located in the stromal cells, but was also more highly expressed in those women who went on to have a successful pregnancy compared to those who did not . During the late proliferative phase, CCNA2 was also highly expressed in epithelial cells of women who became pregnant. A drawback of this research is that no healthy endometrial samples were examined meaning all women were undergoing IVF and had various conditions or factors that would negatively impact pregnancy. However, the correlation between the expression of CCNA2 and ability to achieve a pregnancy was significant. Knockdown of CCNA2 in the study resulted in a significant reduction in the number of endometrial glands in the uteri of mice, and caused infertility (Aljubran et al., 2023).

The ESCRT complex is an overrepresented cellular component in which proteins increased in abundance following treatment with each of miR-340-5p, miR-542-3p or miR-671-5p are significantly enriched. The role of the ESCRT complex in the endometrium in relation to implantation and early pregnancy has not been well described in the literature. The ESCRT complex generally is involved in multivesicular body transport for degradation by lysosomes, by performing membrane scission to produce the multivesicular body. It plays another role during cytokinesis in separation of the daughter cells (Schmidt and Teis, 2012). The ESCRT complex is also able to select and sort multivesicular bodies which are destined for secretion (Guzewska et al., 2023), perhaps identifying a role in cell-cell communication and involvement in endometrial epithelial-stromal cross talk. Furthermore, ESCRT involvement in the

biogenesis of EV secretion could be important for embryo-endometrium signalling during the peri-implantation period and throughout implantation, as previously suggested in pigs (Guzewska et al., 2023). Taken together, these results suggest that the synchronous elevation of miR-340-5p, -542-3p and -671-5p mediated by P4 resulting in increased in abundance of these ESCRT complex associated proteins in the endometrial epithelial cells could be functioning to regulate these processes of cell-cell communication and embryo-endometrial signalling.

Examining the group of proteins which were more abundant in response to overexpression of each of the three miRNAs (Figure 4.18) reveals that Proline rich 11 (PRR11) has the highest fold change of this list in response to both miR-542-3p and miR-671-5p, and the second highest fold change in response to miR-340-5p. Overexpression of PRR11 is characterized in many cancers - breast cancer (Lee et al., 2020), colorectal cancer (Ma et al., 2022), osteosarcoma (Li et al., 2021) and hepatocellular cancer (Qiao et al., 2019), where it promotes proliferation and growth of the cancer, resulting in poor prognosis. This is in contradiction to differentially abundant proteins and their previously discussed mechanisms that miR-340-5p, miR-542-3p and miR-671-5p regulate, which suggest their functions are to downregulate proliferation. Yet, this protein has the largest fold change in the list of proteins common to all three miRNA mimic treatments.

A study into the role of *PRR11* in E2 receptor positive breast cancer demonstrates that overexpression of *PRR11* appears to increase tumour survival despite E2 deprivation treatment (Lee et al., 2020). These tumours are resistant to anti-E2 treatment, and *PRR11* was the only overexpressed gene in the resistant tumours. A suggested mechanism was activation of PI3K pathway, which controls growth, survival and proliferation (Hemmings and Restuccia, 2012). Activation of PI3K in these tumours by *PRR11* was concluded to result in improved growth and survivability. In the endometrium, E2 signalling targets the epithelial cells in the proliferative phase of the cycle to increase proliferation (Yu et al., 2022). During the secretory phase of the menstrual cycle, E2 is very low, and so overexpression of PRR11 in response to upregulated miRNAs caused by P4 production could employ a similar mechanism in activation of the PI3K pathway in the absence of oestrogen, allowing the endometrial epithelial cells to survive. Since proliferation of epithelial cells is reduced at this stage, perhaps proteins previously discussed which are involved in inhibition of proliferation and are also upregulated inflict the opposite effect, meaning that proliferation is tightly regulated but epithelial cells are instructed to survive through PRR11 expression.

To conclude, when comparing altered proteins between miRNAs, there are several proteins common to more than one of the miRNAs. This demonstrates the potential collaborative effect of the miRNAs and their involvement in similar pathways or in regulation of the same functions. This is not entirely unexpected due to the fact that all three miRNAs are upregulated by P4.

Chapter 5 Investigating Functional Roles of Evolutionarily Conserved, Progesterone Regulated MicroRNAs in Implantation

5.1 Introduction

The endometrium is integral for a successful pregnancy to occur - it is the site of embryo implantation, and its normal functioning is vital for maintenance of a pregnancy (Critchley et al., 2020). A major challenge hindering the advancement of our understanding of uterine function and early pregnancy, but also our ability to intervene in infertility and reproductive disorders, is the lack of appropriate in vitro models. Early pregnancy processes, such as implantation, are extremely difficult to study *in vivo* due to ethical issues, along with practical accessibility (Fitzgerald et al., 2021). The UK Human Fertilisation and Embryology Act states that embryo culture *in vitro* is legally limited to 14 days (Human Fertilisation and Embryology Authority, 2008). Some scientists argue that this should be increased to extend research capabilities, with 28 days advocated as an appropriate length (Appleby and Bredenoord, 2018), whereas others concur that 14 days is an appropriate limit (Blackshaw and Rodger, 2021). Animals such as mice provide rudimentary models, which much of our basic understanding is derived from; however mice display major differences - a important one being that mice do not undergo spontaneous, monthly decidualization like humans (Fitzgerald et al., 2021). This therefore, doesn't fully recapitulate all of the processes relevant for human implantation, depending on the nature of the question the investigation addresses. In fact, due to the large inter-species differences in uterine phenotype and implantation strategy, any insights gained into implantation using *in vivo* or *in vitro* animal models are not necessarily applicable to humans or other species. In humans, implantation consists of apposition, adhesion and then invasion; where the blastocyst invades into the underlying stromal layer to establish pregnancy (Ochoa-Bernal and Fazleabas, 2020). Rodents have a less invasive implantation strategy, where an infolding of the endometrial epithelium surrounds the blastocyst (Lee and DeMayo, 2004), again highlighting the limitations of mouse models for studying human implantation. In domestic ruminants like bovine, porcine and ovine; the blastocyst is known instead as a conceptus, which elongates and attaches to the epithelium rather than breaching it (Lee and DeMayo, 2004; McGowen et al., 2014).

Reproducible, physiologically accurate models of the endometrium and embryo implantation would substantially improve the accuracy of the *in vitro* investigations we are able to perform. Consequently, our understanding of the biological processes would improve, opening the door for the development of novel techniques to treat different pathologies. Furthermore, *in vitro* models provide an avenue for testing treatments without the necessity for live animal models - an increasingly relevant concern, before proceeding to human clinical

trials. Furthermore, creating models which can be used with multiple species would be beneficial for studying the molecular pathways which determine the differences observed in implantation strategies between species. In this section, current *in vitro* models and techniques will be discussed.

5.1.1 Two-dimensional Models

Current models to assess implantation in humans include 2D systems to investigate attachment and invasion, and the effects of different treatments on these processes (Fitzgerald et al., 2021). *In vitro* investigation into embryo implantation using primary human endometrial stromal cells and primary hatched blastocysts was carried out by Carver et al., (2003). Blastocysts attached to and invaded the stromal cells, providing valuable insight into the direction in which the blastocyst implants, and showing that hCG production by the blastocyst is significantly increased when cultured in the presence of stromal cells. This method does not fully recapitulate modelling implantation, as the stage of attachment is between blastocyst and endometrial epithelial cells and not the stromal layer. By the time the blastocyst comes into contact with the stromal layer, a cascade of signalling has already been triggered by maternal recognition of pregnancy and attachment to the epithelial cells (Fazleabas et al., 1999). Furthermore, a monolayer of cells does not seem appropriate to study invasion as the blastocyst is unable to invade further than a depth of 1 cell. Stromal cell decidualization is also required for successful implantation in humans (Zhang and Wei, 2021), and the study does not include this process. Another study from the same lab employed similar methods to identify important molecules required for implantation (Grewal et al., 2008), concluding that *Rac1* is necessary for the embryo to successfully implant. Whilst this experiment carries the same drawbacks as the previous one, in this paper decidualization of the stromal cells is performed. This method was also used by Teklenburg et al., (2010) to analyse endometrial cell secretions in the presence of healthy embryos compared with arresting ones. A number of other studies carried out investigations into implantation using a stromal cell model including Holmberg et al., (2012); Gellersen et al., (2013). More recently, culture medium from embryos cultured for ICSI procedures with different developmental competencies was used to assess migration and proliferation of decidualized vs non-decidualized endometrial stromal cells (Berkhout et al., 2018).

Two dimensional models of endometrial epithelial cells can be used to model attachment stage of implantation. Evans et al., (2020) used a range of epithelial cell lines - ECC-1, Ishikawa, Hec-1a and RL95-2 - along with primary endometrial epithelial cells and assessed adherence of trophoblast spheroids following co-culture. Varying attachment rates were observed between different

cell types at different time points. In fact, co-culture of embryos with endometrial epithelial cells prior to embryo transfer has been developed as a clinical programme with the intention of improving implantation in patients with implantation failure (Simón et al., 1999). Attachment assays using endometrial epithelial cells can be used to test IVF techniques to investigate the effect on implantation. EmbryoGlue® is an embryo transfer media which contains a high concentration of hyaluronate that can be used for IVF procedures with the purpose of improving the chance of successful pregnancy (Singh et al., 2015). A 2D model of the endometrial epithelial layer tested this by applying human embryos cultured with or without EmbryoGlue® to a monolayer of Ishikawa cells and assessing attachment (Ruane et al., 2020). This study found that there was no statistically significant advantage of culturing embryos in media with increased hyaluronate. This demonstrates the real life application of 2D endometrial modelling.

Whilst two-dimensional models of the endometrium can give insight into aspects of endometrial function and implantation to a certain extent, by their very nature they omit the multicellular complexity of the endometrium. This means that there is no involvement of the interaction between the different cell types in the endometrium, and does not allow study of invasive implantation due to the monolayer structure (Rawlings, Makwana, Tryfonos, et al., 2021).

5.1.2 Three-dimensional Models

More recently 3D models of the endometrium have been developed using matrices for support (Kim et al., 2005; Lalitkumar et al., 2007; Wang et al., 2012), endometrium on-a-chip (De Bem et al., 2021; Ahn et al., 2021), and organoids derived from primary tissue (Turco et al., 2017; Cindrova-Davies et al., 2021) and are described below.

5.1.2.1 Matrices for 3D cell culture

A matrix consisting of fibrin-agarose was developed to model the endometrium using primary endometrial stromal and epithelial cells as well as performing the same procedure with immortalized cell lines for these cell types (Wang et al., 2012). This structure was used for attachment assays using Jar spheroids (human choriocarcinoma cell line) in the place of an implanting embryo. In this experiment, Jar spheroids were incubated with the 3D model of the endometrium, followed by inverting the plate and centrifuging it upside down to assess attachment. Interestingly, previous research suggests that Jar attachment rates are low compared to alternative spheroid cell types (Grümmer et al., 1994), which highlights the drawbacks of using a cell line over primary embryos. Whilst this model (Wang et al., 2012) does allow incorporation of the

cell to cell cross communication that may be involved in attachment, it would be improved by using human embryos or an invasive cell type to investigate beyond attachment into invasion. There are other components that can be used to form a matrix for 3D cell culture. Collagen is a common component of 3D cell culture matrices. Kim et al., (2005) mixed epithelial cells with collagen, seeding them in a cell culture insert coated with Matrigel which was cultured on top of a stromal layer in a collagen matrix. This technique was used to observe signalling between epithelial and stromal cells important for decidualization in humans and identify key molecules involved in this process. Similarly, collagen was used to seed primary human endometrial stromal cells in an insert, on top of which Matrigel was used to seed the epithelial cells (Lalitkumar et al., 2007). This model was employed to investigate attachment of human blastocysts. Again, to use this 3D model to its full potential it would be intriguing if this could be adapted to study invasion into the underlying stromal compartment.

5.1.2.2 Endometrium on-a-chip

Organ on-a-chip devices have been established for modelling the endometrium. Using an endometrium on-a-chip approach, bovine endometrial cells were seeded in a device with epithelial cells in the top compartment and stromal cells below and treated with different concentrations of glucose or insulin (De Bem et al., 2021). The application of this study was in understanding alteration of these factors in the maternal environment to show the effect on the function of the endometrium. This demonstrates the range of studies that these tools can be utilized for. Another investigation which made use of endometrium on-a-chip technology used a 5 channel device to seed stromal, epithelial and endothelial cells, with the model ready to use after 14 days (Ahn et al., 2021). This study reports creation of an hormonally responsive endometrial model with vascularisation. Xiao et al., (2017) employed microfluidic, endometrium-on-a-chip technology to recreate the human female menstrual cycle *in vitro*. This study used ovarian tissue from mice (as healthy human tissue is inaccessible) to demonstrate follicular development and hormone production in the devices, along with progression of the menstrual cycle. Other chambers of the microfluidic system contained human endometrial tissue, as well as fallopian tube, ectocervix and liver. The endometrial tissue was digested into epithelial and stromal cells and incorporated into scaffolds to maintain long term culture. This system responded in a physiologically accurate way by prolonging P4 production when artificial signals signifying pregnancy were added. This approach provides a method for studying tissue-tissue interactions during the menstrual cycle in humans.

5.1.2.1 Scaffold-based modelling

A polystyrene scaffold has been created with the intention of providing a cost effective, routine and reliable method of 3D cell culture (Knight et al., 2011). This porous polystyrene disk sits inside a plastic insert which is designed to fit into cell culture well plates. Much work has been carried out on using this technology to develop 3D models of different tissues, particularly for skin equivalents (Hill et al., 2015; Costello et al., 2019; Totti et al., 2019). Using Alvetex scaffolds, it was possible to form a 3D *in vitro* model of melanoma skin cancer, which consisted of a dermal fibroblast layer along with epidermal keratinocyte layer with melanoma cells - or without for controls - producing a 3D skin equivalent model to investigate melanoma (Hill et al., 2015). Further work developed the necessity for deposition of extracellular matrix by the dermal component to maintain the structure and differentiation of the epidermal compartment (Costello et al., 2019). These methods were also employed to produce 3D skin models with melanoma, to be used to assess the functionality of immunodiagnostic microneedles (Totti et al., 2019). The Alvetex scaffolds have been used to model glioblastoma, in order to predict treatment outcomes and were superior to 2D culture methods (Gomez-Roman et al., 2017). Studies into modelling the lining of the intestine using Alvetex technology were also performed to improve upon the 'gold-standard' 2D culture systems, resulting in production of a more structurally physiological model (Darling et al., 2020). Alvetex scaffolds have emerged in the reproduction field. They were used to construct a 3D model of the endocervix - which is the inner lining of the cervix. Biopsies from women were used to seed stromal and epithelial cells in the scaffolds, which, once fully formed, were cultured over 28 days with hormones to mimic a menstrual cycle (Arslan et al., 2015). The cells in this culture system were hormone responsive in a physiological way, responding to proliferation cues and production of molecules appropriate to menstrual cycle stage. This method has also been applied to the bovine endometrium, with endometrial stromal cells generating extracellular matrix in the scaffolds and an epithelial layer overlaying the structure (Díez et al., 2023). Applying Alvetex scaffold technology to modelling the human endometrium has not yet been carried out.

5.1.2.2 Organoids

Organoids are 3D modelling structures derived from primary tissue which self-organize to represent a more complex organ (Z. Zhao et al., 2022). They are used to model various tissues including colon (Sato et al., 2011), prostate (Karthaus et al., 2014) and fallopian tube (Kessler et al., 2015). Human endometrial organoids have been developed by Turco et al., (2017) using both endometrial gland tissue and decidual cells. These organoids can be cultured

long-term and passaged, providing a stable *in vitro* endometrial model for research into reproductive conditions and treatments. A drawback of this method is that collection of these cells requires an invasive procedure - especially in humans - unless tissue is collected from other animals from waste sources *i.e.*, food production from animals or veterinary surgeries. However, more recently, organoids have been produced from menstrual flow which respond appropriately to hormonal cues and behave in the same way as those organoids derived from endometrial biopsies (Cindrova-Davies et al., 2021). This advancement makes this technology more accessible, increasing the volume of research that can be carried out with these organoids by improving availability. This could also open the door to *in vitro* personalised treatment investigations due to the ease in which these patient specific models can be collected. Another major advantage of this method of isolating organoids is that they can be easily and non-invasively donated by healthy patients, meaning that investigations into 'normal' implantation can be done, rather than only being able to obtain tissue from patients undergoing investigations for a condition.

Development of oviductal organoids from other species has also been achieved in cow, pig, cat, dog and horse (Lawson et al., 2023). If this technology could be applied to the endometrium, it would introduce the possibility for comparison of endometrial function in these models between different eutherian mammals. This would allow us to improve our understanding of different implantation strategies along with identification of important molecules and signalling pathways relevant to different phenotypes.

5.1.3 Summary

A range of models have been produced to study the function of the reproductive system and embryo implantation. Despite the amount of research into these techniques, there are still gaps in the literature. Firstly, there does not appear to be any research into miRNA involvement in implantation using *in vitro* models. In fact, as discussed in Chapter 2, 3 and 4, there is very little investigation into miRNA involvement in implantation at all. Even the more basic 2D implantation assays investigating attachment of a blastocyst have not yet been used to investigate miRNA involvement in this process. Secondly, whilst some models have been developed incorporating multi-cellular layers to represent the endometrium, it is clear that there is still a requirement for a reproducible, reliable and straightforward human endometrial model to be created. As Alvetex technology has been used for many purposes consistently, as well as to model the bovine endometrium, this appears to be an interesting, promising avenue for generation of a human endometrial model. Finally, the ability to isolate and culture endometrial epithelial organoids from different species would allow us to

compare the inter-species differences in endometrial function and implantation. Both the Alvetex model and organoids derived from other species could consequently be used to investigate miRNA involvement. This chapter intends to address these gaps in the literature.

5.2 Hypothesis and Aims

5.2.1 Hypothesis

We hypothesise that altering the expression of microRNAs in a model of the endometrium will have an effect on embryo implantation and endometrial function.

5.2.2 Aims

This chapter aims to:

1) Determine the functional role of miR-340-5p, miR-542-3p and miR-671-5p in embryo implantation.

2) Develop novel, three-dimensional model(s) of the endometrium as a tool to study endometrial function and embryo implantation.

5.3 Materials and Methods

5.3.1 Cell Culture

For all cell culture processes, a sterile tissue culture hood was used along with 70% ethanol and sterile filtered pipette tips. Cell culture treated flasks of 75cm^2 and 25cm^2 were used to culture cells. Light microscopy was used to assess confluency and quality.

5.3.1.1 Ishikawa (immortalized endometrial epithelial) cell line

Ishikawa cells (ECACC # 99040201 were used as a model of a hormonally responsive epithelial layer of the human endometrium. Cells were maintained in culture and passaged at >70% confluency. This was carried out following the protocol and using the consumables detailed in Section 2.3.1.1;

5.3.1.2 BeWo cell line

BeWo cells (ECACC # 86082803), a human trophoblast cell line derived from a malignant gestational choriocarcinoma in a foetal placenta, were cultured in media which consisted of 1:1 Dulbecco's Modified Eagle Medium (DMEM) and Hams' F12, supplemented with 10% FBS and glutamine, streptomycin and penicillin (GSP). All reagents: media, trypsin, and phosphate buffered saline (without Ca^{2+} / Mg^{2+}) (PBS) were warmed to 37^{o}C in a water bath before being used. Passaging was carried out by aspirating culture media and performing 2 PBS washes to remove traces of media. Five ml of 0.025% trypsin EDTA diluted in PBS was added to the flask and incubated at 37^{o}C for approximately 2-3 min. After incubation, cells were inspected by light microscopy to ensure they had detached from the flask. Culture media was added to the flask at a 1:1 ratio to trypsin to stop enzyme action and cells were centrifuged in a falcon tube at 500 g for 5 min. Following centrifugation, supernatant was removed, and cells were washed in PBS before centrifugation again at 500 g for 5 min. The resulting pellet was resuspended in an appropriate amount of culture media depending on the passaging ratio or plating requirements. BeWo cells were split at a maximum 1:5 ratio, but usually 1:2 or 1:3.

5.3.1.3 Immortalized human endometrial stromal cell line

The human endometrial stromal cell line which is SV40 immortalized (Product T90201, ABM) was cultured and passaged using the same protocol as BeWo cells in Section 5.3.1.2. The only deviation from this protocol is that the media used for culture was Prigrow IV medium (NBS Biologicals) supplemented with 10% FBS and 1% GSP. Pricoat T75 flasks were also used for this cell line which are coated with collagen I extracellular matrix.

5.3.2 Normal 2D endometrium/embryo attachment assay

To model embryo attachment to the endometrium in humans, a 2D model was used. This consists of a monolayer of Ishikawa cells representing the epithelial endometrium - the site of attachment - and spheroids formed from a trophoblast cell line to be used as the embryo. MiRNAs of interest miR-340-5p, miR-542-3p and miR-671-5p were over and under expressed in the Ishikawa cells to investigate their effects on attachment. A schematic workflow for the process is shown in Figure 5.2.

5.3.2.1 MicroRNA mimic or inhibitor transfection

MiRNA mimics and inhibitors for non-targeting mimic, non-targeting inhibitor, miR-340-5p, miR-542-3p and miR-671-5p used in Chapters 2, 3 and 4 were used for transfection of Ishikawa cells for attachment assays.

Mimic and inhibitor transfection was carried out as described in Chapter 2, Section 2.3.2.2, with minor modifications as follows. Ishikawa cells were plated at 60,000 cells per well in a 24 well plate. Mimic and inhibitor treatment volumes were scaled down, as this experiment was carried out in 24 well plates, with the same final concentration of 40nM per mimic/inhibitor/non-targeting control per well. Dharmafect 2 was used for this experiment in place of lipofectamine 2000 as it was important that a cell monolayer with minimal gaps was present in the well for the assay. Lipofectamine 2000 caused visibly patchy cell growth (Figure 5.1) and so Dharmafect 2 was selected for use. Dharmafect 2 volume was 1μl per well as advised in manufacturers' instructions, and confirmation of transfection was carried out by qRT-PCR as described in Chapter 2, Section 2.3.3.4. Treatments were carried out in n=5 biological replicates. A total of 100μl optiMEM with 1μl of Dharmafect 2 and respective miRNA mimic, inhibitor or non-targeting control was added to each well. The plate was rocked to mix and incubated at 37^{o}C, 5% CO_2 for 48 hrs.

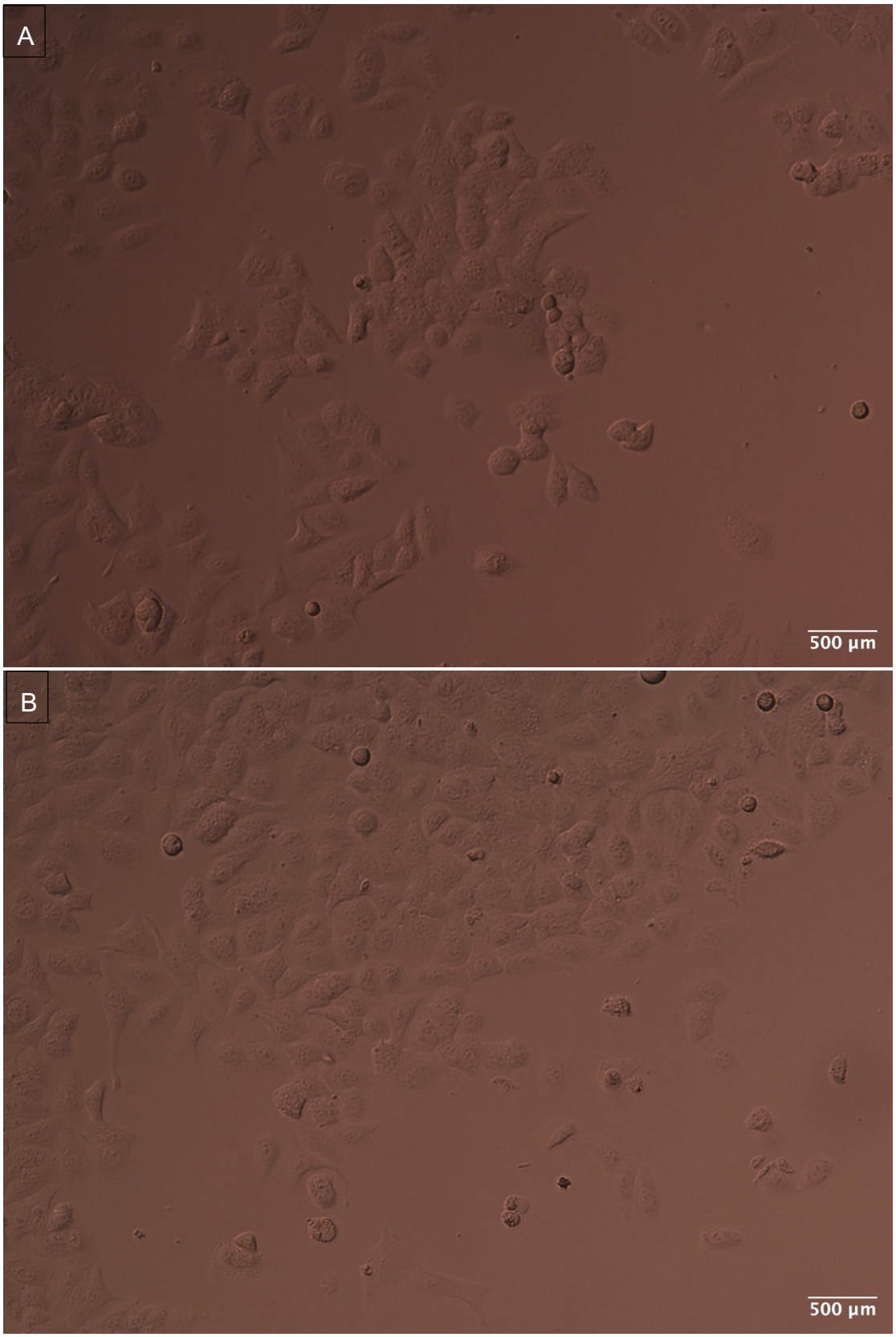

Figure 5.1*: Morphology of Ishikawa cells following transfection with different transfection reagents.*
Cells were plated at 50,000 cells per well in 24 well plate transfected with A) 1µl lipofectamine 2000 or B) 1µl Dharmafect 2 for 24 hours imaged using EVOS microscope brightfield at 20x magnification.

5.3.2.2 Transfection of Ishikawa cells with multiple miRNA mimics and/or inhibitors

To investigate the combinatory effect of differentially expressed miR-340-5p, miR-542-3p and miR-671-5p on attachment, Ishikawa cells were also transfected with every combination of the miRNA mimics and/or inhibitors.

For transfection of Ishikawa cells with more than 1 mimic or inhibitor, an identical protocol was followed as described in Chapter 5, Section 5.3.2.1, with a final concentration of 16nM of each miRNA mimic or inhibitor per well. A list of combinations of mimics and/or inhibitors is supplied in Table 5.1. A control (100μl optiMEM media) and a Dharmafect control (1μl Dharmafect 2 in 100μl optiMEM media was also carried out. For non-targeting controls, concentration of non-targeting mimic or inhibitor was equal to its comparable targeting mimic/inhibitor treatment, *e.g.,* for miR-340-5p mimic (16nM) + miR-542-3p mimic (16nM) and miR-671-5p inhibitor (16nM), the corresponding non-targeting control was non-targeting mimic (32nM) and non-targeting inhibitor (16nM).

Table 5.1: *Table of combinations and concentrations of mimics and inhibitors Ishikawa cells were transfected with for spheroid attachment assays.*

Transfection with 2 mimics/inhibitors	**Transfection with 3 mimics/inhibitors**
Non-targeting mimic (16nM) + non-targeting inhibitor (16nM)	Non-targeting inhibitor (48nM)
miR-340-5p inhibitor (16nM) + miR-542-3p mimic (16nM)	miR-340-5p inhibitor (16nM) + miR-542-3p inhibitor (16nM) + miR-671-5p inhibitor (16nM)
miR-340-5p inhibitor (16nM) + miR-671-5p mimic (16nM)	Non-targeting mimic (32nM) + non-targeting inhibitor (16nM)
miR-340-5p mimic (16nM) + miR-542-3p inhibitor (16nM)	miR-340-5p inhibitor (16nM) + miR-542-3p mimic (16nM) + miR-671-5p mimic (16nM)
miR-340-5p mimic (16nM) + miR-671-5p inhibitor (16nM)	miR-340-5p mimic (16nM) + miR-542-3p- inhibitor (16nM) + miR-671-5p mimic (16nM)
miR-542-3p inhibitor (16nM) + miR-671-5p mimic (16nM)	miR-340-5p mimic (16nM) + miR-542-3p mimic (16nM) + miR-671-5p inhibitor (16nM)
miR-542-3p mimic (16nM) + miR-671-5p inhibitor (16nM)	Non-targeting mimic (16nM) + non-targeting inhibitor (32nM)
Non-targeting mimic (32nM)	miR-340-5p inhibitor (16nM) + miR-542-3p inhibitor (16nM) + miR-671-5p mimic (16nM)
miR-340-5p mimic (16nM) + miR-542-3p mimic (16nM)	miR-340-5p inhibitor (16nM) + miR-542-3p mimic (16nM) + miR-671-5p inhibitor (16nM)

miR-340-5p mimic (16nM) + miR-671-5p mimic (16nM)	miR-340-5p mimic (16nM) + miR-542-3p inhibitor (16nM) + miR-671-5p inhibitor (16nM)
miR-542-3p mimic (16nM) + miR-671-5p mimic (16nM)	Non-targeting mimic (48nM)
Non-targeting inhibitor (32nM)	miR-340-5p mimic + miR-542-3p mimic + miR-671-5p mimic
miR-542-3p inhibitor (16nM) + miR-671-5p inhibitor (16nM)	
miR-340-5p inhibitor (16nM) + miR-671-5p inhibitor (16nM)	
miR-340-5p inhibitor (16nM) + miR-542-3p inhibitor (16nM)	

5.3.2.2 Spheroid production

Polyvinylpyrrolidone (PVP) at a concentration of 10% dissolved in PBS was added to 6 well plates and incubated for 30 min at room temperature. After this incubation, PVP was removed and wells washed with PBS. BeWo cells were lifted from T75 flasks by trypsinization (Chapter 5, Section 5.3.1.2) followed by addition of 5ml of serum and antibiotic free DMEM:F12 media to halt trypsin action and centrifuged at 500 G for 5 min. Supernatant was aspirated and cells resuspended in serum and antibiotic free DMEM:F12 media to wash away any remaining serum. BeWo cells were then plated at 500,000 to 1,000,000 cells per well in 3ml serum and antibiotic free DMEM:F12 media. The plate was then placed on an orbital shaker at 60 rpm and incubated at 37^{o}C, 5% CO_2 for 4 hrs. A P1000 pipette was then used to pipette up and down to break up clumps of spheroids before the plate was returned to the incubator without orbital shaker for overnight incubation at 37^{o}C, 5% CO_2. To harvest spheroids, the contents of the well were passed through a 100μM filter followed by a 40μM filter. One ml of serum and antibiotic free DMEM:F12 media was used to rinse the bottom of each well twice, to collect any remaining spheroids and this was also passed through both filters. The 40μM filter was then inverted over a 50ml falcon and rinsed with serum and antibiotic free DMEM:F12 media and flow through containing spheroids was collected.

5.3.2.3 Attachment assay

Transfected Ishikawa cells in 24 well plates were washed three times with PBS and 500μl of FBS/antibiotic free DMEM:F12 media added to each well. An empty test well was used to estimate appropriate volume of spheroid containing media to add per well to result in approximately 150-200 spheroids per well. This volume of spheroids were then added to the wells and placed in an incubator at 37^{o}C, 5% CO_2 for 1 hr. After incubation, whole wells were imaged by light microscopy in brightfield at 4x objective using an EVOS microscope and images stitched together to form a whole well picture. Media was then aspirated from the wells, and 500μl 4% PFA added for 20 min at room temperature to fix the wells. Following this incubation, formaldehyde was removed and 500μl PBS added to wells, before imaging whole wells once again. Spheroids were counted in both images from 'before' and 'after' fixation, and this was used to calculate percentage spheroid attachment. Data analysis was carried out in R version 4.1 (R Core Team, 2021) and was first checked for outliers by box plot analysis using the Rstatix package identify_outliers (Kassambara, 2023), with any outliers removed, and then normality checked using a Sharpiro-Wilk test.

Statistical analysis was carried out using paired multiple t-tests with Bonferroni correction for multiple testing.

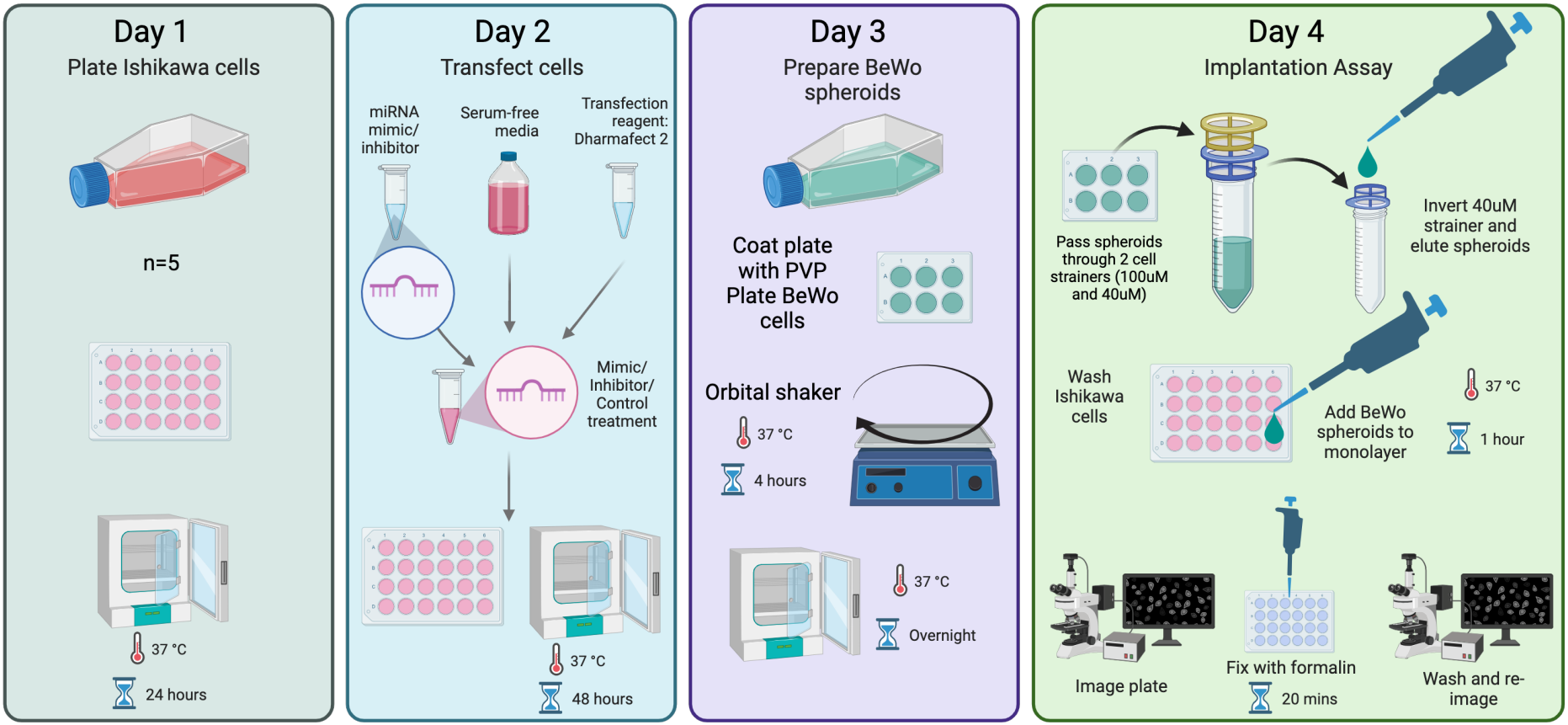

Figure 5.2: *Schematic workflow with stages of attachment assay.*
Day 1: Ishikawa cells are plated at 60,000 cells per well in a 24 well plate and incubated for 24 hours. Day 2: Ishikawa cells are transfected with mimics and inhibitors along with non-targeting controls (40nM) using Dharmafect 2 as a transfection reagent. Day 3: BeWo spheroids are formed using BeWo cells and an orbital shaker. Day 4: spheroids are strained to collect those which are 40-100μM and added to Ishikawa cells, incubated for 1 hour then imaged, fixed with formalin and reimaged.

5.3.3 3D models of the endometrium: Alvetex scaffold model

Figure 5.3 depicts a schematic diagram of the workflow for producing 3D Alvetex scaffold models of the human endometrium. The steps are described below.

5.3.3.1 Optimisation of stromal cell layer

5.3.3.1.1 Seeding scaffolds

Alvetex scaffolds (Generon) were placed in a petri dish and submerged in 70% ethanol for 5 min. Ethanol was then aspirated and replaced with PBS to wash. Scaffolds remained in PBS during preparation of cells. Prior to addition of cells, PBS was aspirated from the scaffolds and they were transferred to wells in a 6 well plate where 1ml warm culture media was added to each scaffold.

Immortalized stromal cells were trypsinised according to protocol in Chapter 5, Section 5.3.1.3. The cell pellet was resuspended to a concentration of 500,000 cells per 100μl. Immediately before seeding the cells in scaffolds, culture media was aspirated. In a dropwise manner, 500,000 cells were added directly to each scaffold and incubated at 37^{o}C, 5% CO_2 for 1 hr to allow cells to adhere. Then,10ml of stromal cell PriGrow IV media supplemented with 10% FBS and 1% GSP was added to the well gently and cells incubated at 37^{o}C, 5% CO_2 for a range of incubation time lengths with the following biological replicates: 7 days (n=1), 14 days (n=1), 21 days (n=1), 25-28 days (n=3), 32-35 days (n=3), and 39 days (n=1). Scaffold numbers with passage information and exact incubation length is listed in Table 5.2. Media was changed twice per week and scaffolds moved to a new 6 well plate once per week.

5.3.3.1.2 Fixing, processing and embedding of Alvetex scaffolds

On the day of collection, media was aspirated and Alvetex scaffold was removed from well insert using forceps. This was then washed 3 times in PBS. Fixing was carried out using 4% formaldehyde for 2 hrs at room temperature before 3 more PBS washes. Scaffolds were then kept in PBS at 4^{o}C until tissue processing. Scaffolds were then placed in cassettes and processed in a tissue processor through the stages listed in Table 5.3. Following processing, scaffolds were cut in half into semi circles using scissors and positioned parallel to each other where they were embedded in paraffin and placed on a cold surface to set. A visual schematic of this process is available in Figure 5.3.

Table 5.2: *Information for Alvetex scaffold seeding of human endometrial stromal cells including scaffold number, cell number, passage number and length of incubation.*

Scaffold	Stromal cell number	Stromal passage number	Incubation length (days)
1	500,000	5	7
2	500,000	5	14
3	500,000	5	21
4	500,000	5	25
5	500,000	5	28
6	500,000	7	28
7	500,000	7	32
8	500,000	7	32
9	500,000	5	35
10	500,000	5	39

Table 5.3: *Table of steps in tissue processing of Alvetex scaffold*

Stage	Solution	Temperature (°C)	Time (hh:mm)
1	70% Ethanol	37	00:30
2	90% Ethanol	37	00:30
3	100% Ethanol	37	00:30
4	100% Ethanol	37	00:30
5	100% Ethanol	37	01:00
6	100% Ethanol	37	01:00
7	100% Ethanol	37	01:00
8	Xylene	37	01:00
9	Xylene	37	01:30
10	Xylene	37	01:30
11	Paraffin wax	65	01:00
12	Paraffin wax	65	01:00

5.3.3.1.5 Sectioning of Alvetex scaffolds

Scaffolds were sectioned using a microtome at a section thickness of 7μm and mounted on slides coated with poly-L-lysine. They were then baked in an oven at 37°C overnight to remove any water.

5.3.3.1.6 Immunofluorescence

Rehydration steps were carried out in a fume cupboard in the following way. Mounted slides were rehydrated by being submerged in 3 changes of Histoclear for 10 min each. Then, the slides were dipped in 3 changes of 100% ethanol 40 times each, followed by 2 changes of 95% ethanol 40 dips each and finally 70% ethanol for 40 dips before being placed in PBS for 5 min. A citrate buffer was used for antigen retrieval (0.01M, 2.941g sodium citrate tribasic dihydrate in 1 litre distilled water pH 6.0), in which slides were submerged and boiled in a microwave for 20 min and then left to cool for a further 20 min. The slides were then placed in PBS for 5 min. A humidity chamber was used for all remaining steps to avoid slides drying out. Each section of tissue was circled with a PAP pen. Bovine serum albumin (BSA) (5%) was made using 0.5g BSA powder and 10mL 1x TBS. A 1x solution of TBS was prepared by 1:10 dilution from a 10x TBS solution made using 0.2M Tris base, 1.5M sodium chloride in distilled water pH 7.4. Then, 60μl of 5% BSA was added to each section and incubated at room temperature for 1 hr to block. Following incubation, blocking solution was removed by tapping slides on paper towels and 60μl of primary antibody was added to appropriate sections. The list of all treatments: controls and primary and secondary antibodies used is shown in Table 5.4. Slides were then incubated at 4°C overnight inside the humidity chamber. The next day, primary antibody was removed from the slides by tapping on paper towel followed by 2 repeats of a 5 min wash in PBS. Then, 60μl of secondary antibody (Table 5.4) was added to corresponding section and incubated at room temperature for 1 hr. Liquid was removed by tapping on paper towel and 2 more 5 min washes in PBS. Washes were carried out with container wrapped in tin foil to avoid light activation of fluorescent antibodies. Fluoromount-G with DAPI was used to mount a coverslip over tissue sections and then slides were left to dry without humidity chamber at 4°C.

Table 5.4: *List of treatments, antibodies and dilutions used for immunofluorescence of Alvetex scaffolds*

Treatment	Primary antibody	Concentration	Secondary antibody and dilution	Concentration
Collagen I	Anti-Collagen I antibody - rabbit polyclonal IgG (Abcam, ab34710)	Stock: 1mg/ml Working: 0.01μg/μl	Alexa Fluor 488 goat anti-rabbit IgG (Thermo, A11034)	Stock: 2mg/ml Working: 0.002μg/μl
Fibronectin	Anti-fibronectin antibody - rabbit polyclonal IgG (Novus Bio, NBP1-91258)	Stock: 1mg/ml Working: 0.01μg/μl	Alexa Fluor 488 goat anti-rabbit IgG (Thermo, A11034)	Stock: 2mg/ml Working: 0.002μg/μl
Vimentin	Anti-Vimentin antibody - mouse monoclonal IgG (Sigma, V6630)	Stock: 5.7mg/ml Working: 0.057μg/μl	Alexa Fluor plus 555 goat anti-mouse IgG (Thermo, A32727)	Stock: 2mg/ml Working: 0.002μg/μl
Cytokeratin 18	Anti-Cytokeratin 18 antibody - rabbit polyclonal IgG (Abcam, ab24561)	Stock: 0.9mg/ml Working: 0.009μg/μl	Alexa Fluor 488 goat anti-rabbit IgG (Thermo, A11034)	Stock: 2mg/ml Working: 0.002μg/μl
Ki67	Anti-human ki67 antibody - monoclonal mouse IgG (Agilent Dako, M7240)	Stock: 46mg/L Working: 0.00046μg/μl	Alexa Fluor plus 555 goat anti-mouse IgG (Thermo, A32727)	Stock: 2mg/ml Working: 0.002μg/μl

IgG control - rabbit	Rabbit IgG control antibody (Vector laboratories, I-1000)	Stock: 5mg/ml Working: 0.02mg/μl	Alexa Fluor 488 goat anti-rabbit IgG (Thermo, A11034)	Stock: 2mg/ml Working: 0.002μg/μl
IgG control - mouse	Mouse IgG control antibody (Vector laboratories, I-2000)	Stock: 2mg/ml Working: 0.02μg/μl	Alexa Fluor plus 555 goat anti-mouse IgG (Thermo, A32727)	Stock: 2mg/ml Working: 0.002μg/μl
Secondary only control (rabbit)	None		Alexa Fluor 488 goat anti-rabbit IgG (Thermo, A11034)	Stock: 2mg/ml Working: 0.002μg/μl
Secondary only control (mouse)	None		Alexa Fluor plus 555 goat anti-mouse IgG (Thermo, A32727)	Stock: 2mg/ml Working: 0.002μg/μl

5.3.3.1.7 Haematoxylin and eosin stain

Slides were de-paraffinized according to the method described in Chapter 5, Section 5.3.3.1.6, until reaching the first submersion in PBS. Cold tap water was used to rinse slides for approximately 3 changes of water before submersion in Hematoxylin for 5 min. Cold tap water was used again to rinse slides under a slow flow rate approximately 4 changes of water. Slides were dipped once in 0.25% acid alcohol then placed immediately in cold water. For 1 min, slides were placed in hot tap water and then rinsed again in cold tap water at a slow flow rate for approximately 4 changes of water. Next, slides were dipped in 95% ethanol 20 times before staining in Eosin for 10 min. Once complete, slides were dehydrated through dipping in 2 changes of 95% ethanol 10 times each, then 3 changes of 100% ethanol 40 times each. Finally, 3 changes of Histoclear were used for 10 min each and a coverslip was mounted using DTP.

5.3.3.1.8 Imaging of Alvetex scaffolds

Haematoxylin and eosin staining was imaged using the Zeiss AX10 microscope by light microscopy using brightfield at 10x objective. No alterations were made to images.

Fluorescent microscopy was carried out using the Zeiss AX10 microscope at 20x objective. Exposure times were as follows: DAPI: 30ms, Collagen I, fibronectin, cytokeratin 300ms, and vimentin and ki67 800ms. Images were edited in Fiji ImageJ. For each image, the 'test image' - that is the one for which the antibody of interest was used *e.g.*, Collagen I - was used to adjust the brightness of itself and its respective controls to remove background fluorescence and make images comparable. This was carried out by histogram analysis of each channel of the test image. The maximum histogram intensity value at which the pixel count was first greater than or equal to 10 was recorded and brightness adjusted to set this value as the maximum. Controls were altered to use this same maximum brightness value.

5.3.3.2 Addition of epithelial cell layer

Ishikawa cells were collected using the method described in Chapter 2, Section 2.3.1.1. Trypan blue stain and light microscopy was used to count cells and they were resuspended in DMEM:F12 media to a concentration of 1,500,000 cells per 100μl. Culture media was removed from the well and 1,500,000 cells (100μl) were added directly to the scaffold in a dropwise manner. Scaffolds were incubated at 37°C, 5% CO_2 for 2 hrs before 10ml media was added gently to each well. Prigrow IV media was changed 3 times per week and scaffolds moved to a new 6 well plate once a week.

Initially, epithelial cells were seeded onto 2 Alvetex scaffolds for 2 different incubation times to produce preliminary data for incubation length, following the optimised stromal incubation length of 35 days. One scaffold (scaffold 11: stromal cells passage 5, Ishikawa cells passage 9) was incubated for 11 days following epithelial layer seeding, and another (scaffold 12: stromal cells passage 5, Ishikawa cells passage 11) was incubated for 4 days.

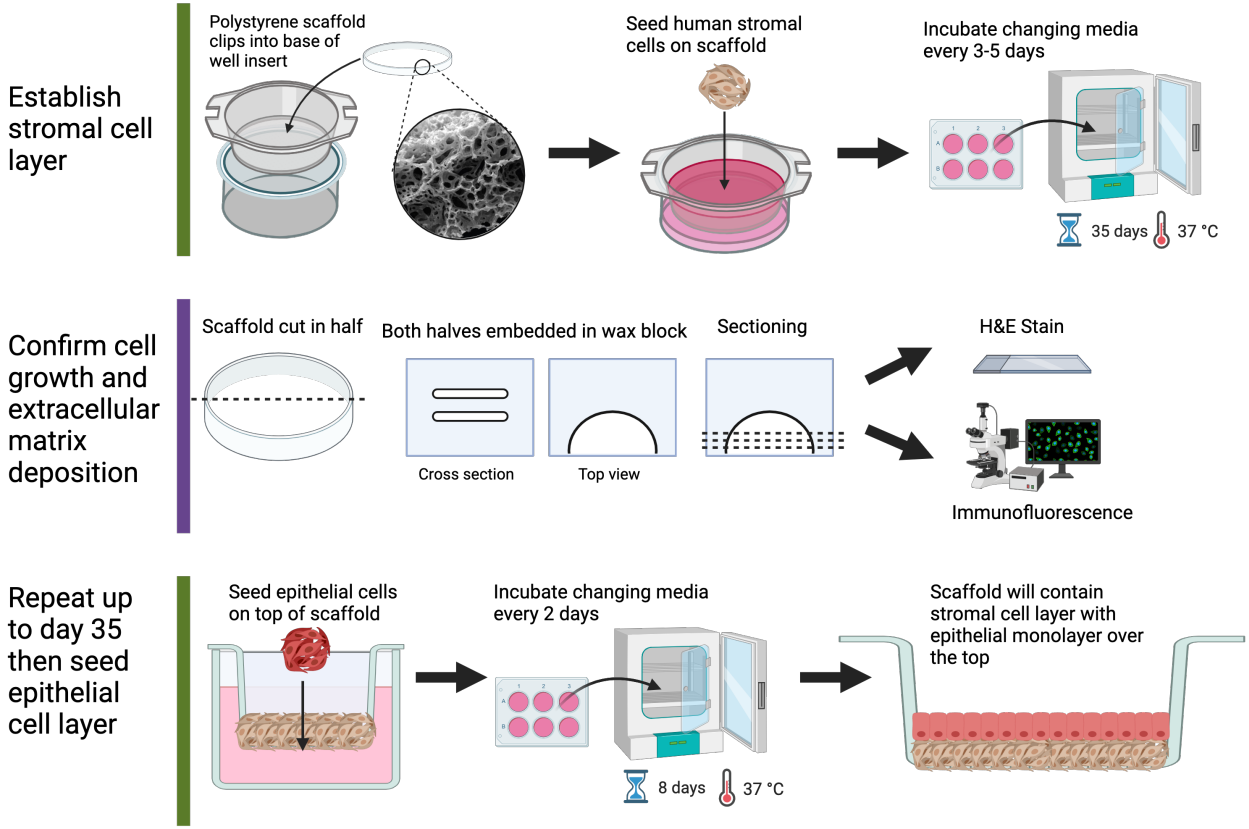

Figure 5.3: *Schematic diagram of workflow for producing 3D model of the human endometrium using Alvetex scaffold.*
The stromal layer is seeded in the scaffold using 500,000 human immortalized endometrial stromal cells before incubating for 35 days. Extracellular matrix deposition should be assessed at this stage by fixing, sectioning and staining scaffold. Once this stage is optimised, new scaffolds can be used to grow stromal layer and then add 1.5 million endometrial epithelial cells (Ishikawa) and incubating for 8 days.

5.3.3.3 Over and under expressing microRNAs of interest in a 3D model of the endometrium

Following this preliminary experiment, 20 scaffolds were seeded with stromal cells for 35 days, followed by addition of Ishikawa cells for 8 days to be used for transfection of miRNA mimics and inhibitors.

5.3.3.3.1 Transfecting Alvetex scaffolds

As the size of the insert is equivalent to a the size of a well in a 24 well plate, the same protocol was used for transfections as described in Chapter 5, Section 5.3.2.1 with the following modifications. The maximum concentration of mimic or inhibitor (50nM) was added to each scaffold. Treatments were as follows, and were carried out in duplicate - 1 scaffold for immunofluorescence and 1 for RNA extraction:

1) Control - 100μl optiMEM media

2) Dharmafect only - 100μl optiMEM media, 1μl Dharmafect

3) Non-targeting mimic - 100μl optiMEM media, 1μl Dharmafect, 50nM non-targeting mimic

4) Non-targeting inhibitor - 100μl optiMEM media, 1μl Dharmafect, 50nM non-targeting inhibitor

5) MiR-340-5p mimic - 100μl optiMEM media, 1μl Dharmafect, 50nM miR-340-5p mimic

6) MiR-340-5p inhibitor - 100μl optiMEM media, 1μl Dharmafect, 50nM miR-340-5p inhibitor

7) MiR-542-3p mimic - 100μl optiMEM media, 1μl Dharmafect, 50nM miR-542-3p mimic

8) MiR-542-3p inhibitor - 100μl optiMEM media, 1μl Dharmafect, 50nM miR-542-3p inhibitor

9) MiR-671-5p mimic - 100μl optiMEM media, 1μl Dharmafect, 50nM miR-671-5p mimic

10) MiR-671-5p inhibitor - 100μl optiMEM media, 1μl Dharmafect, 50nM miR-671-5p inhibitor

11) Combination of miR-340-5p mimic, miR-542-3p mimic, and miR-671-5p mimic - 100μl optiMEM media, 1μl Dharmafect, 16.6nM miR-340-5p mimic, 16.6nM miR-542-3p mimic, 16.6nM miR-671-5p mimic

12) Combination of miR-340-5p inhibitor, miR-542-3p inhibitor, and miR-671-5p inhibitor - 100μl optiMEM media, 1μl Dharmafect, 16.6nM miR-340-5p inhibitor, 16.6nM miR-542-3p inhibitor, 16.6nM miR-671-5p inhibitor

Treatment was added gently directly to the top (epithelial layer) of the Alvetex scaffold. After 3 hrs, scaffolds were washed 3 times with warm PBS and PriGrow IV media supplemented with 10% FBS and 1% GSP added. Scaffolds were incubated at 37°C 5% CO_2 for 48 hrs.

5.3.3.3.2 RNA extraction from Alvetex scaffolds

Media was aspirated from wells and scaffolds were removed from plastic inserts and each placed into a well of a 12 well plate. Next, 700μl QIAZol was added to each well and the plate was placed on an orbital shaker at 100rpm for 10 min at room temperature. Lysates were then pipetted up and down 10 times and transferred to RNAse DNase free eppendorfs. RNA extraction was carried out using the miRNeasy Mini Kit (Qiagen, UK) following manufacturer's instructions. Chloroform (140μl) was added to each tube and shaken vigorously for 15 seconds. Samples were then left at room temperature for 2-3 min before centrifugation at 4°C for 15 min at 12,000 g. All remaining centrifugations were performed at room temperature. The RNA containing upper phase was transferred to a new eppendorf and 525μl 100% ethanol was added before being pipetted into a RNeasy spin column, 700μl at a time. Columns were centrifuged at 8000 g for 15 seconds and flow-through discarded repeatedly until all sample had been passed through the column.

5.3.3.3.3 Analysis of overexpression of miRNAs in Alvetex scaffolds

A miRNA cDNA conversion was performed according to the protocol in Chapter 2, Section 2.3.3.3, followed by a qRT-PCR as detailed in Chapter 2, Section 2.3.3.3.

5.3.3.3.5 Immunofluorescence

Immunofluorescence was carried out on the new scaffolds using the methods described in Chapter 5, Section 5.3.3.1.6, with the addition of Ki67 antibody.

5.3.4 Modelling the Bovine Endometrium: Endometrial Organoids

5.3.4.1 Producing organoids

5.3.4.1.1 Isolating glandular epithelial cells

Bovine cells were isolated from whole reproductive tracts in the following way, based on the method described in (Tinning et al., 2020). On the morning of cell isolation, bovine reproductive tracts were obtained from a local abattoir. Tracts were inspected for damage or infection and the most appropriate tracts selected by examining corpus luteum morphology to determine estrous cycle stage, allowing the correct stage to be selected for specific experiments. Images of tracts for specific experiments are provided in Figure 5.4 and Figure 5.5. After tracts were chosen they were thoroughly washed with 70% ethanol, and placed on paper towels saturated with 70% ethanol in a sterile hood. Sterile hoods, equipment and dissection tools were used for the remainder of the protocol. Endometrial wash (per tract: 25ml PBS and 250ml anti-biotic and anti-mycotic (ABAM)), endometrial strip wash (per tract: 25ml Hanks' Balanced Salt solution (no calcium or magnesium) (HBSS) and 250ml ABAM), stop solution (per tract: 250ml HBSS and 5ml FBS), and HBSS were warmed to 37^{o}C in a water bath prior to use. Before establishing the protocol for producing organoids, an optimisation for digestive solution composition was carried out. This is described in Chapter 5, Section 5.3.5.1.2. For the purpose of this methodology, the digestive solution described here is formed from the composition that was selected due to the outcome of the optimisation. Digestive solution comprised of 50ml HBSS, 50mg bovine serum albumin (BSA) and 25mg collagenase II which was filter sterilised before adding 125μl sterile 4% DNase and 500μl sterile 100X Trypsin EDTA solution.

The uterine horn ipsilateral to the ovary possessing the corpus luteum was used. Removal of ligaments and fat was carried out and the horn was dissected from the uterine body and opened up to expose the endometrium. Endometrial wash (25ml) was poured over the endometrium. The endometrium from this point onwards was not allowed to dry out. Tweezers and scissors were used to dissect the inter-caruncular sections of endometrium from the myometrium and placed into 25ml endometrial strip wash until tissue reaches the 5ml mark. The tissue was washed and the strip wash was poured off and replaced with 25ml HBSS, mixed and poured off. Tissue was then minced using a scalpel blade and added to 25ml fresh HBSS. HBSS was removed and 40ml digestive solution was added. Tubes were incubated in a rocking hot box (37^{o}C) for 1 hr. The solution was then strained inside a sterile hood through a 100μM strainer

above a 40μM strainer into a 50ml falcon tube using a sterile plastic Pasteur pipette to stir the fragments. The 100μM strainer was then discarded and the 40μM strainer inverted over a second falcon. This was rinsed with 5ml stop solution and subjected to centrifugation at 500 g for 5 min. Supernatant was aspirated and pellet resuspended in advanced DMEM/F12 (Life Technologies, 12634010). Cells were centrifuged again at 500 g for 5 min, aspirated and resuspended in advanced DMEM/F12. The volume used for resuspension was dependent on the size of the pellet. An approximate guide to resuspension volumes is shown in Figure 5.6. Cultrex 2 was kept on ice for the duration of plating the organoids. For each well to be plated, 12μl of cell suspension was added to 48μl Cultrex 2 and mixed very gently avoiding bubbles. A droplet of 60μl of this was then pipetted into the centre of the well. Plates were then incubated at 37^{o}C 5% CO_2 for 30 min to allow Cultrex 2 to set. After incubation, droplets were covered with 500μl expansion media - composition in Table 5.5. Expansion media was removed and replaced with fresh every 2-3 days.

Table 5.5: *List of components, concentrations, suppliers and product codes for organoid expansion media.*
Media composition taken from (Turco et al., 2017).

Component	Concentration	Manufacturer	Product Code
Advanced DMEM/F12	1x	Life Technologies	12634010
N2 Supplement	1x	Life Technologies	17502048
B27 Supplement minus vitamin A	1x	Life Technologies	12587010
L-glutamine	2mM	Life Technologies	25030-024
Nicotinamide	10mM	Sigma	N0636
N-Acetyl-L-cysteine	1.25mM	Sigma	A9165-5G
StemMACS	500nM	System Biosciences	A83-01
Primocin	100μg/ml	Invivogen	ant-pm-1
Recombinant human HGF	50ng/ml	Peprotech	100-39
Recombinant human FGF-10	100ng/ml	Peprotech	100-26
Recombinant human Rspondin-1	500ng/ml	Peprotech	120-38
Recombinant human Noggin	100ng/ml	Peprotech	120-10c
Recombinant human EGF	50ng/ml	Peprotech	100-15

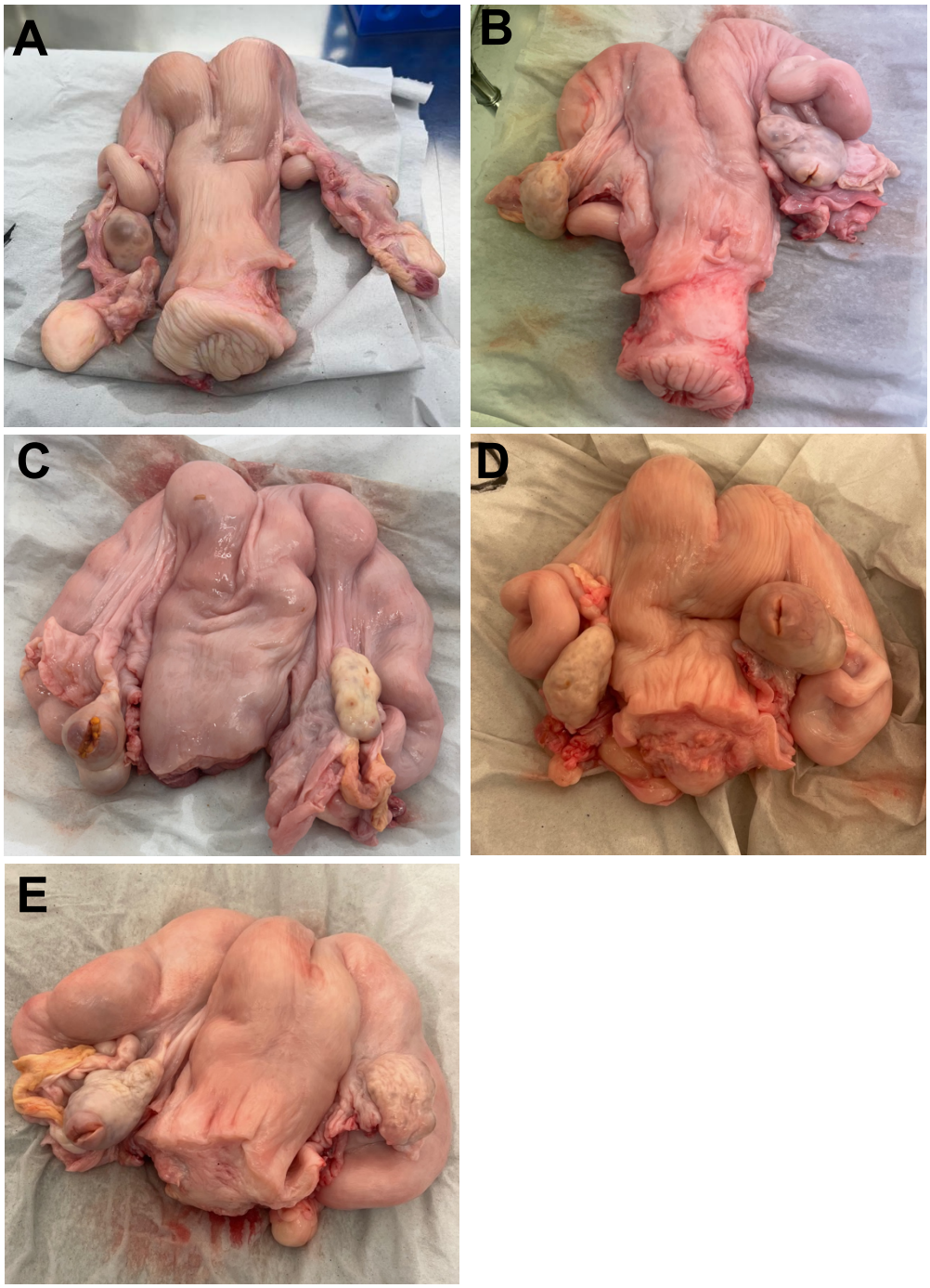

Figure 5.4: *Images of bovine reproductive tracts organoids were derived from which were selected for use in RNASequencing experiment.*
A) Tract 1, **B**) Tract 3, **C**) Tract 4, **D**) Tract 5 and **E**) Tract 6.

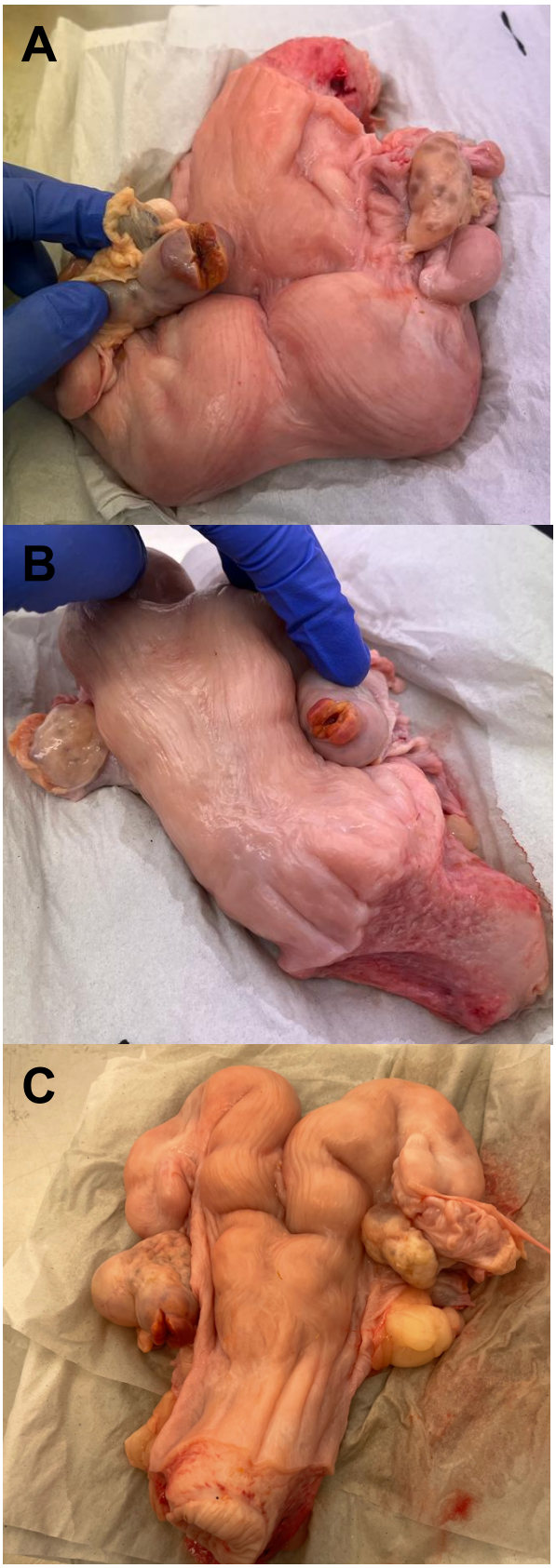

Figure 5.5: *Images of bovine reproductive tracts organoids were derived from which were selected for use in passaging experiment.*
A) n=1, **B**) n=2, **C**) n=3.

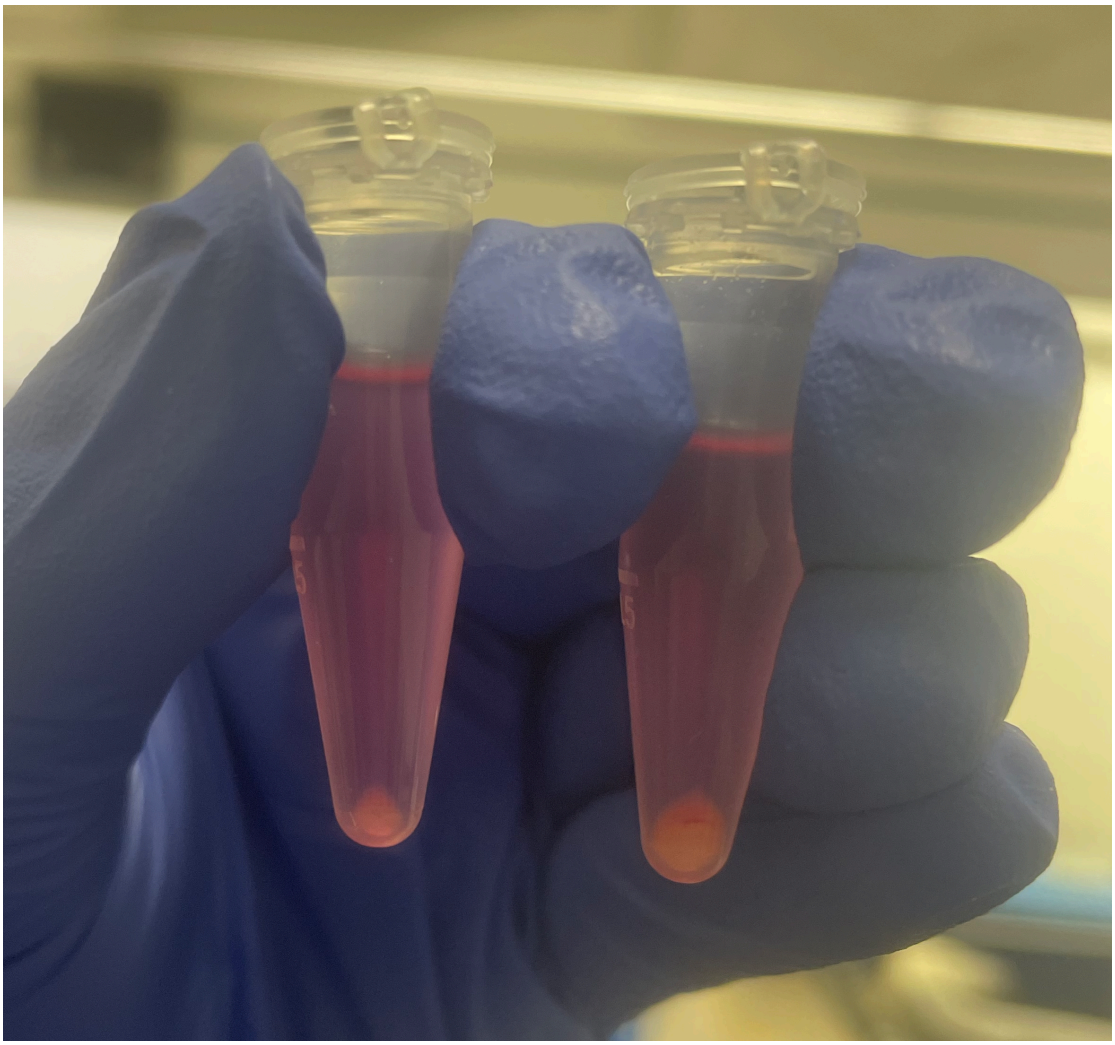

Figure 5.6: *Cell pellets sizes obtained during organoid isolation to be resuspended in Advanced DMEM/F12 for organoid plating.*
Pellets were resuspended in 300μl (left) and 700μl (right).

5.3.4.1.2 Optimising digestion composition and isolation fraction

In order to determine optimal digestion composition for maximum glandular epithelial cell isolation, three combinations of isolation methods at two timepoints were tested. Organoids were isolated in exactly the method described in Chapter 5, Section 5.3.5.1.1, up until digestion. At this point, three different digestion mixtures were produced - compositions are shown in Table 5.6. Each animal was assigned a digestion mix and incubation length of either 30 min or 1 hr for n=3 biological replicates.

Following incubation, contents of the tubes were strained through a 100μM cell strainer over a 40μM cell strainer. To ensure collection of the fraction containing the gland cells, 2 different fractions of the resulting separated digestion were collected for testing. The first fraction which was collected was taken by inverting the 40μM strainer and rinsed with 5ml stop solution. This was then centrifuged for 5 min at 500 g. Supernatant was aspirated and the pellet was snap frozen in liquid nitrogen for analysis. The second fraction was collected by inverting the 100uM strainer and washing with 5ml stop solution. This liquid including tissue chunks was centrifuged at 300 g for 5 min with the intention of separating tissue chunks, whilst leaving gland cells in suspension. Following centrifugation, the supernatant was transferred to a new falcon tube and centrifuged again at 500 g for 5 min. Then, the new supernatant was aspirated and the pellet snap frozen in liquid nitrogen. A schematic showing the processing of different fractions is provided in Figure 5.7.

Table 5.6: *Table of altered components in digestion mixes used for digestion of bovine endometrium to isolate glandular epithelial cells to produce endometrial organoids.*
Components that remained the same in each mix were 50ml HBSS, 50mg bovine serum albumin (BSA) and 500μl sterile 100X Trypsin EDTA solution.

Digestion	**Collagenase II**	**Dispase**	**DNase**	**Reference**
1	0.5mg/ml	N/A	100μg/ml	(Tinning et al., 2020)
2	0.5mg/ml	1mg/ml	100μg/ml	Enzyme concentration from Turco et al., (2017) and DNase concentration from (Tinning et al., 2020)
3	0.5mg/ml	1mg/ml	1μg/ml	(Turco et al., 2017)

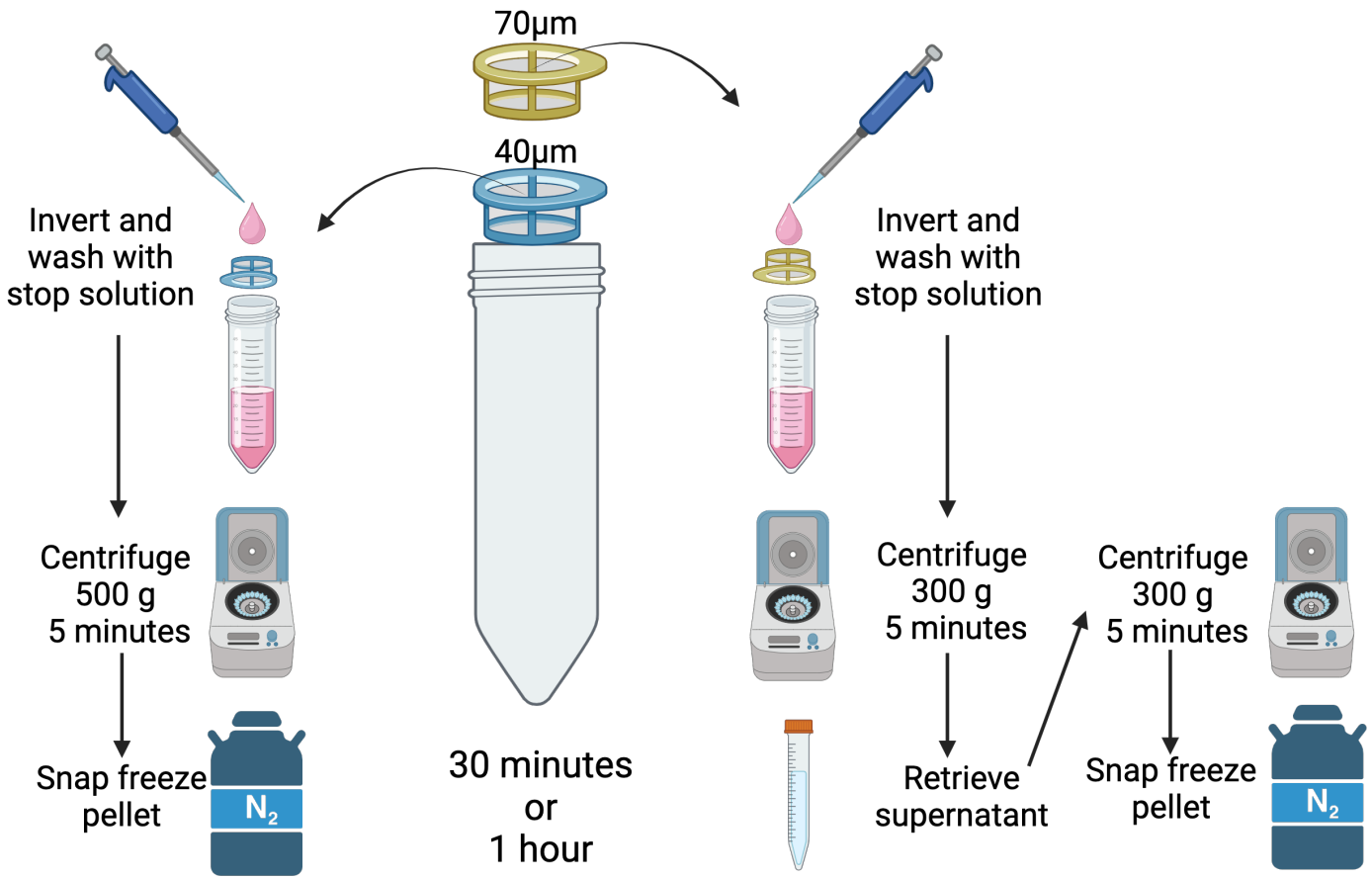

Figure 5.7: *Schematic to show workflow of isolating bovine cells from different fractions of endometrial tissue digestion to determine location of glandular epithelial cells.*
Bovine endometrial tissue was dissected and subjected to different digestion compositions for 30 min or 1 hr before being strained through a 70µM then a 40µM filter and 2 different fractions of digest were isolated for qRT-PCR analysis.

5.3.4.1.3 RNA extraction

Total RNA was extracted using the miRNeasy Micro Kit (Qiagen) following manufacturers protocol. Pellets were thawed on ice and 700μl QIAZol added before vortexing for 1 min to homogenize the cells followed by incubation at room temperature for 5 min. Next, 140μl chloroform was added and tubes shaken vigorously for 15 seconds, before a further room temperature incubation of 3 min. Tubes were centrifuged at 12000 g and 4°C for 15 min to separate RNA, which is present in the upper colourless phase. This phase of approximately 350μl was transferred to another tube carefully without transferring any other phase. A volume of 525μl 100% ethanol was added to the tubes and mixed by pipetting up and down. Then, 700μl each sample was added to corresponding spin columns and centrifuged at 8000 g for 15 seconds. This, and all further centrifugation steps were conducted at room temperature. This step was repeated with the remaining sample. Next, an on column DNase digestion was performed by firstly adding 350μl buffer RWT to the column and centrifuging at 8000 g for 15 seconds before discarding flow through. Per sample, 10μl of DNase I was added to buffer RDD (70μl) and this was added to the column and incubated at room temperature for 15 min. Following this, 350μl buffer RWT was added to wash and centrifuged at 8000 g for 15 seconds, again flow through was discarded. Then, 500μl 80% ethanol was added and the columns were centrifuged for 2 min at 8000 g, discarding flow through. Columns were transferred to a new collection tube and centrifuged at full speed for 5 min with column lids open in order to dry the membrane. The column was finally moved into a collection eppendorf and 14μl DNase and RNase free water was added directly to the membrane. Tubes were centrifuged at full speed for 1 min to elute RNA. RNA concentration was determined using the DeNovix DS-11 FX+ spectrophotometer (DeNovix) by adding 2μl of sample to measure RNA concentration.

5.3.4.1.4 cDNA conversion for mRNA

The High Capacity cDNA Reverse Transcription Kit (Applied Biosystems) was used to carry out a cDNA conversion of RNA samples. Samples were kept on ice for the duration of the set-up, until they were placed in the thermal cycler. Each RNA sample was diluted to 20ng/μl, and 10μl placed in 0.2ml PCR tubes. A master mix was made consisting of: 2μl 10x RT buffer, 0.8μl 25X dNTP mix, 2μl 10x RT random primers, 4.2μl RNase and DNase free water, and 1μl multiscribe RT; per sample. Ten μl of this master mix was added to each of the tubes. A negative RT control was performed for which the RNA was replaced with 10μl of RNA from a pool of all samples and 1μl water was added instead of

multiscribe RT. A positive RT control was carried out for which the RNA was replaced with sterile water. Tubes were centrifuged to ensure contents were at the bottom, then placed into a thermal cycler. They were incubated in the thermal cycler at 25^{o}C for 10 min, 37^{o}C for 120 min, 85^{o}C for 5 min and then held at 4^{o}C until they were collected. cDNA was stored at -20^{o}C short term until it was used.

5.3.4.1.5 Primer design

Primers for gland markers were designed using Primer BLAST. Parameters were set to primer must span an exon-exon junction, with a maximum PCR product size of 100 and minimum of 50. Primer sequences are shown in Table 5.7. The primers which were selected had the fewest unintended targets. Primers were reconstituted to 100μM with DNase and RNase free water according to individual volumes supplied with data sheets for each forward and reverse primer.

Table 5.7: *Table of primer sequences for gland markers*

Gene	Input Accession	Product length (bp)	Exon spanning	Forward sequence (5'-3-)	Reverse sequence (5'-3')
IGFBP1	NM_174554.3	63	Yes	AGCGATGAGGCTACAGATACA	TGAGCTCTCTGGGGACACAT
LIF	NM_173931.1	64	Yes	ACCAGCTGGGACAACTCAAC	CCCTGGGCCGTGTAATAGAG
MUC-1	XM_005203610.4	80	Yes	ACTCCACCTACCACACCCAT	GCCTGCAGAAACCTCCTCAT
KLF5	NM_001083727.1	94	Yes	ACTACTGCGATTACCCAGGC	TTGTACGGCTTCTCACCAGT
FOXA2	XM_025001047.1	72	Yes	GAGCCCGAGGGCTACT	CATGTACGTGTTGCCGT

5.3.4.1.6 Primer validation

A pool of bovine epithelial cell RNA extracted using the method described in Chapter 5, Section 5.3.4.1.3 was used to validate primers. RNA was adjusted by serial dilution with DNase and RNase free water to 10ng/μl, 5ng/μl, 2.5ng/μl and 1.25ng/μl. Into each well, 2μl of cDNA was pipetted. Forward and reverse primers were diluted to 20μM using DNase and RNase free water. For each gene, a primer mix was made comprising of - per well - 2.5μl DNase and RNase water, 0.25μl forward primer, 0.25μl reverse primer and 5μl SYBR green (Roche). Primer mix was pipetted up and down to mix and 8μl added to each well. Plate was sealed using a clear plastic plate seal and covered in tin foil until next steps to avoid light contact. A plate centrifuge was used for 30 seconds to ensure contents of wells were brought to the bottom. The plate was then placed in the LightCycler 96 (Roche). Stages of qRT-PCR reaction are shown in Table 5.8.

Data was processed using LightCycler 96 software to perform absolute quantification of data and then exported to Microsoft Excel to produce graphs for validation.

A qRT-PCR was carried out to select isolation fraction and incubation length using the same method. The only changes to this method was that all cDNA was diluted in DNase and RNase free water to be added to the plate at a concentration of 2.5ng/μl. Data was processed using LightCycler 96 software to perform absolute quantification and then exported to Microsoft Excel for further analysis. Raw CT values were subtracted from 45 (maximum possible value) to obtain raw gene expression, and graphs were plotted using GraphPad Prism.

Table 5.8: *Table listing stages of qRT-PCR reaction*

Stage	**Temperature (°C)**	**Time (s)**
Pre-incubation	95	300
Amplification 45 cycles	95	10
	56	10
	72	10
Melting	95	5
	65	60
	97	Continuous
Cooling	40	10

5.3.4.2 Organoid stability over time

5.3.4.2.1 Passaging organoids

Expansion media already present in the well was pipetted up and down with medium force approximately 4 times using a P1000 pipette set to 300μl to break up the droplet. Contents of wells were transferred to an eppendorf (usually pooling 2 wells) and centrifuged for 6 min at 2400 g. Supernatant was aspirated carefully, leaving approximately 100μl. Next, 150μl advanced DMEM/F12 was added and using a P200 pipette set to 100μl, the contents were pipetted up and down 300 times to break up the organoids. Advanced DMEM/F12 was added (500μl) and centrifuged again for 6 min at 600 g. Supernatant was aspirated once again leaving approximately 100μl. Cells were subjected to repeated up and down pipetting a further 100 times before another centrifugation for 6 min at 1200 g. All supernatant was now removed, and advanced DMEM/F12 was added (12μl per well to be plated). Ice cold Cultrex 2 was then added (48μl per well to be plated) and mixed gently avoiding bubbles. Droplets were plated as described in Chapter 5, Section 5.3.5.1.1. Organoids were usually split in a 1:2 or 1:3 ratio. Passaging for the collection of organoids at different time points as well as imaging of organoids to examine growth was carried out at: passage 0 day 9, passage 1 day 10 and passage 2 day 15.

5.3.4.2.2 Imaging and collection of organoids

Organoids (n=3) were imaged by light microscopy by selecting a random field of view within the droplet. The whole well was inspected visually to ensure relative uniformity of organoids. The time points organoids were imaged at are listed below:

- Passage 0, Day 5, 7 and 9
- Passage 1, Day 7 and 10
- Passage 2, Day 2, 7, 10 and 15
- Passage 3, Day 3, 7, 10 and 14

Organoids (n=3) were collected at different time points listed below:

- Passage 0, Day 2
- Passage 0, Day 5
- Passage 0, Day 7
- Passage 0, Day 9
- Passage 1, Day 10
- Passage 2, Day 15
- Passage 3, Day 14

To collect the organoids, expansion media was removed from wells and 500μl of fridge cold PBS added. This caused the Cultrex 2 to liquify and contents of the well were pipetted up and down approximately 4 times, before transferring to an eppendorf. Tubes were centrifuged at 600 g for 6 min, supernatant aspirated, resuspended in PBS to wash and subjected to another identical centrifuge. The supernatant was aspirated again and pellets snap frozen in liquid nitrogen for RNA extraction.

5.3.4.2.4 Gland marker expression over time and passage

RNA was extracted as described in Chapter 5, Section 5.3.4.1.3 and converted to cDNA as described in Section 5.3.4.1.4. Using validated primers for *LIF*, *MUC-1*, *KLF5*, *FOXA2* and *IGFBP1* (Figure 5.52), a qRT-PCR was performed to analyse expression of gland markers at different time points and over different passages. The qRT-PCR was carried out as described in Chapter 5, Section 5.3.5.1.6, with a cDNA concentration of 2.5ng/μl for each sample. Samples were analysed in technical duplicate. Absolute quantification of the data was carried out using LightCycler96 software and then exported to Microsoft Excel. Raw CT values were subtracted from 45 (maximum possible CT value) to give gene expression values which were plotted on Graphpad Prism. Statistical analysis was not carried out to test for differences as normalization was not performed and the purpose of this experiment was to look for presence or absence of gland markers in each animal.

5.3.4.3 Investigating effect of progesterone on organoids

5.3.4.3.1 Treatment of organoids with progesterone

Organoids (n=5) at passage 0, 8 days post isolation were treated with 1) control - expansion media 2) vehicle - 100% ethanol (20μl) or P4 (10μg/ml - volume 20μl) for 24 hrs at 37^{o}C 5% CO_2 by adding of treatment to expansion media with a final volume added to the well of 500μl.

5.3.4.3.2 Collecting organoids and extracting RNA for RNA sequencing

Organoids were collected in a different way to Chapter 5, Section 5.3.4.2.2, to maximise yield by removal of expansion media from wells and addition of 500μl cell recovery solution before the plate was placed on ice for 1 hr to cause Cultrex 2 to liquify. Contents of wells were transferred to Eppendorfs, pooling 2 wells of the same treatment. Tubes were centrifuged for 6 min at 600 g and supernatant removed, then the pellet was resuspended in 500μl Advanced DMEM/F12 by pipetting up and down approximately 10 times. The tubes were

centrifuged again at 600 g for 6 min and the supernatant removed with the pellet snap frozen in liquid nitrogen. RNA was extracted for RNA sequencing using the method described above in Chapter 5, Section 5.3.5.1.3.

5.3.4.3.4 RNA sequencing

RNA sequencing was carried out by Novogene.(Novogene, Cambridge, UK) Methods described below are based on those supplied by Novogene. Poly-T oligo-attached magnetic beads were used to separate mRNA from total RNA. The mRNA was fragmented, and random hexamer primers were used to first produce the first strand of cDNA, then the second strand. Stages of end repair, A-tailing, adapter ligation, size selection, amplification and purification were carried out to produce the cDNA library. Qubit and RT-PCR were used to quantify the library and a Bioanalyzer 2100 (Agilent Technologies, USA) used for detection of size distribution. An Illumina Novaseq6000 was used to pool libraries and sequence, dependent on library concentration and data amount. Sequencing was carried out by the paired end 150 strategy - which means that a fragment of 150bp is produced from each end of the template resulting in 2 paired reads per target.

5.3.4.3.5 RNASeq data analysis

Initial data analysis was carried out by LeedsOmics. Methods described below for quality control, alignment and differential expression were provided by LeedsOmics. Data analysis was performed in R version 4.1.0.

Quality control was assessed using FastQC (Andrews, 2010) and multiQC (Ewels et al., 2016), with Trimmomatic (Bolger et al., 2014) used to remove adapters and low quality bases (QV<20) from the ends; leaving a minimum read length of 30bp. Downstream analysis was conducted on an average of 23.2 million reads remaining after trimming per sample. The bovine ARS-UCD1.2 release -109 reference genome (retrieved from https://ftp.ensembl.org/pub/release-109/fasta/bos_taurus/dna/Bos_taurus.ARS-UCD1.2.dna.toplevel.fa.gz) was used to map libraries using STAR aligner (Dobin et al., 2013) according to default parameters. Output files generated by STAR aligner were in BAM format and these were used to match read counts to gene features using featureCounts (Liao et al., 2014). The parameters were set to: -p -B -C -M -O --fraction. An annotation file for Bos_taurus.ARS-UCD1.2.109.gtf was downloaded from the same ensembl address.

Differential expression was established from featureCounts matrix using the DeSeq2 negative binomial distribution model through a local fitting type and 0.05 FDR threshold (Love et al., 2014). Pairwise differential expression

comparisons were analysed as follows: 1) vehicle vs control, P4 vs control, P4 vs vehicle. Plotting and graphical representation of the data was produced using the following packages: EdgeR (Robinson et al., 2010) and EnhancedVolcano (Blighe et al., 2019).

Downstream analysis was carried out using WebGestalt for overrepresentation enrichment analysis identifying biological pathways, molecular functions and cellular components associated with differentially expressed genes. Protein-protein interaction networks were predicted by STRING analysis.

5.3.4.3.6 Organoid miRNA analysis

RNA from animals 1, 3 and 4 from the RNASeq experiment was used to examine miRNA expression in bovine organoids with and without P4 treatment. MiRCURY LNA RT Kit (Qiagen) was used to reverse transcribe miRNA into cDNA for qRT-PCR. This was carried out according to the method described in Chapter 2, Section 2.3.3.3.

A qRT-PCR was carried out according to Chapter 2, Section 2.3.3.3 with the following adjustments. Custom miRCURY LNA miRNA PCR Panels (Cat# 339330) were obtained from Qiagen, pre-loaded with primers for conserved eutherian mammal specific miRNAs of interest (Taylor et al., 2023). Samples were carried out in technical duplicate.

The list of miRNAs along with normaliser genes is as follows:

- Hsa-miR-28-3p
- Hsa-miR-127-3p
- Hsa-miR-151a-3p
- Hsa-miR-151a-5p
- Hsa-miR-185-5p
- Hsa-miR-188-5p
- Hsa-miR-324-5p
- Hsa-miR-331-3p
- Hsa-miR-340-5p
- Hsa-miR-378a-3p
- Hsa-miR-423-3p
- Hsa-miR-423-5p
- Hsa-miR-433-3p
- Hsa-miR-505-5p
- Hsa-miR-532-5p
- Hsa-miR-542-3p
- Hsa-miR-660-5p
- Hsa-miR-671-3p

- Hsa-miR-671-5p
- Hsa-miR-708-5p
- 5S rRNA (hsa) – normaliser reference gene

5.4 Results

5.4.1 Normal 2D endometrium/embryo attachment assay

Attachment assays were carried out to determine whether altering expression of miR-340-5p, miR-542-3p and miR-671-5p would have an effect on the attachment stage of implantation. A representative image showing output results is shown in Figure 5.8.

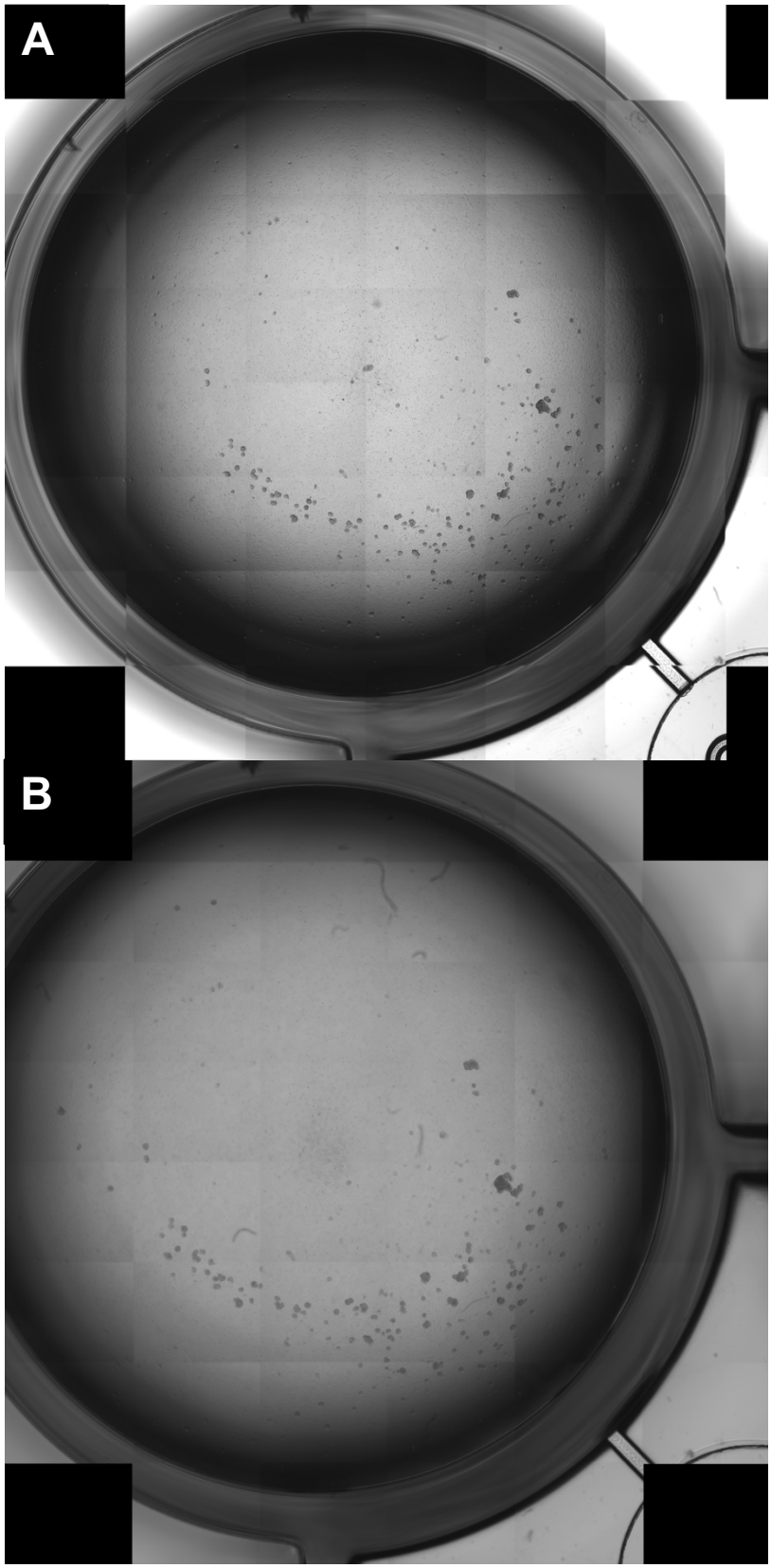

Figure 5.8: *Representative whole well images of attachment assay.* Ishikawa cells (n=5) transfected with miR-340-5p mimic for 48 hrs with BeWo spheroids added to well. Incubated for 1 hr at 37°C 5% CO_2 **A**) Before fixation and **B**) After fixation with formalin followed by PBS wash.

5.4.1.1 Confirmation of transfection using Dharmafect 2 transfection reagent

Expression of miR-340-5p (Figure 5.9), miR-542-3p (Figure 5.10) and miR-671-5p (Figure 5.11) was increased when transfected with their respective mimics by qPCR analysis, using Dharmafect 2 as a transfection reagent. This was carried out to confirm Dharmafect 2 resulted in successful transfection and thus overexpression of miRNAs in Ishikawa cells. As this was proof of principle and this is a widely used protocol in the laboratory, this was carried out with an n=1.

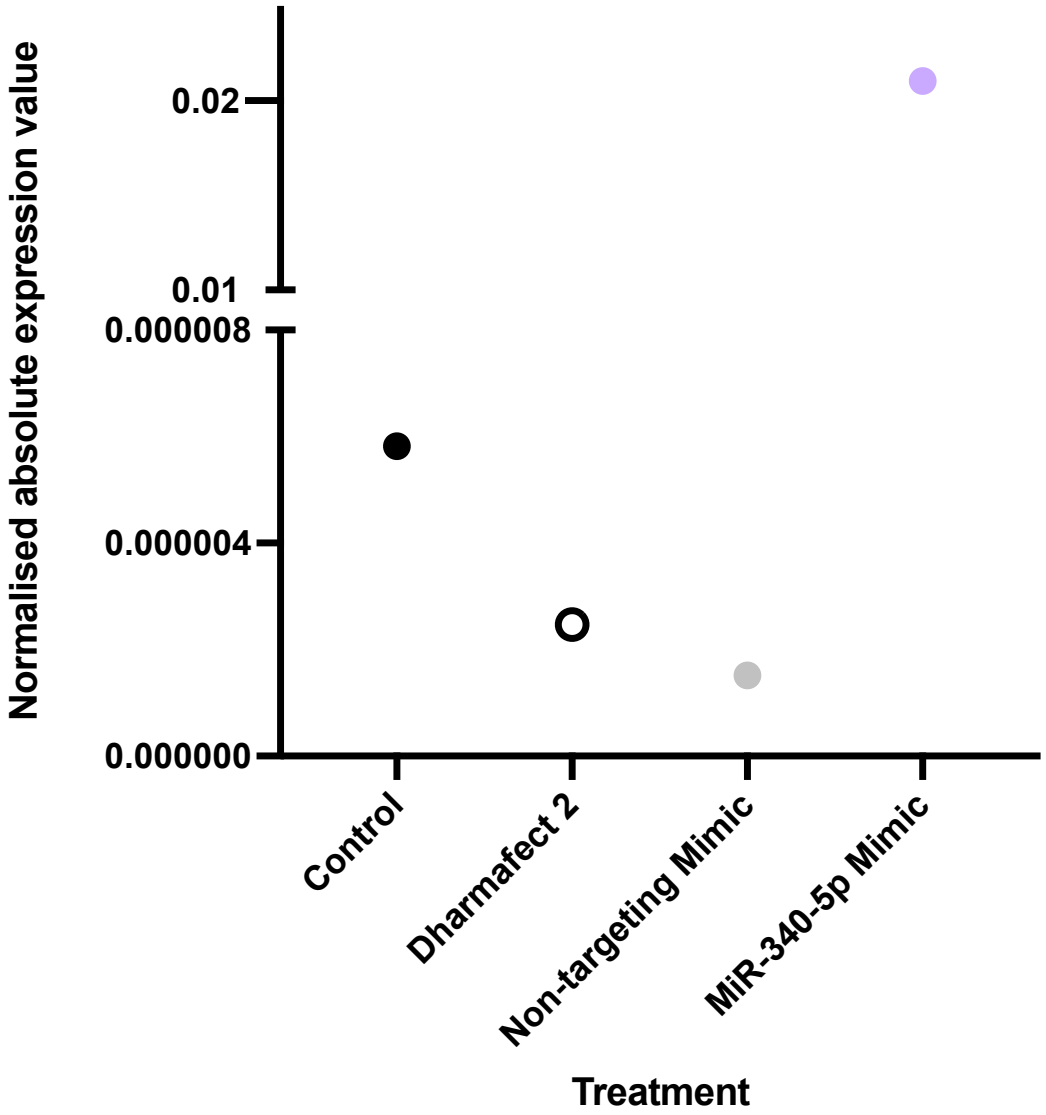

Figure 5.9: *Absolute expression values of miR-340-5p normalised to 5s following endometrial epithelial cell transfection with miR-340-5p mimic.* Treatments were each added to 60,000 Ishikawa cells per well for 48hr (n=1 biological replicates), 0.4ml antibiotic and serum free media and consisted of i) Control - 100μl optiMEM media only, ii) Dharmafect 2 only control - 1μl Dharmafect 2 in 100μl optiMEM media, iii) 40nM of non-targeting mimic, iv) 40nM of miR-340-5p mimic**.**

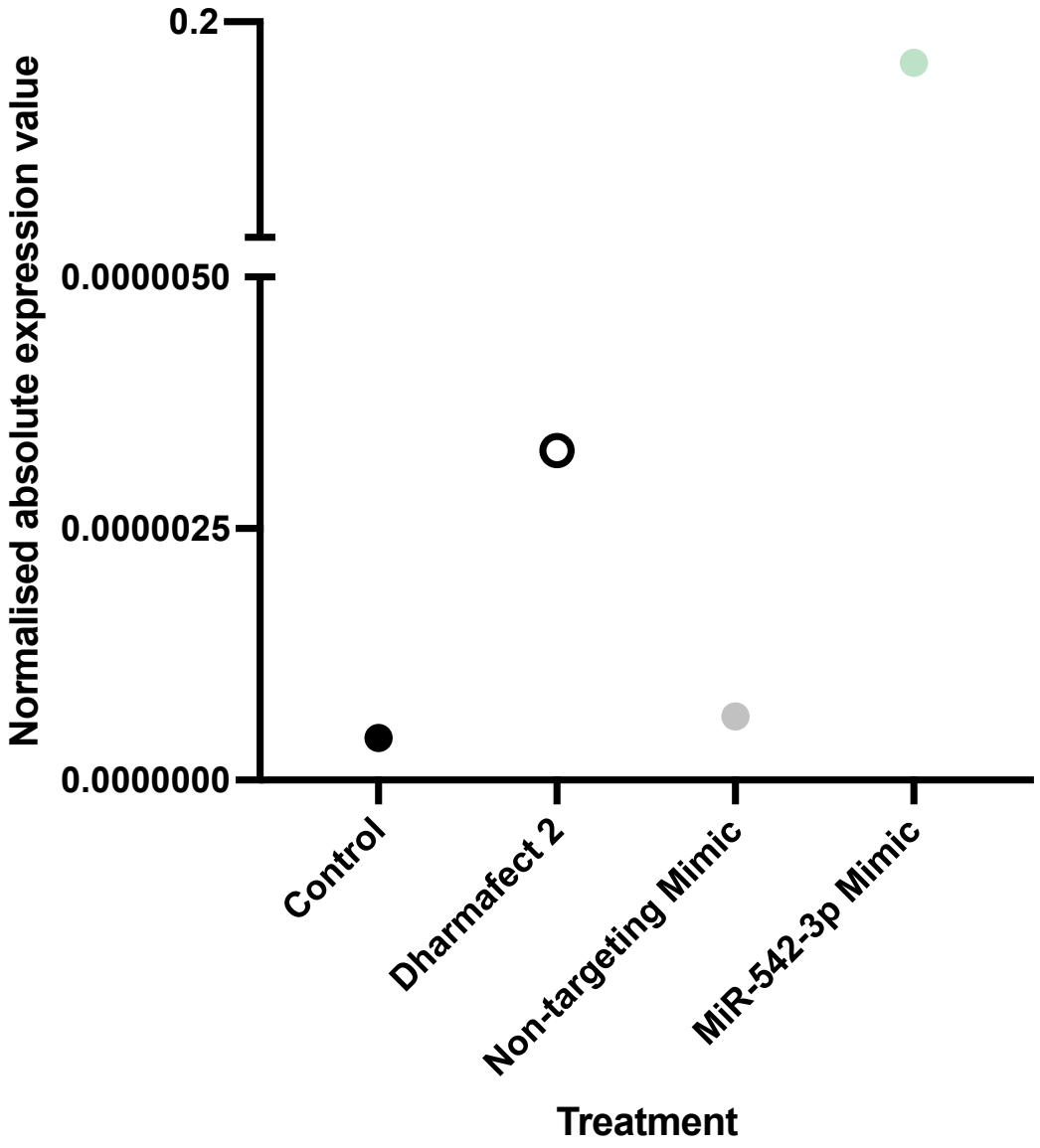

Figure 5.10: *Absolute expression values of miR-542-3p normalised to 5s following endometrial epithelial cell transfection with miR-542-3p mimic.* Treatments were each added to 60,000 Ishikawa cells per well for 48hr (n=1 biological replicates), 0.4ml antibiotic and serum free media and consisted of i) Control - 100μl optiMEM media only, ii) Dharmafect 2 only control - 1μl Dharmafect 2 in 100μl optiMEM media, iii) 40nM of non-targeting mimic, iv) 40nM of miR-542-3p mimic**.**

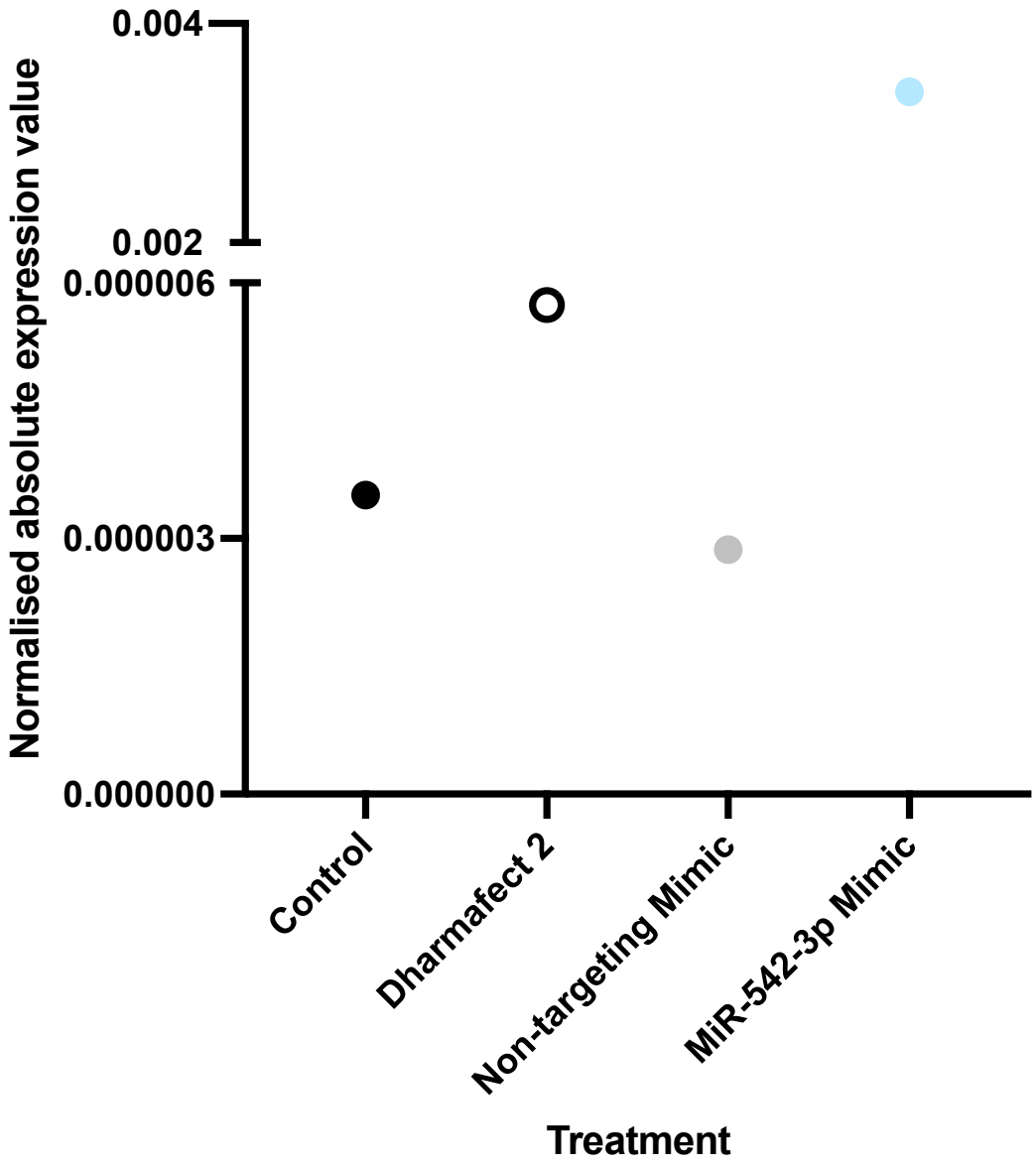

Figure 5.11: *Absolute expression values of miR-671-5p normalised to 5s following endometrial epithelial cell transfection with miR-671-5p mimic.* Treatments were each added to 60,000 Ishikawa cells per well for 48hr (n=1 biological replicates), 0.4ml antibiotic and serum free media and consisted of i) Control - 100μl optiMEM media only, ii) Dharmafect 2 only control - 1μl Dharmafect 2 in 100μl optiMEM media, iii) 40nM of non-targeting mimic, iv) 40nM of miR-671-5p mimic.

5.4.1.2 Optimisation of incubation length and spheroid number

To determine optimal length of incubation and spheroid number for most consistent results, a range of incubation times were tested with two different volumes of spheroids. A percentage spheroid attachment rate of approximately 70% was considered appropriate, as this allowed both significant increases or decreases in attachment to be recognised. An incubation length of 1 hr and a volume of 60μl spheroids - approximately 150-200 spheroids - was selected as this resulted in an average percentage attachment of 69.9% (Figure 5.12).

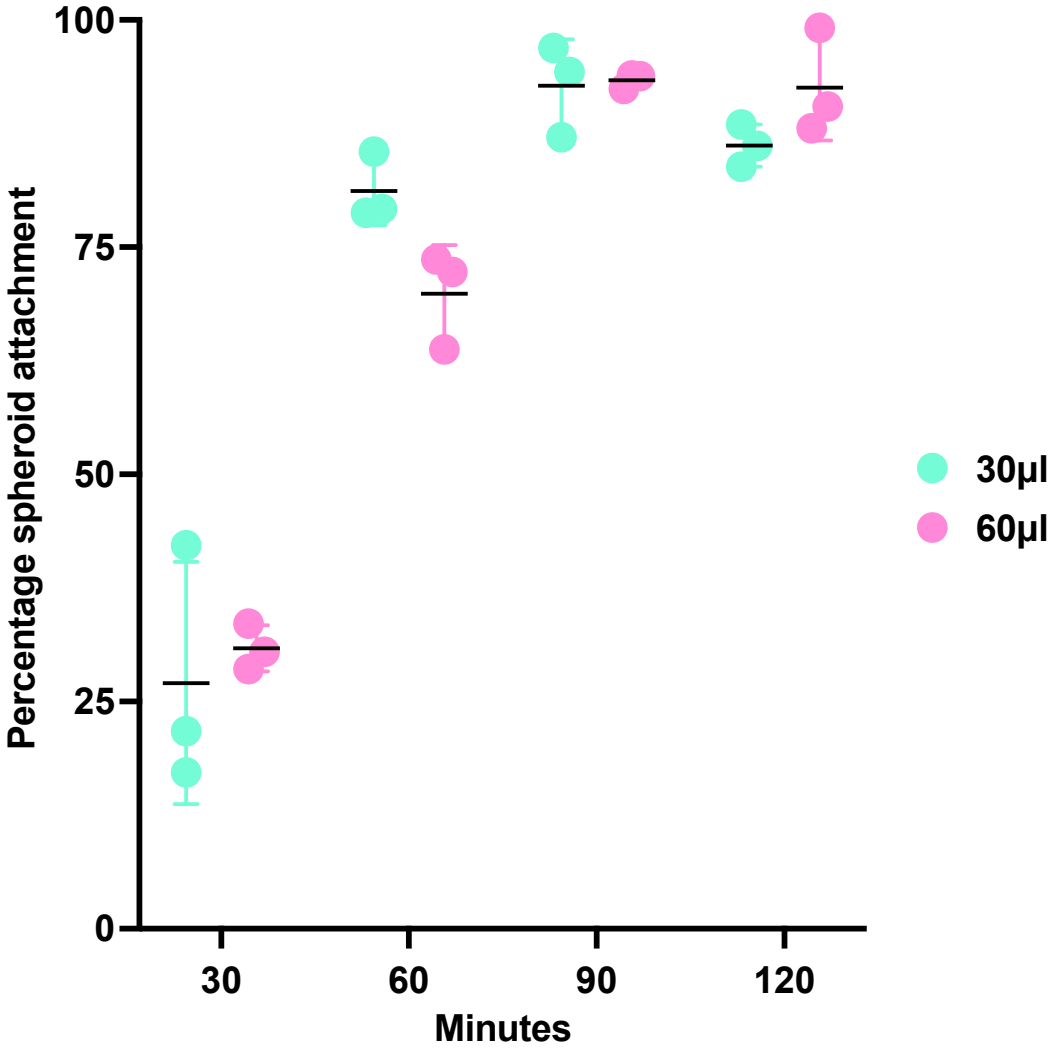

Figure 5.12: *Optimising attachment assay incubation length and spheroid volume.*
Percentage BeWo spheroid attachment (embryo-like model) to Ishikawa cells (n=3) for optimisation of incubation length and spheroid volume. BeWo cells were added to Ishikawa cell monolayers and were subjected to incubations of 30, 60, 120 and 150 min, with volumes of 30µl or 60µl spheroids added to well at each time point.

5.4.1.3 MiR-340-5p

Overexpression of miR-340-5p in endometrial epithelial cells had no significant effect on spheroid attachment (Figure 5.13). However, although non-significant ($p>0.05$), miR-340-5p appeared to increase attachment of the spheroids somewhat.

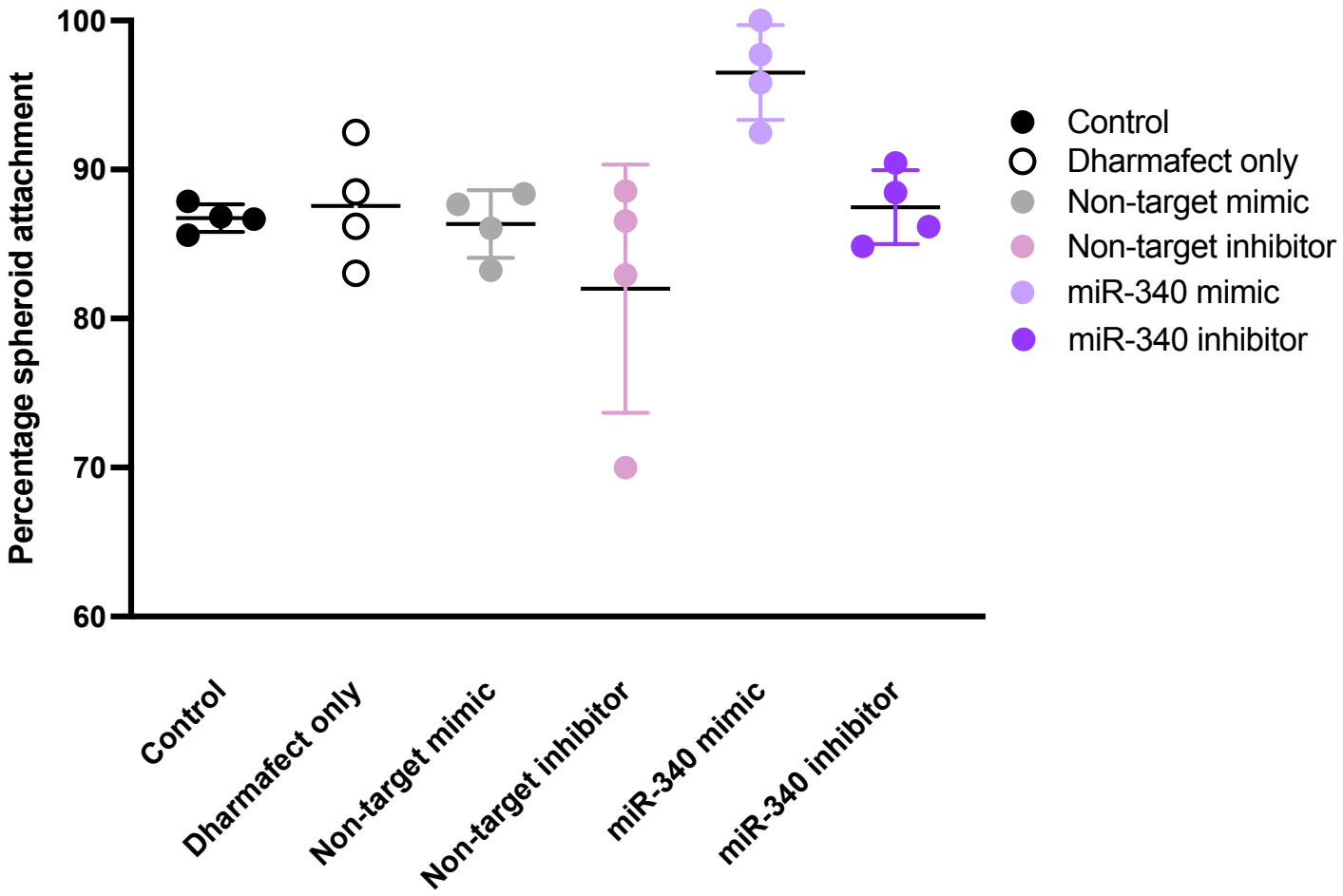

Figure 5.13: *Percentage BeWo spheroid attachment (embryo-like spheroid model) following transfection (48 hrs) of Ishikawa cells (n=4) with miR-340-5p mimic (40nM), inhibitor (40nM) and non-targeting controls (40nM).*
Treatments added to cells using 100μl optiMEM media + 1μl Dharmafect 2, except control - without Dharmafect 2. Statistical significance analysed by multiple t-tests with Bonferroni correction ($p<0.05$).

5.4.1.4 MiR-542-3p

Overexpression of miR-542-3p in endometrial epithelial cells significantly ($p<0.05$) decreased percentage spheroid attachment in comparison to non-targeting mimic and highly significantly ($p<0.01$) decreased percentage spheroid attachment compared to control (Figure 5.14).

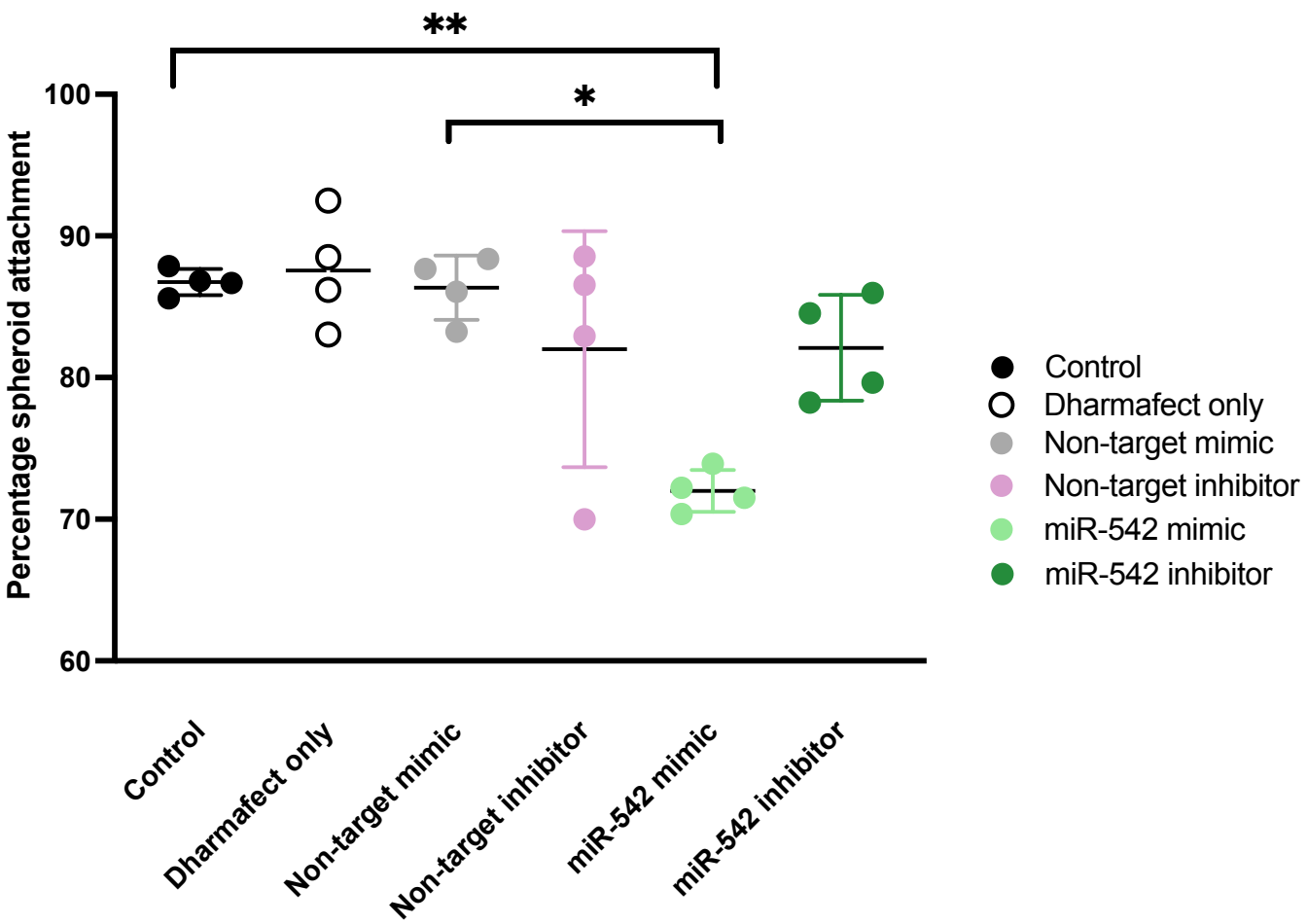

Figure 5.14: *Percentage BeWo spheroid attachment (embryo-like spheroid model) following transfection (48 hrs) of Ishikawa cells (n=4) with miR-542-3p mimic (40nM), inhibitor (40nM) and non-targeting controls (40nM).*
Treatments added to cells using 100μl optiMEM media + 1μl Dharmafect 2, except control - without Dharmafect 2. Statistical significance analysed by multiple t-tests with Bonferroni correction (* = $p<0.05$, ** = $p<0.01$).

5.4.1.5 MiR-671-5p

There were no significant differences in percentage spheroid attachment when over or under expressing miR-671-5p in endometrial epithelial cells (Figure 5.15). Treatment with miR-671-5p inhibitor appears to increase attachment, although non-significantly ($p>0.05$), and treatment with miR-671-5p appears to slightly decrease attachment - again non-significantly ($p>0.05$).

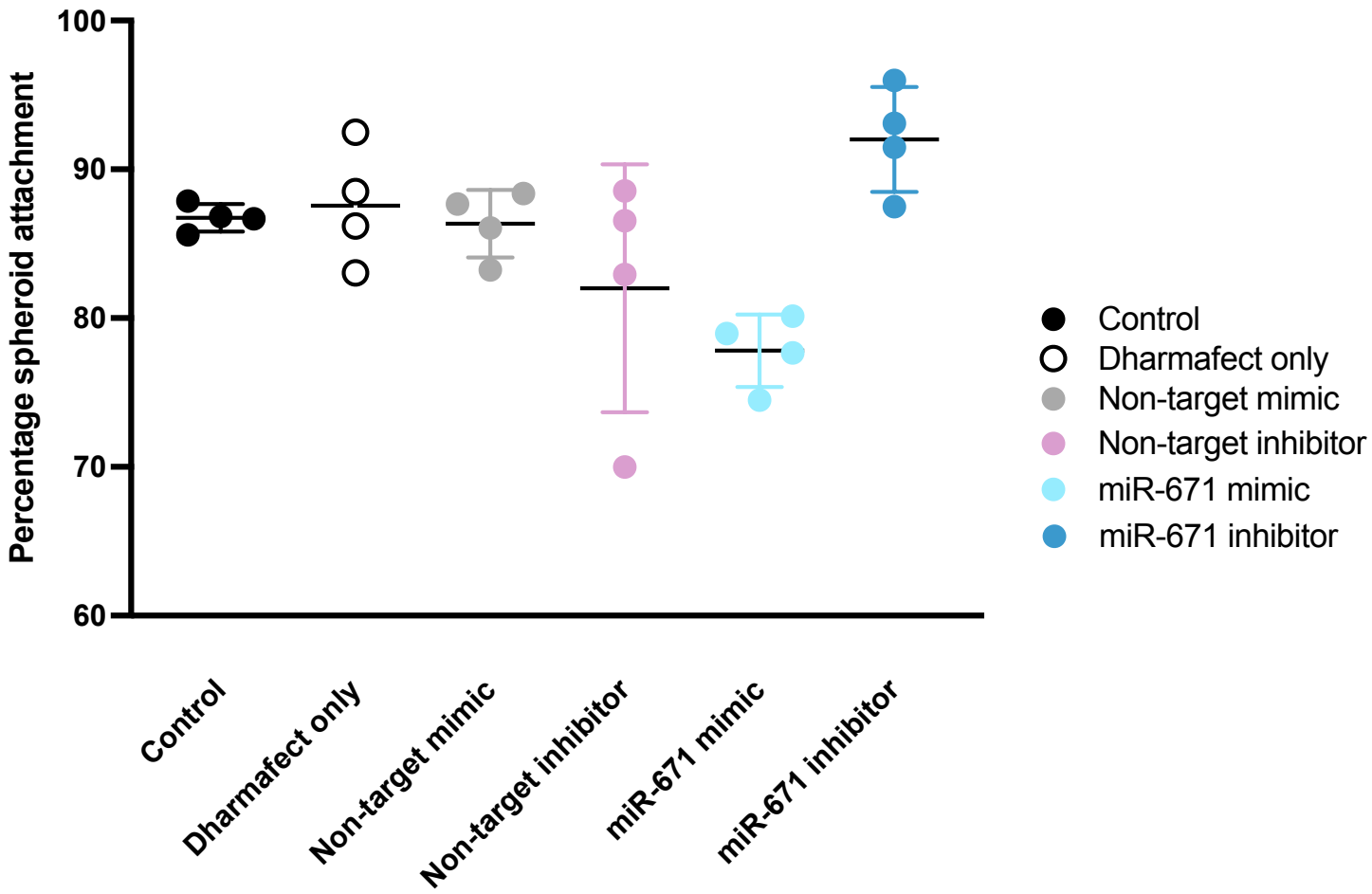

Figure 5.15*: Percentage BeWo spheroid attachment (embryo-like spheroid model) following transfection (48 hrs) of Ishikawa cells (n=4) with miR-671-5p mimic (40nM), inhibitor (40nM) and non-targeting controls (40nM).*
Treatments added to cells using 100μl optiMEM media + 1μl Dharmafect 2, except control - without Dharmafect 2. Statistical significance analysed by multiple t-tests with Bonferroni correction ($p<0.05$).

5.4.1.6 Comparison of effect on attachment between miR-340-5p, miR-542-3p and miR-671-5p

In endometrial epithelial cells, overexpression of miR-542-3p mimic significantly ($p<0.05$) decreased percentage spheroid attachment compared to miR-340-5p mimic treatment (Figure 5.16). MiR-340-5p overexpression significantly ($p<0.05$) increased percentage spheroid attachment in comparison to treatment with miR-671-5p mimic. Also, miR-542-3p overexpression significantly ($p<0.05$) decreased percentage spheroid attachment when compared with miR-671-5p inhibition.

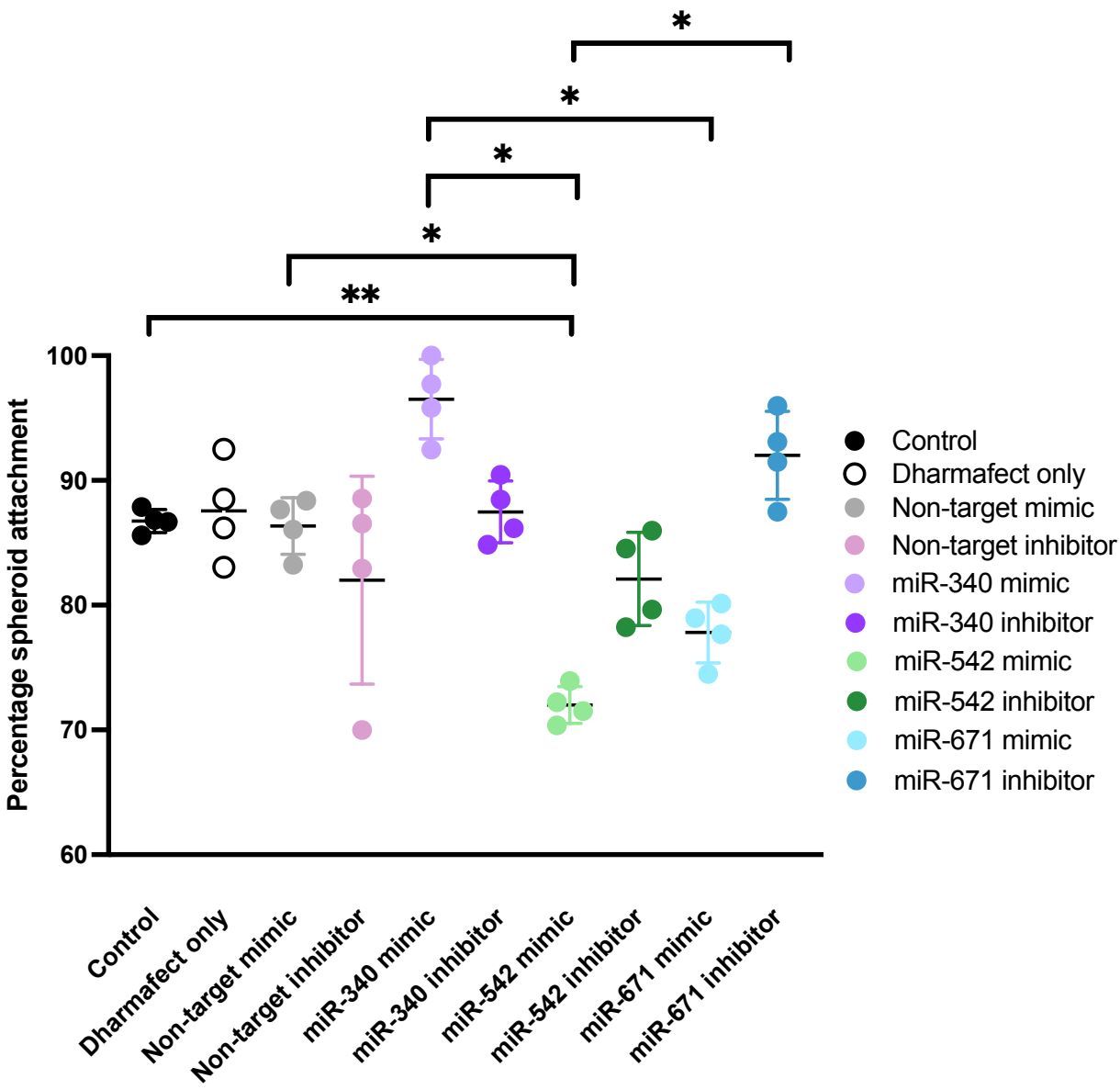

Figure 5.16: *Comparison of spheroid attachment following differential expression of miR-340-5p, miR-542-3p or miR-671-5p.*
Percentage BeWo spheroid attachment following transfection (48 hrs) of Ishikawa cells (n=4) with miR-340-5p/miR-542-3p/miR-671-5p mimic, inhibitor and non-targeting controls. Statistical significance analysed by multiple t-tests with Bonferroni correction (* = $p<0.05$, ** = $p<0.01$).

5.4.1.7 Combinatory effect of miRNA transfections on spheroid attachment

The combined effect of over or under expression of more than one of miR-340-5p, miR-542-3p and miR-671-5p was investigated to determine whether this had an effect on attachment. Since adding 3 times the previously used concentration of mimic or inhibitor exceeded the maximum concentration of miRNA mimic or inhibitor advised for use with Dharmafect 2 transfection reagent, an initial 'proof of principle study' was carried out using lower mimic concentrations. This confirmed that using a lower, and multiple concentrations of miRNA mimics resulted in overexpression of the miRNAs (Figure 5.17). Raw CT values were reduced on average by 10 cycles, which was equivalent to the reduction in raw CT value observed when transfecting with a single miRNA at a higher concentration. Due to the exponential nature of qPCR, this corresponds to a large difference quantitatively. The lower concentrations of mimic or inhibitor were deemed acceptable for use in subsequent attachment assays.

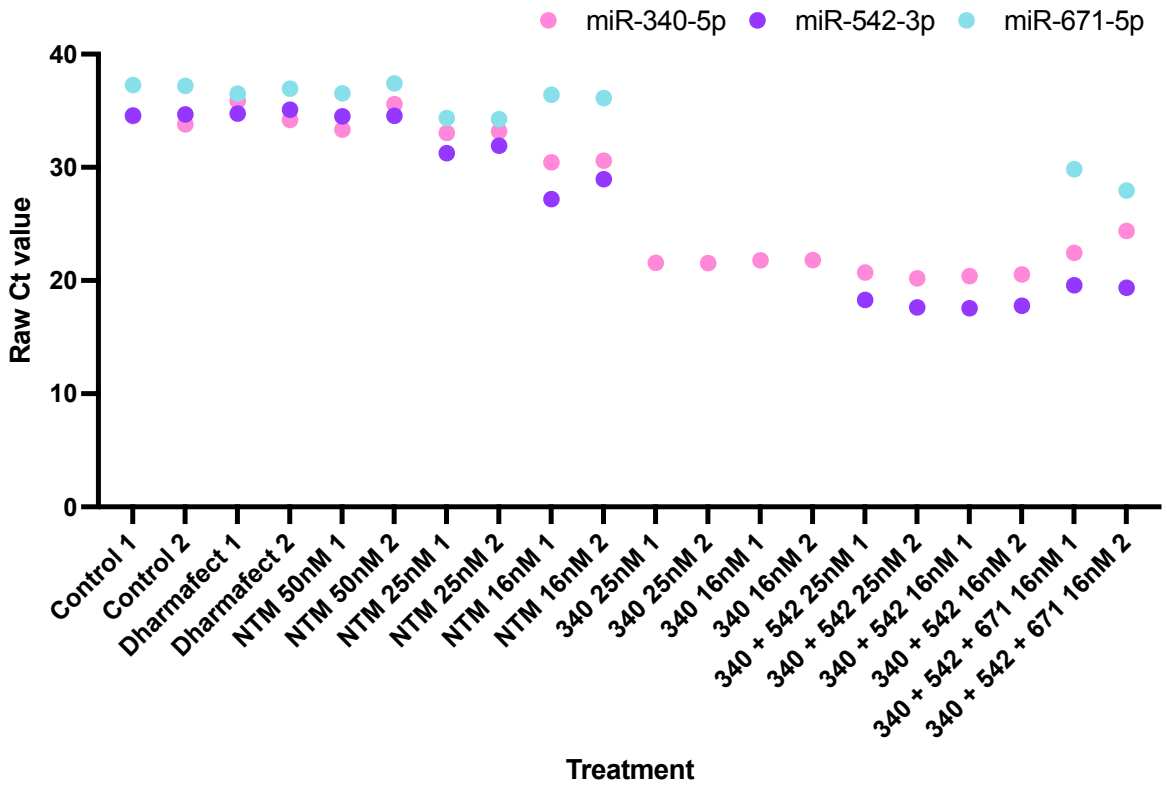

Figure 5.17: *Absolute raw CT expression values of miR-340-5p, miR-542-3p and miR-671-5p following endometrial epithelial cell transfection with different concentrations of miR-340-5p, miR-542-3p, and miR-671-5p mimics.*
Treatments were each added to 60,000 Ishikawa cells per well, for 48hr, (n=2 biological replicates) 400μl antibiotic and serum free media - those with miRNA mimics also included 1μl Dharmafect 2 - and consisted of i) Control - 100μl optiMEM media only, ii) Dharmafect 2 only control - 1μl Dharmafect 2 in 100μl optiMEM media, iii-v) 50nM, 25nM or 16nM of non-targeting mimic, vi-vii) 25nM or 16nM of miR-340-5p mimic, viii-ix) 25nM or 16nM of miR-340-5p and miR-542-3p, and x-xi) 16nM miR-340-5p, miR-542-3p and miR-671-5p.

5.4.1.7.1 The effect of differentially expressing two microRNAs simultaneously on embryo attachment

Transfection of Ishikawa cells (n=4 biological replicates) with 1 mimic and 1 inhibitor for miR-340-5p, miR-542-3p or miR-671-5p resulted in a significant increase ($p<0.05$) in spheroid attachment rate when treated with miR-340-5p inhibitor and miR-542-3p mimic, compared to control (Figure 5.18). Furthermore, miR-340-5p inhibitor with miR-542-3p mimic also significantly ($p<0.05$) increased attachment rate compared to miR-340-5p mimic with miR-671-5p inhibitor.

Ishikawa cells (n=4 biological replicates) which were transfected with 2 mimics from either miR-340-5p, miR-542-3p or miR-671-5p showed no significant differences ($p>0.05$) in embryo attachment rate compared with any controls or other combinations of mimics (Figure 5.19). However, each of the targeting mimic combinations did appear to very slightly increase attachment compared to the non-targeting control, but addition of any mimics (targeting or non-targeting) showed a non-significant decrease in attachment compared to control and Dharmafect only control.

When under expressing 2 miRNAs of miR-340-5p, miR-542-3p and miR-671-5p in Ishikawa cells (n=3 biological replicates), there was significantly decreased attachment ($p<0.05$) when miR-542-3p and miR-671-5p were inhibited compared to control. Furthermore, compared to the Dharmafect only control, there was a significant decrease in attachment following inhibition of miR-542-3p and miR-671-5p, as well as miR-340-5p and miR-671-5p. MiR-542-3p and miR-671-5p inhibition resulted in significantly ($p<0.01$) lower embryo attachment rate than miR-340-5p and miR-671-5p under expression (Figure 5.20).

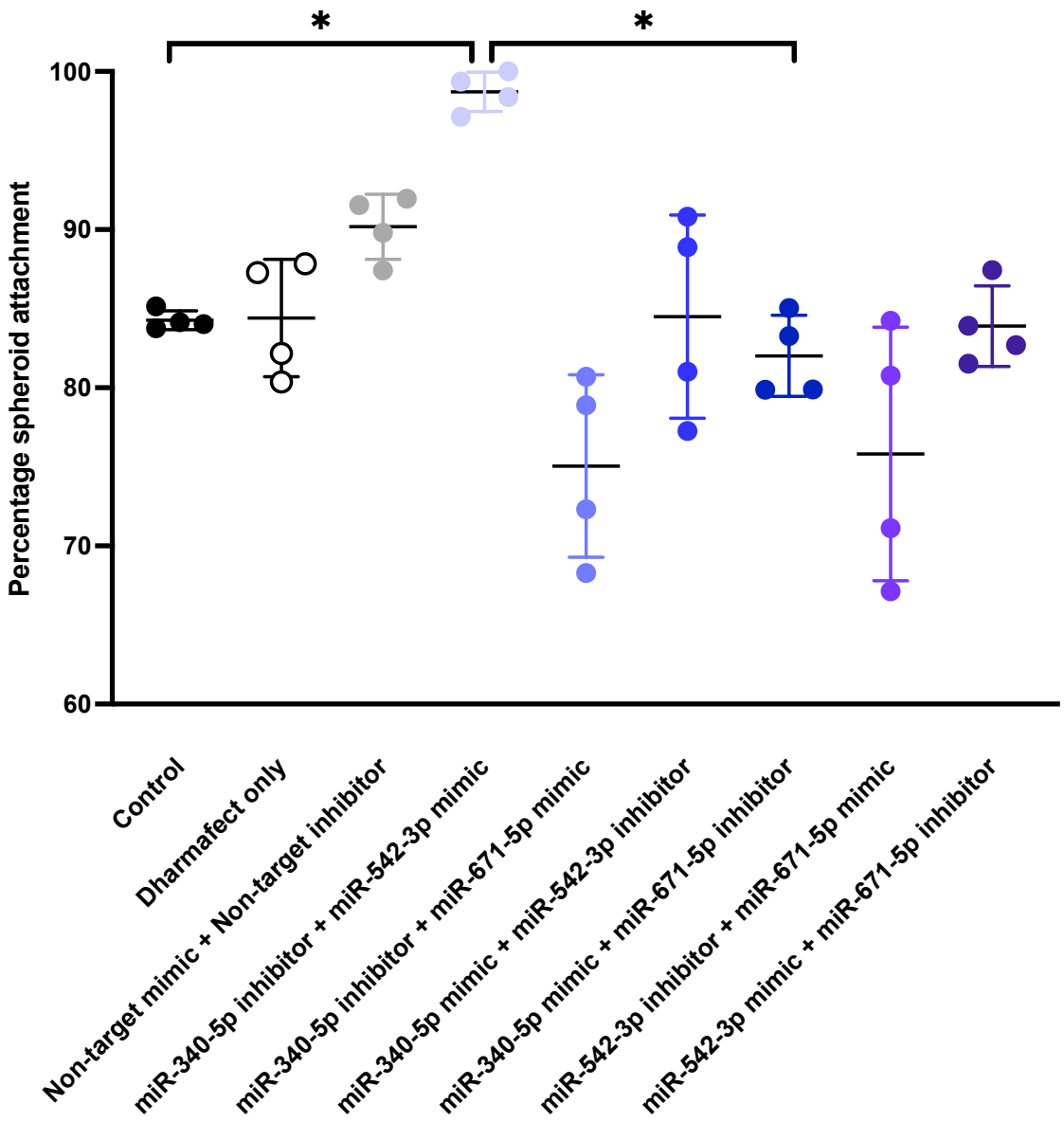

Figure 5.18: *Comparison of spheroid attachment following transfection with 1 mimic and 1 inhibitor of miR-340-5p, miR-542-3p and miR-671-5p.* Percentage BeWo spheroid attachment following transfection (48 hrs) of Ishikawa cells (n=4) with 1 of each miR-340-5p/miR-542-3p/miR-671-5p mimic and inhibitor and non-targeting controls. Statistical significance analysed by multiple t-tests with Bonferroni correction (* = $p<0.05$).

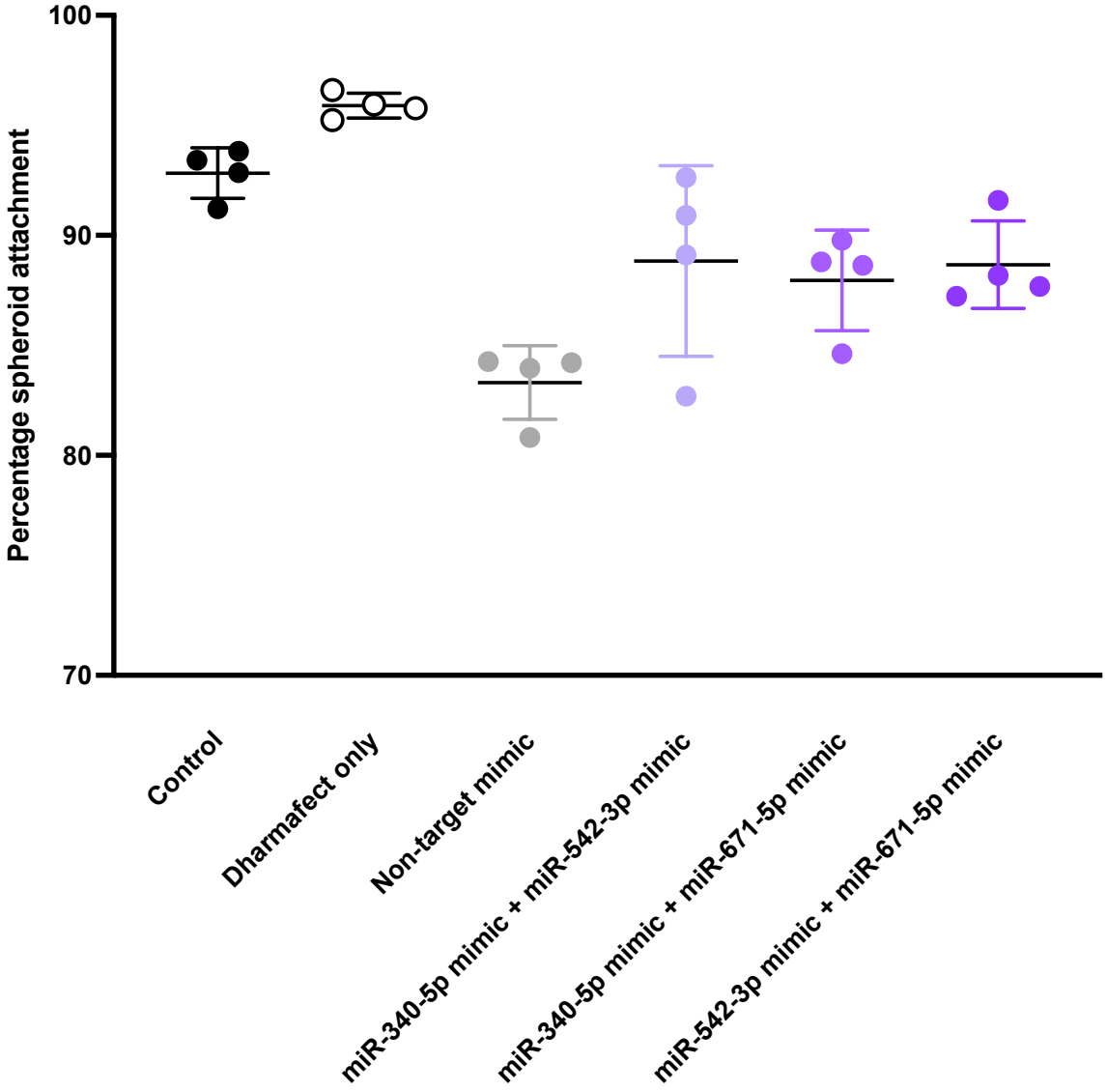

Figure 5.19: *Comparison of spheroid attachment following transfection with 2 mimics for miR-340-5p, miR-542-3p or miR-671-5p.*
Percentage BeWo spheroid attachment following transfection (48 hrs) of Ishikawa cells (n=4) with 2 miR-340-5p/miR-542-3p/miR-671-5p mimics and non-targeting controls. Statistical significance analysed by multiple t-tests with Bonferroni correction (* = $p<0.05$).

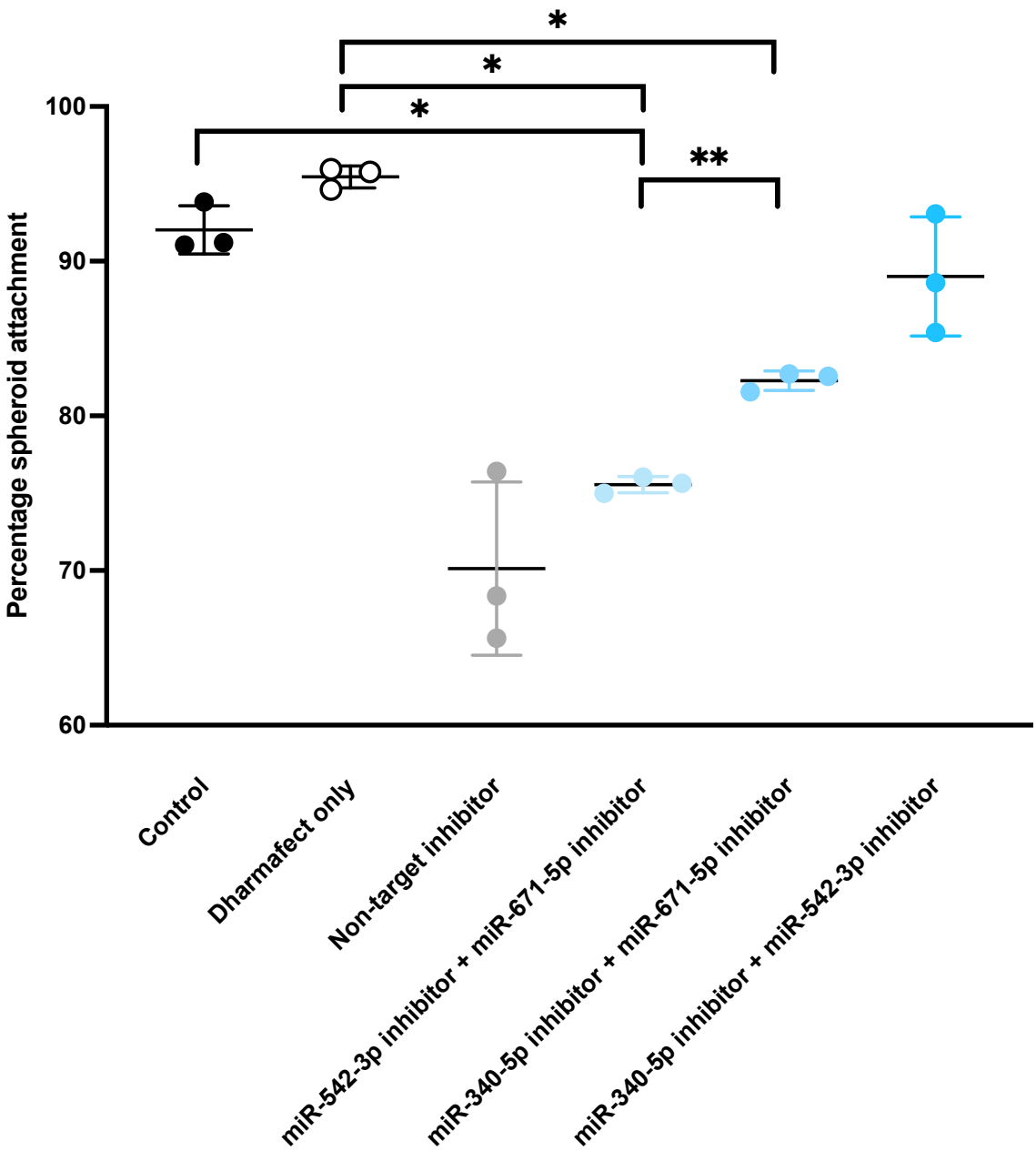

Figure 5.20: *Comparison of spheroid attachment following transfection with 2 inhibitors for miR-340-5p, miR-542-3p or miR-671-5p.*
Percentage BeWo spheroid attachment following transfection (48 hrs) of Ishikawa cells (n=3) with 2 miR-340-5p/miR-542-3p/miR-671-5p inhibitors and non-targeting controls. Statistical significance analysed by multiple t-tests with Bonferroni correction (* = $p<0.05$, ** = $p<0.01$).

5.4.1.7.2 The effect of differentially expressing miR-340-5p, miR-542-3p and miR-671-5p simultaneously on embryo attachment

Simultaneous overexpression of 2 of miR-340-5p, miR-542-3p or miR-671-5p in Ishikawa cells (n=4 biological replicates) whilst under expressing the third miRNA resulted in no significant differences ($p>0.05$) in attachment rate compared to controls or other combinations (Figure 5.21). Similarly, under expressing 2 of the miRNAs with overexpression of the third miRNA had no significant ($p>0.05$) effect on embryo attachment rate (Figure 5.22).

Overexpressing all 3 miRNAs miR-340-5p, miR-542-3p and miR-671-5p in Ishikawa cells (n=5 biological replicates) resulted in a highly significant increase ($p<0.01$) in attachment compared to media only control. However, there was also a significant increase ($p<0.05$) in both non-targeting mimic as well as Dharmafect only control, in comparison to media only control (Figure 5.23). Oppositely, inhibition of miR-340-5p, miR-542-3p and miR-671-5p had no significant ($p>0.05$) effect on embryo attachment to Ishikawa cells (n=4 biological replicates) (Figure 5.24).

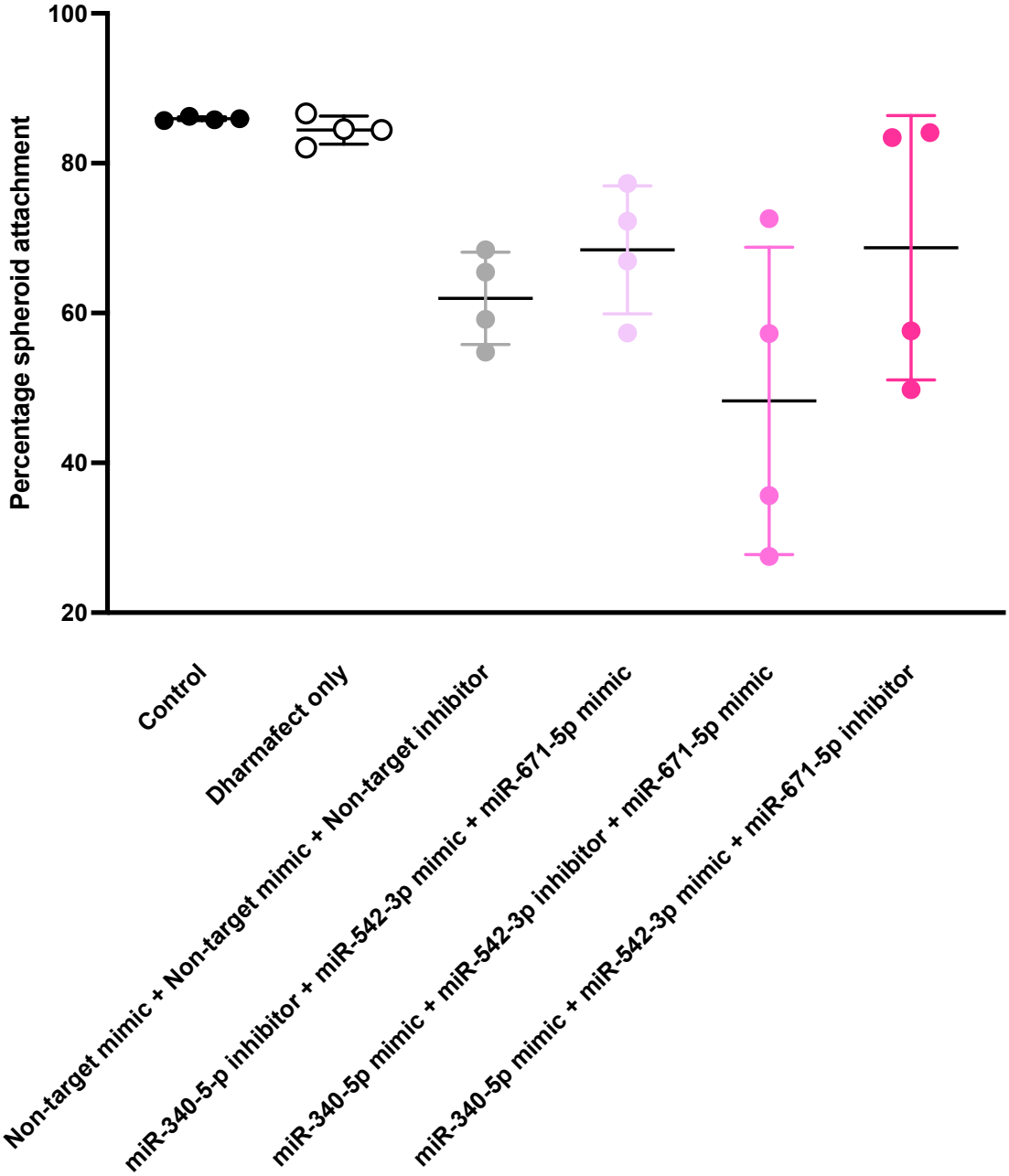

Figure 5.21: *Comparison of spheroid attachment following transfection with 2 mimics for miR-340-5p, miR-542-3p or miR-671-5p, and inhibition of the third.* Percentage BeWo spheroid attachment following transfection (48 hrs) of Ishikawa cells (n=4) with 2 of miR-340-5p/miR-542-3p/miR-671-5p mimics and inhibitor of the third miRNA, and non-targeting controls. Statistical significance analysed by multiple t-tests with Bonferroni correction (* = $p<0.05$).

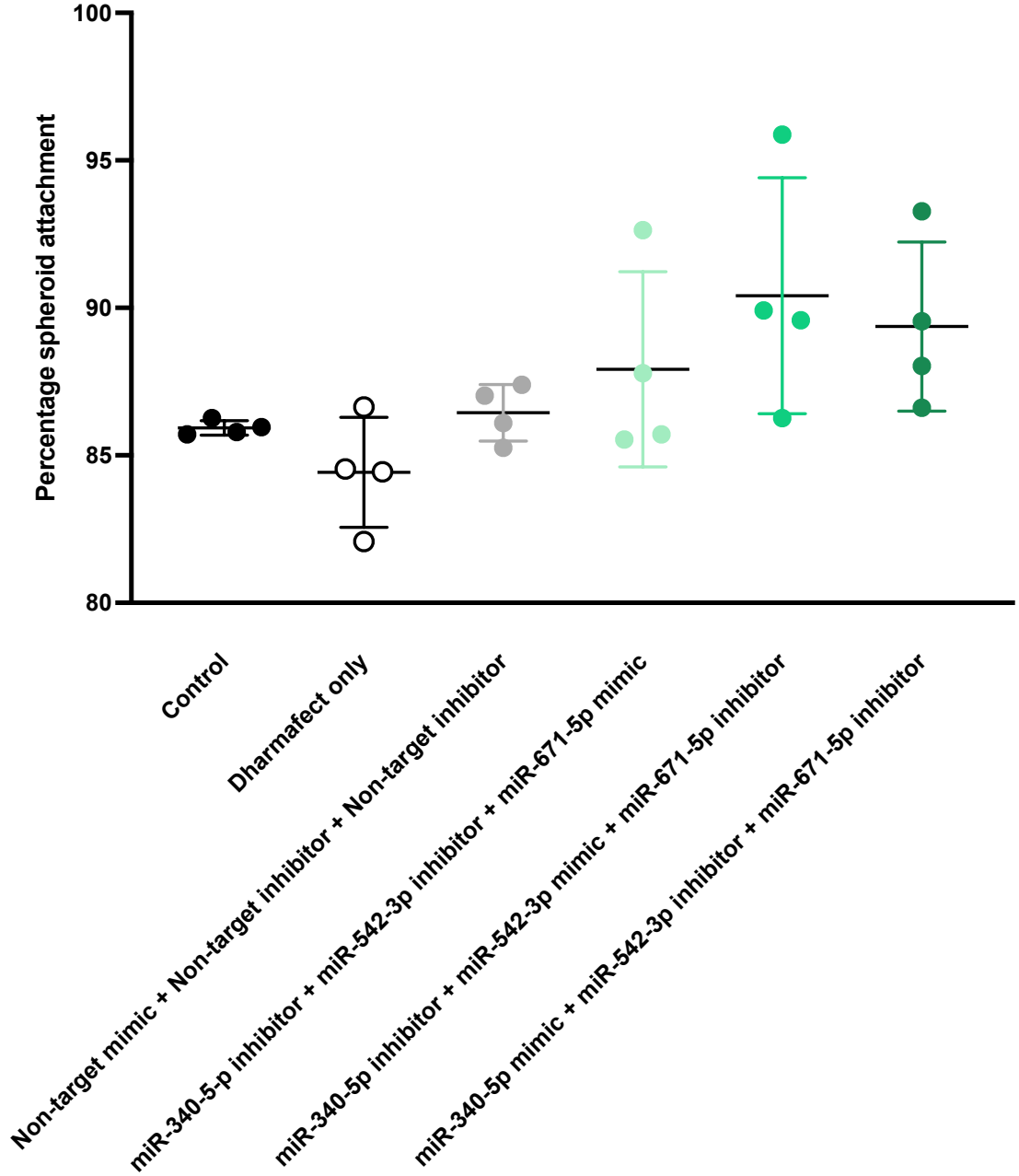

Figure 5.22: *Comparison of spheroid attachment following transfection with 2 inhibitors for miR-340-5p, miR-542-3p or miR-671-5p, and overexpression of the third.*
Percentage BeWo spheroid attachment following transfection (48 hrs) of Ishikawa cells (n=4) with 2 of miR-340-5p/miR-542-3p/miR-671-5p inhibitors and mimic of the third miRNA, and non-targeting controls. Statistical significance analysed by multiple t-tests with Bonferroni correction (* = $p<0.05$).

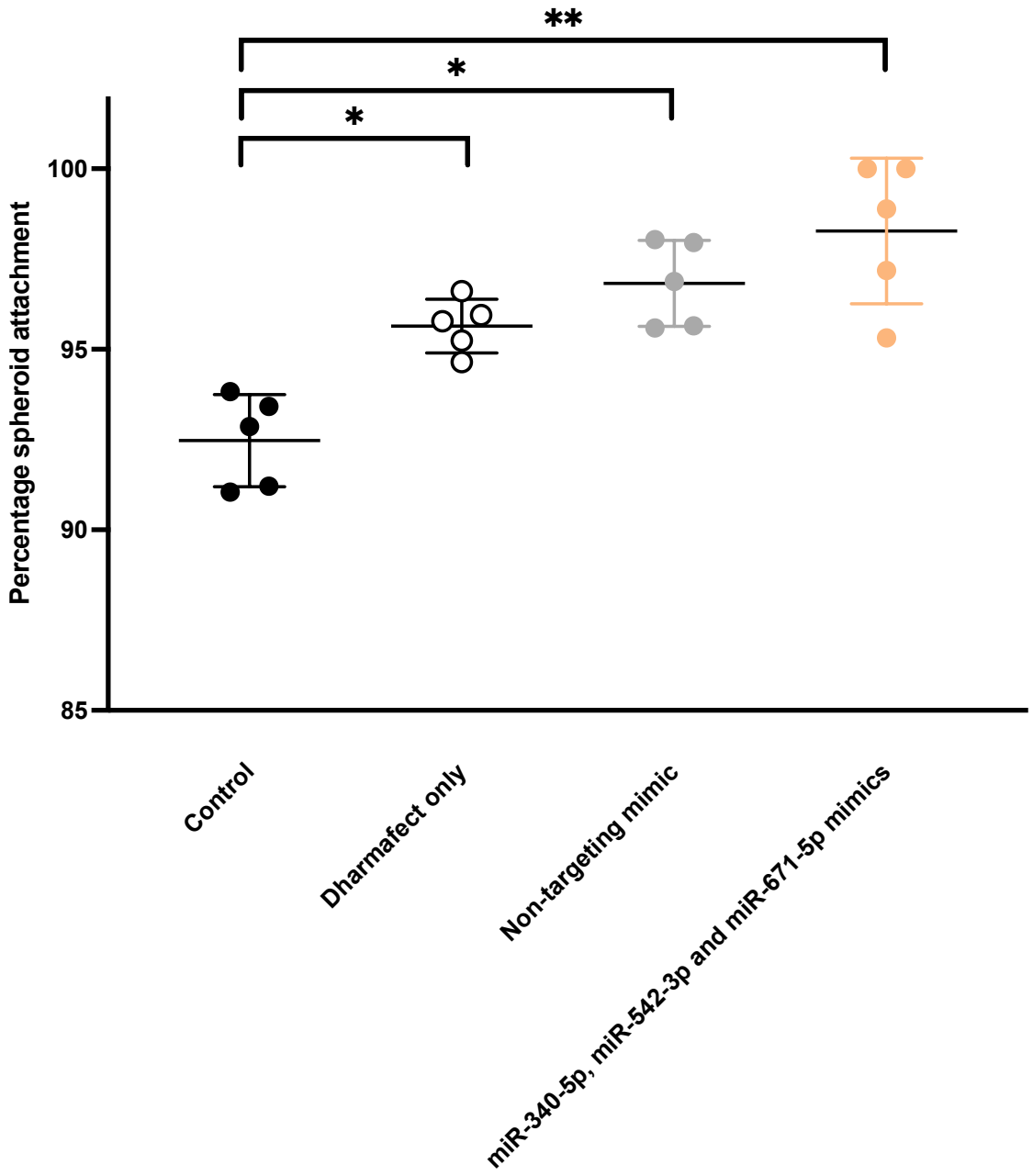

Figure 5.23: *Comparison of spheroid attachment following overexpression of miR-340-5p, miR-542-3p and miR-671-5p.*
Percentage BeWo spheroid attachment following transfection (48 hrs) of Ishikawa cells (n=5) with miR-340-5p, miR-542-3p and miR-671-5p mimics, and non-targeting controls. Statistical significance analysed by multiple t-tests with Bonferroni correction (* = $p<0.05$, ** = $p<0.01$).

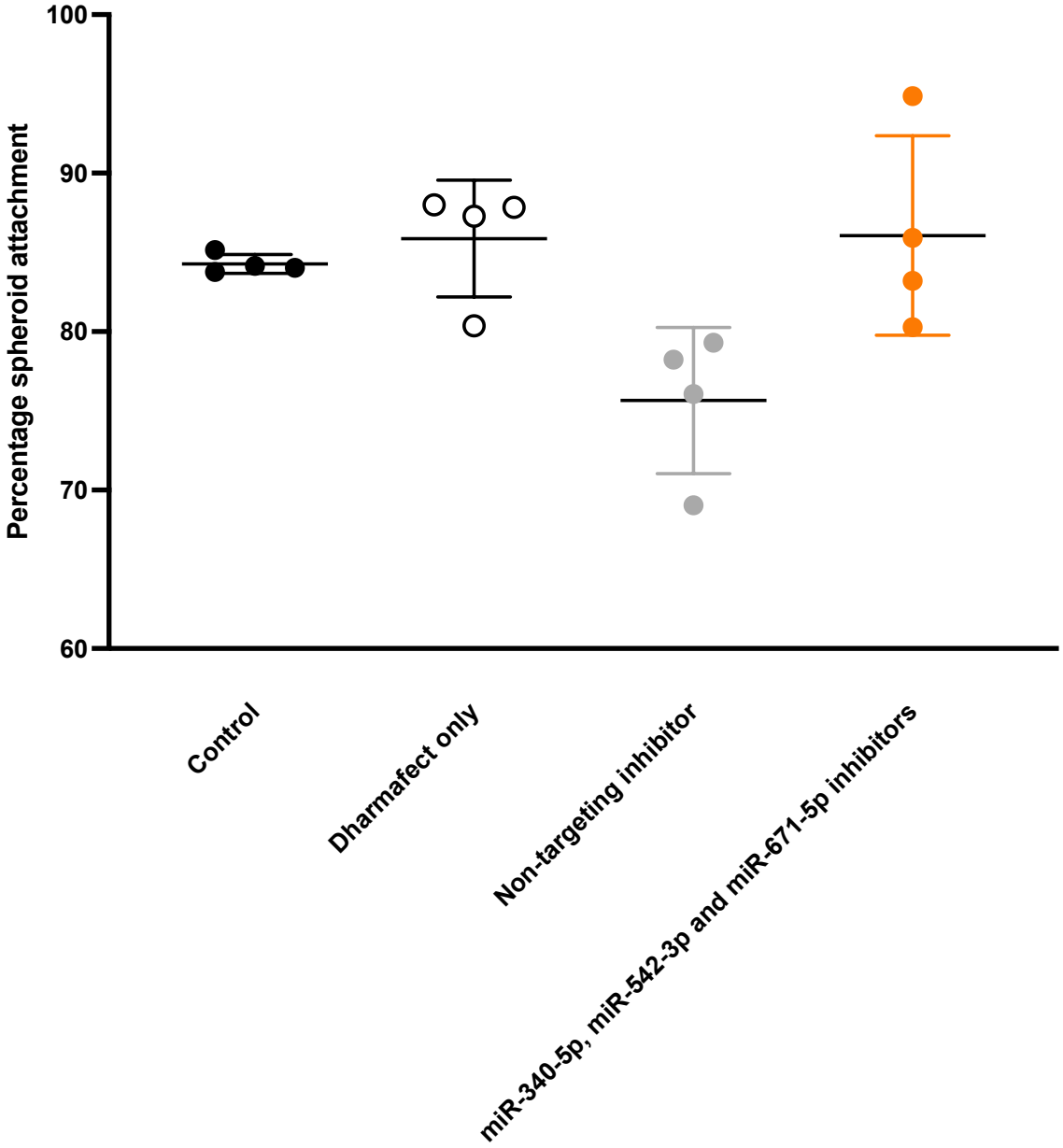

Figure 5.24: *Comparison of spheroid attachment following under expression of miR-340-5p, miR-542-3p and miR-671-5p.*
Percentage BeWo spheroid attachment following transfection (48 hrs) of Ishikawa cells (n=4) with miR-340-5p, miR-542-3p and miR-671-5p inhibitors, and non-targeting controls. Statistical significance analysed by multiple t-tests with Bonferroni correction (* = $p<0.05$).

5.4.2 Modelling the Human Endometrium: Alvetex

5.4.2.1 Optimisation of stromal cell layer

An initial haematoxylin and eosin stain was carried out to show cell density within scaffolds over time (Figure 5.25). There is a clear increase in the density of cells growing within the scaffold from 7 days until 32 days (Figure 5.25A-H), after which point scaffolds appear similar (Figure 5.25I-J). This suggests that the scaffold reaches full density after 32 days. Alvetex scaffolds were stained for extracellular matrix components Collagen I (Figure 5.26) and Fibronectin (Figure 5.27) at different time points of incubation to assess deposition of extracellular matrix inside the scaffold and select optimal incubation length. At day 7 the majority of the scaffold did not survive the immunofluorescence protocol, although there was a small amount of staining for both Collagen I (Figure 5.26A-C) and Fibronectin (Figure 5.27A-C) in the small pieces of scaffold that remained. Collagen I increases from day 14 to day 35 (Figure 5.26D-AA) at which point (Figure 5.26AA) there appears to be the most extracellular matrix deposition and dense cell coverage. This stage was selected as the optimal incubation length for the stromal layer in the Alvetex scaffold, as at day 39 (Figure 5.26AD) there does not appear to be as much Collagen I as day 35 and there are fewer cells. Equally, fibronectin staining increases in the same way between day 14 and 35 (Figure 5.27D-X), with little difference between day 35 (Figure 5.27X) and day 39 (Figure 5.27AA); therefore it was preferable to select day 35 as this would result in a more efficient protocol.

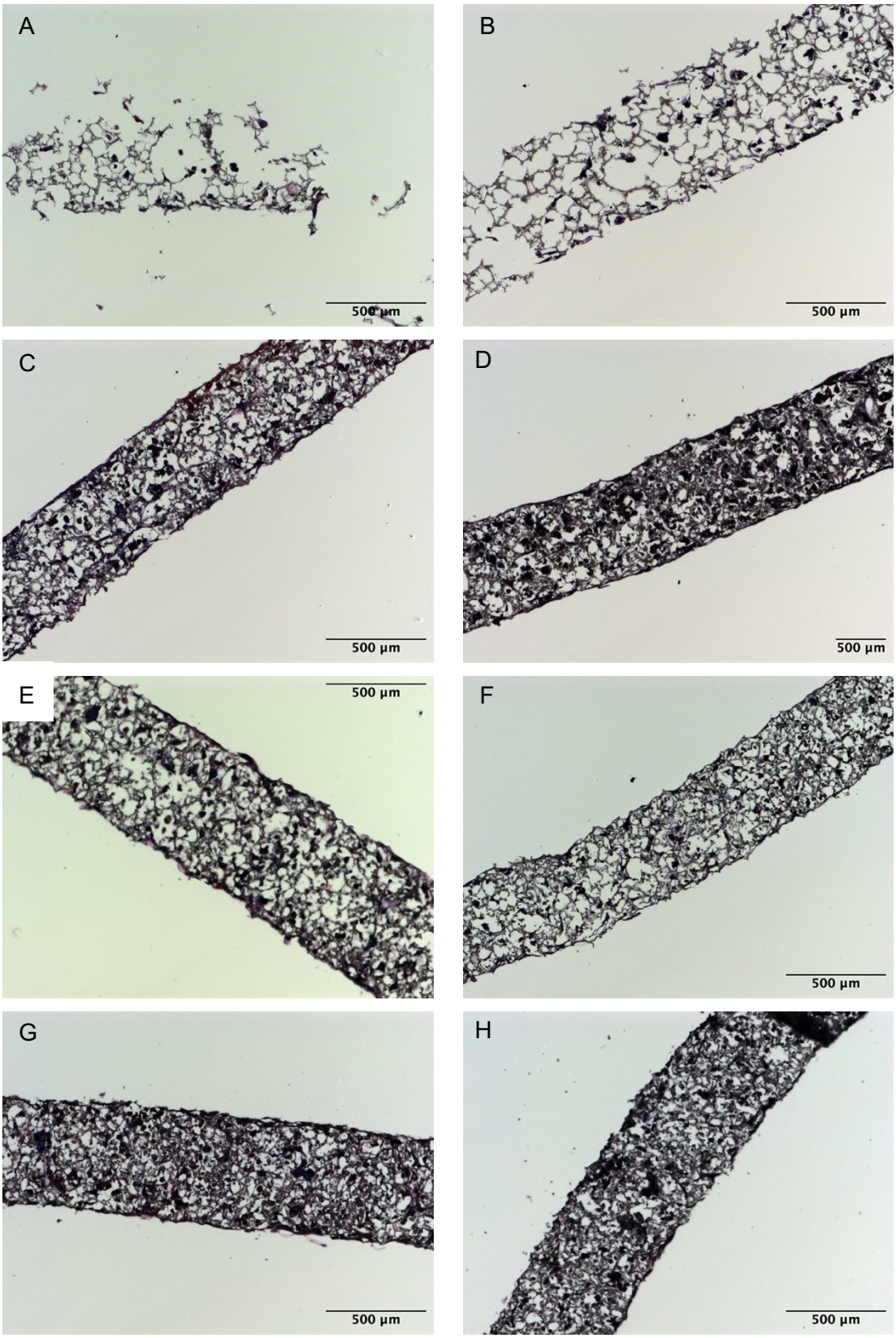
A
500 µm
B
500 µm
C
500 µm
D
500 µm
E
500 µm
F
500 µm
G
500 µm
H
500 µm

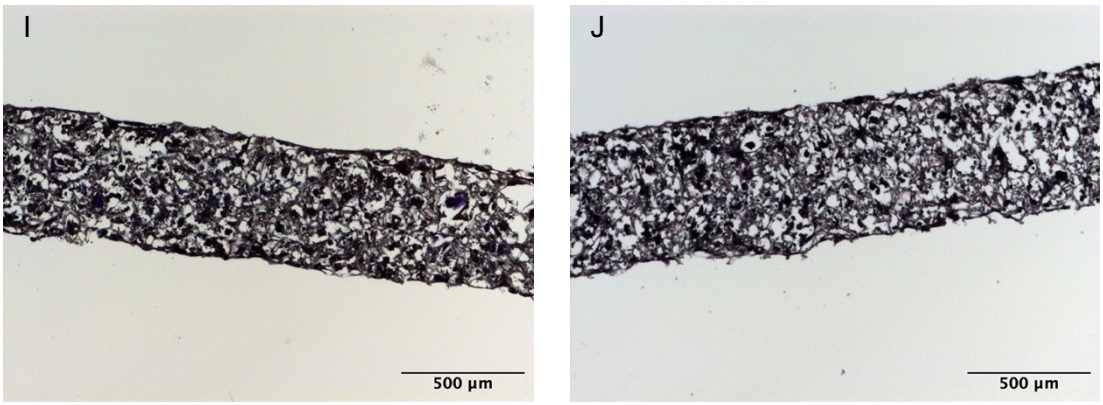

Figure 5.25: *Haematoxylin and eosin stain of Alvetex scaffolds seeded with endometrial stromal cells at different lengths of incubation.*
Light microscopy images of sections of Alvetex scaffold seeded with 500,000 human stromal cells (immortalized cell line) after different lengths of incubation at 37^{o}C 5% CO_2, stained with haematoxylin (pink - cytoplasm) and eosin (blue - nuclei). Incubation lengths of scaffolds were **A**) 7 days, **B**) 14 days, **C**) 21 days, **D**) 25 days, **E**) 28 days, **F**) 28 days, **G**) 32 days, **H**) 32 days, **I**) 35 days and **J**) 39 days.

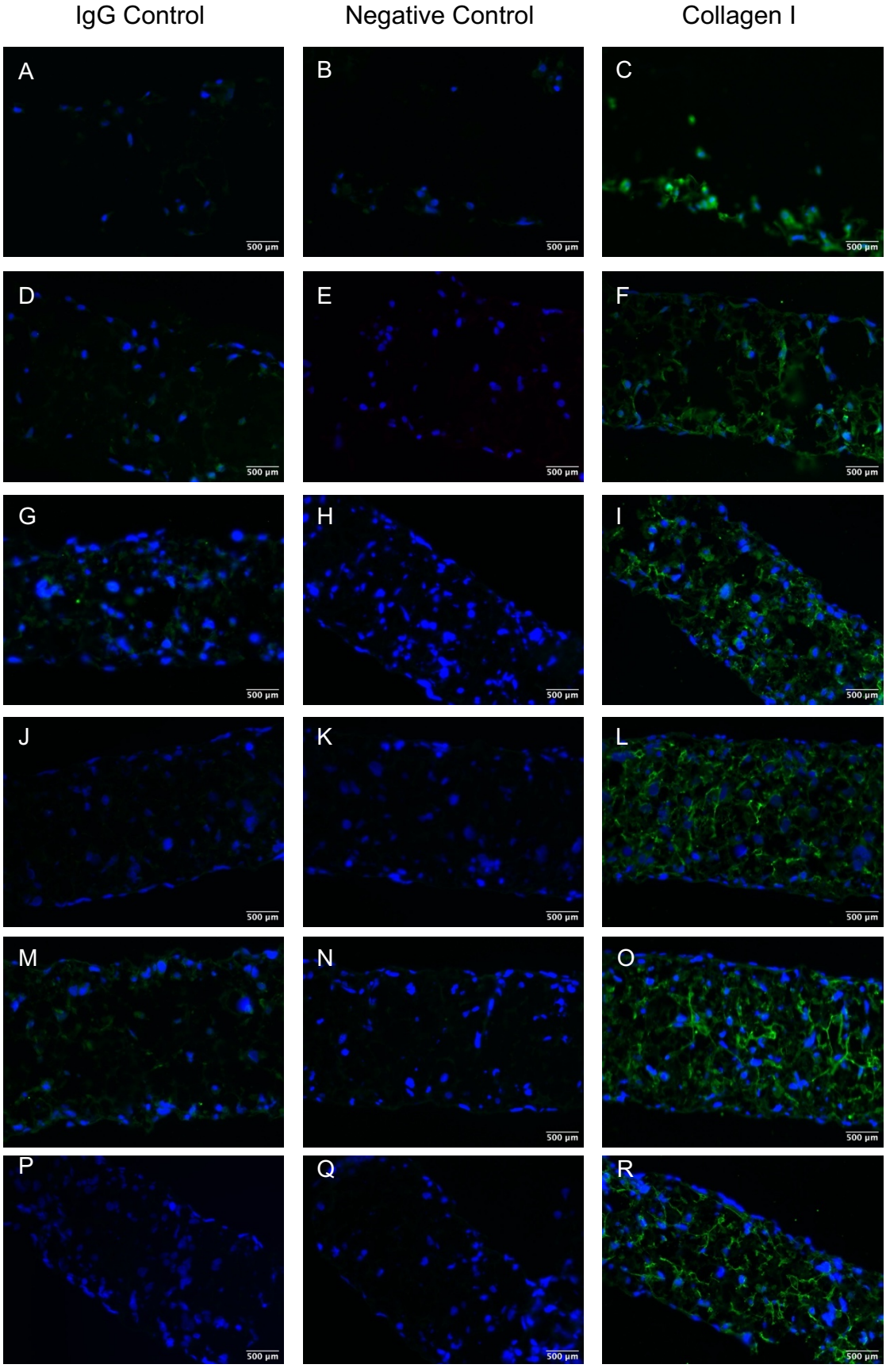
IgG Control
Negative Control
Collagen I
A
B
C
D
E
F
G
H
I
J
K
L
M
N
O
P
Q
R
500 µm

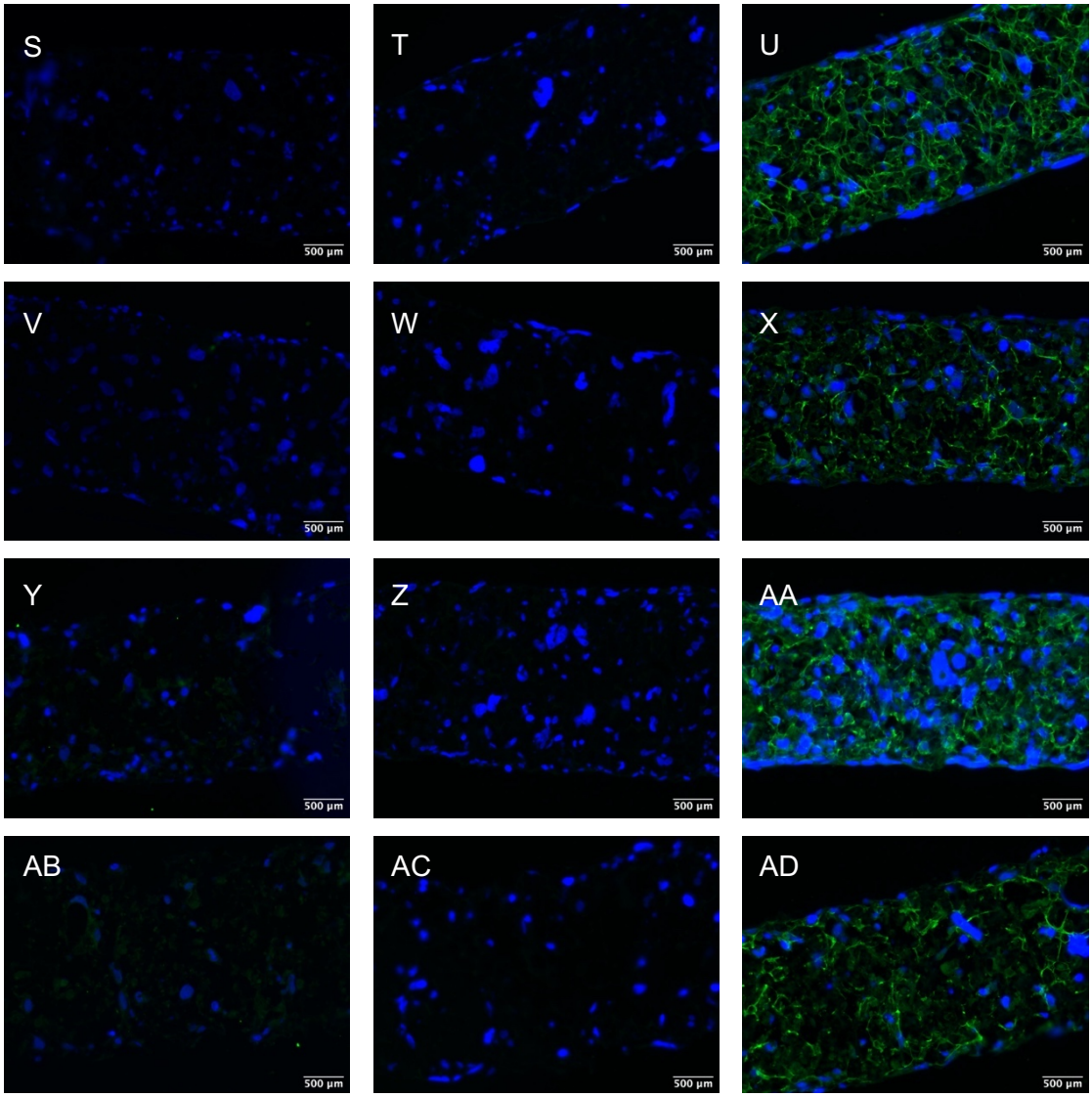

Figure 5.26: *Collagen I expression in Alvetex scaffolds seeded with endometrial stromal cells at different lengths of incubation.*
Fluorescent images of sections of Alvetex scaffold seeded with 500,000 human stromal cells (immortalized cell line) after different lengths of incubation at 37°C 5% CO_2, stained with IgG control (column 1), negative control - secondary antibody only (column 2) or collagen I (green) (column 3). Images of scaffold 1 (**A-C**) incubation for 7 days, 2 (**D-F**) incubation for 14 days, 3 (**G-I**) incubation for 21 days, 4 (**J-L**) incubation for 25 days, 5 (**M-O**) incubation for 28 days, 6 (**P-R**) incubation for 28 days, 7 (**S-U**) incubation for 32 days, 8 (**V-X**) incubation for 32 days, 9 (**Y-AA**)incubation for 35 days and 10 (**AB-AD**) incubation for 39 days. Green = Collagen I, Blue = cell nuclei stained with DAPI.

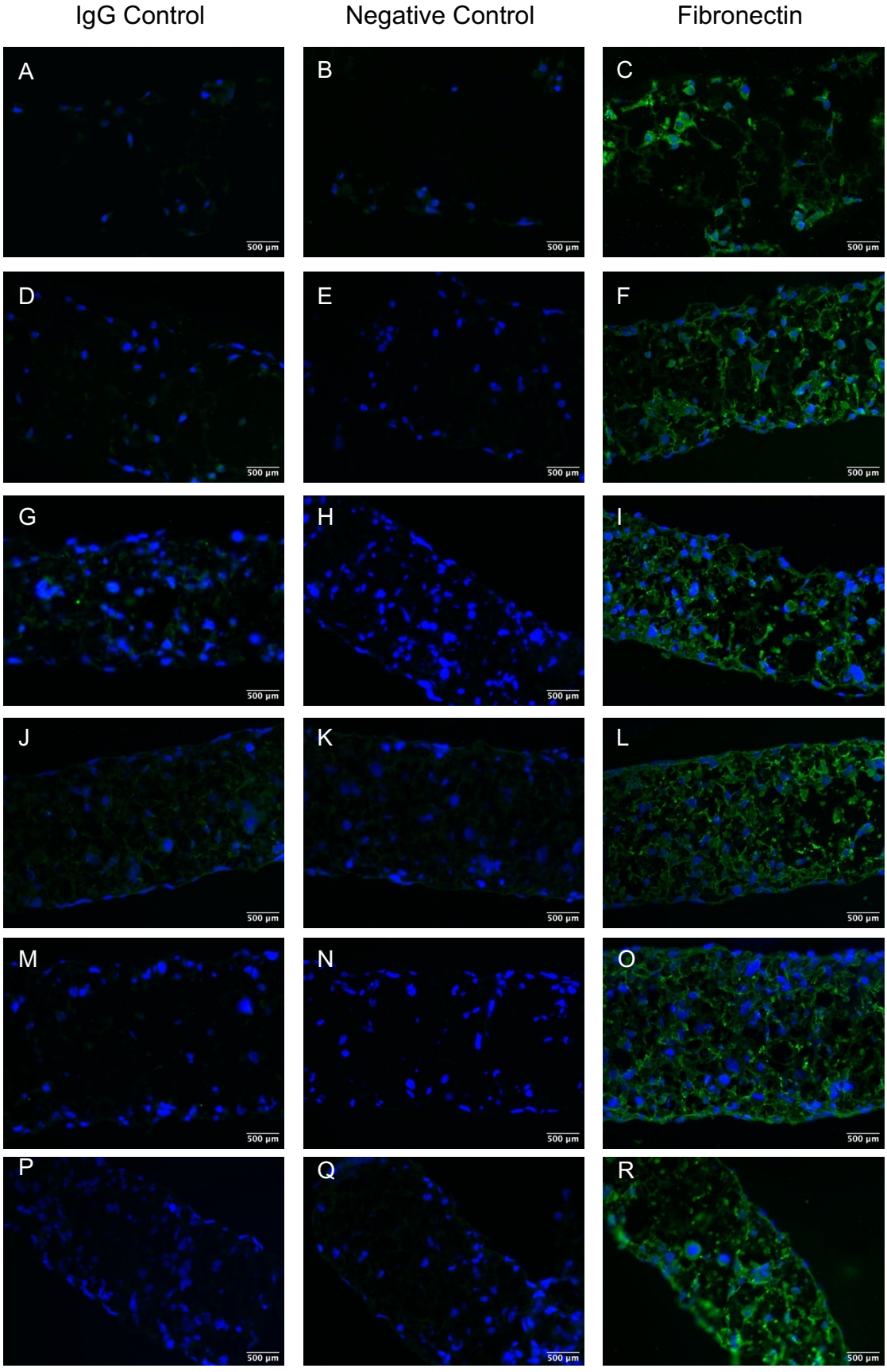
IgG Control
Negative Control
Fibronectin
A
B
C
D
E
F
G
H
I
J
K
L
M
N
O
P
Q
R
500 µm

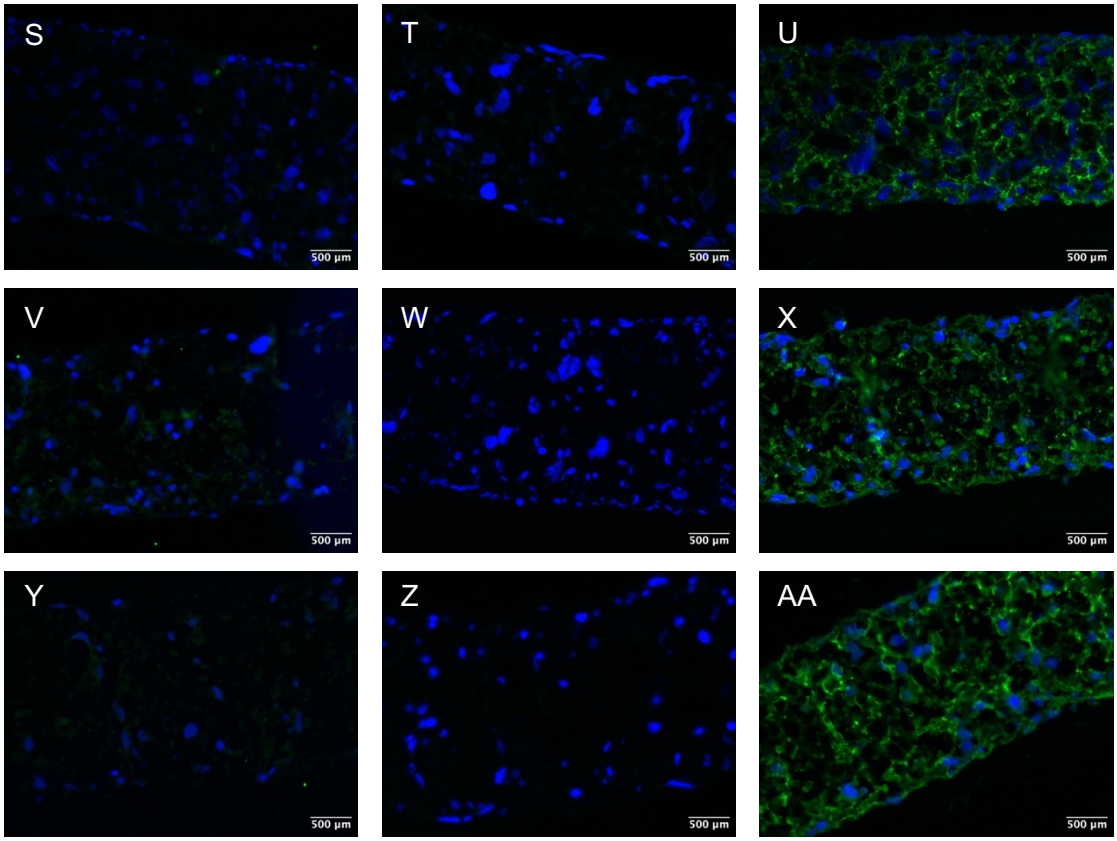

Figure 5.27: *Fibronectin expression in Alvetex scaffolds seeded with endometrial stromal cells at different lengths of incubation.*
Fluorescent images of sections of Alvetex scaffold seeded with 500,000 human stromal cells (immortalized cell line) after different lengths of incubation at 37°C 5% CO_2, stained with IgG control (column 1), negative control - secondary antibody only (column 2) or fibronectin (green) (column 3). Images of scaffold 1 (**A-C**) incubation for 7 days, 2 (**D-F**) incubation for 14 days, 3 (**G-I**) incubation for 21 days, 4 (**J-L**) incubation for 25 days, 5 (**M-O**) incubation for 28 days, 6 (**P-R**) incubation for 28 days, 8 (**V-X**) incubation for 32 days, 9 (**Y-AA**)incubation for 35 days and 10 (**AB-AD**) incubation for 39 days. Green = Fibronectin, Blue = cell nuclei stained with DAPI.

5.4.2.2 Addition of epithelial layer

Ishikawa cells (1.5 million) were added on top of the stromal layer on the Alvetex scaffold after 35 days of culture. DAPI staining of the cell nuclei shows that after 11 days of culture (Scaffold 11), a layer of cells is present on the top of the scaffold (Figure 5.28C, Figure 5.29C and Figure 5.30C). After 4 days of culture (Scaffold 12), a layer of cells is present in some sections but not others, which suggests the epithelial layer is not continuous across the scaffold (Figure 5.28F, Figure 5.30F), however this does not seem to be consistent throughout the scaffold as there does not appear to be a layer of cells along the top of the scaffold in Figure 5.29. Collagen I and fibronectin staining (Figure 5.28 and Figure 5.29) demonstrated the presence of the extracellular matrix throughout the scaffold after addition of epithelial cells. Staining with cytokeratin 18 (Figure 5.30), an epithelial cell marker, illustrates the distribution of the epithelial cells, and shows that they form a layer on top of the scaffold. At day 11, the epithelial cells form a thicker layer, likely due to the nature of being a cell line (Figure 5.30C). Furthermore, the stromal cell layer nuclei staining seems less dense and so this suggests this incubation period is too long. However, at day 4, there is a thinner layer yet this is not always an intact monolayer and can have gaps (Figure 5.30F). Figure 5.31 shows Vimentin staining, a stromal cell marker, throughout the scaffolds. It is clear that after 11 days incubation (Figure 5.31B) following epithelial cell addition, vimentin staining is more towards the bottom of the scaffold, away from the epithelial layer, whereas after 4 days incubation (Figure 5.31D) the vimentin is more widespread throughout the scaffold. For these reasons, a middle option of day 8 was selected for future experiments to aim to have consistent coverage of the epithelial layer with a healthy stromal layer.

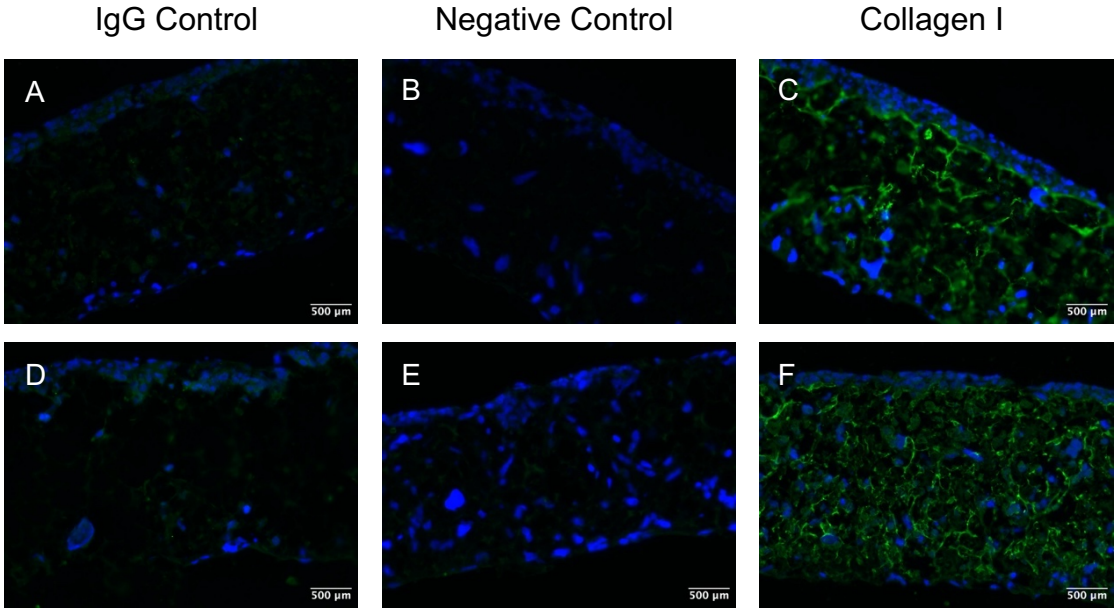

Figure 5.28: *Collagen I expression in Alvetex scaffolds seeded with endometrial stromal and epithelial cells at different lengths of incubation.* Fluorescent images of sections of Alvetex scaffold seeded with 500,000 human stromal cells (immortalized cell line), with 1.5 million endometrial epithelial cells (Ishikawa) cells seeded on top after different lengths of incubation at 37°C 5% CO_2. Cells are stained with IgG control (column 1), negative control - secondary antibody only (column 2) or collagen I (green) (column 3). **A-C**) Images of scaffold 11 (11 days incubation post epithelial layer seeding) and **D-F**) scaffold 12 (4 days incubation post epithelial layer seeding) Green = Collagen I, Blue = cell nuclei stained with DAPI.

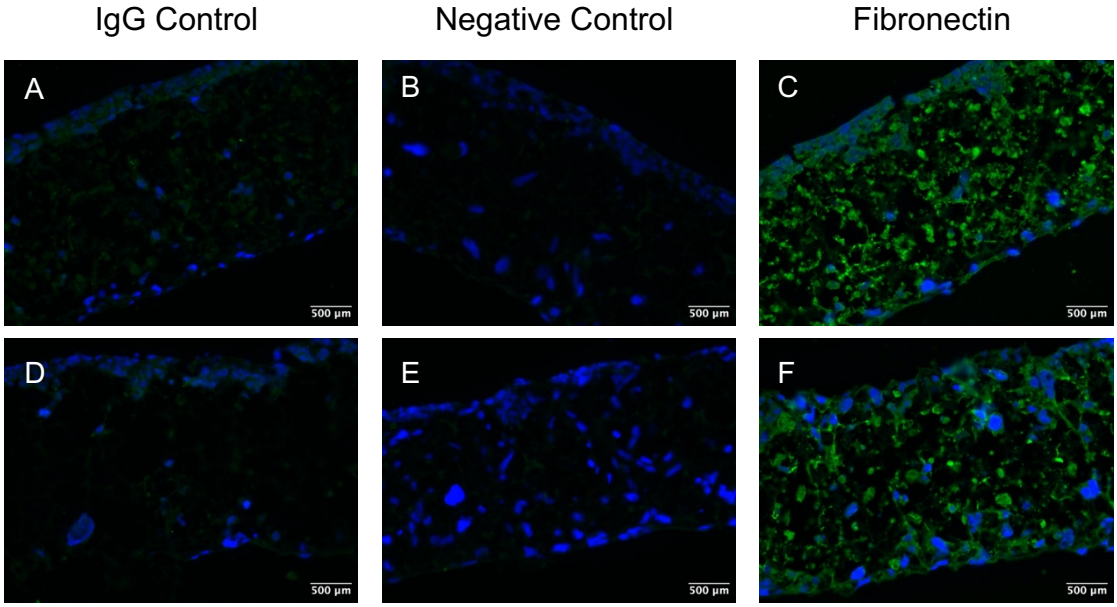

Figure 5.29: *Fibronectin expression in Alvetex scaffolds seeded with endometrial stromal and epithelial cells at different lengths of incubation.* Fluorescent images of sections of Alvetex scaffold seeded with 500,000 human stromal cells (immortalized cell line), with 1.5 million endometrial epithelial cells (Ishikawa) cells seeded on top after different lengths of incubation at 37°C 5% CO_2. Cells are stained with IgG control (column 1), negative control - secondary antibody only (column 2) or fibronectin (green) (column 3). **A-C**) Images of scaffold 11 (11 days incubation post epithelial layer seeding) and **D-F**) scaffold 12 (4 days incubation post epithelial layer seeding) Green = Fibronectin, Blue = cell nuclei stained with DAPI.

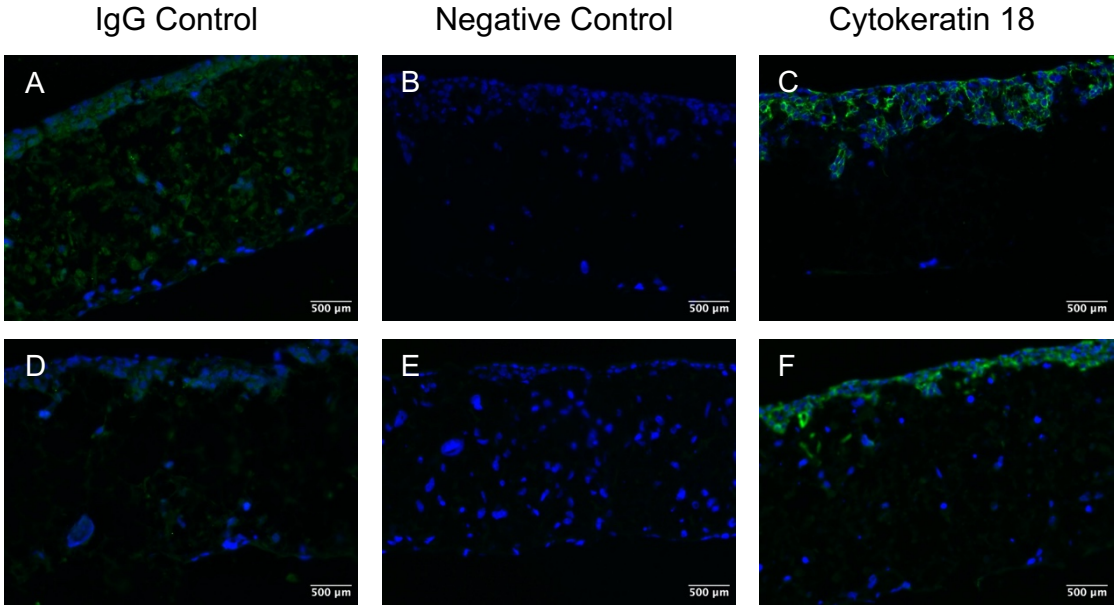

Figure 5.30: *Cytokeratin 18 expression in Alvetex scaffolds seeded with endometrial stromal and epithelial cells at different lengths of incubation.* Fluorescent images of sections of Alvetex scaffold seeded with 500,000 human stromal cells (immortalized cell line), with 1.5 million endometrial epithelial cells (Ishikawa) cells seeded on top after different lengths of incubation at 37°C 5% CO_2. Cells are stained with IgG control (column 1), negative control - secondary antibody only (column 2) or cytokeratin 18 (green) (column 3). **A-C**) Images of scaffold 11 (11 days incubation post epithelial layer seeding) and **D-F**) scaffold 12 (4 days incubation post epithelial layer seeding) Green = Cytokeratin 18, Blue = cell nuclei stained with DAPI.

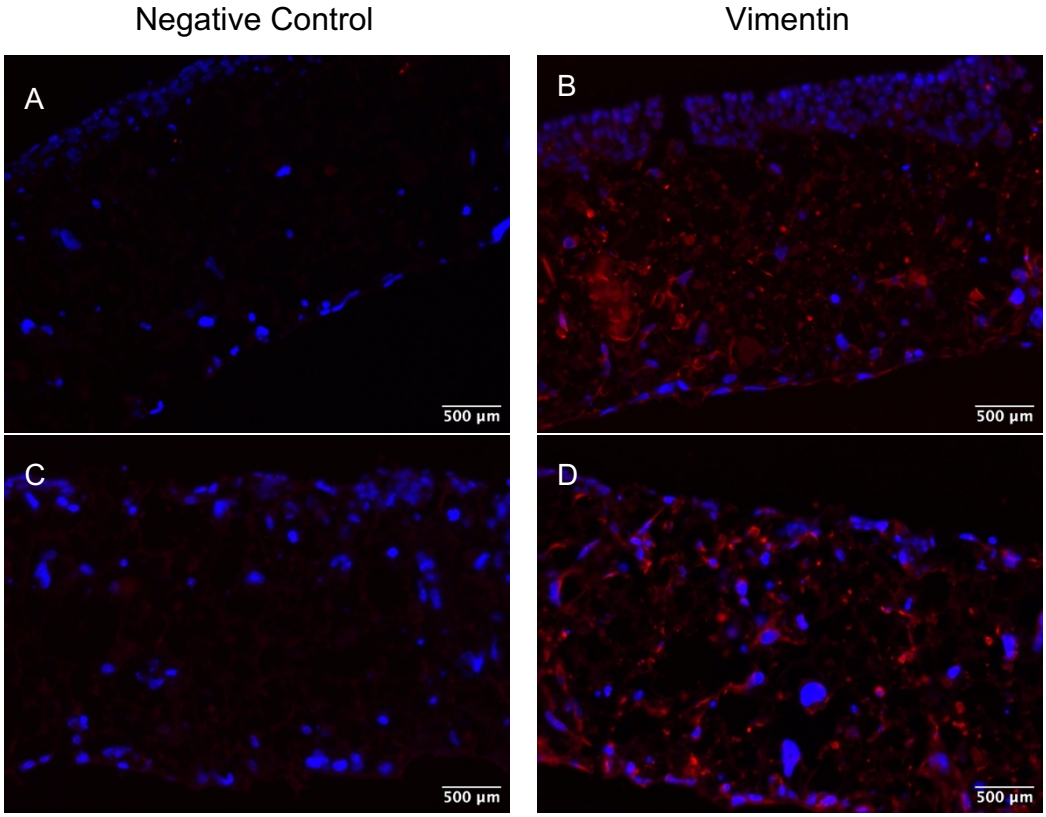

Figure 5.31: *Vimentin expression in Alvetex scaffolds seeded with endometrial stromal and epithelial cells at different lengths of incubation.*
Fluorescent images of sections of Alvetex scaffold seeded with 500,000 human stromal cells (immortalized cell line), with 1.5 million endometrial epithelial cells (Ishikawa) cells seeded on top after different lengths of incubation at 37°C 5% CO_2. Cells are stained with Negative control - secondary antibody only (column 1) or vimentin (red) (column 2). **A-C**) Images of scaffold 11 (11 days incubation post epithelial layer seeding) and **D-F**) scaffold 12 (4 days incubation post epithelial layer seeding). Red = Vimentin, Blue = cell nuclei stained with DAPI.

5.4.2.3 Over or under expressing microRNAs in a 3D model of the endometrium

5.4.2.3.1 Transfecting Alvetex scaffolds with microRNAs

MiR-340-5p (Figure 5.32), miR-542-3p (Figure 5.33) and miR-671-5p (Figure 5.34) were overexpressed in cells from Alvetex scaffolds when a scaffold was transfected with the respective mimic compared to controls. All three miRNAs were also overexpressed compared to controls in the Alvetex scaffold when it was transfected with mimics for all 3 miRNAs. As RNA extracted from Alvetex scaffolds was comprised of both epithelial and stromal cells, a qRT-PCR was performed to determine whether untreated stromal cells expressed any of the 3 miRNAs (Figure 5.35). The immortalized human stromal cell line expresses miR-340-5p and miR-542-3p, however miR-671-5p was not detected.

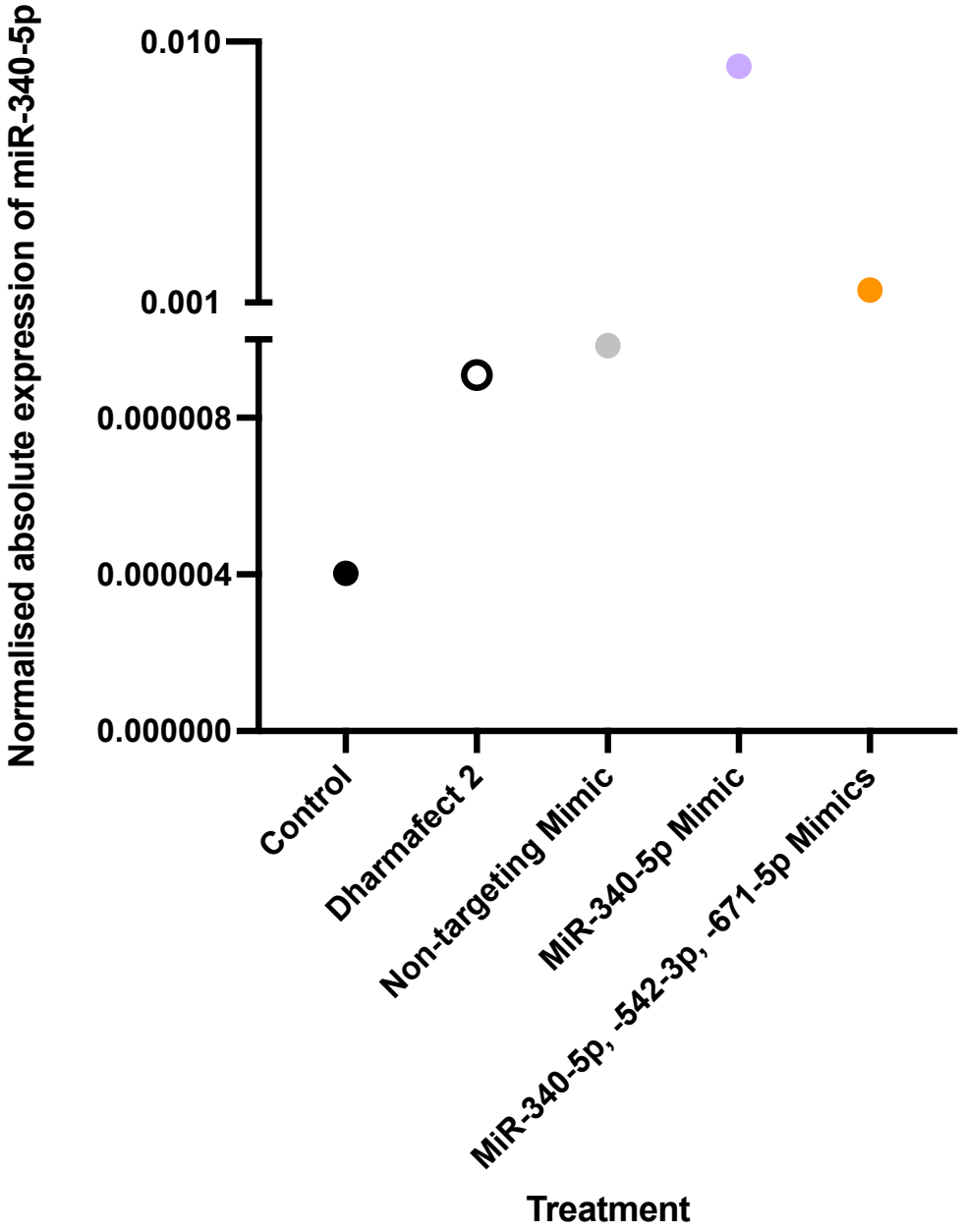

Figure 5.32: *Expression of miR-340-5p, following transfection with miR-340-5p mimic only, or a combination of miR-340-5p, miR-542-3p and miR-671-5p mimics.*
Absolute expression values of miR-340-5p normalised to 5s in Alvetex scaffolds seeded with 500,000 human stromal cells (immortalized cell line) and incubated for 35 days at 37°C 5% CO_2, followed by 1.5 million endometrial epithelial cells (Ishikawa) cells seeded on top for 8 days incubation at 37°C 5% CO_2. Cells were transfected with the following treatments for 3 hrs (n=1) before left to incubate at 37°C 5% CO_2 for 48 hrs. All treatments were added to cells in 100µl optiMEM media: Control - no treatment (black circle), Dharmafect only control - 1µl Dharmafect 2 (empty circle). All further treatments were added to cells in 100µl optiMEM + 1µl Dharmafect 2: 50nM non-targeting mimic (grey circle), 50nM miR-340-5p (light purple circle), 16.6nM miR-340-5p mimic + 16.6nM miR-542-3p mimic + 16.6nM miR-671-5p mimic (orange circle).

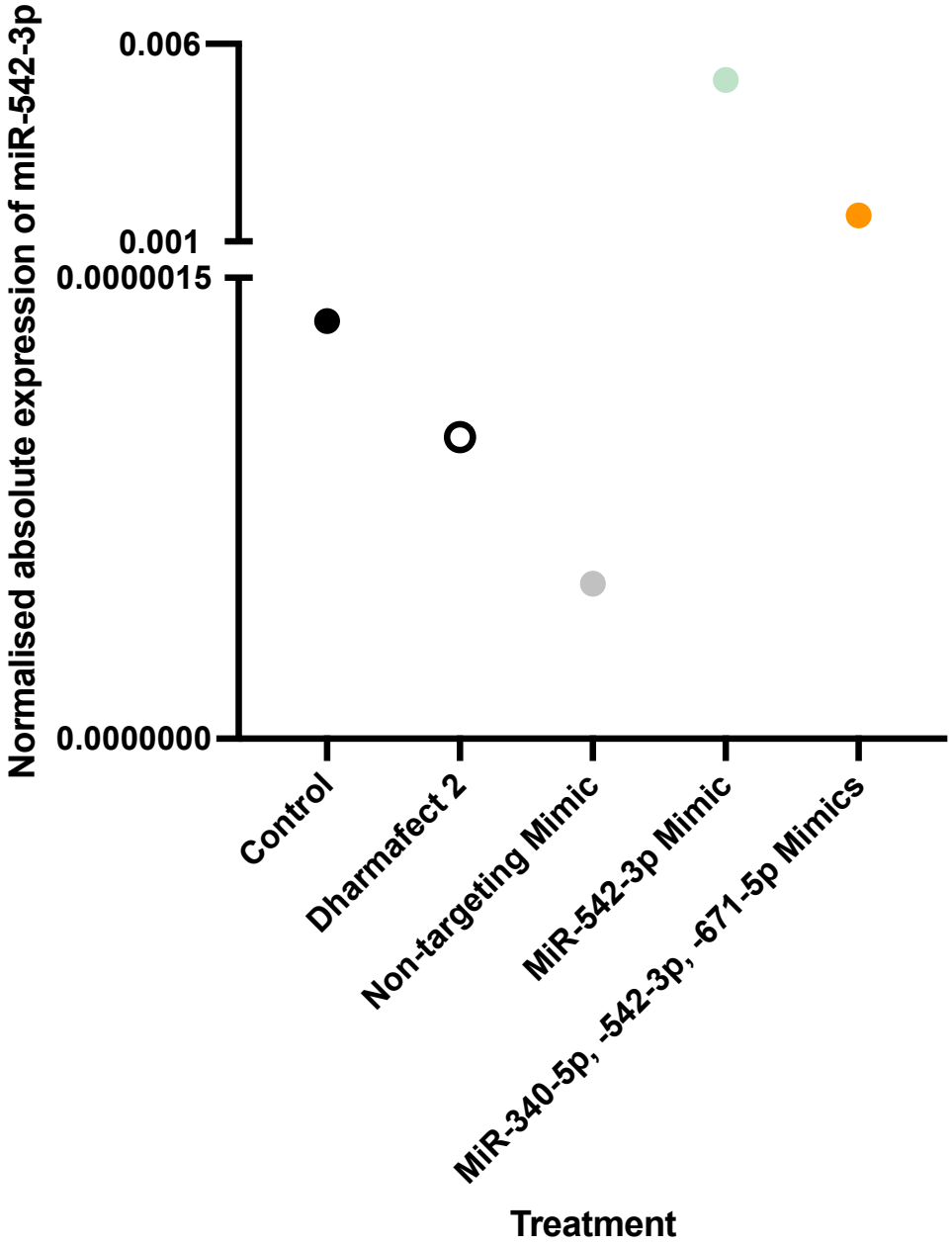

Figure 5.33: *Expression of miR-542-3p, following transfection with miR-542-3p mimic only, or a combination of miR-340-5p, miR-542-3p and miR-671-5p mimics.*
Absolute expression values of miR-542-3p normalised to 5s in Alvetex scaffolds seeded with 500,000 human stromal cells (immortalized cell line) and incubated for 35 days at 37°C 5% CO_2, followed by 1.5 million endometrial epithelial cells (Ishikawa) cells seeded on top for 8 days incubation at 37°C 5% CO_2. Cells were transfected with the following treatments for 3 hrs (n=1) before left to incubate at 37°C 5% CO_2 for 48 hrs. All treatments were added to cells in 100µl optiMEM media: Control - no treatment (black circle), Dharmafect only control - 1µl Dharmafect 2 (empty circle). All further treatments were added to cells in 100µl optiMEM + 1µl Dharmafect 2: 50nM non-targeting mimic (grey circle), 50nM miR-542-3p (light green circle), 16.6nM miR-340-5p mimic + 16.6nM miR-542-3p mimic + 16.6nM miR-671-5p mimic (orange circle).

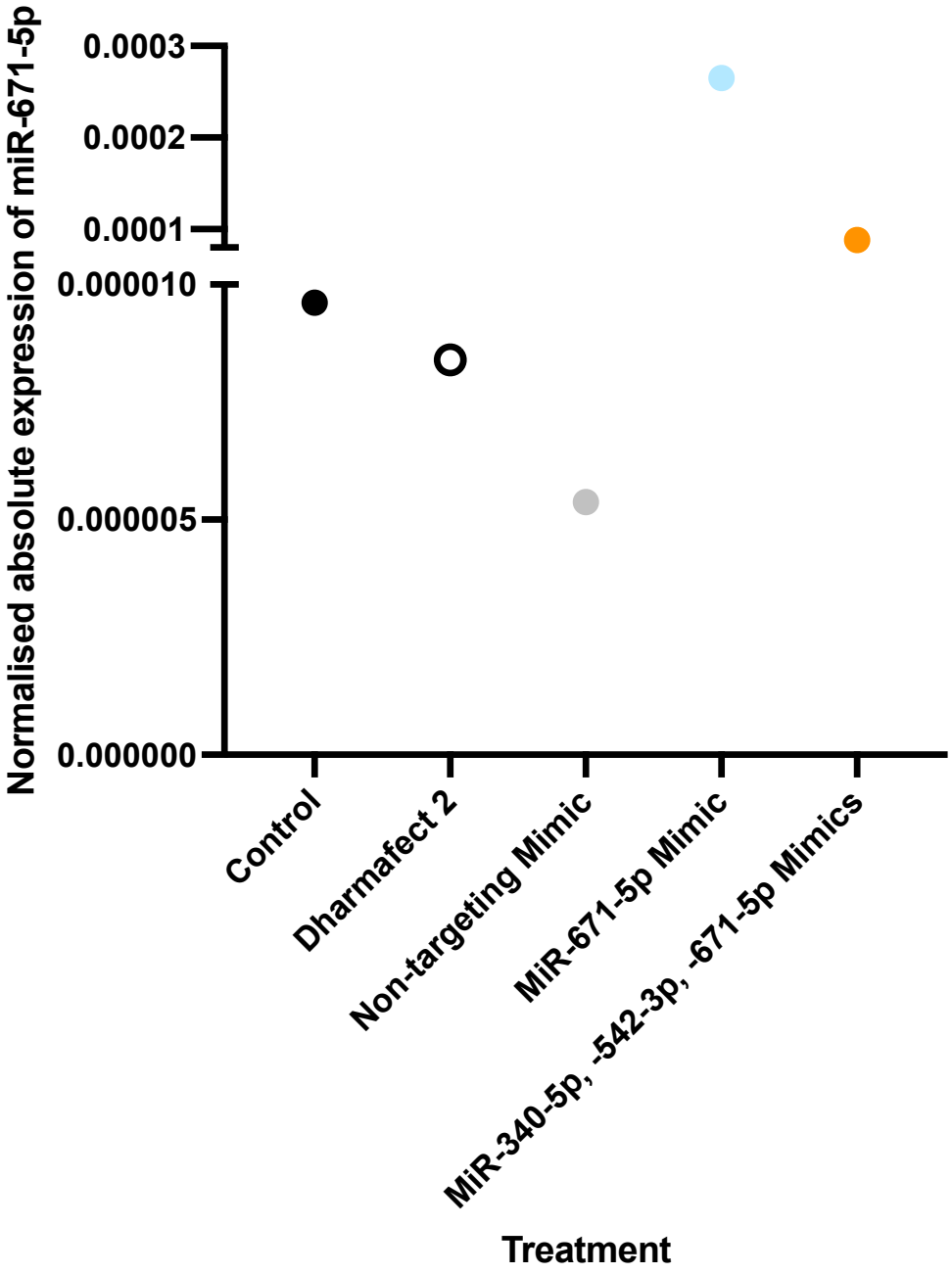

Figure 5.34: *Expression of miR-671-5p, following transfection with miR-671-5p mimic only, or a combination of miR-340-5p, miR-542-3p and miR-671-5p mimics.*
Absolute expression values of miR-671-5p normalised to 5s in Alvetex scaffolds seeded with 500,000 human stromal cells (immortalized cell line) and incubated for 35 days at 37°C 5% CO_2, followed by 1.5 million endometrial epithelial cells (Ishikawa) cells seeded on top for 8 days incubation at 37°C 5% CO_2. Cells were transfected with the following treatments for 3 hrs (n=1) before left to incubate at 37°C 5% CO_2 for 48 hrs. All treatments were added to cells in 100µl optiMEM media: Control - no treatment (black circle), Dharmafect only control - 1µl Dharmafect 2 (empty circle). All further treatments were added to cells in 100µl optiMEM + 1µl Dharmafect 2: 50nM non-targeting mimic (grey circle), 50nM miR-671-5p (light blue circle), 16.6nM miR-340-5p mimic + 16.6nM miR-542-3p mimic + 16.6nM miR-671-5p mimic (orange circle).

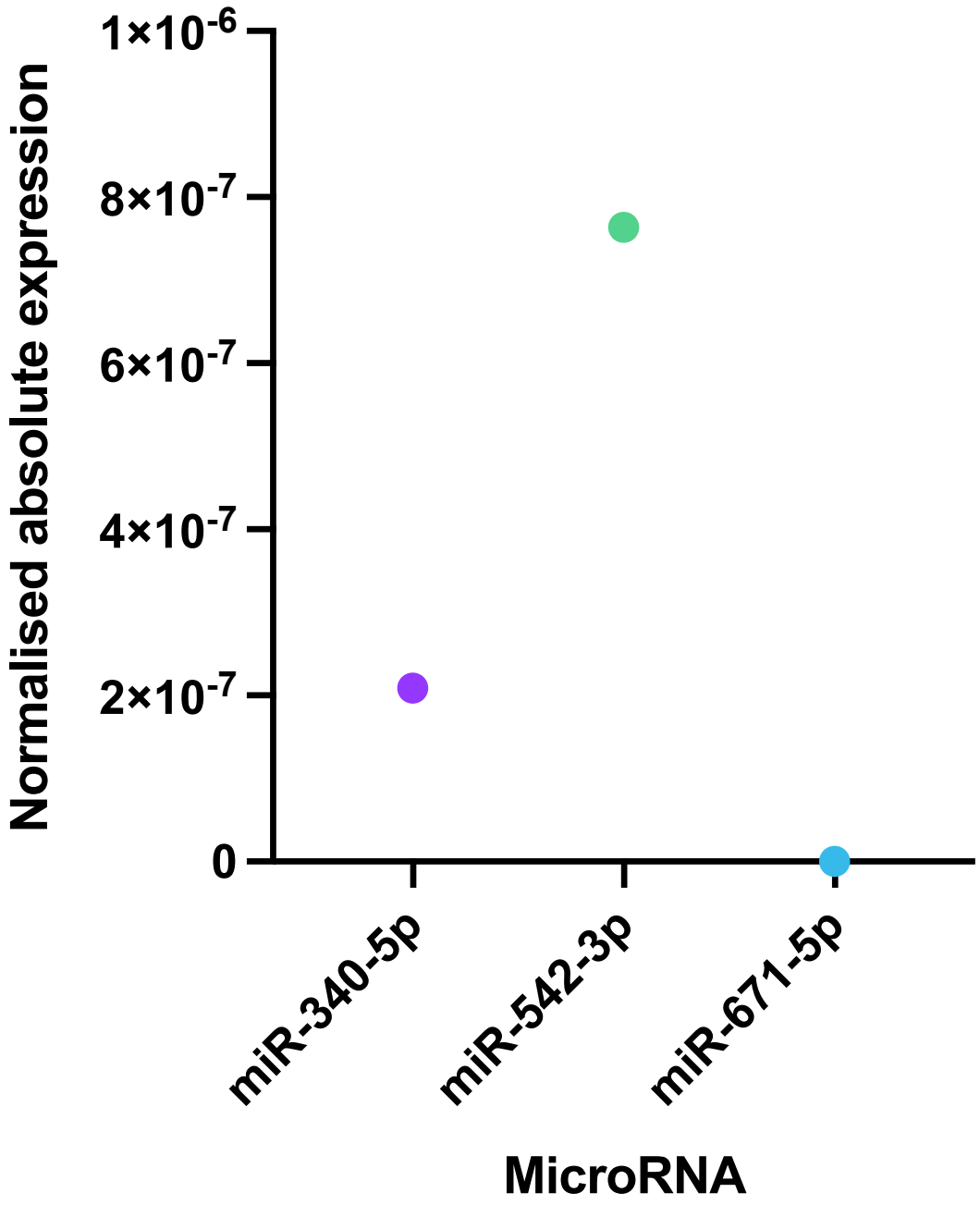

Figure 5.35: *MiR-340-5p, miR-542-3p and miR-671-5p expression in human stromal cell line.*
Absolute expression values (n=1) of miR-340-5p (purple), miR-542-3p (green) and miR-671-5p (blue) normalised to 5s in human stromal cells (immortalized cell line) used for seeding Alvetex scaffolds.

5.4.2.3.2 Extracellular matrix deposition in transfected Alvetex scaffolds

A haematoxylin and eosin stain was carried out to visualise the presence and distribution of cells within the scaffold (Figure 5.36). The layer of cells where the epithelial layer was seeded is dense, however the distribution of cells throughout the rest of the scaffold can be patchy, but does not appear to be linked to specific treatments. Transfected Alvetex scaffolds were stained for collagen I (Figure 5.37) and fibronectin (Figure 5.38) to confirm extracellular matrix structure inside the scaffold following epithelial addition and transfection. DAPI staining in both stains showed a reduction in presence of cell nuclei spread throughout the scaffold, regardless of treatment, in comparison to previous extracellular matrix assessments. Cells were mainly only located at the top or bottom of the scaffold. There also appeared to be less collagen I and fibronectin in comparison to previous experiments. For collagen I, IgG controls for non-specific staining showed some staining. As brightness is adjusted based on the image of the primary antibody under investigation, if collagen I is at a low concentration, the brightness will be increased in the control suggesting there is less difference between the images and therefore not much collagen I present. Fibronectin was present throughout the scaffold in all treatments, displaying fluorescence differently to the controls.

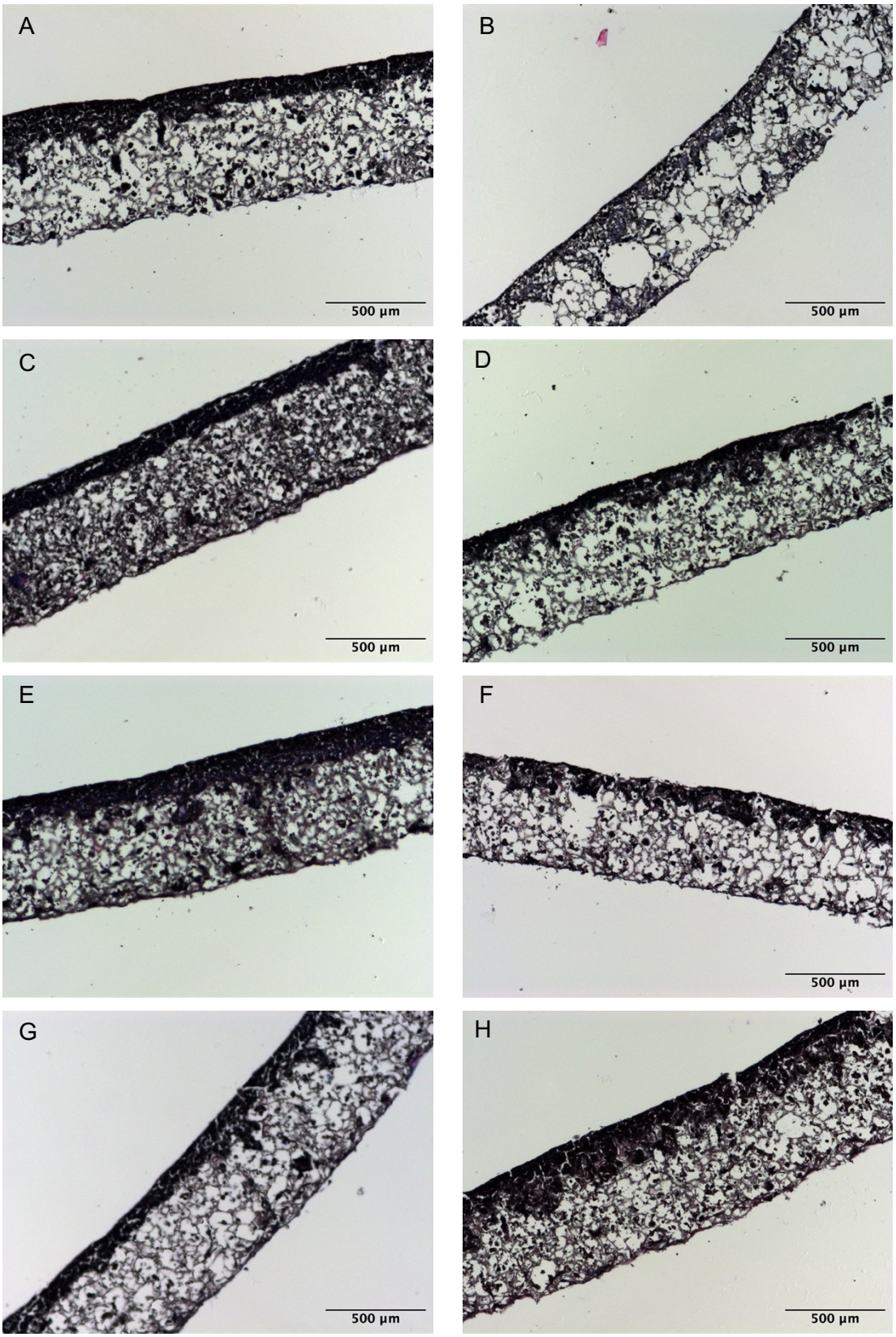
A
500 µm
B
500 µm
C
500 µm
D
500 µm
E
F
500 µm
G
500 µm
H
500 µm

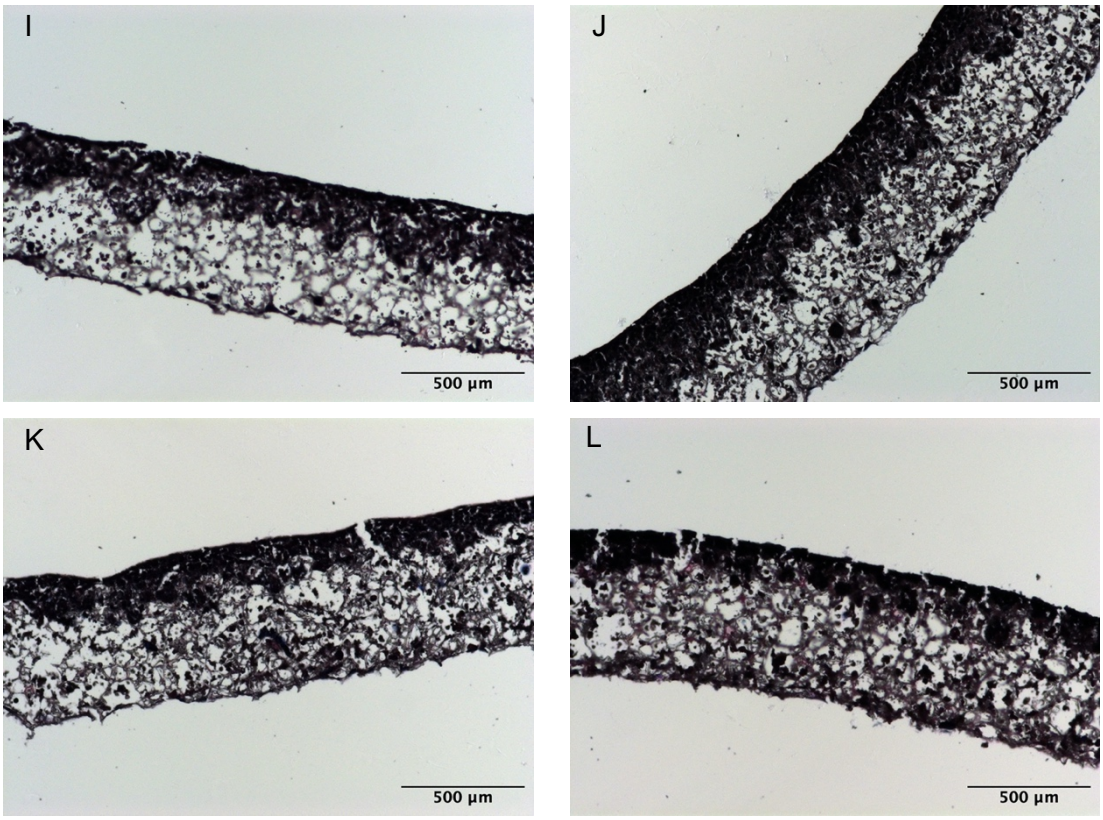

Figure 5.36: *Haematoxylin and eosin stain of Alvetex scaffolds seeded with endometrial stromal and epithelial cells and transfected with mimics and inhibitors for miRNAs of interest.*
Light microscopy images of sections of Alvetex scaffold seeded with 500,000 human stromal cells (immortalized cell line) and incubated for 35 days at 37ºC 5% CO_2, followed by 1.5 million endometrial epithelial cells (Ishikawa) cells seeded on top for 8 days incubation at 37ºC 5% CO_2. Cells were transfected with the following treatments for 3 hrs (n=1) before left to incubate at 37ºC 5% CO_2 for 48 hrs. All treatments were added to cells in 100µl optiMEM media: Control - no treatment (**A**), Dharmafect only control - 1µl Dharmafect 2 (**B**). All further treatments were added to cells in 100µl optiMEM + 1µl Dharmafect 2: 50nM non-targeting mimic (**C**), 50nM non-targeting inhibitor (**D**), 50nM miR-340-5p mimic (**E**), 50nM miR-340-5p inhibitor (**F**), 50nM miR-542-3p mimic (**G**), 50nM miR-542-3p inhibitor (**H**), 50nM miR-671-5p mimic (**I**), 50nM miR-671-5p inhibitor (**J**), 16.6nM miR-340-5p mimic + 16.6nM miR-542-3p mimic + 16.6nM miR-671-5p mimic (**K**), and 16.6nM miR-340-5p inhibitor + 16.6nM miR-542-3p inhibitor + 16.6nM miR-671-5p inhibitor (**L**). Cells are stained with haematoxylin (pink - cytoplasm) and eosin (blue - nuclei).

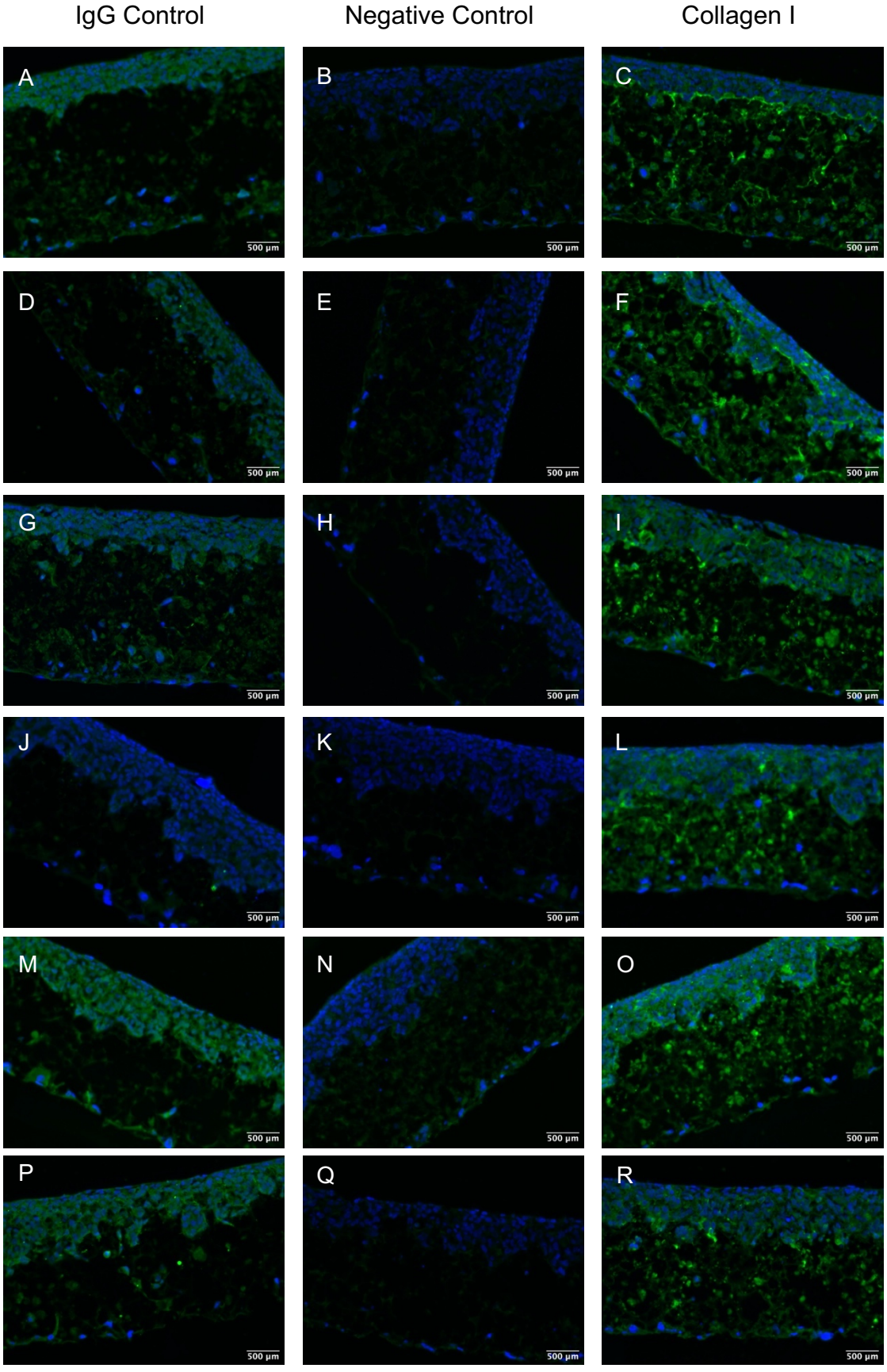
IgG Control
Negative Control
Collagen I
A
B
C
D
E
F
G
H
I
J
K
L
M
N
O
P
Q
R
500 µm

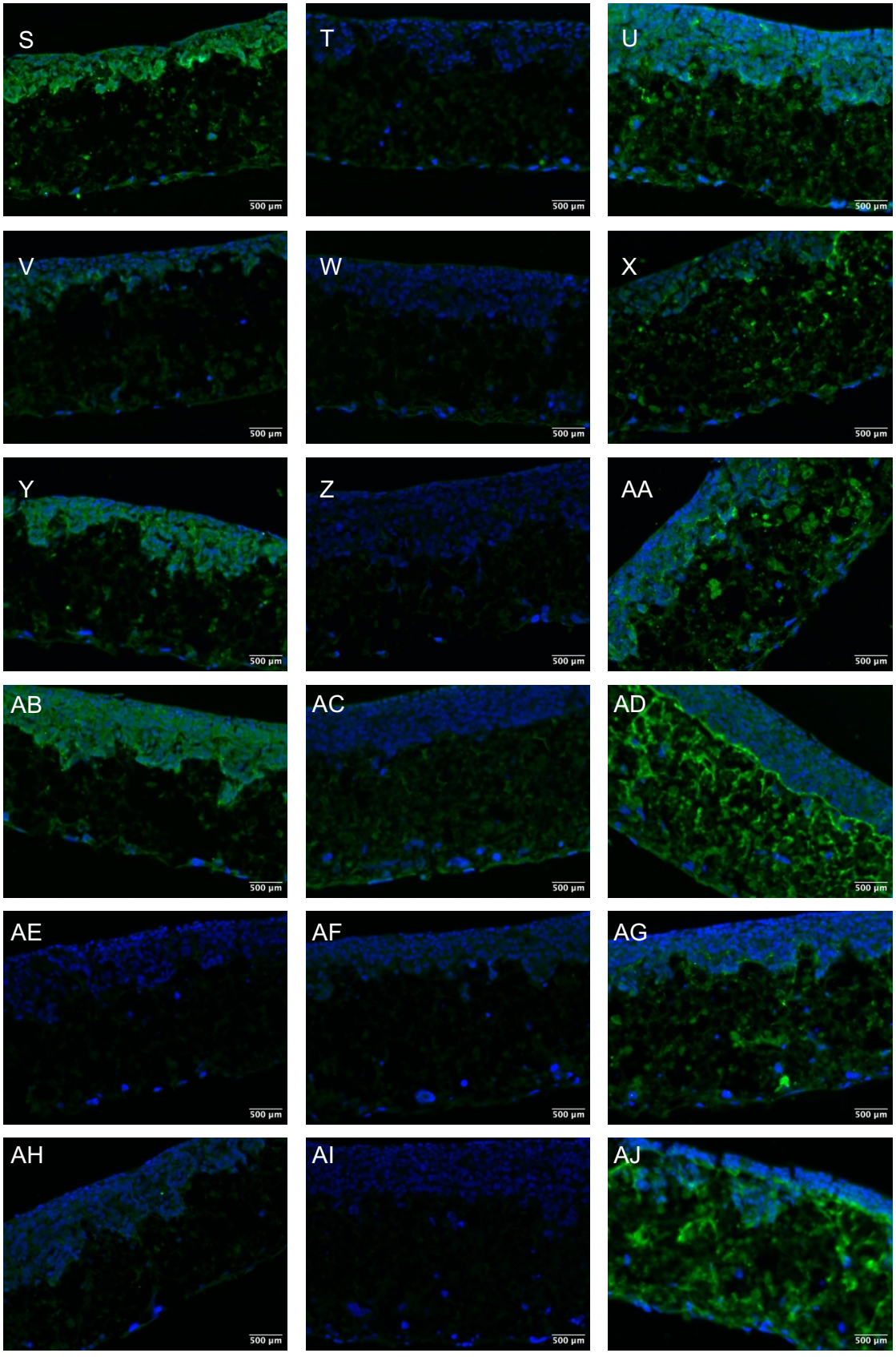
S
T
U
V
W
X
Y
Z
AA
AB
AC
AD
AE
AF
AG
AH
AI
AJ
500 µm

Figure 5.37: *Collagen I expression in Alvetex scaffolds seeded with endometrial stromal and epithelial cells and transfected with mimics and inhibitors for miRNAs of interest.*
Fluorescent images of sections of Alvetex scaffold seeded with 500,000 human stromal cells (immortalized cell line) and incubated for 35 days at 37ºC 5% CO_2, followed by 1.5 million endometrial epithelial cells (Ishikawa) cells seeded on top for 8 days incubation at 37ºC 5% CO_2. Cells were transfected with the following treatments for 3 hrs (n=1) before left to incubate at 37ºC 5% CO_2 for 48 hrs. All treatments were added to cells in 100μl optiMEM media: Control - no treatment (**A-C**), Dharmafect only control - 1μl Dharmafect 2 (**D-F**). All further treatments were added to cells in 100μl optiMEM + 1μl Dharmafect 2: 50nM non-targeting mimic (**G-I**), 50nM non-targeting inhibitor (**J-L**), 50nM miR-340-5p mimic (**M-O**), 50nM miR-340-5p inhibitor (**P-R**), 50nM miR-542-3p mimic (**S-U**), 50nM miR-542-3p inhibitor (**V-X**), 50nM miR-671-5p mimic (**Y-AA**), 50nM miR-671-5p inhibitor (**AB-AD**), 16.6nM miR-340-5p mimic + 16.6nM miR-542-3p mimic + 16.6nM miR-671-5p mimic (**AE-AG**), and 16.6nM miR-340-5p inhibitor + 16.6nM miR-542-3p inhibitor + 16.6nM miR-671-5p inhibitor (**AH-AJ**). Cells are stained with negative IgG control (column 1), negative control - secondary antibody only (column 2) or collagen I (green) (column 3). Green = Collagen I, Blue = cell nuclei stained with DAPI.

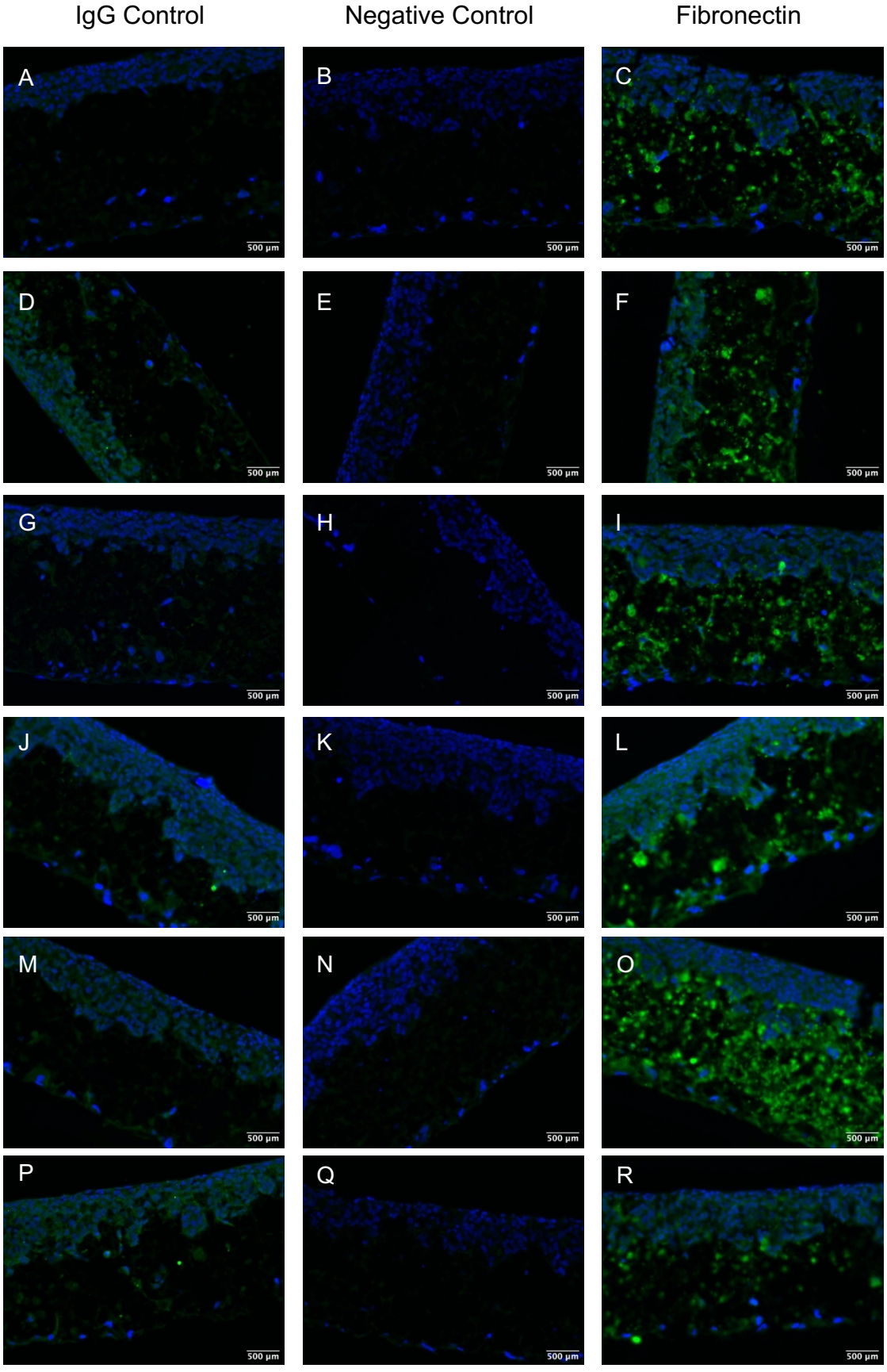
IgG Control
Negative Control
Fibronectin
A
B
C
D
E
F
G
H
I
J
K
L
M
N
O
P
Q
R
500 µm

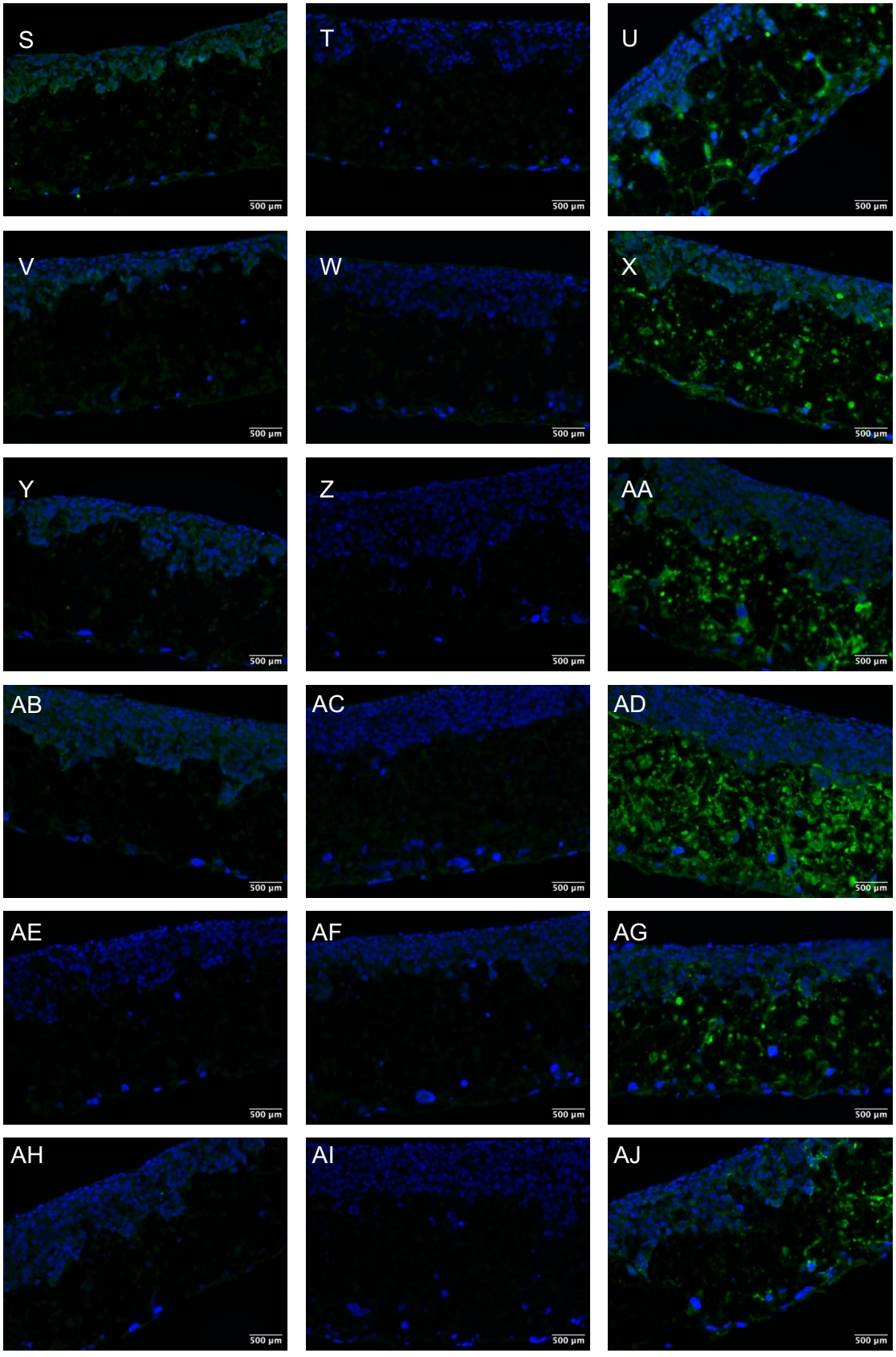
S
T
U
V
W
X
Y
Z
AA
AB
AC
AD
AE
AF
AG
AH
AI
AJ
500 µm

Figure 5.38: *Fibronectin expression in Alvetex scaffolds seeded with endometrial stromal and epithelial cells and transfected with mimics and inhibitors for miRNAs of interest.*
Fluorescent images of sections of Alvetex scaffold seeded with 500,000 human stromal cells (immortalized cell line) and incubated for 35 days at 37ºC 5% CO_2, followed by 1.5 million endometrial epithelial cells (Ishikawa) cells seeded on top for 8 days incubation at 37ºC 5% CO_2. Cells were transfected with the following treatments for 3 hrs (n=1) before left to incubate at 37ºC 5% CO_2 for 48 hrs. All treatments were added to cells in 100μl optiMEM media: Control - no treatment (**A-C**), Dharmafect only control - 1μl Dharmafect 2 (**D-F**). All further treatments were added to cells in 100μl optiMEM + 1μl Dharmafect 2: 50nM non-targeting mimic (**G-I**), 50nM non-targeting inhibitor (**J-L**), 50nM miR-340-5p mimic (**M-O**), 50nM miR-340-5p inhibitor (**P-R**), 50nM miR-542-3p mimic (**S-U**), 50nM miR-542-3p inhibitor (**V-X**), 50nM miR-671-5p mimic (**Y-AA**), 50nM miR-671-5p inhibitor (**AB-AD**), 16.6nM miR-340-5p mimic + 16.6nM miR-542-3p mimic + 16.6nM miR-671-5p mimic (**AE-AG**), and 16.6nM miR-340-5p inhibitor + 16.6nM miR-542-3p inhibitor + 16.6nM miR-671-5p inhibitor (**AH-AJ**). Cells are stained with negative IgG control (column 1), negative control - secondary antibody only (column 2) or fibronectin (green) (column 3). Green = Fibronectin, Blue = cell nuclei stained with DAPI.

5.4.2.3.3 Stromal and epithelial cell distribution in transfected Alvetex scaffolds

Immunofluorescence for cytokeratin and vimentin was carried out to observe the distribution of epithelial and stromal cells within the scaffolds for all transfected Alvetex. Both markers were present in all samples (Figure 5.39-Figure 5.50). Cytokeratin stained the epithelial cells at the top of the scaffold confirming that these cells grew in a layer above the stromal layer, rarely extending into the stromal cells. Vimentin was subtly present throughout the scaffold, most concentrated at the bottom of the scaffold which is where the cell nuclei were more dense. There is some dimmer vimentin staining in the epithelial layer, which could potentially be debris from stromal cells which were previously growing at the top of the scaffold before epithelial cells were seeded, as this staining is not present in controls.

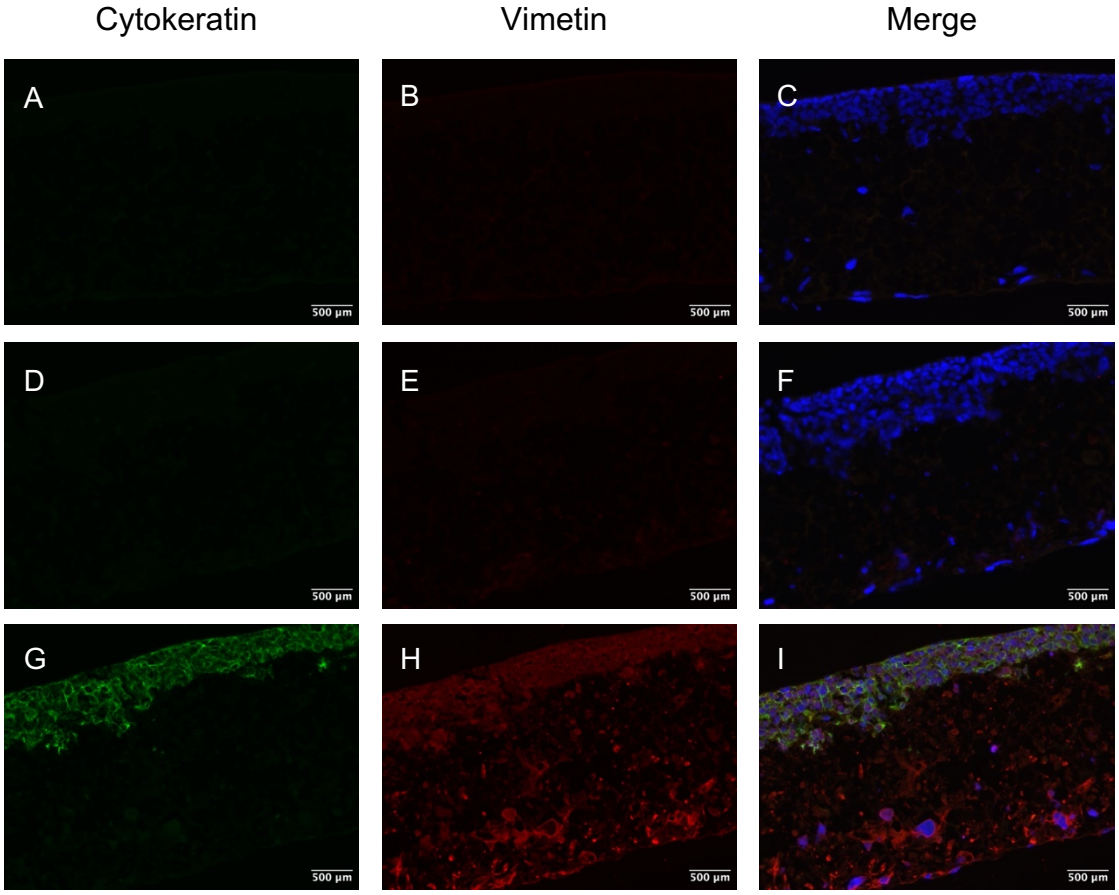

Figure 5.39: *Cytokeratin 18 and Vimentin expression in Alvetex scaffolds seeded with endometrial stromal and epithelial cells - Control*
Fluorescent images of sections of Control Alvetex scaffold seeded with 500,000 human stromal cells (immortalized cell line) and incubated for 35 days at 37ºC 5% CO_2, followed by 1.5 million endometrial epithelial cells (Ishikawa) cells seeded on top for 8 days incubation at 37ºC 5% CO_2. Cells were treated with Control - 100µl optiMEM only for 3 hrs (n=1) before left to incubate at 37ºC 5% CO_2 for 48 hrs. **A-C**) IgG control, **D-F**) Negative control - secondary antibody only, **G-I**) Cytokeratin 18 and Vimentin. Green = Cytokeratin 18, red = Vimentin, blue = nuclei stained with DAPI.

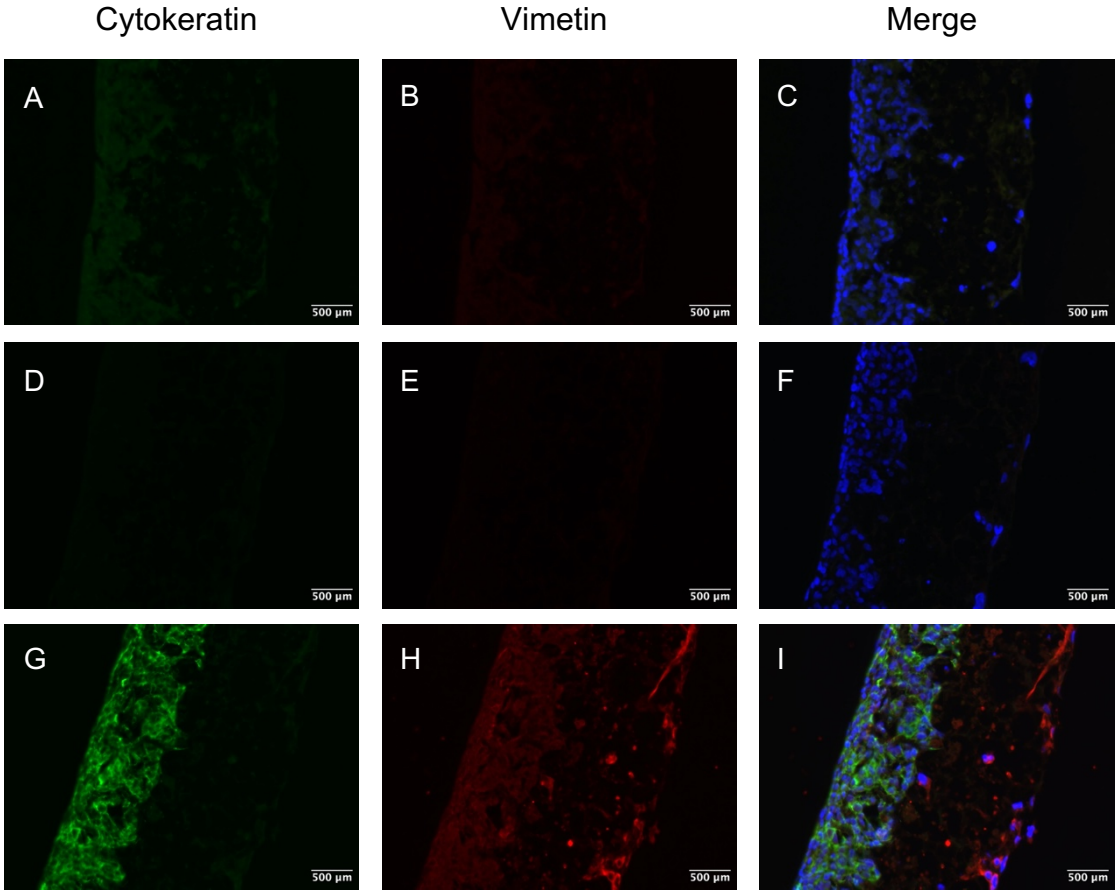

Figure 5.40: *Cytokeratin 18 and Vimentin expression in Alvetex scaffolds seeded with endometrial stromal and epithelial cells - transfection reagent only control.*
Fluorescent images of sections of Dharmafect only Alvetex scaffold seeded with 500,000 human stromal cells (immortalized cell line) and incubated for 35 days at 37°C 5% CO_2, followed by 1.5 million endometrial epithelial cells (Ishikawa) cells seeded on top for 8 days incubation at 37°C 5% CO_2. Cells were treated with Dharmafect only control - 100µl optiMEM + 1µl Dharmafect 2 for 3 hrs (n=1) before left to incubate at 37°C 5% CO_2 for 48 hrs. **A-C**) IgG control, **D-F**) Negative control - secondary antibody only, **G-I**) Cytokeratin 18 and Vimentin. Green = Cytokeratin 18, red = Vimentin, blue = nuclei stained with DAPI.

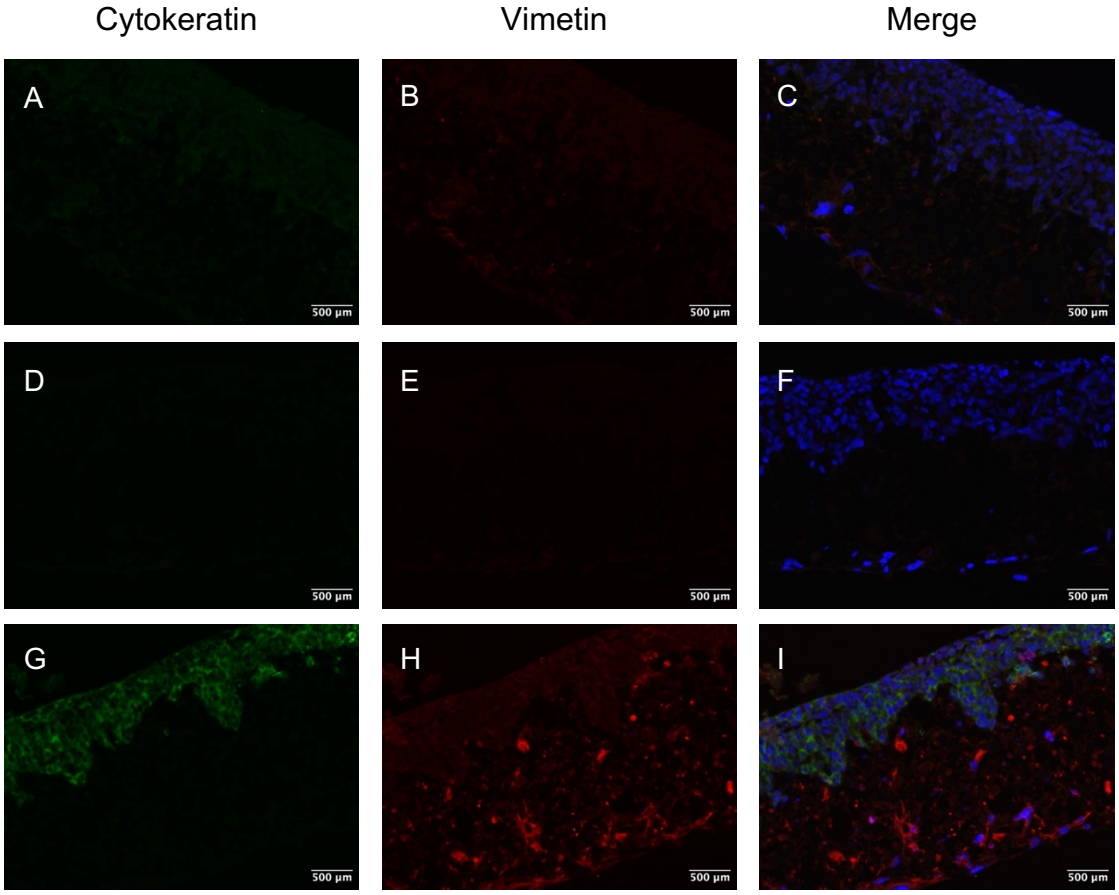

Figure 5.41: *Cytokeratin 18 and Vimentin expression in Alvetex scaffolds seeded with endometrial stromal and epithelial cells transfected with non-targeting mimic*
Fluorescent images of sections of Non-targeting mimic Alvetex scaffold seeded with 500,000 human stromal cells (immortalized cell line) and incubated for 35 days at 37°C 5% CO_2, followed by 1.5 million endometrial epithelial cells (Ishikawa) cells seeded on top for 8 days incubation at 37°C 5% CO_2. Cells were treated with 50nM non-targeting mimic + 100µl optiMEM + 1µl Dharmafect 2 for 3 hrs (n=1) before left to incubate at 37°C 5% CO_2 for 48 hrs. **A-C**) IgG control, **D-F**) Negative control - secondary antibody only, **G-I**) Cytokeratin 18 and Vimentin. Green = Cytokeratin 18, red = Vimentin, blue = nuclei stained with DAPI.

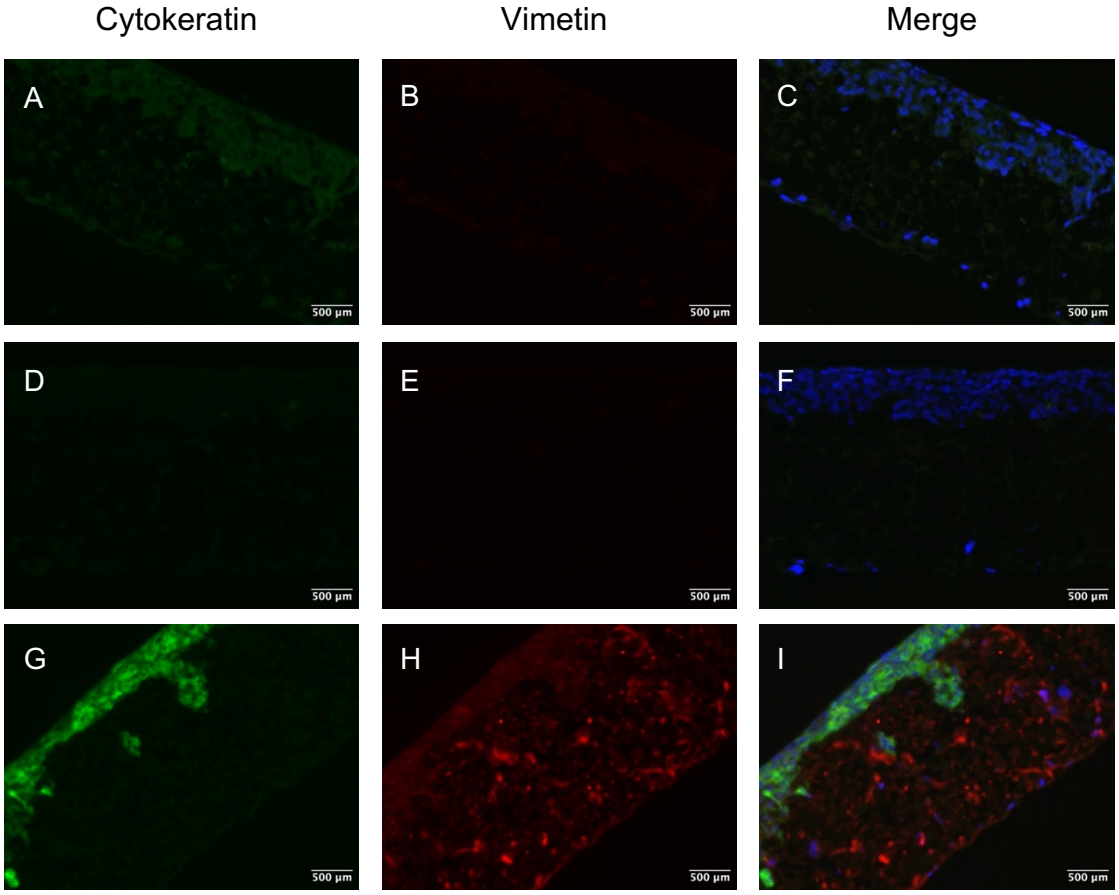

Figure 5.42: *Cytokeratin 18 and Vimentin expression in Alvetex scaffolds seeded with endometrial stromal and epithelial cells transfected with non-targeting inhibitor*
Fluorescent images of sections of Non-targeting inhibitor Alvetex scaffold seeded with 500,000 human stromal cells (immortalized cell line) and incubated for 35 days at 37°C 5% CO_2, followed by 1.5 million endometrial epithelial cells (Ishikawa) cells seeded on top for 8 days incubation at 37°C 5% CO_2. Cells were treated with 50nM non-targeting inhibitor + 100µl optiMEM + 1µl Dharmafect 2 for 3 hrs (n=1) before left to incubate at 37°C 5% CO_2 for 48 hrs. **A-C**) IgG control, **D-F**) Negative control - secondary antibody only, **G-I**) Cytokeratin 18 and Vimentin. Green = Cytokeratin 18, red = Vimentin, blue = nuclei stained with DAPI.

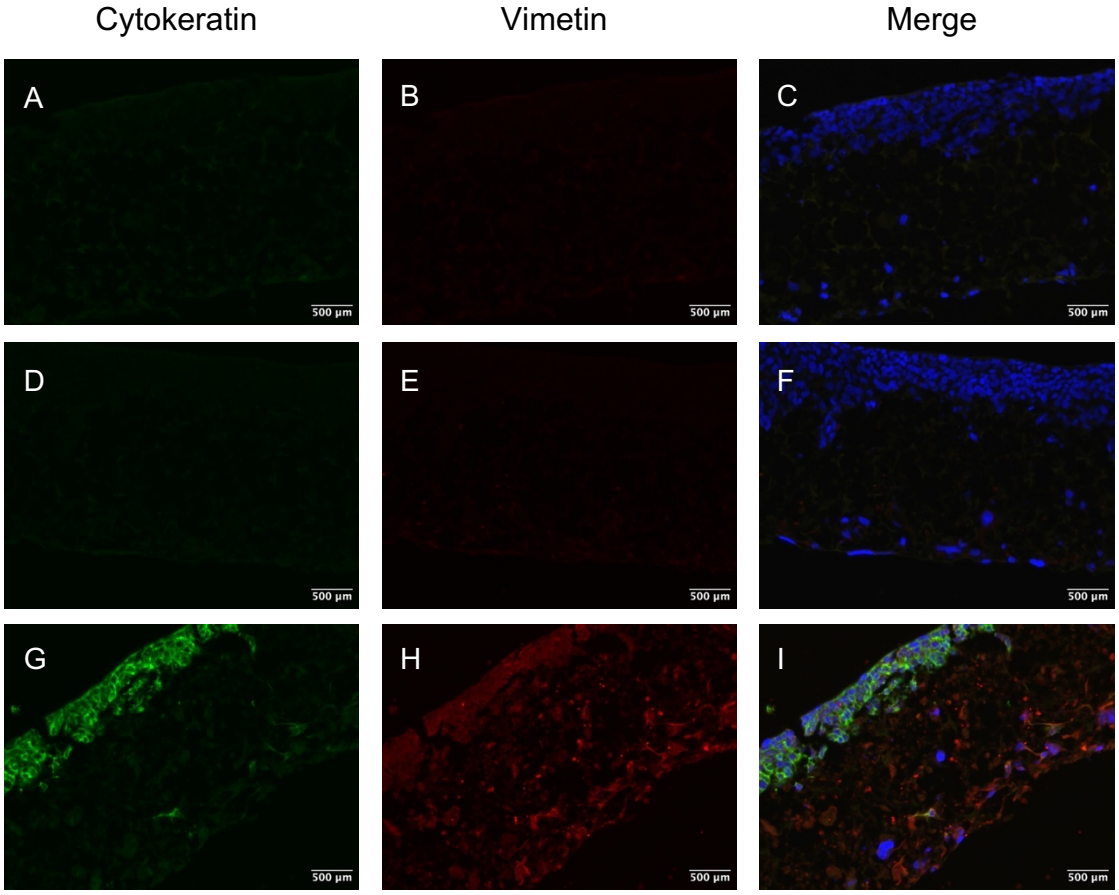

Figure 5.43: *Cytokeratin 18 and Vimentin expression in Alvetex scaffolds seeded with endometrial stromal and epithelial cells transfected with miR-340-5p mimic*

Fluorescent images of sections of overexpressed miR-340-5p Alvetex scaffold seeded with 500,000 human stromal cells (immortalized cell line) and incubated for 35 days at 37oC 5% CO2, followed by 1.5 million endometrial epithelial cells (Ishikawa) cells seeded on top for 8 days incubation at 37oC 5% CO2. Cells were treated with 50nM miR-340-5p mimic + 100ml optiMEM + 1ml Dharmafect 2 for 3 hrs (n=1) before left to incubate at 37oC 5% CO2 for 48 hrs. **A-C**) IgG control, **D-F**) Negative control - secondary antibody only, **G-I**) Cytokeratin 18 and Vimentin. Green = Cytokeratin 18, red = Vimentin, blue = nuclei stained with DAPI.

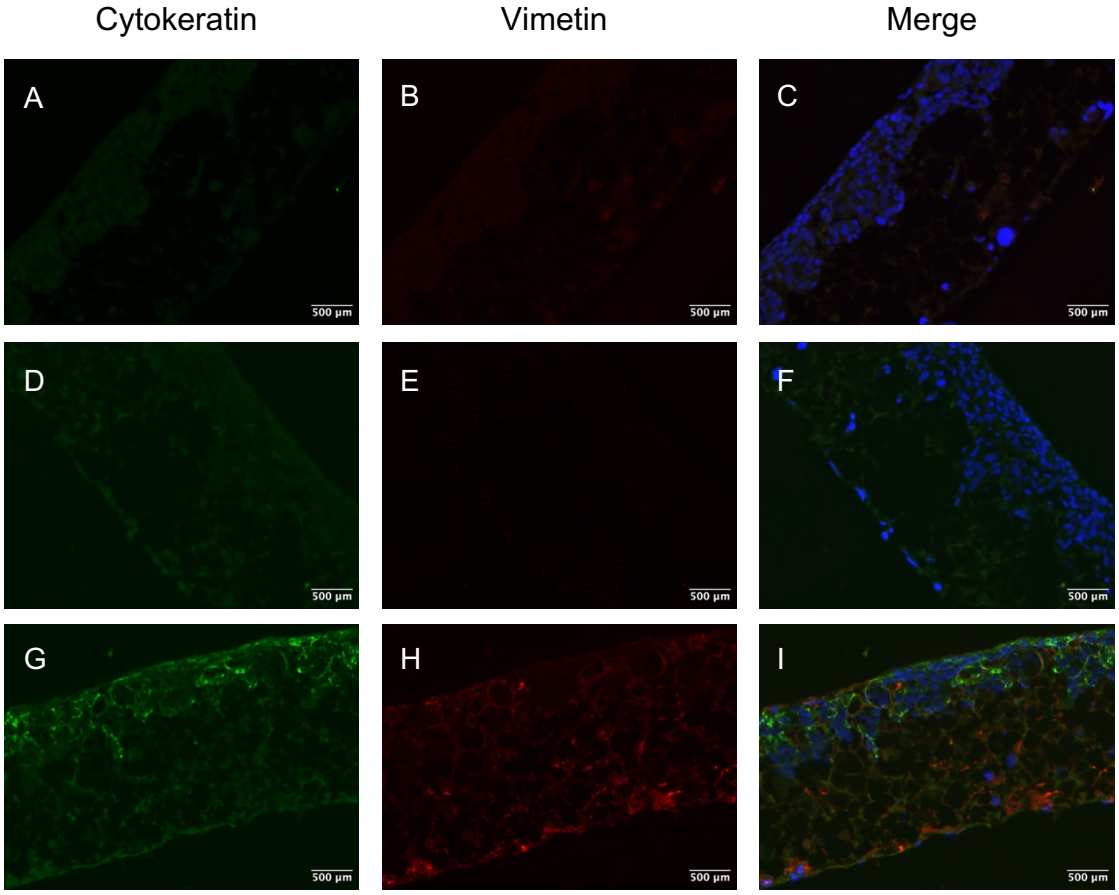

Figure 5.44: *Cytokeratin 18 and Vimentin expression in Alvetex scaffolds seeded with endometrial stromal and epithelial cells transfected with miR-340-5p inhibitor*

Fluorescent images of sections of under expressed miR-340-5p Alvetex scaffold seeded with 500,000 human stromal cells (immortalized cell line) and incubated for 35 days at 37°C 5% CO_2, followed by 1.5 million endometrial epithelial cells (Ishikawa) cells seeded on top for 8 days incubation at 37°C 5% CO_2. Cells were treated with 50nM miR-340-5p inhibitor + 100µl optiMEM + 1µl Dharmafect 2 for 3 hrs (n=1) before left to incubate at 37°C 5% CO_2 for 48 hrs. **A-C**) IgG control, **D-F**) Negative control - secondary antibody only, **G-I**) Cytokeratin 18 and Vimentin. Green = Cytokeratin 18, red = Vimentin, blue = nuclei stained with DAPI.

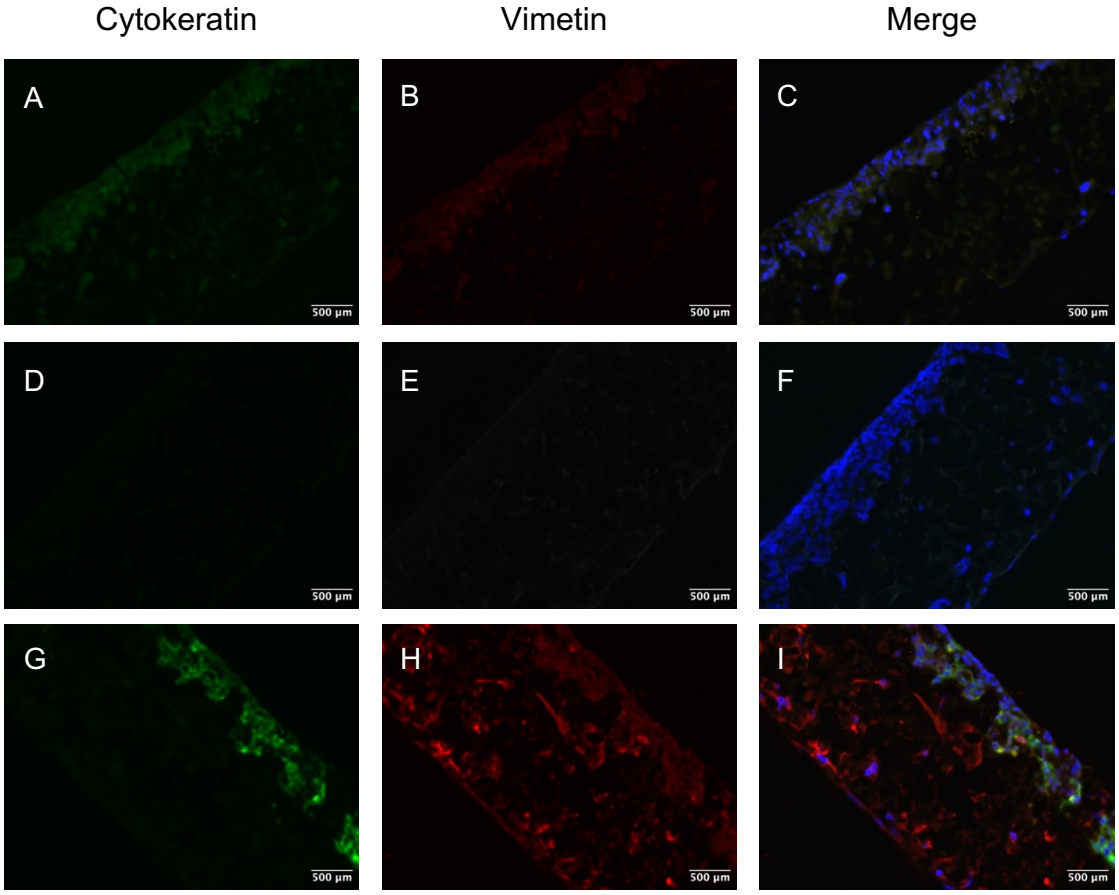

Figure 5.45: *Cytokeratin 18 and Vimentin expression in Alvetex scaffolds seeded with endometrial stromal and epithelial cells transfected with miR-542-3p mimic*

Fluorescent images of sections of overexpressed miR-542-3p Alvetex scaffold seeded with 500,000 human stromal cells (immortalized cell line) and incubated for 35 days at 37oC 5% CO2, followed by 1.5 million endometrial epithelial cells (Ishikawa) cells seeded on top for 8 days incubation at 37oC 5% CO2. Cells were treated with 50nM miR-542-3p mimic + 100ml optiMEM + 1ml Dharmafect 2 for 3 hrs (n=1) before left to incubate at 37oC 5% CO2 for 48 hrs. **A-C**) IgG control, **D-F**) Negative control - secondary antibody only, **G-I**) Cytokeratin 18 and Vimentin. Green = Cytokeratin 18, red = Vimentin, blue = nuclei stained with DAPI.

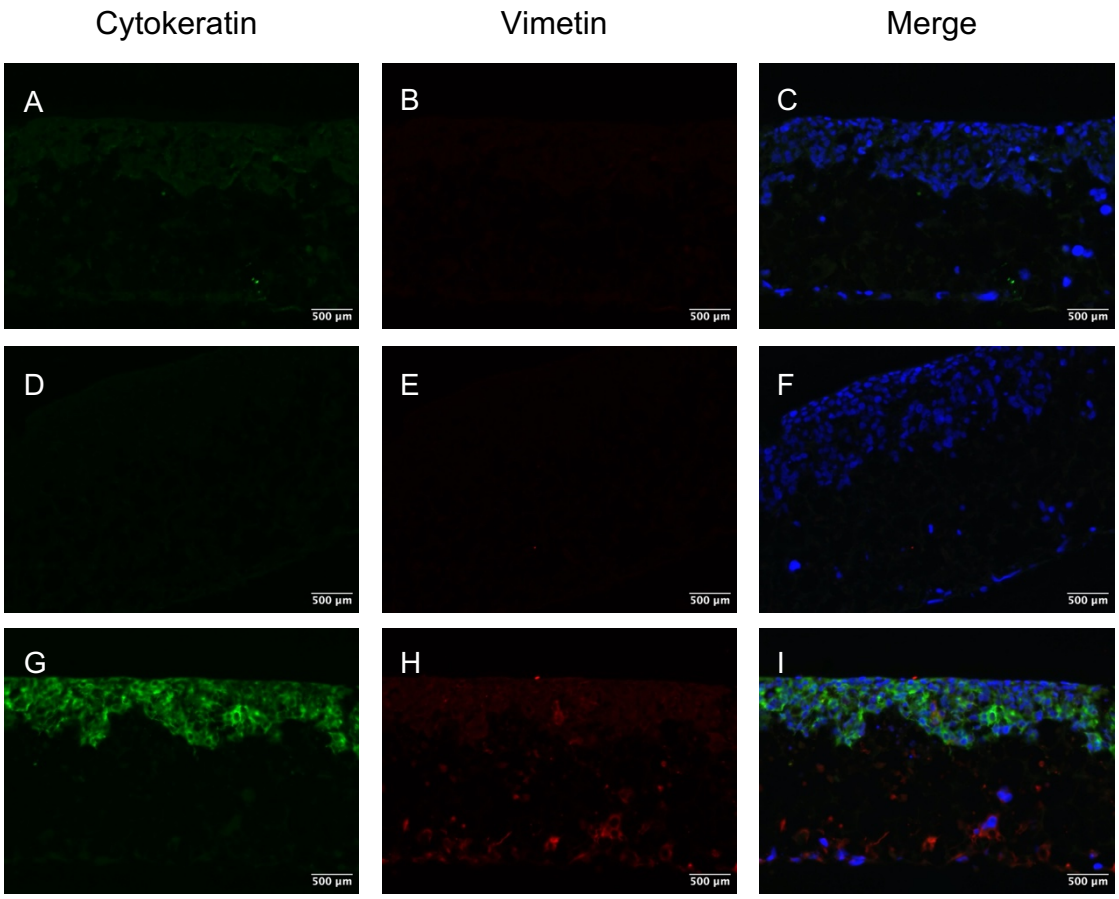

Figure 5.46: *Cytokeratin 18 and Vimentin expression in Alvetex scaffolds seeded with endometrial stromal and epithelial cells transfected with miR-542-3p inhibitor*

Fluorescent images of sections of under expressed miR-542-3p Alvetex scaffold seeded with 500,000 human stromal cells (immortalized cell line) and incubated for 35 days at 37°C 5% CO_2, followed by 1.5 million endometrial epithelial cells (Ishikawa) cells seeded on top for 8 days incubation at 37°C 5% CO_2. Cells were treated with 50nM miR-542-3p inhibitor + 100µl optiMEM + 1µl Dharmafect 2 for 3 hrs (n=1) before left to incubate at 37°C 5% CO_2 for 48 hrs. **A-C**) IgG control, **D-F**) Negative control - secondary antibody only, **G-I**) Cytokeratin 18 and Vimentin. Green = Cytokeratin 18, red = Vimentin, blue = nuclei stained with DAPI.

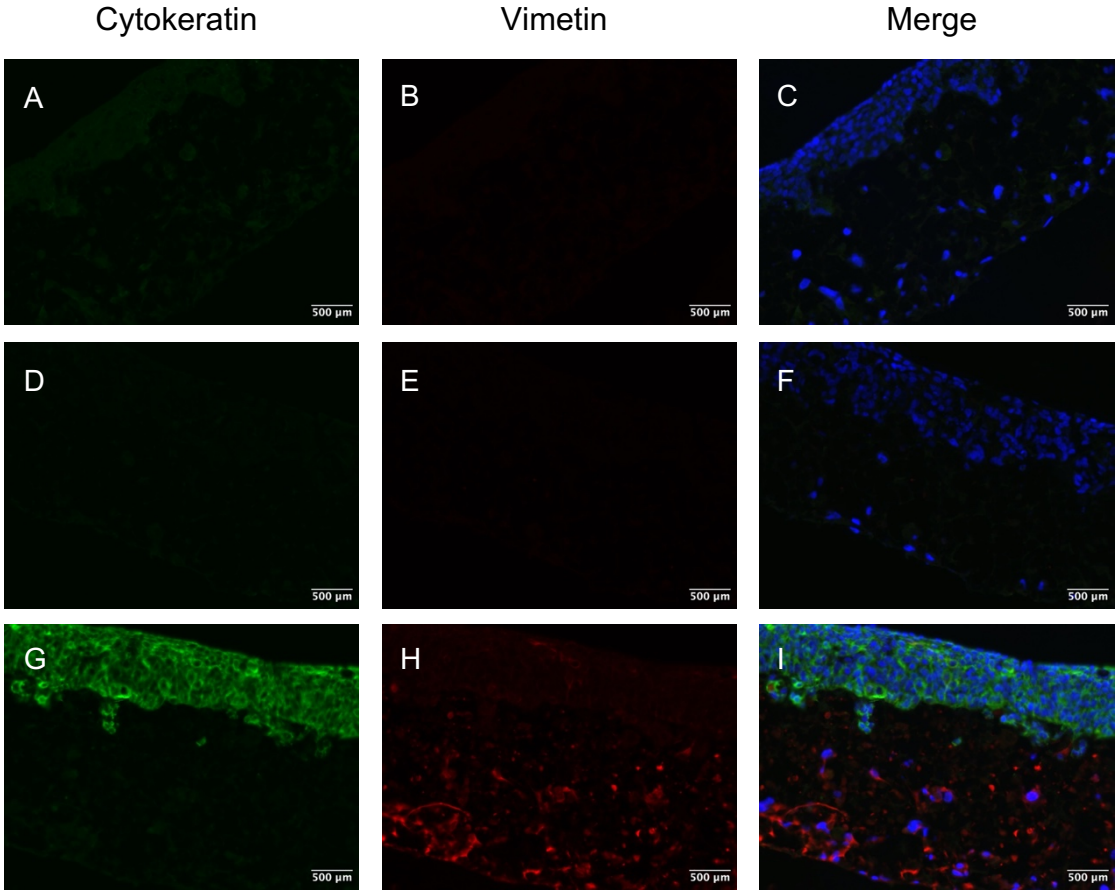

Figure 5.47: *Cytokeratin 18 and Vimentin expression in Alvetex scaffolds seeded with endometrial stromal and epithelial cells transfected with miR-671-5p mimic*

Fluorescent images of sections of overexpressed miR-671-5p Alvetex scaffold seeded with 500,000 human stromal cells (immortalized cell line) and incubated for 35 days at 37oC 5% CO2, followed by 1.5 million endometrial epithelial cells (Ishikawa) cells seeded on top for 8 days incubation at 37oC 5% CO2. Cells were treated with 50nM miR-671-5p mimic + 100ml optiMEM + 1ml Dharmafect 2 for 3 hrs (n=1) before left to incubate at 37oC 5% CO2 for 48 hrs. **A-C**) IgG control, **D-F**) Negative control - secondary antibody only, **G-H**) Cytokeratin 18 and Vimentin. Green = Cytokeratin 18, red = Vimentin, blue = nuclei stained with DAPI.

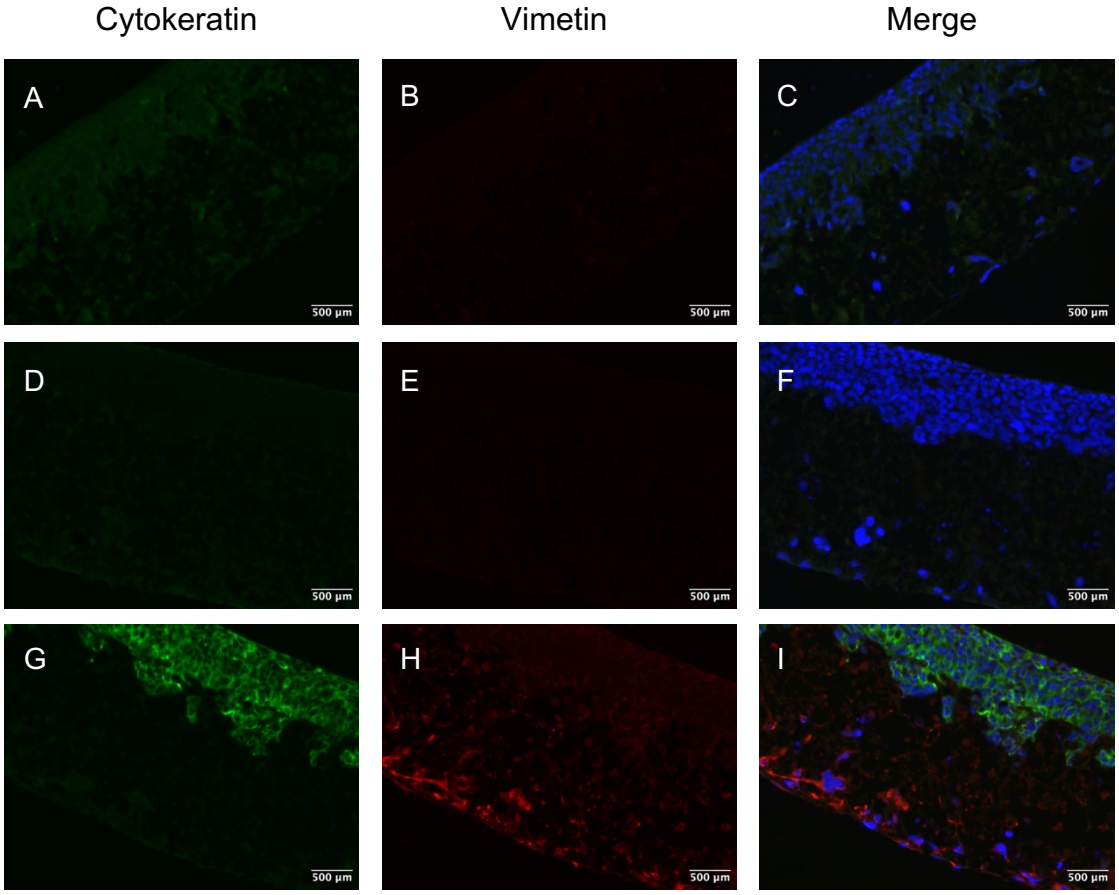

Figure 5.48: *Cytokeratin 18 and Vimentin expression in Alvetex scaffolds seeded with endometrial stromal and epithelial cells transfected with miR-671-5p inhibitor*
Fluorescent images of sections of under expressed miR-671-5p Alvetex scaffold seeded with 500,000 human stromal cells (immortalized cell line) and incubated for 35 days at 37°C 5% CO_2, followed by 1.5 million endometrial epithelial cells (Ishikawa) cells seeded on top for 8 days incubation at 37°C 5% CO_2. Cells were treated with 50nM miR-671-5p inhibitor + 100µl optiMEM + 1µl Dharmafect 2 for 3 hrs (n=1) before left to incubate at 37°C 5% CO_2 for 48 hrs. **A-C**) IgG control, **D-F**) Negative control - secondary antibody only, **G-H**) Cytokeratin 18 and Vimentin. Green = Cytokeratin 18, red = Vimentin, blue = nuclei stained with DAPI.

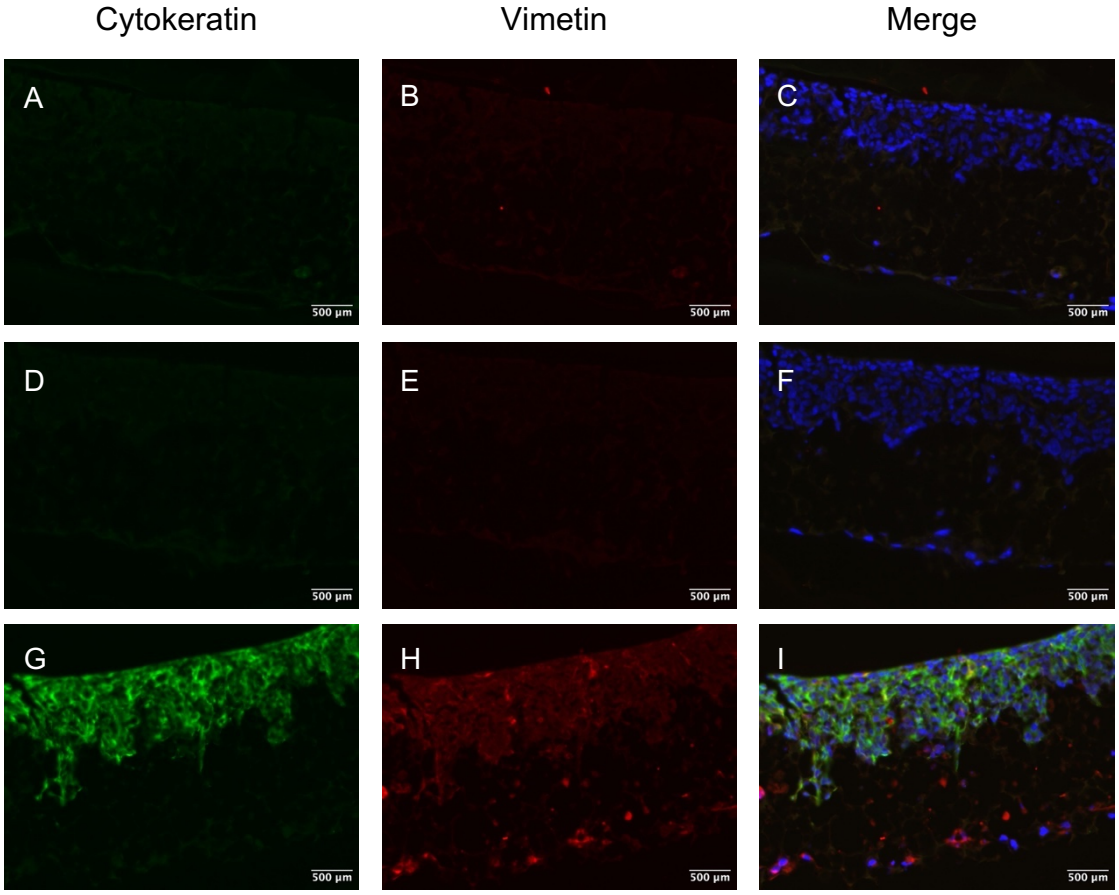

Figure 5.49: *Cytokeratin 18 and Vimentin expression in Alvetex scaffolds seeded with endometrial stromal and epithelial cells transfected with miR-340-5p, miR-542-3p and miR-671-5p mimics*
Fluorescent images of sections of overexpressed miR-340-5p, miR-542-3p and miR-671-5p Alvetex scaffold seeded with 500,000 human stromal cells (immortalized cell line) and incubated for 35 days at 37ºC 5% CO_2, followed by 1.5 million endometrial epithelial cells (Ishikawa) cells seeded on top for 8 days incubation at 37ºC 5% CO_2. Cells were treated with 16.6nM miR-340-5p mimic + 16.6nM miR-542-3p mimic + 16.6nM miR-671-5p mimic + 100µl optiMEM + 1µl Dharmafect 2 for 3 hrs (n=1) before left to incubate at 37ºC 5% CO_2 for 48 hrs. **A-C**) IgG control, **D-F**) Negative control - secondary antibody only, **G-H**) Cytokeratin 18 and Vimentin. Green = Cytokeratin 18, red = Vimentin, blue = nuclei stained with DAPI.

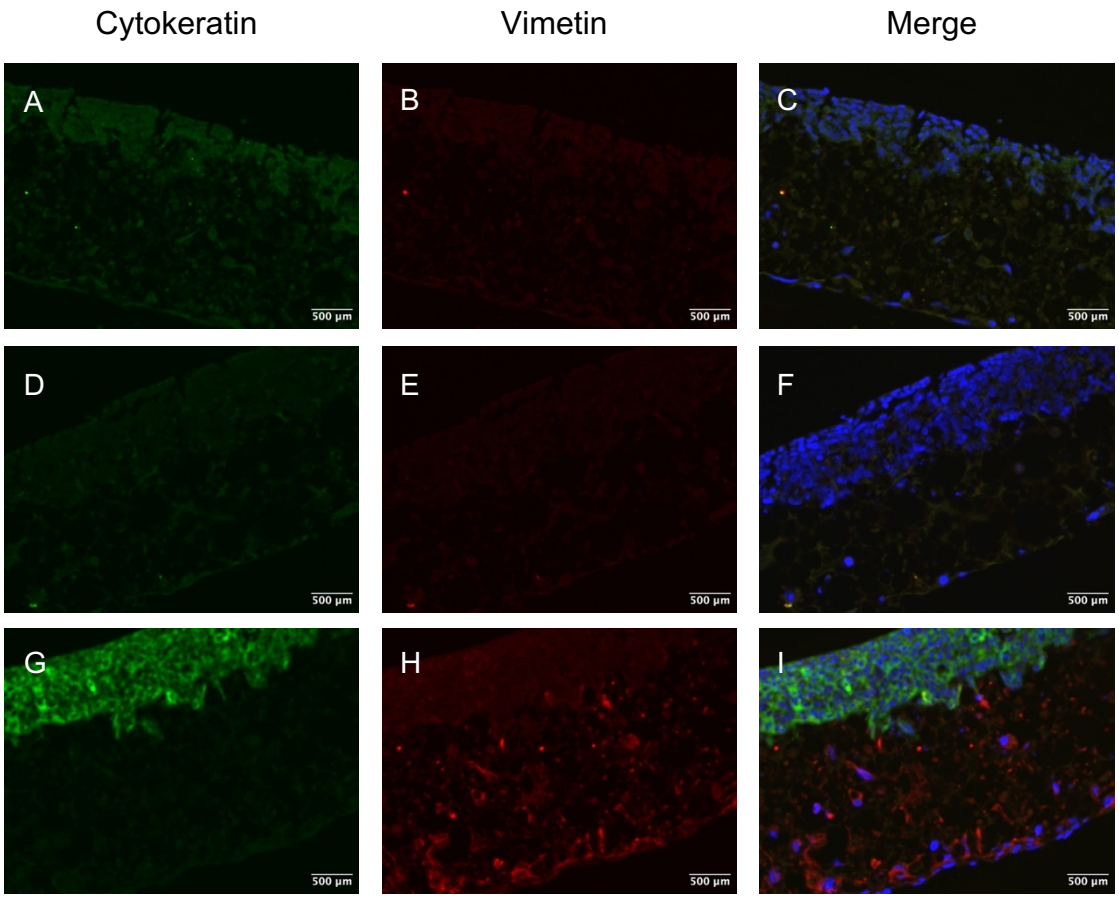

Figure 5.50: *Cytokeratin 18 and Vimentin expression in Alvetex scaffolds seeded with endometrial stromal and epithelial cells transfected with miR-340-5p, miR-542-3p and miR-671-5p inhibitors*
Fluorescent images of sections of under expressed miR-340-5p, miR-542-3p and miR-671-5p Alvetex scaffold seeded with 500,000 human stromal cells (immortalized cell line) and incubated for 35 days at 37ºC 5% CO_2, followed by 1.5 million endometrial epithelial cells (Ishikawa) cells seeded on top for 8 days incubation at 37ºC 5% CO_2. Cells were treated with 16.6nM miR-340-5p inhibitor + 16.6nM miR-542-3p inhibitor + 16.6nM miR-671-5p inhibitor + 100µl optiMEM + 1µl Dharmafect 2 for 3 hrs (n=1) before left to incubate at 37ºC 5% CO_2 for 48 hrs. **A-C**) IgG control, **D-F**) Negative control - secondary antibody only, **G-H**) Cytokeratin 18 and Vimentin. Green = Cytokeratin 18, red = Vimentin, blue = nuclei stained with DAPI.

5.4.2.3.4 Assessing proliferation in transfected Alvetex scaffolds

Cells were stained for proliferation marker Ki67 to observe cell proliferation following treatment with miRNAs of interest (Figure 5.51). Alvetex transfections were only carried out with 1 biological replicate so no quantitative or statistical analysis was carried out, rather this was a preliminary stain to provide an approximation of cell proliferation following transfection. This was also due to the fact that only 1 image from a section of the scaffold was taken so this may not be wholly representative. However these images provide some tentative results. MiR-340-5p (Figure 5.51M-O) mimic appears to reduce proliferation in the epithelial layer compared to miR-340-5p inhibition (Figure 5.51P-R) as there is less ki67 staining. MiR-542-3p overexpression (Figure 5.51S-U) also seems to reduce proliferation in the epithelial layer compared to miR-542-3p inhibition (Figure 5.51V-X). Conversely, proliferation is approximately equal following miR-671-5p over (Figure 5.51Y-AA) or under expression (Figure 5.51AB-AD). Interestingly, when miR-340-5p, miR-542-3p and miR-671-5p are all overexpressed, there is no ki67 expression, suggesting halted proliferation (Figure 5.51AE-AG). This is in contrast to inhibition of all 3 miRNAs, where there is a large amount of ki67 staining, which means that proliferation is occurring (Figure 5.51).

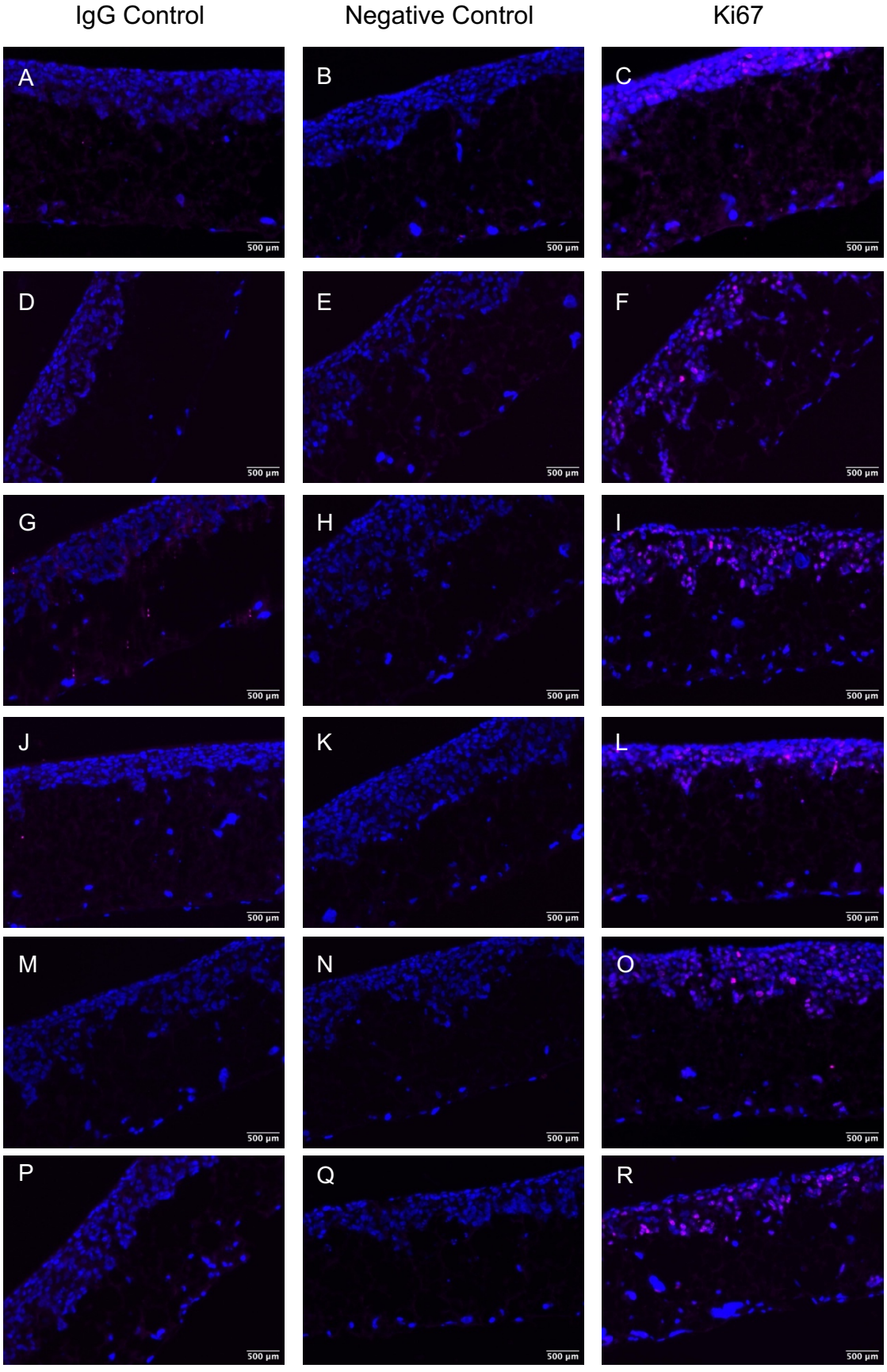
IgG Control
Negative Control
Ki67
A
B
C
D
E
F
G
H
I
J
K
L
M
N
O
P
Q
R
500 µm

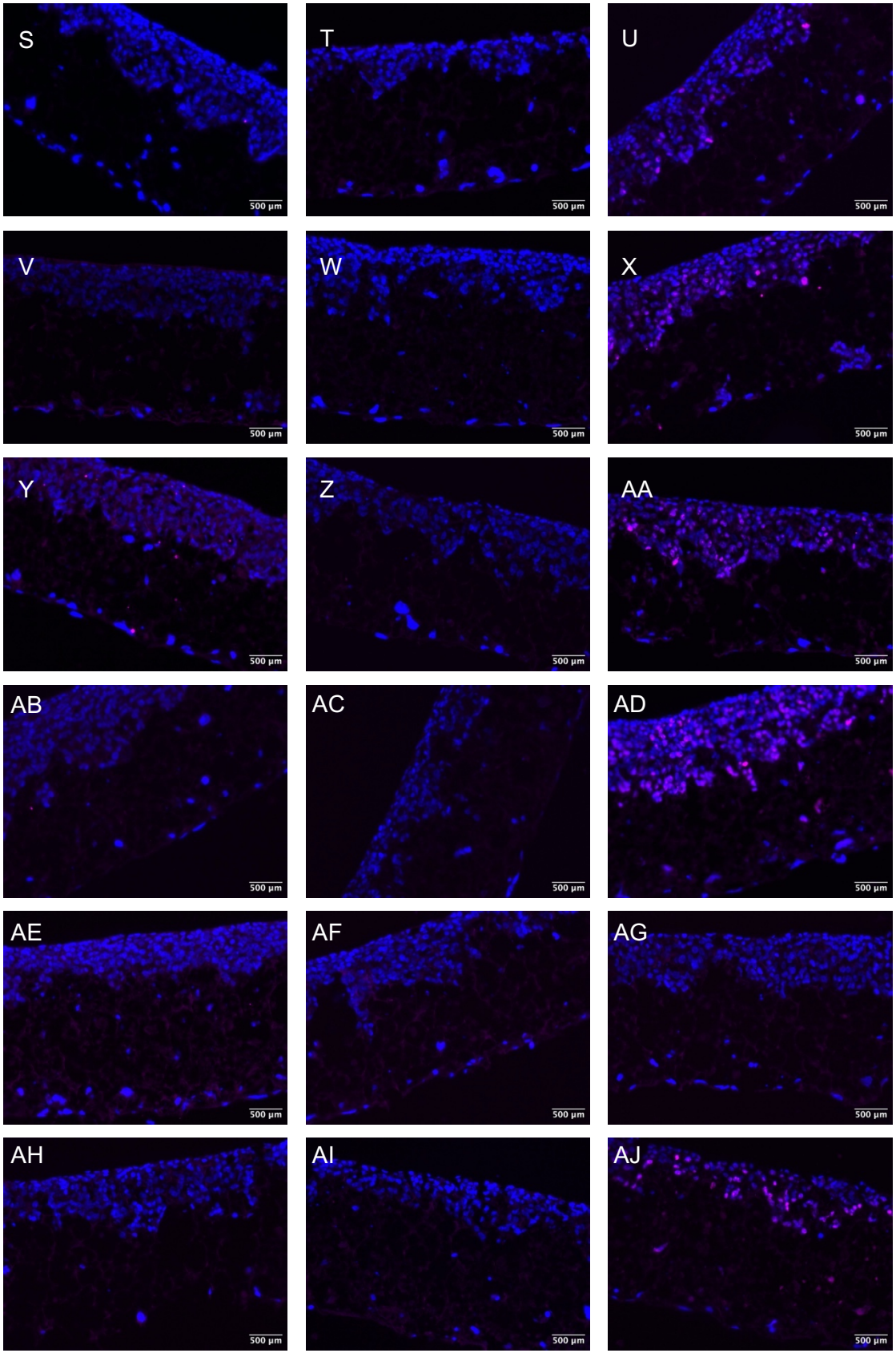
S
T
U
V
W
X
Y
Z
AA
AB
AC
AD
AE
AF
AG
AH
AI
AJ
500 µm

Figure 5.51: *Ki67 expression in Alvetex scaffolds seeded with endometrial stromal and epithelial cells and transfected with mimics and inhibitors for miRNAs of interest.*
Fluorescent images of sections of Alvetex scaffold seeded with 500,000 human stromal cells (immortalized cell line) and incubated for 35 days at 37ºC 5% CO_2, followed by 1.5 million endometrial epithelial cells (Ishikawa) cells seeded on top for 8 days incubation at 37ºC 5% CO_2. Cells were transfected with the following treatments for 3 hrs (n=1) before left to incubate at 37ºC 5% CO_2 for 48 hrs. All treatments were added to cells in 100μl optiMEM media: Control - no treatment (**A-C**), Dharmafect only control - 1μl Dharmafect 2 (**D-F**). All further treatments were added to cells in 100μl optiMEM + 1μl Dharmafect 2: 50nM non-targeting mimic (**G-I**), 50nM non-targeting inhibitor (**J-L**), 50nM miR-340-5p mimic (**M-O**), 50nM miR-340-5p inhibitor (**P-R**), 50nM miR-542-3p mimic (**S-U**), 50nM miR-542-3p inhibitor (**V-X**), 50nM miR-671-5p mimic (**Y-AA**), 50nM miR-671-5p inhibitor (**AB-AD**), 16.6nM miR-340-5p mimic + 16.6nM miR-542-3p mimic + 16.6nM miR-671-5p mimic (**AE-AG**), and 16.6nM miR-340-5p inhibitor + 16.6nM miR-542-3p inhibitor + 16.6nM miR-671-5p inhibitor (**AH-AJ**). Cells are stained with negative IgG control (column 1), negative control - secondary antibody only (column 2) or Ki67 (purple) (column 3). Purple = Ki67, Blue = cell nuclei stained with DAPI.

5.4.3 Modelling the Bovine Endometrium: Endometrial Organoids

5.4.3.1 Producing Organoids

5.4.3.1.1 Primer validation

Five primers were validated for use in measuring expression of gland markers in selecting the correct digestion mix and incubation length, as well as to measure in bovine organoids. These were *KLF5, MUC1, LIF, FOXA2* and *IGFBP1*. Graphs demonstrating standard curves for these primers are shown in Figure 5.52. *FOXA2* did not produce expected results for validation, however was still selected to be used as a gland marker as the pool of RNA for which the validations were carried out on was not purely glandular cells, and the CT values for *FOXA2* still showed the exponential expression pattern expected for a primer to be validated.

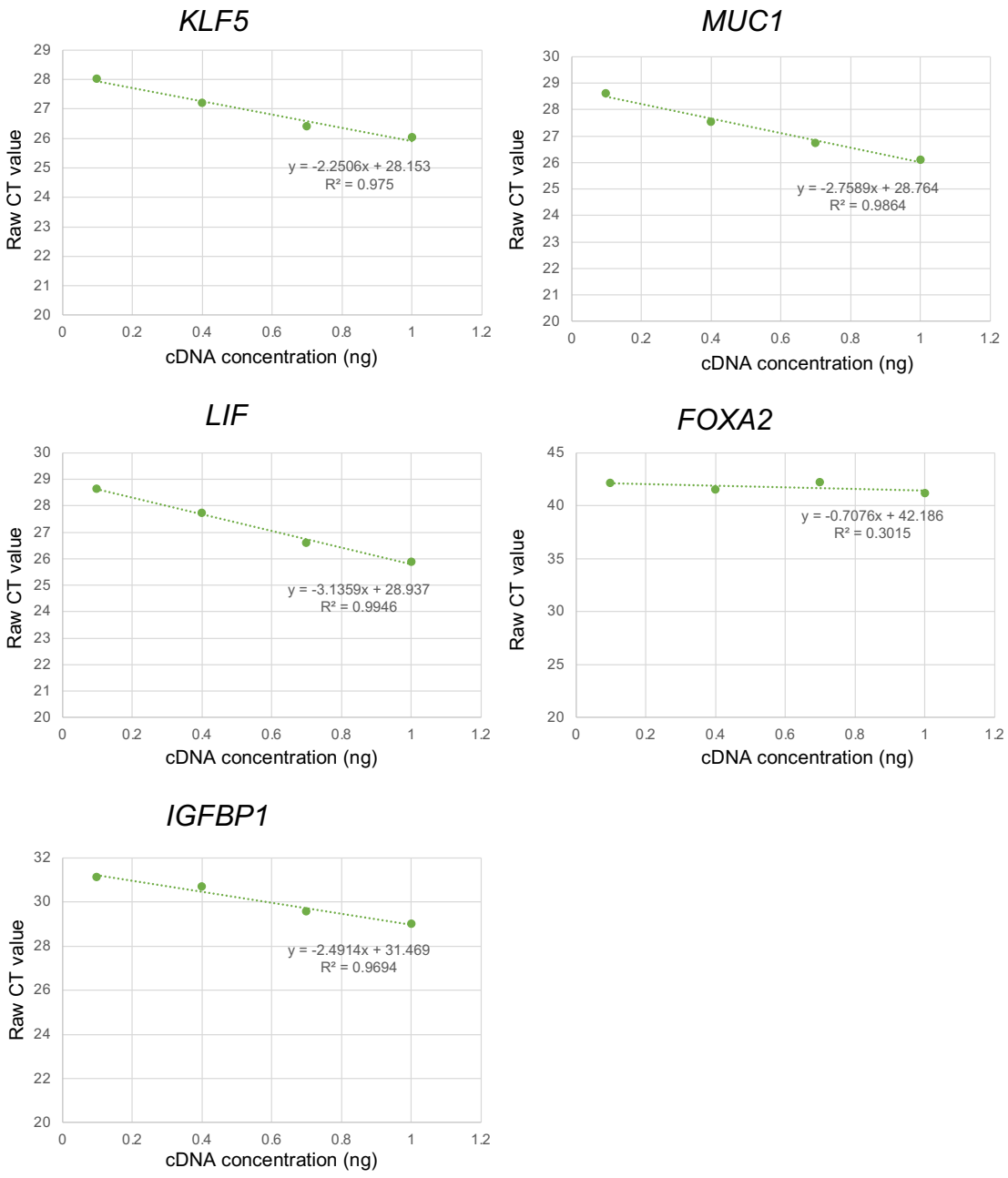

Figure 5.52: *Gland marker primer validation.*
Graphs showing PCR results for primer validation of *KLF5, MUC1, LIF, FOXA2* and *IGFBP1* in bovine epithelial cells (n=1) at concentrations of 10ng/μl, 5ng/μl, 2.5ng/μl and 1.25ng/μl.

5.4.3.1.2 Optimisation of digestion mix and incubation length

Three different digestion compositions (Table 5.6) were used for digesting bovine endometrium (n=3) for analysis of gland markers *LIF* (Figure 5.53)*, MUC1* (Figure 5.54)*, KLF5* (Figure 5.55)*, FOXA2* (Figure 5.56) and *IGFBP1* (Figure 5.57). Two time points of 30 min and 1 hr were used, and different fractions of the digestion were collected (Figure 5.7). Consistently, gland marker expression is lowest using Digestion 3, and each gland marker is absent from 1 or more samples using this digestion (Figure 5.53-Figure 5.57). Gland marker expression is similar in most cases for Digestion 1 and Digestion 2, therefore Digestion 1 was selected for digestion composition as there are less components whilst still resulting in the same glandular marker expression. Cells taken from the 70μM strainer fraction (Figure 5.7) exhibit lower expression of all gland markers for each animal at both time points than those taken from the 40μM strainer. *FOXA2* and *IGFBP1* expression in animal 3 (blue) using the 70μM strainer is not detected at all (Figure 5.56 and Figure 5.57). For these reasons, cells isolated and collected by inversion of the 40μM strainer were selected for use. Expression of all gland markers for each animal were higher following a 1 hr incubation compared to a 30 min incubation. Overall, the conditions selected were: 1 hr incubation, Digestion mix 1, cells taken from 40μM strainer.

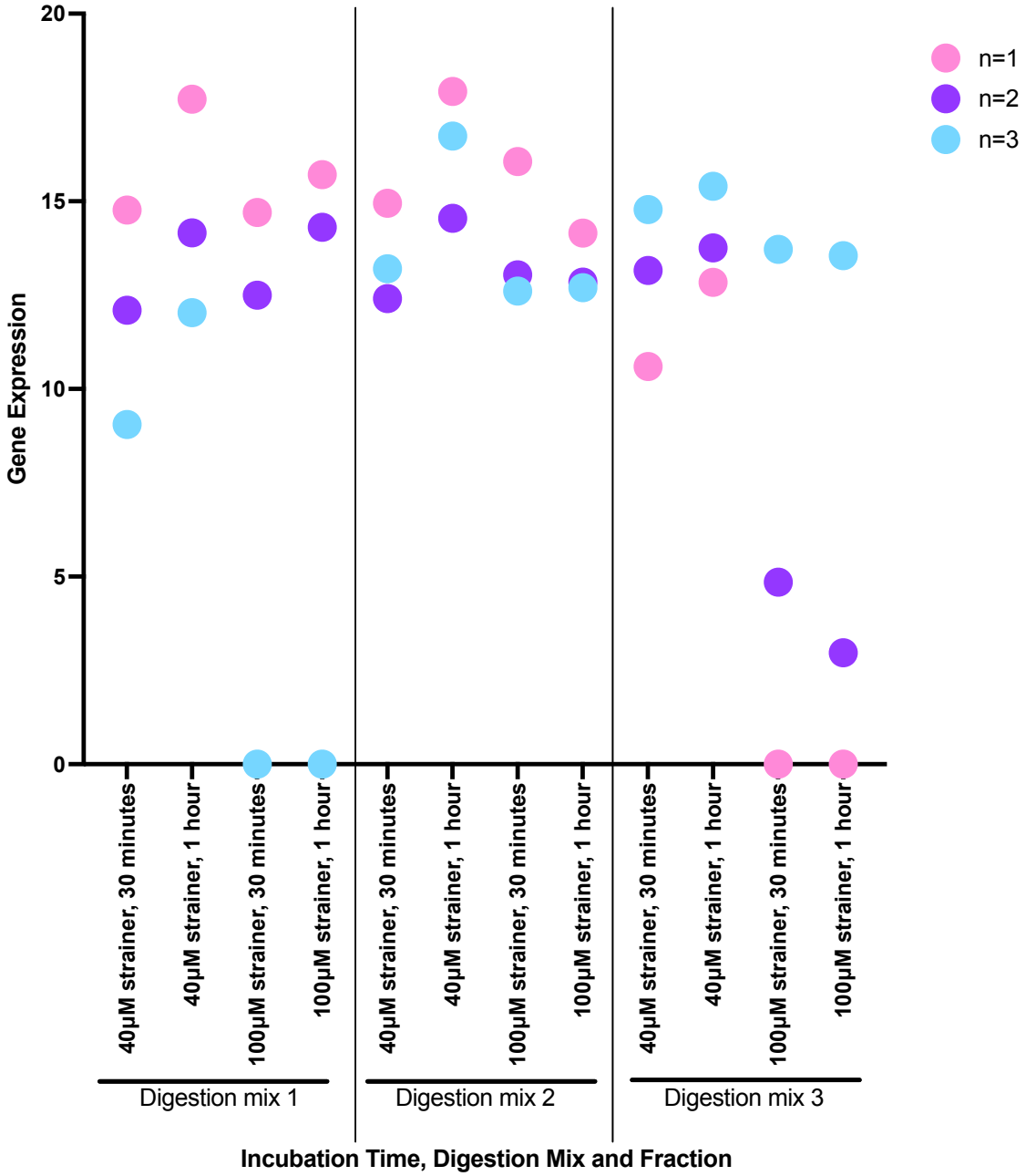

Figure 5.53: *LIF expression in cells isolated from bovine endometrium using different methods of isolation.*
Comparison of *LIF* gene expression in cells isolated from the 40µM strainer or the 70µM strainer from bovine endometrium (n=3) following either 30 min or 1 hr incubation at 37oC 5% CO2 in digestion mix 1 (0.5mg/ml collagenase II, 100µg/ml DNase), 2 (0.5mg/ml collagenase II, 1mg/ml dispase, 100µg/ml DNase) or 3 (0.5mg/ml collagenase II, 1mg/ml dispase, 1µg/ml DNase).

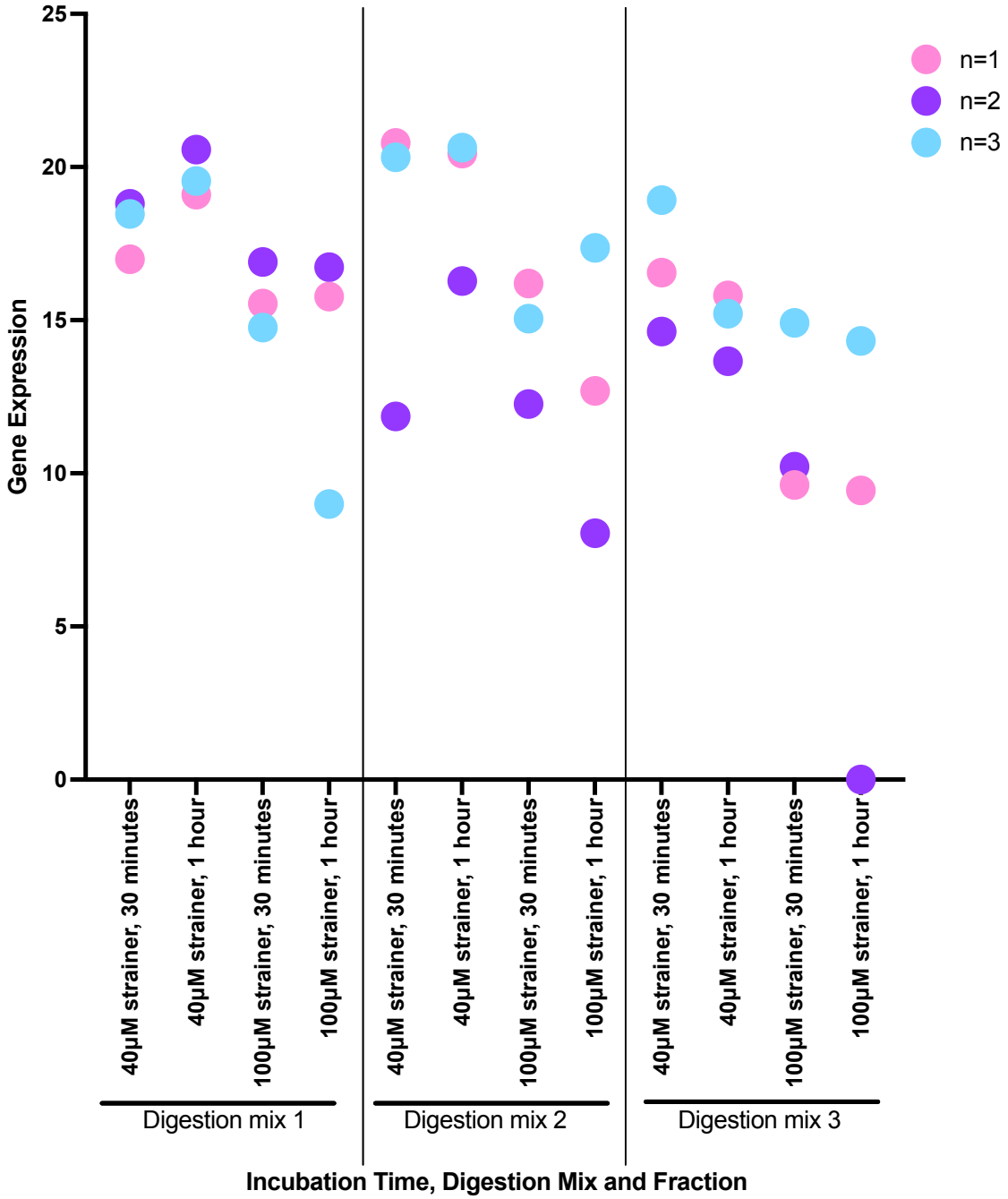

Figure 5.54: *MUC1 expression in cells isolated from bovine endometrium using different methods of isolation.*
Comparison of *MUC1* gene expression in cells isolated from the 40µM strainer or the 70µM strainer from bovine endometrium (n=3) following either 30 min or 1 hr incubation at 37oC 5% CO2 in digestion mix 1 (0.5mg/ml collagenase II, 100µg/ml DNase), 2 (0.5mg/ml collagenase II, 1mg/ml dispase, 100µg/ml DNase) or 3 (0.5mg/ml collagenase II, 1mg/ml dispase, 1µg/ml DNase).

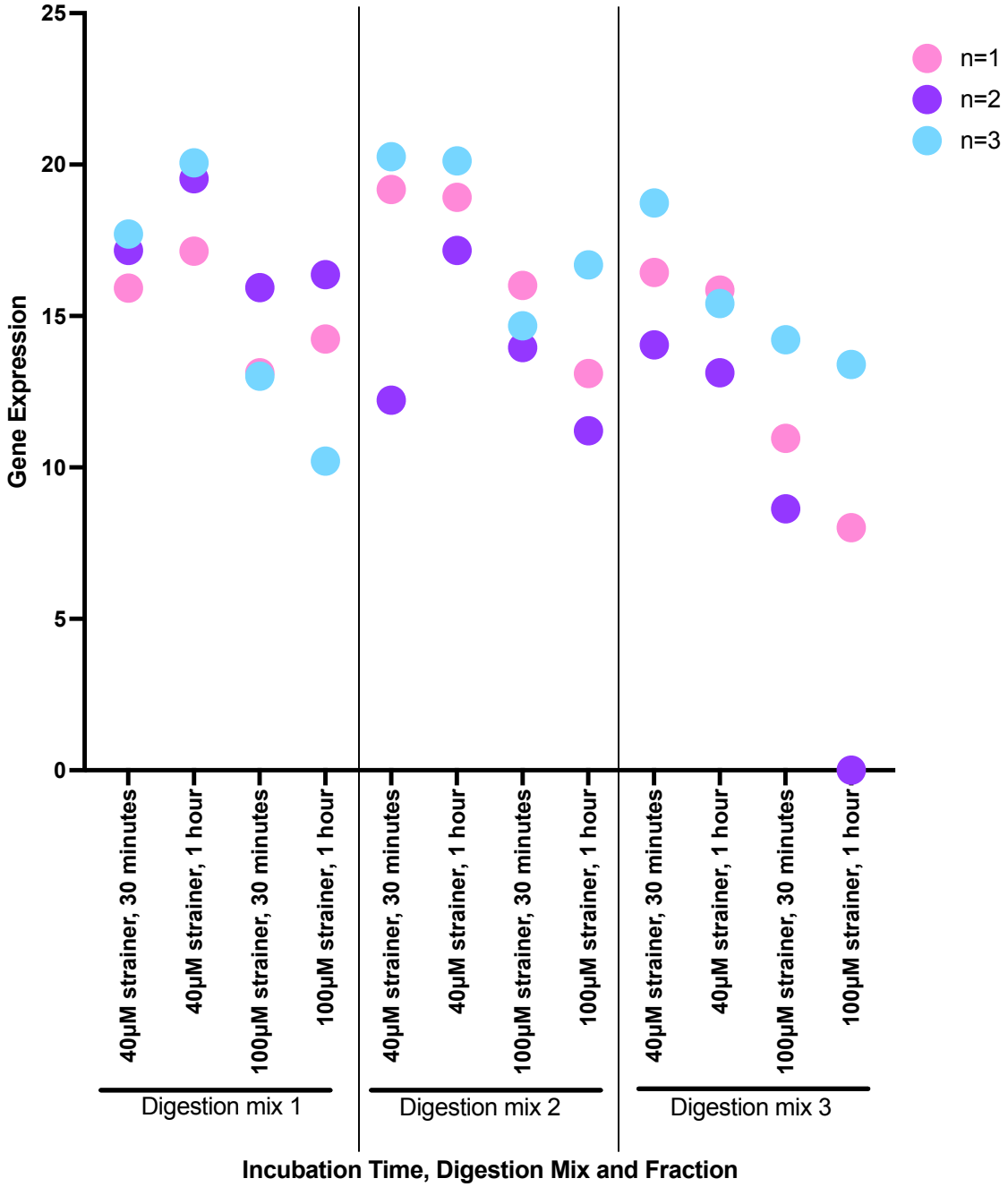

Figure 5.55: *KLF5 expression in cells isolated from bovine endometrium using different methods of isolation.*
Comparison of *KLF5* gene expression in cells isolated from the 40µM strainer or the 70µM strainer from bovine endometrium (n=3) following either 30 min or 1 hr incubation at 37oC 5% CO2 in digestion mix 1 (0.5mg/ml collagenase II, 100µg/ml DNase), 2 (0.5mg/ml collagenase II, 1mg/ml dispase, 100µg/ml DNase) or 3 (0.5mg/ml collagenase II, 1mg/ml dispase, 1µg/ml DNase).

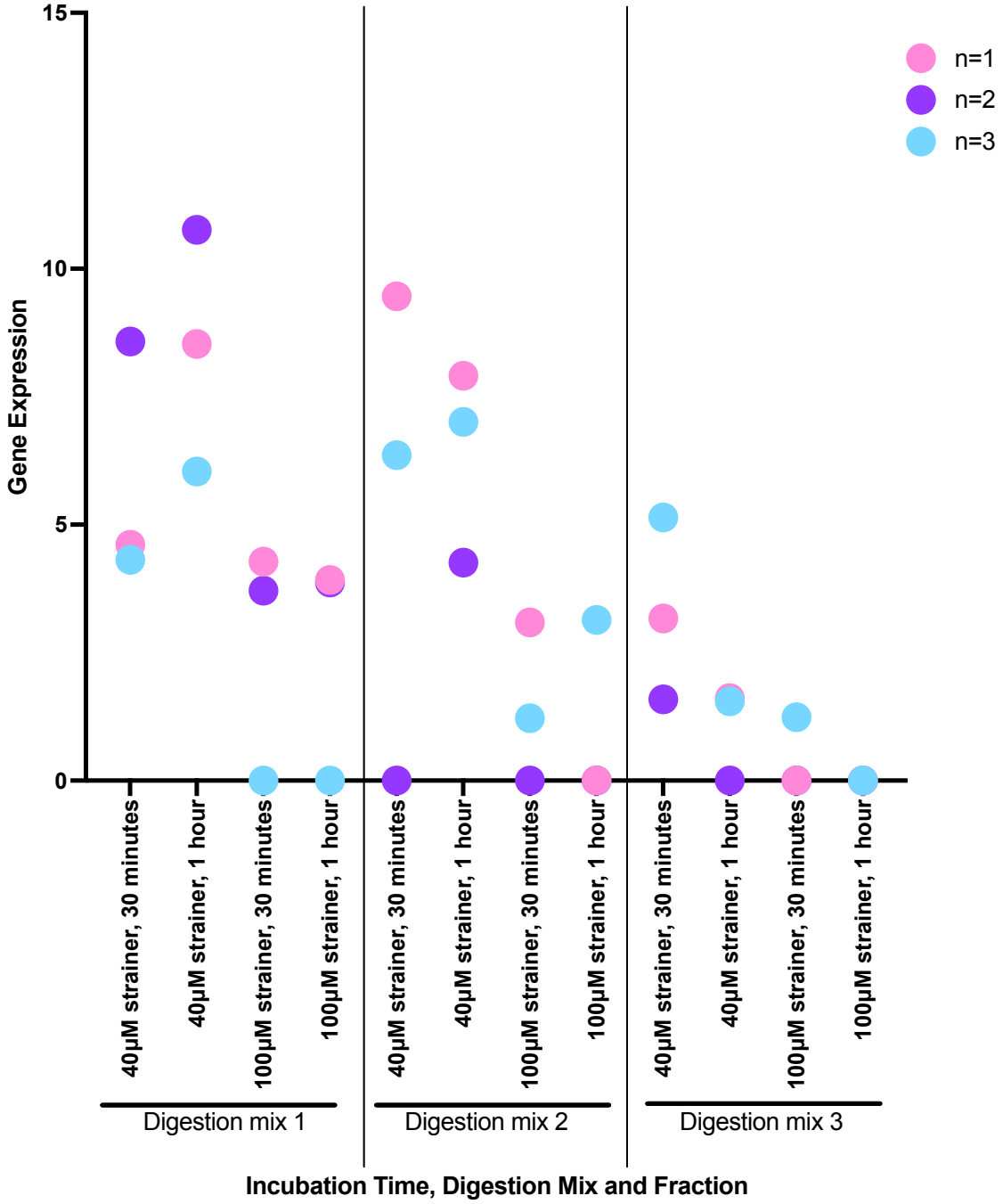

Figure 5.56: *FOXA2 expression in cells isolated from bovine endometrium using different methods of isolation.*
Comparison of *FOXA2* gene expression in cells isolated from the 40µM strainer or the 70µM strainer from bovine endometrium (n=3) following either 30 min or 1 hr incubation at 37oC 5% CO2 in digestion mix 1 (0.5mg/ml collagenase II, 100µg/ml DNase), 2 (0.5mg/ml collagenase II, 1mg/ml dispase, 100µg/ml DNase) or 3 (0.5mg/ml collagenase II, 1mg/ml dispase, 1µg/ml DNase).

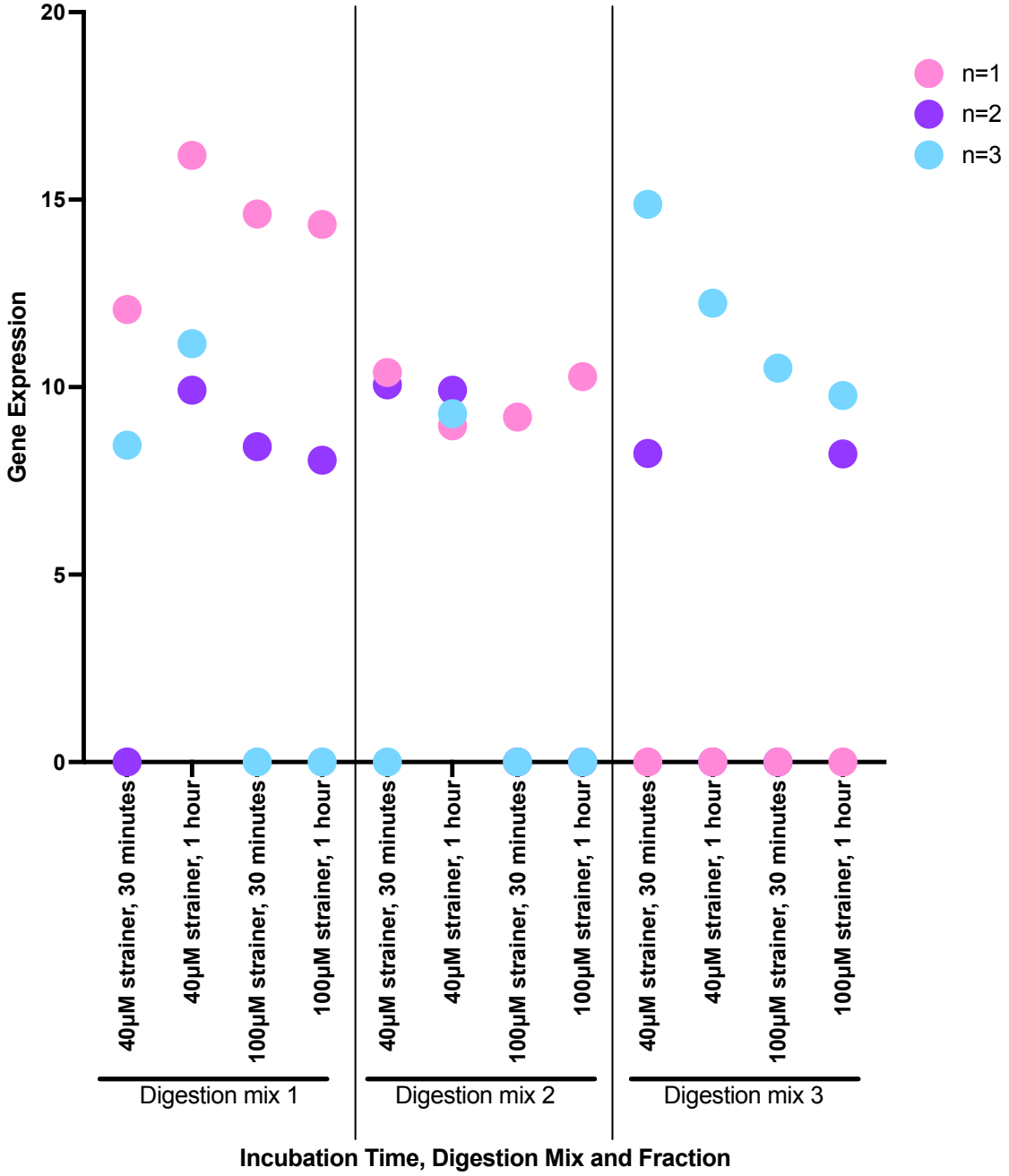

Figure 5.57: *IGFBP1 expression in cells isolated from bovine endometrium using different methods of isolation.*
Comparison of *IGFBP1* gene expression in cells isolated from the 40µM strainer or the 70µM strainer from bovine endometrium (n=3) following either 30 min or 1 hr incubation at 37oC 5% CO2 in digestion mix 1 (0.5mg/ml collagenase II, 100µg/ml DNase), 2 (0.5mg/ml collagenase II, 1mg/ml dispase, 100µg/ml DNase) or 3 (0.5mg/ml collagenase II, 1mg/ml dispase, 1µg/ml DNase).

5.4.3.1.3 Bovine organoids over time and passage

Bovine endometrial organoids for n=3 animals were grown and imaged at regular time points to assess growth and determine whether they were able to survive passaging, reform and continue to grow. Images of organoids produced from cells isolated from animal 1 are shown at passage 0 and passage 1 in Figure 5.58, passage 2 in Figure 5.59 and passage 3 in Figure 5.60. Images for animal 2 are provided in Figure 5.61 for passage 0 and 1, Figure 5.62 for passage 2 and Figure 5.63 for passage 3. Similar trends are observed for all animals. Figure 5.64 depicts organoids produced from animal 3 at passage 0 and 1, with Figure 5.65 showing passage 2 and Figure 5.66 showing passage 3 timepoints. Between day 5-9 (Panels A-C Figure 5.58, Figure 5.61, Figure 5.64), each animal shows growth in size of organoids; though animal 2 and 3 develop larger organoids than animal 1. Throughout passage 1, at passage 1 + 5, +7 and +10 days (Panels D-F Figure 5.58, Figure 5.61 and Figure 5.64) there is again growth of size of organoids observed in all 3 animals. During passage 2, animal 2 and 3 demonstrate some growth in organoid size (Figure 5.62 and Figure 5.65), although over a longer period of time the organoids do not expand to the size they reached in passage 0 and passage 1. Animal 1 displays minimal growth throughout passage 2 (Figure 5.59). Growth of organoids is poor across all animals during passage 3, where there is little to no growth observed for any animal at any stage (Figure 5.60, Figure 5.63 and Figure 5.66).

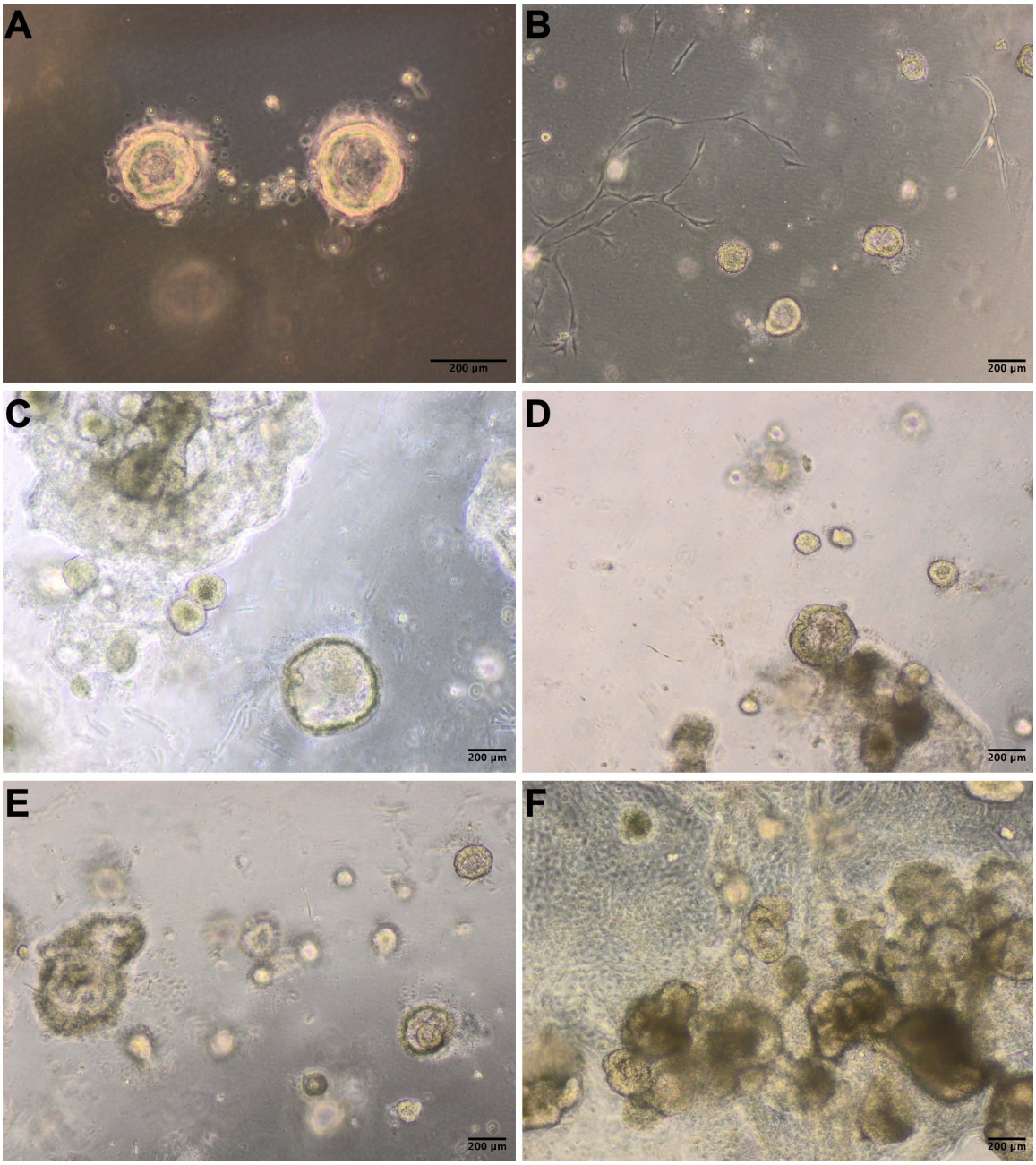

Figure 5.58: *Light microscopy images of bovine endometrial organoids (n=1) at different time points of growth during passage 0 and passage 1.*
A) Day 5, **B**) Day 7, **C**) Day 9, **D**) Passage 1 + 5 days, **E**) Passage 1 + 7 days **F**) Passage 1 + 10 days.

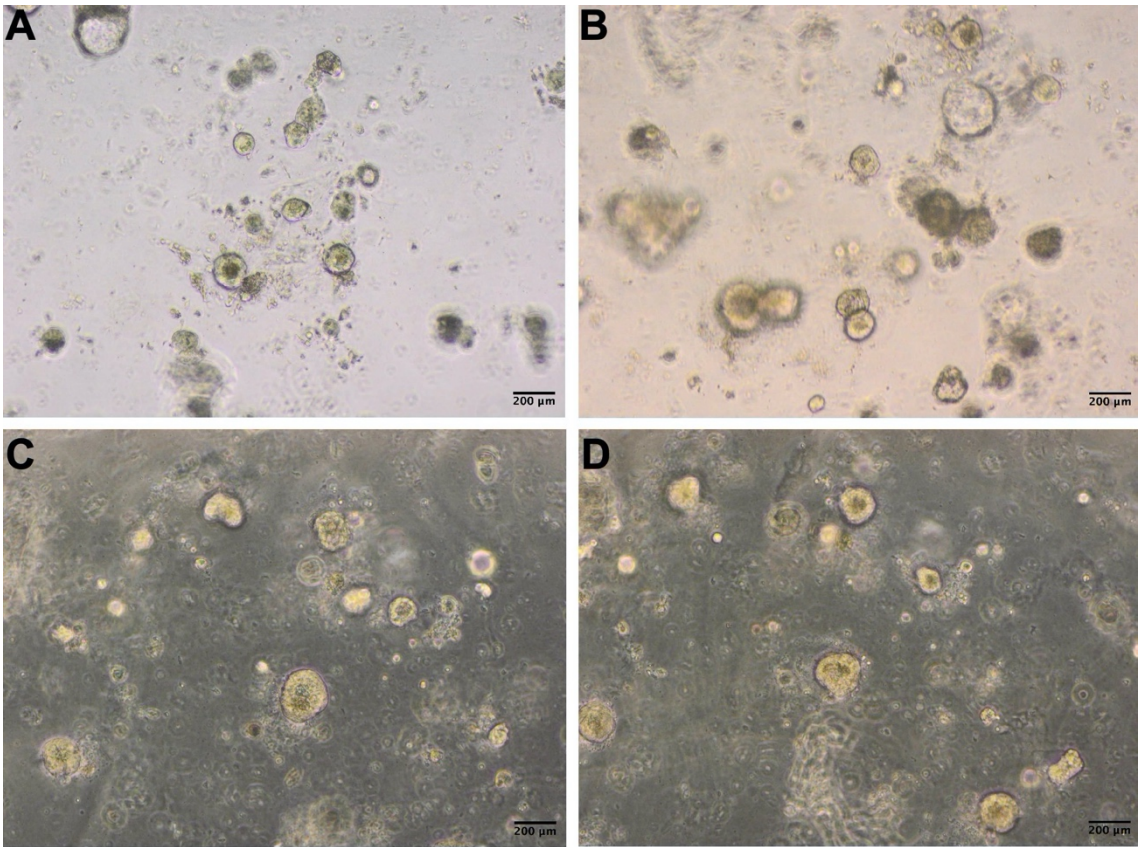

Figure 5.59: *Light microscopy images of bovine endometrial organoids (n=1) at different time points of growth during passage 2.*
A) Passage 2 + 2 days, **B**) Passage 2 + 7 days, **C**) Passage 2 + 10 days, **D**) Passage 2 + 15 days.

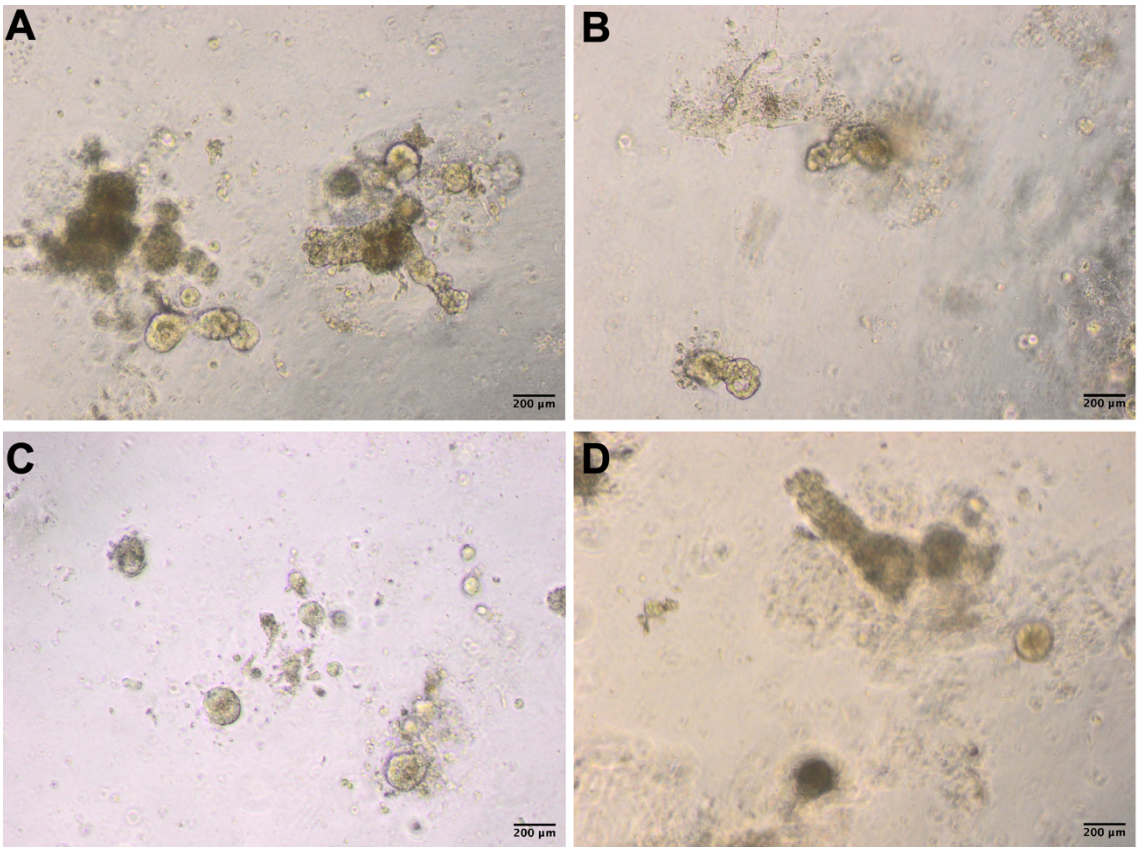

Figure 5.60: *Light microscopy images of bovine endometrial organoids (n=1) at different time points of growth during passage 3.*
A) Passage 3 + 3 days, **B**) Passage 3 + 7 days, **C**) Passage 3 + 10 days, **D**) Passage 3 + 14 days.

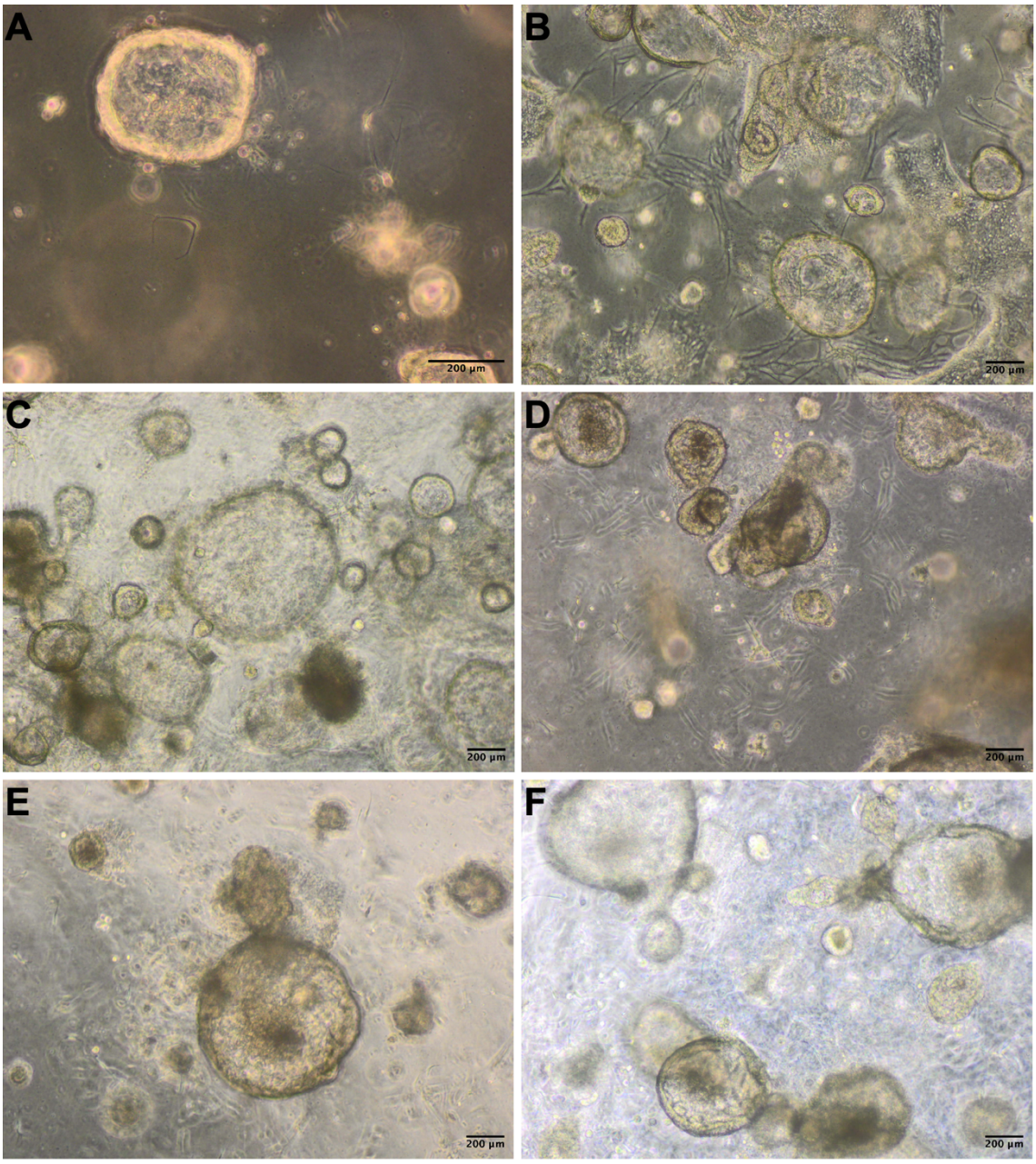

Figure 5.61: *Light microscopy images of bovine endometrial organoids (n=2) at different time points of growth during passage 0 and passage 1.*
A) Day 5, **B**) Day 7, **C**) Day 9, **D**) Passage 1 + 5 days, **E**) Passage 1 + 7 days **F**) Passage 1 + 10 days.

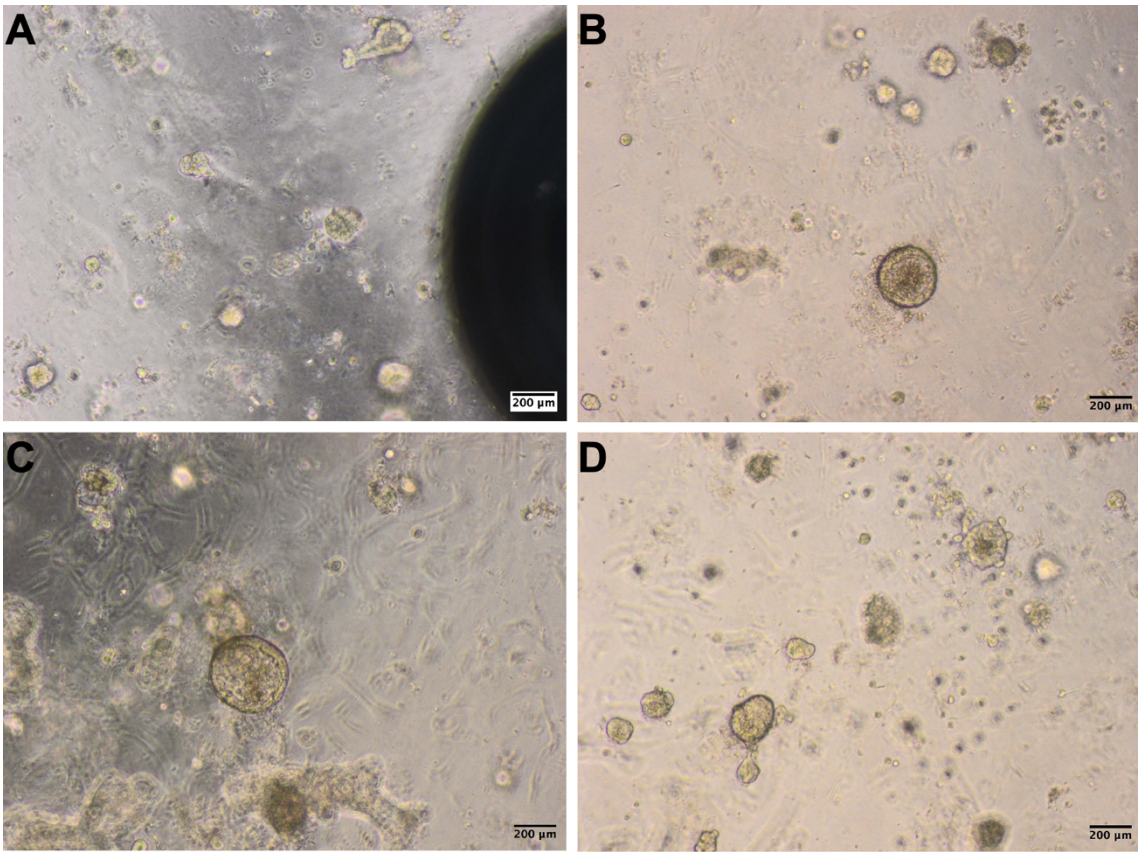

Figure 5.62: *Light microscopy images of bovine endometrial organoids (n=2) at different time points of growth during passage 2.*
A) Passage 2 + 2 days, **B**) Passage 2 + 7 days, **C**) Passage 2 + 10 days, **D**) Passage 2 + 15 days.

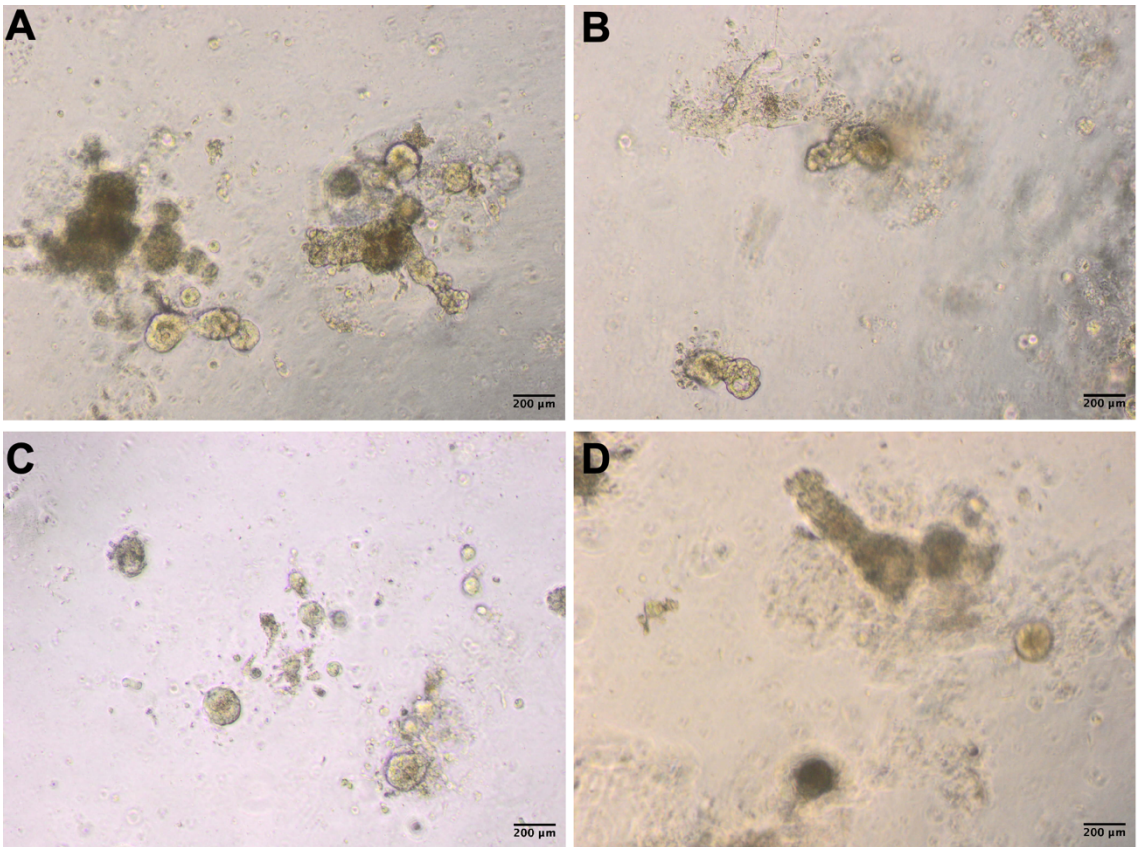

Figure 5.63: *Light microscopy images of bovine endometrial organoids (n=2) at different time points of growth during passage 3.*
A) Passage 3 + 3 days, **B**) Passage 3 + 7 days, **C**) Passage 3 + 10 days, **D**) Passage 3 + 14 days.

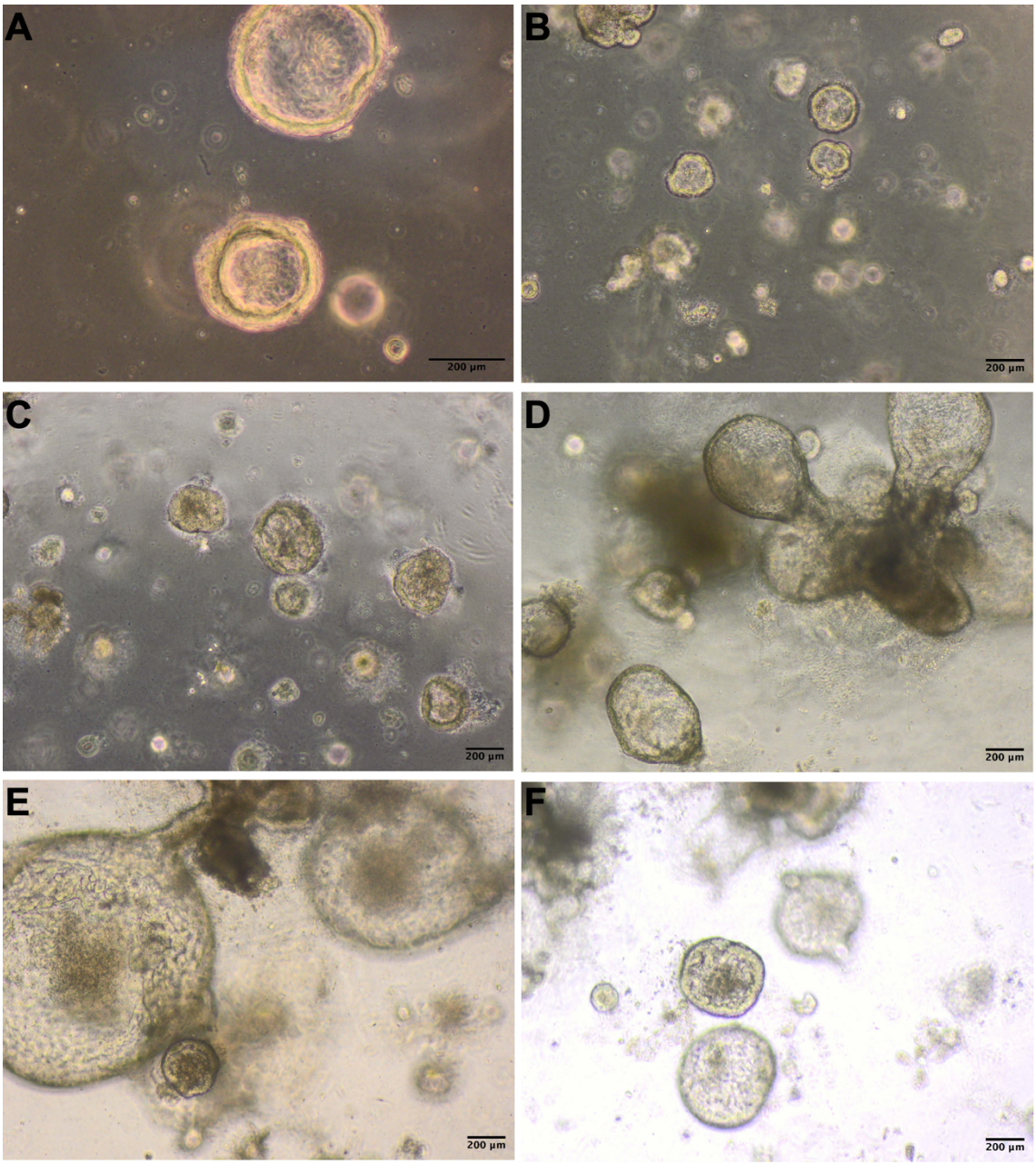

Figure 5.64: *Light microscopy images of bovine endometrial organoids (n=3) at different time points of growth during passage 0 and passage 1.*
A) Day 5, **B**) Day 7, **C**) Day 9, **D**) Passage 1 + 5 days, **E**) Passage 1 + 7 days **F**) Passage 1 + 10 days.

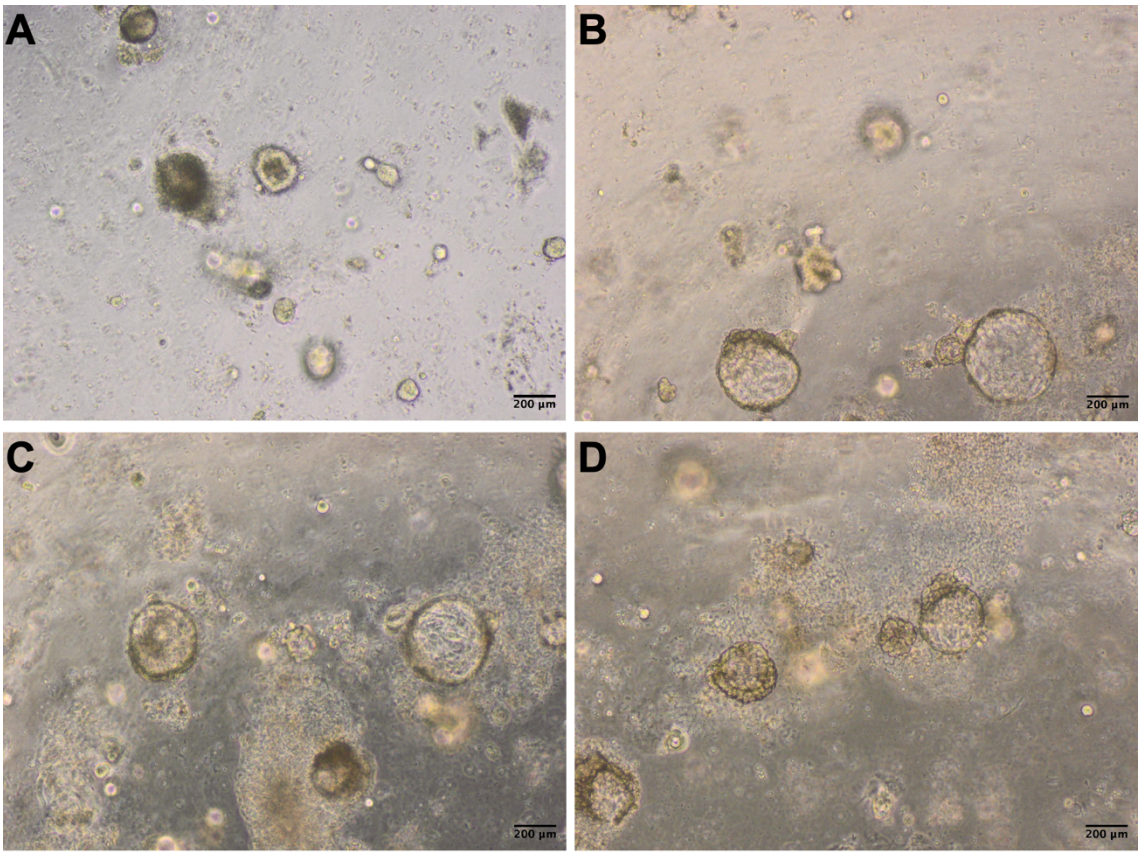

Figure 5.65: *Light microscopy images of bovine endometrial organoids (n=3) at different time points of growth during passage 2.*
A) Passage 2 + 2 days, **B**) Passage 2 + 7 days, **C**) Passage 2 + 10 days, **D**) Passage 2 + 15 days.

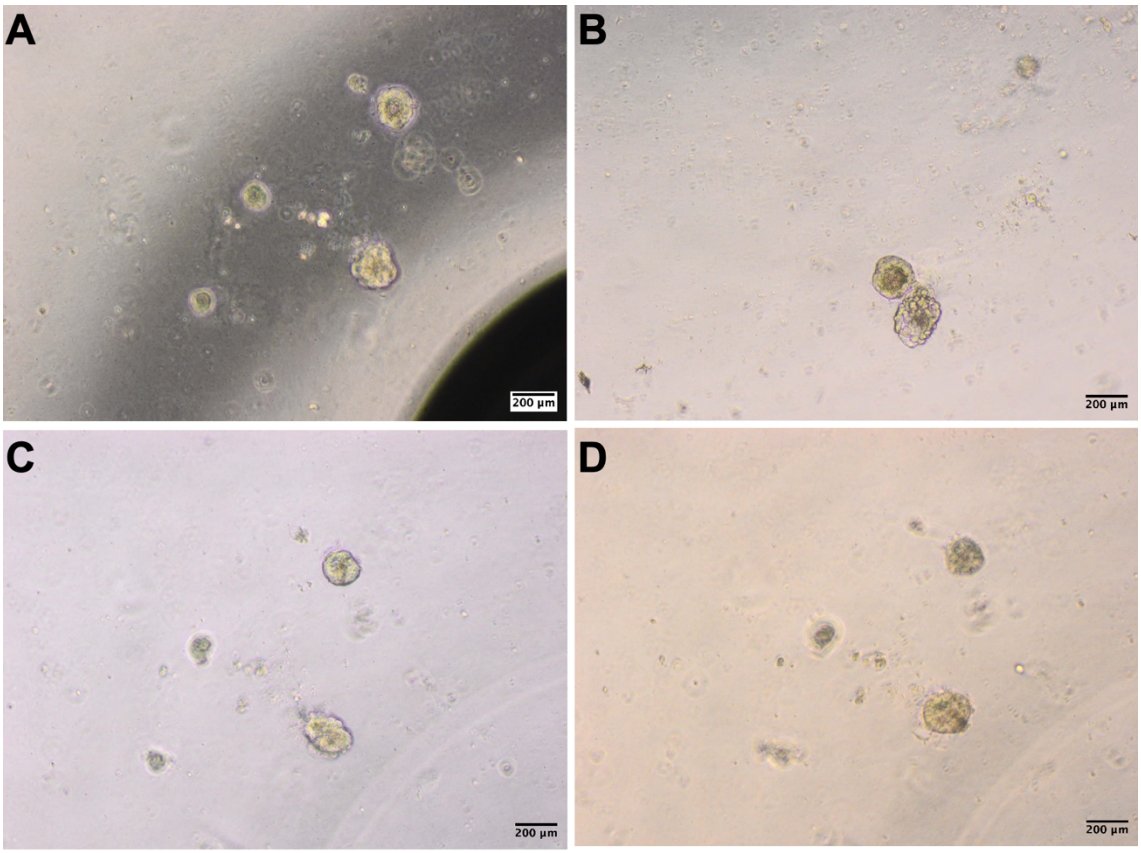

Figure 5.66: *Light microscopy images of bovine endometrial organoids (n=3) at different time points of growth during passage 3.*
A) Passage 3 + 3 days, **B**) Passage 3 + 7 days, **C**) Passage 3 + 10 days, **D**) Passage 3 + 14 days.

5.4.3.1.4 Gland marker expression over time

Raw CT values were used to test gland marker expression as a preliminary method to determine whether these genes were expressed in the bovine endometrial organoids. All 5 markers: *KLF5, MUC1, LIF, FOXA2* and *IGFBP1* were expressed in all animals (n=3), but not always at every time point tested (Figure 5.67). *FOXA2* was not expressed at passage 3 in any animal, and this gene exhibits large variation in expression between animals at early stages of growth. In fact, at day 2, day 5 and day 7 for all genes, expression appears to be very different between animals. At day 9 and passage 1, gene expression of these 5 gland markers becomes more similar for each animal. Expression of all these genes is reduced at passage 3.

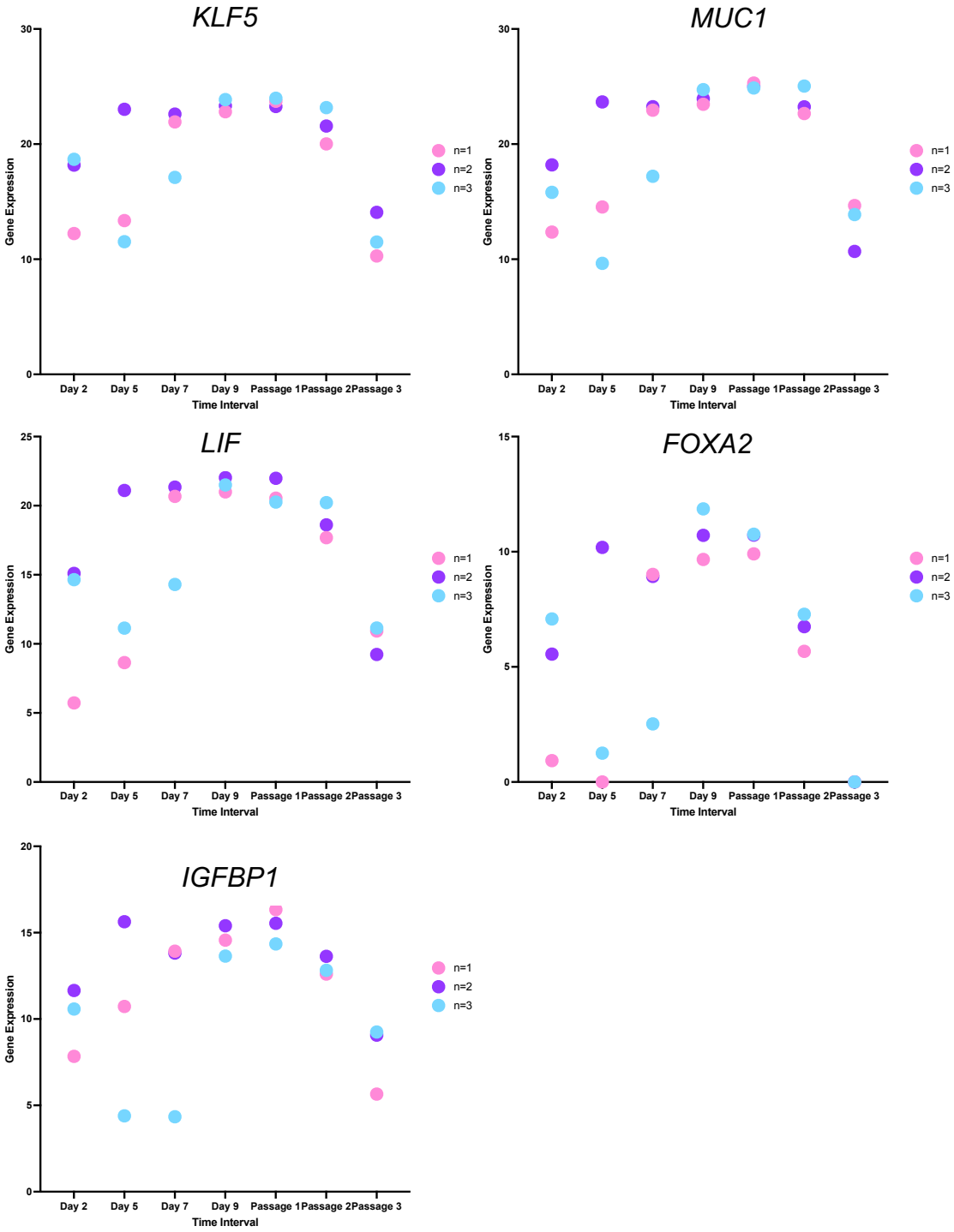

Figure 5.67: *Gland marker expression in bovine endometrial organoids at different time points*
Raw gene expression (raw CT value subtracted from 45 - maximum CT value) of gland markers in bovine endometrial organoids (n=3) at the following points of growth post isolation: day 2, day 7, day 9, passage 1, passage 2 and passage 3.

5.4.3.2 RNA sequencing of progesterone treated bovine organoids

5.4.3.2.1 PCA plot

Principal component analysis (PCA) demonstrated separation of the P4 treated samples from the control and vehicle control, demonstrating P4 had an effect on the transcriptional response of organoids (Figure 5.68). Data points for the P4 treated organoids are all towards the top of the graph, whereas the controls and vehicles are all located lower down, and separate between the left hand side of the PCA and the right hand side. Each control sample clusters with its corresponding vehicle control - emphasising the similarity of these samples which suggests the vehicle has minimal effect. Biological replicate has an effect on the variance of the data as each control point with its corresponding vehicle control data point is separated from the other animals controls. Biological replicate also exhibits an effect on the P4 treated organoids as for each animal, the P4 treated organoids are separated and each one is located diagonally upwards and left of its corresponding controls.

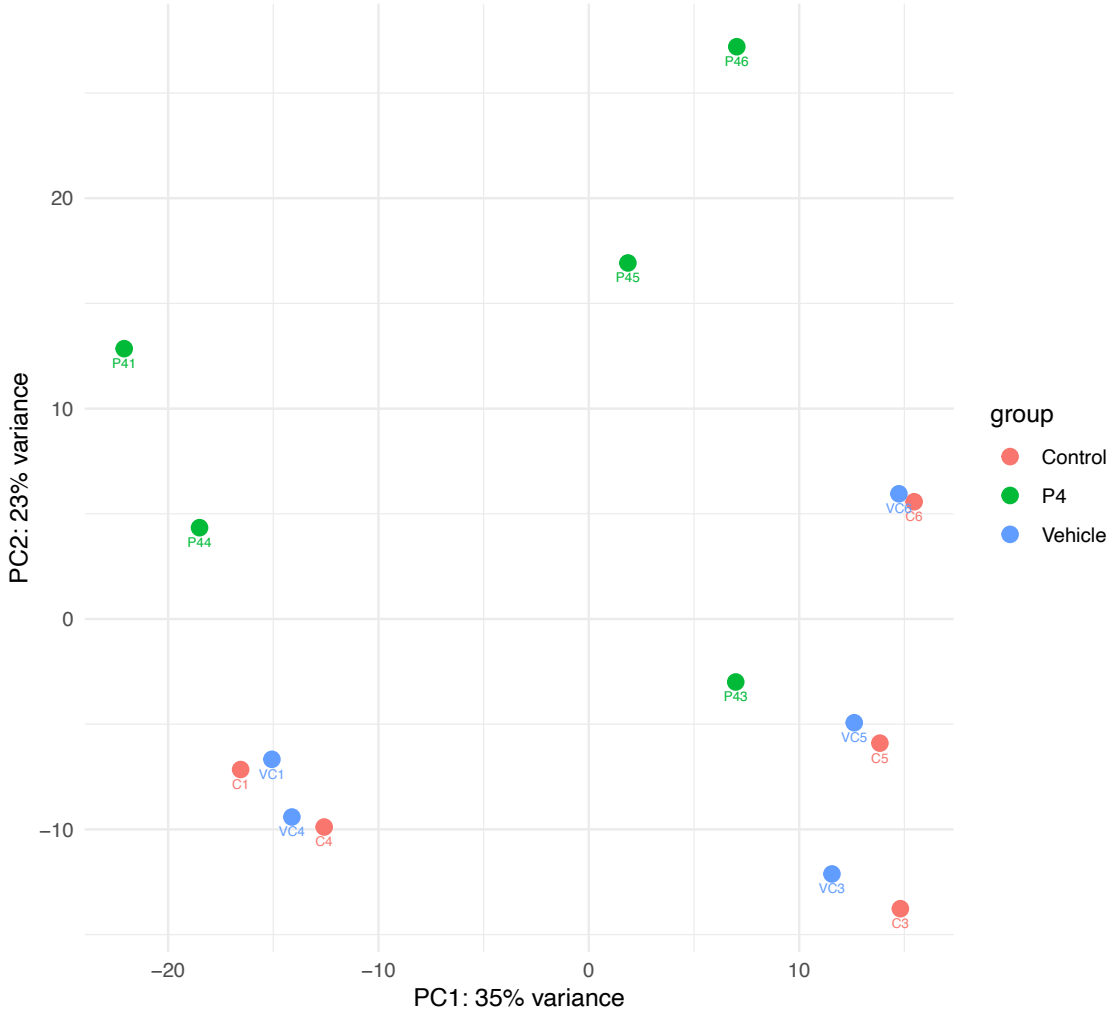

Figure 5.68: *PCA plot (PC1 and PC2) for progesterone treated bovine endometrial organoids.*
PCA (principal component analysis) plot of PC1 and PC2 for bovine endometrial organoids at passage 0 (n=5) isolated from primary bovine endometrium, treated for 24 hrs with no treatment (control - C - red), vehicle (100% ethanol at equal volume to P4 - VC - blue) or 10μg/ml progesterone (P4 - green). Organoids were incubated for 24 hours before collection and subjected to RNA extraction and RNA Sequencing. Biological repeats are depicted by the number 1-5 following C, VC or P4. PCA plot produced by LeedsOmics.

5.4.3.2.2 Differentially expressed genes in bovine organoids in response to P4

Figure 5.69 is a volcano plot which provides a visual representation of differentially expressed genes in bovine endometrial organoids following 24 hr treatment with 10μg/ml P4 compared to ethanol control (100% ethanol of equal volume to P4 treatment). Genes which are significantly differentially expressed are shown in blue ($p<0.05$) and yellow (Log_2Fold Change) and those which are highly significantly differentially expressed are shown in red ($p<0.05$ and Log_2Fold Change).

A total of 373 transcripts were significantly upregulated (padj<0.05 or log_2fold change >0.05) in organoids treated with 10μg/ml P4 compared to vehicle control. The upregulated gene with the highest fold change was Growth Regulation by Oestrogen in Breast Cancer 1 (*GREB1*). Genes which are significantly upregulated by P4 treatment were significantly overrepresented (FDR<0.05) in biological processes of positive regulation of protein localization to both plasma membrane and cell periphery, for which the same 6 genes overlap with the process gene set (Figure 5.70). These 6 genes are also overrepresented in the biological process of positive regulation of protein localization to membrane, along with 2 other genes. The cellular components for which these genes are overrepresented are apical membrane and apical part of cell (Figure 5.70). STRING network analysis to investigate predicted protein-protein interactions showed that the majority of upregulated genes interact with other upregulated genes (Figure 5.71).

There were 240 genes significantly downregulated in response to 10μg/ml P4 treatment compared with the vehicle control. The differentially expressed downregulated gene with the largest negative fold change was C-X-C Motif Chemokine Ligand 10 (*CXCL10*). Significantly downregulated genes (padj<0.05 or log_2fold change <-0.05) were significantly overrepresented (FDR<0.05) in biological processes of cilium organization (10 genes), microtubule bundle formation (6 genes) and cytoskeleton organization (21 genes) (Figure 5.72). Twenty eight genes were also significantly overrepresented in the mitochondria (Figure 5.72). STRING network analysis to represent predicted protein protein interactions results in a large number of interactions between genes downregulated in response to P4 (Figure 5.73).

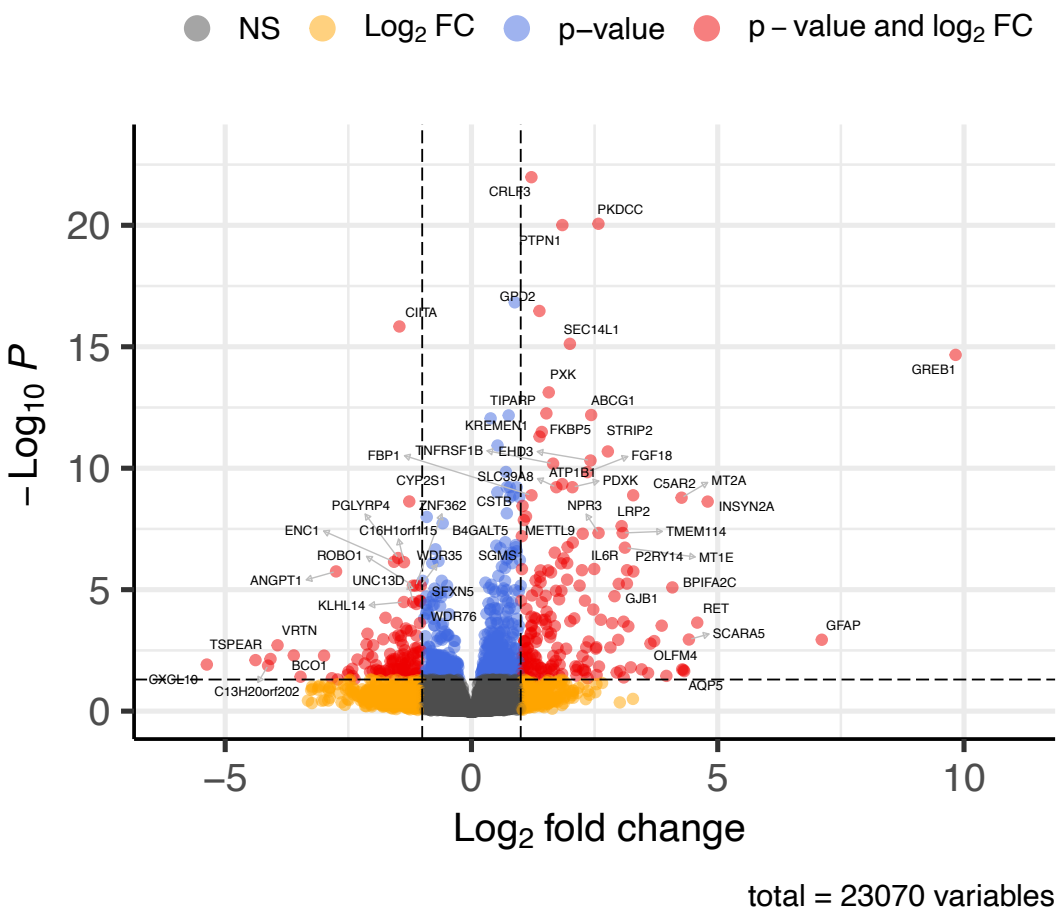

Figure 5.69: *Volcano plot of differentially expressed genes in bovine endometrial organoids (n=5) treated for 24 hrs with vehicle control - ethanol, compared with 10μg/ml progesterone.*
Significance is depicted by yellow - Log_2 fold change, blue - p<0.05 and red p<0.05 and Log_2 fold change. Genes most or least significantly differentially expressed are labelled. Produced by LeedsOmics.

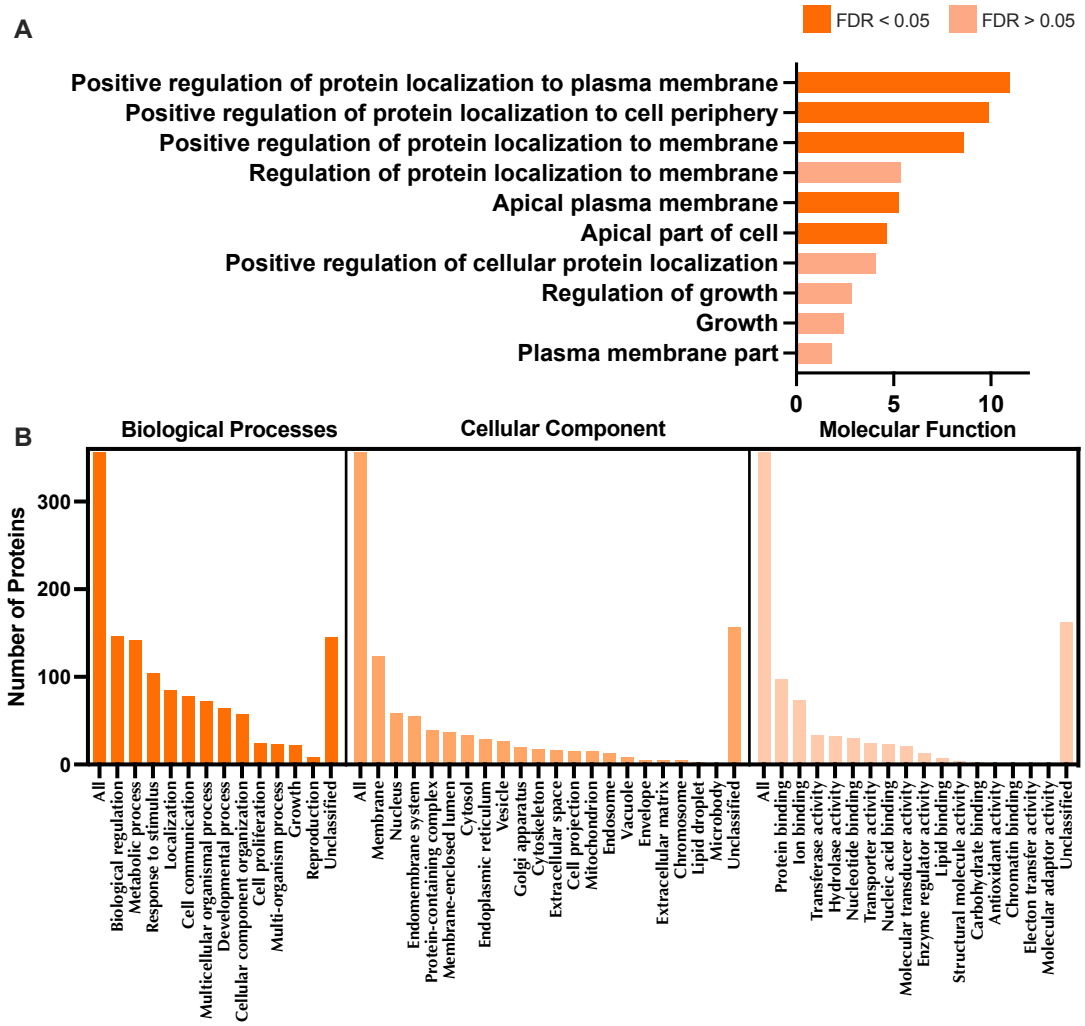

Figure 5.70: *Differentially expressed genes significantly upregulated (padj<0.05 or log$_2$fold change >0.05) in bovine endometrial organoids (n=5) following 24 hr treatment with progesterone.*
A) Enriched KEGG pathways associated with upregulated mRNA following treatment for 24 hrs with 10μg/ml progesterone (FDR<0.05). **B**) WebGestalt overrepresentation analysis of biological process, cellular component, and molecular function categories for identified significantly upregulated mRNAs (padj<0.05 or log$_2$fold change >0.05) in response to treatment of bovine endometrial organoids with 10μg/ml progesterone for 24 hrs. (Supplementary Table 36).

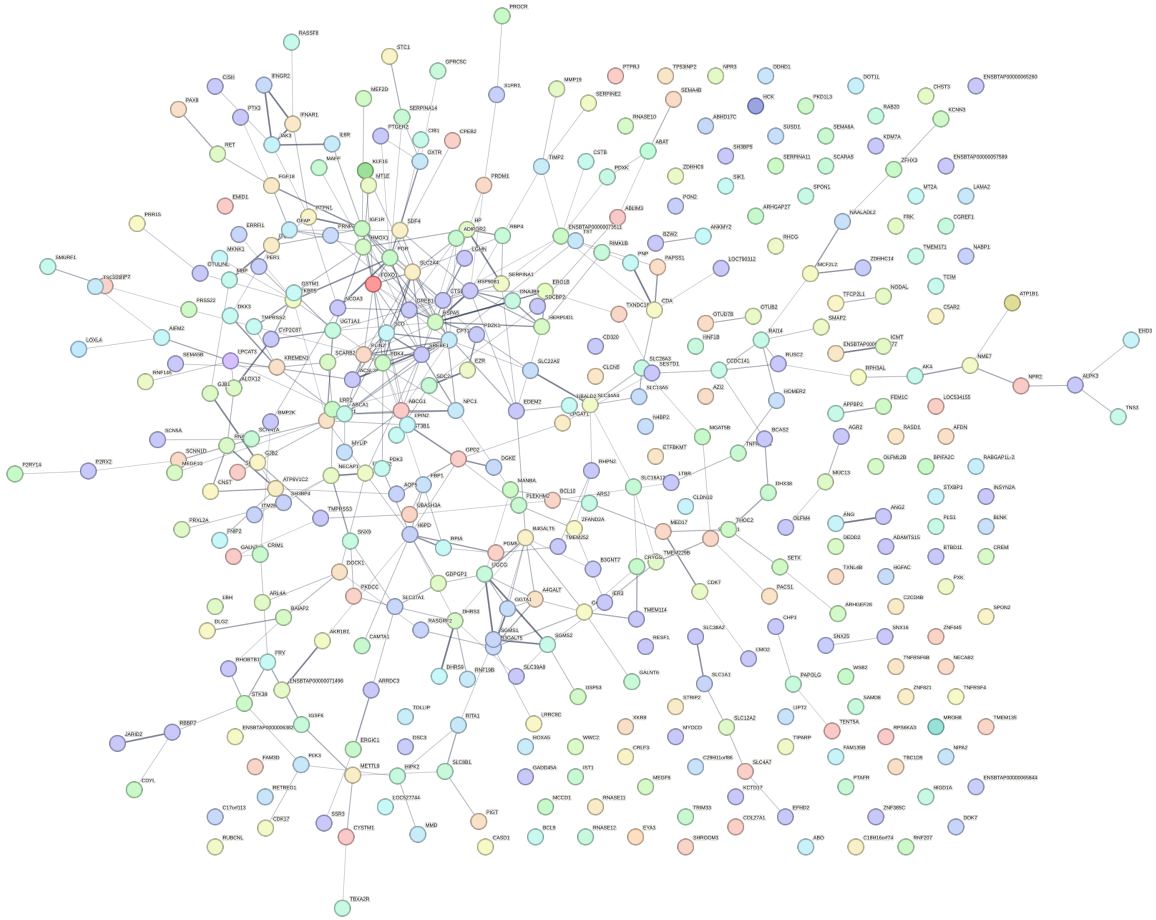

Figure 5.71: *String interaction network analysis for significantly upregulated genes (padj<0.05 or log_2fold change >0.05) following treatment of bovine endometrial organoids (n=5) with 10μg/ml progesterone for 24 hrs.*

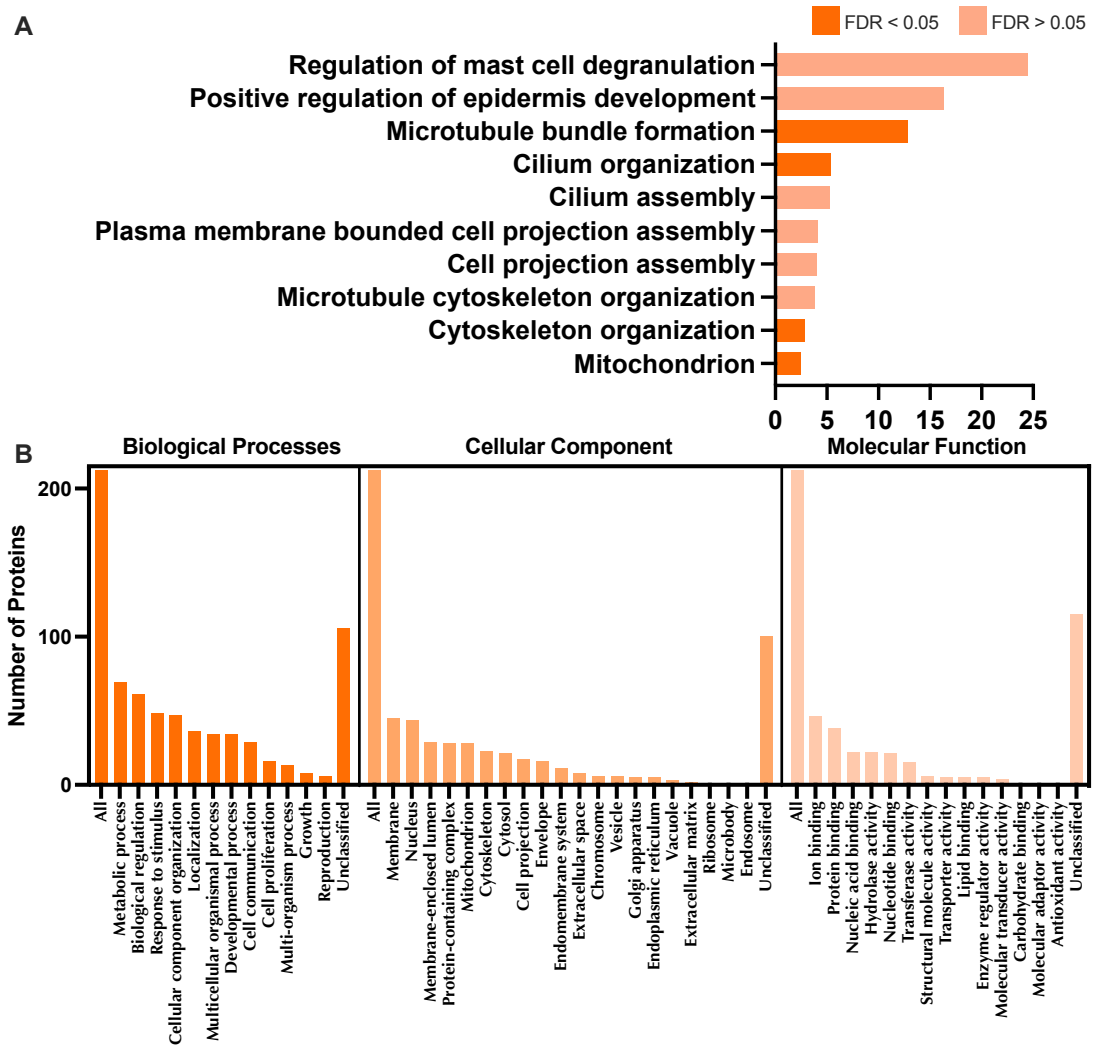

Figure 5.72: *Differentially expressed genes significantly downregulated (padj<0.05 or log$_2$fold change <-0.05) in bovine endometrial organoids (n=5) following 24 hr treatment with progesterone.*
A) Enriched KEGG pathways associated with downregulated mRNA following treatment for 24 hrs with 10μg/ml progesterone (FDR<0.05). (Supplementary table 37). **B**) WebGestalt overrepresentation analysis of biological process, cellular component, and molecular function categories for identified significantly upregulated mRNAs (padj<0.05 or log$_2$fold change <-0.05) in response to treatment of bovine endometrial organoids with 10μg/ml progesterone for 24 hrs. (Supplementary Table 37).

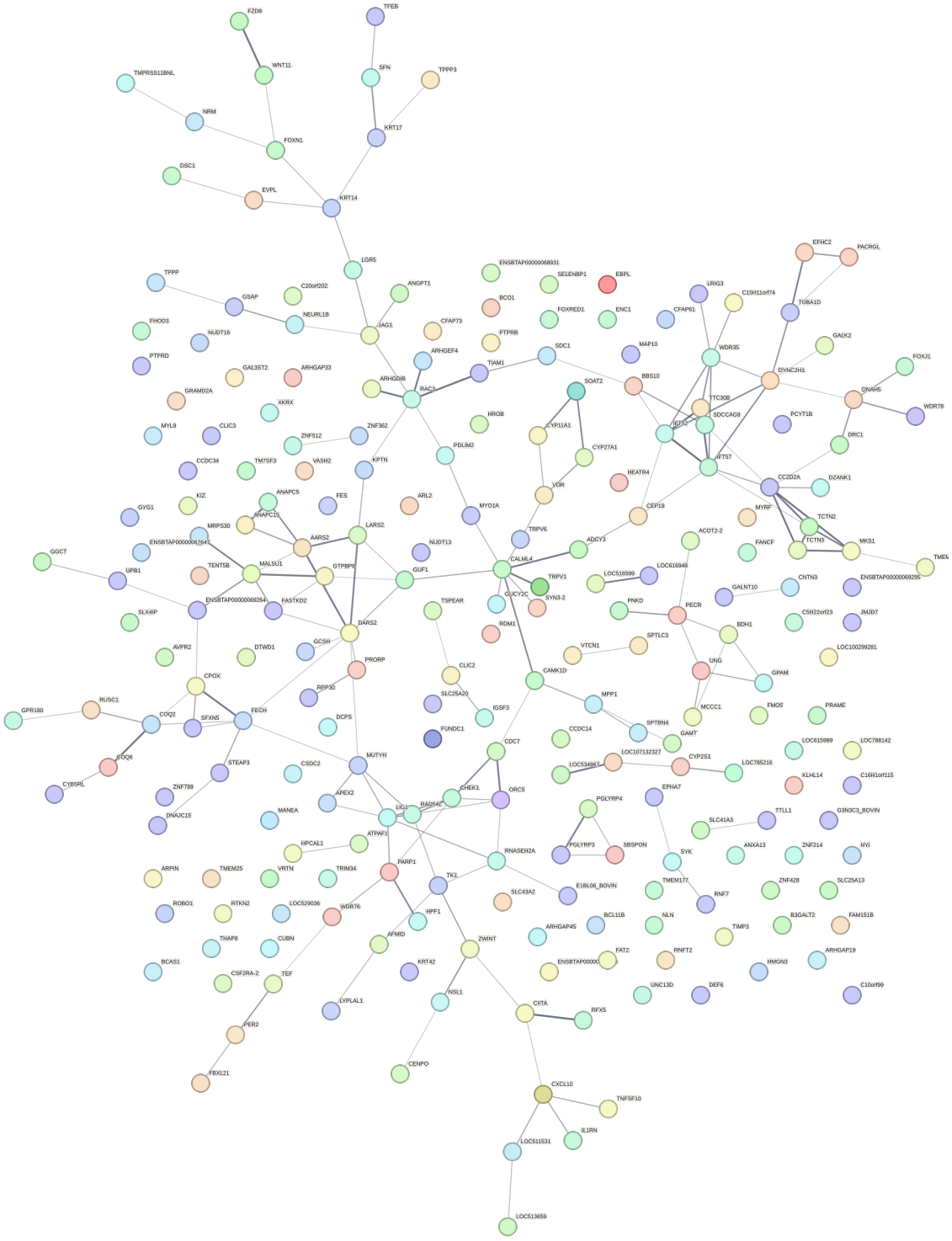

Figure 5.73: *String interaction network analysis for significantly downregulated genes (padj<0.05 or log_2fold change <-0.05) following treatment of bovine endometrial organoids (n=5) with 10μg/ml progesterone for 24 hrs.*

5.4.3.3 Conserved microRNA expression in progesterone treated organoids

Both miR-378a-3p and miR-708-5p were significantly reduced ($p<0.05$) in expression in response to treatment with 10μg/ml P4 in comparison to control (Figure 5.74). However, they were not significantly differentially expressed compared to vehicle control (ethanol). None of the other miRNAs were differentially expressed in response to P4 in bovine glandular epithelial endometrial organoids. Nonetheless this data shows that conserved microRNAs are expressed in these cells.

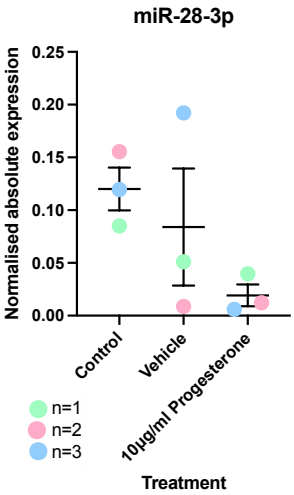
miR-28-3p
Normalised absolute expression
0.25
0.20
0.15
0.10
0.05
0.00
Control
Vehicle
10µg/ml Progesterone
n=1
n=2
n=3
Treatment

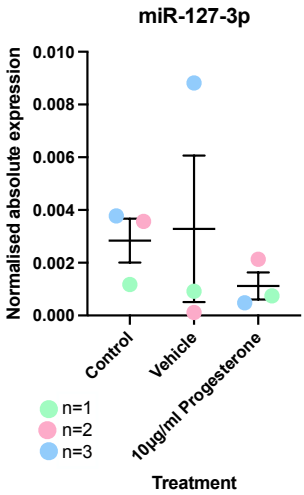
miR-127-3p
Normalised absolute expression
0.010
0.008
0.006
0.004
0.002
0.000
Control
Vehicle
10µg/ml Progesterone
n=1
n=2
n=3
Treatment

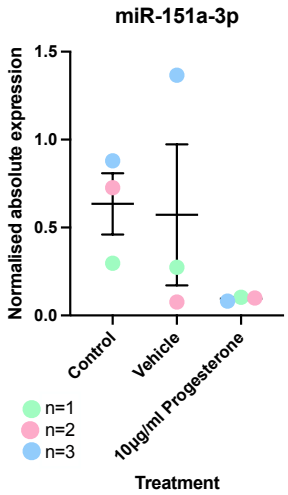
miR-151a-3p
Normalised absolute expression
1.5
1.0
0.5
0.0
Control
Vehicle
10µg/ml Progesterone
n=1
n=2
n=3
Treatment

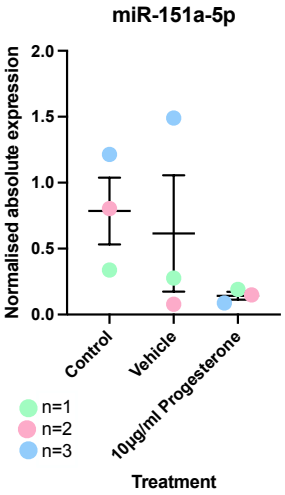
miR-151a-5p
Normalised absolute expression
2.0
1.5
1.0
0.5
0.0
Control
Vehicle
10µg/ml Progesterone
n=1
n=2
n=3
Treatment

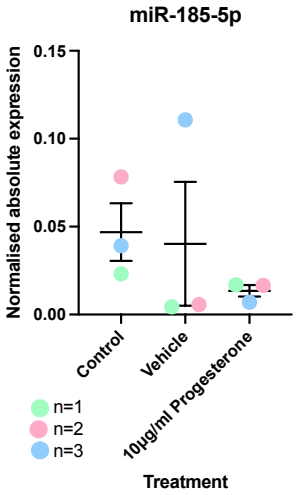
miR-185-5p
Normalised absolute expression
0.15
0.10
0.05
0.00
Control
Vehicle
10µg/ml Progesterone
n=1
n=2
n=3
Treatment

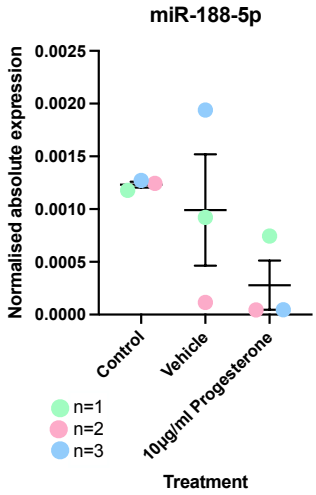
miR-188-5p
Normalised absolute expression
0.0025
0.0020
0.0015
0.0010
0.0005
0.0000
Control
Vehicle
10µg/ml Progesterone
n=1
n=2
n=3
Treatment

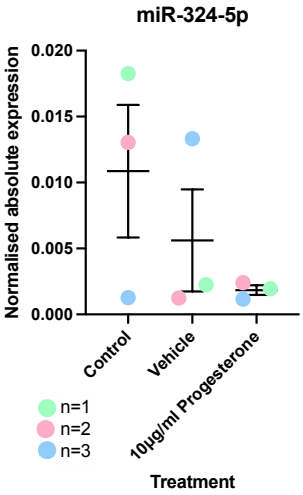
miR-324-5p
Normalised absolute expression
0.020
0.015
0.010
0.005
0.000
Control
Vehicle
10µg/ml Progesterone
n=1
n=2
n=3
Treatment

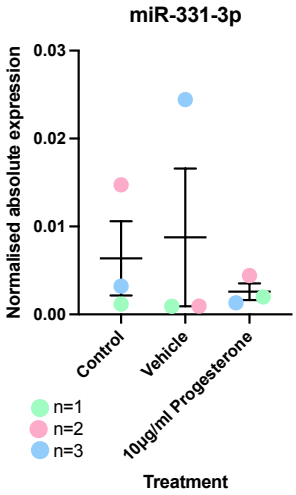
miR-331-3p
Normalised absolute expression
0.03
0.02
0.01
0.00
Control
Vehicle
10µg/ml Progesterone
n=1
n=2
n=3
Treatment

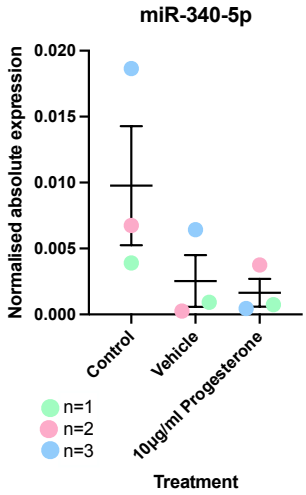
miR-340-5p
Normalised absolute expression
0.020
0.015
0.010
0.005
0.000
Control
Vehicle
10µg/ml Progesterone
n=1
n=2
n=3
Treatment

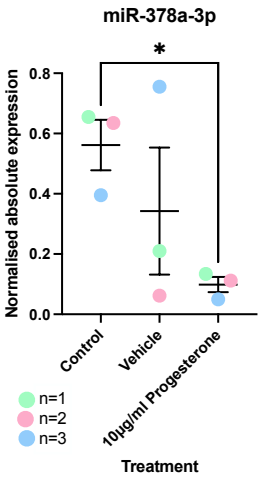
miR-378a-3p
*
Normalised absolute expression
0.8
0.6
0.4
0.2
0.0
Control
Vehicle
10µg/ml Progesterone
n=1
n=2
n=3
Treatment

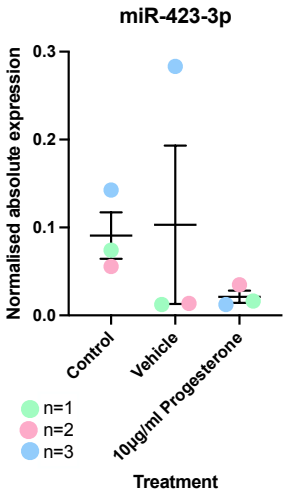
miR-423-3p
Normalised absolute expression
0.3
0.2
0.1
0.0
Control
Vehicle
10µg/ml Progesterone
n=1
n=2
n=3
Treatment

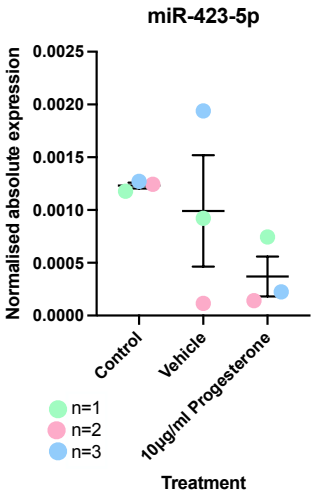
miR-423-5p
Normalised absolute expression
0.0025
0.0020
0.0015
0.0010
0.0005
0.0000
Control
Vehicle
10µg/ml Progesterone
n=1
n=2
n=3
Treatment

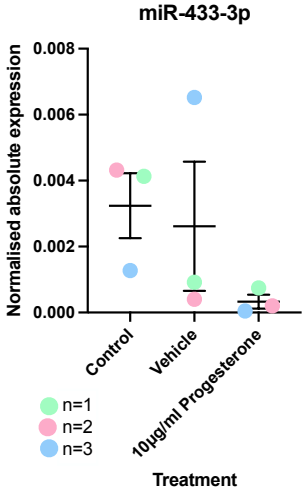
miR-433-3p
Normalised absolute expression
0.008
0.006
0.004
0.002
0.000
Control
Vehicle
10µg/ml Progesterone
n=1
n=2
n=3
Treatment

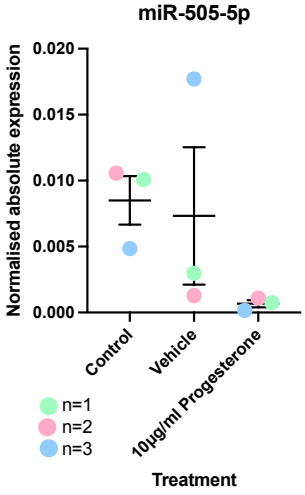
miR-505-5p
Normalised absolute expression
0.020
0.015
0.010
0.005
0.000
Control
Vehicle
10µg/ml Progesterone
n=1
n=2
n=3
Treatment

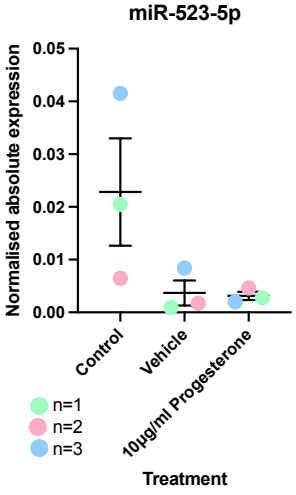
miR-523-5p
Normalised absolute expression
0.05
0.04
0.03
0.02
0.01
0.00
Control
Vehicle
10µg/ml Progesterone
n=1
n=2
n=3
Treatment

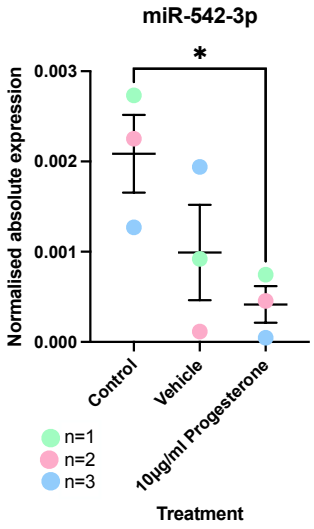
miR-542-3p
*
Normalised absolute expression
0.003
0.002
0.001
0.000
Control
Vehicle
10µg/ml Progesterone
n=1
n=2
n=3
Treatment

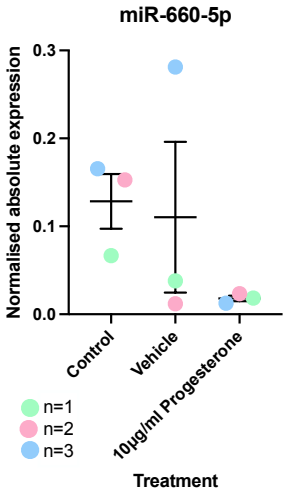
miR-660-5p
Normalised absolute expression
0.3
0.2
0.1
0.0
Control
Vehicle
10µg/ml Progesterone
n=1
n=2
n=3
Treatment

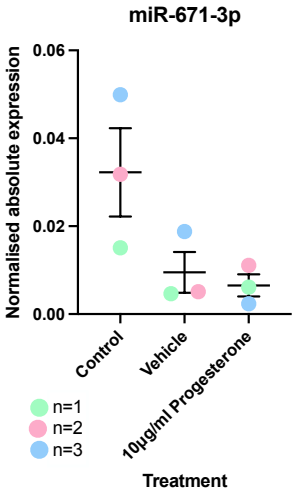
miR-671-3p
Normalised absolute expression
0.06
0.04
0.02
0.00
Control
Vehicle
10µg/ml Progesterone
n=1
n=2
n=3
Treatment

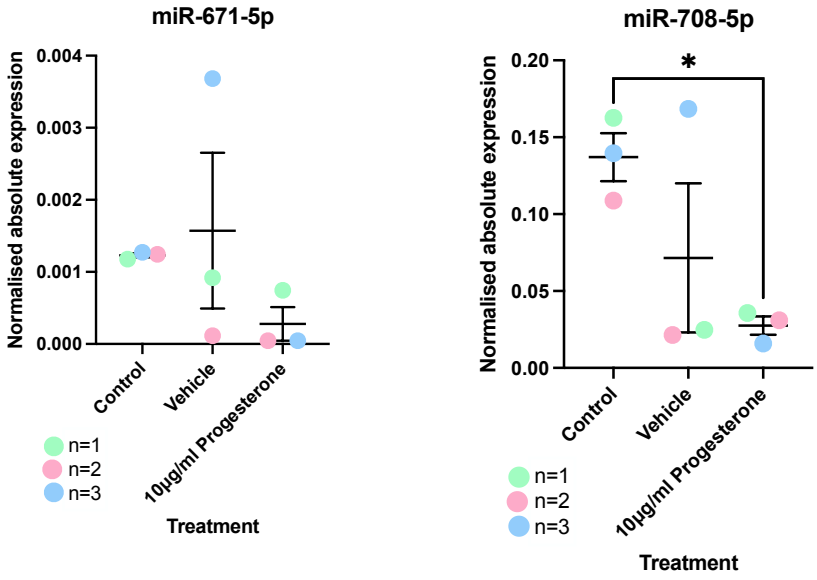

Figure 5.74: *Expression of selected microRNAs of interest in bovine endometrial organoids.*
Bovine organoids (n=3) treated for 24 hrs with 1) control, 2) vehicle - ethanol (volume equal to that of progesterone treatment added to well) or 3) 10µg/ml progesterone. Expression quantified by qRT-PCR and values normalised to 5s. Differences in expression were determined using an ANOVA with Tukey's multiple comparisons test where statistical significance was met when the adjusted p value <0.05.

5.5 Discussion

This chapter has demonstrated that expression of conserved, progesterone regulated miRNAs can be altered and this has consequences for the attachment stage of implantation. This was achieved using a 2D model to analyse attachment of trophoblast spheroids to endometrial epithelial cells. Furthermore, a 3D, multicellular model of the endometrium has been successfully generated using Alvetex scaffolds. Observations show that the stromal cell layer deposits extracellular matrix creating a tissue like structure, on top of which an epithelial layer can grow. It has also been shown that it is possible to transfect these endometrial models with miRNAs of interest, and stain for a proliferation marker to assess the effect of over or under expressing these miRNAs on cell proliferation. Finally, endometrial epithelial organoids have been derived from primary bovine endometrium for the first time, and their ability to survive passaging has been assessed. Conserved miRNA expression in these organoids has been investigated.

5.5.1 Normal 2D endometrium/embryo attachment assay

The 2D attachment assay used here provides a method for modelling blastocyst attachment to endometrial epithelial cells. However, this model is not without its drawbacks. Due to the monolayer set up, any stages of implantation beyond attachment cannot be studied, as invasion is not possible in a single layer cell culture. In comparison to attachment assays carried out using stromal cell monolayers (Carver et al., 2003; Grewal et al., 2008), this method is more physiologically relevant as the blastocyst would attach to the endometrial cells, not the stromal cells. Using cell lines is also less favourable than primary cells, however Ishikawa cells are an hormonally responsive representative *in vitro* cell line of the endometrial epithelium (Mo et al., 2006). Furthermore, BeWo cells are a choriocarcinoma cell line and are trophoblast cells, which are the cells surrounding the inner cell mass of the embryo which attach to the epithelium, making them an appropriate cell line for this experiment. BeWo cells also secrete hCG, required for implantation and produced by embryos *in vivo* (Rothbauer et al., 2017). It is ethically complicated to use primary embryos for experimental work, and in most cases those undergoing *in vitro* fertilisation to produce embryos are doing so because of an underlying fertility issue, so are not ideal candidates for studying successful, physiologically 'normal' implantation. Recently, models which can be used for investigating implantation termed 'blastoids' have been developed from induced pluripotent stem cells (Kagawa et al., 2022). The introduction of ground-breaking, physiologically appropriate methods such as this suggests that more primitive cell line spheroid

models may become obsolete in the near future. Due to time and cost constraints, it was not possible to employ this technology for this experiment. Much of this experiment was also carried out prior to the introduction of blastoids. Notwithstanding, BeWo spheroids - and spheroids formed of other embryo-like cell lines - are widely used in attachment assays throughout the field (Huang et al., 2017; Ruane et al., 2020), and characterisation has deemed it a worthwhile model (Abaidoo et al., 2010). Another unexpected disadvantage of this attachment assay is the high attachment rate in the controls. Ideally, an attachment rate of around 70% should be appropriate for controls, as was observed in the optimisation experiments. This would allow for an attachment rate which could be improved upon or inhibited following addition of miRNA mimics or inhibitors. Incubation time should perhaps be reduced to lower control attachment rates to achieve this. Interestingly though, Ishikawa cells used for similar experiments assessing attachment showed much lower attachment rates of only 37% after 2 hrs of incubation with trophectoderm spheroids produced from trophectoderm stem cells isolated from human embryos (Evans et al., 2020). The spheroids do not reach even 80% attachment until 6 hrs of incubation. This makes it evident that the type of cells forming the spheroid have a large impact on attachment rate. As the spheroids are filtered and collected at sizes between 40μM and 100μM, perhaps variation in the number of spheroids of different sizes within this range has an effect on attachment. For example, if the proportion of larger spheroids (closest to 100μM) compared to smaller spheroids (closest to 40μM) was higher in the experiment than in the optimisation, perhaps this caused the higher attachment rate in the controls, and vice versa. Notwithstanding, this does not diminish the significant results and conclusions drawn from this experiment as treatments with miRNA mimics and inhibitors were compared to the corresponding controls carried out at the same time. However, due to the higher attachment rate observed in the controls, some attachment rates which were increased may appear non-significant as they reach 100% attachment. MiR-671-5p inhibition does not significantly increase attachment, however the attachment rate appears to be elevated following under expression of miR-671-5p. This is in agreement with a study analysing miRNA presence in uterine fluid from patients with recurrent implantation failure (RIF), miR-671-5p was significantly upregulated when compared to healthy patients (von Grothusen et al., 2022). MiR-542-3p overexpression significantly reduces attachment rate of trophoblast spheroids to Ishikawa cells. In Chapter 3, proteomic analysis demonstrates that Survivin is increased in Ishikawa cells following overexpression of miR-542-3p. Survivin is an apoptosis inhibitor, and apoptosis is required at the stage of attachment (Galán et al., 2000). These results functionally support the mechanistic

conclusions drawn in Chapter 3, which suggest that upregulation of miR-542-3p causes upregulation of survivin, which inhibits apoptosis - resulting in reduced attachment, as apoptosis is required for attachment. Oppositely, reduction of apoptosis is required for apposition stage of implantation, at which time P4 is also elevated. This suggests that miR-542-3p is overexpressed in response to P4, inhibiting apoptosis to aid in apposition stage of attachment. Clearly, other regulatory mechanisms must be involved during attachment stage for successful implantation to occur, as transfection with miR-542-3p mimic alone has a negative impact. In fact, when miR-542-3p overexpression is combined with miR-340-5p inhibition, attachment rate was significantly increased. This suggests that there is cooperation between the targets of these miRNAs which results in increased embryo attachment. This indicates that embryo attachment and consequently implantation is not mediated by a single miRNA. An error occurred in carrying out some implantation assays - those cells which were transfected with 2 mimics and 1 inhibitor, or 2 inhibitors and 1 mimic (Figure 5.21 and Figure 5.22) had their media aspirated before they were imaged due to a computer error during imaging. As each assay's controls were carried out at the same time and thus subjected to the same treatment, these results are comparable within their own assay. However, some spheroids may have been removed when media was aspirated before imaging and so the attachment rate may not be wholly representative. Overexpressing miR-340-5p, miR-542-3p and miR-671-5p seemed to result in an increase in embryo attachment, suggesting that the combination of increased expression of these 3 miRNAs in response to P4 at this stage of the menstrual cycle facilitates endometrial receptivity to embryo implantation. This may provide a reason for why miR-542-3p alone decreases attachment and miR-671-5p is elevated in RIF patients, whereas overexpression of all 3 miRNAs together results in increased attachment. This could be because each miRNA perhaps controls different mechanisms *i.e.,* miR-542-3p upregulation is important for successful apposition, with miR-340-5p and miR-671-5p controlling other aspects of implantation; and a collaborative effect of overexpression of all 3 alters the proteome to facilitate implantation. Further biological replicates are required to understand the true effect of differentially expressing miR-340-5p, miR-542-3p and miR-671-5p simultaneously on embryo attachment, as well as assays that allow investigation into other aspects of implantation - such as invasion.

5.5.2 Modelling the Human Endometrium: Alvetex

Using Alvetex technology to model the endometrium is a process that has already been achieved in a bovine model (Díez et al., 2023). This has not yet been performed using human cells. Applying these principles to establish a

model of an human endometrium in an Alvetex scaffold results in a multi-cellular model which can be used to investigate endometrial function and test novel treatment therapies. In the endocervix model using Alvetex technology, hormone treatment was used to mimic the menstrual cycle (Arslan et al., 2015), which could be an application for the established endometrial model. This technology provides this solution to longer experiments due to the ability to perform longer term cell culture.

Interestingly, cell nucleus density in the centre of the scaffold is low following epithelial cell addition. Vimentin staining is also scarce throughout the scaffold, with more vimentin present at the bottom of the scaffold. A potential reason for this could have been the process of transfecting the cells, where they are not fully submerged in media for 3 hours whilst the transfection takes place, so this may have had a negative effect on the cells. Furthermore, the epithelial layer is very thick, so this may be causing a barrier which is stopping media nutrients accessing the stromal layer. This could explain why there are more cells present at the bottom of the scaffold, as these cells are in contact with the media. Díez et al., (2023) used the same Alvetex scaffold to model the bovine endometrium and found similar results. The distribution of vimentin was also located towards the bottom of the scaffold, and there were fewer cells in the centre of the scaffold.

Transfection of the Alvetex scaffolds does not provide conclusive results as there is only 1 biological replicate and only 1 representative image was taken from each section. However, it is fascinating that in the scaffold which was transfected with mimics for miR-340-5p, miR-542-3p and miR-671-5p, ki67 does not appear to be expressed. Ki67 is a proliferation marker which is expressed at all cell cycle stages of an actively proliferating cell (Sun and Kaufman, 2018). This seems to reinforce the conclusions drawn from Chapter 2 and 3, that miR-340-5p and miR-542-3p have an inhibitory effect on proliferation. Indeed, in the scaffolds which were transfected with a single mimic for each of miR-340-5p and miR-542-3p, ki67 expression seems to be reduced compared to their respective inhibitors. This is not the case for miR-671-5p mimic, which appears to show no difference in ki67 expression whether over or under expressed. Due to these individual results, it is remarkable to observe the apparent combinatory effect of over expressing all 3 miRNAs on cell proliferation.

5.5.3 Modelling the Bovine Endometrium: Endometrial Organoids

Here, it has been demonstrated that 3D organoids can be produced from bovine endometrium. Organoid production from endometrial epithelial gland cells in bovine are a great model for studying endometrial function and implantation, as uterine gland secretions are vital for implantation and fertility (Kelleher et al., 2019). Over the observed time course of organoid development, animal 1 exhibits much slower growth. The reason for this could be that the glandular epithelial cells were not plated densely enough. Therefore, as all passaging was carried out on the same day irrespective of organoid size between animals, perhaps these organoids never reached appropriate size or cell density and so were consistently smaller throughout the experiment time course. Nevertheless, this may just highlight the high level of variability between animals. Across all 3 animals, there is no growth at passage 3. This demonstrates the limited longevity of the organoids, emphasising that experiments using these organoids should be carried out at the earlier passages. Previous work using cells isolated from primary bovine tissue in our lab already determined that primary epithelial and stromal cells are unable to be kept in culture for extended periods of time and should be used at early passages. Clearly, organoid cultures using these cells are no different to this. However, no optimisation of expansion media was carried out for these organoids. The components of the expansion media were taken directly from (Turco et al., 2017), which is optimised for supporting human endometrial organoid culture. Given more time, optimisation of the components of this media would be a favourable course of action and may support better growth and/or allow later passaging. Future potential roles for bovine endometrial epithelial organoids would be to incorporate stromal cells to produce endometrial assembloids, a process which has been achieved in human organoids (Rawlings, Makwana, Taylor, et al., 2021).

Gland marker expression levels were quantified in the organoids, however this data was not normalised, and was a simplified, rudimentary investigation into their expression, essentially just to show presence or absence. Despite this, at many stages of growth, expression of gland markers appears similar between animals. With this in mind, there is a large variation in expression of gland markers at the early stages of growth <9 days; which could be due to the different speeds for which these cells grow, perhaps because of animal-to-animal variation or differences in plating densities, as these are estimated.

RNASeq data shows highest upregulation of *GREB1* following treatment with P4. This is interesting, as in the human this has also been characterised as a P4 regulated gene (Camden et al., 2017). However, the results of that investigation found that *GREB1* was necessary for stromal cell decidualization, which is a process which does not happen in non-invasive implantation, as

occurs in bovine (MacIntyre et al., 2002). In other systems, *GREB1* has been found to be oestrogen upregulated in mice (Laviolette et al., 2014), as well as necessary for hormone induced growth of breast cancer (Rae et al., 2005) and prostate cancer (Rae et al., 2006). Therefore, it would be possible that this gene which is upregulated in response to P4 treatment in bovine organoids is involved in regulation of growth and proliferation.

For both the list of genes that were upregulated as well as those that were downregulated, following downstream Webgestalt analysis there were many genes which were uncharacterised when analysing involvement in biological processes, cellular components or molecular functions. This spotlights the lack of research into bovine gene functions. This could explain the lack of significantly enriched processes associated with these genes, and the fact that very few are reproduction related, due to the scarcity of research into bovine reproduction. Additionally, in the STRING network analysis; whilst there are many predicted protein-protein interactions, there are many which do not appear to interact - likely due to lack of research in this field.

Janus kinase 3 (*JAK3*) is another gene which is upregulated in response to P4 treatment. *JAK3* is a modulator of immune response, and its inhibition in the human intestine resulted in increased immune response (Wang et al., 2013). It is known that during pregnancy in multiple species including bovine, the immune response has to be controlled in order to allow immune tolerance to the developing offspring (Oliveira et al., 2012). Considering P4 is elevated at the time of implantation, and *JAK3* is overexpressed in response to P4, this could function to reduce a negative immune response against the conceptus.

Positive regulation of protein localization to membrane is a significantly overrepresented biological process associated with genes upregulated in response to P4 treatment. This suggests that P4 induces production of proteins necessary for implantation of the conceptus and localization of these to the site of implantation at the membrane. One of the proteins that fall into this category is ezrin - a membrane protein involved in cellular adhesion (Pujuguet et al., 2003). These results suggest ezrin may be upregulated in endometrial epithelial gland cells during implantation to assist in adhesion of the conceptus. Curiously, another study stated that ezrin was downregulated in implantation - finding a decrease at day 20, and re-emergence at day 35. Perhaps temporal control of ezrin is necessary for successful implantation in bovine.

It is interesting to see that many of the miRNAs conserved across eutherian mammals (Taylor et al., 2023) are expressed in these bovine organoids. Due to the large variation between individuals already known, a larger sample size would perhaps provide more conclusive evidence. Furthermore, the vehicle

treatment appears to have a profound effect on the expression of many of the miRNAs. As this vehicle was 100% ethanol, perhaps using a different vehicle for P4 such as water would be beneficial to look at the P4 treatment specific effects which are not influenced by the vehicle.

5.5.4 Summary

This chapter has employed various techniques in order to model the endometrium in human and cow. As discussed in Chapter 1, these two species display very different phenotypes in aspects of early pregnancy and implantation strategies, despite both undergoing mono-ovulation. In order to fully understand the mechanisms involved, appropriate models are required in both species to unravel the signalling and interaction networks underpinning early pregnancy. The human Alvetex model aims to provide insight into implantation beyond attachment, displaying a 3D multicellular model allowing for invasion assays and improving on monolayer models to allow investigation of the endometrium in a tissue like structure. In contrast, the bovine organoids to model the endometrium by deriving organoids from endometrial gland cells does not recapitulate the multicellular nature of the endometrium, however allows for studying of gland cell secretion and embryo interaction. The ideal comparison to gather useful data would be to compare these models with their counterpart in the opposite species, which have already been developed (Turco et al., 2017; Díez et al., 2023). RNASeq data provided here from bovine organoid response to P4 would be interesting to compare to RNASeq data of human organoids treated with P4, to decipher whether there are differences in signalling between the two species. This could potentially identify targets for further investigation which may be responsible for some of the diverse phenotypes observed in early pregnancy. It is well known in the field and clear from the literature that much more research has been directed towards understanding human early pregnancy events, with some bovine models used to understand processes they share, such as ovulation (Adams and Pierson, 1995). Use of RNASeq data produced from bovine organoids here could provide valuable insights for not only expanding the understanding of bovine early pregnancy events; but, in conjunction with human data, could increase our knowledge of similarity or differences with human processes.

Future work to expand on experiments carried out in this chapter would investigate blastocyst attachment and invasion in Alvetex scaffolds, as this would be possible due to the multi-cellular structure. More optimisation of bovine endometrial organoid processes are required, for expansion media, growth and passaging. This would potentially result in the ability to study implantation using this tool, and could lead to the production of assembloids by the addition of stromal cells. With these further stages of development, a reliable, reproducible, multicellular model of the endometrium in humans can be achieved, and a 3D organoid based model of the bovine endometrium can be improved upon to be used in research into implantation and endometrial

function. Furthermore, development of a bovine Alvetex model and utilisation of existing human endometrial organoids will allow comparison between species to unravel the molecules responsible for the different implantation strategies.

In summary, this chapter has used a 2D embryo attachment model to study the impact of differential expression of conserved miRNAs on human implantation. Furthermore, it has demonstrated the production of 2 novel, 3D models of the endometrium - a scaffold based multicellular human endometrium model and a glandular spheroid bovine model, to address the lack of available models. Here, it has been shown that these models can be used to study miRNA expression, and they have future potential to model implantation to improve our understanding in this process.

Chapter 6 Discussion and Future Directions

6.1 Discussion

Events in early pregnancy are synchronised and tightly controlled; requiring an appropriately developed embryo to interact with an optimally primed endometrium (Critchley et al., 2020). It is thought that endometrial receptivity is responsible for around two thirds of failed implantation events in humans, with the other third attributable to the embryo (Achache and Revel, 2006). Human embryo implantation is surprisingly inefficient, with implantation rates averaging only 20-25% for natural conception and 25% for IVF patients (Simon and Laufer, 2012). The inability to conceive causes a huge impact on patients' wellbeing, not only psychologically but financially due to the high cost of assisted reproductive treatment (Greil et al., 2010). This is only further exacerbated in patients with recurrent implantation failure. Poor efficiency observed in early pregnancy is not exclusive to humans, with approximately 50% of fertilised bovine embryos lost within the first weeks of pregnancy (Imakawa et al., 2022), the majority of which occur during the preimplantation period (Tinning et al., 2023). This has a negative effect on food security, with meat and dairy industries suffering financially and a knock-on effect on the climate and their contribution to environmental damage. These factors highlight the necessity for improved understanding of the signaling molecules and mechanisms behind early pregnancy events. Only with a clear perception of the biology governing these processes, can we hope to identify targets for intervention.

MiRNAs are short, non-coding molecules which regulate up to 60% of protein coding genes and are involved in a multitude of processes throughout the body, including reproduction (Shu et al., 2017; Hayder et al., 2018). Novel miRNAs often emerge at times of developmental innovation, such as the introduction of a new organ, such as the placenta (Hosseini et al., 2018). A group of miRNAs which evolved coincident with the eutherian mammals and were subsequently conserved across all extant species studied were identified by our group (Taylor et al., 2023). It is likely that these miRNAs play a role in reproductive events and the conservation and diversification of implantation strategies observed across the eutherian mammals, with all 13 associated in the literature with various reproductive functions (discussed in Chapter 1, Section 1.9.5). MiRNAs miR-340-5p, -542-3p and -671-5p are each individually significantly upregulated in response to P4 (Edge et al., 2023), of which elevated concentration is characteristic in the secretory phase hormone profile in eutherian mammals (Nagy et al., 2021). Other miRNAs are also found to be regulated in response to P4 and E2. MiR-125b and miR-133a were both upregulated by P4 in the endometrial epithelium (C. Chen et al., 2016; Pan et al., 2017), whilst in stromal

cells - miR-181b, let-7c and let-7e were upregulated by E2 (Reed et al., 2018). Further to this, a correlation has been shown between downregulation of miR-30b, -125b, -424 and -451 with high blood concentration of P4 in patients undergoing IVF compared to those with average P4 (R. Li et al., 2011). The fact that miRNAs are expressed or inhibited in response to hormones required for pregnancy suggests that they may be involved in regulating some of the key processes in pregnancy including endometrial receptivity and implantation. For example, in the mouse uterus, it was discovered that prostaglandin-endoperoxide synthase 2 (*PTGS2)* which is a gene associated with successful implantation, was downregulated by miR-101a (Chakrabarty et al., 2007). Furthermore, in the human endometrium, Altmäe et al., (2013) established that miR-30b and miR-30d were upregulated during the window of receptivity, whilst miR-494 and miR-923 expression was reduced. These findings indicate that miRNAs are important for establishing endometrial receptivity, and/or have roles in pregnancy. Considering that miR-340-5p, -542-3p and -671-5p are regulated by P4 and are conserved across all extant eutherian mammal species studied; it is likely that they may have specific relevance to early pregnancy events.

This thesis is comprised of two major approaches to unravel the involvement of 3 evolutionarily conserved, P4 regulated miRNAs in the intricate events required for successful pregnancy:

1) investigating the effect of these miRNAs in the endometrium by proteomic analysis; and

2) modelling the endometrium and implantation

The first approach sought to test the hypothesis that these miRNAs would modify protein coding regions of the genome, potentially facilitating receptivity to implantation in humans. The second approach aimed to evaluate the hypothesis that altering these miRNAs in a model of the endometrium would have a functional effect on embryo implantation; and to develop a novel, 3D model of the endometrium.

In this thesis, the proteomic impact of altering concentrations of evolutionarily conserved, P4 regulated miRNAs is demonstrated. MiR-340-5p results in a number of mechanistic responses when overexpressed, with altered proteins demonstrating much involvement in regulation of the cell cycle. In fact, some proteins - NRAS, Notch2, STAT3, PTRH2 and CAAP (discussed in Chapter 2, Section 2.5) - which are differentially abundant following overexpression suggest miR-340-5p participates in controlling endometrial epithelial proliferation - specifically inhibition of it - during early pregnancy. During the menstrual cycle, in the proliferative phase, the epithelial layer of the

endometrium proliferates and thickens in response to E2, whilst P4 in the secretory phase halts proliferation (Marquardt et al., 2019). Therefore, it is reasonable to suggest that a P4 induced increase in expression of miR-340-5p may be regulating proliferation, due to its targets showing overrepresentation in cell cycle processes; as well as negatively regulating proliferation in endometrial cancer (Xie et al., 2016). Other miRNAs have been shown to regulate proliferation in endometrial tissue - miR-92a-3p overexpression caused reduced proliferation in endometrial stromal cells in endometriosis (Zhu et al., 2023). This miRNA is also implicated in controlling proliferation in breast cancer cells, functioning in the opposite way, where its overexpression increased proliferation (Jinghua et al., 2021). The two opposite functions of the same miRNA in different systems highlights the functional plasticity of miRNAs, in that they are able to perform different roles depending on the cell type and environment. In addition to these studies, miR-135a upregulation also resulted in increased proliferation in endometrial cancer (Wang et al., 2020). In fact, a study found that miR-133a was upregulated in response to P4, and in a similar mimic/inhibitor experiment also using Ishikawa cells, they discovered that miR-133a reduced proliferation (Pan et al., 2017). These studies demonstrate that miRNAs are involved in regulating proliferation in multiple processes associated with the endometrium, and in particular, that miRNAs which are upregulated by P4 are capable of controlling proliferation in the secretory phase. Proteomic analysis in this thesis also leads to the suggestion that P4 induced upregulated miR-542-3p is modulating proliferation in the secretory phase endometrium. Interestingly, the results show that the protein which has the highest fold change in abundance in response to each of miR-340-5p overexpression, miR-542-3p overexpression or miR-671-5p is *PRR11*, which the literature points towards being a proliferation promoter. However, most of these studies focus on *PRR11* in cancer (Lee et al., 2020), and it is well known that cancer cells influence their own survival and proliferation by hijacking of cellular processes (Baghban et al., 2020); so it is possible that *PRR11* may have other functions in the non-cancerous endometrium. Similarly, this study was conducted in Ishikawa cells, which are derived from cancerous cells - regularly used for modelling endometrial cancer (Devor et al., 2020); and so this may have some effect on the results.

Different claudin proteins were differentially abundant in response to each of the 3 miRNAs, suggesting that claudins may play a role in early pregnancy events Claudins are a group of transmembrane proteins that are components of TJs between epithelial cells, controlling permeability of the epithelium (Serafini et al., 2009). There are 24 claudin genes in mammals, and knockout mouse models provide evidence for their roles in maintaining tissue structure (Lal-Nag and

Morin, 2009). MiR-340-5p overexpression elevates claudin 4 abundance, whilst miR-542-3p overexpression downregulates claudin 1, and miR-671-5p upregulates claudin 7. As discussed in Chapter 2, CLDN4 is increased at the time of implantation and then reduces (Riesewijk et al., 2003). It was suggested in Chapter 2 that this decrease following implantation perhaps aids in the process of invasion, as reduction of CLDN4 disrupts TJ formation (Shang et al., 2012; Bhurke et al., 2016). It would be interesting to determine whether overexpression of all 3 miRNAs has the same effect on claudin expression as each one does individually. Claudin 1, 4 and 7 have all found to be increased during the secretory phase in the endometrium previously (Sobel et al., 2006; Gaetje et al., 2008). Claudin 7 was also observed to improve adhesion in lung cancer cells (Kim Hyung et al., 2019). In other systems, claudin expression is under miRNA control; *i.e.*, miR-195-5p downregulation results in increased claudin 2 expression in inflammatory bowel disease, which then decreased claudin 1 also (Scalavino et al., 2022). Therefore, it is possible that miRNAs are controlling TJs in the endometrium to control and facilitate appropriate embryo implantation.

Endometrial epithelial cells are known to secrete proteins involved in cross talk with the preimplantation embryo, demonstrated in the endometrial epithelial cell line ECC1, which secreted EVs containing proteins important for implantation, having a positive effect on pregnancy success (Greening et al., 2016). Fibulin 1 (FBLN1) was one protein that was discovered in the EV cargo and is regulated during the menstrual cycle and linked to cell adhesion and migration (Okada et al., 2014). Heparan sulphate proteoglycan 2 (HSPG2) and complement decay-accelerating factor (CD55) are other proteins identified which have previously been found to be important for successful implantation. Similar results are seen in Ishikawa cells, as well as primary endometrial epithelial cells, where EV contents consisted of many proteins associated with adhesion and implantation (Segura-Benítez et al., 2022). It is therefore possible that many of the proteins found to be altered by miR-340-5p, miR-542-3p and miR-671-5p which are enriched in adhesion processes may be subsequently secreted in EVs to partake in endometrial/embryo cross talk. Certainly, many of the significantly enriched biological processes for proteins altered in abundance by each of the 3 miRNAs included protein transport and localisation. This suggests that transport, and so secretion, of proteins is upregulated at this time to aid in this process.

Additionally, it has been shown that secretions from the epithelial layer of the endometrium can communicate with, and have an impact on, the stromal layer. Fitzgerald et al., (2023) used endometrial organoids to analyse the basolateral

secreted protein cargo, applying these proteins to primary stromal cells to examine the effect; concluding that cystatin C (CST3) influenced decidualisation. This provides evidence that proteins produced in the epithelium have roles in stromal cell functions. Many of the significantly enriched biological processes that proteins altered by conserved, P4 regulated miRNAs in the endometrial epithelium were found to be involved in centre around ER stress, which is elevated during decidualisation - a stromal cell specific process. The ER is the site of protein production, from folding and modifying to degrading and localising. ER stress occurs when there is a disparity between the ER protein processing capacity and the protein requirements of the cell (McMahon et al., 2017). This causes misfolded proteins to congregate, activating the UPR, which deals with this by 1) slowing or halting protein production, 2) degrading misfolded proteins or 3) expanding ER machinery to accommodate increased protein production (Read and Schröder, 2021). It is known that ER stress and the UPR occur during stromal cell decidualisation in preparation for implantation (Soczewski et al., 2020). It is interesting that ER stress and UPR has been linked to successful implantation - with recurrent implantation failure patients producing less UPR markers than fertile women (Grasso et al., 2018). Alternatively, women who suffer from recurrent pregnancy loss - importantly after implantation was successful; produce more UPR markers. These negative pregnancy outcomes potentially demonstrate the consequences of ER stress and UPR which is not controlled tightly enough (Soczewski et al., 2023). Taken together, this evidence suggests that ER stress and UPR is vital for implantation by correct decidualisation and priming of the endometrium, but must be effectively controlled.

In this proteomic analysis, proteins altered by miR-671-5p were heavily associated with ER stress and UPR, with miR-542-3p altered proteins also implicated. MiRNAs in the literature are associated with ER stress in other systems. In hepatocellular cancer, ER stress induced UPR is inhibited following miR-122 overexpression, resulting in a rise in apoptosis (Yang et al., 2011). ER stress in reproductive systems has been occasionally linked to miRNA control; in pig embryos, miR-210 upregulation was negatively correlated with embryo development (Ridlo et al., 2021). Investigation into miRNAs involved in ER stress and UPR during decidualisation was carried out by Soczewski et al., (2023), discovering that miR-17-5p, miR-21-5p and miR193b-3p were all downregulated following ER stress induction as well as when human endometrial stromal cells underwent decidualisation. This suggested that these miRNAs may be associated with ER stress and UPR and perhaps their downregulation is important for management of these processes. Proteomic data demonstrated in this thesis for proteins increased in abundance by

overexpression of miR-671-5p and decreased in abundance by inhibition are significantly enriched in ER and UPR processes. This suggests that upregulation of this miRNA is increasing production of proteins to control this, whereas miRNAs identified by Soczewski et al., (2023) appear to be modulating ER stress through their downregulation. As miRNAs most commonly function by repression of mRNA translation, it is likely that reducing expression of these miRNAs stops inhibition of the translation of proteins relevant to ER stress. In a similar fashion to the work carried out in this thesis, it would be interesting to investigate which proteins are increased in abundance when these 3 miRNAs are downregulated simultaneously to investigate whether they are ER associated and if they overlap with those altered in response to miR-671-5p.

As discussed in Chapter 3, survivin was found to be upregulated in response to miR-542-3p overexpression, and downregulated by inhibition. The function of this was suggested to reduce apoptosis of endometrial epithelial cells during implantation. Interestingly, this protein was found to be miRNA regulated, as well as implicated in ER stress in human umbilical vein endothelial cells (HUVECs) (Chatterjee et al., 2021). They discovered that miR-494 significantly reduced the presence of survivin, which is linked to a reduction in ER stress response. This mechanism was also observed in colon cancer cells where inhibition of survivin resulted in a decrease in ER stress markers (Gundamaraju et al., 2018).This may mean that miR-542-3p upregulated survivin is potentially functioning to increase ER stress response in the endometrium.

During analysis of proteomic data, proteins altered in abundance in Ishikawa cells were compared to RNASeq data from primary human endometrial biopsies (Lipecki et al., 2022) to confirm presence of proteins in human endometrium. As Ishikawa cells are a cancerous cell line, this comparison sought to increase confidence in results obtained from proteomic investigation. A total of 36 women were involved in the study, aged between 31-36, with between 0 and 9 previous losses. Outcomes recorded in the study included live birth, ongoing pregnancy or miscarriage. The comparison of the data presented in this thesis with this RNASeq data is not necessarily completely accurate due to the presence of multiple other cell types present in an endometrial biopsy. Whilst Ishikawa cells here are intended to represent the endometrial epithelium, an endometrial biopsy will also contain stromal cells, blood cells and immune cells which may affect results. However, as a simple method of comparison to understand how many proteins identified were also present in the endometrium as a whole, the data was useful. Furthermore, all of the biopsies were at the correct stage of the menstrual cycle, being collected 4-12 days following ovulation, meaning they were physiologically relevant P4 primed endometrial cells.

The second approach taken in this thesis centred around modelling the endometrium in order to investigate the functional roles of the conserved, P4 regulated miRNAs (Chapter 5). The first model used a 2D Ishikawa cell monolayer and embryo-like spheroids formed from a trophoblast cell line to model embryo attachment to the endometrial epithelium. The main finding of this experiment was that miR-542-3p overexpression significantly reduced embryo attachment rates. Other miRNAs appeared to have an effect on attachment; miR-340-5p overexpression non-significantly increased attachment rates, as did inhibition of miR-671-5p. MiR-671-5p has been found to be upregulated in patients with RIF, as compared with fertile patients (von Grothusen et al., 2022), which is in agreement with the results of this attachment assay. As miR-542-3p is increased in response to P4, which is elevated during the window of implantation, it is unlikely that miR-542-3p is involved in the attachment stage of implantation. This is due to the results of the attachment assay demonstrating that overexpression of miR-542-3p decreases embryo attachment rate. As discussed in more detail in Chapter 5, Section 5.5.1 and Chapter 3, Section 3.5, miR-542-3p may be involved in apposition stages of implantation through regulating apoptosis by modifying abundance of Survivin, an apoptosis inhibitor. The results of these studies suggest that miR-542-3p could upregulate *Survivin* to inhibit apoptosis during apposition, which is required at this stage of implantation (Galán et al., 2000). Another miRNA - miR-181 - was also found to inhibit embryo implantation in mice (Chu et al., 2015). Mechanistically, this occurred by miR-181 downregulation of leukaemia inhibitory factor (*LIF*), where readministering *LIF* reverses the inhibitory effect on implantation. MiR-181 was specifically downregulated on day 4 following insemination; which is the point at which implantation would occur. Expression of miR-181 was then returned to usual by day 6. Perhaps miR-542-3p expression is increased by P4 in the secretory phase of the menstrual cycle in humans, but is reduced specifically at the time of implantation to reverse its inhibitory effect on embryo attachment. If that was the case, increased miR-542-3p expression before the point of implantation could be a mechanism to stop the embryo attaching to the endometrium at an inappropriate time. Interestingly, when combined with under expression of miR-340-5p, miR-542-3p significantly increases embryo attachment rate. Furthermore, overexpressing miR-340-5p, miR-542-3p and miR-671-5p appears to cause an increase in embryo attachment. Taken together, these results suggest that upregulation of these 3 miRNAs simultaneously may facilitate implantation by altering the proteome of the endometrium to establish endometrial receptivity. MiRNAs are found to function collaboratively, thought to result in 'fine tuning' of protein production (Skommer et al., 2014; Chen et al., 2017). Proteomic analysis of individually

overexpressed miR-340-5p, miR-542-3p and miR-671-5p discovered that 122 targets were altered by all 3 miRNAs, with larger numbers of confirmed targets shared between 2 of the 3 miRNAs. These 122 proteins are significantly involved in multiple stages of the cell cycle, suggesting that upregulation of these miRNAs collaboratively facilitates embryo attachment by contributing to endometrial receptivity through controlling endometrial epithelial cell proliferation.

This thesis is the first study to use Alvetex scaffold technology to model the human endometrium *in vitro*, which is detailed in Chapter 5. Whilst this method is not yet fully optimised, the early stages of development demonstrate that it is possible to culture endometrial stromal cells in the scaffold which deposit extracellular matrix. Furthermore, endometrial epithelial cells can be seeded on top of this, which grow in a layer on top of the stromal cells, representing the structure of the endometrium. This process has been carried out recently using bovine endometrial cells (Díez et al., 2023). The fact that this technology can be applied to multiple species provides an avenue for comparative investigations into endometrial function and implantation. It was possible to transfect the scaffold with mimics and inhibitors for miR-340-5p, miR-542-3p and miR-671-5p; meaning this technology can be used for investigation into miRNA functionality in the endometrium. From proteomic analysis, it appeared that miR-340-5p and miR-542-3p were involved in controlling proliferation of the endometrial epithelium. For this reason, ki67 - a proliferation marker - was measured in the Alvetex scaffolds. Fascinatingly, in a scaffold which overexpressed miR-340-5p, miR-542-3p and miR-671-5p, proliferation appeared to be completely inhibited, and in those scaffolds overexpressing a single miRNA of either miR-340-5p or miR-542-3p, proliferation of epithelial cells seemed to be slightly reduced compared to scaffolds where these miRNAs were reduced. This study requires further investigation, as it was only carried out in a single biological replicate but is preliminary data to suggest that these evolutionarily conserved, P4 regulated miRNAs are involved in controlling proliferation, and evidence that they may function in combination with each other. Taken together, the proteomic analysis identifying protein targets along with observed reduction in epithelial proliferation in the Alvetex model forms a basis for concluding that miR-340-5p, miR-542-3p and miR-671-5p downregulate proliferation in the endometrial epithelium in the secretory phase following their upregulation in response to P4. It is known that epithelial proliferation is halted in the secretory phase (Marquardt et al., 2019), and this thesis provides the suggestion that these miRNAs may be responsible for this.

In recent years, organoids have emerged as a 3D modelling technique in many biological systems, from kidneys (Takasato et al., 2016) to brain (Sun et al., 2021), and including the human endometrium (Turco et al., 2017). Some organoid models have been developed for modelling bovine systems; with reproduction related examples including mammary gland organoids (Martignani et al., 2018) and testicular organoids (Cortez et al., 2022). This thesis is the first time that bovine organoids modelling the endometrium have been derived. Modelling the bovine endometrium by creating organoids from epithelial glands is vitally important to understanding endometrial function and implantation, as animal gland knockout models such as in goats show that glands are required for successful implantation (Gray et al., 2001). Similarly to the Alvetex scaffolds, as discussed in Chapter 5, these bovine endometrial organoids are at an early stage of development which require further optimisation. Longevity of the organoids in culture is poor - with organoids showing no further growth from passage 3. Optimisation of the culture media could be carried out to see if the lifespan could be extended, perhaps taking inspiration from the pre-mentioned bovine organoid models, as the media composition used was taken from the human endometrial organoids (Turco et al., 2017). The bovine organoids were responsive to P4 treatment, which resulted in upregulated expression of 373 genes, and downregulation of 240 genes. Furthermore, the organoids were shown to express many of miRNAs that are conserved amongst the eutherian mammals. The production of these organoids demonstrates, for the first time, the derivation of hormone responsive, bovine endometrial organoids to model the endometrium, which may be used for studying endometrial function and embryo interactions. As this model already exists in humans (Turco et al., 2017), these models could be used comparatively to advance our understanding in the inter-species differences in endometrial receptivity.

6.2 Complications, Solutions, and Future Directions

The proteomic analysis described in this thesis demonstrates the effect of over or under expressing conserved, P4 regulated miRNAs on the proteome of the endometrial epithelium. The data produced is very large and provides many avenues for future research. Further in-depth analysis of specific groups of proteins could be investigated, for example - focusing on the list of proteins altered by miR-671-5p and implicated in ER stress response. It would be interesting to examine proteins significantly altered by these miRNAs in primary cells - as a cell line is not completely representative of a normal endometrium, although it does display many of the characteristics such as functional P4 receptors (Mo et al., 2006). If there was access to primary tissue, analysing abundance of the proteins found to be altered, along with miRNA expression in tissue from recurrent implantation failure (RIF) patients would provide further insight into dysregulated pathways and proteins which may contribute to RIF. This may identify miRNA regulated proteins responsible for failed implantation and identify therapeutic targets. Analysis of EV cargo secreted from epithelial cells transfected with miRNA mimics and inhibitors for miR-340-5p, miR-542-3p and miR-671-5p is the next logical step for this research. It is of particular interest to determine whether the proteins involved in ER stress are amongst those secreted, as this thesis concludes that these proteins are involved in epithelial/stromal cross talk to control the ER stress response to decidualisation. Furthermore, this would also provide insight into whether adhesion proteins are secreted in response to P4 upregulation of these miRNAs which may contribute to endometrial/embryonic communication to facilitate implantation.

As much of the data presented here, particularly for miR-340-5p (Chapter 2) and miR-542-3p (Chapter 3), points towards the involvement of these conserved, P4 regulated miRNAs playing a role in controlling proliferation in the epithelial layer of the endometrium, a future direction would be to conduct proliferation assays. An ATP concentration assay using a biomarker such as luciferase could be used to investigate this. This would be possible to do following transfection with these miRNA mimics and inhibitors to determine whether there is a significantly difference in the cells proliferative activity when these miRNAs are over or under expressed. It would also be possible to transfect with all 3 miRNA mimics to investigate proliferation under the collaborative effect of their overexpression which occurs in response to P4. In fact, transfecting endometrial epithelial cells with all 3 miRNA mimics and conducting a similar proteomic analysis presented in this thesis would be beneficial to understanding the roles of P4 regulated miRNAs. This would

provide insight into alterations in protein abundance in the endometrium when all 3 miRNAs are overexpressed - as was found to occur in response to P4.

In this thesis, stromal cell expression of miR-340-5p, miR-542-3p and miR-671-5p was investigated in a stromal cell line, with no prior treatments. It would be interesting to study whether treatment with P4 causes a similar effect in stromal cells as it does in the epithelial cells, as this may play a role in decidualisation. Conducting qPCR to measure expression of all 13 conserved miRNAs in the stromal cells both with and without P4 would allow us to understand whether different miRNAs are changed in the stromal layer in response to P4.

The 2D implantation assay provides insight into whether altering conserved, P4 regulated miRNAs has an effect on attachment of embryos. However, as this is a 2D culture system, no conclusions can be drawn concerning implantation beyond attachment. Furthermore, this system is non-sterile, due to logistic issues in the laboratory, which is not ideal and may introduce variability. It is difficult to distribute the spheroids evenly throughout the well, and those which are further from the middle appear to attach less frequently than those in the middle. This could be because the Ishikawa cells are more densely populated in the middle of the well, despite efforts to maintain an evenly confluent monolayer across the whole plate. These solutions may be solved by using microfluidic devices which would be sealed, sterile units. This could be achieved with basic microfluidic devices similar to those used by De Bem et al., (2021), or alternatively I have identified a method used for other systems, which could be adapted for studying attachment. The Bioflux instrument (Fluxion) is a type of microfluidic device which can also control shear flow rates. This is usually used for vessel on a chip development, as well as biofilm production and host-pathogen interactions (Tremblay et al., 2015). Unfortunately, channels in the commercially available plates were too narrow to accommodate BeWo spheroids and so it was not possible to carry this experiment out within the scope of this thesis. However, if plates with wider channels were produced, this technology could be employed to study attachment in a high throughput manner - as a single plate has multiple channels and can all be controlled at once. Furthermore, being able to easily and reliably control shear flow would allow these investigations to be carried out under flow in the device, to recapitulate flow of fluid in the uterus. Another drawback of the spheroid attachment model was that the percentage embryo attachment rates in the controls were too high, as there should be room for improvement or deterioration of the attachment rate. Optimisations were carried out to achieve a control attachment rate of approximately 70%, which was not observed in the experiment. Reduction in

incubation time may solve this issue, or alternately this could be down to the previously mentioned distribution of the spheroids within the well.

Development of Alvetex scaffold for endometrial modelling is at the early stages of optimisation. It is clear that some work is required to select the most suitable cell number or timing for seeding the epithelial layer, as shown in Chapter 5, the epithelial layer is very thick, and the stromal layer does not seem dense enough. The epithelial layer also appears to breach the stromal layer in places. As Ishikawa cells are formed from a cancer line, invasiveness is a hallmark of cancer, and this may play a role in how they behave in the Alvetex (Hanahan, 2022). Although, other studies have suggested that the Ishikawa cells are poorly invasive, whilst finding that they can become more invasive when using fibronectin as a chemoattractant (Meng et al., 2007), which has been shown to be deposited in the Alvetex scaffolds by immunofluorescence. This may influence the invasiveness of these cells and cause them to breach into the stromal layer, particularly if the stromal layer is not as dense. An alternative cell type could be used which does not derive from a cancer line, or ideally primary cells. Using a patient's primary endometrial stromal and epithelial cells may provide a personalised medicine approach using Alvetex technology for modelling the patient's own endometrium; potentially allowing for testing of therapeutics to improve fertility. It could be that the Ishikawa cells are forming glandular structures in the endometrial model, as the cell line is representative of endometrial luminal and glandular epithelial cells, and Ishikawa cells have been previously shown to develop gland-like structures (Fitzgerald et al., 2021).

As discussed in Chapter 5, following addition of epithelial cell layer, there appears to be less dense nuclei in the stromal layer. This could be due to a number of reasons: 1) transfection protocol - during the transfection, cells were incubated for 3 hours during which they were not fully submerged in media. In this time, media was only added to the top of the insert to perform the transfection. To rule this out, it would require an experiment to be carried out that compares those inserts which have remained in media with those who were subjected to the transfection protocol (without actual transfection reagents) to determine whether this has an effect. I would expect this reason to be unlikely as the cause as during epithelial cell seeding a similar process is carried out and the cells not submerged in media for 2 hours, but as seen in Chapter 5, after 4 days the stromal layer demonstrates a similar appearance to before the addition of epithelial cells. Suggested reason 2) the epithelial layer thickens and produces a barrier which means internal stromal cells do not have access to nutrients. The evidence from the Alvetex results suggests this is a likely explanation as there seems to be nuclei present at the bottom of the scaffold -

where the cells would be in contact with media, but few nuclei in the middle of the scaffold. *In vivo*, the endometrium would be vascularised so the cells further into the tissue would receive nutrients - which this model does not have. Potential reason 3) stromal cells cannot persist in culture in the Alvetex model for this length of time. This is another likely reason and to disprove this would require a stromal only model to test the density of the stromal layer in the maximum incubation time (stromal + epithelial seeding time points). To resolve this issue, perhaps alternative cells could be used, or epithelial layer seeded earlier to reduce incubation time - the latter of these suggestions, though, may result in more observed invasion of the epithelial cells due to a less developed extracellular matrix.

Once optimised fully, immediate future directions for the Alvetex technology to model the endometrium would be to stain for high fold change proteins in the transfected models. It would be interesting to carry out immunofluorescence to investigate proteins such as *PRR11* which is highly upregulated in response to each of miR-340-5p, miR-542-3p and miR-671-5p. The Alvetex endometrium would also provide a multi-cellular, 3D model for studying decidualisation. Furthermore, inducing decidualisation and studying ER stress and UPR in these models, particularly following transfection with miR-671-5p would be fascinating. It would be possible to study expression of UPR markers such as sXBP1 and CHOP (Grasso et al., 2018) to investigate whether miR-671-5p is playing a role.

Another use for this technology would be to use the 3D Alvetex endometrium for an implantation assay, which would allow us to study stages of invasion. BeWo spheroids would not be an appropriate model for this, as they have been shown to be non-invasive into stromal cells (Grümmer et al., 1994). Alternatively, mouse embryos could be used to investigate whether over or under expression of miRNAs has an effect on implantation through to the stages of invasion. Again, this type of technology carried out with primary patient cells could lead to personalised medicine implantation assays to model the events of implantation in the patient’s own cells.

Organoids are an *in vitro* model that have been developed as a solution to investigating the endometrium. Here, it is shown for the first time that bovine endometrial organoids can be derived from bovine endometrial epithelial cells. This is at a very early stage of development and a number of further optimisations are required to validate this system. The organoids demonstrate varied growth and poor results following passaging. As the expansion media was taken from Turco et al., (2017), which is optimised for human organoids, each growth factor and concentration should be tested and optimised with bovine organoids for improved growth. The next steps of developing these

organoids would be to measure PR and ER expression, as well as response to E2, and to stain for polarity, to ensure cells are oriented correctly. Reversing the polarity of the bovine organoids is a future investigation that would broaden the potential of this model. Very recently, and only currently in pre-print format, a study has reported reversing polarity of human endometrial organoids so that their apical membrane is facing outwards (Ahmad et al., 2023). This makes the organoids more applicable for use in embryo interaction experiments, as the site of blastocyst attachment is on the outside, as well as co-culture systems to examine endometrial-embryo communication. This would be a particularly useful physiological system to use bovine organoids for with the preimplantation period being longer. The bovine organoids show presence of all miRNAs from eutherian mammal conserved miRNA families Taylor et al., (2023). The organoids were treated with P4, however for miRNA expression, the vehicle appears to affect expression resulting in no significant differences between the vehicle and P4 treatment. This could be reduced perhaps by using a P4 treatment for which the vehicle is water, rather than ethanol. It would be interesting to compare the bovine organoid miRNA expression to that of human organoids to determine whether their expression is significantly different between species. Unfortunately, due to long delays in availability of Matrigel, it was not possible to carry out this comparison. Cultrex 2 which was used for bovine organoids did not support growth of human organoids, hypothesised to be due to the change from long term culture in Matrigel. Another suggestion for investigation of these organoids concerning miRNA expression would be to treat each species with their respective maternal recognition molecules - hCG for human and IFNT for bovine - to observe the effect of this on the expression of miRNAs, and the differences between the species. It may also be possible to add human or bovine organoids to Alvetex scaffolds to produce gland structures within the 3D modelled endometrium to develop a more physiologically accurate model.

A further future direction that this work forms the basis of would be to study the expression of the conserved miRNAs (Taylor et al., 2023) in the placental tissue. The rationale for this would be that many of these miRNAs are implicated in placental tissue and pathologies involving the placenta (discussed in Chapter 1). It would be fascinating to investigate their involvement in placental development - studying their expression from early pregnancy to term, as well as comparing this to their expression in different conditions such as preeclampsia. This would further deduce the roles of these conserved miRNAs and could begin to explain some of the vast phenotypic and strategic differences observed between the placenta in various species of Eutherians.

6.3 Conclusions

The early events of pregnancy which are tightly controlled both temporally and spatially still lack comprehensive understanding. Part of the reason for this is that the tissues and cells required to study these processes are, by their very nature, inaccessible. Increasing our understanding of the molecular processes behind successful pregnancy, as well as developing novel *in vitro* models to study functional roles, is crucially important for the advancement of fertility treatment and intervention, along with improving industries such as meat and dairy production.

MiR-340-5p, miR-542-3p and miR-671-5p are conserved miRNAs found to be upregulated in response to P4 in endometrial epithelial cells. This project sought to investigate their roles in pregnancy in eutherian mammals. Over or under expression of each of these 3 miRNAs results in alterations in the endometrial epithelial proteome, with lists of proteins that are changed produced which could be of potential interest for future research. Comparisons of *in vitro* confirmed proteins with those which are predicted targets has highlighted the unreliability of target prediction tools for miRNAs. Downstream analysis of altered proteins for over or under expression of each miRNA has revealed pathways and processes in which these proteins are involved, which suggests these miRNAs are regulating them. This data suggests that miR-340-5p regulates proliferation in the endometrial epithelial layer, along with association in *Notch* signalling pathways which may facilitate adhesion. MiR-542-3p may be controlling apoptosis to modulate successful implantation and is also implicated in proliferation. Proteins altered in response to differential expression of miR-671-5p are heavily associated with ER stress and UPR; which is a key function during decidualisation of stromal cells. This suggests miR-671-5p may be influencing protein production in the epithelial layer to be transported to modulate stromal ER stress. Proteins altered in abundance by differential expression of each of the 3 miRNAs are linked to symbiont process. The protein with the largest fold change that is more abundant in response to each of the 3 miRNAs is a proliferation control protein, suggesting that all 3 of the miRNAs have a role in proliferation.

A 2D implantation assay was used to investigate functional roles of the miRNAs in the endometrial epithelium. This revealed that miR-542-3p overexpression significantly reduces blastocyst attachment, whilst miR-340-5p overexpression and miR-671-5p inhibition appear to increase the attachment rate. Oppositely, when both overexpressing miR-542-3p and under expressing miR-340-5p, embryo attachment is significantly increased. Overexpressing miR-340-5p, miR-

542-3p and miR671-5p simultaneously appears to increase embryo attachment, however this was not fully conclusive.

This thesis also describes development of a novel 3D, multicellular human endometrial model. This incorporates a stromal layer which deposits extracellular matrix and an epithelial layer. This may provide avenues for investigating implantation beyond attachment, which could potentially be used for testing therapeutic methods to treat recurrent implantation failure.

A second approach to *in vitro* modelling of the endometrium was carried out to produce bovine endometrial organoids. Whilst endometrial organoids have been developed in humans, this is the first time this has been achieved in bovine. This model is at a very early stage of optimisation, nevertheless it shows promising results in the expression of gland markers, ability to undergo minimal passaging and expression of conserved miRNAs. This is a promising model for comparative research into endometrial function and receptivity between humans and cows; perhaps unravelling the functions of conserved miRNAs across different eutherian mammals.

References

Abaidoo, C.S., Warren, M.A., Andrews, P.W. and Boateng, K.A. 2010. A Quantitative Assessment of the Morphological Characteristics of BeWo Cells as an in vitro Model of Human Trophoblast Cells. *International Journal of Morphology*. **28**, pp.1047–1058.

Abedal-Majed, M.A. and Cupp, A.S. 2019. Livestock animals to study infertility in women. *Animal frontiers : the review magazine of animal agriculture*. **9**(3), pp.28–33.

Achache, H. and Revel, A. 2006. Endometrial receptivity markers, the journey to successful embryo implantation. *Human Reproduction Update*. **12**(6), pp.731–746.

Adams, G.P. and Pierson, R.A. 1995. Bovine model for study of ovarian follicular dynamics in humans. *Theriogenology*. **43**(1), pp.113–120.

Afratis, N.A., Nikitovic, D., Multhaupt, H.A.B., Theocharis, A.D., Couchman, J.R. and Karamanos, N.K. 2017. Syndecans – key regulators of cell signaling and biological functions. *The FEBS Journal*. **284**(1), pp.27–41.

Aghajanova, L., Hamilton, A.E. and Giudice, L.C. 2008. Uterine receptivity to human embryonic implantation: histology, biomarkers, and transcriptomics. *Seminars in cell & developmental biology*. **19**(2), pp.204–211.

Ahmad, V., Yeddula, S.G.R., Telugu, B.P., Spencer, T.E. and Kelleher, A.M. 2023. Development of Polarity-Reversed Endometrial Epithelial Organoids. *bioRxiv : the preprint server for biology*.

Ahn, J., Yoon, M.-J., Hong, S.-H., Cha, H., Lee, D., Koo, H.S., Ko, J.-E., Lee, J., Oh, S., Jeon, N.L. and Kang, Y.-J. 2021. Three-dimensional microengineered vascularised endometrium-on-a-chip. *Human Reproduction*. **36**(10), pp.2720–2731.

Alarcon, V.B. and Marikawa, Y. 2022. Trophectoderm formation: regulation of morphogenesis and gene expressions by RHO, ROCK, cell polarity, and HIPPO signaling. *Reproduction*. **164**(4), pp.R75–R86.

Ali, A., Hadlich, F., Abbas, M.W., Iqbal, M.A., Tesfaye, D., Bouma, G.J., Winger, Q.A. and Ponsuksili, S. 2021. MicroRNA-mRNA Networks in Pregnancy Complications: A Comprehensive Downstream Analysis of Potential Biomarkers. *International journal of molecular sciences*. **22**(5).

Aljubran, F., Shumacher, K., Graham, A., Gunewardena, S., Marsh, C., Lydic, M., Holoch, K. and Nothnick, W.B. 2023. Endometrial cyclin A2 deficiency is associated with human female infertility and is recapitulated in a conditional knockout mouse model. *bioRxiv*., 2023.06.16.545284.

Altmäe, S., Koel, M., Võsa, U., Adler, P., Suhorutšenko, M., Laisk-Podar, T., Kukushkina, V., Saare, M., Velthut-Meikas, A., Krjutškov, K., Aghajanova, L., Lalitkumar, P.G., Gemzell-Danielsson, K., Giudice, L., Simón, C. and Salumets, A. 2017. Meta-signature of human endometrial receptivity: a meta-analysis and validation study of transcriptomic biomarkers. *Scientific Reports*. **7**(1), p.10077.

Altmäe, S., Martinez-Conejero, J.A., Esteban, F.J., Ruiz-Alonso, M., Stavreus-Evers, A., Horcajadas, J.A. and Salumets, A. 2013. MicroRNAs miR-30b,

miR-30d, and miR-494 Regulate Human Endometrial Receptivity. *Reproductive Sciences*. **20**(3), pp.308–317.

Andrews, S. 2010. FASTQC. A quality control tool for high throughput sequence data.

Annese, T., Tamma, R., De Giorgis, M. and Ribatti, D. 2020. microRNAs Biogenesis, Functions and Role in Tumor Angiogenesis . *Frontiers in Oncology* . **10**.

Anthwal, N., Joshi, L. and Tucker, A.S. 2013. Evolution of the mammalian middle ear and jaw: adaptations and novel structures. *Journal of anatomy*. **222**(1), pp.147–160.

Anton, L., Olarerin-George, A.O., Schwartz, N., Srinivas, S., Bastek, J., Hogenesch, J.B. and Elovitz, M.A. 2013. miR-210 Inhibits Trophoblast Invasion and Is a Serum Biomarker for Preeclampsia. *The American Journal of Pathology*. **183**(5), pp.1437–1445.

Appleby, J.B. and Bredenoord, A.L. 2018. Should the 14-day rule for embryo research become the 28-day rule? *EMBO Molecular Medicine*. **10**(9), p.e9437.

Arslan, S.Y., Yu, Y., Burdette, J.E., Pavone, M.E., Hope, T.J., Woodruff, T.K. and Kim, J.J. 2015. Novel Three Dimensional Human Endocervix Cultures Respond to 28-Day Hormone Treatment. *Endocrinology*. **156**(4), pp.1602–1609.

Arteaga-Vázquez, M., Caballero-Pérez, J. and Vielle-Calzada, J.-P. 2006. A family of microRNAs present in plants and animals. *The Plant cell*. **18**(12), pp.3355–3369.

Ashary, N., Tiwari, A. and Modi, D. 2018. Embryo Implantation: War in Times of Love. *Endocrinology*. **159**(2), pp.1188–1198.

Baghban, R., Roshangar, L., Jahanban-Esfahlan, R., Seidi, K., Ebrahimi-Kalan, A., Jaymand, M., Kolahian, S., Javaheri, T. and Zare, P. 2020. Tumor microenvironment complexity and therapeutic implications at a glance. *Cell Communication and Signaling*. **18**(1), p.59.

Bahramy, A., Zafari, N., Izadi, P., Soleymani, F., Kavousi, S. and Noruzinia, M. 2021. The Role of miRNAs 340-5p, 92a-3p, and 381-3p in Patients with Endometriosis: A Plasma and Mesenchymal Stem-Like Cell Study B. Durmaz, ed. *BioMed Research International*. **2021**, p.5298006.

Barbieri, R.L. 2014. The Endocrinology of the Menstrual Cycle BT - Human Fertility: Methods and Protocols *In*: Z. Rosenwaks and P. M. Wassarman, eds. New York, NY: Springer New York, pp.145–169. Available from: https://doi.org/10.1007/978-1-4939-0659-8_7.

Bartel, D.P. 2009. MicroRNAs: Target Recognition and Regulatory Functions. *Cell*. **136**(2), pp.215–233.

Basavaraja, R., Przygrodzka, E., Pawlinski, B., Gajewski, Z., Kaczmarek, M.M. and Meidan, R. 2017. Interferon-tau promotes luteal endothelial cell survival and inhibits specific luteolytic genes in bovine corpus luteum. *Reproduction*. **154**(5), pp.559–568.

Bauersachs, S., Ulbrich, S.E., Gross, K., Schmidt, S.E.M., Meyer, H.H.D., Wenigerkind, H., Vermehren, M., Sinowatz, F., Blum, H. and Wolf, E. 2006.

Embryo-induced transcriptome changes in bovine endometrium reveal species-specific and common molecular markers of uterine receptivity. *Reproduction*. **132**(2), pp.319–331.

De Bem, T.H.C., Tinning, H., Vasconcelos, E.J.R., Wang, D. and Forde, N. 2021. Endometrium On-a-Chip Reveals Insulin- and Glucose-induced Alterations in the Transcriptome and Proteomic Secretome. *Endocrinology*. **162**(6), p.bqab054.

Benson, G. V, Lim, H., Paria, B.C., Satokata, I., Dey, S.K. and Maas, R.L. 1996. Mechanisms of reduced fertility in Hoxa-10 mutant mice: uterine homeosis and loss of maternal Hoxa-10 expression. *Development (Cambridge, England)*. **122**(9), pp.2687–2696.

Berkhout, R.P., Lambalk, C.B., Huirne, J., Mijatovic, V., Repping, S., Hamer, G. and Mastenbroek, S. 2018. High-quality human preimplantation embryos actively influence endometrial stromal cell migration. *Journal of assisted reproduction and genetics*. **35**(4), pp.659–667.

Bernard, D.J., Fortin, J., Wang, Y. and Lamba, P. 2010. Mechanisms of FSH synthesis: what we know, what we don't, and why you should care. *Fertility and Sterility*. **93**(8), pp.2465–2485.

Bhurke, A.S., Bagchi, I.C. and Bagchi, M.K. 2016. Progesterone-Regulated Endometrial Factors Controlling Implantation. *American Journal of Reproductive Immunology*. **75**(3), pp.237–245.

Bi, L., Yang, Q., Yuan, J., Miao, Q., Duan, L., Li, F. and Wang, S. 2016. MicroRNA-127-3p acts as a tumor suppressor in epithelial ovarian cancer by regulating the BAG5 gene. *Oncology reports*. **36**(5), pp.2563–2570.

Bianco-Miotto, T., Craig, J.M., Gasser, Y.P., van Dijk, S.J. and Ozanne, S.E. 2017. Epigenetics and DOHaD: from basics to birth and beyond. *Journal of Developmental Origins of Health and Disease*. **8**(5), pp.513–519.

Bischof, P. and Campana, A. 1997. Trophoblast differentiation and invasion: its significance for human embryo implantation. *Early pregnancy : biology and medicine : the official journal of the Society for the Investigation of Early Pregnancy*. **3**(2), pp.81–95.

Blackshaw, B.P. and Rodger, D. 2021. Why we should not extend the 14-day rule. *Journal of Medical Ethics*. **47**(10), 712 LP – 714.

Blighe, K., Rana, S. and Lewis, M. 2019. EnhancedVolcano: publication-ready volcano plots with enhanced colouring and labeling.

Boeddeker, S.J., Baston-Buest, D.M., Altergot-Ahmad, O., Kruessel, J.S. and Hess, A.P. 2014. Syndecan-1 knockdown in endometrial epithelial cells alters their apoptotic protein profile and enhances the inducibility of apoptosis. *Molecular Human Reproduction*. **20**(6), pp.567–578.

Bolger, A.M., Lohse, M. and Usadel, B. 2014. Trimmomatic: a flexible trimmer for Illumina sequence data. *Bioinformatics (Oxford, England)*. **30**(15), pp.2114–2120.

Boon, R.A. and Vickers, K.C. 2013. Intercellular transport of microRNAs. *Arteriosclerosis, thrombosis, and vascular biology*. **33**(2), pp.186–192.

Bora, G. and Yaba, A. 2021. The role of mitogen-activated protein kinase signaling pathway in endometriosis. *Journal of Obstetrics and Gynaecology*

Research. **47**(5), pp.1610–1623.

Borchert, G.M., Lanier, W. and Davidson, B.L. 2006. RNA polymerase III transcribes human microRNAs. *Nature Structural & Molecular Biology*. **13**(12), pp.1097–1101.

Braakman, I. and Bulleid, N.J. 2011. Protein Folding and Modification in the Mammalian Endoplasmic Reticulum. *Annual Review of Biochemistry*. **80**(1), pp.71–99.

Bradley, S.E., Johnson, A.E., Le, I.P., Oosterhouse, E., Hledin, M.P., Marquez, G.A. and Burnatowska-Hledin, M. 2010. Phosphorylation of VACM-1/Cul5 by protein kinase A regulates its neddylation and antiproliferative effect. *The Journal of biological chemistry*. **285**(7), pp.4883–4895.

Brooks, K., Burns, G. and Spencer, T.E. 2014. Conceptus elongation in ruminants: roles of progesterone, prostaglandin, interferon tau and cortisol. *Journal of animal science and biotechnology*. **5**(1), p.53.

Broughton, J.P., Lovci, M.T., Huang, J.L., Yeo, G.W. and Pasquinelli, A.E. 2016. Pairing beyond the Seed Supports MicroRNA Targeting Specificity. *Molecular cell*. **64**(2), pp.320–333.

Burris, H.H., Gerson, K.D., Woodward, A., Redhunt, A.M., Ledyard, R., Brennan, K., Baccarelli, A.A., Hecht, J.L., Collier, A.-R.Y. and Hacker, M.R. 2023. Cervical microRNA expression and spontaneous preterm birth. *American Journal of Obstetrics & Gynecology MFM*. **5**(1), p.100783.

Bushati, N. and Cohen, S.M. 2007. microRNA Functions. *Annual Review of Cell and Developmental Biology*. **23**(1), pp.175–205.

Cai, M., Kolluru, G.K. and Ahmed, A. 2017. Small Molecule, Big Prospects: MicroRNA in Pregnancy and Its Complications. *Journal of pregnancy*. **2017**, p.6972732.

Camden, A.J., Szwarc, M.M., Chadchan, S.B., DeMayo, F.J., O'Malley, B.W., Lydon, J.P. and Kommagani, R. 2017. Growth regulation by estrogen in breast cancer 1 (GREB1) is a novel progesterone-responsive gene required for human endometrial stromal decidualization. *Molecular human reproduction*. **23**(9), pp.646–653.

Carson, D.D., Lagow, E., Thathiah, A., Al-Shami, R., Farach-Carson, M.C., Vernon, M., Yuan, L., Fritz, M.A. and Lessey, B. 2002. Changes in gene expression during the early to mid-luteal (receptive phase) transition in human endometrium detected by high-density microarray screening. *Molecular Human Reproduction*. **8**(9), pp.871–879.

Cartwright, J.E., Fraser, R., Leslie, K., Wallace, A.E. and James, J.L. 2010. Remodelling at the maternal–fetal interface: relevance to human pregnancy disorders. *REPRODUCTION*. **140**(6), pp.803–813.

Carver, J., Martin, K., Spyropoulou, I., Barlow, D., Sargent, I. and Mardon, H. 2003. An in-vitro model for stromal invasion during implantation of the human blastocyst. *Human Reproduction*. **18**(2), pp.283–290.

Catalanotto, C., Cogoni, C. and Zardo, G. 2016. MicroRNA in Control of Gene Expression: An Overview of Nuclear Functions. *International journal of molecular sciences*. **17**(10), p.1712.

Chakrabarty, A., Tranguch, S., Daikoku, T., Jensen, K., Furneaux, H. and Dey,

S.K. 2007. MicroRNA regulation of cyclooxygenase-2 during embryo implantation. *Proceedings of the National Academy of Sciences*. **104**(38), pp.15144–15149.

Charnock-Jones, D.S., Sharkey, A.M., Fenwick, P. and Smith, S.K. 1994. Leukaemia inhibitory factor mRNA concentration peaks in human endometrium at the time of implantation and the blastocyst contains mRNA for the receptor at this time. *Journal of reproduction and fertility*. **101**(2), pp.421–426.

Chatterjee, N., Fraile-Bethencourt, E., Baris, A., Espinosa-Diez, C. and Anand, S. 2021. MicroRNA-494 Regulates Endoplasmic Reticulum Stress in Endothelial Cells . *Frontiers in Cell and Developmental Biology* . **9**.

Cheloufi, S., Dos Santos, C.O., Chong, M.M.W. and Hannon, G.J. 2010. A dicer-independent miRNA biogenesis pathway that requires Ago catalysis. *Nature*. **465**(7298), pp.584–589.

Chen, C., Zhao, Y., Yu, Y., Li, R. and Qiao, J. 2016. MiR-125b regulates endometrial receptivity by targeting MMP26 in women undergoing IVF-ET with elevated progesterone on HCG priming day. *Scientific reports*. **6**, p.25302.

Chen, J., Wang, M., Guo, M., Xie, Y. and Cong, Y.-S. 2013. miR-127 regulates cell proliferation and senescence by targeting BCL6. *PloS one*. **8**(11), p.e80266.

Chen, L., Wang, D., Wu, Z., Ma, L. and Daley, G.Q. 2010. Molecular basis of the first cell fate determination in mouse embryogenesis. *Cell Research*. **20**(9), pp.982–993.

Chen, Q., Ni, Y., Han, M., Zhou, W.-J., Zhu, X.-B. and Zhang, A.-J. 2020. Integrin-linked kinase improves uterine receptivity formation by activating Wnt/β-catenin signaling and up-regulating MMP-3/9 expression. *American journal of translational research*. **12**(6), pp.3011–3022.

Chen, S., Sun, K.-X., Liu, B.-L., Zong, Z.-H. and Zhao, Y. 2016. MicroRNA-505 functions as a tumor suppressor in endometrial cancer by targeting TGF-alpha. *Molecular cancer*. **15**, p.11.

Chen, X., Zhao, W., Yuan, Y., Bai, Y., Sun, Y., Zhu, W. and Du, Z. 2017. MicroRNAs tend to synergistically control expression of genes encoding extensively-expressed proteins in humans. *PeerJ*. **5**, p.e3682.

Chu, B., Zhong, L., Dou, S., Wang, J., Li, J., Wang, M., Shi, Q., Mei, Y. and Wu, M. 2015. miRNA-181 regulates embryo implantation in mice through targeting leukemia inhibitory factor. *Journal of Molecular Cell Biology*. **7**(1), pp.12–22.

Cindrova-Davies, T., Zhao, X., Elder, K., Jones, C.J.P., Moffett, A., Burton, G.J. and Turco, M.Y. 2021. Menstrual flow as a non-invasive source of endometrial organoids. *Communications Biology*. **4**(1), p.651.

Cirkovic, A., Stanisavljevic, D., Milin-Lazovic, J., Rajovic, N., Pavlovic, V., Milicevic, O., Savic, M., Kostic Peric, J., Aleksic, N., Milic, Nikola, Stanisavljevic, T., Mikovic, Z., Garovic, V. and Milic, Natasa 2021. Preeclamptic Women Have Disrupted Placental microRNA Expression at the Time of Preeclampsia Diagnosis: Meta-Analysis . *Frontiers in Bioengineering and Biotechnology* . **9**.

Clemente, M., Fuente, J. de La, Fair, T., Naib, A. Al, Gutierrez-Adan, A., Roche, J.F., Rizos, D. and Lonergan, P. 2009. Progesterone and conceptus elongation in cattle: a direct effect on the embryo or an indirect effect via the endometrium? *REPRODUCTION*. **138**(3), pp.507–517.

Cole, L.A. 2010. Biological functions of hCG and hCG-related molecules. *Reproductive biology and endocrinology : RB&E*. **8**, p.102.

Cook, J., Bennett, P.R., Kim, S.H., Teoh, T.G., Sykes, L., Kindinger, L.M., Garrett, A., Binkhamis, R., MacIntyre, D.A. and Terzidou, V. 2019. First Trimester Circulating MicroRNA Biomarkers Predictive of Subsequent Preterm Delivery and Cervical Shortening. *Scientific reports*. **9**(1), p.5861.

Corbacho, A.M., Martínez De La Escalera, G. and Clapp, C. 2002. Roles of prolactin and related members of the prolactin/growth hormone/placental lactogen family in angiogenesis. *The Journal of endocrinology*. **173**(2), pp.219–238.

Cork, B.A., Tuckerman, E.M., Li, T.C. and Laird, S.M. 2002. Expression of interleukin (IL)-11 receptor by the human endometrium in vivo and effects of IL-11, IL-6 and LIF on the production of MMP and cytokines by human endometrial cells in vitro. *Molecular human reproduction*. **8**(9), pp.841–848.

Cortez, J., Leiva, B., Torres, C.G., Parraguez, V.H., De los Reyes, M., Carrasco, A. and Peralta, O.A. 2022. Generation and Characterization of Bovine Testicular Organoids Derived from Primary Somatic Cell Populations. *Animals*. **12**(17).

Costa, M.A. 2016. The endocrine function of human placenta: an overview. *Reproductive BioMedicine Online*. **32**(1), pp.14–43.

Costello, L., Fullard, N., Roger, M., Bradbury, S., Dicolandrea, T., Isfort, R., Bascom, C. and Przyborski, S. 2019. Engineering a Multilayered Skin Equivalent: The Importance of Endogenous Extracellular Matrix Maturation to Provide Robustness and Reproducibility BT - Skin Tissue Engineering: Methods and Protocols *In*: S. Böttcher-Haberzeth and T. Biedermann, eds. New York, NY: Springer New York, pp.107–122. Available from: https://doi.org/10.1007/978-1-4939-9473-1_9.

Critchley, H.O.D., Kelly, R.W., Brenner, R.M. and Baird, D.T. 2001. The endocrinology of menstruation – a role for the immune system. *Clinical Endocrinology*. **55**(6), pp.701–710.

Critchley, H.O.D., Maybin, J.A., Armstrong, G.M. and Williams, A.R.W. 2020. Physiology of the endometrium and regulation of menstruation. *Physiological Reviews*. **100**(3), pp.1149–1179.

Cuman, C., Menkhorst, E., Winship, A., Van Sinderen, M., Osianlis, T., Rombauts, L.J. and Dimitriadis, E. 2014. Fetal–maternal communication: the role of Notch signalling in embryo implantation. *REPRODUCTION*. **147**(3), pp.R75–R86.

d'Hauterive, S.P., Close, R., Gridelet, V., Mawet, M., Nisolle, M. and Geenen, V. 2022. Human Chorionic Gonadotropin and Early Embryogenesis: Review. *International Journal of Molecular Sciences*. **23**(3).

Dai, B. and Jiang, J. 2021. Increased miR-188-3p in Ovarian Granulosa Cells of Patients with Polycystic Ovary Syndrome T. Huang, ed. *Computational and Mathematical Methods in Medicine*. **2021**, p.5587412.

Darling, N.J., Mobbs, C.L., González-Hau, A.L., Freer, M. and Przyborski, S. 2020. Bioengineering Novel in vitro Co-culture Models That Represent the Human Intestinal Mucosa With Improved Caco-2 Structure and Barrier Function . *Frontiers in Bioengineering and Biotechnology* . **8**.

Dennery, P.A. 2010. Oxidative stress in development: Nature or nurture? *Free Radical Biology and Medicine*. **49**(7), pp.1147–1151.

Devor, E.J., Gonzalez-Bosquet, J., Thiel, K.W. and Leslie, K.K. 2020. Genomic characterization of five commonly used endometrial cancer cell lines. *International journal of oncology*. **57**(6), pp.1348–1357.

Devoto, L., Kohen, P., Muñoz, A. and Strauss, J.F. 2009. Human corpus luteum physiology and the luteal-phase dysfunction associated with ovarian stimulation. *Reproductive BioMedicine Online*. **18**, pp.S19–S24.

Díez, M.C., Przyborski, S., del Cerro, A., Alonso-Guervós, M., Iglesias-Cabo, T., Carrocera, S., García, M.A., Fernández, M., Alonso, L. and Muñoz, M. 2023. Generation of a novel three-dimensional scaffold-based model of the bovine endometrium. *Veterinary Research Communications*.

Dobin, A., Davis, C.A., Schlesinger, F., Drenkow, J., Zaleski, C., Jha, S., Batut, P., Chaisson, M. and Gingeras, T.R. 2013. STAR: ultrafast universal RNA-seq aligner. *Bioinformatics (Oxford, England)*. **29**(1), pp.15–21.

Donoghue, P.C.J. and Purnell, M.A. 2005. Genome duplication, extinction and vertebrate evolution. *Trends in Ecology & Evolution*. **20**(6), pp.312–319.

Dorostghoal, M., Ghaffari, H.-O.-A., Marmazi, F. and Keikhah, N. 2018. Overexpression of Endometrial Estrogen Receptor-Alpha in The Window of Implantation in Women with Unexplained Infertility. *International journal of fertility & sterility*. **12**(1), pp.37–42.

Van Dort, C., Zhao, P., Parmelee, K., Capps, B., Poel, A., Listenberger, L., Kossoris, J., Wasilevich, B., Murrey, D., Clare, P. and Burnatowska-Hledin, M. 2003. VACM-1, a cul-5 gene, inhibits cellular growth by a mechanism that involves MAPK and p53 signaling pathways. *American Journal of Physiology-Cell Physiology*. **285**(6), pp.C1386–C1396.

Doyle, M., Badertscher, L., Jaskiewicz, L., Güttinger, S., Jurado, S., Hugenschmidt, T., Kutay, U. and Filipowicz, W. 2013. The double-stranded RNA binding domain of human Dicer functions as a nuclear localization signal. *RNA (New York, N.Y.)*. **19**(9), pp.1238–1252.

Dunwell, T.L., Paps, J. and Holland, P.W.H. 2017. Novel and divergent genes in the evolution of placental mammals. *Proceedings. Biological sciences*. **284**(1864), p.20171357.

Edge, J.C., Hume, L., Tinning, H., Wang, D., Taylor, A.S., Ovchinnikov, V., Geijer-Simpson, A. V, Vrljicak, P., Brosens, J.J., Lucas, E.S., Simpson, N.A.B., Shillito, J., Forbes, K., O'Connell, M.J. and Forde, N. 2023. MicroRNAs emerging coordinate with placental mammals alter pathways in endometrial epithelia important for endometrial function. *iScience*. **26**(4), p.106339.

Elhag, D.A. and Al Khodor, S. 2023. Exploring the potential of microRNA as a diagnostic tool for gestational diabetes. *Journal of Translational Medicine*. **21**(1), p.392.

Ellwanger, D.C., Büttner, F.A., Mewes, H.-W. and Stümpflen, V. 2011. The

sufficient minimal set of miRNA seed types. *Bioinformatics (Oxford, England)*. **27**(10), pp.1346–1350.

Elovitz, M.A., Brown, A.G., Anton, L., Gilstrop, M., Heiser, L. and Bastek, J. 2014. Distinct cervical microRNA profiles are present in women destined to have a preterm birth. *American Journal of Obstetrics and Gynecology*. **210**(3), 221.e1-221.e11.

Emera, D., Romero, R. and Wagner, G. 2012. The evolution of menstruation: A new model for genetic assimilation. *BioEssays*. **34**(1), pp.26–35.

Enciso, M., Aizpurua, J., Rodríguez-Estrada, B., Jurado, I., Ferrández-Rives, M., Rodríguez, E., Pérez-Larrea, E., Climent, A.B., Marron, K. and Sarasa, J. 2021. The precise determination of the window of implantation significantly improves ART outcomes. *Scientific Reports*. **11**(1), p.13420.

Enders, A.C., Blankenship, T.N., Lantz, K.C. and Enders, S.S. 1998. Morphological variation in the interhemal areas of chorioallantoic placentae: A review. *Placenta*. **19**, pp.1–19.

Evans, J., Walker, K.J., Bilandzic, M., Kinnear, S. and Salamonsen, L.A. 2020. A novel 'embryo-endometrial' adhesion model can potentially predict 'receptive' or 'non-receptive' endometrium. *Journal of assisted reproduction and genetics*. **37**(1), pp.5–16.

Evans, R.W. and Leavitt, W.W. 1980. Progesterone inhibition of uterine nuclear estrogen receptor: dependence on RNA and protein synthesis. *Proceedings of the National Academy of Sciences*. **77**(10), pp.5856–5860.

Ewels, P., Magnusson, M., Lundin, S. and Käller, M. 2016. MultiQC: summarize analysis results for multiple tools and samples in a single report. *Bioinformatics (Oxford, England)*. **32**(19), pp.3047–3048.

Fallen, S., Baxter, D., Wu, X., Kim, T.-K., Shynlova, O., Lee, M.Y., Scherler, K., Lye, S., Hood, L. and Wang, K. 2018. Extracellular vesicle RNAs reflect placenta dysfunction and are a biomarker source for preterm labour. *Journal of cellular and molecular medicine*. **22**(5), pp.2760–2773.

Fan, H.-Y., Liu, Z., Shimada, M., Sterneck, E., Johnson, P.F., Hedrick, S.M. and Richards, J.S. 2009. MAPK3/1 (ERK1/2) in ovarian granulosa cells are essential for female fertility. *Science (New York, N.Y.)*. **324**(5929), pp.938–941.

Fauser, B.C. and Van Heusden, A.M. 1997. Manipulation of human ovarian function: physiological concepts and clinical consequences. *Endocrine reviews*. **18**(1), pp.71–106.

Fazleabas, A.T., Donnelly, K.M., Srinivasan, S., Fortman, J.D. and Miller, J.B. 1999. Modulation of the baboon (Papio anubis) uterine endometrium by chorionic gonadotrophin during the period of uterine receptivity. *Proceedings of the National Academy of Sciences*. **96**(5), pp.2543–2548.

Fazleabas, A.T. and Kim, J.J. 2003. What Makes an Embryo Stick? *Science*. **299**(5605), pp.355–356.

Fierro-González, J.C., White, M.D., Silva, J.C. and Plachta, N. 2013. Cadherin-dependent filopodia control preimplantation embryo compaction. *Nature Cell Biology*. **15**(12), pp.1424–1433.

Fiore, D., Donnarumma, E., Roscigno, G., Iaboni, M., Russo, V., Affinito, A.,

Adamo, A., De Martino, F., Quintavalle, C., Romano, G., Greco, A., Soini, Y., Brunetti, A., Croce, C.M. and Condorelli, G. 2016. miR-340 predicts glioblastoma survival and modulates key cancer hallmarks through down-regulation of NRAS. *Oncotarget*. **7**(15), pp.19531–19547.

Firmin, J. and Maître, J.-L. 2021. Morphogenesis of the human preimplantation embryo: bringing mechanics to the clinics. *Seminars in Cell & Developmental Biology*. **120**, pp.22–31.

Fitzgerald, H.C., Kelleher, A.M., Ranjit, C., Schust, D.J. and Spencer, T.E. 2023. Basolateral secretions of human endometrial epithelial organoids impact stromal cell decidualization. *Molecular Human Reproduction*. **29**(4), p.gaad007.

Fitzgerald, H.C., Schust, D.J. and Spencer, T.E. 2021. In vitro models of the human endometrium: evolution and application for women's health. *Biology of reproduction*. **104**(2), pp.282–293.

Forde, N., Beltman, M.E., Lonergan, P., Diskin, M., Roche, J.F. and Crowe, M.A. 2011. Oestrous cycles in Bos taurus cattle. *Animal Reproduction Science*. **124**(3), pp.163–169.

Forde, N. and Lonergan, P. 2017. Interferon-tau and fertility in ruminants. *Reproduction*. **154**(5), pp.F33–F43.

Furukawa, S., Kuroda, Y. and Sugiyama, A. 2014. A comparison of the histological structure of the placenta in experimental animals. *Journal of toxicologic pathology*. **27**(1), pp.11–18.

Gaetje, R., Holtrich, U., Engels, K., Kissler, S., Rody, A., Karn, T. and Kaufmann, M. 2008. Differential expression of claudins in human endometrium and endometriosis. *Gynecological Endocrinology*. **24**(8), pp.442–449.

Galán, A., O'Connor, J.E., Valbuena, D., Herrer, R., Remohí, J., Pampfer, S., Pellicer, A. and Simón, C. 2000. The Human Blastocyst Regulates Endometrial Epithelial Apoptosis in Embryonic Adhesion1. *Biology of Reproduction*. **63**(2), pp.430–439.

Gao, F., Bian, F., Ma, X., Kalinichenko, V. V and Das, S.K. 2015. Control of regional decidualization in implantation: Role of FoxM1 downstream of Hoxa10 and cyclin D3. *Scientific Reports*. **5**(1), p.13863.

Garrido-Gómez, T., Dominguez, F., Quiñonero, A., Estella, C., Vilella, F., Pellicer, A. and Simon, C. 2012. Annexin A2 is critical for embryo adhesiveness to the human endometrium by RhoA activation through F-actin regulation. *The FASEB Journal*. **26**(9), pp.3715–3727.

Garrido-Gomez, T., Quiñonero, A., Dominguez, F., Rubert, L., Perales, A., Hajjar, K.A. and Simon, C. 2020. Preeclampsia: a defect in decidualization is associated with deficiency of Annexin A2. *American Journal of Obstetrics and Gynecology*. **222**(4), 376.e1-376.e17.

Gauster, M., Moser, G., Wernitznig, S., Kupper, N. and Huppertz, B. 2022. Early human trophoblast development: from morphology to function. *Cellular and Molecular Life Sciences*. **79**(6), p.345.

Ge, Q., Zhu, Y., Li, H., Tian, F., Xie, X. and Bai, Y. 2015. Differential expression of circulating miRNAs in maternal plasma in pregnancies with fetal macrosomia. *International journal of molecular medicine*. **35**(1), pp.81–91.

Gebremedhn, S., Salilew-Wondim, D., Hoelker, M., Held-Hoelker, E., Neuhoff, C., Tholen, E., Schellander, K. and Tesfaye, D. 2018. Exploring maternal serum microRNAs during early pregnancy in cattle. *Theriogenology*. **121**, pp.196–203.

Gellersen, B. and Brosens, J. 2003. Cyclic AMP and progesterone receptor cross-talk in human endometrium: a decidualizing affair. *The Journal of endocrinology*. **178**(3), pp.357–372.

Gellersen, B. and Brosens, J.J. 2014. Cyclic Decidualization of the Human Endometrium in Reproductive Health and Failure. *Endocrine Reviews*. **35**(6), pp.851–905.

Gellersen, B., Wolf, A., Kruse, M., Schwenke, M. and Bamberger, A.-M. 2013. Human endometrial stromal cell-trophoblast interactions: mutual stimulation of chemotactic migration and promigratory roles of cell surface molecules CD82 and CEACAM1. *Biology of reproduction*. **88**(3), p.80.

Genbacev, O.D., Prakobphol, A., Foulk, R.A., Krtolica, A.R., Ilic, D., Singer, M.S., Yang, Z.-Q., Kiessling, L.L., Rosen, S.D. and Fisher, S.J. 2003. Trophoblast L-selectin-mediated adhesion at the maternal-fetal interface. *Science (New York, N.Y.)*. **299**(5605), pp.405–408.

Georgadaki, K., Khoury, N., Spandidos A., D. and Zoumpourlis, V. 2016. The molecular basis of fertilization (Review). *Int J Mol Med*. **38**(4), pp.979–986.

Germeyer, A., Klinkert, M.S., Huppertz, A.-G., Clausmeyer, S., Popovici, R.M., Strowitzki, T. and von Wolff, M. 2007. Expression of syndecans, cell–cell interaction regulating heparan sulfate proteoglycans, within the human endometrium and their regulation throughout the menstrual cycle. *Fertility and Sterility*. **87**(3), pp.657–663.

Gilad, S., Meiri, E., Yogev, Y., Benjamin, S., Lebanony, D., Yerushalmi, N., Benjamin, H., Kushnir, M., Cholakh, H., Melamed, N., Bentwich, Z., Hod, M., Goren, Y. and Chajut, A. 2008. Serum MicroRNAs Are Promising Novel Biomarkers. *PLOS ONE*. **3**(9), p.e3148.

Girsh, E., Milvae, R.A., Wang, W. and Meidan, R. 1996. Effect of endothelin-1 on bovine luteal cell function: role in prostaglandin F2alpha-induced antisteroidogenic action. *Endocrinology*. **137**(4), pp.1306–1312.

Giudice, L.C. 1999. Potential biochemical markers of uterine receptivity. *Human Reproduction*. **14**(suppl_2), pp.3–16.

Gleeson, L.M., Chakraborty, C., McKinnon, T. and Lala, P.K. 2001. Insulin-Like Growth Factor-Binding Protein 1 Stimulates Human Trophoblast Migration by Signaling through α5β1 Integrin via Mitogen-Activated Protein Kinase Pathway1. *The Journal of Clinical Endocrinology & Metabolism*. **86**(6), pp.2484–2493.

Gomez-Roman, N., Stevenson, K., Gilmour, L., Hamilton, G. and Chalmers, A.J. 2017. A novel 3D human glioblastoma cell culture system for modeling drug and radiation responses. *Neuro-Oncology*. **19**(2), pp.229–241.

Gougeon, A. 2003. Dynamics for Human Growth: Morphologic, Dynamic and Functional Aspects. *The ovary*. **2**, pp.25–43.

Graham, J.D. and Clarke, C.L. 1997. Physiological Action of Progesterone in Target Tissues*. *Endocrine Reviews*. **18**(4), pp.502–519.

Grasso, E., Gori, S., Soczewski, E., Fernández, L., Gallino, L., Vota, D., Martínez, G., Irigoyen, M., Ruhlmann, C., Lobo, T.F., Salamone, G., Mattar, R., Daher, S., Leirós, C.P. and Ramhorst, R. 2018. Impact of the Reticular Stress and Unfolded Protein Response on the inflammatory response in endometrial stromal cells. *Scientific reports*. **8**(1), p.12274.

Gray, C.A., Bartol, F.F., Tarleton, B.J., Wiley, A.A., Johnson, G.A., Bazer, F.W. and Spencer, T.E. 2001. Developmental Biology of Uterine Glands1. *Biology of Reproduction*. **65**(5), pp.1311–1323.

Green, C., Chatterjee, R., McGarrigle, H.H., Ahmed, F. and Thomas, N.S. 2000. p107 is active in the nucleolus in non-dividing human granulosa lutein cells. *Journal of Molecular Endocrinology*. **25**(3), pp.275–286.

Greening, D.W., Nguyen, H.P.T., Elgass, K., Simpson, R.J. and Salamonsen, L.A. 2016. Human Endometrial Exosomes Contain Hormone-Specific Cargo Modulating Trophoblast Adhesive Capacity: Insights into Endometrial-Embryo Interactions1. *Biology of Reproduction*. **94**(2), pp.1-15,38.

Greil, A.L., Slauson-Blevins, K. and McQuillan, J. 2010. The experience of infertility: a review of recent literature. *Sociology of Health & Illness*. **32**(1), pp.140–162.

Grewal, S., Carver, J.G., Ridley, A.J. and Mardon, H.J. 2008. Implantation of the human embryo requires Rac1-dependent endometrial stromal cell migration. *Proceedings of the National Academy of Sciences of the United States of America*. **105**(42), pp.16189–16194.

Grimson, A., Farh, K.K.-H., Johnston, W.K., Garrett-Engele, P., Lim, L.P. and Bartel, D.P. 2007. MicroRNA targeting specificity in mammals: determinants beyond seed pairing. *Molecular cell*. **27**(1), pp.91–105.

von Grothusen, C., Frisendahl, C., Modhukur, V., Lalitkumar, P.G., Peters, M., Faridani, O.R., Salumets, A., Boggavarapu, N.R. and Gemzell-Danielsson, K. 2022. Uterine fluid microRNAs are dysregulated in women with recurrent implantation failure. *Human Reproduction*. **37**(4), pp.734–746.

Grümmer, R., Hohn, H.-P., Mareel, M.M. and Denker, H.-W. 1994. Adhesion and invasion of three human choriocarcinoma cell lines into human endometrium in a three-dimensional organ culture system. *Placenta*. **15**(4), pp.411–429.

Gu, W., Xu, Y., Xie, X., Wang, T., Ko, J.-H. and Zhou, T. 2014. The role of RNA structure at 5' untranslated region in microRNA-mediated gene regulation. *RNA (New York, N.Y.)*. **20**(9), pp.1369–1375.

Gude, N.M., Roberts, C.T., Kalionis, B. and King, R.G. 2004. Growth and function of the normal human placenta. *Thrombosis Research*. **114**(5–6), pp.397–407.

Guernsey, M.W., Chuong, E.B., Cornelis, G., Renfree, M.B. and Baker, J.C. 2017. Molecular conservation of marsupial and eutherian placentation and lactation A. Rokas, ed. *eLife*. **6**, p.e27450.

Guerra-Assunção, J.A. and Enright, A.J. 2012. Large-scale analysis of microRNA evolution. *BMC Genomics*. **13**(1), p.218.

Guillomot, M., Fléchon, J.-E. and Wintenberger-Torres, S. 1981. Conceptus attachment in the Ewe: an ultrastructural study. *Placenta*. **2**(2), pp.169–

181.

Gundamaraju, R., Vemuri, R., Chong, W.C., Myers, S., Norouzi, S., Shastri, M.D. and Eri, R. 2018. Interplay between Endoplasmic Reticular Stress and Survivin in Colonic Epithelial Cells. *Cells*. **7**(10).

Gundling Jr, W.E. and Wildman, D.E. 2015. A review of inter- and intraspecific variation in the eutherian placenta. *Philosophical transactions of the Royal Society of London. Series B, Biological sciences*. **370**(1663), p.20140072.

Guo, J., Zhou, W., Sacco, M., Downing, P., Dimitriadis, E. and Zhao, F. 2023. Using organoids to investigate human endometrial receptivity. *Frontiers in endocrinology*. **14**, p.1158515.

Guo, L., Liu, Y., Guo, Y., Yang, Y. and Chen, B. 2018. MicroRNA-423–5p inhibits the progression of trophoblast cells via targeting IGF2BP1. *Placenta*. **74**, pp.1–8.

Guzewska, M.M., Szuszkiewicz, J. and Kaczmarek, M.M. 2023. Extracellular vesicles: Focus on peri-implantation period of pregnancy in pigs. *Molecular Reproduction and Development*. **90**(7), pp.634–645.

Hamilton, M.J., Davidson, A.D., Sibly, R.M. and Brown, J.H. 2011. Universal scaling of production rates across mammalian lineages. *Proceedings. Biological sciences*. **278**(1705), pp.560–566.

Han, S.W., Lei, Z.M. and Rao, C.V. 1999. Treatment of human endometrial stromal cells with chorionic gonadotropin promotes their morphological and functional differentiation into decidua. *Molecular and Cellular Endocrinology*. **147**(1), pp.7–16.

Hanahan, D. 2022. Hallmarks of Cancer: New Dimensions. *Cancer Discovery*. **12**(1), pp.31–46.

Harapan, H. and Andalas, M. 2015. The role of microRNAs in the proliferation, differentiation, invasion, and apoptosis of trophoblasts during the occurrence of preeclampsia—A systematic review. *Tzu Chi Medical Journal*. **27**(2), pp.54–64.

Hayder, H., O'Brien, J., Nadeem, U. and Peng, C. 2018. MicroRNAs: crucial regulators of placental development. *Reproduction*. **155**(6), pp.R259–R271.

Heimberg, A.M., Sempere, L.F., Moy, V.N., Donoghue, P.C.J. and Peterson, K.J. 2008. MicroRNAs and the advent of vertebrate morphological complexity. *Proceedings of the National Academy of Sciences*. **105**(8), pp.2946–2950.

Hemmings, B.A. and Restuccia, D.F. 2012. PI3K-PKB/Akt pathway. *Cold Spring Harbor perspectives in biology*. **4**(9), p.a011189.

Hertel, J., Lindemeyer, M., Missal, K., Fried, C., Tanzer, A., Flamm, C., Hofacker, I.L., Stadler, P.F. and 2005, T.S. of B.C.L. 2004 and 2006. The expansion of the metazoan microRNA repertoire. *BMC Genomics*. **7**(1), p.25.

Hill, D.S., Robinson, N.D.P., Caley, M.P., Chen, M., O'Toole, E.A., Armstrong, J.L., Przyborski, S. and Lovat, P.E. 2015. A Novel Fully Humanized 3D Skin Equivalent to Model Early Melanoma Invasion. *Molecular Cancer Therapeutics*. **14**(11), pp.2665–2673.

Hiraoka, T., Hirota, Y., Fukui, Y., Gebril, M., Kaku, T., Aikawa, S., Hirata, T.,

Akaeda, S., Matsuo, M., Haraguchi, H., Saito-Kanatani, M., Shimizu-Hirota, R., Takeda, N., Yoshino, O., Fujii, T. and Osuga, Y. 2020. Differential roles of uterine epithelial and stromal STAT3 coordinate uterine receptivity and embryo attachment. *Scientific reports*. **10**(1), p.15523.

Holmberg, J.C., Haddad, S., Wünsche, V., Yang, Y., Aldo, P.B., Gnainsky, Y., Granot, I., Dekel, N. and Mor, G. 2012. An In Vitro Model for the Study of Human Implantation. *American Journal of Reproductive Immunology*. **67**(2), pp.169–178.

Hong, L., Yu, T., Xu, H., Hou, N., Cheng, Q., Lai, L., Wang, Q., Sheng, J. and Huang, H. 2018. Down-regulation of miR-378a-3p induces decidual cell apoptosis: a possible mechanism for early pregnancy loss. *Human reproduction (Oxford, England)*. **33**(1), pp.11–22.

Hong, X., Luense, L.J., McGinnis, L.K., Nothnick, W.B. and Christenson, L.K. 2008. Dicer1 Is Essential for Female Fertility and Normal Development of the Female Reproductive System. *Endocrinology*. **149**(12), pp.6207–6212.

Horne, A.W., White, J.O., Margara, R.A., Williams, R., Winston, R.M.L. and Lalani, E.-N. 2001. MUC 1: a genetic susceptibility to infertility? *The Lancet*. **357**(9265), pp.1336–1337.

Hosseini, M.K., Gunel, T., Gumusoglu, E., Benian, A. and Aydinli, K. 2018. MicroRNA expression profiling in placenta and maternal plasma in early pregnancy loss. *Molecular medicine reports*. **17**(4), pp.4941–4952.

Huang, K., Chen, G., Fan, W. and Hu, L. 2020. miR-23a-3p increases endometrial receptivity via CUL3 during embryo implantation. *Journal of Molecular Endocrinology*. **65**(2), pp.35–44.

Huang, L., Shen, Z., Xu, Q., Huang, X., Chen, Q. and Li, D. 2013. Increased levels of microRNA-424 are associated with the pathogenesis of fetal growth restriction. *Placenta*. **34**(7), pp.624–627.

Huang, X., Liu, H. and Li, R. 2017. Prostaglandin E(2) promotes BeWo spheroids implantation in RL95-2 cell monolayers. *Gynecological endocrinology : the official journal of the International Society of Gynecological Endocrinology*. **33**(7), pp.548–552.

Hughes, P., Marshall, D., Reid, Y., Parkes, H. and Gelber, C. 2007. The costs of using unauthenticated, over-passaged cell lines: how much more data do we need? *BioTechniques*. **43**(5), pp.575–586.

Human Fertilisation and Embryology Authority 2008. Human Fertilisation and Embryology Act.

Hunter, M.G., Robinson, R.S., Mann, G.E. and Webb, R. 2004. Endocrine and paracrine control of follicular development and ovulation rate in farm species. *Animal Reproduction Science*. **82**–**83**, pp.461–477.

Huntzinger, E. and Izaurralde, E. 2011. Gene silencing by microRNAs: contributions of translational repression and mRNA decay. *Nature Reviews Genetics*. **12**(2), pp.99–110.

Huyen, D. V and Bany, B.M. 2011. Evidence for a conserved function of heart and neural crest derivatives expressed transcript 2 in mouse and human decidualization. *Reproduction (Cambridge, England)*. **142**(2), pp.353–368.

Ibáñez-Ventoso, C., Vora, M. and Driscoll, M. 2008. Sequence relationships

among C. elegans, D. melanogaster and human microRNAs highlight the extensive conservation of microRNAs in biology. *PloS one*. **3**(7), pp.e2818–e2818.

Imakawa, K., Bai, R., Fujiwara, H., Ideta, A., Aoyagi, Y. and Kusama, K. 2017. Continuous model of conceptus implantation to the maternal endometrium. *Journal of Endocrinology*. **233**(1), pp.R53–R65.

Imakawa, K., Matsuno, Y. and Fujiwara, H. 2022. New Roles for EVs, miRNA and lncRNA in Bovine Embryo Implantation . *Frontiers in Veterinary Science* . **9**.

Ioannidis, J. and Donadeu, F.X. 2016. Circulating miRNA signatures of early pregnancy in cattle. *BMC Genomics*. **17**(1), p.184.

Ito, M., Sferruzzi-Perri, A.N., Edwards, C.A., Adalsteinsson, B.T., Allen, S.E., Loo, T.-H., Kitazawa, M., Kaneko-Ishino, T., Ishino, F., Stewart, C.L. and Ferguson-Smith, A.C. 2015. A trans-homologue interaction between reciprocally imprinted miR-127 and Rtl1 regulates placenta development. *Development (Cambridge, England)*. **142**(14), pp.2425–2430.

Iwata, K., Yumoto, K., Sugishima, M., Mizoguchi, C., Kai, Y., Iba, Y. and Mio, Y. 2014. Analysis of compaction initiation in human embryos by using time-lapse cinematography. *Journal of assisted reproduction and genetics*. **31**(4), pp.421–426.

Jabbour, H.N. and Critchley, H.O. 2001. Potential roles of decidual prolactin in early pregnancy. *Reproduction*. **121**(2), pp.197–205.

Jasper, M.J., Tremellen, K.P. and Robertson, S.A. 2007. Reduced expression of IL-6 and IL-1α mRNAs in secretory phase endometrium of women with recurrent miscarriage. *Journal of Reproductive Immunology*. **73**(1), pp.74–84.

Jiang, Y., Liao, Y., He, H., Xin, Q., Tu, Z., Kong, S., Cui, T., Wang, B., Quan, S., Li, B., Zhang, S. and Wang, H. 2015. FoxM1 Directs STAT3 Expression Essential for Human Endometrial Stromal Decidualization. *Scientific Reports*. **5**(1), p.13735.

Jinghua, H., Qinghua, Z., Chenchen, C., Lili, C., Xiao, X., Yunfei, W., Zhengzhe, A., Changxiu, L. and Hui, H. 2021. MicroRNA miR-92a-3p regulates breast cancer cell proliferation and metastasis via regulating B-cell translocation gene 2 (BTG2). *Bioengineered*. **12**(1), pp.2033–2044.

Jonczyk, A.W., Piotrowska-Tomala, K.K. and Skarzynski, D.J. 2019. Effects of prostaglandin F2α (PGF2α) on cell-death pathways in the bovine corpus luteum (CL). *BMC Veterinary Research*. **15**(1), p.416.

Kagawa, H., Javali, A., Khoei, H.H., Sommer, T.M., Sestini, G., Novatchkova, M., Scholte op Reimer, Y., Castel, G., Bruneau, A., Maenhoudt, N., Lammers, J., Loubersac, S., Freour, T., Vankelecom, H., David, L. and Rivron, N. 2022. Human blastoids model blastocyst development and implantation. *Nature*. **601**(7894), pp.600–605.

Kajihara, T., Brosens, J.J. and Ishihara, O. 2013. The role of FOXO1 in the decidual transformation of the endometrium and early pregnancy. *Medical Molecular Morphology*. **46**(2), pp.61–68.

Kamijo, S., Hamatani, T., Sasaki, H., Suzuki, H., Abe, A., Inoue, O., Iwai, M., Ogawa, S., Odawara, K., Tanaka, K., Mikashima, M., Suzuki, M., Miyado,

K., Matoba, R., Odawara, Y. and Tanaka, M. 2022. MicroRNAs secreted by human preimplantation embryos and IVF outcome. *Reproductive Biology and Endocrinology*. **20**(1), p.130.

Kang, Y.-J., Lees, M., Matthews, L.C., Kimber, S.J., Forbes, K. and Aplin, J.D. 2015. miR-145 suppresses embryo–epithelial juxtacrine communication at implantation by modulating maternal IGF1R. *Journal of Cell Science*. **128**(4), pp.804–814.

Karthaus, W.R., Iaquinta, P.J., Drost, J., Gracanin, A., van Boxtel, R., Wongvipat, J., Dowling, C.M., Gao, D., Begthel, H., Sachs, N., Vries, R.G.J., Cuppen, E., Chen, Y., Sawyers, C.L. and Clevers, H.C. 2014. Identification of multipotent luminal progenitor cells in human prostate organoid cultures. *Cell*. **159**(1), pp.163–175.

Kassambara, A. 2023. rstatix: Pipe-Friendly Framework for Basic Statistical Tests.

Kelleher, A.M., DeMayo, F.J. and Spencer, T.E. 2019. Uterine Glands: Developmental Biology and Functional Roles in Pregnancy. *Endocrine reviews*. **40**(5), pp.1424–1445.

Kessler, M., Hoffmann, K., Brinkmann, V., Thieck, O., Jackisch, S., Toelle, B., Berger, H., Mollenkopf, H.-J., Mangler, M., Sehouli, J., Fotopoulou, C. and Meyer, T.F. 2015. The Notch and Wnt pathways regulate stemness and differentiation in human fallopian tube organoids. *Nature communications*. **6**, p.8989.

Kim Hyung, D., Lu, Q. and Chen, Y. 2019. Claudin-7 modulates cell-matrix adhesion that controls cell migration, invasion and attachment of human HCC827 lung cancer cells. *Oncol Lett*. **17**(3), pp.2890–2896.

Kim, M.R., Park, D.W., Lee, J.H., Choi, D.S., Hwang, K.J., Ryu, H.S. and Min, C.K. 2005. Progesterone-dependent release of transforming growth factor-beta1 from epithelial cells enhances the endometrial decidualization by turning on the Smad signalling in stromal cells. *Molecular Human Reproduction*. **11**(11), pp.801–808.

Kishi, H., Kitahara, Y., Imai, F., Nakao, K. and Suwa, H. 2018. Expression of the gonadotropin receptors during follicular development. *Reproductive medicine and biology*. **17**(1), pp.11–19.

Klisch, K. and Mess, A. 2007. Evolutionary Differentiation of Cetartiodactyl Placentae in the Light of the Viviparity-Driven Conflict Hypothesis. *Placenta*. **28**(4), pp.353–360.

Knight, E., Murray, B., Carnachan, R. and Przyborski, S. 2011. Alvetex®: Polystyrene Scaffold Technology for Routine Three Dimensional Cell Culture BT - 3D Cell Culture: Methods and Protocols *In*: J. W. Haycock, ed. Totowa, NJ: Humana Press, pp.323–340. Available from: https://doi.org/10.1007/978-1-60761-984-0_20.

Knox, K. and Baker, J.C. 2008. Genomic evolution of the placenta using co-option and duplication and divergence. *Genome Research* . **18**(5), pp.695–705.

Kokkinos, M.I., Murthi, P., Wafai, R., Thompson, E.W. and Newgreen, D.F. 2010. Cadherins in the human placenta – epithelial–mesenchymal transition (EMT) and placental development. *Placenta*. **31**(9), pp.747–755.

Kozieł, M.J., Kowalska, K. and Piastowska-Ciesielska, A.W. 2020. Claudins: New Players in Human Fertility and Reproductive System Cancers. *Cancers*. **12**(3).

Kumar, P. and Sait, S.F. 2011. Luteinizing hormone and its dilemma in ovulation induction. *Journal of human reproductive sciences*. **4**(1), pp.2–7.

Kuokkanen, S., Chen, B., Ojalvo, L., Benard, L., Santoro, N. and Pollard, J.W. 2010. Genomic Profiling of MicroRNAs and Messenger RNAs Reveals Hormonal Regulation in MicroRNA Expression in Human Endometrium1. *Biology of Reproduction*. **82**(4), pp.791–801.

Kwon, M.J. 2013. Emerging roles of claudins in human cancer. *International journal of molecular sciences*. **14**(9), pp.18148–18180.

Lal-Nag, M. and Morin, P.J. 2009. The claudins. *Genome biology*. **10**(8), p.235.

Lalitkumar, P.G.L., Lalitkumar, S., Meng, C.X., Stavreus-Evers, A., Hambiliki, F., Bentin-Ley, U. and Gemzell-Danielsson, K. 2007. Mifepristone, but not levonorgestrel, inhibits human blastocyst attachment to an in vitro endometrial three-dimensional cell culture model. *Human Reproduction*. **22**(11), pp.3031–3037.

Large, M.J. and DeMayo, F.J. 2012. The regulation of embryo implantation and endometrial decidualization by progesterone receptor signaling. *Molecular and cellular endocrinology*. **358**(2), pp.155–165.

Latendresse, G. and Founds, S. 2015. The Fascinating and Complex Role of the Placenta in Pregnancy and Fetal Well-being. *Journal of Midwifery & Women's Health*. **60**(4), pp.360–370.

Laviolette, L.A., Hodgkinson, K.M., Minhas, N., Perez-Iratxeta, C. and Vanderhyden, B.C. 2014. 17β-estradiol upregulates GREB1 and accelerates ovarian tumor progression in vivo. *International Journal of Cancer*. **135**(5), pp.1072–1084.

Lawson, E.F., Ghosh, A., Blanch, V., Grupen, C.G., Aitken, R.J., Lim, R., Drury, H.R., Baker, M.A., Gibb, Z. and Tanwar, P.S. 2023. Establishment and characterization of oviductal organoids from farm and companion animals†. *Biology of Reproduction*. **108**(6), pp.854–865.

Lee, H., Han, S., Kwon, C.S. and Lee, D. 2016. Biogenesis and regulation of the let-7 miRNAs and their functional implications. *Protein & cell*. **7**(2), pp.100–113.

Lee, K., Guerrero-Zotano, A.L., Servetto, A., Sudhan, D.R., Lin, C.-C., Formisano, L., Jansen, V.M., González-Ericsson, P., Sanders, M.E., Stricker, T.P., Raj, G., Dean, K.M., Fiolka, R., Cantley, L.C., Hanker, A.B. and Arteaga, C.L. 2020. Proline rich 11 (PRR11) overexpression amplifies PI3K signaling and promotes antiestrogen resistance in breast cancer. *Nature Communications*. **11**(1), p.5488.

Lee, K., Jeong, J., Kwak, I., Yu, C.-T., Lanske, B., Soegiarto, D.W., Toftgard, R., Tsai, M.-J., Tsai, S., Lydon, J.P. and DeMayo, F.J. 2006. Indian hedgehog is a major mediator of progesterone signaling in the mouse uterus. *Nature Genetics*. **38**(10), pp.1204–1209.

Lee, K.Y. and DeMayo, F.J. 2004. Animal models of implantation. *Reproduction*. **128**(6), pp.679–695.

Lee, R.C., Feinbaum, R.L. and Ambros, V. 1993. The C. elegans heterochronic gene lin-4 encodes small RNAs with antisense complementarity to lin-14. *Cell*. **75**(5), pp.843–854.

Lee, Y., Kim, M., Han, J., Yeom, K.-H., Lee, S., Baek, S.H. and Kim, V.N. 2004. MicroRNA genes are transcribed by RNA polymerase II. *The EMBO journal*. **23**(20), pp.4051–4060.

Légaré, C., Clément, A.-A., Desgagné, V., Thibeault, K., White, F., Guay, S.-P., Arsenault, B.J., Scott, M.S., Jacques, P.-É., Perron, P., Guérin, R., Hivert, M.-F. and Bouchard, L. 2022. Human plasma pregnancy-associated miRNAs and their temporal variation within the first trimester of pregnancy. *Reproductive Biology and Endocrinology*. **20**(1), p.14.

Lejeune, B., Van Hoeck, J. and Leroy, F. 1981. Transmitter role of the luminal uterine epithelium in the induction of decidualization in rats. *Reproduction*. **61**(1), pp.235–240.

Lessey, B.A., Killam, A.P., Metzger, D.A., Haney, A.F., Greene, G.L. and McCarty JR., K.S. 1988. Immunohistochemical Analysis of Human Uterine Estrogen and Progesterone Receptors Throughout the Menstrual Cycle*. *The Journal of Clinical Endocrinology & Metabolism*. **67**(2), pp.334–340.

Lessey, B.A. and Young, S.L. 2019a. Chapter 9 - Structure, Function, and Evaluation of the Female Reproductive Tract *In*: J. F. Strauss and R. L. B. T.-Y. and J. R. E. (Eighth E. Barbieri, eds. Philadelphia: Elsevier, pp.206-247.e13. Available from: https://www.sciencedirect.com/science/article/pii/B9780323479127000093.

Lessey, B.A. and Young, S.L. 2019b. What exactly is endometrial receptivity? *Fertility and Sterility*. **111**(4), pp.611–617.

Li, J., Chigurupati, S., Agarwal, R., Mughal, M.R., Mattson, M.P., Becker, K.G., Wood, W.H. 3rd, Zhang, Y. and Morin, P.J. 2009. Possible angiogenic roles for claudin-4 in ovarian cancer. *Cancer biology & therapy*. **8**(19), pp.1806–1814.

Li, J., Shao, W. and Feng, H. 2019. MiR-542-3p, a microRNA targeting CDK14, suppresses cell proliferation, invasiveness, and tumorigenesis of epithelial ovarian cancer. *Biomedicine & Pharmacotherapy*. **110**, pp.850–856.

Li, K., Yu, H., Zhao, C., Li, J., Tan, R. and Chen, L. 2021. Down-regulation of PRR11 affects the proliferation, migration and invasion of osteosarcoma by inhibiting the Wnt/β-catenin pathway. *Journal of Cancer*. **12**(22), pp.6656–6664.

Li, L., Sun, Y., Wu, J., Li, X., Luo, M. and Wang, G. 2015. The global effect of heat on gene expression in cultured bovine mammary epithelial cells. *Cell stress & chaperones*. **20**(2), pp.381–389.

Li, Q., Kannan, A., DeMayo, F.J., Lydon, J.P., Cooke, P.S., Yamagishi, H., Srivastava, D., Bagchi, M.K. and Bagchi, I.C. 2011. The Antiproliferative Action of Progesterone in Uterine Epithelium Is Mediated by Hand2. *Science*. **331**(6019), pp.912–916.

Li, Q., Liu, W., Chiu, P.C.N. and Yeung, W.S.B. 2020. Mir-let-7a/g Enhances Uterine Receptivity via Suppressing Wnt/β-Catenin Under the Modulation of Ovarian Hormones. *Reproductive Sciences*. **27**(5), pp.1164–1174.

Li, R., Qiao, J., Wang, L., Li, L., Zhen, X., Liu, P. and Zheng, X. 2011.

MicroRNA array and microarray evaluation of endometrial receptivity in patients with high serum progesterone levels on the day of hCG administration. *Reproductive Biology and Endocrinology*. **9**(1), p.29.

Li, Z., Wong, K.Y., Calin, G.A., Chng, W.-J., Chan, G.C.-F. and Chim, C.S. 2019. Epigenetic silencing of miR-340-5p in multiple myeloma: mechanisms and prognostic impact. *Clinical epigenetics*. **11**(1), p.71.

Li, Z., Xu, R. and Li, N. 2018. MicroRNAs from plants to animals, do they define a new messenger for communication? *Nutrition & Metabolism*. **15**(1), p.68.

Lian, J., Zhu, X., Du, J., Huang, B., Zhao, F., Ma, C., Guo, R., Zhang, Y., Ji, L., Yahaya, B.H. and Lin, J. 2023. Extracellular vesicle-transmitted miR-671-5p alleviates lung inflammation and injury by regulating the AAK1/NF-κB axis. *Molecular Therapy*. **31**(5), pp.1365–1382.

Liao, Y., Smyth, G.K. and Shi, W. 2014. featureCounts: an efficient general purpose program for assigning sequence reads to genomic features. *Bioinformatics (Oxford, England)*. **30**(7), pp.923–930.

Liao, Y., Wang, J., Jaehnig, E.J., Shi, Z. and Zhang, B. 2019. WebGestalt 2019: gene set analysis toolkit with revamped UIs and APIs. *Nucleic acids research*. **47**(W1), pp.W199–W205.

Lim, H., Paria, B.C., Das, S.K., Dinchuk, J.E., Langenbach, R., Trzaskos, J.M. and Dey, S.K. 1997. Multiple Female Reproductive Failures in Cyclooxygenase 2–Deficient Mice. *Cell*. **91**(2), pp.197–208.

Lin, J.-C., Kuo, C.-Y., Tsai, J.-T. and Liu, W.-H. 2021. miR-671-5p Inhibition by MSI1 Promotes Glioblastoma Tumorigenesis via Radioresistance, Tumor Motility and Cancer Stem-like Cell Properties. *Biomedicines*. **10**(1).

Lipecki, J., Mitchell, A.E., Muter, J., Lucas, E.S., Makwana, K., Fishwick, K., Odendaal, J., Hawkes, A., Vrljicak, P., Brosens, J.J. and Ott, S. 2022. EndoTime: non-categorical timing estimates for luteal endometrium. *Human Reproduction*. **37**(4), pp.747–761.

Liu, D., Lin, L., Wang, Y., Chen, Lu, He, Y., Luo, Y., Qi, L., Guo, Y., Chen, Liwei, Han, Z., Li, G., Li, Q., Liu, Z., Chen, P. and Guo, H. 2020. PNO1, which is negatively regulated by miR-340-5p, promotes lung adenocarcinoma progression through Notch signaling pathway. *Oncogenesis*. **9**(5), p.58.

Liu, J., Guo, S., Zhang, T., Ma, X., Wu, Z., Jiang, K., Zhang, X., Guo, X. and Deng, G. 2020. MiR-505 as an anti-inflammatory regulator suppresses HMGB1/NF-κB pathway in lipopolysaccharide-mediated endometritis by targeting HMGB1. *International Immunopharmacology*. **88**, p.106912.

Liu, N., Okamura, K., Tyler, D.M., Phillips, M.D., Chung, W.-J. and Lai, E.C. 2008. The evolution and functional diversification of animal microRNA genes. *Cell Research*. **18**(10), pp.985–996.

Liu, X., Zhao, H., Li, W., Bao, H., Qu, Q. and Ma, D. 2020. Up-regulation of miR-145 may contribute to repeated implantation failure after IVF–embryo transfer by targeting PAI-1. *Reproductive BioMedicine Online*. **40**(5), pp.627–636.

Logan, P.C., Ponnampalam, A.P., Steiner, M. and Mitchell, M.D. 2013. Effect of cyclic AMP and estrogen/progesterone on the transcription of DNA methyltransferases during the decidualization of human endometrial

stromal cells. *Molecular Human Reproduction*. **19**(5), pp.302–312.

Lonergan, P. and Forde, N. 2014. Maternal-embryo interaction leading up to the initiation of implantation of pregnancy in cattle. *animal*. **8**(s1), pp.64–69.

Lorenzi, T., Turi, A., Morroni, M., Vitali, A., Tranquilli, A.L., David, G., Castellucci, M. and Marzioni, D. 2011. Modulation of syndecans in the uterus throughout the menstrual cycle: comparison between endometrium and myometrium. *Fertility and Sterility*. **95**(8), pp.2608-2611.e1.

Loscalzo, G., Scheel, J., Ibañez-Cabellos, J.S., García-Lopez, E., Gupta, S., García-Gimenez, J.L., Mena-Mollá, S., Perales-Marín, A. and Morales-Roselló, J. 2021. Overexpression of microRNAs miR-25-3p, miR-185-5p and miR-132-3p in Late Onset Fetal Growth Restriction, Validation of Results and Study of the Biochemical Pathways Involved. *International journal of molecular sciences*. **23**(1).

Love, M.I., Huber, W. and Anders, S. 2014. Moderated estimation of fold change and dispersion for RNA-seq data with DESeq2. *Genome Biology*. **15**(12), p.550.

Lovely, L.P., Fazleabas, A.T., Fritz, M.A., McAdams, D.G. and Lessey, B.A. 2005. Prevention of Endometrial Apoptosis: Randomized Prospective Comparison of Human Chorionic Gonadotropin Versus Progesterone Treatment in the Luteal Phase. *The Journal of Clinical Endocrinology & Metabolism*. **90**(4), pp.2351–2356.

Luo, L., Ye, G., Nadeem, L., Fu, G., Yang, B.B., Honarparvar, E., Dunk, C., Lye, S. and Peng, C. 2012. MicroRNA-378a-5p promotes trophoblast cell survival, migration and invasion by targeting Nodal. *Journal of Cell Science*. **125**(13), 3124 LP – 3132.

Ma, H., Yang, W., Wang, X. and Dai, G. 2022. PRR11 Promotes Proliferation and Migration of Colorectal Cancer through Activating the EGFR/ERK/AKT Pathway via Increasing CTHRC1. *Annals of clinical and laboratory science*. **52**(1), pp.86–94.

Ma, L., Benson, G. V, Lim, H., Dey, S.K. and Maas, R.L. 1998. Abdominal B (AbdB) Hoxa genes: regulation in adult uterus by estrogen and progesterone and repression in müllerian duct by the synthetic estrogen diethylstilbestrol (DES). *Developmental biology*. **197**(2), pp.141–154.

Macfarlane, L.-A. and Murphy, P.R. 2010. MicroRNA: Biogenesis, Function and Role in Cancer. *Current genomics*. **11**(7), pp.537–561.

MacIntyre, D.M., Lim, H.C., Ryan, K., Kimmins, S., Small, J.A. and MacLaren, L.A. 2002. Implantation-Associated Changes in Bovine Uterine Expression of Integrins and Extracellular Matrix1. *Biology of Reproduction*. **66**(5), pp.1430–1436.

Maître, J.-L. 2017. Mechanics of blastocyst morphogenesis. *Biology of the Cell*. **109**(9), pp.323–338.

Marinić, M. and Lynch, V.J. 2020. Relaxed constraint and functional divergence of the progesterone receptor (PGR) in the human stem-lineage. *PLOS Genetics*. **16**(4), p.e1008666.

Marquardt, R.M., Kim, T.H., Shin, J.-H. and Jeong, J.-W. 2019. Progesterone and Estrogen Signaling in the Endometrium: What Goes Wrong in Endometriosis? *International journal of molecular sciences*. **20**(15), p.3822.

Martignani, E., Accornero, P., Miretti, S. and Baratta, M. 2018. Bovine Mammary Organoids: A Model to Study Epithelial Mammary Cells BT - Epithelial Cell Culture: Methods and Protocols *In*: M. Baratta, ed. New York, NY: Springer New York, pp.137–144. Available from: https://doi.org/10.1007/978-1-4939-8600-2_14.

Maslar, I.A., Powers-Craddock, P. and Ansbacher, R. 1986. Decidual Prolactin Production by Organ Cultures of Human Endometrium: Effects of Continuous and Intermittent Progesterone Treatment1. *Biology of Reproduction*. **34**(4), pp.741–750.

Matsumoto, H., Zhao, X., Das, S.K., Hogan, B.L.M. and Dey, S.K. 2002. Indian Hedgehog as a Progesterone-Responsive Factor Mediating Epithelial–Mesenchymal Interactions in the Mouse Uterus. *Developmental Biology*. **245**(2), pp.280–290.

Mattick, J.S. 2001. Non-coding RNAs: the architects of eukaryotic complexity. *EMBO reports*. **2**(11), pp.986–991.

McCracken, J.A., Custer, E.E. and Lamsa, J.C. 1999. Luteolysis: A Neuroendocrine-Mediated Event. *Physiological Reviews*. **79**(2), pp.263–323.

McCreight, J.C., Schneider, S.E., Wilburn, D.B. and Swanson, W.J. 2017. Evolution of microRNA in primates. *PLOS ONE*. **12**(6), p.e0176596.

McGee, E.A. and Hsueh, A.J.W. 2000. Initial and Cyclic Recruitment of Ovarian Follicles*. *Endocrine Reviews*. **21**(2), pp.200–214.

McGowen, M.R., Erez, O., Romero, R. and Wildman, D.E. 2014. The evolution of embryo implantation. *The International journal of developmental biology*. **58**(2–4), pp.155–161.

McMahon, M., Samali, A. and Chevet, E. 2017. Regulation of the unfolded protein response by noncoding RNA. *American Journal of Physiology-Cell Physiology*. **313**(3), pp.C243–C254.

Meijer, H.A., Smith, E.M. and Bushell, M. 2014. Regulation of miRNA strand selection: follow the leader? *Biochemical Society Transactions*. **42**(4), pp.1135–1140.

Meng, Y.G., Han, W.D., Zhao, Y.L., Huang, K., Si, Y.L., Wu, Z.Q. and Mu, Y.M. 2007. Induction of the LRP16 gene by estrogen promotes the invasive growth of Ishikawa human endometrial cancer cells through the downregulation of E-cadherin. *Cell Research*. **17**(10), pp.869–880.

Meseguer, M., Aplin, J.D., Caballero-Campo, P., O'Connor, J.E., Martín, J.C., Remohí, J., Pellicer, A. and Simón, C. 2001. Human Endometrial Mucin MUC1 Is Up-Regulated by Progesterone and Down-Regulated In Vitro by the Human Blastocyst1. *Biology of Reproduction*. **64**(2), pp.590–601.

Messinis, I.E., Messini, C.I. and Dafopoulos, K. 2009. Luteal-phase endocrinology. *Reproductive BioMedicine Online*. **19**, pp.15–29.

Michael Roberts, R., Xie, S. and Mathialagan, N. 1996. Maternal Recognition of Pregnancy1. *Biology of Reproduction*. **54**(2), pp.294–302.

Millar, A.A. and Waterhouse, P.M. 2005. Plant and animal microRNAs: similarities and differences. *Functional & Integrative Genomics*. **5**(3), pp.129–135.

Miura, K., Miura, S., Yamasaki, K., Higashijima, A., Kinoshita, A., Yoshiura, K. and Masuzaki, H. 2010. Identification of Pregnancy-Associated MicroRNAs in Maternal Plasma. *Clinical Chemistry*. **56**(11), pp.1767–1771.

Mo, B., Vendrov, A.E., Palomino, W.A., DuPont, B.R., Apparao, K.B.C. and Lessey, B.A. 2006. ECC-1 Cells: A Well-Differentiated Steroid-Responsive Endometrial Cell Line with Characteristics of Luminal Epithelium1. *Biology of Reproduction*. **75**(3), pp.387–394.

Mohammed, J., Siepel, A. and Lai, E.C. 2014. Diverse modes of evolutionary emergence and flux of conserved microRNA clusters. *RNA* . **20**(12), pp.1850–1863.

Montiel, J.F., Kaune, H. and Maliqueo, M. 2013. Maternal-fetal unit interactions and eutherian neocortical development and evolution. *Frontiers in neuroanatomy*. **7**, p.22.

Moustafa, S. and Young, S.L. 2020. Diagnostic and therapeutic options in recurrent implantation failure. *F1000Research*. **9**.

Nagy, B., Szekeres-Barthó, J., Kovács, G.L., Sulyok, E., Farkas, B., Várnagy, Á., Vértes, V., Kovács, K. and Bódis, J. 2021. Key to Life: Physiological Role and Clinical Implications of Progesterone. *International journal of molecular sciences*. **22**(20).

Napso, T., Yong, H.E.J., Lopez-Tello, J. and Sferruzzi-Perri, A.N. 2018. The Role of Placental Hormones in Mediating Maternal Adaptations to Support Pregnancy and Lactation. *Frontiers in physiology*. **9**, p.1091.

Navid, F. and Colbert, R.A. 2017. Causes and consequences of endoplasmic reticulum stress in rheumatic disease. *Nature Reviews Rheumatology*. **13**(1), pp.25–40.

Ng, S.-W., Norwitz, G.A., Pavlicev, M., Tilburgs, T., Simón, C. and Norwitz, E.R. 2020. Endometrial Decidualization: The Primary Driver of Pregnancy Health. *International journal of molecular sciences*. **21**(11).

Nguyen, H.P.T., Simpson, R.J., Salamonsen, L.A. and Greening, D.W. 2016. Extracellular Vesicles in the Intrauterine Environment: Challenges and Potential Functions. *Biology of reproduction*. **95**(5), p.109.

Nicholson, M.D.O., Lindsay, L.A. and Murphy, C.R. 2010. Ovarian hormones control the changing expression of claudins and occludin in rat uterine epithelial cells during early pregnancy. *Acta Histochemica*. **112**(1), pp.42–52.

Nievelt, A.F.H. van and Smith, K.K. 2005. To replace or not to replace: the significance of reduced functional tooth replacement in marsupial and placental mammals. *Paleobiology*. **31**(2), pp.324–346.

Niswender, G.D., Juengel, J.L., Silva, P.J., Rollyson, M.K. and McIntush, E.W. 2000. Mechanisms Controlling the Function and Life Span of the Corpus Luteum. *Physiological Reviews*. **80**(1), pp.1–29.

O'Brien, J., Hayder, H., Zayed, Y. and Peng, C. 2018. Overview of MicroRNA Biogenesis, Mechanisms of Actions, and Circulation. *Frontiers in endocrinology*. **9**, p.402.

Ochoa-Bernal, M.A. and Fazleabas, A.T. 2020. Physiologic Events of Embryo Implantation and Decidualization in Human and Non-Human Primates.

International journal of molecular sciences. **21**(6).

Oggero, S., Austin-Williams, S. and Norling, L.V. 2019. The Contrasting Role of Extracellular Vesicles in Vascular Inflammation and Tissue Repair . *Frontiers in Pharmacology* . **10**, p.1479.

Ogoyama, M., Ohkuchi, A., Takahashi, H., Zhao, D., Matsubara, S. and Takizawa, T. 2021. LncRNA H19-Derived miR-675-5p Accelerates the Invasion of Extravillous Trophoblast Cells by Inhibiting GATA2 and Subsequently Activating Matrix Metalloproteinases. *International journal of molecular sciences*. **22**(3).

Okada, C., Yamashita, E., Lee, S.J., Shibata, S., Katahira, J., Nakagawa, A., Yoneda, Y. and Tsukihara, T. 2009. A high-resolution structure of the pre-microRNA nuclear export machinery. *Science (New York, N.Y.)*. **326**(5957), pp.1275–1279.

Okada, H., Tsuzuki, T. and Murata, H. 2018. Decidualization of the human endometrium. *Reproductive medicine and biology*. **17**(3), pp.220–227.

Okada, H., Tsuzuki, T., Shindoh, H., Nishigaki, A., Yasuda, K. and Kanzaki, H. 2014. Regulation of decidualization and angiogenesis in the human endometrium: Mini review. *Journal of Obstetrics and Gynaecology Research*. **40**(5), pp.1180–1187.

Okano, A. 1997. Maternal Recognition of Pregnancy in Pigs. *Journal of Reproduction and Development*. **43**(6), pp.j83–j90.

Oliveira, L.J., Barreto, R.S.N., Perecin, F., Mansouri-Attia, N., Pereira, F.T. V and Meirelles, F. V 2012. Modulation of Maternal Immune System During Pregnancy in the Cow. *Reproduction in Domestic Animals*. **47**(s4), pp.384–393.

Oliveros, J.C. n.d. Venny. An interactive tool for comparing lists with Venn's diagrams. Available from: https://bioinfogp.cnb.csic.es/tools/venny/index.html.

Oshima, K., Watanabe, H., Yoshihara, K., Kojima, T., Dochi, O., Takenouchi, N., Fukushima, M. and Komatsu, M. 2003. Gene expression of leukemia inhibitory factor (LIF) and macrophage colony stimulating factor (M-CSF) in bovine endometrium during early pregnancy. *Theriogenology*. **60**(7), pp.1217–1226.

Pan, J. -l., Yuan, D. -z., Zhao, Y. -b., Nie, L., Lei, Y., Liu, M., Long, Y., Zhang, J. -h., Blok, L.J., Burger, C.W. and Yue, L. -m. 2017. Progesterone-induced miR-133a inhibits the proliferation of endometrial epithelial cells. *Acta Physiologica*. **219**(3), pp.685–694.

Pan, X.-Y., Li, X., Weng, Z.-P. and Wang, B. 2009. Altered expression of claudin-3 and claudin-4 in ectopic endometrium of women with endometriosis. *Fertility and Sterility*. **91**(5), pp.1692–1699.

Paoli, P., Giannoni, E. and Chiarugi, P. 2013. Anoikis molecular pathways and its role in cancer progression. *Biochimica et Biophysica Acta (BBA) - Molecular Cell Research*. **1833**(12), pp.3481–3498.

Papari, E., Noruzinia, M., Kashani, L. and Foster, W.G. 2020. Identification of candidate microRNA markers of endometriosis with the use of next-generation sequencing and quantitative real-time polymerase chain reaction. *Fertility and sterility*. **113**(6), pp.1232–1241.

Paria, B.C., Reese, J., Das, S.K. and Dey, S.K. 2002. Deciphering the Cross-Talk of Implantation: Advances and Challenges. *Science*. **296**(5576), pp.2185–2188.

Park, J.-Y., Su, Y.-Q., Ariga, M., Law, E., Jin, S.-L.C. and Conti, M. 2004. EGF-Like Growth Factors As Mediators of LH Action in the Ovulatory Follicle. *Science*. **303**(5658), pp.682–684.

Park, O.-K. and Mayo, K.E. 1991. Transient Expression of Progesterone Receptor Messenger RNA in Ovarian Granuiosa Cells after the Preovulatory Luteinizing Hormone Surge. *Molecular Endocrinology*. **5**(7), pp.967–978.

Parr, E.L., Tung, H.N. and Parr, M.B. 1987. Apoptosis as the mode of uterine epithelial cell death during embryo implantation in mice and rats. *Biology of reproduction*. **36**(1), pp.211–225.

Pasquinelli, A.E., Reinhart, B.J., Slack, F., Martindale, M.Q., Kuroda, M.I., Maller, B., Hayward, D.C., Ball, E.E., Degnan, B., Müller, P., Spring, J., Srinivasan, A., Fishman, M., Finnerty, J., Corbo, J., Levine, M., Leahy, P., Davidson, E. and Ruvkun, G. 2000. Conservation of the sequence and temporal expression of let-7 heterochronic regulatory RNA. *Nature*. **408**(6808), pp.86–89.

Paul, P., Chakraborty, A., Sarkar, D., Langthasa, M., Rahman, M., Bari, M., Singha, R.K.S., Malakar, A.K. and Chakraborty, S. 2018. Interplay between miRNAs and human diseases. *Journal of Cellular Physiology*. **233**(3), pp.2007–2018.

Pawar, S., Starosvetsky, E., Orvis, G.D., Behringer, R.R., Bagchi, I.C. and Bagchi, M.K. 2013. STAT3 regulates uterine epithelial remodeling and epithelial-stromal crosstalk during implantation. *Molecular endocrinology (Baltimore, Md.)*. **27**(12), pp.1996–2012.

Perez, T.D. and Nelson, W.J. 2004. Cadherin adhesion: mechanisms and molecular interactions. *Handbook of experimental pharmacology*. (165), pp.3–21.

Pineles, B.L., Romero, R., Montenegro, D., Tarca, A.L., Han, Y.M., Kim, Y.M., Draghici, S., Espinoza, J., Kusanovic, J.P., Mittal, P., Hassan, S.S. and Kim, C.J. 2007. Distinct subsets of microRNAs are expressed differentially in the human placentas of patients with preeclampsia. *American Journal of Obstetrics and Gynecology*. **196**(3), 261.e1-261.e6.

Place, R.F., Li, L.-C., Pookot, D., Noonan, E.J. and Dahiya, R. 2008. MicroRNA-373 induces expression of genes with complementary promoter sequences. *Proceedings of the National Academy of Sciences*. **105**(5), pp.1608–1613.

Prasanth, K. V and Spector, D.L. 2007. Eukaryotic regulatory RNAs: an answer to the ‘genome complexity’ conundrum. *Genes & Development* . **21**(1), pp.11–42.

Pujuguet, P., Del Maestro, L., Gautreau, A., Louvard, D. and Arpin, M. 2003. Ezrin regulates E-cadherin-dependent adherens junction assembly through Rac1 activation. *Molecular biology of the cell*. **14**(5), pp.2181–2191.

Qiao, W., Wang, H., Zhang, X. and Luo, K. 2019. Proline-rich protein 11 silencing inhibits hepatocellular carcinoma growth and epithelial-

mesenchymal transition through β-catenin signaling. *Gene*. **681**, pp.7–14.

Qu, X., Fang, Y., Zhuang, S. and Zhang, Y. 2021. Micro-RNA miR-542-3p suppresses decidualization by targeting ILK pathways in human endometrial stromal cells. *Scientific Reports*. **11**(1), p.7186.

Queckbörner, S., Syk Lundberg, E., Gemzell-Danielsson, K. and Davies, L.C. 2020. Endometrial stromal cells exhibit a distinct phenotypic and immunomodulatory profile. *Stem Cell Research & Therapy*. **11**(1), p.15.

R Core Team 2021. R: A language and environment for statistical computing. *R Foundation for Statistical Computing, Vienna, Austria*.

Radi, Z.A., Marusak, R.A. and Morris, D.L. 2009. Species Comparison of the Role of p38 MAP Kinase in the Female Reproductive System. *Journal of toxicologic pathology*. **22**(2), pp.109–124.

Rae, J.M., Johnson, M.D., Cordero, K.E., Scheys, J.O., Larios, J.M., Gottardis, M.M., Pienta, K.J. and Lippman, M.E. 2006. GREB1 is a novel androgen-regulated gene required for prostate cancer growth. *The Prostate*. **66**(8), pp.886–894.

Rae, J.M., Johnson, M.D., Scheys, J.O., Cordero, K.E., Larios, J.M. and Lippman, M.E. 2005. GREB1 is a critical regulator of hormone dependent breast cancer growth. *Breast Cancer Research and Treatment*. **92**(2), pp.141–149.

Raheem, K.A. 2017. An insight into maternal recognition of pregnancy in mammalian species. *Journal of the Saudi Society of Agricultural Sciences*. **16**(1), pp.1–6.

Rana, S., Lemoine, E., Granger, J.P. and Karumanchi, S.A. 2019. Preeclampsia. *Circulation Research*. **124**(7), pp.1094–1112.

Rankin, A. and Clauss, N. 2021. Evolution of Live Birth in Mammals (140 MYA) BT - Encyclopedia of Evolutionary Psychological Science *In*: T. K. Shackelford and V. A. Weekes-Shackelford, eds. Cham: Springer International Publishing, pp.2554–2559. Available from: https://doi.org/10.1007/978-3-319-19650-3_711.

Rawlings, T.M., Makwana, K., Taylor, D.M., Molè, M.A., Fishwick, K.J., Tryfonos, M., Odendaal, J., Hawkes, A., Zernicka-Goetz, M. and Hartshorne, G.M. 2021. Modelling the impact of decidual senescence on embryo implantation in human endometrial assembloids. *Elife*. **10**, p.e69603.

Rawlings, T.M., Makwana, K., Tryfonos, M. and Lucas, E.S. 2021. Organoids to model the endometrium: implantation and beyond. *Reproduction and Fertility*. **2**(3), pp.R85–R101.

Read, A. and Schröder, M. 2021. The Unfolded Protein Response: An Overview. *Biology*. **10**(5).

Reed, B.G., Babayev, S.N., Chen, L.X., Carr, B.R., Word, R.A. and Jimenez, P.T. 2018. Estrogen-regulated miRNA-27b is altered by bisphenol A in human endometrial stromal cells. *Reproduction*. **156**(6), pp.559–567.

Reinhart, B.J., Slack, F.J., Basson, M., Pasquinelli, A.E., Bettinger, J.C., Rougvie, A.E., Horvitz, H.R. and Ruvkun, G. 2000. The 21-nucleotide let-7 RNA regulates developmental timing in Caenorhabditis elegans. *Nature*.

403(6772), pp.901–906.

Rekker, K., Saare, M., Roost, A.M., Salumets, A. and Peters, M. 2013. Circulating microRNA Profile throughout the Menstrual Cycle. *PLOS ONE*. **8**(11), p.e81166.

Renfree, M.B. 2010. Review: Marsupials: Placental Mammals with a Difference. *Placenta*. **31**, pp.S21–S26.

Revel, A., Achache, H., Stevens, J., Smith, Y. and Reich, R. 2011. MicroRNAs are associated with human embryo implantation defects. *Human reproduction*. **26**(10), pp.2830–2840.

Reynolds, L.P., Grazul-Bilska, A.T. and Redmer, D.A. 2000. Angiogenesis in the corpus luteum. *Endocrine*. **12**(1), pp.1–9.

Reza, A.M.M.T., Choi, Y.-J., Han, S.G., Song, H., Park, C., Hong, K. and Kim, J.-H. 2019. Roles of microRNAs in mammalian reproduction: from the commitment of germ cells to peri-implantation embryos. *Biological Reviews*. **94**(2), pp.415–438.

Richards, J.S., Russell, D.L., Robker, R.L., Dajee, M. and Alliston, T.N. 1998. Molecular mechanisms of ovulation and luteinization. *Molecular and Cellular Endocrinology*. **145**(1), pp.47–54.

Ridlo, M.R., Kim, E.H. and Kim, G.A. 2021. MicroRNA-210 Regulates Endoplasmic Reticulum Stress and Apoptosis in Porcine Embryos. *Animals : an open access journal from MDPI*. **11**(1).

Riesewijk, A., Martín, J., van Os, R., Horcajadas, J.A., Polman, J., Pellicer, A., Mosselman, S. and Simón, C. 2003. Gene expression profiling of human endometrial receptivity on days LH+2 versus LH+7 by microarray technology. *Molecular Human Reproduction*. **9**(5), pp.253–264.

Roberts, R.M., Green, J.A. and Schulz, L.C. 2016. The evolution of the placenta. *Reproduction (Cambridge, England)*. **152**(5), pp.R179–R189.

Robinson, M.D., McCarthy, D.J. and Smyth, G.K. 2010. edgeR: a Bioconductor package for differential expression analysis of digital gene expression data. *Bioinformatics (Oxford, England)*. **26**(1), pp.139–140.

Robker, R.L., Hennebold, J.D. and Russell, D.L. 2018. Coordination of Ovulation and Oocyte Maturation: A Good Egg at the Right Time. *Endocrinology*. **159**(9), pp.3209–3218.

Roche, J.F. 1996. Control and regulation of folliculogenesis--a symposium in perspective. *Reviews of Reproduction*. **1**(1), pp.19–27.

Rodríguez-Rodríguez, P., Ramiro-Cortijo, D., Reyes-Hernández, C.G., López de Pablo, A.L., González, M.C. and Arribas, S.M. 2018. Implication of Oxidative Stress in Fetal Programming of Cardiovascular Disease . *Frontiers in Physiology* . **9**.

Romero-Ruiz, A., Avendaño, M.S., Dominguez, F., Lozoya, T., Molina-Abril, H., Sangiao-Alvarellos, S., Gurrea, M., Lara-Chica, M., Fernandez-Sanchez, M., Torres-Jimenez, E., Perdices-Lopez, C., Abbara, A., Steffani, L., Calzado, M.A., Dhillo, W.S., Pellicer, A. and Tena-Sempere, M. 2019. Deregulation of miR-324/KISS1/kisspeptin in early ectopic pregnancy: mechanistic findings with clinical and diagnostic implications. *American Journal of Obstetrics & Gynecology*. **220**(5), 480.e1-480.e17.

Rongxin, S., Pengfei, L., Li, S., Xiaochen, J. and Yihe, H. 2019. MicroRNA-340-5p suppresses osteosarcoma development by down-regulating the Wnt/β-catenin signaling pathway via targeting the STAT3 gene. *European review for medical and pharmacological sciences*. **23**(3), pp.982–991.

Rothbauer, M., Patel, N., Gondola, H., Siwetz, M., Huppertz, B. and Ertl, P. 2017. A comparative study of five physiological key parameters between four different human trophoblast-derived cell lines. *Scientific Reports*. **7**(1), p.5892.

Ruane, P.T., Buck, C.J., Babbington, P.A., Aboussahoud, W., Berneau, S.C., Westwood, M., Kimber, S.J., Aplin, J.D. and Brison, D.R. 2020. The effects of hyaluronate-containing medium on human embryo attachment to endometrial epithelial cells in vitro. *Human reproduction open*. **2020**(2), p.hoz033.

Ruby, J.G., Jan, C.H. and Bartel, D.P. 2007. Intronic microRNA precursors that bypass Drosha processing. *Nature*. **448**(7149), pp.83–86.

Sánchez, J.M., Mathew, D.J., Passaro, C., Fair, T. and Lonergan, P. 2018. Embryonic maternal interaction in cattle and its relationship with fertility. *Reproduction in Domestic Animals*. **53**(S2), pp.20–27.

Sato, T., Stange, D.E., Ferrante, M., Vries, R.G.J., Van Es, J.H., Van den Brink, S., Van Houdt, W.J., Pronk, A., Van Gorp, J., Siersema, P.D. and Clevers, H. 2011. Long-term expansion of epithelial organoids from human colon, adenoma, adenocarcinoma, and Barrett's epithelium. *Gastroenterology*. **141**(5), pp.1762–1772.

Satokata, I., Benson, G. and Maas, R. 1995. Sexually dimorphic sterility phenotypes in Hoxa10-deficient mice. *Nature*. **374**(6521), pp.460–463.

Scalavino, V., Piccinno, E., Lacalamita, A., Tafaro, A., Armentano, R., Giannelli, G. and Serino, G. 2022. miR-195-5p Regulates Tight Junctions Expression via Claudin-2 Downregulation in Ulcerative Colitis. *Biomedicines*. **10**(4).

Schmidt, O. and Teis, D. 2012. The ESCRT machinery. *Current biology : CB*. **22**(4), pp.R116-20.

Schroeder, M., Jakovcevski, M., Polacheck, T., Drori, Y., Luoni, A., Roeh, S., Zaugg, J., Ben-Dor, S., Albrecht, C. and Chen, A. 2018. Placental miR-340 mediates vulnerability to activity based anorexia in mice. *Nature Communications*. **9**.

Segura-Benítez, M., Carbajo-García, M.C., Corachán, A., Faus, A., Pellicer, A. and Ferrero, H. 2022. Proteomic analysis of extracellular vesicles secreted by primary human epithelial endometrial cells reveals key proteins related to embryo implantation. *Reproductive biology and endocrinology : RB&E*. **20**(1), p.3.

Sempere, L.F., Cole, C.N., Mcpeek, M.A. and Peterson, K.J. 2006. The phylogenetic distribution of metazoan microRNAs: insights into evolutionary complexity and constraint. *Journal of Experimental Zoology Part B: Molecular and Developmental Evolution*. **306B**(6), pp.575–588.

Serafini, P.C., Silva, I.D.C.G., Smith, G.D., Motta, E.L.A., Rocha, A.M. and Baracat, E.C. 2009. Endometrial claudin-4 and leukemia inhibitory factor are associated with assisted reproduction outcome. *Reproductive Biology and Endocrinology*. **7**(1), p.30.

Seshagiri, P.B., Sen Roy, S., Sireesha, G. and Rao, R.P. 2009. Cellular and molecular regulation of mammalian blastocyst hatching. *Journal of Reproductive Immunology*. **83**(1), pp.79–84.

Seshagiri, P.B., Vani, V. and Madhulika, P. 2016. Cytokines and Blastocyst Hatching. *American Journal of Reproductive Immunology*. **75**(3), pp.208–217.

Shahbazi, M.N. 2020. Mechanisms of human embryo development: from cell fate to tissue shape and back. *Development (Cambridge, England)*. **147**(14).

Shang, X., Lin, X., Alvarez, E., Manorek, G. and Howell, S.B. 2012. Tight Junction Proteins Claudin-3 and Claudin-4 Control Tumor Growth and Metastases. *Neoplasia*. **14**(10), pp.974-IN22.

Shekibi, M., Heng, S. and Nie, G. 2022. MicroRNAs in the Regulation of Endometrial Receptivity for Embryo Implantation. *International Journal of Molecular Sciences*. **23**(11), p.6210.

Shi, C., Shen, H., Fan, L.-J., Guan, J., Zheng, X.-B., Chen, X., Liang, R., Zhang, X.-W., Cui, Q.-H., Sun, K.-K., Zhao, Z.-R. and Han, H.-J. 2017. Endometrial MicroRNA Signature during the Window of Implantation Changed in Patients with Repeated Implantation Failure. *Chinese Medical Journal*. **130**(5), pp.566–573.

Shu, J., Silva, B.V.R. e., Gao, T., Xu, Z. and Cui, J. 2017. Dynamic and Modularized MicroRNA Regulation and Its Implication in Human Cancers. *Scientific Reports*. **7**(1), p.13356.

Sidow, A. 1996. Gen(om)e duplications in the evolution of early vertebrates. *Current Opinion in Genetics & Development*. **6**(6), pp.715–722.

Simon, A. and Laufer, N. 2012. Assessment and treatment of repeated implantation failure (RIF). *Journal of assisted reproduction and genetics*. **29**(11), pp.1227–1239.

Simón, C., Mercader, A., Garcia-Velasco, J., Nikas, G., Moreno, C., Remohí, J. and Pellicer, A. 1999. Coculture of Human Embryos with Autologous Human Endometrial Epithelial Cells in Patients with Implantation Failure1. *The Journal of Clinical Endocrinology & Metabolism*. **84**(8), pp.2638–2646.

Singh, H. and Aplin, J.D. 2015. Endometrial apical glycoproteomic analysis reveals roles for cadherin 6, desmoglein-2 and plexin b2 in epithelial integrity. *Molecular Human Reproduction*. **21**(1), pp.81–94.

Singh, M., Chaudhry, P. and Asselin, E. 2011. Bridging endometrial receptivity and implantation: network of hormones, cytokines, and growth factors. *Journal of Endocrinology*. **210**(1), pp.5–14.

Singh, N., Gupta, M., Kriplani, A. and Vanamail, P. 2015. Role of Embryo Glue as a transfer medium in the outcome of fresh non-donor in-vitro fertilization cycles. *Journal of human reproductive sciences*. **8**(4), pp.214–217.

Skinner, M.K. 2005. Regulation of primordial follicle assembly and development. *Human Reproduction Update*. **11**(5), pp.461–471.

Skinner, M.K., Schmidt, M., Savenkova, M.I., Sadler-Riggleman, I. and Nilsson, E.E. 2008. Regulation of granulosa and theca cell transcriptomes during ovarian antral follicle development. *Molecular reproduction and*

development. **75**(9), pp.1457–1472.

Skommer, J., Rana, I., Marques, F.Z., Zhu, W., Du, Z. and Charchar, F.J. 2014. Small molecules, big effects: the role of microRNAs in regulation of cardiomyocyte death. *Cell death & disease*. **5**(7), p.e1325.

Sobel, G., Németh, J., Kiss, A., Lotz, G., Szabó, I., Udvarhelyi, N., Schaff, Z. and Páska, C. 2006. Claudin 1 differentiates endometrioid and serous papillary endometrial adenocarcinoma. *Gynecologic Oncology*. **103**(2), pp.591–598.

Soczewski, E., Grasso, E., Gallino, L., Hauk, V., Fernández, L., Gori, S., Paparini, D., Perez Leirós, C. and Ramhorst, R. 2020. Immunoregulation of the decidualization program: focus on the endoplasmic reticulum stress. *Reproduction*. **159**(4), pp.R203–R211.

Soczewski, E., Murrieta-Coxca, J.M., Miranda, L., Fuentes-Zacarías, P., Gutiérrez-Samudio, R., Grasso, E., Marti, M., Leirós, C.P., Morales-Prieto, D., Markert, U.R. and Ramhorst, R. 2023. miRNA associated with endoplasmic reticulum stress and unfolded protein response during decidualization. *Reproductive BioMedicine Online*., p.103289.

Spencer, T.E. 2013. Early pregnancy: Concepts, challenges, and potential solutions. *Animal Frontiers*. **3**(4), pp.48–55.

Spencer, T.E. and Gray, C.A. 2006. Sheep uterine gland knockout (UGKO) model. *Methods in molecular medicine*. **121**, pp.85–94.

Staun-Ram, E. and Shalev, E. 2005. Human trophoblast function during the implantation process. *Reproductive Biology and Endocrinology*. **3**(1), p.56.

Stefanoska, I., Jovanović Krivokuća, M., Vasilijić, S., Ćujić, D. and Vićovac, L. 2013. Prolactin stimulates cell migration and invasion by human trophoblast in vitro. *Placenta*. **34**(9), pp.775–783.

Stefanski, A.L., Martinez, N., Peterson, L.K., Callahan, T.J., Treacy, E., Luck, M., Friend, S.F., Hermesch, A., Maltepe, E., Phang, T., Dragone, L.L. and Winn, V.D. 2019. Murine trophoblast-derived and pregnancy-associated exosome-enriched extracellular vesicle microRNAs: Implications for placenta driven effects on maternal physiology. *PLOS ONE*. **14**(2), p.e0210675.

Stewart, C.L., Kaspar, P., Brunet, L.J., Bhatt, H., Gadi, I., Köntgen, F. and Abbondanzo, S.J. 1992. Blastocyst implantation depends on maternal expression of leukaemia inhibitory factor. *Nature*. **359**(6390), pp.76–79.

Stirm, L., Huypens, P., Sass, S., Batra, R., Fritsche, L., Brucker, S., Abele, H., Hennige, A.M., Theis, F., Beckers, J., Hrabě de Angelis, M., Fritsche, A., Häring, H.-U. and Staiger, H. 2018. Maternal whole blood cell miRNA-340 is elevated in gestational diabetes and inversely regulated by glucose and insulin. *Scientific reports*. **8**(1), p.1366.

Stocco, C., Telleria, C. and Gibori, G. 2007. The Molecular Control of Corpus Luteum Formation, Function, and Regression. *Endocrine Reviews*. **28**(1), pp.117–149.

Su, R.-W. and Fazleabas, A.T. 2015. Implantation and Establishment of Pregnancy in Human and Nonhuman Primates. *Advances in anatomy, embryology, and cell biology*. **216**, pp.189–213.

Sun, N., Meng, X., Liu, Y., Song, D., Jiang, C. and Cai, J. 2021. Applications of brain organoids in neurodevelopment and neurological diseases. *Journal of Biomedical Science*. **28**(1), p.30.

Sun, Q. and Zhu, E. 2023. Molecular mechanism and diagnostic marker investigation of endoplasmic reticulum stress on periodontitis. *BMC oral health*. **23**(1), p.135.

Sun, X. and Kaufman, P.D. 2018. Ki-67: more than a proliferation marker. *Chromosoma*. **127**(2), pp.175–186.

Tabas, I. and Ron, D. 2011. Integrating the mechanisms of apoptosis induced by endoplasmic reticulum stress. *Nature cell biology*. **13**(3), pp.184–190.

Takamoto, N., Zhao, B., Tsai, S.Y. and DeMayo, F.J. 2002. Identification of Indian Hedgehog as a Progesterone-Responsive Gene in the Murine Uterus. *Molecular Endocrinology*. **16**(10), pp.2338–2348.

Takasato, M., Er, P.X., Chiu, H.S., Maier, B., Baillie, G.J., Ferguson, C., Parton, R.G., Wolvetang, E.J., Roost, M.S., Lopes, S.M.C. de S. and Little, M.H. 2016. Erratum: Kidney organoids from human iPS cells contain multiple lineages and model human nephrogenesis. *Nature*. **536**(7615), p.238.

Tamm, K., Rõõm, M., Salumets, A. and Metsis, M. 2009. Genes targeted by the estrogen and progesterone receptors in the human endometrial cell lines HEC1A and RL95-2. *Reproductive biology and endocrinology : RB&E*. **7**, p.150.

Tan, X., Li, Z., Ren, S., Rezaei, K., Pan, Q., Goldstein, A.T., Macri, C.J., Cao, D., Brem, R.F. and Fu, S.W. 2019. Dynamically decreased miR-671-5p expression is associated with oncogenic transformation and radiochemoresistance in breast cancer. *Breast cancer research : BCR*. **21**(1), p.89.

Tang, Q., Wu, W., Xu, X., Huang, L., Gao, Q., Chen, H., Sun, H., Xia, Y., Sha, J., Wang, X., Chen, D. and Xu, Q. 2013. miR-141 contributes to fetal growth restriction by regulating PLAG1 expression. *PloS one*. **8**(3), p.e58737.

Taraborrelli, S. 2015. Physiology, production and action of progesterone. *Acta Obstetricia et Gynecologica Scandinavica*. **94**(S161), pp.8–16.

Taylor, A.S., Tinning, H., Ovchinnikov, V., Edge, J., Smith, W., Pullinger, A.L., Sutton, R.A., Constantinides, B., Wang, D., Forbes, K., Forde, N. and O'Connell, M.J. 2023. A burst of genomic innovation at the origin of placental mammals mediated embryo implantation. *Communications Biology*. **6**(1), p.459.

Taylor, A.S., Tinning, H., Ovchinnikov, V., Smith, W., Pullinger, A.L., Sutton, R.A., Constantinides, B., Wang, D., Forde, N. and O'Connell, M.J. 2021. A burst of regulatory and protein innovation at the origin of placental mammals drove the emergence of placenta and underpins divergent early pregnancy strategies in modern mammals. *bioRxiv*., 2021.07.22.453388.

Teeli, A.S., Leszczyński, P., Krishnaswamy, N., Ogawa, H., Tsuchiya, M., Śmiech, M., Skarzynski, D. and Taniguchi, H. 2019. Possible Mechanisms for Maintenance and Regression of Corpus Luteum Through the Ubiquitin-Proteasome and Autophagy System Regulated by Transcriptional Factors. *Frontiers in endocrinology*. **10**, p.748.

Teklenburg, G., Salker, M., Molokhia, M., Lavery, S., Trew, G., Aojanepong, T., Mardon, H.J., Lokugamage, A.U., Rai, R., Landles, C., Roelen, B.A.J., Quenby, S., Kuijk, E.W., Kavelaars, A., Heijnen, C.J., Regan, L., Brosens, J.J. and Macklon, N.S. 2010. Natural selection of human embryos: decidualizing endometrial stromal cells serve as sensors of embryo quality upon implantation. *PloS one*. **5**(4), p.e10258.

Ticconi, C., Zicari, A., Belmonte, A., Realacci, M., Rao, C.V. and Piccione, E. 2007. Pregnancy-Promoting Actions of HCG in Human Myometrium and Fetal Membranes. *Placenta*. **28**, pp.S137–S143.

Timofeeva, A. V, Gusar, V.A., Kan, N.E., Prozorovskaya, K.N., Karapetyan, A.O., Bayev, O.R., Chagovets, V. V, Kliver, S.F., Iakovishina, D.Y., Frankevich, V.E. and Sukhikh, G.T. 2018. Identification of potential early biomarkers of preeclampsia. *Placenta*. **61**, pp.61–71.

Tinning, H., Edge, J.C., DeBem, T.H.C., Deligianni, F., Giovanardi, G., Pensabene, V., Meirelles, F. V and Forde, N. 2023. Review: Endometrial function in pregnancy establishment in cattle. *animal*. **17**, p.100751.

Tinning, H., Taylor, A., Wang, D., Constantinides, B., Sutton, R., Oikonomou, G., Velazquez, M.A., Thompson, P., Treumann, A., O'Connell, M.J. and Forde, N. 2020. The role of CAPG in molecular communication between the embryo and the uterine endometrium: Is its function conserved in species with different implantation strategies? *bioRxiv*., 2020.02.19.953794.

Tochigi, H., Kajihara, T., Mizuno, Yosuke, Mizuno, Yumi, Tamaru, S., Kamei, Y., Okazaki, Y., Brosens, J.J. and Ishihara, O. 2017. Loss of miR-542-3p enhances IGFBP-1 expression in decidualizing human endometrial stromal cells. *Scientific Reports*. **7**(1), p.40001.

Tolomeo, M. and Cascio, A. 2021. The Multifaced Role of STAT3 in Cancer and Its Implication for Anticancer Therapy. *International journal of molecular sciences*. **22**(2).

Totti, S., Ng, K.W., Dale, L., Lian, G., Chen, T. and Velliou, E.G. 2019. A novel versatile animal-free 3D tool for rapid low-cost assessment of immunodiagnostic microneedles. *Sensors and Actuators B: Chemical*. **296**, p.126652.

Tremblay, Y.D.N., Vogeleer, P., Jacques, M. and Harel, J. 2015. High-throughput microfluidic method to study biofilm formation and host-pathogen interactions in pathogenic Escherichia coli. *Applied and environmental microbiology*. **81**(8), pp.2827–2840.

Tsutsumi, R. and Webster, N.J.G. 2009. GnRH pulsatility, the pituitary response and reproductive dysfunction. *Endocrine journal*. **56**(6), pp.729–737.

Turco, M.Y., Gardner, L., Hughes, J., Cindrova-Davies, T., Gomez, M.J., Farrell, L., Hollinshead, M., Marsh, S.G.E., Brosens, J.J., Critchley, H.O., Simons, B.D., Hemberger, M., Koo, B.-K., Moffett, A. and Burton, G.J. 2017. Long-term, hormone-responsive organoid cultures of human endometrium in a chemically defined medium. *Nature Cell Biology*. **19**(5), pp.568–577.

Vogel, C. and Chothia, C. 2006. Protein family expansions and biological complexity. *PLoS computational biology*. **2**(5), p.e48.

Wallach, E.E., Shoham, Z., Schachter, M., Loumaye, E., Weissman, A.,

MacNamee, M. and Insler, V. 1995. The luteinizing hormone surge—the final stage in ovulation induction: modern aspects of ovulation triggering. *Fertility and Sterility*. **64**(2), pp.237–251.

Walter, P. and Ron, D. 2011. The Unfolded Protein Response: From Stress Pathway to Homeostatic Regulation. *Science*. **334**(6059), pp.1081–1086.

Wan, Y., Huang, J., Song, Y., Gu, C., Kong, J., Zuo, L. and Chen, J. 2022. hsa-miR-340-5p inhibits epithelial-mesenchymal transition in endometriosis by targeting MAP3K2 and inactivating MAPK/ERK signaling. *Open medicine (Warsaw, Poland)*. **17**(1), pp.566–576.

Wang, H., Brown, J., Gao, S., Liang, S., Jotwani, R., Zhou, H., Suttles, J., Scott, D.A. and Lamont, R.J. 2013. The Role of JAK-3 in Regulating TLR-Mediated Inflammatory Cytokine Production in Innate Immune Cells. *The Journal of Immunology*. **191**(3), pp.1164–1174.

Wang, H., Pilla, F., Anderson, S., Martínez-Escribano, S., Herrer, I., Moreno-Moya, J.M., Musti, S., Bocca, S., Oehninger, S. and Horcajadas, J.A. 2012. A novel model of human implantation: 3D endometrium-like culture system to study attachment of human trophoblast (Jar) cell spheroids. *Molecular Human Reproduction*. **18**(1), pp.33–43.

Wang, J., Zhang, L., Jiang, W., Zhang, R., Zhang, B., Silayiding, A. and Duan, X. 2020. MicroRNA-135a promotes proliferation, migration, invasion and induces chemoresistance of endometrial cancer cells. *European Journal of Obstetrics & Gynecology and Reproductive Biology: X*. **5**, p.100103.

Weatherbee, B.A.T., Cui, T. and Zernicka-Goetz, M. 2021. Modeling human embryo development with embryonic and extra-embryonic stem cells. *Developmental biology*. **474**, pp.91–99.

Wei, J.-W., Huang, K., Yang, C. and Kang, C.-S. 2017. Non-coding RNAs as regulators in epigenetics (Review). *Oncol Rep*. **37**(1), pp.3–9.

Wei, Q., Guo, Z., Chen, D. and Jia, X. 2020. MiR-542-3p Suppresses Neuroblastoma Cell Proliferation and Invasion by Downregulation of KDM1A and ZNF346. *Open life sciences*. **15**, pp.173–184.

Wessels, J.M., Edwards, A.K., Khalaj, K., Kridli, R.T., Bidarimath, M. and Tayade, C. 2013. The microRNAome of pregnancy: deciphering miRNA networks at the maternal-fetal interface. *PloS one*. **8**(11), p.e72264.

Wetendorf, M. and DeMayo, F.J. 2012. The progesterone receptor regulates implantation, decidualization, and glandular development via a complex paracrine signaling network. *Molecular and cellular endocrinology*. **357**(1–2), pp.108–118.

Wightman, B., Ha, I. and Ruvkun, G. 1993. Posttranscriptional regulation of the heterochronic gene lin-14 by lin-4 mediates temporal pattern formation in C. elegans. *Cell*. **75**(5), pp.855–862.

Wildman, D.E., Chen, C., Erez, O., Grossman, L.I., Goodman, M. and Romero, R. 2006. Evolution of the mammalian placenta revealed by phylogenetic analysis. *Proceedings of the National Academy of Sciences of the United States of America*. **103**(9), 3203 LP – 3208.

Wu, L. and Belasco, J.G. 2008. Let Me Count the Ways: Mechanisms of Gene Regulation by miRNAs and siRNAs. *Molecular Cell*. **29**(1), pp.1–7.

Wu, Z., Wu, Q., Wang, C., Wang, X., Huang, J., Zhao, J., Mao, S., Zhang, G., Xu, X. and Zhang, N. 2011. miR-340 inhibition of breast cancer cell migration and invasion through targeting of oncoprotein c-Met. *Cancer*. **117**(13), pp.2842–2852.

Xiao, S., Coppeta, J.R., Rogers, H.B., Isenberg, B.C., Zhu, J., Olalekan, S.A., McKinnon, K.E., Dokic, D., Rashedi, A.S., Haisenleder, D.J., Malpani, S.S., Arnold-Murray, C.A., Chen, K., Jiang, M., Bai, L., Nguyen, C.T., Zhang, J., Laronda, M.M., Hope, T.J., Maniar, K.P., Pavone, M.E., Avram, M.J., Sefton, E.C., Getsios, S., Burdette, J.E., Kim, J.J., Borenstein, J.T. and Woodruff, T.K. 2017. A microfluidic culture model of the human reproductive tract and 28-day menstrual cycle. *Nature Communications*. **8**(1), p.14584.

Xie, W., Qin, W., Kang, Y., Zhou, Z. and Qin, A. 2016. MicroRNA-340 Inhibits Tumor Cell Proliferation and Induces Apoptosis in Endometrial Carcinoma Cell Line RL 95-2. *Medical science monitor : international medical journal of experimental and clinical research*. **22**, pp.1540–1546.

Yang, C., Wang, M.-H., Zhou, J.-D. and Chi, Q. 2017. Upregulation of miR-542-3p inhibits the growth and invasion of human colon cancer cells through PI3K/AKT/survivin signaling. *Oncol Rep*. **38**(6), pp.3545–3553.

Yang, F., Zhang, Ling, Wang, F., Wang, Yue, Huo, X., Yin, Y., Wang, Yu-qi, Zhang, Lin and Sun, S. 2011. Modulation of the Unfolded Protein Response Is the Core of MicroRNA-122-Involved Sensitivity to Chemotherapy in Hepatocellular Carcinoma. *Neoplasia*. **13**(7), pp.590-IN4.

Yang, J.-S., Maurin, T., Robine, N., Rasmussen, K.D., Jeffrey, K.L., Chandwani, R., Papapetrou, E.P., Sadelain, M., O'Carroll, D. and Lai, E.C. 2010. Conserved vertebrate mir-451 provides a platform for Dicer-independent, Ago2-mediated microRNA biogenesis. *Proceedings of the National Academy of Sciences*. **107**(34), pp.15163–15168.

Yang, Q., Gu, W.-W., Gu, Y., Yan, N.-N., Mao, Y.-Y., Zhen, X.-X., Wang, J.-M., Yang, J., Shi, H.-J., Zhang, X. and Wang, J. 2018. Association of the peripheral blood levels of circulating microRNAs with both recurrent miscarriage and the outcomes of embryo transfer in an in vitro fertilization process. *Journal of translational medicine*. **16**(1), p.186.

Ye, J., Luo, W., Luo, L., Zhai, L. and Huang, P. 2022. MicroRNA-671-5p inhibits cell proliferation, migration and invasion in non-small cell lung cancer by targeting MFAP3L. *Molecular medicine reports*. **25**(1).

Yoon, S., Choi, Y.-C., Lee, S., Jeong, Y., Yoon, J. and Baek, K. 2010. Induction of growth arrest by miR-542-3p that targets survivin. *FEBS Letters*. **584**(18), pp.4048–4052.

Young, S.L. 2013. Oestrogen and progesterone action on endometrium: a translational approach to understanding endometrial receptivity. *Reproductive biomedicine online*. **27**(5), pp.497–505.

Yu, K., Huang, Z.-Y., Xu, X.-L., Li, J., Fu, X.-W. and Deng, S.-L. 2022. Estrogen Receptor Function: Impact on the Human Endometrium. *Frontiers in endocrinology*. **13**, p.827724.

Yuan, J., Ji, H., Xiao, F., Lin, Z., Zhao, X., Wang, Z., Zhao, J. and Lu, J. 2017. MicroRNA-340 inhibits the proliferation and invasion of hepatocellular

carcinoma cells by targeting JAK1. *Biochemical and Biophysical Research Communications*. **483**(1), pp.578–584.

Yung, Y., Aviel-Ronen, S., Maman, E., Rubinstein, N., Avivi, C., Orvieto, R. and Hourvitz, A. 2014. Localization of luteinizing hormone receptor protein in the human ovary. *Molecular Human Reproduction*. **20**(9), pp.844–849.

Zeleznik, A.J. 2004. The physiology of follicle selection. *Reproductive biology and endocrinology : RB&E*. **2**, p.31.

Zhang, X. and Wei, H. 2021. Role of Decidual Natural Killer Cells in Human Pregnancy and Related Pregnancy Complications. *Frontiers in immunology*. **12**, p.728291.

Zhao, M., Zhang, W.-Q. and Liu, J.-L. 2017. A study on regional differences in decidualization of the mouse uterus. *Reproduction*. **153**(5), pp.645–653.

Zhao, R., Fu, J., Zhu, L., Chen, Y. and Liu, B. 2022. Designing strategies of small-molecule compounds for modulating non-coding RNAs in cancer therapy. *Journal of hematology & oncology*. **15**(1), p.14.

Zhao, Z., Chen, X., Dowbaj, A.M., Sljukic, A., Bratlie, K., Lin, L., Fong, E.L.S., Balachander, G.M., Chen, Z., Soragni, A., Huch, M., Zeng, Y.A., Wang, Q. and Yu, H. 2022. Organoids. *Nature Reviews Methods Primers*. **2**(1), p.94.

Zhong, Y., Zhu, F. and Ding, Y. 2019. Differential microRNA expression profile in the plasma of preeclampsia and normal pregnancies. *Experimental and therapeutic medicine*. **18**(1), pp.826–832.

Zhou, W., Santos, L. and Dimitriadis, E. 2020. Characterization of the role for cadherin 6 in the regulation of human endometrial receptivity. *Reproductive biology and endocrinology : RB&E*. **18**(1), p.66.

Zhu, B., Tian, T. and Zhao, M. 2020. MiR-645 promotes proliferation and migration of non-small cell lung cancer cells by targeting TP53I11. *European review for medical and pharmacological sciences*. **24**(11), pp.6150–6156.

Zhu, J., Xu, Z., Wu, P., Zeng, C., Peng, C., Zhou, Y. and Xue, Q. 2023. MicroRNA-92a-3p Inhibits Cell Proliferation and Invasion by Regulating the Transcription Factor 21/Steroidogenic Factor 1 Axis in Endometriosis. *Reproductive Sciences*. **30**(7), pp.2188–2197.

Zhu, M., Leung, C.Y., Shahbazi, M.N. and Zernicka-Goetz, M. 2017. Actomyosin polarisation through PLC-PKC triggers symmetry breaking of the mouse embryo. *Nature Communications*. **8**(1), p.921.

Zhu, Z., Luo, L., Xiang, Q., Wang, J., Liu, Y., Deng, Y. and Zhao, Z. 2020. MiRNA-671-5p Promotes prostate cancer development and metastasis by targeting NFIA/CRYAB axis. *Cell Death & Disease*. **11**(11), p.949.